

Vicente Gilabert Pérez

Vulcanismo del Decán, impacto de  
Chicxulub, control orbital y  
extinción masiva de los  
foraminíferos planctónicos: Un  
estudio multidisciplinar a través del  
tránsito Cretácico-Paleógeno

Director/es

Arz Sola, José Antonio  
Arenillas Sierra, Ignacio

<http://zaguan.unizar.es/collection/Tesis>

© Universidad de Zaragoza  
Servicio de Publicaciones

ISSN 2254-7606



**Universidad**  
Zaragoza

Tesis Doctoral

VULCANISMO DEL DECÁN, IMPACTO DE  
CHICXULUB, CONTROL ORBITAL Y EXTINCIÓN  
MASIVA DE LOS FORAMINÍFEROS  
PLANCTÓNICOS: UN ESTUDIO  
MULTIDISCIPLINAR A TRAVÉS DEL TRÁNSITO  
CRETÁCICO-PALEÓGENO

Autor

Vicente Gilabert Pérez

Director/es

Arz Sola, José Antonio  
Arenillas Sierra, Ignacio

**UNIVERSIDAD DE ZARAGOZA**  
**Escuela de Doctorado**

Programa de Doctorado en Geología

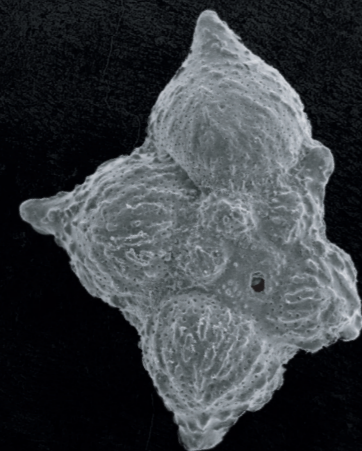
2022





Vicente Gilabert Pérez es un especialista en el estudio de los foraminíferos planctónicos del tránsito Cretácico–Paleógeno, así como en el estudio de los cambios paleoclimáticos, paleoambientales y paleobiológicos de este mismo intervalo temporal. Durante el doctorado, complementó su formación con otras disciplinas como el estudio de isótopos estables y el análisis de series temporales, permitiendo de esta manera una mayor precisión en la reconstrucción de este periodo de la historia de la Tierra.

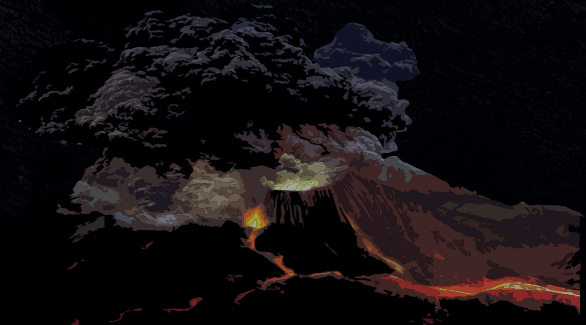
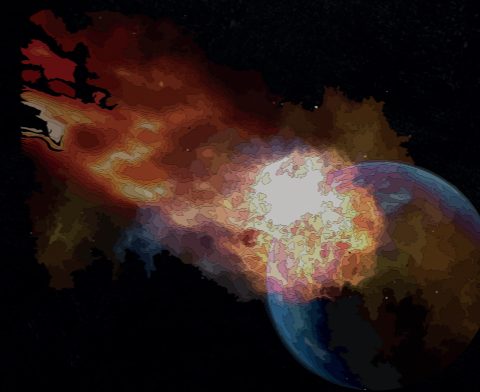
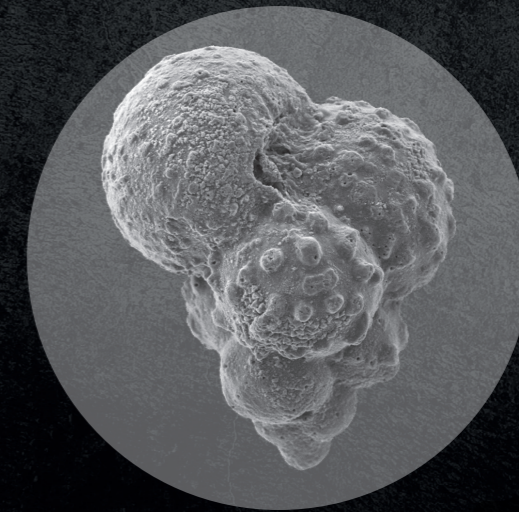
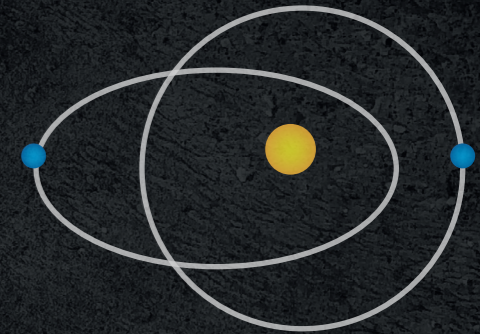
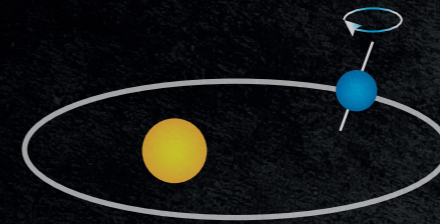
Vicente se licenció en Geología en 2013, completó el Máster en Geología: Técnicas y aplicaciones en 2015 en la Universidad de Zaragoza. En 2017 Inició sus estudios de doctorado bajo la dirección de Ignacio Arenillas Sierra y José Antonio Arz Sola. Durante este periodo, ha realizado varias estancias internacionales (México D.F, Oxford y Rennes), colaborado en la elaboración de artículos, capítulos de libros y otros tipos de publicaciones, además de asistir a congresos de ambito nacional e internacional.



Vulcanismo del Decán,, impacto de Chicxulub, control orbital y extinción masiva de los foraminíferos planctónicos: un estudio multidisciplinar a través del tránsito Cretácico–Paleógeno

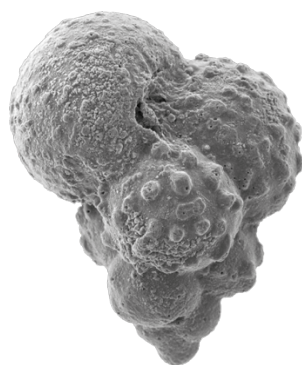
# VULCANISMO DEL DECÁN, IMPACTO DE CHICXULUB, CONTROL ORBITAL Y EXTINCIÓN MASIVA DE LOS FORAMINÍFEROS PLANCTÓNICOS: UN ESTUDIO MULTIDISCIPLINAR A TRAVÉS DEL TRÁNSITO CRETÁCICO-PALEÓGENO.

Vicente Gilabert Pérez  
2022



# **Vulcanismo del Decán, impacto de Chicxulub, control orbital y extinción masiva de los foraminíferos planctónicos: un estudio multidisciplinar a través del tránsito Cretácico–Paleógeno.**

Vicente Gilabert Pérez  
2022



Tesis Doctoral dirigida por:

José Antonio Arz Sola e Ignacio Arenillas Sierra

Área de Paleontología, Departamento de Ciencias de la Tierra

Facultad de Ciencias, Universidad de Zaragoza



Departamento de  
Ciencias de la Tierra  
**Universidad Zaragoza**



Instituto Universitario de Investigación  
en Ciencias Ambientales  
de Aragón  
**Universidad Zaragoza**



Esta tesis se presenta en formato de compendio de publicaciones. Para cumplir con la normativa vigente en la Universidad de Zaragoza, la tesis se compone de cinco artículos científicos publicados en revistas incluidas en el *Journal Citation Reports* (JCR).

Arenillas, I., Arz, J. A., **Gilabert**, V., 2017. Revalidation of the genus *Chiloguembelitria* Hofker: Implications for the evolution of early Danian planktonic foraminifera. *Journal of African Earth Sciences* 134, 435–456, <https://doi.org/10.1016/j.jafrearsci.2017.07.011>.

Arenillas, I., Arz, J. A., **Gilabert**, V., 2018. Blooms of aberrant planktic foraminifera across the K/Pg boundary in the Western Tethys: causes and evolutionary implications. *Paleobiology* 44, (3), 460–489. <https://doi.org/10.1017/pab.2018.16>.

**Gilabert**, V., Arz, J.A., Arenillas, I., Robinson, S.A., and Ferrer, D., 2021. Influence of the Latest Maastrichtian Warming Event on planktic foraminiferal assemblages and ocean carbonate saturation at Caravaca, Spain. *Cretaceous Research* 125, 104844. <https://doi.org/10.1016/j.cretres.2021.104844>.

**Gilabert**, V., Arenillas, I., Arz, J.A., Batenburg, S., Robinson, S.A., 2021. Multiproxy analysis of paleoenvironmental, paleoclimatic and paleoceanographic changes during the Early Danian in the Caravaca section (Spain). *Palaeogeography, Palaeoclimatology, Palaeoecology* 576, 110513. <https://doi.org/10.1016/j.palaeo.2021.110513>.

**Gilabert**, V., Batenburg, S.J., Arenillas, I., Arz, J.A., 2021. Contribution of orbital forcing and Deccan volcanism to global climatic and biotic changes across the KP/B at Zumaia, Spain. *Geology*, <https://doi.org/10.1130/G49214.1>. Publicado *online* como *Early Publication* el 30 de Agosto del 2021 (pendiente de asignación de volumen).

Como se indica en el Reglamento sobre Tesis Doctorales de la Universidad de Zaragoza, en el Apéndice que figura tras el listado de referencias bibliográficas se incluye información sobre el factor de impacto de las revistas y las áreas temáticas correspondientes a estas cinco publicaciones, junto con una breve justificación de la contribución del doctorando en cada uno de los trabajos realizados en coautoría.



Esta tesis doctoral se postula para la obtención de mención internacional ya que durante el transcurso del doctorado se han realizado dos estancias de investigación que suman una duración de tres meses y una semana (99 días), de los cuales dos meses completos (61 días) se realizaron en el *Department of Earth Sciences de la University of Oxford* (Reino Unido), bajo la tutela del Doctor Stuart Alan Robinson. Durante esta estancia se llevaron a cabo análisis geoquímicos que permitieron generar una gran cantidad de datos de isótopos estables y calcimetrías, que fueron comparados con los datos micropaleontológicos. La integración de estos datos y su análisis y discusión resultaron esenciales para la caracterización de los eventos paleoclimáticos estudiados en esta tesis.

La segunda estancia, con una duración total de 38 días, se realizó en la *Université de Rennes I* (Francia), bajo la tutela de la Doctora Sietske Batenburg. El objetivo principal fue la adquisición de nuevos conocimientos para el análisis de series temporales. Esta estancia fue también de gran utilidad, ya que permitió integrar en un marco astrocronológico todos los eventos paleoclimáticos y paleobiológicos estudiados y proponer relaciones temporales entre todos ellos con una alta resolución temporal.

Las publicaciones que integran esta tesis doctoral están incluidas en el capítulo **4. Resultados** en su versión original y en el idioma en el que han sido publicadas (inglés). El cuerpo principal de esa memoria de tesis es el castellano, mientras que el resumen y las conclusiones se presentan tanto en castellano como en inglés.

El doctorando ha colaborado en la publicación de otros artículos y capítulos de libro que **no forman parte del compendio**. Algunas están relacionadas con la obtención de edades numéricas para el límite K/Pg mediante datación radiométrica  $^{40}\text{Ar}/^{39}\text{Ar}$  en vidrios de impacto de la isla colombiana de Gorgonilla (Renne et al., 2018) o con la publicación detallada de la estratigrafía, sedimentología y bioestratigrafía de esta sección (Bermúdez et al., 2019). Además, tanto los artículos de Metsana-Oussaid et al. (2019), como de Fendley et al. (2020) ha formado parte de las respectivas tesis doctorales de las primeras autoras, mientras que la publicación de Arenillas et al. (2021) en *Geosciences* no pertenece a una revista catalogada en el JCR. Las referencias de estos artículos son las siguientes:

Renne, P.R., Arenillas, I., Arz, J.A., Vajda, V., **Gilabert, V.**, Bermúdez, H.D., 2018. Multi-proxy record of the Chicxulub impact at the Cretaceous- Paleogene boundary from Gorgonilla Island, Colombia. *Geology* 46, (6), 547–550, <https://doi.org/10.1130/G40224.1>.

Bermúdez, H.D., Arenillas, I., Arz, J.A., Vajda, V., Renne, P.R., **Gilabert, V.**, Rodríguez, J.V., 2019. The Cretaceous/Paleogene boundary deposits on Gorgonilla Island. En: Gómez, J., Mateus–Zabala, D. (Eds.), *The Geology of Colombia, Volume 3 Paleogene – Neogene*. Servicio Geológico Colombiano, Publicaciones Geológicas Especiales 37, pp. 1–19. Bogotá, <https://doi.org/10.32685/pub.esp.37.2019.01>.

Metsana-Oussaid, F., Belhai, D., Arenillas, I., Arz, J.A., **Gilabert, V.**, 2019. New sections of the Cretaceous–Paleogene transition in the southwestern Tethys (Médéa, northern Algeria): planktic foraminiferal biostratigraphy and biochronology. *Arabian Journal of Geosciences* 12, (217), 1–34, <https://doi.org/10.1007/s12517-019-4402-4>.

Fendley, I.M., Sprain, C.J., Renne, P.R., Arenillas, I., Arz, J.A., **Gilabert, V.**, Self, S., Vanderkluyesen, L., Pande, K., Smit, J., Mittal, T., 2020. No Cretaceous-Paleogene Boundary in Exposed Rajahmundry Traps: A Refined Chronology of the Longest Deccan Lava Flows From  $^{40}\text{Ar}/^{39}\text{Ar}$  Dates, Magnetostratigraphy, and Biostratigraphy. *Geochemistry, Geophysics, Geosystems* 21, (9), e2020GC009149, <https://doi.org/10.1029/2020GC009149>.

Arenillas, I., **Gilabert, V.**, Arz, J.A., 2021. New Biochronological scales of planktic foraminifera for the early Danian based on high resolution biostratigraphy. *Geosciences* 11(11), 479, <https://doi.org/10.3390/geosciences11110479>.



## **AGRADECIMIENTOS**

*Esta tesis doctoral se ha beneficiado de la ayuda BES-2016-077800 financiada por el Ministerio de Ciencia e Innovación, la Agencia Estatal de Investigación/10.13039/501100011033 y por el “Fondo Social Europeo Invierte en tu futuro”. El desarrollo de esta tesis se ha beneficiado de los proyectos de I+D+I CGL2015-64422-P y PGC2018-093890-BI00, ambos financiados por el Ministerio de Ciencia e Innovación, la Agencia Estatal de Investigación/10.13039/501100011033/ y el “Fondo Europeo de Desarrollo Regional, Una manera de hacer Europa”. Además, se ha contado con las ayudas de la Unión europea a través del Fondo Europeo de Desarrollo Regional al Gobierno de Aragón (ayudas al grupo de investigación de Diputación general de Aragón E33\_17R y E33\_20R) “Extinción y reconstrucción paleoambiental desde el Cretácico al Cuaternario”.*

*Quiero agradecer profundamente a mis directores de tesis José Antonio Arz e Ignacio Arenillas, su excelente labor como directores Su dedicación, profesionalidad, meticulosidad y sobre todo su paciencia han influido enormemente en mi formación académica, ayudándome a apreciar la visión crítica pero constructiva del mundo científico. En el aspecto meramente académico y profesional no puedo manifestar más que mi satisfacción por haber tenido la oportunidad de trabajar codo con codo con dos excelentes científicos. Pero es en el lado humano de ambos, Nacho y Arz, donde me han demostrado su mayor valía. Creo que no me quedo corto al decir que son dos personas maravillosas con las que me siento afortunado de poder haber pasado este tiempo junto a ellos. En estos años hemos compartido muchos y muy difíciles momentos y, aunque también ha habido muchos buenos, creo que las relaciones se curten ante la adversidad. Es por ello que para mí son mucho más que unos excelentes directores y magníficas personas: son amigos de verdad y ojalá que lo sean para siempre.*

*Mis más sinceros agradecimientos a José Ignacio Canudo (Universidad de Zaragoza), Francisco Javier Sierro (Universidad de Salamanca), Carolina Nañez (Servicio Geológico Minero Argentino), Jaime Humberto Urrutia (Universidad Nacional Autónoma de México) y a Ana Rosa Soria (Universidad de Zaragoza) por acceder a formar parte del tribunal de esta tesis. También agradecer a las personas que accedieron a actuar como revisores externos en la evaluación de esta tesis Carlos Sánchez*

*(Universidad Nacional de Colombia) y Uxue Villanueva (Universidad Nacional Autónoma de México).*

*Gracias también al Programa de Doctorado en Geología y al Departamento de Ciencias de la Tierra, en los que se ha desarrollado esta tesis, y al Servicio General de Apoyo a la Investigación-SAI de la Universidad de Zaragoza. Extiendo los agradecimientos a todos los profesores del área de Paleontología, con quienes a lo largo de todos los años que llevo en esta casa he tenido el placer de coincidir y que en mayor o menor medida son responsables de los pasos que me han llevado hasta aquí.*

*Agradecer a la dirección del Geoparque de la Costa Vasca - Geoparkea, personada en Asier Hilario quien siempre nos facilitó nuestra labor en los muestreos de la sección de Zumaia, sobre todo en aquel lejano muestreo del Santoniense-Campaniense. Gracias también a Juan Cruz Larrasoña por la ayuda prestada en el laborioso muestreo a taladro de Zumaia y por su ayuda en los análisis paleomagnéticos.*

*Durante estos casi cinco años de gestación de la tesis he tenido la oportunidad de viajar “internacionalmente” lo que me ha permitido conocer a muchas personas que han contribuido en mi desarrollo académico y personal. Empiezo por los encantadores Manuel Grajales-Nishimura y Carmen Rosales, muchas gracias por vuestro recibimiento en nuestra visita a ese gran país que es México, fue un placer tener la oportunidad de conocerlos y de platicar de tan variados temas con ustedes.*

*Agradecer a Stuart Robinson la invitación para realizar una estancia de dos meses en la Universidad de Oxford. Muchas gracias por ayudarme a conocer a tanta gente fantástica como Sietske Batenburg, Hugh Jenkyns, Lauren O'Connor, Stephen Wyatt y Cristopher Day. A estos dos últimos muchas gracias por la ayuda en los centenares de análisis geoquímicos. No me olvido de mis compadres latinos Alfredo, Cesar, Felix y Felipe que tan buenos ratos me hicieron pasar durante mi estancia en Oxford (mención especial a las tremendas barbacoas que nos marcamos). Aunque de entre todas las personas que allí conocí quiero destacar a Sietske, cuyo entusiasmo y profesionalidad, alegría y determinación junto con el hecho de compartir trabajo en Zumaia facilitaron una rápida conexión a nivel personal y profesional, que espero continúe por mucho tiempo.*

*En este sentido he de agradecer de nuevo a Sietske que me acogiese para realizar una estancia de un mes y medio en Rennes (Francia), que pese a la situación pandémica fue muy productiva. Aprovecho para agradecerle junto a Mathieu, Charlotte, Jean Paul, Militza los buenos momentos que me hicieron vivir durante mi estancia en Rennes, a pesar de que en lo personal mi situación estaba lejos de ser la mejor.*

*Antes de mencionar a todos los compañeros de fatigas de la tesis quiero hacer mención a todos mis compañeros de promoción y alrededores: gracias por hacer de mi paso por la licenciatura posiblemente los mejores años de mi vida, gracias a todos de corazón. Ahora sí, muchas gracias a todos con los que he compartido despacho, cafés cervezas y momentos, gracias Manu, Lucía, Edu, Jara, Raquel, Carmen, Toni, Julia, Pablo, Ester, Esteve, Fernando, Alba, Álvaro, Gaby, Elisa, Christian, Samuel, Miguel, Diego C., Luismi, Edu P., Gasca, Diego T., Alberto, Pere, Dani perdón de antemano si me olvido de alguien, ¡no volverá a ocurrir!*

*Gracias también a mis amigos de siempre, los irreductibles andorranos, con quienes pasar cualquier rato es un placer. Hacen fácil lo difícil y difícil lo fácil, con ellos siempre hay cabida para un banquete o para las conversaciones más ingeniosas y divertidas aderezadas puntualmente con reflexiones metafísicas, gracias a todos (Victor/Puchico, Javi F./Popi, Jorge/Chopi, Eloy/Cherokee, Álvaro/Tyson, Alberto A./Mendo, Fran, Juan F./ Pozo, Adri, Carlos/Luchi, Edu A./ Costal, Fran M./Moya, Jesús/Chapu, José Luis/Kopon, Marcos/Meji, Alejandro/Rati, Oscar/ Zaera, Javier Q./Kiki, Sergio/Bolintxe, Javier B./Chapis).*

*Gracias a mi familia, quienes siempre han estado apoyándome a pesar de que aun después de tantos años siguen pensando que lo mío son los dinosaurios. También a mis tíos Rosa, Amparo, Pedro, Jose Luis, a mis primos Marta, Miriam, Héctor y Marina y a mi abuela Ana. Gracias además a mi ya oficial familia alcorisana, a mi suegra María Jesús, y a mis cuñados Christian y Sergio.*

*Especial agradecimiento a mis padres y mi hermana (Vicente, Asunción y Cristina), por ellos he tenido la oportunidad de llegar hasta aquí y por ello les estaré siempre agradecido. Gracias por señalarme el camino cuando esta desorientado, por recordarme*

*una vocación olvidada, por vuestro apoyo, paciencia y por estar a mi lado siempre que lo he necesitado.*

*No me olvido de aquellas personas que ya no están entre nosotros y que siempre tuvieron palabras de afecto, cariño y apoyo. Por desgracia su pérdida será irremplazable. Desde aquí os agradezco profundamente: gracias Varela, gracias Tía Dori, gracias Yayo Antonio y muchas gracias Eduardo mi querido suegro. A ti Eduardo te quiero dar un agradecimiento especial, ya que desde el primer momento recibí tu apoyo en la decisión de iniciarme en este difícil viaje. Siempre recordaré tu gran corazón, templanza y paciencia, tu sonrisa en el día de la boda de tu hija y las lágrimas de emoción en tus ojos por mis minúsculos éxitos profesionales.*

*Por último, pero no por ello menos importante, quiero agradecer a la persona que siempre ha estado a mi lado, alentándome en los momentos más difíciles, ayudándome en todo lo posible, sacrificándose conmigo y que aún estando hundido siempre conseguía sacarme una sonrisa. Esta tesis te la dedico a ti mi querida Estibaliz. Es en los duros momentos cuando se demuestra el verdadero valor de una persona y creo que en este sentido me has demostrado que eres la persona más valiosa y valiente que jamás he conocido. Gracias por querer compartir la vida conmigo y por hacerme cada día mejor persona. Gracias por todo Esti, sin ti, esto no hubiera sido posible.*

*A los que estuvieron, están  
y estarán siempre ahí*





## ÍNDICE

RESUMEN	13
ABSTRACT	15
INTRODUCCIÓN	17
1.1. Foraminíferos Planctónicos	19
1.2. Evolución del clima tipo invernadero desde el Cretácico Tardío al Eoceno	20
1.3. Eventoestratigrafía a través tránsito Cretácico–Paleógeno	23
1.3.1. Registro global de temperaturas y principales relaciones isotópicas a través del límite K/Pg	25
1.3.2. Principales modelos eruptivos del vulcanismo del Decán a través del límite K/Pg	27
1.3.3. El impacto de Chicxulub: edad, estratigrafía y efectos paleoambientales	32
2. OBJETIVOS	37
3. MATERIALES Y MÉTODOS	41
3.1. Localidades estudiadas	43
3.2. Métodos de laboratorio y tratamiento de muestras micropaleontológicas	45
3.3. Taxonomía y bioestratigrafía	46
3.4. Análisis cuantitativo	49
3.5. Análisis morfoestadístico	51
3.6. Análisis de la susceptibilidad magnética	52
3.7. Análisis geoquímico (%CaCO <sub>3</sub> , TOC, $\delta^{13}\text{C}$ y $\delta^{18}\text{O}$ )	52
3.8. Elaboración de nuevo material gráfico de síntesis	54
4. RESULTADOS	55
4.1. Revalidation of the genus <i>Chiloguembeltria</i> Hofker: Implications for the evolution of early Danian	57
4.3. Influence of the Latest Maastrichtian Warming Event on planktic foraminiferal assemblages and ocean carbonate saturation at Caravaca, Spain.	111
4.4. Multiproxy analysis of paleoenvironmental, paleoclimatic and paleoceanographic changes during the Early Danian in the Caravaca section (Spain)	134
4.5 Contribution of orbital forcing and Deccan volcanism to global climatic and biotic changes across the KPB at Zumaia, Spain	154
5. DISCUSIÓN	161
5.1 El evento de calentamiento del Maastrichtiense tardío (LMWE)	163
5.1.1 Caracterización isotópica, calibración temporal y causas más probables	163
5.1.2. Episodios de disolución del CaCO <sub>3</sub>	167
5.1.3. Influencia sobre las asociaciones de foraminíferos planctónicos	169
5.2. El enfriamiento progresivo en los últimos 100 ka del Maastrichtiense	171
5.3. El evento del límite K/Pg.	172
5.3.1 Definición y edad del límite Cretácico/Paleógeno	172

5.3.2. Modelo de extinción y de supervivencia de los foraminíferos planctónicos _____	173
5.4.2. Radiaciones evolutivas y reconocimiento de acmé-estadios _____	178
5.4.3. Episodios de apogeo de Chiloguembelitra y vulcanismo del Decán _____	180
<b>5.5. Los eventos Dan-C2 y LC29n _____</b>	<b>182</b>
5.5.1. Características principales y calibración temporal _____	182
5.5.2. Efectos en las asociaciones de foraminíferos planctónicos. _____	185
<b>6. CONCLUSIONES _____</b>	<b>187</b>
<b>BIBLIOGRAFÍA _____</b>	<b>195</b>
<b>ANEXOS _____</b>	<b>225</b>
<b>Anexo I. Material suplementario de Arenillas et al. (2018) _____</b>	<b>227</b>
<b>Anexo II. Material suplementario de Gilabert et al. (2021a) _____</b>	<b>241</b>
<b>Anexo III. Material suplementario de Gilabert et al. (2021b) _____</b>	<b>245</b>
<b>Anexo IV. Material suplementario de Gilabert et al. (2021c) _____</b>	<b>249</b>
<b>Anexo V. (Material suplementario elaborado para esta tesis doctoral) _____</b>	<b>276</b>
<b>APÉNDICE I. Listado de trabajos que componen esta tesis doctoral. _____</b>	<b>291</b>
<b>APÉNDICE II. Cartas de aceptación. _____</b>	<b>293</b>

## **RESUMEN**

El intervalo de un millón de años a través del límite Cretácico/Paleógeno es un breve periodo de la historia de la Tierra en el que se sucedieron varios eventos destacables, uno de los cuales con la capacidad de alterar irreversiblemente la evolución de la vida en el planeta: el conocido como evento de extinción masiva del límite K/Pg. Durante este intervalo de tiempo, la Tierra se encontraba en un estado climático de tipo invernadero relativamente suave y óptimo para la vida. Este estado climático se vio alterado transitoriamente por los cambios ambientales desencadenados por el impacto del asteroide de Chicxulub y por episodios cortos de calentamiento climático y de perturbación en el ciclo del carbono (denominados en sentido amplio como eventos hipertermales). Los eventos analizados son conocidos por sus siglas en inglés como LMWE (*Latest Maastrichtian Warming Event*), Dan-C2 y LC29n (*Lower C29n*), y han sido relacionados por algunos autores con las principales fases eruptivas de la Gran Provincia Ígnea del Decán (India).

Esta tesis tiene como objetivo analizar e interpretar la respuesta paleobiológica de los foraminíferos planctónicos ante los cambios paleoambientales y paleoclimáticos provocados por el LMWE, el impacto de Chicxulub, el Dan-C2 y el LC29n, para así obtener nuevas evidencias acerca del papel que jugó el vulcanismo masivo del Decán en las extinciones de finales del Maastrichtiense y en la posterior radiación evolutiva durante el Daniense inferior. Para ello, se han analizado cuantitativamente las asociaciones de foraminíferos planctónicos del tránsito K–Pg en cuatro localidades: Caravaca y Zumaia (España) y El Kef y Aïn Settara (Túnez). Las secciones de Caravaca y Zumaia se estudiaron multidisciplinariamente, obteniendo también datos geoquímicos ( $\delta^{13}\text{C}$ ,  $\delta^{18}\text{O}$  y  $\text{CaCO}_3$ ) y paleomagnéticos (susceptibilidad magnética). Por último, mediante calibraciones magneto- y astrocronológicas, se han datado todos los eventos paleoclimáticos, paleoambientales y paleobiológicos reconocidos. Las técnicas de calibración astrocronológica han permitido, además, valorar el papel jugado por el forzamiento orbital en los eventos analizados.

Los resultados han sido publicados en los cinco artículos seleccionados para esta tesis doctoral, y se resumen del siguiente modo: 1) se ha identificado un evento de extinción masiva catastrófica de foraminíferos planctónicos coincidiendo con el límite K/Pg, el cual se ha relacionado con el impacto de Chicxulub; (2) los eventos LMWE, Dan-C2 y LC29n tuvieron una influencia débil y transitoria en la diversidad y en la estructura de las

asociaciones de foraminíferos planctónicos; (3) el LMWE fue causado por la coincidencia temporal del último máximo de excentricidad larga del Maastrichtiense y una elevada tasa de desgasificación en el Decán; (4) el evento Dan-C2 estuvo relacionado con los dos máximos de excentricidad corta del primer máximo de excentricidad larga del Daniense, pero no con el vulcanismo del Decán; (5) el evento LC29n fue un evento menor relacionado con un máximo de excentricidad corta, que no produjo un cambio climático o ambiental relevante; y, por último, (6) la principal señal paleobiológica relacionada con el vulcanismo del Decán en el Daniense es un intervalo de estrés ecológico previo al evento Dan-C2 registrada como un incremento brusco en la abundancia relativa de guembelítridos triseriados (*Chiloguembelitra*) y en la tasa de conchas de foraminíferos planctónicos con crecimientos aberrantes.

**ABSTRACT**

The one million year interval across the Cretaceous/Paleogene (K/Pg) boundary is a very short period of Earth history on which several important events occurred, one of whom irreversibly shaped the evolution of life on Earth: the so-called K/Pg boundary mass extinction event. During this time interval, the Earth was in a relatively mild greenhouse state, optimal for the development of life. This climate state was disrupted by the environmental changes triggered by the impact of the Chicxulub asteroid and by transient events of global warming and carbon cycle perturbation (broadly referred to as hyperthermal events). The analyzed events are the LMWE (Latest Maastrichtian Warming Event), the Dan-C2, and the Lower C29n (LC29n), which have been mechanistically linked by some authors to the main eruptive phases of the Large Igneous Province of the Deccan Traps (India).

This PhD thesis aims to analyze and interpret the paleobiological response of planktic foraminifera to the paleoenvironmental and paleoclimatic changes caused by the LMWE, the Chicxulub impact, the Dan-C2 and the LC29n, in order to obtain new evidence about the role that massive Deccan volcanism played in the late Maastrichtian extinction and the subsequent evolutionary radiation during the early Danian. For this purpose, planktic foraminiferal assemblages from four well-known localities of the K–Pg transition have been quantitatively studied: Caravaca and Zumaia (Spain), El Kef and Aïn Settara (Tunisia). Additionally, both the Caravaca and Zumaia sections were studied with a multidisciplinary approach, generating geochemical data ( $\delta^{13}\text{C}$ ,  $\delta^{18}\text{O}$  y  $\text{CaCO}_3$ ) and paleomagnetic data (magnetic susceptibility). Finally, all paleoclimatic, paleoenvironmental and paleobiological events have been dated by magnetostratigraphic and astrochronological calibration. Additionally, the cyclostratigraphic age models allow evaluating the contribution of orbital forcing to all analyzed events.

The results have been published in the five articles selected for this PhD thesis, and are summarized as follows: 1) a catastrophic mass extinction event of planktic foraminifera has been recognized at the K/Pg boundary, which has been linked to the Chicxulub impact; (2) the LMWE, Dan-C2 and LC29n events had a weak and transitory influence on the diversity and structure of the planktic foraminiferal assemblages; (3) the LMWE was triggered by the temporal co-occurrence of the last long eccentricity maximum of the Maastrichtian and a high rate of degassing in the Deccan; (4) the Dan-C2 event has been linked to the two short eccentricity maxima within the first long

eccentricity maximum of the Danian, but not to the Deccan volcanism; (5) the LC29n event was a minor event related to a short eccentricity maximum, which did not produce a relevant climatic or environmental change; and finally (6) the main paleobiological signal linked to the Deccan volcanism during the Danian is an interval of ecological stress prior to the Dan-C2 event recorded as an increase in the relative abundance of the triserial guembelitrid (*Chiloguembelitra*) and to the index of planktic foraminiferal tests with aberrant growths.

***Capítulo 1.***  
***Introducción***





## 1. INTRODUCCIÓN

### 1.1. Foraminíferos Planctónicos

Los foraminíferos planctónicos son microorganismos marinos heterótrofos, pertenecientes al reino Protista, que recubren su cuerpo unicelular con elaboradas conchas calcíticas y que habitan en la parte superior de la columna de agua. El citoplasma contenido en el interior de sus conchas presenta los típicos orgánulos de las células eucariotas junto a una serie de cuerpos fibrilares que ayudan a controlar la flotabilidad de las mismas. En el exterior de la concha, el citoplasma se estira en hebras delgadas anastomosadas llamadas rizopodios, que pueden extenderse a varias veces el diámetro total de la concha permitiéndoles la adquisición activa de alimento (ver detalle sobre biología de este grupo de protozoos en Hemleben et al., 1989).

Aunque los foraminíferos aparecieron por primera vez en el dominio bentónico durante el Cámbrico, no es hasta el Jurásico, y sobre todo durante el Cretácico, cuando colonizaron exitosamente el dominio pelágico (Loeblich y Tappan, 1987). La gran variedad de características morfológicas de sus conchas, así como de las diferentes estructuras observables en la pared o superficie de las mismas, ha permitido el reconocimiento de centenares de morfoespecies de foraminíferos planctónicos desde el Cretácico hasta la actualidad (BouDagher-Fadel, 2015).

Los foraminíferos planctónicos son unos excelentes fósiles-guía debido a su alta abundancia, rápida evolución y amplia distribución biogeográfica (Bé, 1977; Vincent y Berger, 1981; Aze et al., 2011; BouDagher-Fadel, 2015). Su estudio proporciona un registro bioestratigráfico relativamente continuo durante los últimos ~100 millones de años (Ma) (Schiebel et al., 2018). Dado que su tasa de evolución ha sido relativamente alta, su estudio permite identificar en el registro estratigráfico numerosos eventos de primera y última aparición (Olsson et al., 1999; Arenillas et al., 2004). Su amplia distribución latitudinal permite reconocer muchos biohorizontes-guía (datos de primer y último registro) que ayudan a establecer correlaciones cronológicas entre localidades a escala global (McGowran, 2008; Schiebel et al., 2018). Es por ello que los foraminíferos planctónicos se consideran como uno de los mejores marcadores biocronoestratigráficos del Cretácico y del Cenozoico (Kucera et al., 2007).

Estos organismos son también unos excelentes indicadores paleoambientales, paleoclimáticos y paleoceanográficos (Schiebel et al., 2018). Cada grupo está adaptado a unas condiciones ecológicas determinadas de temperatura y profundidad, y su

distribución biogeográfica dependerá de la latitud y batimetría a las que esté adaptado (Hart, 1980; Schiebel y Hemleben, 2005). Estos organismos se hallan afectados también por la distribución de las corrientes marinas y, por ello, son buenos marcadores de cambios paleoceanográficos (Premoli Silva y Sliter, 1999; MacLeod et al., 2001). Adicionalmente, los estudios biométricos y tafonómicos nos pueden brindar información acerca de las condiciones ambientales en las que habitaron estos microorganismos (p. ej., Malmgren y Kennett 1978; Berger et al., 1982; Malmgren, 1987; Kucera et al., 1997; Schindt et al., 2006).

Además, el estudio geoquímico e isotópico de sus conchas calcíticas proporciona información sobre temperatura, salinidad, oxigenación y cantidad de nutrientes en los océanos (Kucera et al., 2007). Las reconstrucciones paleoclimáticas basadas en los cambios de las relaciones isotópicas ( $\delta^{18}\text{O}$  y  $\delta^{13}\text{C}$ ) de sus conchas a lo largo del tiempo geológico ha permitido la reconstrucción detallada de los principales cambios climáticos acontecidos desde el Cretácico hasta la actualidad (D'Hondt y Zachos, 1993; Abramovich et al., 2003; Pearson et al., 2009; Aze et al., 2011; Petrizzo et al., 2020). Por todas estas razones, a los foraminíferos planctónicos se les considera una de las herramientas geológicas más útiles en las reconstrucciones paleoclimáticas, paleoceanográficas y paleoambientales (Schiebel et al., 2018).

Desde que los foraminíferos colonizaron los medios pelágicos, sus conchas constituyen una gran parte de los sedimentos calcáreos marinos en las principales cuencas oceánicas (Berger et al., 1982). En la actualidad, los foraminíferos planctónicos son responsables de la producción de aproximadamente el 25% del carbonato cálcico ( $\text{CaCO}_3$ ) de los océanos (Schiebel, 2002), lo que permite deducir el papel determinante de estos microorganismos en las condiciones geoquímicas de los océanos actuales y pasados. Además de ser importantes organismos calcificadores pelágicos, se encargan de transportar enormes cantidades de carbono orgánico al fondo marino (Henahan et al. 2016), por lo que también son esenciales en el ciclo del carbono (Wu y Berger, 1989; Milliman 1993; Henahan et al., 2019).

## 1.2. Evolución del clima tipo invernadero desde el Cretácico Tardío al Eoceno

El intervalo del Cretácico Tardío al Eoceno es una continuación del estado climático de tipo invernadero (*greenhouse*) que se inició en el Cretácico Temprano (Littler et al., 2011; Friedrich et al., 2012; Petrizzo et al., 2020). A lo largo de los 65 Ma que dura este

intervalo *greenhouse* se produjeron variaciones climáticas significativas que permiten diferenciar hasta 3 subestados climáticos: invernadero-cálido, invernadero-templado e invernadero-fresco (Zachos et al., 2008; O'Brien et al., 2017; Huber et al., 2018; Westerhold et al., 2020; Fig. 1). En el Cretácico Tardío se alcanzaron temperaturas extremadamente altas en el medio marino, registrándose hasta 20°C en profundidades batiales (Huber et al., 2018). Estas temperaturas tan elevadas caracterizaron el intervalo desde el Cenomaniense tardío hasta el Campaniense más temprano (entre ~97 y 82 Ma), cuando el sistema climático fue del tipo invernadero cálido (Huber et al., 1995, 2018; Friedrich et al., 2012; Fig. 1). Por el contrario, durante el Campaniense (83,6–72,1 Ma), el clima fue enfriándose gradualmente hasta convertirse en un clima invernadero templado con temperaturas de ~6–8 °C en profundidades batiales (Clarke y Jenkyns, 1999; Huber et al., 2018). Esta tendencia de enfriamiento gradual prosiguió durante el Maastrichtiense (72,1–66 Ma), momento en el que tuvo lugar la transición de un estado climático de invernadero templado a uno de invernadero fresco (Cramer et al., 2009; Linnert et al., 2014; Huber et al., 2018; Fig. 1).

Las condiciones generales de *greenhouse* impidieron la formación de casquetes polares permanentes (Huber et al., 2002; Miller et al., 2005; MacLeod et al., 2013), favoreciendo que la flora y fauna termofílica habitase en latitudes altas (Frakes et al., 1992; Francis y Frakes, 1993; Tarduno et al., 1998), y causando que el nivel del mar fuese entre 75 y 250 m más alto que en la actualidad (Miller et al., 2005; Haq, 2014). Algunos de los cambios oceánicos más representativos a lo largo de los casi 34 Ma que abarca el Cretácico Tardío son los eventos anóxicos oceánicos (OAEs por sus siglas en inglés). El OAE2 de hace ~94 Ma representa el mayor episodio de anoxia oceánica global de los OAEs reconocidos en el Cretácico Superior, siendo comparable a su homólogo del Cretácico Inferior: el OAE1 de hace ~120 Ma (Jenkyns et al., 1994; Kuypers et al., 1999; Jenkyns, 2010; O'Brien et al., 2017). El OAE2 marcó además el inicio de un cambio climático conocido como el Máximo Térmico del Cretácico (KTM por sus siglas en inglés) (Poulsen et al., 2003; O'Brien et al., 2017; Huber et al., 2018; Fig. 1). No obstante, son los cambios climáticos del Maastrichtiense tardío los que han recibido una mayor atención por parte de la comunidad científica, debido principalmente a que a finales de este periodo se produjo la extinción masiva del límite Cretácico/Paleógeno (límite K/Pg).

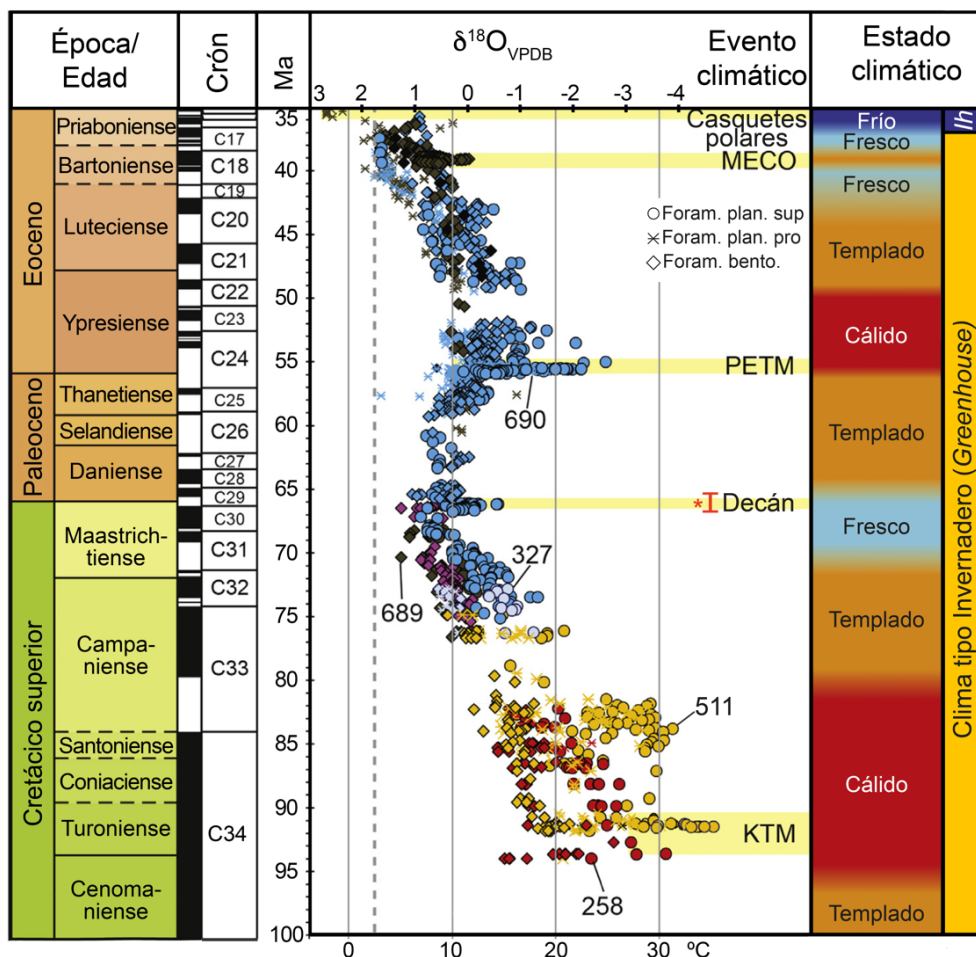
El estado climático de invernadero templado-fresco típico del Maastrichtiense e iniciado en el Campaniense, culminó en el Paleoceno medio (~60 Ma), momento en el que se produjo un punto de inflexión (Cramer et al., 2011; Westerhold et al., 2020). A

partir de este momento, el Paleoceno se caracteriza por un ascenso gradual de las temperaturas globales con la vuelta a un estado climático tipo invernadero templado, que finalizó con el evento del Máximo Térmico del límite Paleoceno/Eoceno (PETM por sus siglas en inglés), momento en el que se alcanzó la máxima temperatura de todo el Paleógeno (Zachos et al., 1993, 2008; Westerhold et al., 2011). Con el PETM (~56 Ma) se estableció un nuevo estado climático invernadero cálido conocido como el Óptimo Climático del Eoceno Temprano (EECO por sus siglas en inglés), y que persistió hasta hace 49 Ma (~54–49 Ma) (Westerhold et al., 2020). Tras el EECO, tuvo lugar un enfriamiento gradual hasta alcanzar de nuevo el estado de invernadero fresco en el Eoceno medio ~42 Ma (Zachos et al., 2008; Huber et al., 2018; Westerhold et al., 2020), siendo brevemente interrumpido por el Óptimo climático del Eoceno medio (MECO) (Rivero-Cuesta et al., 2020), durante el que se estableció de nuevo un sistema climático de invernadero templado. Tras el MECO se produce un retorno a las condiciones de enfriamiento generalizado que culminó en el tránsito Eoceno–Oligoceno, marcando la transición hacia un estado climático frío o de tipo congelador (*icehouse*) (Zachos et al., 1996, 2001; Coxall et al., 2005; Lear et al., 2008; Westerhold et al., 2020; Fig.1).

Superpuestos a estas tendencias climáticas generales, durante el Paleoceno y el Eoceno aparecen registrados numerosos eventos de calentamiento climático global, conocidos como eventos hipertermales, los cuales quedan marcados en el registro estratigráfico como excursiones isotópicas negativas (Kennett y Stott, 1991; Thomas y Shackleton, 1996; Zachos et al., 2006; Norris et al., 2013). Los hipertermales suelen tener una duración breve desde el punto de vista de la escala de tiempo geológico, aproximadamente de 100 mil años (ka), y usualmente están asociados con grandes perturbaciones del ciclo del carbono, acidificación de los océanos, disolución de carbonatos en aguas profundas, perturbaciones del ciclo hidrológico y un aumento de la erosión continental (ver p. ej. Thomas et al., 2000; Cramer et al., 2003; Zachos et al., 2010; McInerney y Wing, 2011; Lauretano et al., 2015; Zeebe et al., 2017; Giorgioni et al., 2019).

La mayoría de los hipertermales del Paleógeno fueron desencadenados por cambios en el movimiento orbital de excentricidad de la Tierra (Cramer et al., 2003; Zachos et al., 2010; Lauretano et al., 2015; Foster et al., 2018). Sin embargo, algunos de ellos no parecen coincidir con cambios orbitales como, por ejemplo, el PETM (Cramer et al., 2003; Zachos et al., 2010; Littler et al., 2014). Al igual que el PETM, algunos de estos eventos hipertermales se han relacionado con diversos factores modificadores del clima

tales como la liberación del metano contenido en los clatratos de las rocas sedimentarias marinas, la combustión de materia orgánica, el derretimiento del permafrost en altas latitudes o una intensa desgasificación de origen volcánico (Zachos et al., 2005; McInerney y Wing, 2011; Barnet et al., 2019).



**Figura 1.** Evolución del  $\delta^{18}\text{O}$  a lo largo del intervalo Cretácico Superior–Eoceno (modificado de Huber et al., 2018). Los círculos hacen referencia a foraminíferos planctónicos superficiales, las cruces a foraminíferos planctónicos profundos y los rombos a foraminíferos bentónicos; el color hace referencia a la localidad de procedencia. KTM = Máximo Térmico del Cretácico; PETM = Máximo Térmico del límite Paleoceno-Eoceno; MECO = Optimo Climático del Eoceno medio; \* = intervalo estudiado en esta tesis; *Ih* = Clima tipo congelador (*Icehouse*).

### 1.3. Eventoestratigrafía a través tránsito Cretácico–Paleógeno

El intervalo de tiempo estudiado en esta tesis doctoral (~66,4–65,4 Ma) es uno de los periodos más excepcionales de la historia reciente del planeta Tierra, en el que se sucedieron relevantes eventos geológicos como el impacto de un gran asteroide o el

emplazamiento de una Gran Provincia Ígnea (GPI), junto con el desarrollo de algunos eventos hipertermales. De todos ellos, el evento que ha atraído la mayor atención de la comunidad científica desde hace más de 40 años es el impacto del asteroide de Chicxulub en lo que hoy es la Península del Yucatán (México) (Hildebrand et al., 1991). El impacto de Chicxulub se considera usualmente el principal responsable de la última de las cinco grandes extinciones masivas del Fanerozoico (p. ej. Smit, 1999; Kring, 2007; Schulte et al., 2010), que afectó a alrededor del 30% de los géneros y el 75% de las especies marinas (Raup y Sepkoski 1982).

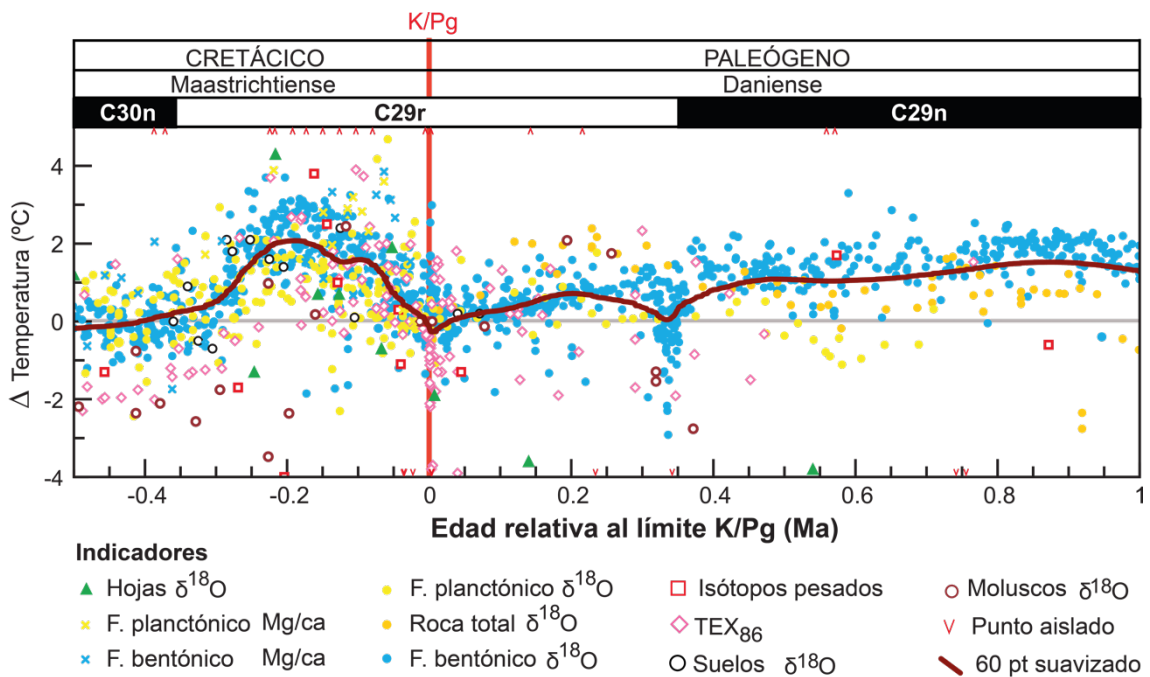
En el caso de los foraminíferos planctónicos algunos autores defienden que más del 90% de especies se extinguieron en coincidencia con el límite K/Pg en un evento de extinción en masa catastrófico (Smit, 1999; Arenillas et al., 2000, 2006; Schulte et al., 2010; Lowery et al., 2018; Hull et al., 2020). Otros autores han propuesto que un conjunto amplio de especies de foraminíferos planctónicos maastrichtienses se extinguieron en un intervalo temporal amplio, siguiendo un patrón de extinción masiva gradual (Keller, 1988; Canudo et al., 1991; Keller et al., 1993, 1995; MacLeod y Keller, 1994; Luciani, 1997). Los defensores de esta hipótesis han propuesto múltiples causas climático-ambientales para explicar este patrón de extinción como son, por ejemplo, una combinación de episodios de vulcanismo masivo, enfriamiento climático y caída del nivel del mar a finales del Maastrichtiense (Keller, 1988, Stinnesbeck et al., 1996; Li y Keller, 1998a,b) y múltiples impactos meteoríticos (Keller, 2003a, 2005; Keller et al., 2003).

Probablemente, el principal proceso que potencialmente podría desencadenar un modelo de extinción masiva gradual es el vulcanismo de la GPI del Decán, ya que es el único fenómeno que se prolongó durante cientos de miles de años a través del límite K/Pg (Courtilot et al., 1988; Chenet et al., 2008; Keller et al., 2010, 2016, 2020). Sin embargo, durante décadas ha sido difícil establecer un vínculo directo entre la actividad volcánica y las alteraciones de los ecosistemas, debido en parte al grado de incertidumbre inherente a las dataciones radiométricas disponibles para las principales fases eruptivas (Courtilot et al., 1986; Vandamme et al., 1991; Chenet et al., 2007). Esta problemática ha sido parcialmente resuelta en trabajos recientes que han aportado nuevas dataciones radiométricas de los episodios volcánicos del Decán, basadas en los métodos  $^{40}\text{Ar}/^{39}\text{Ar}$  (Renne et al., 2015; Sprain et al., 2019) y U-Pb (Schoene et al., 2015, 2019). Esta acumulación de datos ha permitido determinar con mayor precisión la duración del vulcanismo de Decán en <1 Ma y establecer una correlación más robusta entre los episodios volcánicos del Decán y los cambios biológicos, climáticos e isotópicos que

acontecieron en el tránsito K–Pg (Barnet et al., 2018; Hull et al., 2020; Fendley et al., 2020; Hernandez Nava et al., 2021).

1.3.1. Registro global de temperaturas y principales relaciones isotópicas a través del límite K/Pg

La reciente publicación de una de las mayores recopilaciones de indicadores de paleotemperaturas a lo largo de 1 Ma a través del límite K/Pg (Hull et al., 2020), ha contribuido de forma importante a la reconstrucción de la temperatura global de la Tierra durante este periodo. Este compendio combina los cambios de temperatura de más de 50 localidades repartidas por todo el planeta, tanto en paleoambientes continentales como marinos, dando como resultado una curva de variación de temperatura ( $\Delta T$ ) promedio global (Fig. 2).



**Figura 2.** Integración de múltiples indicadores climáticos y paleotermómetros que reflejan los cambios de temperatura globales a través del límite K/Pg. La línea curva granate es la resultante de una transformación rápida de Fourier de 60 puntos y refleja la tendencia global de la variación de temperatura (modificado de Hull et al., 2020). F. = foraminíferos.

Tal y como se observa en la Fig. 2, las relaciones isotópicas del oxígeno ( $\delta^{18}\text{O}$ ) y los valores del  $\text{TEX}_{86}$  encontrados a finales del Maastrichtiense reflejan un episodio de calentamiento climático global conocido como el Evento de Calentamiento del



Maastrichtiense Tardío (LMWE por sus siglas en inglés), que se inició ~300 ka antes del límite K/Pg (Barrera y Savin, 1999; MacLeod et al., 2005; Huber et al., 2018). El LMWE fue un evento transitorio ya que, tras su finalización, se recuperó durante los últimos ~150 ka del Maastrichtiense la tendencia climática general de lento enfriamiento progresivo que caracteriza esta edad de la historia geológica (Barnet et al., 2018) (Figs. 1 y 2).

Aunque el corto e intenso enfriamiento generalizado del planeta, asociado al impacto meteorítico del límite K/Pg, ha sido verificado con el paleotermómetro  $\text{TEX}_{86}$  a partir de muestreos de alta resolución (Vellekoop et al., 2014, 2016, Fig. 2), éste se refleja en la curva de  $\Delta T$  de Hull et al. (2020) debido a su breve duración, estimada en tan sólo unos meses o pocos años (Brugger et al., 2017). Esta curva tampoco refleja adecuadamente otros cambios en la temperatura de la superficie de los océanos de corta duración, ya que está basada principalmente en el registro isotópico de foraminíferos bentónicos.

En comparación con el detallado conocimiento del clima de los últimos cientos de miles de años previos al límite K/Pg, el número de datos isotópicos y de paleotemperaturas para los primeros cientos de miles de años del Daniense es menor, lo que ha dificultado históricamente su estudio en detalle. Esto se debe en parte a que la tasa de sedimentación en este intervalo suele ser más baja, provocando secciones más condensadas y con frecuentes hiatos (Olsson et al., 2002; D'Hondt, 2005; Jones et al., 2019). Por estas razones, la curva de  $\Delta T$  de Hull et al. (2020) para el Daniense inferior se basa principalmente en los registros isotópicos del *Ocean Drilling program* ODP 1262 en el Atlántico Sur, en el que se ha demostrado la continuidad sedimentaria a través del límite K/Pg (Barnet et al., 2019).

Los primeros eventos netamente desmarcados de la influencia del impacto de Chicxulub fueron los hipertermales (tomado aquí este término en sentido amplio) Dan-C2 (Quillévére et al., 2008) y LC29n (Coccioni et al., 2010). Las excursiones isotópicas negativas del carbono ( $\delta^{13}\text{C}$ ) y del oxígeno ( $\delta^{18}\text{O}$ ) (CIE y OIE, por sus siglas en inglés) asociadas a estos dos eventos solo se evidencian en los registros isotópicos obtenidos en roca total y sobre conchas de foraminíferos planctónicos, los cuales permiten analizar los cambios ambientales acontecidos en la parte superficial del océano para ambientes pelágicos (Coccioni et al., 2010). Estos eventos se han reconocido en realidad en muy pocas localidades del Atlántico y del Tetis, y no se muestran con claridad en la Fig. 2. Además, no se ha observado un calentamiento generalizado del fondo oceánico durante el Dan-C2 y el LC29n, lo que ha provocado que la naturaleza hipertermal de los mismos

haya sido recientemente cuestionada (Barnet et al., 2019; Hull et al., 2020; Arreguín-Rodríguez et al., 2021).

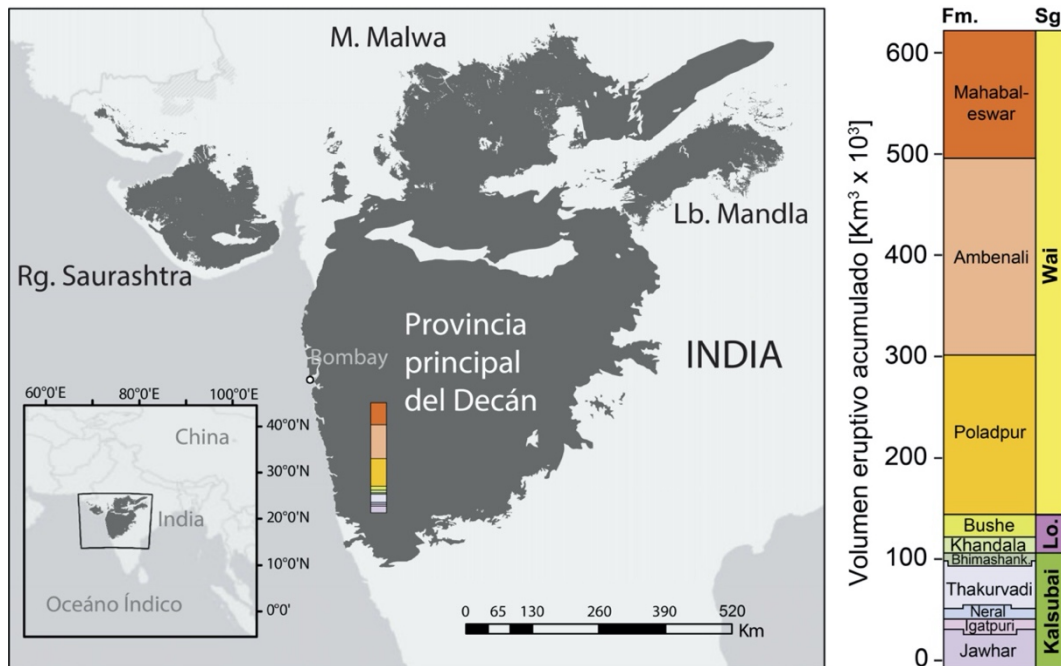
En la actualidad, se sigue explorando no solo las repercusiones paleobiológicas de los cambios paleoclimáticos y paleoambientales asociados a los eventos LMWE, límite K/Pg, Dan-C2 y LC29n, sino también cuáles fueron los mecanismos que los desencadenaron (Barnet et al., 2018, 2019; Lowery et al., 2018, 2021; Hull et al., 2020; Fendley et al., 2020; Keller et al., 2020; Krhal et al., 2020). En esta tesis se han reconocido y analizado estos eventos tras estudiar el registro isotópico ( $\delta^{13}\text{C}$  y  $\delta^{18}\text{O}$  sobre roca total) de las secciones de Caravaca y Zumaia (Capítulos 4.3, 4.4, 4.5; Gilabert et al., 2021a,b,c). Con ello se ha contribuido a establecer cuál es la relación de cada uno de ellos con el vulcanismo masivo del Decán, el impacto de Chicxulub y el forzamiento orbital.

### 1.3.2. Principales modelos eruptivos del vulcanismo del Decán a través del límite K/Pg

A la GPI del Decán también se la conoce como las Traps del Decán (*Deccan Traps*, en inglés), distinguiéndose una región o provincia ígnea principal, que acumula la mayor parte de las coladas basálticas, y otras subregiones menores (Jay y Widdowson, 2008; Manu Prasanth et al., 2019). La provincia principal aflora en la Meseta del Decán (centro-este de la India) con unas coordenadas aproximadas de  $\sim 73^\circ\text{--}78^\circ$  N y  $\sim 16\text{--}22^\circ$  E, mientras que las subregiones volcánicas de Saurashtra, la meseta de Malwa y el lóbulo de Mandla, se ubican respectivamente hacia el NO, N y NE de la provincia principal (Jay y Widdowson, 2008; Eddy et al., 2020; Hernandez Nava et al., 2021; Fig. 3). Las coladas basálticas de la provincia principal del Decán afloran en las conocidas como *Western Ghats* de la India, presentan un espesor actual máximo de 3500 m y ocupan una extensión aproximada de  $5 \times 10^5$  km<sup>2</sup>. Se estima que los volúmenes eruptivos de las coladas de basaltos oscilaron entre 0.6 y  $1.5 \times 10^6$  km<sup>3</sup> (Jay y Widdowson, 2008; Self et al., 2008; Richards et al., 2015).

Desde el punto de vista estratigráfico, la provincia principal del Decán se puede subdividir en tres Subgrupos (Sgs.) con sus respectivas formaciones, que en orden cronológico son: 1) el Sg. Kalsubai, compuesto por las Fms. Jawhar, Igatpuri, Neral, Thakurvadi y Bhimashankar; 2) el Sg. Lonavala, que incluye las Fms. Khandala y Bushe; y 3) el Sg. Wai, compuesto por las Fms. Poladpur, Ambenali y Mahabaleswar. Cada formación se caracteriza por la acumulación de grandes flujos toleíticos compuestos, con disposiciones subhorizontales y espesores variables, en los que la composición química y mineralógica de cada uno de ellos permite su reconocimiento como formaciones

individuales (Chenet et al., 2008). Quizá la característica más destacable de la volcanoestratigrafía del Decán es que las formaciones del Sg. Wai representan el ~75% del volumen total de las coladas basálticas emitidas por el vulcanismo del Decán (Renne et al., 2015; Richards et al., 2015; Schoene et al., 2015, 2019; Sprain et al., 2019).



**Figura 3.** Localización geográfica y extensión de las Traps del Decán en India (modificado de Hernandez Nava et al., 2021). En la columna estratigráfica se indican las formaciones volcanoestratigráficas del Decán, los subgrupos en las que se agrupan y el volumen eruptivo acumulado para cada formación (modificado de Schoene et al., 2019). Rg. = Región; M.= Meseta; Lb = Lóbulo; Fm. = Formación; Sg. = Subgrupo; Lo. = Lonavala.

La mejora en la precisión de las dataciones radiométricas recientes (Schoene et al., 2019; Sprain et al., 2019) ha permitido asignar a los Sg. Kalsubai y Lonavala una edad Maastrichtiense superior, comprendida entre el límite de los magnetocrones C30n/C29r y el límite K/Pg. Sin embargo, existen grandes discrepancias en cuanto a la edad de la Fm. Poladpur, la más antigua del Sg. Wai. Esta formación ha sido datada, utilizando el método U-Pb, como Maastrichtiense terminal por Schoene et al. (2015, 2019) y, utilizando el método <sup>40</sup>Ar/<sup>39</sup>Ar, como Daniense basal por Renne et al. (2015) y Sprain et al. (2019). Ambos métodos de datación radiométrica no sólo sugieren edades distintas para la Fm. Poladpur, sino también dos modelos eruptivos bastante diferentes entre sí (Fig. 4) y que se describen a continuación:

### 1) Modelo de mega-pulsos eruptivos

Las dataciones U-Pb de Schoene et al. (2015, 2019) sugieren la emisión de las coladas basálticas del Decán en fases discretas, en grandes pulsos eruptivos con una intensidad variable en el tiempo (Schoene et al., 2019). Este modelo fue originalmente propuesto por Chenet et al. (2007, 2008), quienes diferenciaron tres fases eruptivas: la primera, situada en la parte basal del magnetocrón C30n, la segunda y principal en el intervalo Maastrichtiense del magnetocrón C29r, y la tercera alrededor de la base del magnetocrón C29n, ya en el Daniense. Sus partidarios sostienen que la mayor tasa eruptiva ocurrió antes del límite K/Pg, desencadenando un cambio global sobre el clima y los ecosistemas en los últimos cientos de miles de años del Maastrichtiense que podría explicar las extinciones previas al límite K/Pg que caracterizan el modelo de extinción masiva gradual que ellos defienden (Courtilot, 1999; Stüben et al., 2003; Keller et al., 2008; Keller et al., 2011; Punekar et al., 2014a). La versión actualizada de este modelo eruptivo (Schoene et al., 2019, 2021) no habla de tres fases sino de cuatro mega-pulsos eruptivos concentrados en un intervalo de ~700 ka en torno al límite K/Pg (Fig. 4A).

Schoene et al. (2019, 2021) asignan con dataciones U-Pb una edad de  $66,016 \pm 0,050$  Ma para el límite K/Pg, tras recalibrar el mismo conjunto de datos de Clyde et al. (2016) procedentes de la Cuenca de Denver (Colorado), que originalmente arrojaban una edad de  $66,021 \pm 0,24/0,039$  Ma. Para estos autores, el primer mega-pulso se emitió entre ~66,3 Ma y ~66,15 Ma, propiciando el emplazamiento de los Sgs. Kalsubai y Lonavala. El segundo mega-pulso, que se corresponde con el emplazamiento de la Fm. Poladpur del Sg. Wai, se produjo entre ~66,10 y 66,04 Ma, concluyendo ~30 ka antes del límite K/Pg. El tercer y cuarto mega-pulso, ligados al emplazamiento de las formaciones danienses Ambenali y Mahabaleswar, ocurrieron de acuerdo a sus dataciones entre ~65,9 y ~65,8 Ma y entre ~65,6 y 65,5 Ma, respectivamente. Según Schoene et al. (2019, 2021), el mega-pulso de la Fm. Poladpur es el que registra la mayor tasa eruptiva de toda la secuencia eruptiva, mientras que los intervalos de tiempo entre el segundo y el tercer mega-pulso y entre el tercer y cuarto mega-pulso, de aproximadamente 100 ka y 200 ka respectivamente, se caracterizarían por una relativa quiescencia eruptiva (Fig. 4A).

### 2) Modelo de erupción casi-continua

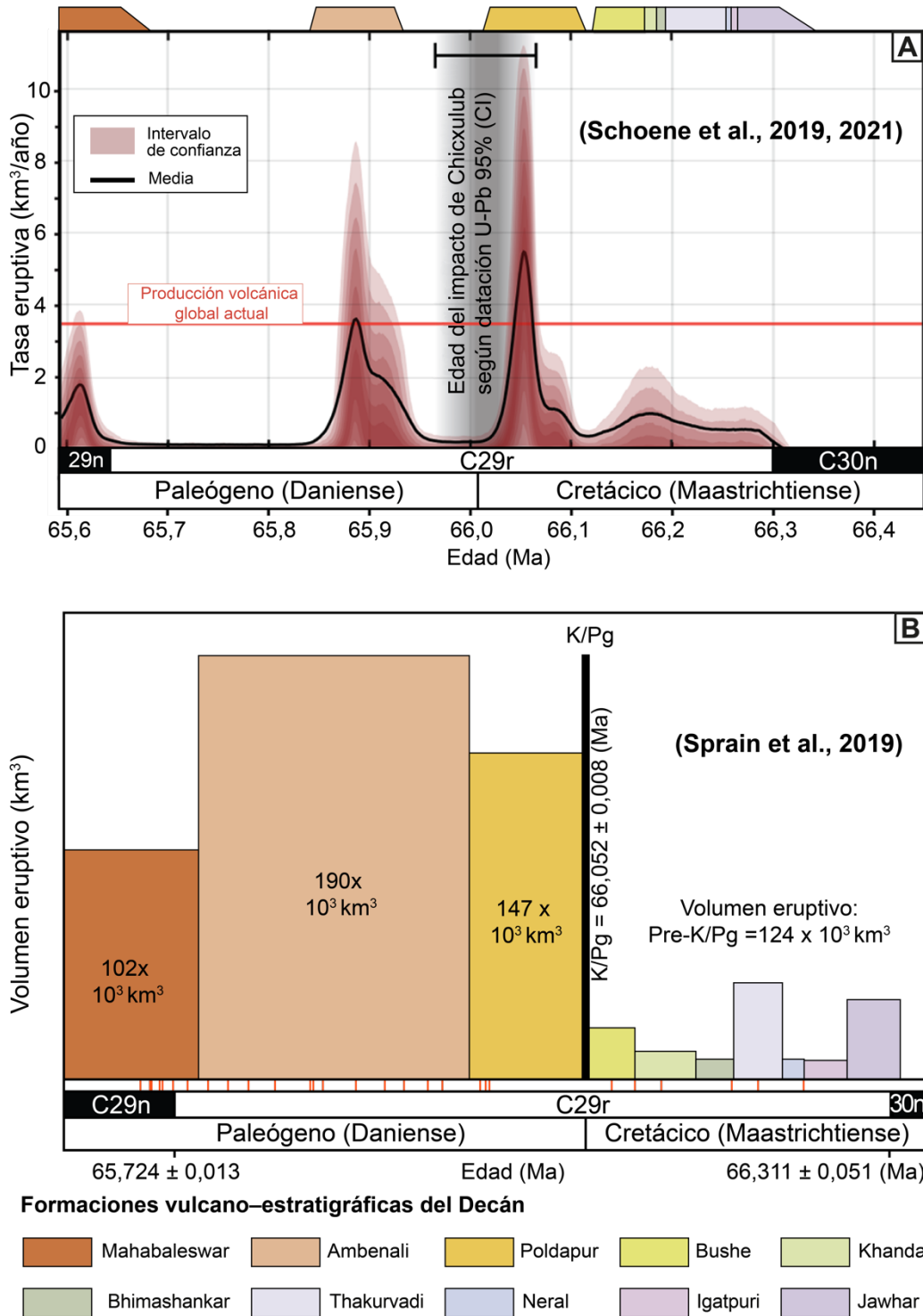
Las dataciones  $^{40}\text{Ar}/^{39}\text{Ar}$  de Renne et al. (2015) y de Sprain et al. (2019) sugieren un modelo eruptivo diferente (Fig. 4B), según el cual las coladas basálticas del Decán se emitieron con un ritmo bastante homogéneo en el tiempo (sin la existencia de mega-

pulsos apreciables) y durante el  $\sim 1$  Ma que duró la formación de la provincia ígnea principal del Decán (Sprain et al., 2019). El emplazamiento relativamente continuo de las formaciones de los Sgs. Kalsubai y Lonavala, así como de gran parte de la Fm. Poladpur del Sg. Wai, se infiere por la escasez de paleosuelos identificados en su interior (Chenet et al., 2008, 2009; Jay et al., 2009; Renne et al., 2015). Por el contrario, los paleosuelos son mucho más frecuentes en el resto de formaciones más modernas del Sg. Wai (Fig. 4B), lo que refleja una tasa eruptiva más variable. Esta diferencia en el emplazamiento parece sugerir un cambio en el sistema magmático del Decán, produciéndose un cambio desde erupciones de poco volumen, pero de elevada frecuencia, a erupciones de baja frecuencia, pero de elevado volumen (Renne et al., 2015; Richards et al., 2015; Sprain et al., 2019).

Los partidarios de este modelo sitúan el límite K/Pg entre los Sgs. Lonavala y Wai, ya que, de acuerdo a las dataciones  $^{40}\text{Ar}/^{39}\text{Ar}$  de Sprain et al. (2018), el límite K/Pg tiene una edad de  $66,052 \text{ Ma} \pm 0,008/0,043$ , la cual es casi indistinguible a la asignada al límite estratigráfico entre ambos subgrupos, que es de  $66,03 \pm 0,04 \text{ Ma}$  (Sprain et al., 2019). Es en este momento cuando se produjo el cambio en el sistema eruptivo, el cual quedó reflejado como cambios en la morfología, en el volumen y en la geoquímica de los flujos de lava de los Sgs. Kalsubai y Lonavala respecto a los del Sg. Wai. Este cambio tan relevante llevó a plantear la hipótesis de una posible aceleración de la tasa eruptiva en el Decán provocada por el impacto de Chicxulub (Renne et al., 2015; Richards et al., 2015).

Los cambios climáticos y ambientales más comúnmente relacionados con el vulcanismo del Decán son: calentamiento climático, pulsos de enfriamiento, perturbación del ciclo del carbono, lluvia ácida, disolución de carbonatos y acidificación oceánica (ver por ejemplo Li y Keller, 1998a,b; Keller, 2003a; Wignall, 2005; Gertsch et al., 2011; Keller et al., 2012, 2020; Henehan et al., 2016; Punekar et al., 2014a,b, 2016). Sin embargo, la interpretación de los cambios climáticos y ambientales ligados al vulcanismo del Decán difiere en función del modelo eruptivo que se escoja.

En esta tesis, se ha comparado la cronología asignada por otros autores a las formaciones de las Traps del Decán, con diversos indicadores micropaleontológicos, geoquímicos y paleomagnéticos calibrados temporalmente. Esto ha permitido evaluar la influencia del vulcanismo del Decán considerando ambos modelos eruptivos en los eventos paleobiológicos, paleoambientales y paleoclimáticos identificados a lo largo del  $\sim 1$  Ma estudiado (ver capítulos 4.2, 4.3, 4.4, 4.5; Arenillas et al., 2018; Gilabert et al., 2021a,b,c).

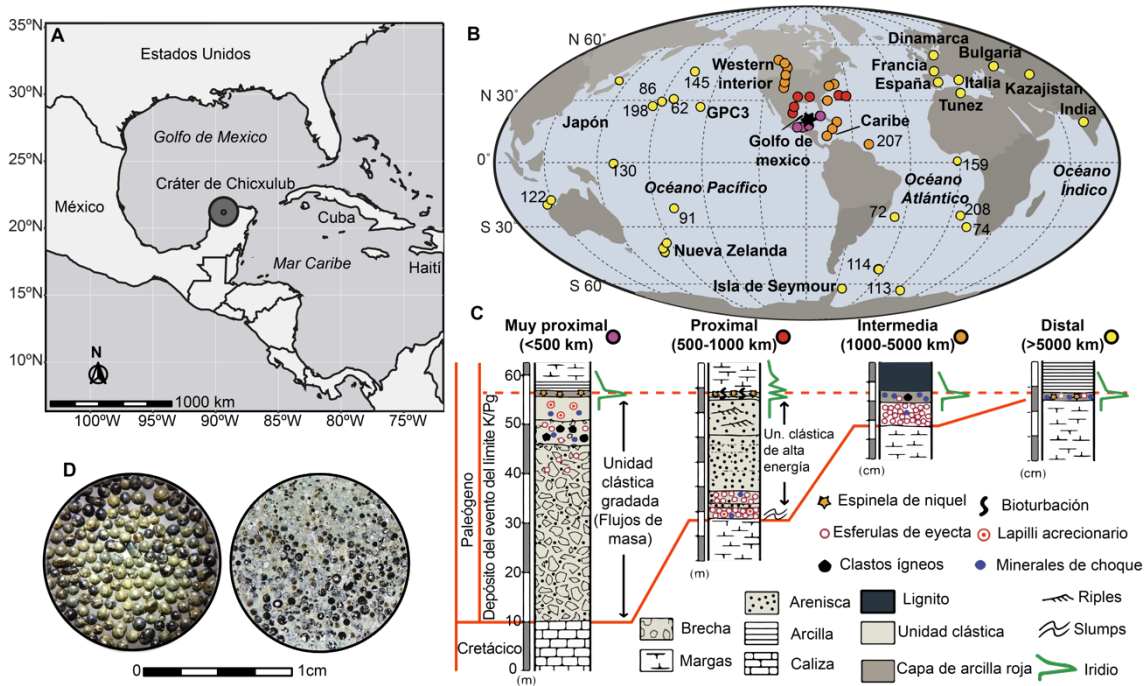


**Figura 4.** Principales modelos eruptivos y de edad para las formaciones volcano-estratigráficas de las Traps del Decán: **A)** Modelo de mega-pulsos eruptivos (modificado de Schoene et al., 2019, 2021); **B)** Modelo de erupción casi-continua (modificado de Sprain et al., 2019). Las dataciones U-Pb de la Fig. 4A indican que el mayor pulso volcánico antecedió al límite K/Pg, mientras que las dataciones  $^{40}\text{Ar}/^{39}\text{Ar}$  de la Fig. 4B indican que lo precedió. En el modelo de Sprain et al. (2019), se muestra con finas líneas verticales rojas la posición aproximada de los paleosuelos reconocidos por Chenet et al. (2008, 2009) y por Jay et al. (2009) a lo largo de la serie eruptiva del Decán.

### 1.3.3. El impacto de Chicxulub: edad, estratigrafía y efectos paleoambientales

La identificación del cráter de impacto de ~180 km de diámetro enterrado bajo la localidad de Chicxulub, península del Yucatán, México (Hilderbrand et al., 1991; Fig. 5A) es considerada como una de las evidencias más contundentes de que el impacto de un asteroide causó la extinción masiva catastrófica del límite K/Pg, teoría inicialmente propuesta por Alvarez et al. (1980) y por Smit y Hertogen (1980). El eyecta de impacto generado (vidrios de impacto, cuarzos de choque, espinelas de níquel, iridio, etc.) se distribuyó globalmente, acumulándose en una unidad estratigráfica que separa los materiales maastrichtienses y danienses y que tiende a ser más fina a medida que nos alejamos del cráter de Chicxulub (Smit, 1999; Claeys et al., 2002; Molina et al., 2009; Schulte et al., 2010; Fig. 5B,C).

La composición química de las rocas andesíticas del interior de la estructura de impacto de Chicxulub se demostró similar a la de los vidrios de impacto de secciones proximales como las de Haití, sugiriendo una más que probable relación co-genética entre ambas (Hildebrand et al., 1991). Desde fechas tempranas, la coincidencia del impacto de Chicxulub con el límite K/Pg ha sido criticada utilizando argumentos estratigráficos y micropaleontológicos en estudios llevados a cabo en localidades del Golfo de México y El Caribe, que indicarían que el impacto antecede en 200 ó 300 ka al límite K/Pg (p. ej. Ward et al., 1992; Keller et al., 1997, 2004, 2009; Keller, 2003a; Stinnesbeck et al., 2004). Sin embargo, estos argumentos han sido criticados en otras publicaciones análogas, las cuales demuestran que el impacto tuvo lugar en coincidencia con el límite K/Pg (p. ej. Sharpton et al., 1992; Smit et al., 1996; Smit 1999; Soria et al., 2001; Arz et al., 2004; Arenillas et al., 2006; Molina et al., 2009; Schulte et al., 2010; Paull et al., 2014; Urrutia-Fucugauchi et al., 2016; Lowery et al., 2018). Entre los principales trabajos que han confirmado una relación causa-efecto, Renne et al. (2013), aplicaron la técnica de datación  $^{40}\text{Ar}/^{39}\text{Ar}$  a vidrios de impacto de Beloc (Haití) y a bentonitas cercanas al límite K/Pg en Hell Creek (Montana), con lo que demostraron que el nivel de extinción en masa, el límite K/Pg y el impacto de Chicxulub tuvieron lugar dentro de un corto intervalo de tan solo 32 ka, estableciendo una nueva edad para el límite K/Pg de  $66,043 \pm 0,043$  Ma. La sincronía entre el impacto de Chicxulub y el límite K/Pg fue confirmada posteriormente por Renne et al. (2018) mediante la datación  $^{40}\text{Ar}/^{39}\text{Ar}$  de los vidrios de impacto de la isla de Gorgonilla (Pacífico colombiano) (Fig. 5D), que arrojaron una edad de  $66,051 \pm 0,031$  Ma para el límite K/Pg.



**Figura 5.** A) Localización geográfica de la estructura de impacto (cráter) de Chicxulub; B-C) Localización geográfica de las principales localidades donde se registra el límite K/Pg y estratigrafía variable de las unidades clásticas asociadas al impacto de Chicxulub según la distancia al centro del cráter de Chicxulub (modificado de Schulte et al., 2010); D) Fotografías de detalle de vidrios de impacto de la localidad de Gorgonilla, Colombia (Bérmudez y Cui, 2020).

La estratigrafía del tránsito K-Pg es compleja debido a la gran cantidad de energía y procesos geológicos implicados. Las localidades de paleoambientes marinos se pueden clasificar en función de su proximidad o lejanía al centro de la estructura de impacto de Chicxulub en cuatro grupos principales: 1) Secciones muy proximales, situadas a <500 km de distancia; están caracterizadas por depósitos de brechas enriquecidas en eyecta, de hasta varios centenares de metros de espesor (Urrutia-Fucugauchi et al., 1996; Takayama et al., 2000; Grajales-Nishimura et al., 2003; Arenillas et al., 2006; Urrutia et al., 2008); 2) Secciones proximales, entre 500–1000 km de distancia; están caracterizadas por unidades clásticas con estructuras sedimentarias que reflejan procesos de alta energía, como tsunamis y flujos de gravedad (Smit et al., 1996; Soria et al., 2001; DePalma et al., 2019); 3) Secciones intermedias, entre 1000–5000 km de distancia; están caracterizadas por una capa de 2 a 10 cm de espesor rica en vidrios de impacto, sobre la cual se deposita una fina capa <1 mm rica en iridio y otros elementos del grupo de los platinoideos, cuarzos de impacto y espinelas de níquel (Norris et al., 1999; Schulte et al., 2009; Renne et al., 2018). 4) Secciones distales, situadas a >5000 km de distancia; están caracterizadas por



una fina capa de arcilla roja rica en eyecta de impacto. Si existe continuidad sedimentaria en la parte basal del Daniense, sobre la capa que contiene el eyecta se reconoce en ambientes pelágicos una capa de arcilla oscura de espesor variable (Smit, 1982, 1999; Dupuis et al., 2001; Molina et al., 2006, 2009). De acuerdo a esta agrupación, las secciones de Caravaca, Zumaia, El Kef y Aïn Settara son del cuarto grupo, es decir, secciones pelágicas distales.

En cuanto a las perturbaciones ambientales asociadas, se estima que el impacto de Chicxulub liberó a la estratosfera ~325 gigatoneladas (Gt) de azufre y ~425 Gt de CO<sub>2</sub> procedentes de las rocas de la plataforma carbonatada-evaporítica del Yucatán, así como otros volátiles e ingentes cantidades de polvo y ceniza (Schulte et al., 2010; Artemieva et al., 2017). El efecto combinado de la bola de fuego asociada al propio impacto y la reentrada de los materiales de eyecta desde la estratosfera provocó un enorme pulso térmico en la troposfera, el cual pudo persistir durante horas o días y alcanzar miles de km desde el punto de impacto (Goldin y Melosh, 2009; Morgan et al., 2013). Tras este breve pulso térmico, los materiales en suspensión en la atmósfera causaron una reducción abrupta de la luz solar, iniciando un breve invierno de impacto con una duración aproximada de varios meses o unos pocos años en los que las temperaturas globales disminuyeron al menos unos 7 °C (Vellekoop et al., 2014, 2016) o, según recientes modelizaciones climáticas, incluso hasta 28 °C (Brugger et al., 2017). Además, el bloqueo de la luz solar debió inhibir la fotosíntesis, provocando el colapso de las cadenas tróficas terrestres y marinas (Zachos et al., 1989, Toon et al., 1997, D'Hondt et al., 1998, Coxall et al., 2006; Birch et al., 2021).

Las consecuencias derivadas de la liberación de aerosoles y materiales volatilizados procedentes tanto de la plataforma del Yucatán como del asteroide debieron ocasionar además la destrucción de la capa de ozono, la emisión de toxinas y metales pesados, así como la reducción catastrófica de los organismos calcificadores pelágicos (Smit, 1982, Arenillas et al., 2000a,b; Bown, 2005) y el subsecuente calentamiento climático y acidificación de los océanos (Smit y Romein, 1985; Hsü y McKenzie, 1985; Kring, 2007; Alegret et al., 2012; Henehan et al., 2019). El brusco descenso del contenido en CaCO<sub>3</sub>, del  $\delta^{18}\text{O}$  y del  $\delta^{13}\text{C}$  que caracterizan la quimioestratigrafía de ambientes marinos son un reflejo de estos últimos procesos (Zachos et al. 1989; D'Hondt et al. 1998; Schulte et al., 2010; Henehan et al., 2016). La recuperación de la productividad oceánica fue relativamente rápida (Sepúlveda et al., 2009; Lowery et al., 2018, 2021). Sin embargo, la

diversidad no alcanzó valores similares a los de finales del Cretácico hasta de 3 a 10 Ma después (Aze et al., 2011; Birch et al., 2016, 2021; Lowery y Fraas, 2019).

En esta tesis, el estudio detallado de las asociaciones de foraminíferos planctónicos y de los indicadores geoquímicos a través del límite K/Pg ha permitido evaluar la contribución del impacto de Chicxulub tanto en el evento de extinción masiva, como en la subsiguiente radiación evolutiva y en los cambios ambientales que caracterizaron el comienzo del Daniense (Capítulos 4.1, 4.2, 4.4, 4.5; Arenillas et al., 2017, 2018; Gilabert et al., 2021b,c).



# *Capítulo 2.*

---

## *Objetivos*



## 2. OBJETIVOS

El principal objetivo de esta tesis doctoral es el de profundizar en el conocimiento acerca del papel jugado por el vulcanismo del Decán, el impacto de Chicxulub y otros factores en la extinción masiva y en la radiación evolutiva de los foraminíferos planctónicos a través del tránsito Cretácico-Paleógeno (K–Pg). Se pretende así plantear una detallada calibración temporal de los principales eventos paleobiológicos y paleoambientales acontecidos durante 1 Ma a través del límite K/Pg, determinando de forma precisa las posibles relaciones causa-efecto entre todos ellos. En concreto, se han marcado los siguientes objetivos específicos<sup>1</sup>:

- I. Analizar bioestratigráficamente el tránsito K–Pg en cuatro de las secciones consideradas como más completas y expandidas del mundo: El Kef, Aïn Settara, Caravaca y Zumaia [Arenillas et al., 2018; Gilabert et al., 2021a,b,c].
- II. Precisar la edad de los biohorizontes-guía de las principales biozonas y acmé-estadios de foraminíferos planctónicos mediante calibraciones magnetocronológicas y astrocronológicas [Gilabert et al., 2021a,b,c].
- III. Reconocer y correlacionar a escala global los principales eventos isotópicos del tránsito Cretácico-Paleógeno (LMWE, límite K/Pg, Dan-C2 y LC29n) [Gilabert et al., 2021a,b,c].
- IV. Calibrar astrocronológicamente la duración del LMWE, y de los eventos Dan-C2 y LC29n [Gilabert et al., 2021c].
- V. Interpretar las evidencias de acidificación oceánica y de cambios en la estructura de la columna del agua a lo largo del intervalo estudiado [Gilabert et al., 2021a,b].
- VI. Ponderar las repercusiones paleoambientales del LMWE, K/Pg, Dan-C2 y LC29n y su influencia en las asociaciones de foraminíferos planctónicos [Arenillas et al., 2018; Gilabert et al., 2021a,b,c].
- VII. Determinar si existen evidencias paleobiológicas de un aumento de las condiciones de estrés ambiental vinculadas exclusivamente al vulcanismo del Decán [Arenillas et al., 2018; Gilabert et al., 2021a,b,c].
- VIII. Comprobar la validez del taxón *Chiloguembelitra* y evaluar las implicaciones filogenéticas que esto conlleva [Arenillas et al., 2017].

---

<sup>1</sup> En cada objetivo específico se indica en que [artículo/s], se ha abordado el objetivo en cuestión.

- IX. Evaluar las variaciones en la tasa de formas aberrantes de foraminíferos planctónicos y sus causas [Arenillas et al., 2018; Gilabert et al., 2021b].
- X. Interpretar las contribuciones relativas del vulcanismo del Decán y del forzamiento orbital en los cambios climáticos y biológicos en el Maastrichtiense superior y Daniense inferior [Arenillas et al., 2018; Gilabert et al., 2021a,b,c].

***Capítulo 3.***  
 ***Materiales y***  
 ***Métodos***





### 3. MATERIALES Y MÉTODOS

La metodología usada en esta tesis doctoral se aborda en cada uno de los artículos que la componen y que se han reunido en el capítulo de Resultados. Sin embargo, y dada la variedad de técnicas empleadas, se ha considerado necesario redactar a continuación un apartado de materiales y métodos siguiendo un orden lógico en función de la tipología de las técnicas utilizadas.

#### 3.1. Localidades estudiadas

En esta tesis doctoral se han analizado muestras provenientes de cuatro secciones estratigráficas muy conocidas internacionalmente por el debate sobre los patrones de extinción de foraminíferos planctónicos en torno al límite K/Pg, y consideradas como cuatro de las secciones más completas y continuas del tránsito K–Pg: Caravaca (Murcia) y Zumaia (Guipúzcoa) en España, y El Kef y Aïn Settara en Túnez. Las secciones tunecinas y Caravaca pertenecen al Tetis occidental, mientras que Zumaia se localiza en una zona de transición entre el Tetis y el Atlántico Norte (Tabla 1).

	<b>El Kef</b> (Arenillas et al., 2017, 2018)	<b>Aïn Settara</b> (Arenillas et al., 2018)	<b>Caravaca</b> (Gilabert et al., 2021a,b)	<b>Zumaia</b> (Gilabert et al., 2021c)
<b>Coordenadas</b>	36° 09' 13" N 08° 38' 54" W	35° 07' 59" N 09° 49' 59" W	38° 04' 36" N 01° 52' 42" W	42° 18' 00" N 02° 15' 30" W
<b>Dominio</b>	Tetis occidental	Tetis occidental	Tetis occidental	Tetis–Atlántico Norte
<b>Paleo-profundidad</b>	Batial superior-medio	Batial superior-medio	Batial medio	Batial medio-profundo
<b>Tipo de análisis</b>	Foraminíferos planctónicos	Foraminíferos planctónicos	Foraminíferos planctónicos, $\delta^{13}\text{C}$ , $\delta^{18}\text{O}$ , SM, $\text{CaCO}_3$	Foraminíferos planctónicos, $\delta^{13}\text{C}$ , SM, $\text{CaCO}_3$
<b>Eventos reconocidos</b>	Límite K/Pg	Límite K/Pg	Límite K/Pg, LMWE, Dan-C2	Límite K/Pg, LMWE, Dan-C2; LC29n

**Tabla 1:** Resumen de la localización geográfica, paleogeográfica y paleobatimétrica de las secciones estudiadas en esta tesis doctoral, así como el tipo de análisis realizados y los eventos estudiados en cada una de ellas. Para mayor información consultar los artículos mencionados en esta tabla. SM = susceptibilidad magnética.

Las muestras de El Kef y Aïn Settara fueron proporcionadas por los directores de tesis, mientras que las de Caravaca y Zumaia se recogieron en varias campañas de campo (Fig.6) en las que se realizaron muestreos de alta resolución, se levantaron columnas

estratigráficas anotando la posición de las muestras recolectadas y se llevaron a cabo las observaciones estratigráficas y/o sedimentológicas pertinentes. Además, se tomaron fotografías detalladas de todos los tramos litológicos para llevar un mejor control de la posición de las muestras.

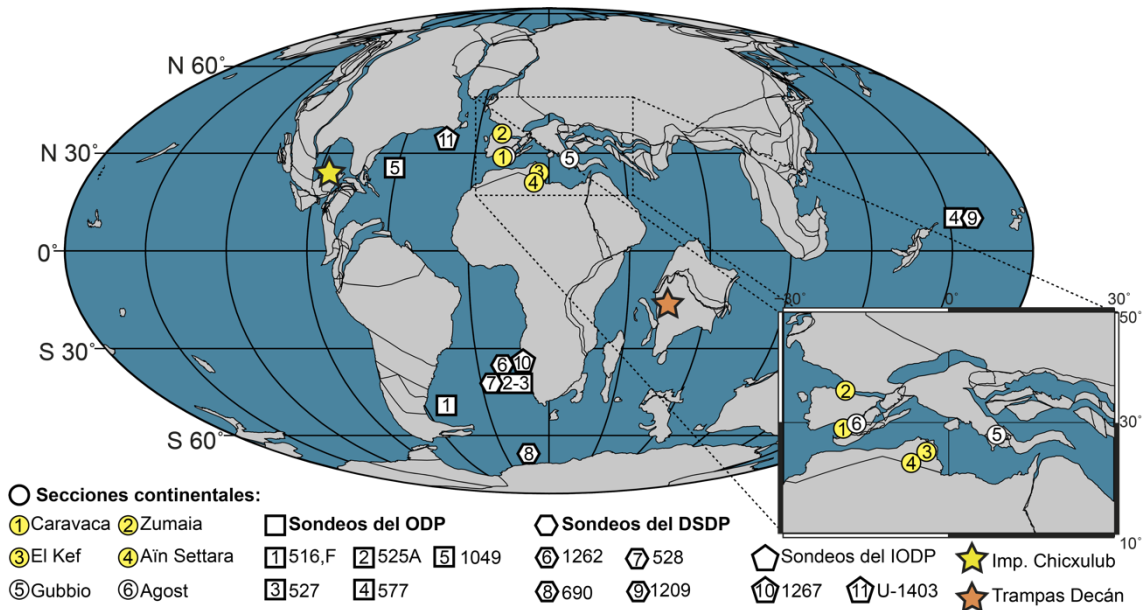


**Figura 6.** Toma de muestras en las secciones de Caravaca (A) y Zumaia (B,C)

Las secciones estudiadas se caracterizan por ser muy completas, continuas y expandidas en el intervalo analizado. La sección de El Kef fue designada como la sección-tipo del *Global boundary Stratotype Section and Point* (GSSP) de la base del Daniense (Cowie et al., 1989; Molina et al., 2006), mientras que el resto fueron designadas como secciones auxiliares del mismo (Molina et al., 2009). A pesar de haber sido extensamente estudiadas en los últimos 40 años (p. ej., Smit, 1982; Canudo et al., 1991; Keller, 1996; Kaiho et al., 1999; Arenillas et al., 2000a,b; Arz et al. 2000; Lamolda et al., 2005; Gallala et al., 2009; Batenburg et al., 2012 o Font et al., 2018), estas secciones todavía poseen un gran potencial para extraer información micropaleontológica y geoquímica y para ampliar el conocimiento sobre los cambios paleoclimáticos, paleoambientales y paleobiológicos a lo largo de este intervalo de tiempo de la historia de la Tierra, a tenor de los resultados obtenidos en los artículos en los que se basa esta tesis doctoral.

Para una mejor caracterización e interpretación global de estos cambios, ha sido necesario, además, comparar los resultados obtenidos con los de otros autores, en éstas y en otras localidades repartidas en ambos hemisferios (Fig. 7). La mayoría de estas localidades con las que se han comparado los resultados pertenecen a sondeos profundos de las expediciones del *Ocean Drilling program* (ODP), del *Deep Sea Drilling Project* (DSDP) y del *Integrated Ocean Drilling Program* (IODP). Además, se han integrado

datos de otras secciones bien conocidas del Tetis, como las de Gubbio (Contessa-Highway y Bottaccione, Italia) y Agost (Alicante).



**Figura 7.** Localización geográfica de las secciones estudiadas en esta tesis doctoral (círculos en amarillo) y de otras localidades con las que se realizaron comparaciones y correlaciones del registro micropaleontológico, isotópico y paleomagnético.

### 3.2. Métodos de laboratorio y tratamiento de muestras micropaleontológicas

Para la extracción del residuo concentrado de foraminíferos planctónicos, se ha seguido el procedimiento estándar del método del levigado adaptado a las características litológicas particulares de cada afloramiento. En rocas poco endurecidas, como las de Caravaca, se inició con una primera molienda mecánica mediante mortero. Seguidamente se procedió a la disgregación química de la muestra, sumergiéndola en una solución de agua oxigenada (H<sub>2</sub>O<sub>2</sub>) diluida al 10%. El tiempo para la disgregación fue de 2 horas para las muestras del Maastrichtiense y de 3–4 horas para las del Daniense. Finalmente, la muestra disgregada se hizo pasar por una torre de tamices de luz de malla de 1 mm, 100 μm y 63 μm bajo un flujo de agua corriente, y el residuo concentrado de foraminíferos fue secado en un horno a una temperatura <50 °C y recogido en un frasco de plástico cilíndrico convenientemente siglado. Entre muestra y muestra, los tamices se sumergieron en una solución de azul de metileno (C<sub>16</sub>H<sub>18</sub>ClN<sub>3</sub>S) con el fin de reconocer ejemplares contaminados en las muestras procesadas. Dado que para la sección de Caravaca se planteó realizar un análisis del índice de fragmentación de las conchas de

foraminíferos planctónicos, el proceso de molienda y el paso a través de la torre de tamices se realizó con la máxima delicadeza posible para evitar un sesgo en su interpretación tafonómica.

En el caso de las muestras de Zumaia, el procedimiento seguido fue el mismo que el descrito anteriormente, variando tan solo la técnica de disgregación química. En este caso, se utilizó la técnica descrita por Lirer (2000) para la extracción de microfósiles en rocas carbonatadas muy endurecidas. Para ello, tras la molienda se empleó ácido acético glacial ( $\text{CH}_3\text{COOH}$ ) diluido al 80% y se dejó actuar durante 3–4 horas.

En todas las localidades analizadas, las muestras han sido estudiadas cuantitativamente empleando para ello generalmente la fracción  $>63 \mu\text{m}$ . Cada muestra de residuo concentrado fue cuarteada usando un microcuarteador tipo Otto para obtener alícuotas estadísticamente representativas de al menos 300 ejemplares de foraminíferos planctónicos. Al mismo tiempo, se extrajeron y contabilizaron el número de foraminíferos bentónicos que, a diferencia de los planctónicos, no se determinaron taxonómicamente. Los ejemplares fueron fijados en celdillas micropaleontológicas estándar de 60 unidades usando goma de tragacanto, y almacenadas para asegurar su preservación y posterior consulta. Una parte del material figurado en las publicaciones fue etiquetado convenientemente y depositado en el Museo de Ciencias Naturales de la Universidad de Zaragoza (material etiquetado como MPZ 2016/108 a MPZ 2016/119 y como MPZ 2019/1 a MPZ 2019/21). Complementariamente, algunos ejemplares de especies y géneros clave de foraminíferos planctónicos fueron seleccionados para su fotografiado bajo el microscopio electrónico de barrido (MEB) modelo JEOL JSM 6400, en el Servicio de Microscopía de la Universidad de Zaragoza.

### 3.3. Taxonomía y bioestratigrafía



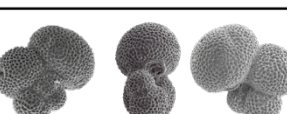
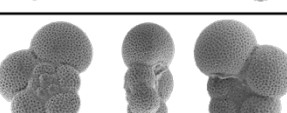
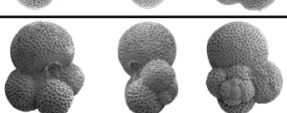

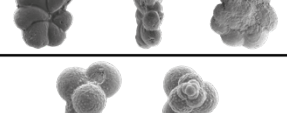
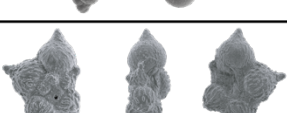
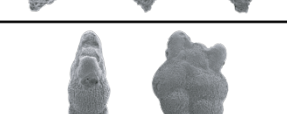
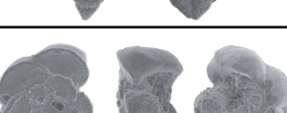

Los ejemplares de foraminíferos planctónicos han sido clasificados a nivel de especie y de género. Para la clasificación de los taxones del Maastrichtiense se han utilizado las propuestas taxonómicas de Robaszynski et al. (1983–1984) y de Caron (1985) para la diagnosis de especies trocoespiraladas, la de Nederbragt (1991) para las especies seriadas y multiseriadas, y la de Smith y Pessagno (1973) para las especies planoespiraladas. Las descripciones y figuraciones de los taxones analizados fueron comparadas con las proporcionadas en tesis doctorales como las de Arz (1996) y Pérez-Rodríguez (2013). En la clasificación de los taxones del Daniense se ha tenido en cuenta el atlas de

foraminíferos planctónicos del Paleoceno de Olsson et al. (1999). Sin embargo, este monográfico tiene una tendencia al agrupamiento de especies y/o géneros (taxonomía tipo "lumper"), sobre todo en la parte basal del Daniense.

En esta tesis doctoral se ha seguido, por el contrario, una taxonomía más diferenciadora (tipo "splitter") como la propuesta en la tesis doctoral de Arenillas (1996), la cual se basó en los esquemas taxonómicos de Bolli (1957, 1966), Luterbacher (1964), Luterbacher y Premoli Silva (1964), Stainforth et al. (1975), Blow (1979), y Toumarkine y Luterbacher (1985). La propuesta de Arenillas (1996) fue actualizada a lo largo de las siguientes décadas en numerosos trabajos de revisión taxonómica y filogenética, que también han sido tenidos en cuenta (Arenillas y Arz 2013a,b, 2017; Arenillas et al., 2010, 2016a, 2017, 2018). Por último, también se ha consultado la información alojada en la web <https://www.mikrotax.org/pforams/> (Young et al., 2017), en la que se puede encontrar una gran cantidad de información acerca de los foraminíferos planctónicos del Mesozoico y Cenozoico.

La biozonación empleada en esta tesis doctoral se ha resumido en la Fig. 8. Para los materiales de edad Maastrichtiense se ha seguido la biozonación alfanumérica de Li y Keller (1998a) y la biozonación binomial de Arz y Molina (2002). Para el Daniense, se ha utilizado la biozonación de Arenillas et al. (2004), la cual fue actualizada en Metsana-Oussaid et al. (2019). Con el objetivo de facilitar la comprensión de los lectores, en los artículos que componen esta tesis doctoral se ha comparado la escala de Arenillas et al. (2004) con la biozonación alfanumérica estándar de Berggren y Pearson (2005), la cual fue actualizada por Wade et al. (2011). En ocasiones (p. ej. en Fig. 1 de Arenillas et al., 2018), se ha mencionado también la biozonación de Keller et al. (1995).

En esta tesis también se ha realizado bioestratigrafía cuantitativa, lo que ha permitido reconocer los tres acmé-estadios de foraminíferos planctónicos (PFAS por sus siglas en inglés) del Daniense inferior definidos por Arenillas et al. (2006): PFAS-1, caracterizado por el dominio del género triseriado *Guembelitra*; PFAS-2, caracterizado por el dominio de las especies trocoespinaladas diminutas de *Palaeoglobigerina* y *Parvularugoglobigerina*; y PFAS-3, caracterizado por el dominio de las especies biseriadas de *Woodringina* y *Chiloguembelina* (ver su equivalencia con las biozonas en Fig. 8). Estos tres acmé-estadios permiten minimizar la influencia en las interpretaciones bioestratigráficas de los potenciales problemas taxonómicos a nivel específico que dependen de la taxonomía empleada por los diferentes autores (Arenillas et al., 2018; Gilabert et al., 2021b,c).

ESTADIO	Biozonas			Acmé-estadios	Biohorizontes y bioeventos clave	Especies índice			
	(A)	(B)	(C)						
DANIENSE INFERIOR	Parasubbotina pseudobulloidis	<i>Globanomalina compressa</i>	P1c	3	└ DPR <i>G. compressa</i> (11) └ DPR de <i>S. triloculinoides</i> (10) └ DPR de <i>P. varianta</i> (9) └ DUR de <i>Pv. eugubina</i> └ DPR de <i>P. pseudobulloidis</i> (8)	 (11)			
		<i>Subbotina triloculinoides</i>	P1b			P1c	 (10)		
			<i>Eoglobigerina trivialis</i>				P1a	P1b	 (9)
		P1b				 (8)			
		Pv. eugubina	<i>Eoglobigerina simplicissima</i>			Pα	P1a	└ DPR <i>E. simplicissima</i> (7) └ DPR de <i>Pv. eugubina</i> (6)	 (7)
			<i>Pv. sabina</i>			Pα	P1a	└ DPR de <i>Pv. eugubina</i> (6)	 (6)
	Gb. cretacea (4)	<i>Pv. longiapertura</i>	P0	P0	└ DPR de <i>Pv. longiapertura</i> (5) └ Extinción del límite K/Pg = DUR de <i>Pt. hantkeninoides</i>			 (5)	
	MAASTRICHTIENSE SUPERIOR	Abathomphalus mayaroensis			<i>Plummerita hantkeninoides</i>	CF1	1	└ DPR de <i>Pt. hantkeninoides</i> (3)	 (4)
			<i>Pseudoguembelina hariaensis</i> (2)	CF2		 (3)			
		 (2)							
		CF3			└ DUR de <i>Gna. gansseri</i> (1)	 (1)			
(D)		(E)							

**Figura 8.** Comparativa de las principales biozonaciones de foraminíferos planctónicos empleadas en esta tesis doctoral: (A) Arenillas et al. (2004); (B) Wade et al. (2011); (C) Keller et al. (1995); (D) Arz y Molina (2002); (E) Li y Keller (1998a). DPR = Dato de Primer Registro (o de registro más bajo); DUR = Dato de Último Registro (o de registro más alto). Gna. = *Gansserina*; Mh. = *Muricohedbergella*; Pv. = *Parvularugoglobigerina*; Gb. = *Guembelitra*.

### 3.4. Análisis cuantitativo

El análisis cuantitativo de las asociaciones de foraminíferos planctónicos es la herramienta fundamental utilizada en esta tesis doctoral. Además del reconocimiento de acmé-zonas, ha permitido llevar a cabo un análisis de la diversidad de foraminíferos planctónicos en cada intervalo de tiempo, evaluando en cada muestra la riqueza específica (S), el índice de Shanon-Weaver ( $H'$ ), el índice de Simpson ( $1/\lambda$ ) y la equitabilidad (E). Para ello, se ha utilizado el software PAST versión 4.0.3 (Hammer et al., 2001). Complementariamente, las bases de datos generadas por el análisis cuantitativo han permitido obtener reconstrucciones paleoambientales y paleoclimáticas precisas, así como identificar los cambios de la estructura de la parte superior de la columna de agua y los eventos paleobiológicos que se suceden en el intervalo de tiempo estudiado.

Ya que en esta tesis doctoral no se han realizado análisis isotópicos directamente sobre conchas de foraminíferos planctónicos, para reconstruir el hábitat batimétrico de cada una de sus especies se ha consultado el banco de datos de paleobiología isotópica de foraminíferos planctónicos recopilados por numerosos autores (p. ej., D'Hondt y Zachos, 1993; D'Hondt y Arthur, 1995; Olsson et al., 1999; Abramovich et al., 2003; Isaza-Londoño et al., 2006; Aze et al., 2011; Birch et al., 2012; Ashckenazi-Polivoda et al., 2014; Falzoni et al., 2014, 2016; Petrizzo et al., 2020). Con esta información, se han propuesto diversas reconstrucciones del estado y/o estructura de la parte superior de la columna de agua. Por ejemplo, en Gilabert et al. (2021a, Tabla 1) se asignó a cada uno de los géneros de foraminíferos planctónicos del Maastrichtiense de Caravaca un hábitat concreto de profundidad, en función de su preferencia a habitar la capa de mezcla, la capa intermedia o la termoclina. Posteriormente se empleó el índice profundo/superficial (P/S) como un indicador del estado de la columna de agua. Valores altos del índice P/S se interpretaron como una termoclina más profunda y expandida y una columna de agua térmicamente bien estratificada con hábitats batimétricos mejor definidos y estables. Valores bajos del índice P/S se interpretaron como una capa de mezcla más expandida y una termoclina más adelgazada, provocando una pérdida en la estratificación térmica de la columna de agua y la proliferación de especies generalistas que comúnmente habitan en la capa de mezcla.

$$P/S (\%) = \frac{(\text{Habitantes de termoclina})}{(\text{Habitantes de termoclina} + \text{habitantes de capa de mezcla})} \times 100$$



Por otra parte, la identificación de acmés o episodios de apogeo de especies generalistas y oportunistas es un buen indicador de aumentos de estrés ambiental en los ecosistemas. Los ejemplos más comunes de este tipo de acmés para el intervalo Maastrichtiense–Daniense son los asociados a los géneros *Heterohelix*, *Guembelitra* y *Chiloguembelitra* (p. ej., Kroon y Nederbragt, 1990; Puneekar et al., 2014a,b; Arenillas et al., 2018; Gilabert et al., 2021b,c). De igual manera, y aunque es un indicador más habitual en foraminíferos bentónicos (Yanko et al., 1998), el brusco aumento de la tasa de ejemplares con malformaciones (conchas aberrantes) es otro indicador que se ha utilizado por primera vez como evidencia directa de condiciones de elevado estrés ambiental a través del tránsito K–Pg (Arenillas et al., 2018; Gilabert et al., 2021b). La tasa o índice de foraminíferos aberrantes (FAI en siglas inglesas) se calcula de la siguiente manera:

$$\text{FAI (\%)} = \frac{\text{Aberrantes}}{\text{Aberrantes} + \text{Conchas normales}} \times 100$$

Otro indicador utilizado fue el índice de fragmentación de las conchas de foraminíferos planctónicos. Es un indicador tafonómico muy útil para evaluar los cambios en el estado de saturación del carbonato cálcico (Berger et al., 1982; Malmgren, 1987; Hennehan et al., 2016). Para contabilizar un resto de concha como fragmento se ha considerado que su grado de preservación es  $<2/3$  de la concha completa. Para calcular el índice de fragmentación se triaron en cada muestra todos los restos reconocibles de conchas de foraminíferos planctónicos (con un promedio de  $\sim 765$  restos por muestra entre fragmentos y conchas completas) hasta completar aproximadamente lo que serían unos 500 ejemplares de conchas completas para el Maastrichtiense (Gilabert et al., 2021a) y unos 360 en promedio para el Daniense (Gilabert et al., 2021b). El índice de fragmentación (FI en siglas inglesas) se calcula de la siguiente manera:

$$\text{FI (\%)} = \frac{\text{Fragmentos}}{\text{Fragmentos} + \text{Conchas completas}} \times 100$$

Por último, el índice planctónico/bentónico (P/B) es un índice muy útil para estimar la paleobatimetría y la distancia de la línea de costa, permitiendo reconocer ambientes sublitorales o neríticos internos ( $<10\%$ ), medios y externos (20–60%), batial superior (60–90%) y batial medio (80–99%) (Gibson 1989). No obstante, en esta tesis doctoral el

índice P/B se ha utilizado como un indicador auxiliar al FI para evaluar los cambios en el estado de saturación del CaCO<sub>3</sub>. El índice P/B complementa la información del índice de fragmentación porque los foraminíferos bentónicos son más resistentes que los planctónicos a los procesos de disolución (Berger et al., 1982). Por tanto, un descenso de este índice, sin otras evidencias de cambios paleobatimétricos relevantes, puede reflejar episodios de disolución de carbonatos, como los provocados por el ascenso de la lisoclina. Cuando se producen estos episodios de disolución, se puede reconocer una fuerte relación lineal inversa entre los índices FI y P/B (Kucera et al., 1997). El índice P/B se calcula de la siguiente manera:

$$P/B (\%) = \frac{F. \text{planctónicos}}{F. \text{planctónicos} + F. \text{bentónicos}} \times 100$$

### 3.5. Análisis morfoestadístico

Se han realizado distintos análisis morfoestadísticos univariantes, bivariantes y multivariantes para determinaciones taxonómicas y estudios paleoambientales, usando para ello el software PAST versiones 3.1.1 y 4.0.3 (Hammer et al., 2001). En Arenillas et al. (2017) se analizó biométricamente el ángulo de convexidad en vista axial ( $\alpha$ ), longitud (L), anchura (W) y altura (H) de la concha de 124 ejemplares de *Chiloguembelitra*, con el objetivo de comprobar el número de especies (morfoespecies) de este género en el Daniense inferior. Sobre estos ejemplares se midieron también la longitud (CL), anchura (CW) y altura (CH) de la última cámara. Con dichas variables biométricas se obtuvo el diámetro medio de la cámara ( $CAD = (CL \times CW \times CH)^{1/3}$ ) y la relación H/L. El parámetro  $\alpha$  y la relación H/L se analizaron de manera univariante y bivariante, permitiendo identificar al menos tres morfoespecies de *Chiloguembelitra*. Además, se realizó un análisis de componentes principales (PCA) y un análisis clúster aglomerativo (modo R), que contribuyó a la determinación de dichas especies.

En Gilabert et al. (2021a) se aplicó un análisis univariante de la altura (H) y longitud (L) de 507 ejemplares de *Contusotruncana contusa* y de la altura (H) y anchura (W) de 507 ejemplares de *Pseudoguembelina hariaensis*, con el objetivo de identificar episodios de enanismo de sus conchas. El análisis biométrico de ambas especies se basó en 10 ejemplares por cada muestra, seleccionado aleatoriamente sobre una muestra cuarteada y estadísticamente significativa en la fracción de >100 micras, para evitar el posible sesgo

provocado por la medición de ejemplares juveniles. En las muestras en las que no se alcanzó la cantidad de 10 ejemplares durante el primer triado, se procedió a repetir el proceso de cuarteado del residuo restante hasta completar dicha cantidad.

En Gilabert et al. (2021b) se efectuó un análisis clúster aglomerativo de las asociaciones de foraminíferos planctónicos del Daniense en la sección de Caravaca, basado en el índice de similaridad de Bray-Curtis. El objetivo de este análisis fue el de reconocer los 3 acmé-estadios PFAS de Arenillas et al. (2006) y evaluar su posible división en subestadios estadísticamente representativos, contribuyendo de esta manera a una mejor caracterización de los PFAS y su posterior interpretación paleoambiental.

### 3.6. Análisis de la susceptibilidad magnética

En Caravaca y en Zumaia se analizó la susceptibilidad magnética con el objetivo de conseguir una precisa caracterización litológica de los afloramientos, esencial para el reconocimiento de la ciclicidad en la secuencia estratigráfica (Gilabert et al., 2021c) y para evaluar la posible influencia de los procesos de disolución en las muestras de roca a lo largo de la serie estratigráfica (Gilabert et al., 2021b). Para medir la susceptibilidad magnética, las muestras fueron trituradas con un mortero de ágata hasta obtener fragmentos de un volumen lo más próximo posible al del bote de plástico cilíndrico empleado ( $10 \text{ cm}^3$ ), en el que se introdujo el fragmento para su posterior medida. La susceptibilidad magnética se midió con un susceptómetro tipo Kappabridge KLY-35, aplicando un campo alterno de 300 A/m con una frecuencia de 875 Hz. Los valores de susceptibilidad magnética se han obtenido en función de la masa de cada muestra ( $\text{m}^3/\text{kg}$ ).

### 3.7. Análisis geoquímico (%CaCO<sub>3</sub>, TOC, $\delta^{13}\text{C}$ y $\delta^{18}\text{O}$ )

El análisis del contenido en carbonato de calcio (%CaCO<sub>3</sub>) es una excelente fuente de información, no sólo para evaluar el estado de saturación del CaCO<sub>3</sub> oceánico, sino también para reconocer ciclicidad en la sedimentación. Para medir el %CaCO<sub>3</sub> de una muestra, se han utilizado dos técnicas. En el caso de las muestras de Caravaca, estas se procesaron en el *Department of Earth Sciences* de la *University of Oxford* durante una estancia pre-doctoral. En este caso se calculó previamente el contenido en carbono orgánico e inorgánico de cada una de las muestras. Para ello, las rocas se trituraron y pesaron en una báscula de precisión modelo Sartorius, realizando duplicados de cada una de ellas. Después, uno de los duplicados de cada muestra se introdujo en un horno a

420 °C durante 12 horas, con el objetivo de calcinar y eliminar todo el carbono orgánico. A continuación, los duplicados de muestras (calcínada y no calcínada) se introdujeron sucesivamente en un coulombímetro tipo Strohlein Coulomat 702. La diferencia resultante de los valores obtenidos para cada duplicado nos proporcionó una estimación del carbono orgánico total (TOC). Desafortunadamente, en la mayoría de muestras, este parámetro quedó por debajo del umbral de detección del instrumental y esta estimación no fue de utilidad. Asumiendo por tanto que el resto del carbono está presente como  $\text{CaCO}_3$ , el último paso fue multiplicar el contenido en carbono inorgánico de la muestra pre-horneada por 8,3 siguiendo la ecuación de Stax y Stein (1993). Las muestras de Zumaia fueron analizadas en el Departamento de Ciencias de la Tierra de la Universidad de Zaragoza, usando un manocalcímetero. El análisis de  $\% \text{CaCO}_3$  se realizó en una cápsula cuya presión interna es independiente de la presión atmosférica, añadiendo 5 ml de HCl 5M a un gramo de muestra machacada; posteriormente se midió el aumento de la presión del  $\text{CO}_2$  liberado por la muestra tras producirse la reacción química.

Los análisis de las relaciones isotópicas  $\delta^{13}\text{C}$  y  $\delta^{18}\text{O}$ , junto con los modelos de edad propuestos, conforman el núcleo principal de evidencias para reconocer y caracterizar los episodios y eventos paleoambientales estudiados en esta tesis doctoral (Gilabert et al., 2021a,b,c). Los análisis de los isótopos estables del carbono y el oxígeno ( $\delta^{13}\text{C}$  y  $\delta^{18}\text{O}$ ) en Caravaca y Zumaia se realizaron sobre roca total. Para ello se usó un dispositivo GasBench y/o Kiel (en función de la disponibilidad) acoplados a un espectrómetro de masas del tipo ThermoFisher Delta V. Las relaciones isotópicas publicadas están expresadas según la anotación delta estándar ( $\delta^{13}\text{C}$  y  $\delta^{18}\text{O}$ ) en partes por mil (‰) en la escala de *Vienna PeeDee Belemnite* (VPDB). La calibración de las muestras a la escala VPDB se realizó mediante la repetición múltiple de los análisis, comparándolo con el estándar del mármol de Carrara (NOCZ), siendo los valores promedio en la escala VPDB de -1,90‰ para el oxígeno y 2,18‰ para el carbono. El  $\delta^{18}\text{O}$  estándar NOCZ se calibró a la escala VDPB mediante comparación con los estándares NBS19 y NBS18, que para los isótopos del oxígeno tienen asignados valores de -2,20‰ y -23,01‰ respectivamente. Por otro lado, el  $\delta^{13}\text{C}$  fue calibrado a la escala VPDB, comparándolo con los análisis del estándar NBS19 que tiene asignado un valor de 1,95‰. Todos los análisis han sido repetidos múltiples veces sugiriendo una reproducibilidad de  $\pm 1\sigma$  de  $<0,1$  para ambas relaciones isotópicas ( $\delta^{13}\text{C}$  y  $\delta^{18}\text{O}$ ).

**3.8. Elaboración de nuevo material gráfico de síntesis**

A lo largo de la memoria se ha tratado de integrar los resultados obtenidos en cada uno de los cinco artículos que componen esta tesis doctoral. Para ello, se han elaborado nuevas figuras y tablas que no han sido publicadas previamente, pero que recogen los resultados clave proyectados bajo el mismo modelo de edad, que es el que se ha obtenido mediante la calibración astrocronológica de horizontes isotopo- y bioestratigráficos en Zumaia (Gilabert et al., 2021c, y Tablas Anexas 1 y 2). Con ello se han podido establecer nuevas relaciones temporales para los eventos y/o episodios paleoclimáticos, paleoambientales y paleobiológicos que no fueron reconocidos en algunas de las publicaciones relacionadas con esta tesis, lo que ha enriquecido el capítulo de discusión de los resultados. Las figuras se elaboraron con la ayuda del software RStudio™, un entorno de desarrollo integrado para el lenguaje de programación R™, dedicado a la computación estadística y a la elaboración de gráficos. Este software permite manejar grandes cantidades de datos como los ilustrados en algunas de las figuras. Tras su elaboración con RStudio™, las figuras fueron maquetadas utilizando los programas Adobe Illustrator™ y/o Adobe Photoshop™.

***Capítulo 4.***  
***Resultados***

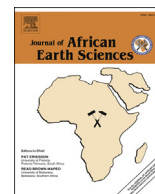


## 4. RESULTADOS

### 4.1. Revalidation of the genus *Chiloguembelitra* Hofker: Implications for the evolution of early Danian

Arenillas, I., Arz, J. A., **Gilbert**, V., 2017. Revalidation of the genus *Chiloguembelitra* Hofker: Implications for the evolution of early Danian planktonic foraminifera. *Journal of African Earth Sciences* 134, 435–456.  
<https://doi.org/10.1016/j.jafrearsci.2017.07.011>.





# Revalidation of the genus *Chiloguembeltria* Hofker: Implications for the evolution of early Danian planktonic foraminifera



Ignacio Arenillas<sup>a,\*</sup>, José A. Arz<sup>a</sup>, Vicente Gilabert<sup>b</sup>

<sup>a</sup> Departamento de Ciencias de la Tierra, Instituto Universitario de Investigación en Ciencias Ambientales de Aragón, Universidad de Zaragoza, E-50009 Zaragoza, Spain

<sup>b</sup> Departamento de Ciencias de la Tierra, Universidad de Zaragoza, E-50009 Zaragoza, Spain

## ARTICLE INFO

### Article history:

Received 24 August 2016

Received in revised form

15 May 2017

Accepted 17 July 2017

Available online 18 July 2017

### Keywords:

Guembeltriids

Wall texture

K/Pg boundary

Morphostatistical analysis

Tunisia

## ABSTRACT

*Guembeltria* is the only planktonic foraminiferal genus whose survival from the mass extinction event of the Cretaceous/Paleogene (K/Pg) boundary has been clearly proven. The evolution of *Guembeltria* after the K/Pg boundary led to the appearance of two guembeltriid lineages in the early Danian: one biserial, represented by *Woodringina* and culminating in *Chiloguembelina*, and the other trochospiral, represented by *Trochoguembeltria* and culminating in *Globoconusa*. We have re-examined the genus *Chiloguembeltria*, another guembeltriid descended from *Guembeltria* and whose taxonomic validity had been questioned, it being considered a junior synonym of the latter. Nevertheless, *Chiloguembeltria* differs from *Guembeltria* mainly in the wall texture (pustulate to rugose vs. pore-mounded) and the position of the aperture (umbilical-extraumbilical to extraumbilical vs. umbilical). *Chiloguembeltria* shares its wall texture with *Trochoguembeltria* and some of the earliest specimens of *Woodringina*, suggesting that it played an important role in the evolution of early Danian guembeltriids, as it seems to be the most immediate ancestor of both trochospiral and biserial lineages. Morphological and morphostatistical analyses of *Chiloguembeltria* discriminate at least five species: *Chg. danica*, *Chg. irregularis*, and three new species: *Chg. hofkeri*, *Chg. trilobata* and *Chg. biseriata*.

© 2017 Elsevier Ltd. All rights reserved.

## 1. Introduction

The mass extinction event of the Cretaceous/Paleogene (K/Pg) boundary 66 million years ago eliminated almost all species of Maastrichtian planktonic foraminifera (Smit, 1990; Arenillas et al., 2002; Molina et al., 2006, 2009), leaving vacant most of the pelagic niches and triggering in the early Danian the most important radiation in their evolutionary history. One of the most passionate debates in the Earth Sciences focuses on the paleobiological and paleoenvironmental changes that occurred before, during and after this extinction, as well as its relation with the massive eruptions in the Deccan volcanic province in India (Chenet et al., 2007; Schoene et al., 2015) and/or with the Chicxulub asteroid impact on Yucatan in Mexico (Hildebrand et al., 1991; Schulte et al., 2010).

Numerous new species of trochospiral and biserial planktonic foraminifera originated after the K/Pg boundary (Luterbacher and

Premoli Silva, 1964; Smit, 1982; Canudo et al., 1991; Liu and Olsson, 1992; Molina et al., 1998). This evolutionary radiation happened in two pulses (Arenillas et al., 2000b, 2004). The first occurred between approximately 5 and 20 kyr after the K/Pg boundary (Arenillas et al., 2016b), with the appearance of species belonging to the parvularugoglobigerinids (*Parvularugoglobigerina* Hofker, 1978, and *Palaeoglobigerina* Arenillas, Arz and Nájuez, 2007) and biserial taxa (*Woodringina* Loeblich and Tappan, 1957, and *Chiloguembelina* Loeblich and Tappan, 1956). The second evolutionary radiation occurred between approximately 37 and 80 kyr after the K/Pg boundary, giving rise to species belonging to *Trochoguembeltria* Arenillas, Arz and Nájuez, 2012, *Eoglobigerina* Morozova, 1959, *Parasubbotina* Olsson, Hemleben, Berggren and Liu, 1992, *Globanomalina* Haque, 1956, and *Praemurica* Olsson, Hemleben, Berggren and Liu 1992 (Arenillas et al., 2010, 2012; Arenillas and Arz, 2013a, 2013b, 2017). Other genera appear shortly afterwards, such as *Subbotina* Brotzen and Pozaryska, 1961, and *Globoconusa* Khalilov, 1956.

One of the presumed ancestors of the earliest Danian taxa was *Guembeltria* Cushman, 1933, the only planktonic foraminiferal genus whose survival from the K/Pg mass extinction event has been

\* Corresponding author.

E-mail addresses: [ias@unizar.es](mailto:ias@unizar.es) (I. Arenillas), [josearz@unizar.es](mailto:josearz@unizar.es) (J.A. Arz), [vgilabert@unizar.es](mailto:vgilabert@unizar.es) (V. Gilabert).

clearly proven (Smit, 1982; Olsson et al., 1999; Arenillas et al., 2000a; Ashckenazi-Polivoda et al., 2014; Arenillas et al., 2016a). There is a general consensus that *Guembelitra* is the ancestor of microperforate genera such as *Woodringina* and *Globoconusa* (Olsson et al., 1999; Arenillas and Arz, 2000; Arenillas et al., 2010; Koutsoukos, 2014). For the latter, Arenillas et al. (2012, 2016b) proposed the evolutionary lineage *Guembelitra*-*Trochoguembelitra*-*Globoconusa*, instead of the more direct derivation of *Globoconusa* from *Guembelitra*. *Woodringina*, with a mixed triserial-biserial test, is in turn the ancestor of the wholly biserial genus *Chiloguembelina*.

*Guembelitra* species were r-strategy opportunists that inhabited surface-water environments (Nederbragt, 1991) and bloomed during the stressful times of Maastrichtian global warming events associated with the Deccan Traps eruptions (Pardo and Keller, 2008). *Guembelitra* also bloomed immediately after the Chicxulub impact, during approximately the first 10 or 15 kyr of the Danian (acme-stage PFAS-1 of Arenillas et al., 2006). Another, later bloom of triserial guembelitriids has been recognized in the early Danian of Egypt, Israel, Tunisia and India. This was related to a global warming episode linked to the last phase of Deccan volcanism (Punekar et al., 2014).

The main object of the present study is *Chiloguembelitra* Hofker, 1978, another guembelitriid that originated in the first evolutionary radiation and whose taxonomic validity has been questioned, it being considered a junior synonym of *Guembelitra* (e.g. D'Hondt, 1991; MacLeod, 1993). However, *Chiloguembelitra* may be key to elucidating the evolutionary relationships among the earliest Danian guembelitriids. Arenillas et al. (2010) suggested that *Chiloguembelitra* includes at least three species: *Chg. danica* Hofker, 1978, *Chg. irregularis* (Morozova, 1961) and *Ch. cf. cretacea*. However, studies of its morphologic variability and species diversity have not been conducted so far.

In this paper, we document new specimens assignable to the genus *Chiloguembelitra* mainly from the El Kef section (Tunisia) in order to assess its taxonomic validity, advance the understanding of its phylogenetic relationships with *Guembelitra*, *Woodringina* and other genera, and determine its species diversity. This review will also help to date and correlate the climatic warming episodes of the early Danian. The bloom of triserial guembelitriids linked to the last volcanic phase of the Deccan has been ascribed to *Guembelitra* (Punekar et al., 2014). Nevertheless, it could in fact be an acme of *Chiloguembelitra*, which replaced *Guembelitra* in the early Danian, occupying the same ecological niche. Considering *Chiloguembelitra* and *Guembelitra* as separate genera will make it possible to differentiate more easily the possible Danian blooms of *Chiloguembelitra* from the PFAS-1 episode (acme of *Guembelitra* immediately after the K/Pg boundary), recognize and calibrate possible hiatuses in lower Danian sections, and interpret and correlate more accurately the paleoenvironmental changes occurring after the K/Pg boundary extinction event.

## 2. Material and methods

Samples for this study were selected from the lower Danian of the El Kef section, Tunisia, which is the Global boundary Stratotype Section and Point for the base of the Danian Stage (Molina et al., 2006). All studied rock samples were disaggregated in water with diluted H<sub>2</sub>O<sub>2</sub>, washed through a 63- $\mu$ m sieve, then oven-dried at 50 °C. Analyzed specimens were mounted on microslides for a permanent record and identification. Planktonic foraminifera were picked from the residues and selected for scanning electron microscopy (SEM), using the JEOL JSM 6400 and Zeiss MERLIN FE-SEM of the Electron Microscopy Service of the Universidad de Zaragoza (Spain). The type-specimens of the new species described in this

paper were deposited in the Museo de Ciencias Naturales of the Universidad de Zaragoza (Aragon Government, Spain). In addition to El Kef, specimens from other localities have also been taken into account for taxonomic studies, such as those from Elles and Aïn Settara (Tunisia), Caravaca and Agost (Spain), Ben Gurion (Israel), Lynn Creek (Mississippi), Nye Klov (Denmark) and Bajada del Jagüel (Argentina).

For taxonomical and evolutionary studies, we have relied on morphological, morphostatistical, ontogenetic and textural criteria, and a high-resolution biostratigraphy. The morphostatistical studies were based on 124 specimens of *Chiloguembelitra* randomly chosen from lower Danian sample KF19.50 of El Kef (Table 1), 7.5 m above the K/Pg boundary. The foraminiferal preservation in El Kef is good enough to analyze the wall texture, although corroded and recrystallized surfaces can be observed. The ranges of the studied taxa were established after reviewing the high-resolution biostratigraphic data from the El Kef section (Arenillas et al., 2000a), which allowed us to pinpoint the first appearance of the taxa. We used the planktonic foraminiferal zonation of Arenillas et al. (2004) and Berggren and Pearson (2005); their equivalence is shown in Fig. 1. Notably, the former is based on complete and greatly expanded Tunisian and Spanish K/Pg sections such as El Kef, Aïn Settara, Elles, Caravaca, Agost and Zumaia (see Molina et al., 2009). Biomagnetostratigraphical calibrations allowed Arenillas et al. (2004) to date the zonal boundaries of their biochronological scale (Fig. 1). The section studied at El Kef spans only up to the *Subbotina triloculinoides* Subzone (*Parasubbotina pseudo-bulloides* Zone) of Arenillas et al. (2004), or Subzone P1b of Berggren and Pearson (2005). For this reason, the range tops of some species have been determined after reviewing previous biostratigraphic studies at Spanish localities such as Caravaca, Agost and Zumaia (see Molina et al., 1998).

## 3. Taxonomic and phylogenetic remarks

All the planktonic foraminiferal taxa studied here have usually been considered to belong to the family Guembelitriidae Montanaro-Gallitelli, 1957, except for *Chiloguembelina* of the family Chiloguembelinidae Reiss, 1963 (Loeblich and Tappan, 1987; Olsson et al., 1999), and *Trochoguembelitra* and *Globoconusa*, which have recently been included in the family Globoconusidae BouDagher-Fadel, 2012 (see Arenillas et al., 2016b). Guembelitriidae traditionally includes planktonic foraminifera with triserial tests, at least in their juvenile stage. Its type-genus, *Guembelitra*, is the only one universally accepted as belonging to it. The other genera included within guembelitriids show serial reduction (*Woodringina*) or proliferation (*Guembelitriella* Tappan, 1940) throughout their ontogeny. *Guembelitriella* was proposed to include irregular multiserial forms in the adult stage, being triserial in the early stage. However, the systematic position of this genus is problematic, since Longoria (1974) and Georgescu (2009) considered that its type-species, *Guembelitriella graysonensis* Tappan, 1940, exhibits a trochospirally coiled test and is morphologically closer to benthic *Praebulimina* Hofker, 1953, than to *Guembelitra*. The *Guembelitriella*-type multiserial forms of the K-Pg transition, assigned to *Guembelitriella postcretacea* Pandey, 1981, were not considered in the taxonomies of Arenillas et al. (2007) and Arz et al. (2010) because they apparently belong to aberrant forms of *Guembelitra*. According to these authors, all survivor guembelitriids from the K/Pg boundary event belong to *Guembelitra*.

### 3.1. Upper Cretaceous triserial guembelitriids

*Guembelitra* is characterized by a test that is wholly triserial (Fig. 2), microperforate and with a pore-mounded wall texture

**Table 1**

Biometric measurements (in microns) of *Chiloguembelitra* specimens, and biometric indices H/L and CAD/H. Arithmetic means in bold type. L, test length; W, test width; H, test height; CAD, chamber average diameter;  $\alpha$ , test convexity angle measured in axial view.

<i>Chiloguembelitra danica</i>							
Specimen	L	W	H	CAD	$\alpha$	H/L	CAD/H
1	83.4	83.0	104.7	57.2	64.4	125.6	54.6
2	102.5	104.8	146.3	69.1	60.9	142.7	47.2
3	102.4	101.6	137.0	62.2	65.5	133.8	45.4
4	96.8	92.1	121.3	60.6	69.5	125.3	49.9
5	88.1	85.1	124.7	65.0	63.6	141.6	52.2
6	87.8	84.7	122.3	59.0	59.9	139.2	48.2
7	85.4	86.2	121.7	57.8	72.9	142.5	47.5
8	107.5	90.7	140.9	70.0	68.9	131.0	49.7
9	88.1	81.4	110.0	61.3	71.2	125.0	55.7
10	87.1	87.8	115.7	56.6	68.7	132.8	48.9
11	97.8	102.0	123.1	61.7	68.6	125.9	50.1
12	89.1	87.2	127.1	57.7	60.4	142.6	45.4
13	79.8	79.4	111.7	57.7	67.4	140.0	51.7
14	80.9	85.6	112.1	57.0	65.3	138.5	50.8
15	90.4	88.4	113.1	60.9	72.8	125.1	53.9
16	80.2	82.5	102.0	58.6	73.6	127.1	57.5
17	89.6	90.2	125.0	65.3	70.4	139.5	52.3
18	94.1	94.7	134.6	64.4	67.7	143.1	47.9
19	94.2	89.9	128.6	63.8	70.3	136.5	49.6
20	70.4	70.4	92.6	44.0	65.3	131.5	47.5
21	83.6	83.4	120.7	59.3	62.8	144.3	49.1
22	77.3	67.1	103.7	53.0	69.3	134.2	51.1
23	77.1	69.5	97.6	50.8	68.6	126.6	52.0
24	92.9	89.9	130.4	68.3	65.0	140.4	52.4
25	75.2	76.1	104.0	45.6	60.4	138.3	43.8
26	88.9	85.5	126.2	61.8	70.2	142.0	49.0
27	72.6	74.4	95.9	46.5	66.7	132.2	48.5
28	74.7	77.0	106.1	50.9	69.4	142.1	48.0
29	85.1	83.6	123.4	59.8	60.5	144.9	48.4
30	80.3	71.4	106.9	53.3	70.0	133.1	49.9
31	73.9	69.3	104.0	46.2	61.5	140.7	44.5
32	78.3	79.4	107.0	51.8	61.8	136.7	48.4
33	103.7	106.7	151.3	63.0	69.6	145.8	41.6
34	92.0	92.2	133.1	51.9	65.5	144.7	39.0
35	80.2	83.4	110.2	51.2	62.3	137.4	46.5
36	90.0	96.8	126.4	61.6	67.1	140.4	48.7
37	103.3	97.3	128.2	62.6	67.7	124.1	48.9
38	84.0	85.1	119.7	56.3	64.8	142.5	47.1
39	108.8	104.1	139.6	70.0	67.8	128.4	50.1
40	99.6	95.9	138.1	64.0	64.2	138.7	46.3
41	90.7	89.5	121.9	56.1	67.1	134.4	46.0
42	89.1	86.1	116.0	50.9	69.5	130.1	43.9
43	93.9	88.9	127.4	66.2	64.6	135.7	52.0
44	104.8	104.8	136.7	64.0	64.7	130.4	46.8
45	88.7	91.6	126.5	64.2	70.4	142.6	50.7
46	84.0	80.2	105.3	52.5	63.6	125.5	49.9
47	94.1	93.5	117.3	51.0	65.9	124.7	43.5
48	75.7	58.2	108.8	51.0	68.7	143.7	46.9
49	83.0	77.8	112.6	56.0	62.6	135.6	49.7
50	77.8	88.1	112.6	54.1	62.5	144.7	48.1
51	92.2	91.0	130.8	61.3	63.8	141.9	46.8
52	97.4	96.4	132.2	58.0	63.9	135.6	43.9
53	84.7	88.9	122.3	49.4	69.6	144.3	40.4
54	107.7	102.8	154.1	78.7	65.9	143.1	51.1
55	89.6	93.1	127.2	67.9	69.8	142.0	53.4
56	104.0	107.0	134.9	69.0	66.7	129.7	51.1
57	102.5	92.1	134.0	63.9	67.9	130.7	47.7
58	99.0	82.5	132.8	63.0	66.3	134.2	47.5
59	82.0	83.9	114.8	57.0	68.3	140.1	49.7
60	101.6	102.0	139.2	69.1	64.8	137.0	49.6
61	87.9	85.8	122.5	52.2	65.1	139.5	42.6
62	91.4	88.2	124.7	63.5	67.4	136.5	50.9
63	104.5	102.7	139.8	63.4	66.2	133.8	45.4
64	91.8	93.0	130.3	67.1	64.3	141.9	51.5
65	88.9	88.2	118.0	57.9	66.4	132.8	49.1
66	88.5	89.1	121.1	59.1	66.1	136.9	48.7
67	92.5	88.2	127.1	59.6	67.6	137.3	46.9
<b>Average</b>	<b>89.6</b>	<b>87.9</b>	<b>122.1</b>	<b>59.2</b>	<b>66.5</b>	<b>136.3</b>	<b>48.6</b>

*Chiloguembelitra trilobata* sp. nov.

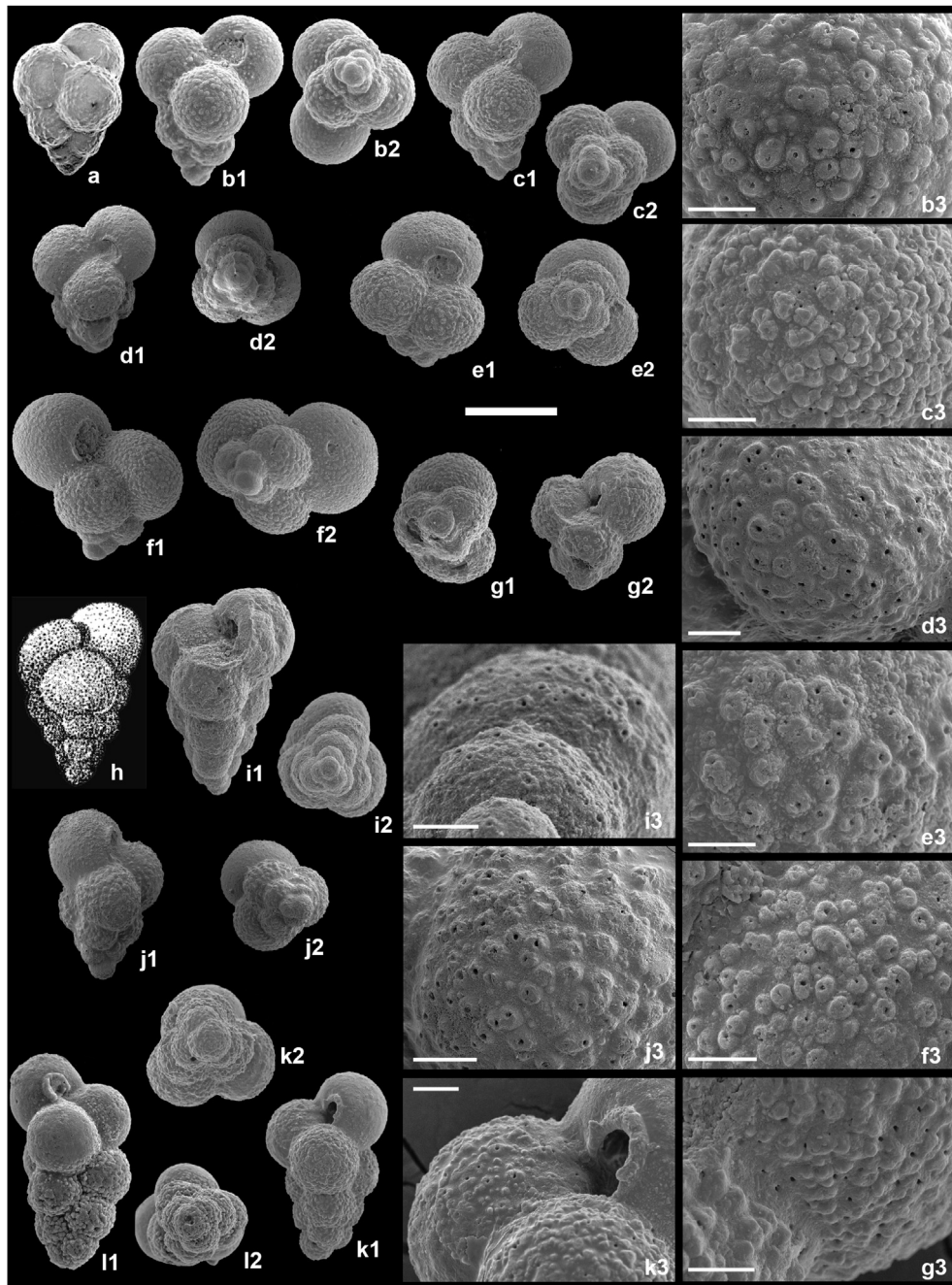
Specimen	L	W	H	CAD	$\alpha$	H/L	CAD/H
1	87.0	84.9	96.6	60.4	82.1	111.0	62.5
2	85.8	83.1	94.2	57.7	83.1	109.7	61.2
3	93.2	98.0	110.6	63.9	90.7	118.8	57.8
4	84.9	83.9	96.8	58.8	96.0	114.1	60.7
5	81.1	79.2	95.2	63.4	90.1	117.3	66.6
6	93.7	93.2	101.4	63.1	98.8	108.3	62.2
7	91.4	87.3	98.3	65.8	97.3	107.6	66.9
8	85.8	77.7	97.1	62.3	85.2	113.3	64.1
9	83.0	84.0	98.9	58.2	87.0	119.2	58.9
10	98.7	94.5	103.9	61.1	85.5	105.3	58.8
11	101.8	95.8	115.3	71.4	103.2	113.3	61.9
12	81.5	83.7	90.1	59.6	88.1	110.5	66.2
13	87.0	79.2	87.1	66.5	89.2	100.1	76.3
14	89.2	85.4	101.5	69.4	90.0	113.8	68.4
15	89.6	94.4	106.5	67.3	85.5	118.9	63.2
16	87.9	79.5	93.6	62.7	99.7	106.4	67.0
17	95.3	84.7	106.3	62.8	87.7	111.5	59.1
18	86.1	77.2	93.1	61.6	85.6	108.0	66.2
19	95.4	86.7	105.4	67.2	93.6	110.6	63.8
20	86.8	77.6	100.5	66.1	94.4	115.7	65.8
21	88.7	84.5	100.7	69.6	91.1	113.5	69.1
22	87.5	84.7	96.1	59.2	91.7	109.7	61.7
23	87.5	79.2	99.1	63.7	92.4	113.3	64.2
24	83.2	84.5	91.8	61.2	94.0	110.4	66.7
25	95.5	91.0	106.3	62.8	90.0	111.3	59.1
<b>Average</b>	<b>89.1</b>	<b>85.4</b>	<b>99.5</b>	<b>63.4</b>	<b>90.9</b>	<b>111.7</b>	<b>63.9</b>

*Chiloguembelitra hofkeri* sp. nov.

Specimen	L	W	H	CAD	$\alpha$	H/L	CAD/H
1	92.7	91.6	140.4	64.3	53.2	151.4	45.8
2	86.1	92.9	141.9	59.7	45.6	164.8	42.1
3	89.9	99.6	141.5	65.7	48.0	157.4	46.4
4	90.5	92.6	148.6	58.9	44.3	164.2	39.7
5	106.0	105.6	170.0	70.9	48.0	160.4	41.7
6	78.4	77.4	119.7	59.5	49.4	152.7	49.7
7	80.9	75.2	126.9	53.1	50.8	156.9	41.8
8	94.0	94.1	159.9	61.7	45.5	170.0	38.6
9	82.5	77.8	128.4	53.1	48.3	155.8	41.4
10	95.3	98.3	149.8	59.0	47.4	157.2	39.4
11	84.0	82.6	126.8	56.4	56.7	150.9	44.5
12	98.9	97.0	154.7	61.1	51.4	156.5	39.5
13	76.4	78.1	115.6	48.3	55.8	151.3	41.8
14	84.9	85.3	128.5	55.8	52.8	151.2	43.4
15	82.3	85.8	125.3	53.1	53.9	152.3	42.4
16	88.9	92.1	138.7	60.6	52.3	156.0	43.7
17	80.9	81.9	125.9	54.6	54.1	155.8	43.3
18	80.2	85.1	127.6	56.8	52.8	159.2	44.5
19	81.3	81.6	123.3	54.2	53.9	151.7	44.0
20	102.2	103.6	158.9	67.2	49.4	155.5	42.3
21	110.7	114.1	179.1	69.1	50.4	161.7	38.6
22	90.3	95.3	142.9	63.6	52.1	158.3	44.5
23	107.2	110.0	167.7	66.0	50.3	156.4	39.4
<b>Average</b>	<b>89.8</b>	<b>91.2</b>	<b>141.0</b>	<b>59.7</b>	<b>50.7</b>	<b>156.9</b>	<b>42.5</b>

(Loeblich and Tappan, 1987; Olsson et al., 1999; Georgescu et al., 2011), its type-species being *Guembelitra cretacea* Cushman, 1933. After carrying out a morphostatistical analysis, Arz et al. (2010) proposed three species in *Guembelitra* for the upper Maastrichtian: *G. cretacea* (Fig. 2(a)–(d)), *G. blowi* Arz et al., 2010 (Fig. 2(e)–(g)), and *G. dammula* Voloshina, 1961 (Fig. 2(h)–(k)). Before being described, *G. blowi* was usually named as *Guembelitra trifolia* (Morozova, 1961) because Blow (1979) used the specific name *trifolia* for the low-spined triserial morphotypes. However, the holotype of *Globigerina* (*Eoglobigerina*) *trifolia* Morozova, 1961, is an early Danian trochospiral form that Olsson et al. (1999) later considered to be *Globoconusa*. On the other hand, Cretaceous specimens of *G. dammula* have usually been attributed to *Guembelitra danica* (Hofker, 1978) (e.g. MacLeod, 1993). Arenillas et al. (2007) and Arz et al. (2010) pointed out the possible existence of



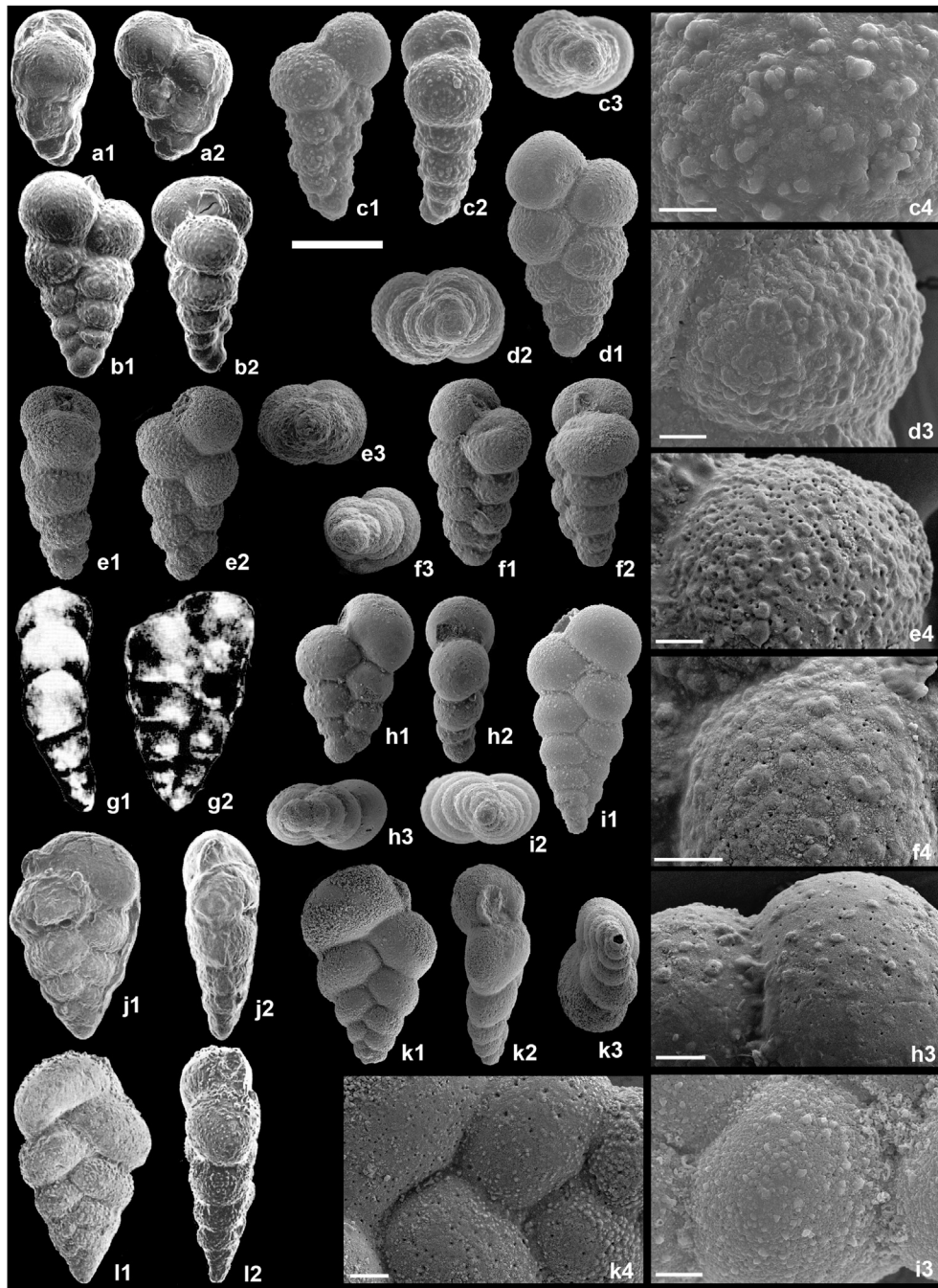


**Fig. 2.** Holotypes and specimens of *Guembelitra* spp. (scale bar = 100 µm; scale bar of detail SEM-micrographs = 10 µm). (a) *Guembelitra cretacea* Cushman, holotype, Upper Cretaceous, Guadalupe County, Texas, U.S.A. (SEM-micrograph from Olsson et al., 1999). (b) *Guembelitra cretacea* Cushman, sample KF13.50 (1.5 m above K/Pg boundary), *Pv. longiapertura* Subzone (*G. cretacea* Zone), El Kef, Tunisia. (c) *Guembelitra cretacea* Cushman, sample KF11 (1 m below K/Pg boundary), *P. hantkeninoides* Subzone (*A. mayaroensis* Zone), El Kef, Tunisia. (d) *Guembelitra cretacea* Cushman, sample KF 12.05 (5 cm above K/Pg boundary), *H. holmdelensis* Subzone (*G. cretacea* Zone), El Kef, Tunisia. (e) *Guembelitra blowi* Arz, Arenillas and Nández, holotype, sample KF4.50 (7.5 m below K/Pg boundary), *P. hantkeninoides* Subzone (*A. mayaroensis* Zone), El Kef, Tunisia. (f) *Guembelitra blowi* Arz, Arenillas and Nández, hypotype, sample JA680 (19 cm below K/Pg boundary), *A. mayaroensis* Zone, Bajada del Jagüel, Argentina. (g) *Guembelitra blowi* Arz, Arenillas and Nández, hypotype, sample KF11 (1 m below K/Pg boundary), *P. hantkeninoides* Subzone (*A. mayaroensis* Zone), El Kef, Tunisia. (h) *Guembelitra dammula* Voloshina, holotype, Maastrichtian, Volin-Podolsk Plateau, western Russia. (i) *Guembelitra dammula* Voloshina, sample KF11 (1 m below K/Pg boundary), *P. hantkeninoides* Subzone (*A. mayaroensis* Zone), El Kef, Tunisia. (j) *Guembelitra dammula* Voloshina, sample KF13.00 (1 m above K/Pg boundary), *Pv. longiapertura* Subzone (*G. cretacea* Zone), El Kef, Tunisia. (k) *Guembelitra dammula* Voloshina, sample KF13.25 (1.25 m above K/Pg boundary), *Pv. longiapertura* Subzone (*G. cretacea* Zone), El Kef, Tunisia.

*Guembelitra*. The evolution of *Guembelitra* from *Neobulimina* would be similar to that from *Praeplanctonia* to *Archaeoguembelitra* in the late Albian. However, the occurrence of clear *G. cretacea* specimens in Santonian sediments means that additional studies are required to define more adequately the stratigraphical distributions of *G. turrita* and *N. newjerseyensis* as presumed ancestors of *G. cretacea* (see Georgescu et al., 2011).

### 3.2. Biserial and trochospiral lineages of Danian guembelitriids

The Paleogene biserial lineage descending from *Guembelitra* includes *Woodringina* and *Chiloguembelina* (Fig. 3). *Woodringina* clusters Danian species with a triserial juvenile stage followed by biserially arranged chambers. Its type-species is *W. claytonensis* Loeblich and Tappan, 1957. The description of its wall texture has



**Fig. 3.** Holotypes and specimens of *Woodringina* spp. and *Chiloguembelina* spp. (scale bar = 100  $\mu\text{m}$ ; scale bar of detail SEM-micrographs = 10  $\mu\text{m}$ ). (a) *Woodringina claytonensis* Loeblich and Tappan, holotype, lower Danian, Clayton Fm., Alabama, U.S.A. (SEM-micrograph from Olsson et al., 1999). (b) *Woodringina hornerstownensis* Olsson, holotype, upper Danian, Hornerstown Fm., New Jersey, U.S.A. (SEM-micrograph from Olsson et al., 1999). (c) *Woodringina hornerstownensis* Olsson, sample AEA 6.90 (5.9 m above K/Pg boundary), *S. triloculinooides* Subzone (*P. pseudobulloides* Zone), Elles, Tunisia. (d) *Woodringina hornerstownensis* Olsson, sample KF 20.50 (8.5 m above K/Pg boundary), *E. trivialis* Subzone (*P. pseudobulloides* Zone), El Kef, Tunisia. (e) *Woodringina hornerstownensis* Olsson, sample KF 19.50 (7.5 m above K/Pg boundary), *E. trivialis* Subzone (*P. pseudobulloides* Zone), El Kef, Tunisia. (f) *Woodringina hornerstownensis* Olsson, sample KF 19.50 (7.5 m above K/Pg boundary), *E. trivialis* Subzone (*P. pseudobulloides* Zone), El Kef, Tunisia. (g) *Chiloguembelina taurica* Morozova, holotype, lower Danian, Tarkhankhut Peninsula, eastern Crimea. (h) *Chiloguembelina taurica* Morozova, sample KF 21.95 (9.95 m above K/Pg boundary), lower part of the *E. trivialis* Subzone (*P. pseudobulloides* Zone), El Kef, Tunisia. (i) *Chiloguembelina taurica* Morozova, sample 14 cc, *P. pseudobulloides* Zone, Site 305 Shatsky Rise, North Pacific. (j) *Gümbelina midwayensis* Cushman, holotype, Eocene, Midway Fm., Alabama, U.S.A. (SEM-micrograph from Olsson et al., 1999). (k) *Chiloguembelina midwayensis* (Cushman), sample KF 19.50 (7.5 m above K/Pg boundary), *E. trivialis* Subzone (*P. pseudobulloides* Zone), El Kef, Tunisia. (l) *Gümbelina morsei* Kline, holotype, Danian, Porters Creek Clay (Midway series), Alabama, U.S.A. (SEM-micrograph from Olsson et al., 1999).

varied from one author to another, but it is usually considered to be pustulate with a variable density of pustules, giving an appearance that is smoother if low density or more muricate if high density. Although Loeblich and Tappan (1957) described it as very finely hispid, Loeblich and Tappan (1987) later depicted it as smooth.

Olsson et al. (1999) and BouDagher-Fadel (2012, 2015) also suggested a smooth wall for *Woodringina*, though sometimes bearing pore-mounds, at least in the juvenile stage. Arenillas et al. (2007) proposed for *Woodringina* a papillate wall, with imperforate blunt pustules, and suggested that its pustules are ontogenetically linked

to modified pore-mounds, which are only present in the most primitive forms (assigned herein to *Chiloguembeltria biseriata* sp. nov.). *Woodringina* is considered the intermediate taxon between *Guembeltria* and *Chiloguembelina* (Olsson et al., 1999). *Chiloguembelina* is characterized by a wholly biserial test, and its wall texture was originally described as smooth or hispid (Loeblich and Tappan, 1956), or as granulate by Loeblich and Tappan (1987). Olsson et al. (1999), Huber et al. (2006) and BouDagher-Fadel (2012, 2015) described it as having with numerous small pustules, and Arenillas et al. (2007) as having a finely or moderately papillate surface, with blunt pustules. Four species of *Woodringina* and *Chiloguembelina* have been considered here: *W. claytonensis* Loeblich and Tappan, 1957 (Figs. 3(a) and 14(e)–(h)), *W. hornerstownensis* Olsson, 1960 (Fig. 3(b)–(f)), *Ch. taurica* Morozova, 1961 (Fig. 3(g)–(i)), and *Ch. midwayensis* (Cushman, 1940) (Fig. 3(j)–(k)).

Various trochospiral genera from the earliest Danian have also been linked to or included in the family Guembeltriidae (Olsson et al., 1999; Arenillas et al., 2007, 2012), such as *Parvularugoglobigerina*, *Palaeoglobigerina*, *Trochoguembeltria*, and *Globoconusa*. The first two have recently been excluded from the guembeltriids (BouDagher-Fadel, 2012; Arenillas and Arz, 2013a, 2013b), and a benthic origin has been proposed for them (Brinkhuis and Zachariasse, 1988; Arenillas and Arz, 2017). The Paleogene trochospiral lineage descending from *Guembeltria* includes to *Trochoguembeltria* and *Globoconusa* (Fig. 4). The genus *Trochoguembeltria*, whose type-species is *Guembeltria? alabamensis* Liu and Olsson, 1992, was proposed by Arenillas et al. (2012) in order to include trochospiral specimens with a pustulate to rugose wall texture (with decentred pore-mounds and perforate rugosities) previously assigned to *Parvularugoglobigerina* (e.g. Olsson et al., 1999), restricting the latter genus only to species with a smooth wall texture, such as *Pv. eugubina* (Luterbacher and Premoli Silva, 1964) and *Pv. longiapertura* (Blow, 1979). *Trochoguembeltria* may be triserial in the juvenile stage, at least in some specimens of *T. alabamensis*, revealing its triserial evolutionary origin. Arenillas et al. (2012) suggested that *Trochoguembeltria* is the ancestor of the pustulate-walled *Globoconusa*. After carrying out a morphostatistical analysis of *Trochoguembeltria*, Arenillas et al. (2016b) proposed four species: *T. alabamensis* (Liu and Olsson, 1992) (Fig. 4(a)–(c)), *T. extensa* (Blow, 1979) (Fig. 4(d)–(e)), *T. liuae* Arenillas, Arz and Nájuez, 2016 (Fig. 4(f)), and *T. olsoni* Arenillas, Arz and Nájuez, 2016 (Fig. 4(g)). Moreover, three species have been considered in *Globoconusa*: *Gc. daubjergensis* Brönnimann, 1953 (type-species, Fig. 4(h)–(i)), *Gc. conusa* Khalilov, 1956 (Fig. 4(j)–(k)), and *Gc. victori* Koutsoukos, 2014. The classification of BouDagher-Fadel (2012, 2015) still retained the genus *Postrugoglobigerina* Salaj, 1986, basing it on characters similar to those attributed to *Trochoguembeltria*. However, *Postrugoglobigerina* has been regarded as a *nomen dubium non conservandum* due to the holotypes and type-material of its species have been lost and are of doubtful application (see discussion in Arenillas et al., 2012). Olsson et al. (1999) and Arenillas et al. (2012, 2016b) considered *Postrugoglobigerina* a junior synonym of *Parvularugoglobigerina*. The latter has also usually been included in Guembeltriidae because *Guembeltria* was considered its direct ancestor (Olsson et al., 1999), but recent taxonomic proposals include it, together with *Globanomalina*, in the family Globanomalinidae Loeblich and Tappan, 1984 (e.g. BouDagher-Fadel, 2012).

#### 4. Textural variability in lower Danian guembeltriids

The wall texture of upper Maastrichtian guembeltriids is usually described as pore-mounded (Loeblich and Tappan, 1987; Olsson et al., 1999; Georgescu et al., 2011). The typical pore-mounds of *Guembeltria* are blunt pustules (papilla-type) marked

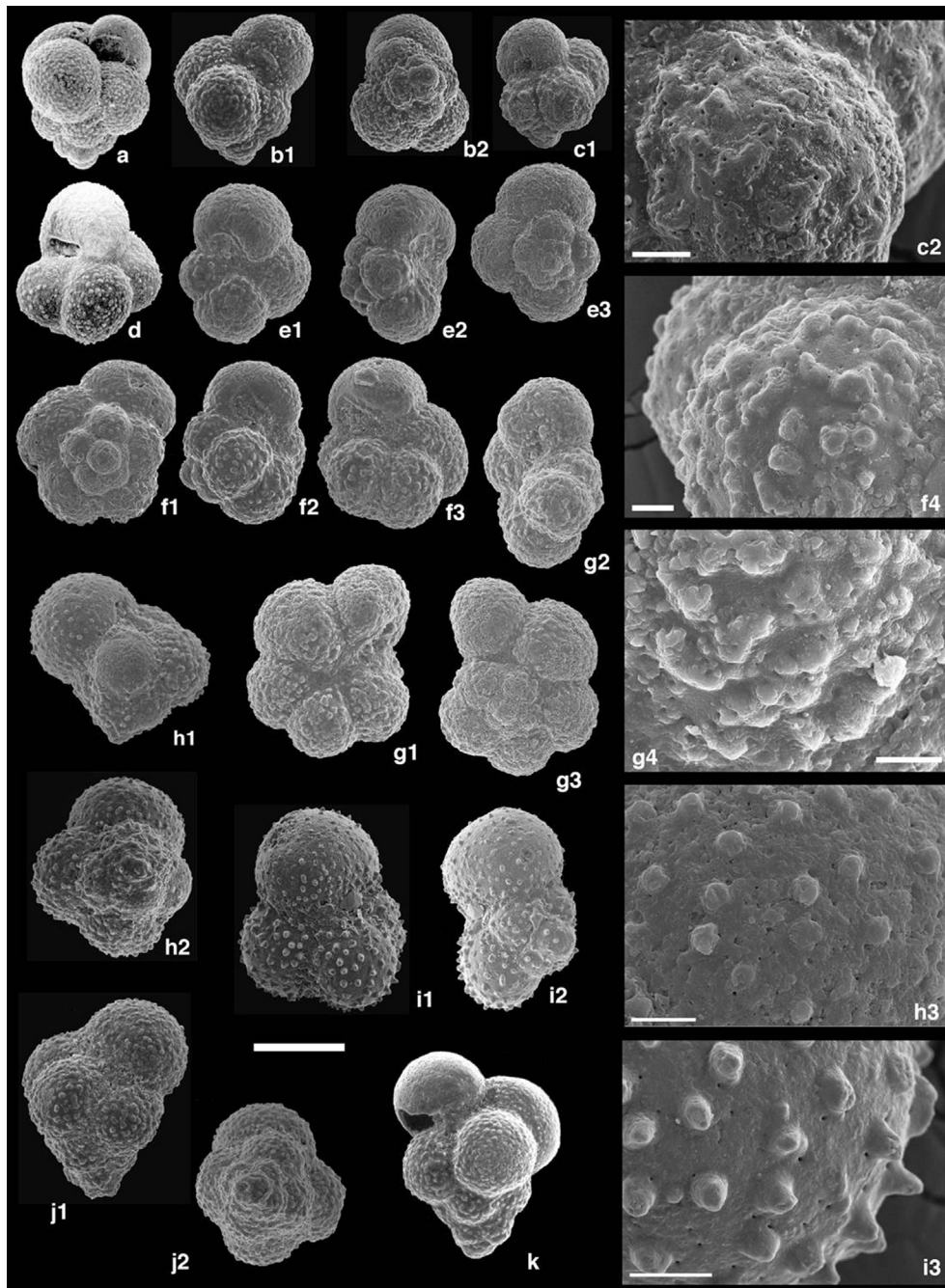
by a more or less centered pore (Fig. 5(a)). However, Loeblich and Tappan (1987) and Arenillas et al. (2007, 2010) reported that the microtextural variability among guembeltriids of the lowermost Danian is greater than in the upper Maastrichtian. For example, the most immediate descendants from *Guembeltria*, i.e. *Woodringina* (Fig. 5(e)) and *Trochoguembeltria* (Fig. 5(d)), already had a different type of wall texture (a pustulate or rugose wall), although this clearly evolved from the typical pore-mounded wall of *Guembeltria* (Arenillas et al., 2012, 2016b).

These textural variations may consist of irregular pore-mounds with decentered pores, imperforate pustules that may be blunt or sharp, and a high or low density of pore-mounds and/or imperforate pustules on the surface. Moreover, pore-mounds and blunt pustules can coalesce, generating small, non-aligned rugae or ridges (a rugose wall). Some of these variations can be mixed in a single specimen. In the case of triserial guembeltriids, these other types of wall texture have usually been considered part of the microtextural variability in *Guembeltria* (e.g. Olsson et al., 1999). Although part of this variability could have an ecophenotypic or ontogenetic origin, it has also been related to pseudocryptic speciation, which resulted in species only distinguished by their wall surface under the scanning electron microscope (Arenillas et al., 2010).

##### 4.1. Wall textures in lower Danian guembeltriids

Arenillas et al. (2007, 2010, 2012) and Arz et al. (2010) studied and illustrated the textural variability of the guembeltriids of the K-Pg transition, including examples of wall texture assignable to *Chiloguembeltria*. Among the earliest Danian guembeltriids, the following wall textures were recognized:

- 1) Pore-mounded wall, or papillate wall with pore-mounds (Fig. 5(a)): wall texture characterized by blunt pore-mounds irregularly distributed, generally with one pore per papilla, approximately centered (regular pore-mounds), and sometimes two pores per papilla; the density of pore-mounds is variable and, when the density is high, the pore-mounds can be fused at their bases; this is the wall surface typical of Maastrichtian specimens of *Guembeltria* from tropical to temperate latitudes in both oceanic and neritic environments, and also in lowermost Danian specimens.
- 2) Pustulate/papillate to rugose wall, with irregular, decentered pore-mounds, imperforate blunt pustules (papilla-type), and imperforate and perforate rugosities (Fig. 5(c)–(d)): wall surface characterized mainly by rugosities with or without multiple pores, produced by the coalescence of pore-mounds or imperforate blunt pustules; the pustules may also be sharp (Fig. 5(g)); it is microperforate with tiny pores within the rugosities and isolated pore-mounds, and in the smooth surface; pores in rugosities and pore-mounds are very decentered, often situated in the basal part of the ridges or mounds; in specimens with a higher pore density, the rugosities tend to be smaller and more crowded (muricate-type); all these types of pustules and rugosities may be found in a single specimen; this is typical of *Chiloguembeltria* and *Trochoguembeltria*.
- 3) Pustulate wall, with small blunt pustules (Fig. 5(e)–(f)): wall surface with blunt pustules and tiny pores scattered over the smooth surface of the wall; this is typical of *Woodringina* and *Chiloguembelina*; in specimens – mainly of *Woodringina* – with higher pore density, the pustules tend to be smaller and more crowded (muricate-type); in specimens – mainly of *Chiloguembelina* – with low pustule density or smaller pustule size, the wall surface looks smooth.

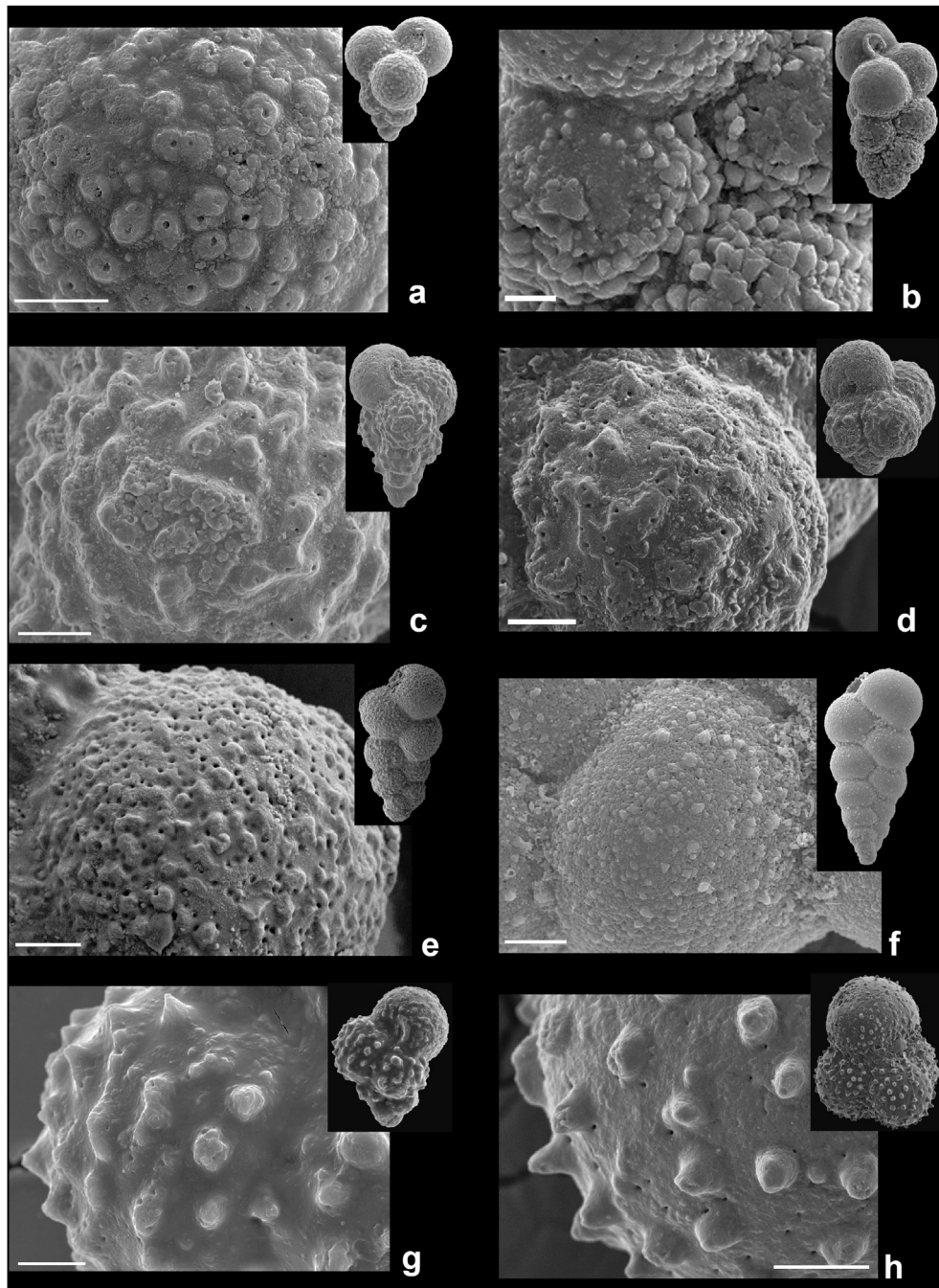


**Fig. 4.** Holotypes and specimens of *Trochoguembeltria* spp. and *Globoconusa* spp. (scale bar = 100  $\mu$ m; scale bar of detail SEM-micrographs = 10  $\mu$ m). (a) *Trochoguembeltria alabamensis*, holotype, Millers Ferry, Alabama, U.S.A. (SEM-micrograph from Liu and Olsson, 1992). (b) *Trochoguembeltria alabamensis*, sample KF24.80 (12.8 m above the K/Pg boundary), *S. triloculinoidea* Subzone (*P. pseudobulloides* Zone), El Kef, Tunisia. (c) *Trochoguembeltria alabamensis*, sample KF20.50 (8.5 m above the K/Pg boundary), middle part of the *E. trivialis* Subzone (*P. pseudobulloides* Zone), El Kef, Tunisia. (d) *Trochoguembeltria extensa*, holotype, Zone P1, DSDP Leg 6, South Pacific (SEM-micrographs from Blow, 1979). (e) *Trochoguembeltria extensa*, sample KF18.50 (6.5 m above the K/Pg boundary), upper part of the *E. simplicissima* Subzone (*Pv. eugubina* Zone), El Kef, Tunisia. (f) *Trochoguembeltria liauae*, holotype, sample KF20.50 (8.5 m above the K/Pg boundary), middle part of the *E. trivialis* Subzone (*P. pseudobulloides* Zone), El Kef, Tunisia. (g) *Trochoguembeltria olssoni*, holotype, sample KF20.50 (8.5 m above the K/Pg boundary), middle part of the *E. trivialis* Subzone (*P. pseudobulloides* Zone), El Kef, Tunisia. (h) *Globoconusa daubjergensis* (Brönnimann), sample BG1000–4.25, *S. triloculinoidea* Subzone (*P. pseudobulloides* Zone), Ben Gurion, Israel. (i) *Globoconusa daubjergensis*, sample BJ56 + 110, middle part of the *E. trivialis* Subzone (*P. pseudobulloides* Zone), Bajada del Jagüel, Argentina. (j) *Globoconusa conusa* Khalilov, sample BG1000–4.25, *S. triloculinoidea* Subzone (*P. pseudobulloides* Zone), Ben Gurion, Israel. (k) *Globoconusa conusa*, sample NSB88, middle part of the *E. trivialis* Subzone (*P. pseudobulloides* Zone), *Acarinina uncinata* Zone (or Zone P2), Sidi Naseur, Kalaat Senan, Tunisia.

4) Pustulate wall, with sharp pustules (Fig. 5(h)): wall surface with sharp pustules and small pores scattered over the smooth surface of the wall; the pustules may also be blunt; both sharp and blunt pustules may be found in a single specimen; the density of pustules is usually low; this is typical of *Globoconusa*.

Additionally, Loeblich and Tappan (1987) and Arenillas et al. (2010) distinguished a granular or granulate wall in guembeltriids or in evolutionarily and/or ecologically associated taxa (e.g. *Chiloguembelina* and/or *Parvularugoglobigerina*). This is characterized by minute calcite crystallites with in a mosaic or jagged shape





**Fig. 5.** Wall textural details of *Guembelitrina*, *Chiloguembelitra*, *Trochoguembelitra*, *Globoconusa*, *Woodringina* and *Chiloguembelina* (scale bars = 10  $\mu$ m). (a) *Guembelitrina cretacea* Cushman, sample KF13.5 (1.5 m above K/Pg boundary), *Pv. longiapertura* Subzone (*G. cretacea* Zone), El Kef, Tunisia. (b) *Guembelitrina dammula* Voloshina, sample KF13.00 (1 m above K/Pg boundary), *Pv. longiapertura* Subzone (*G. cretacea* Zone), El Kef, Tunisia. (c) *Chiloguembelitra hofkeri* sp. nov., sample KF 20.50 (8.5 m above K/Pg boundary), *E. trivialis* Subzone (*P. pseudobulloides* Zone), El Kef, Tunisia. (d) *Trochoguembelitra alabamensis*, sample KF20.50 (8.5 m above the K/Pg boundary), middle part of the *E. trivialis* Subzone (*P. pseudobulloides* Zone), El Kef, Tunisia. (e) *Woodringina hornerstownensis* Olsson, sample KF 19.50 (7.5 m above K/Pg boundary), *E. trivialis* Subzone (*P. pseudobulloides* Zone), El Kef, Tunisia. (f) *Chiloguembelina taurica* Morozova, sample 14 cc, *P. pseudobulloides* Zone, Site 305 Shatsky Rise, North Pacific. (g) *Chiloguembelitra danica* Hofker, sample KF 20.50 (8.5 m above K/Pg boundary), *E. trivialis* Subzone (*P. pseudobulloides* Zone), El Kef, Tunisia. (h) *Globoconusa daubjergensis*, sample BJ56 + 110, middle part of the *E. trivialis* Subzone (*P. pseudobulloides* Zone), Bajada del Jagüel, Argentina.

over the entire test surface (Fig. 5(b)). Salaj (1986) defined at El Kef two new Danian species of *Guembelitrina* (*G. besbesi* and *G. azzouzi*) that were also described as having small pustules, referring probably to a granulate wall texture. Although these species were later considered junior synonyms of *G. cretacea* (Olsson et al., 1999) and should be regarded as *nomina dubia non conservanda* like the *Postrugoglobigerina* species (see discussion in Arenillas et al., 2012),

this is not the last time that this wall texture has been recognized in guembelitrinids. Arz et al. (2010) and Arenillas et al. (2010) suggested that – unlike the specimens of other taxa in the same samples of Tunisian sections – the wall surface of many Maasrichtian and Danian specimens of *Guembelitrina* is covered by a secondary granular crust (Fig. 2(c), (g)). Without ruling out the recrystallization processes which are usual in Tunisian sections, the

authors postulated that the granular wall could also be related to gametogenetic calcification, i.e. a secondary outer calcite crust covering the normal pore-mounded surface. Some specimens of guembeltriids show a granulate surface in all chambers except in the last ones (e.g. Fig. 2(l)), suggesting the likelihood of such a proposal. However, due to the inability to demonstrate the difference between the diagenetically modified gametogenetic calcification and the recrystallization itself, the suggestion of a granular crust is here considered highly speculative for now.

#### 4.2. Wall texture in *Chiloguembeltria*

Loeblich and Tappan (1987) considered that the main diagnostic character of *Chiloguembeltria* is its wall texture, which made it possible to differentiate it from *Guembeltria*. Hofker (1978) specified its wall texture by studying the type-species *Chg. danica*, describing it as having small blunt pustules. Studying topotypes of *Chg. danica*, Loeblich and Tappan (1987) concluded that *Chiloguembeltria* has a surface that is finely pustulose but lacks pore-mounds. Later, Arenillas et al. (2010) described it as papillate to rugose, with perforate or imperforate pustules and rugosities, and BouDagher-Fadel (2012, 2015) as muricate, i.e. surface possessing high density of pustules.

Kroon and Nederbragt (1990), D'Hondt (1991), MacLeod (1993), Jenkins et al. (1998) and Olsson et al. (1999) among others have proposed, however, that *Chiloguembeltria* is a junior synonym of *Guembeltria*, claiming that both genera bear pore-mounds. MacLeod (1993) illustrated Maastrichtian specimens assigned to *Guembeltria danica* exhibiting well-developed pore-mounds, and suggested that both *G. cretacea* and *Chg. danica* – although distinct species – belong to the genus *Guembeltria*, *Chiloguembeltria* being a junior synonym. However, Maastrichtian specimens morphologically similar to the holotype of *Chg. danica* have recently been attributed to *G. dammula* (Arz et al., 2010). Because the holotype of *Chg. danica* cannot be found (depository not given by the author), Jenkins et al. (1998) chose topotypes of *Chg. danica* and designated a neotype. They conclude that these type-specimens bear pore-mounds similar to those of *Guembeltria*, supporting the idea that the two genera are synonymous. However, the specimens that they illustrated are poorly preserved and seem to have imperforate pustules and rugosities, including the neotype of *Chg. danica* selected by them. For these reasons, Arz et al. (2010) concluded that the presence of regular pore-mounds in *Chg. danica* is very dubious, and proposed that their taxonomy should be clarified by carrying out a more profound study of the wall texture and morphology of this genus and other Danian guembeltriids.

### 5. Morphological variability in lower Danian guembeltriids

#### 5.1. Gross morphology

At the genus level, the serial guembeltriids were usually classified in accordance with their chamber arrangement (Fig. 6(a)), distinguishing the wholly triserial forms (*Guembeltria*) and the triserial-biserial mixed forms (*Woodringina*). The types of wall texture identified seemed to fit well with these two genera, *Guembeltria* having a pore-mounded wall (usually with regular pore-mounds) and *Woodringina* a papillate or pustulate wall (usually with a high density of blunt pustules).

At the species level, the main diagnostic criterion used in guembeltriids is the spire height, bearing in mind that triserial and biserial are spiral forms with three and two chambers per whorl respectively (Tyszkla, 2006; Fig. 6). In *Guembeltria* (Arz et al., 2010), three species were distinguished according to whether they are low-spired (*G. blowi*, or *G. trifolia* for some authors), medium-spired

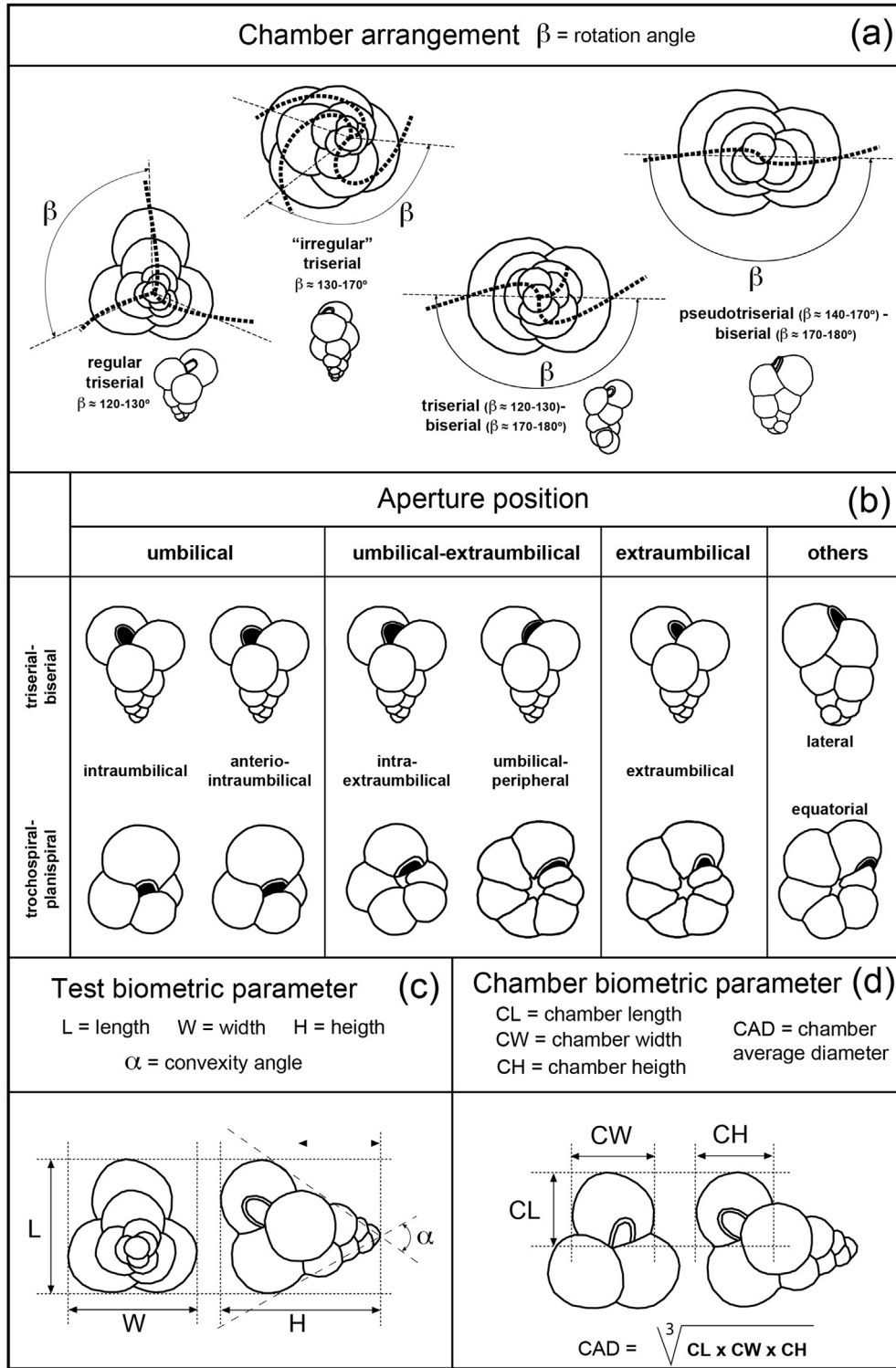
(*G. cretacea*), or high-spired (*G. dammula*, or *G. danica* for some authors). Triserial guembeltriids of irregular appearance (twisted test) have usually been classified within *G. irregularis* (herein *Chiloguembeltria irregularis*). The separation of regular and “irregular” triserial guembeltriids can be established using the rotation angle  $\beta$ , so that when  $\beta$  is approximately between 120° and 130° they have a regular appearance (with some twisting when further away from 120°) and when more than 130° they have an irregular appearance (Fig. 6(a)). In the adult stage, the spire height of *Chg. irregularis* is great, similar to that of *G. dammula* or that of the original holotype of *Chg. danica*.

In *Woodringina* (Olsson et al., 1999; Arenillas et al., 2007), two species have been distinguished according to whether they are low-spired (*W. claytonensis*) or high-spired (*W. hornerstownensis*). The triserial juvenile stage of many specimens of *W. claytonensis* and *W. hornerstownensis*, mainly the most modern ones, is greatly shrunken (pseudotriserial,  $\beta \approx 140\text{--}170^\circ$ ) or absent (biserial,  $\beta \approx 170\text{--}180^\circ$ ) (Fig. 6(a)). Those that have a gross morphology similar to *W. claytonensis* have been assigned to *Woodringina kelleri* MacLeod, 1993, and those similar to *W. hornerstownensis* have usually been assigned to *Chiloguembelina morsei* (Kline, 1943) or *Chiloguembelina* cf. *morsei* (e.g. D'Hondt, 1991; Olsson et al., 1999; Arenillas and Arz, 2000; Arenillas et al., 2000a, 2000b). MacLeod (1993) remarked that *W. kelleri* differs from *W. claytonensis* in its laterally compressed adult chambers, and especially in its large, elongate aperture. Olsson et al. (1999) considered *W. kelleri* to be a junior synonym of *W. claytonensis* adducing that the differences proposed by MacLeod (1993) appear insufficient to warrant maintenance of *W. kelleri* as a separate taxon. Arenillas et al. (2007) considered *Ch. morsei* (Fig. 3(l)) to be a junior synonym of *Chiloguembelina midwayensis* (Cushman, 1940), since their holotypes are almost indistinguishable, and re-assigned the high-spired specimens with a shrunken triserial initial stage within the morphological variability of *W. hornerstownensis*.

Considering how species are discriminated in *Guembeltria* and *Woodringina*, it is consistent to expect the existence of several species within *Chiloguembeltria* distinguishable only by the spire height, as proposed Arenillas et al. (2010). In addition to *Chg. danica* (sensu the original holotype of Hofker, 1978) and *Chg. irregularis*, Arenillas et al. (2010) suggested the existence of a new pseudocryptic species in the early Danian similar to *G. cretacea* but with rugose wall, which was provisionally named *Ch. cf. cretacea* (assigned herein to *Chg. danica* sensu the neotype of Jenkins et al., 1998).

#### 5.2. Aperture position and shape

Another of the criteria used to distinguish *Guembeltria* and *Chiloguembeltria* is the position and shape of the aperture (Hofker, 1978), because the *Chiloguembeltria* aperture was originally described as more similar to that of *Chiloguembelina* than to that of *Guembeltria*. Following the terminologies of Li (1987), Li et al. (1992) and BouDagher-Fadel (2012) for describing the position and morphology of the aperture, Arenillas et al. (2016b) considered two types of apertural position in triserial-trochospiral tests: umbilical and umbilical-extraumbilical (Fig. 6(b)), subdividing the first into two subtypes: intraumbilical and anterio-intraumbilical, and the second into another two subtypes: intra-extraumbilical and umbilical-peripheral. The apertures outside the umbilicus may also be subdivided into three other subtypes (Fig. 6(b)): extraumbilical, equatorial (in spiral tests) and lateral (in biserial tests). According to this terminology, most of the *Chiloguembeltria* specimens present umbilical-peripheral or extraumbilical (rarely intra-extraumbilical) apertures, or lateral ones if they have a more developed biserial stage. This diagnostic character separates *Chiloguembeltria* from



**Fig. 6.** (a) Types of chamber arrangement. (b) Types of aperture position. (c–d) Biometric parameters, abbreviations and descriptive terms used for the morphological analysis of the *Chiloguembelitra* tests.

*Guembelitra*, whose species usually have intraumbilical or anterio-intraumbilical apertures.

The apertures of the studied planktonic foraminifera have the following morphologies: (a) a rounded, wide arch, (b) a marginally/laterally elongate, wide arch, and (c) a high arch (like a loop). Most of the *Chiloguembelitra* specimens exhibit apertures with a

marginally or laterally elongate, wide arch, but rounded apertures similar to those of *Guembelitra* and *Trochoguembelitra* are also frequent. The apertural shape in *Chiloguembelitra* is almost identical to that of *Woodringina*, although species of the latter tend to acquire an aperture with a higher arch, as in *Chiloguembelina*. The aperture of all these genera is surrounded by a thin imperforate lip,

although some tend to acquire a thicker lip as in *Chiloguembelina*.

## 6. Morphostatistical analysis of wholly triserial *Chiloguembelitra*

The biometric and morphostatistical analysis has been applied to “regular”, wholly triserial specimens (Fig. 6(a)) of *Chiloguembelitra*. The identification of other species in *Chiloguembelitra* was based on qualitative morphological criteria, i.e. their gross morphology: a strongly twisted, triserial test for *Chg. irregularis*, and a biserial final stage for *Chg. biseriata* sp. nov.

### 6.1. Biometric parameters and indices and morphostatistical analyses

The biometric parameters used to delimit species are the following (Fig. 6(c)–(d); Table 1): convexity angle ( $\alpha$ ) measured in axial view; length (L), width (W) and height (H) of the test; and length (CL), width (CW) and height (CH) of the chamber, used to calculate the chamber average diameter  $CAD = (CL \times CW \times CH)^{1/3}$ . In addition, we used the biometric indices H/L and CAD/H (Table 1). Other biometric indices have been explored, but these have not given consistent results for separating species.

For morphostatistical analyses, the software used was the program PAST, version 3.11, by Hammer et al. (2001). The biometric parameters and indices were treated statistically using the following analyses:

- 1) Univariate analyses: Two of the above-mentioned biometric indices ( $\alpha$  and H/L) were analyzed in an univariate manner in order to ascertain whether these biometric variables are useful for discriminating species; the results of the univariate analyses were displayed as histograms of 20 bins (Fig. 7). Mixture analysis was applied to each biometric variable in order to identify two or more univariate normal distributions (Gaussian bell-shaped curves) based on a pooled univariate sample; this method is used to identify species and study differences between them; Kernel density estimates were also plotted on histograms.
- 2) Bivariate analyses: Variables  $\alpha$  vs H/L were used to make bivariate analyses. Kernel density estimates allowed us to make smooth maps of point density in XY graphs (Fig. 8); the density estimate is based on a Gaussian function, and scales give an estimate of the number of points per area, not a probability density.
- 3) Multivariate analyses: R-mode cluster analysis and principal component analysis (PCA) were used; the cluster analyses were based on Bray-Curtis index measures among all specimens using the values of the above-mentioned biometric indices/parameters ( $\alpha$ , H/L and CAD/H) in order to find groupings that might represent species (Fig. 9). The PCA was applied to the values of the three biometric indices/parameters (original variables). Such an analysis finds hypothetical variables (components) that account for as much of the variance in the multidimensional data as possible by reducing the data set to two variables (the two most important components) through a routine that finds eigenvalues and eigenvectors (i.e. components) of the variance-covariance correlation matrix. All the original data points were plotted as an XY graph in the coordinate system given by the two most important components (PC1 and PC2) to enhance visualization of the data sets representing the possible species (Fig. 10); 95% confidence ellipses, which assume a bivariate normal distribution, and convex hulls, which are the smallest convex polygons containing all points, were presented in the scatter diagram.

### 6.2. Results of the morphostatistical analysis

The morphological and morphostatistical analyses discriminate at least three species within *Chiloguembelitra*. Whether or not the statistically identified morphogroups are biological species is a question that we do not intend to clarify. Nevertheless, there is no doubt that the three identified species fall within the concept of morphospecies, which is based on overall morphological similarity, and defined as the smallest morphogroup that is consistently and persistently distinct.

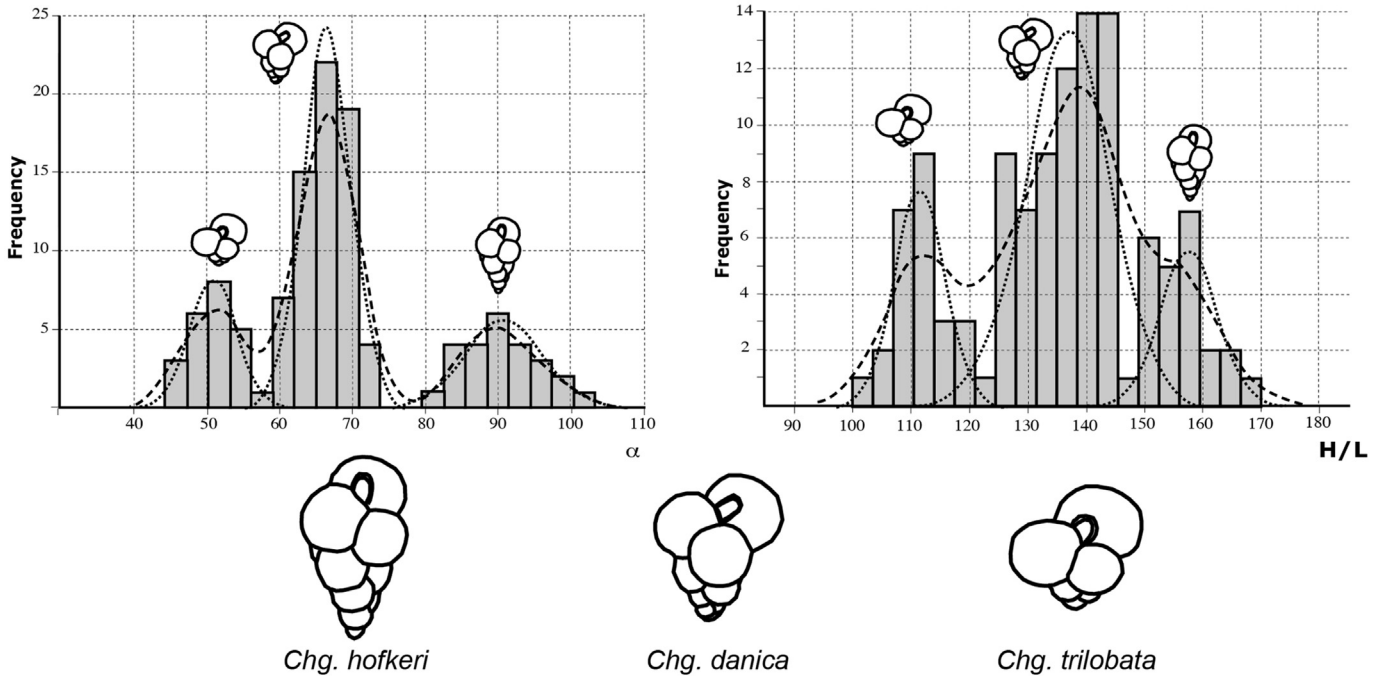
Frequency distributions of the univariate analyses (Fig. 7), calculated for all measured specimens and represented in plot histograms of 20 bins, suggest three morphogroups of *Chiloguembelitra*, as also suggested by Gaussian bells and Kernel density estimates. Both  $\alpha$  and H/L variates seem to distinguish three groups, a low-spined group, assigned to *Chg. trilobata* sp. nov., a medium-spined group, assigned to *Chg. danica*, and a high-spined group, assigned to *Chg. hofkeri* sp. nov. Bivariate analyses (Fig. 8) also strongly suggest that the genus *Chiloguembelitra* contains the three above-mentioned species; these are well observable in the Kernel density maps.

Cluster analysis (Fig. 9), based on the Bray-Curtis similarity index, produced dendrograms with two primary clusters, one grouping the morphotypes with a low-spined test (*Chg. trilobata* sp. nov.), and the other those with a high-medium-spined test, which is subdivided into two sub-clusters, one grouping medium-spined (*Chg. danica*) and the other high-spined morphogroups (*Chg. hofkeri* sp. nov.). The two resulting dendrograms, one based on  $\alpha$  and H/L variables (Fig. 9(a)) and the other on  $\alpha$ , H/L and CAD/H variables (Fig. 9(b)), made it possible to discriminate the three above-mentioned species. The principal component analysis (PCA) based on  $\alpha$ , H/L and CAD/H variables showed similar results to those of the cluster analysis (Fig. 10). The principal component PC1 explains 94.5% of the variance. The PCA scatter diagram, where X and Y are the principal components PC1 and PC2, distinguishes three sets of points of higher density. We specified three groups of specimens, clustering them subjectively by their gross morphology. These are approximately equivalent to those obtained by the PCA. Except for the intermediate and/or anomalous specimens, the convex hulls and 95% confidence ellipses clearly delimit the three above-mentioned species. Their main characteristics are easily recognizable under the stereomicroscope.

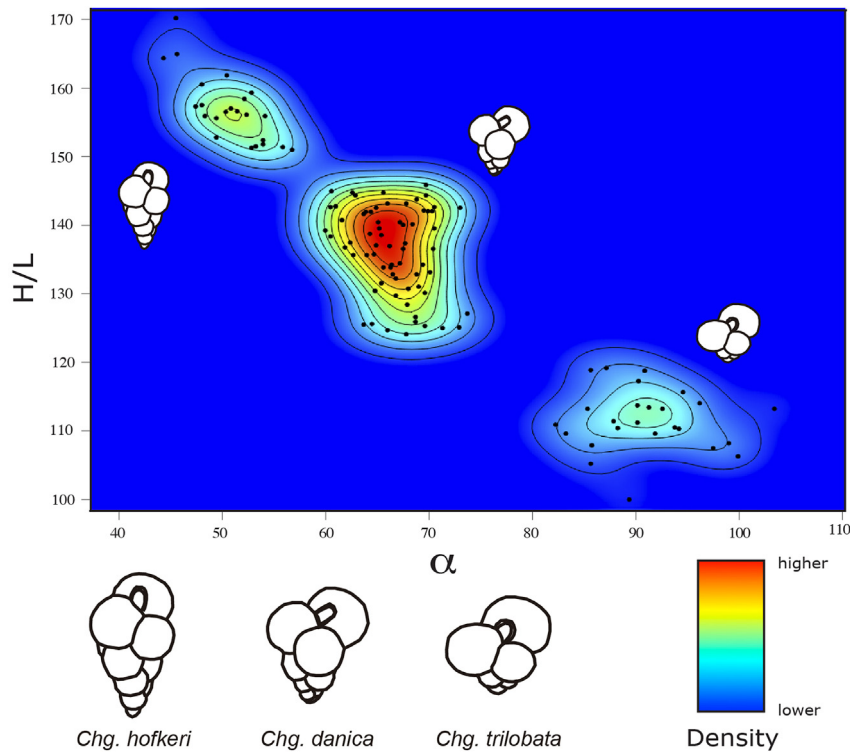
## 7. Paleontological systematics

Olsson et al. (1999) showed that the phyletic relationship of *Trochoguembelitra* (*Parvularugoglobigerina* according to them), *Globoconusa*, *Woodringina*, and *Chiloguembelina* with *Guembelitra* indicates that trochospiral and biserial chamber arrangements evolved divergently within the planktonic foraminifera. Such relationships are not clearly accounted for by taxonomic schemes, which separate serial and trochospiral morphotypes at the superfamily level (e.g. Loeblich and Tappan, 1987). It is broadly accepted that *Chiloguembelina* is lineally derived from *Guembelitra*, via *Woodringina* (Olsson, 1970; Li and Radford, 1991; Liu and Olsson, 1992; D'Hondt, 1991). The phylogenetic relationship between *Chiloguembelina* and *Guembelitra* indicates that *Guembelitriidae* constitutes a paraphyletic family because it does not include descendant species assigned to the family *Chiloguembelinidae* (Olsson et al., 1999). Moreover, BouDagher-Fadel (2012, 2015) assigned the trochospiral *guembelitriids* *Trochoguembelitra* (*Postrugoglobigerina* according to the author) and *Globoconusa* to the family *Globoconusidae*.

The new evidence reported here indicates that it is advisable to reconsider the validity of the genus *Chiloguembelitra*, as its wall



**Fig. 7.** Univariate analyses based on biometric variables  $\alpha$  and H/L to delimit the *Chiloguembeltria* species, displayed as histograms of 20 bins; thick dotted lines are the Kernel density estimations; fine dot lines are univariate normal distributions (Gaussian bell-shaped curves) based on mixture analysis.

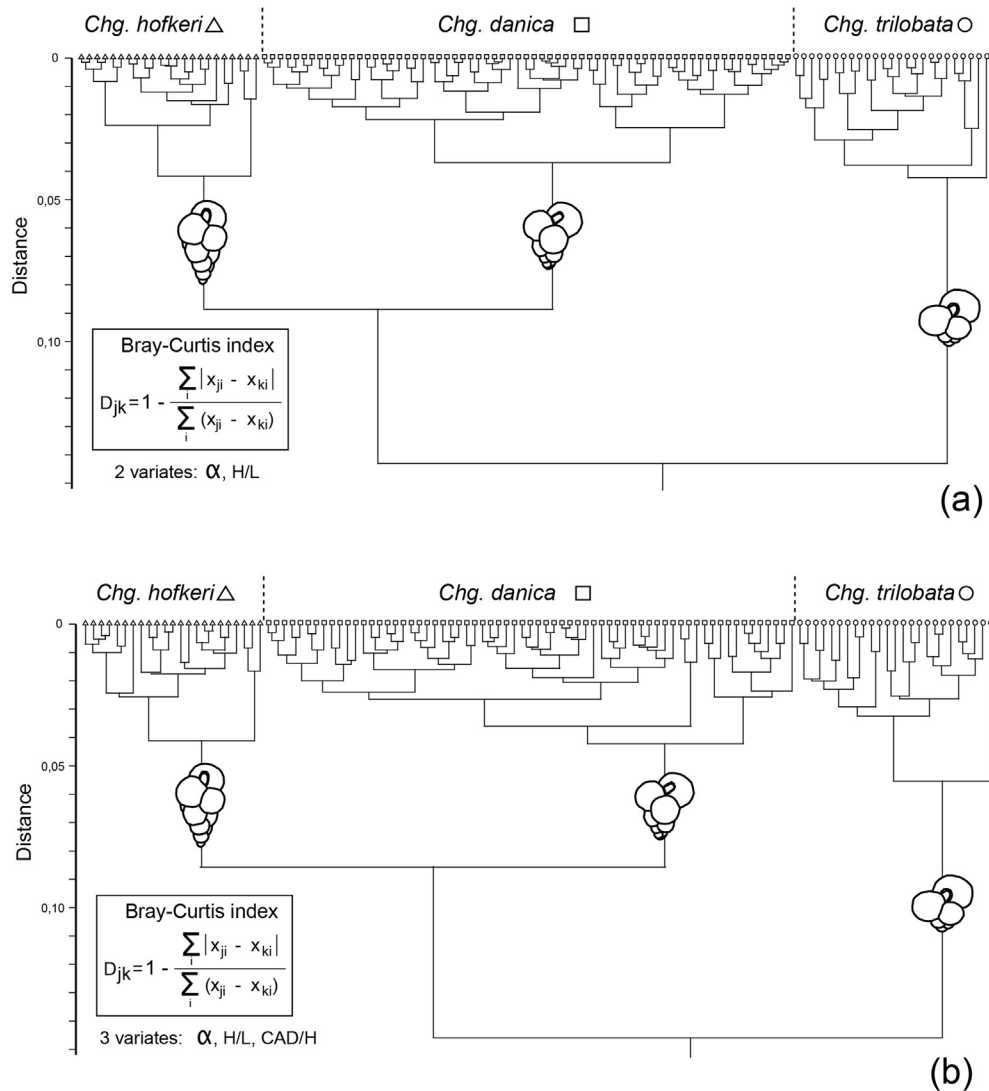


**Fig. 8.** Bivariate analyses based on Kernel density estimations from paired variables  $\alpha$  vs. H/L, and plotted in smooth map of point density; colour scale with deep red for highest density and dark blue for lowest. (For interpretation of the references to colour in this figure legend, the reader is referred to the web version of this article.)

texture is distinguishable from those of *Guembeltria*, and very similar to those described in *Trochoguembeltria* and in some of the earliest specimens of *Woodringina*. Furthermore, the position of its aperture also differs from that of *Guembeltria*. *Chiloguembeltria* should be assigned to the family Guembeltriidae together with

*Guembeltria* and *Woodringina*. The proposed phylogenetic relationships of these genera are illustrated in Fig. 11.

The family Guembeltriidae is usually included in the superfamily Heterohelicoidea Cushman, 1927, which has been excluded from the order Globigerinida Delage and Hérouard, 1896, in more



**Fig. 9.** R-mode cluster analysis based on Bray-Curtis index and applied to the values of the biometric variables measured in all SEM-photographed *Chiloguembeltria* specimens. (a) Cluster for biometric variables  $\alpha$  and H/L; (b) Cluster for biometric variables  $\alpha$ , H/L and CAD/H.  $D_{jk}$  = Bray-Curtis index value between specimen j and specimen k;  $x_{ji}$  = value of the variable i (biometric index/parameter i) of the specimen j;  $x_{ki}$  = value of the variable i (biometric index/parameter i) of the specimen k.

recent taxonomies (e.g. BouDagher-Fadel, 2012), and included separately in the order Heterohellicida Fursenko, 1958. However, if it is confirmed that *Guembeltria* evolved from the benthic *Neobulimina* or a similar buliminid, as Georgescu et al. (2011) proposed, the family Guembeltriidae should also be excluded from the superfamily Heterohelicoidea and the order Heterohellicida.

? Order **Heterohellicida** Fursenko, 1958

? Superfamily **Heterohelicoidea** Cushman, 1927

Family **Guembeltriidae** Montanaro-Gallitelli, 1957

Genus ***Chiloguembeltria*** Hofker, 1978, emended

**Type description.** Test small, elongate, wholly triserial. All foramina and the aperture are placed axially and perpendicular to the sutures, are slit-like elongate, with a distinct lip which is crenulate at the axial side of the border of the apertures, as in *Chiloguembelina*. It is like a *Guembelina* in which the biserial part is not yet developed, and may be the true ancestor of that genus. Both *Chiloguembeltria* and *Chiloguembelina* are monolamellar.

**Emended description.** Test small, subconical, wholly triserial tending to biserial, or with an undeveloped biserial final stage.

Chambers subspherical or globular. Outline lobate, with incised sutures. Aperture interiomarginal, umbilical-extraumbilical to extraumbilical (in the middle part of the suture between the last and the penultimate chamber), rounded or elongate arch, generally asymmetrical, with an imperforate lip. Wall calcareous, hyaline, microperforate, pustulate to rugose, with irregular or decentered pore-mounds, imperforate blunt pustules (papilla-type), occasionally sharp pustules, and both perforate and imperforate rugosities; rugosities and pustules irregularly distributed.

**Remarks.** *Chiloguembeltria* was originally described in the lower Danian as having a wholly triserial test, as *Guembeltria*, but with an aperture more similar to that of the biserial genus *Chiloguembelina*. Hofker (1978) and Loeblich and Tappan (1987) showed that the main diagnostic characters of *Chiloguembeltria* are its aperture shape (similar to *Chiloguembelina*) and its wall texture with imperforate blunt pustules. Kroon and Nederbragt (1990), D'Hondt (1991), MacLeod (1993), Jenkins et al. (1998) and Olsson et al. (1999) suggested that *Chiloguembeltria* is a junior synonym of *Guembeltria*, after concluding that its species bear pore-mounds similar to those of *Guembeltria*. However, well-preserved Danian specimens of *Chg. danica* from DSDP Site 47.2, Shatsky Rise (North

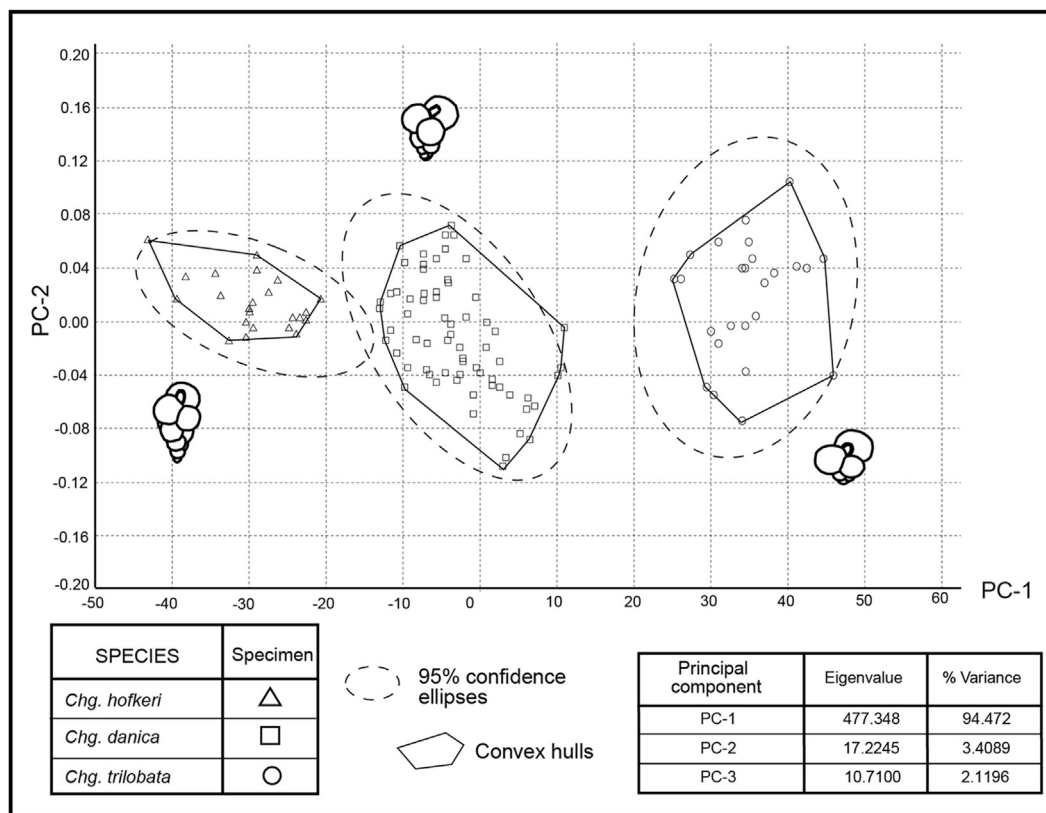


Fig. 10. Principal components analysis (PCA), applied to the values of biometric variables ( $\alpha$ , H/L and CAD/H) in all *Chiloguembeltria* specimens.

Pacific) exhibit imperforate blunt pustules and rugosities (Loeblich and Tappan, 1987), which is different from the wall texture of Maastrichtian specimens. Arz et al. (2010) and BouDagher-Fadel (2012, 2015) argued that *Chiloguembeltria* is a valid taxon, since its wall texture and apertural position differ from *Guembeltria*. Arenillas et al. (2010) described its wall texture as pustulate/papillate to rugose, and BouDagher-Fadel (2012, 2015) as muricate (a surface with a high density of pustules).

#### *Chiloguembeltria danica* Hofker, 1978

(Fig. 5(g); Fig. 12(c)–(g))

non 1978 *Chiloguembeltria danica* Hofker, p. 60, holotype: pl. 4, Fig. 14.

non 1987 *Guembeltria danica* (Hofker); Loeblich and Tappan, p. 452, part, topotype: pl. 484, Fig. 8.

non 1993 *Guembeltria danica* (Hofker); MacLeod, pl. 3, Figs. 1 and 5.

1998 *Guembeltria danica* (Hofker); Jenkins et al., p. 64, part, neotype: pl. 1, Fig. 1; topotype: pl. 1, Fig. 5.

non 2007 *Guembeltria danica* (Hofker); Arenillas et al., p. 38, Figs. 13.14–17.

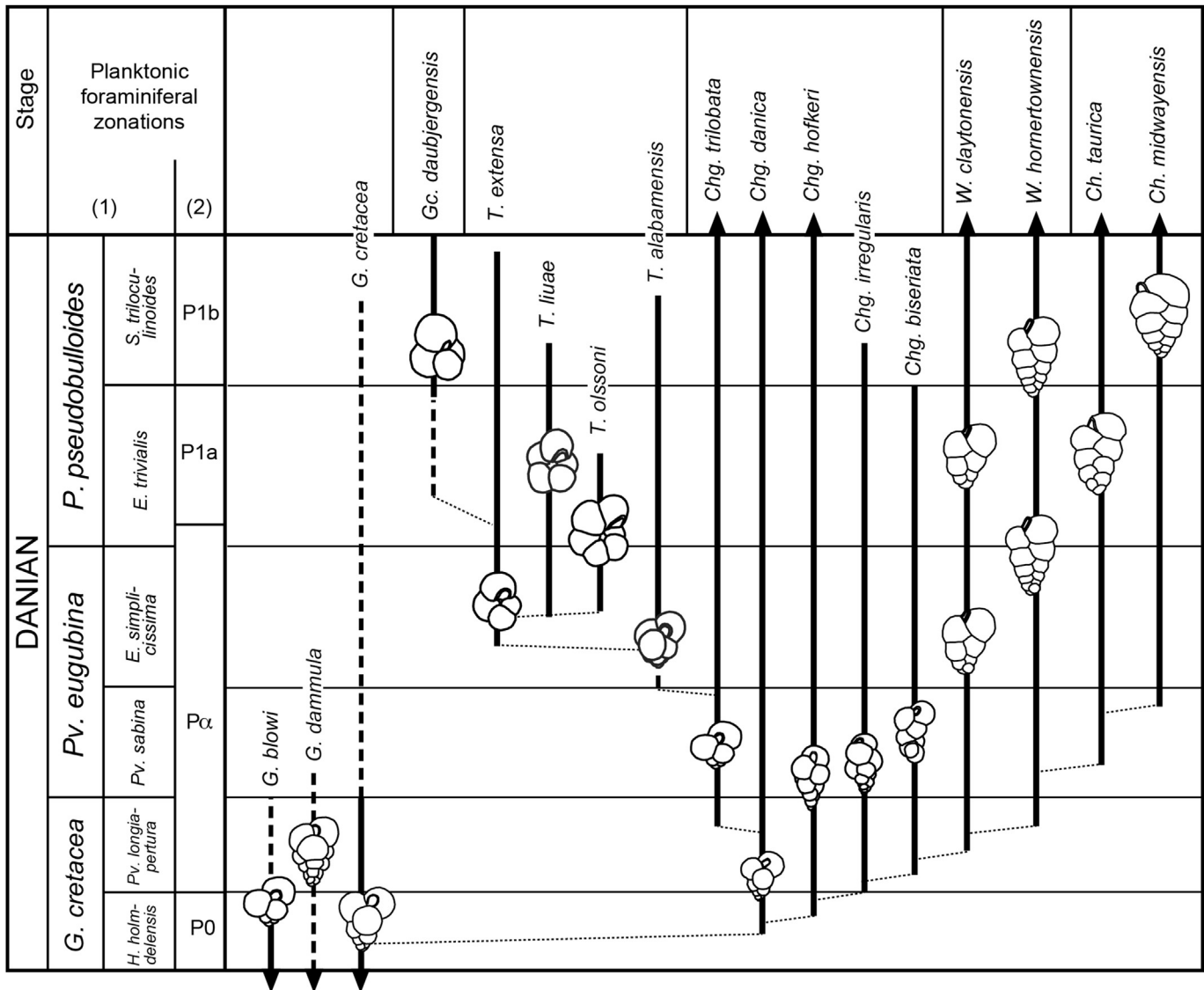
**Type description.** Test small, elongate, with triserially arranged chambers throughout. Chambers globular, with distinctly depressed sutures in between, gradually increasing in size so that the whole test remains slender. Walls thin, consisting of only one lamella, without secondary thickening. Walls finely perforate, with small blunt pustules. Aperture high, elongate, narrow, with protruding lip at the axial side of the aperture, as in *Chiloguembelina*. Length of test up to 0.1 mm; larger breadth near the apertural end 0.05 mm.

**Emended description.** Test subconical, medium-spined although higher than wide or long. Triserial arrangement, often

slightly twisted, with 9–12 subspherical chambers distributed in 3–4 spiral whorls, with a moderate rate of chamber enlargement. Outline subtriangular, lobate, with incised sutures. Aperture interiomarginal, umbilical-extraumbilical to extraumbilical, rounded or elongate, generally asymmetrical, surrounded by an imperforate lip. Wall surface microperforate, pustulate to rugose, with isolated, decentered pore-mounds, perforate and/or imperforate rugosities, and blunt pustules (papilla-type) and/or sharp pustules. Adult size range 100–150  $\mu$ m in height.

**Occurrence.** Lowermost Danian, from the upper part of Zone P0 to the lower part of Zone P1c of Berggren and Pearson (2005), i.e. from the upper part of the *Hedbergella holmdelensis* Subzone (*Guembeltria cretacea* Zone) to the lower part of the *Globanomalina compressa* Subzone (*Parasubbotina pseudobulloides* Zone) of Arenillas et al. (2004). It is very frequent in the *Eoglobigerina trivialis* Subzone (*Parasubbotina pseudobulloides* Zone), i.e. in P1a (Fig. 1).

**Remarks.** Kroon and Nederbragt (1990) suggested that *Chg. danica* is a junior synonym of *G. cretacea*, assuming that it bears pore-mounds. However, the presence of regular pore-mounds in *Chg. danica* is doubtful (Hofker, 1978; Loeblich and Tappan, 1987; Arz et al., 2010; Arenillas et al., 2010; BouDagher-Fadel, 2012, 2015). Morphologically, *G. dammula* is very similar to the original illustration of the holotype of *Chg. danica*. Since many authors have considered that *Guembeltria* and *Chiloguembeltria* are synonymous genera, the Maastrichtian high-spined guembeltriids assigned to *Guembeltria dammula* Voloshina, 1961, by Arz et al. (2010) have frequently been named *Guembeltria danica* (e.g. MacLeod, 1993). In any case, *G. dammula* was originally defined from Maastrichtian beds and has priority in date of publication over the species defined by Hofker (1978). The neotype selected by Jenkins et al. (1998) for *Chg. danica* (Fig. 12(c)) has a medium-spined test similar to that of *G. cretacea*, thus not reflecting the original



**Fig. 11.** Proposed phylogenetic relationships of *Guembelitra*, *Chiloguembelitra*, *Trochoguembelitra*, *Globoconusa*, *Woodringina* and *Chiloguembelina* based on evidence reported here and previous phylogenetic studies (see Arenillas et al., 2012, 2016b); thick dotted lines indicate doubtful range, based probably on reworked specimens. (1) Arenillas et al. (2004); (2) Berggren and Pearson (2005).

morphology (high-spired test) of the Hofker's holotype (Fig. 12(a)). Nevertheless, the designated neotype has priority according to the Article 75 of International Code of Zoological Nomenclature, so that the name "danica" should be used to refer to *Chiloguembelitra* specimens with a medium-spired test.

#### ***Chiloguembelitra irregularis* (Morozova, 1961)**

(Fig. 12(i)–(n))

1961 *Guembelitra irregularis* Morozova, p. 17–18, pl. 1, Figs. 9–10.

1987 *Guembelitra danica* (Hofker); Loeblich and Tappan, p. 452, part, pl. 484, Figs. 7 and 9.

1993 *Guembelitra irregularis* Morozova; MacLeod, pt. 3, Figs. 2–4, 6–7.

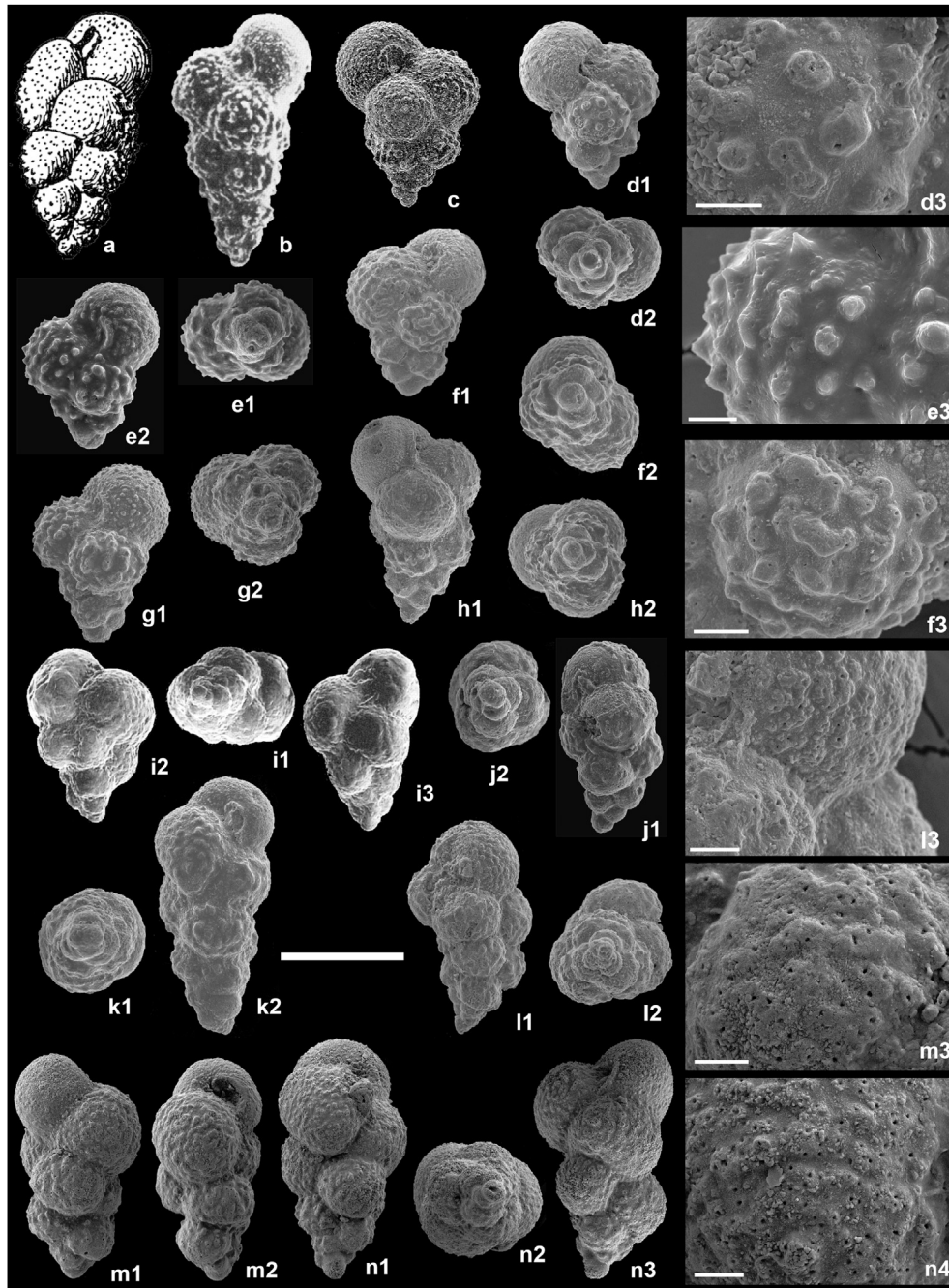
1998 *Guembelitra danica* (Hofker); Jenkins et al., p. 64, part, pl. 1, Figs. 4 and 6.

2007 *Guembelitra? irregularis* Morozova; Arenillas et al., p. 38–39, Figs. 13.9–13.

**Type description.** Test high, height two to three times exceeding the diameter. Initial end pointed, initial angle about 30°. Apertural end rounded. Spire consists of seven to eight whorls. The number of chambers in each whorl is not uniform, sometimes two and a half, sometimes three, so the chambers do not form regular rows. In all mature forms there are 17–20 subspheroidal chambers. Sutures deep. Aperture semilunate, basal. Wall smooth, semi-transparent. Surface weakly rough [Translation from the Russian].

**Emended description.** Test elongated, subconical, high-spired. Triserial arrangement, twisted with irregular appearance, with 11–17 subspherical chambers distributed in 3.5–5.5 spiral whorls, with low rate of chamber enlargement. Outline subtriangular, lobate, with incised sutures. Aperture interiomarginal, usually extraumbilical, rounded or elongate, generally asymmetrical, with an imperforate lip. Wall surface microperforate, pustulate to rugose, with isolated, decentered pore-mounds, perforate and/or imperforate rugosities, and blunt pustules (papilla-type). Adult size range 120–180 µm in height.





**Fig. 12.** Holotypes and specimens of *Chiloguembeltria danica* Hofker and *Chiloguembeltria irregularis* Morozova (scale bar = 100  $\mu$ m; scale bar of detail SEM-micrographs = 10  $\mu$ m). (a) *Chiloguembeltria danica* Hofker, invalid holotype (considered here as *Chg. hofkeri* sp. nov.), middle Danian, DSDP Leg 6 Shatsky Rise, northern Pacific. (b) *Chiloguembeltria danica* Hofker (considered here as *Chg. hofkeri* sp. nov.), topotype of *Loeblich and Tappan* (1987), Danian, DSDP Site 472, Shatsky Rise, northern Pacific. (c) *Chiloguembeltria danica* Hofker, neotype of *Jenkins et al.* (1998), Danian, DSDP Leg 6, Shatsky Rise, northern Pacific. (d) *Chiloguembeltria danica* Hofker, sample KF 20.50 (8.5 m above K/Pg boundary), *E. trivialis* Subzone (*P. pseudobulloides* Zone), El Kef, Tunisia. (e) *Chiloguembeltria danica* Hofker, sample KF 20.50 (8.5 m above K/Pg boundary), *E. trivialis* Subzone (*P. pseudobulloides* Zone), El Kef, Tunisia. (f) *Chiloguembeltria danica* Hofker, sample KF 20.50 (8.5 m above K/Pg boundary), *E. trivialis* Subzone (*P. pseudobulloides* Zone), El Kef, Tunisia. (g) *Chiloguembeltria danica* Hofker, sample KF 20.50 (8.5 m above K/Pg boundary), *E. trivialis* Subzone (*P. pseudobulloides* Zone), El Kef, Tunisia. (h) *Chiloguembeltria hofkeri* sp. nov., sample KF 20.50 (8.5 m above K/Pg boundary), *E. trivialis* Subzone (*P. pseudobulloides* Zone), El Kef, Tunisia. (i) *Guembeltria irregularis* Morozova, Holotype, lower Danian, Tarkhankut, Crimea (SEM-micrographs from *Olsson et al.*, 1999). (j) *Chiloguembeltria irregularis* (Morozova), sample KF 20.50 (8.5 m above K/Pg boundary), *E. trivialis* Subzone (*P. pseudobulloides* Zone), El Kef, Tunisia. (k) *Chiloguembeltria irregularis* (Morozova), sample STW+45 + 47 (46 cm above K/Pg boundary), *Pv. longiapertura* Subzone (*G. cretacea* Zone), Ain Settara, Tunisia. (l) *Chiloguembeltria irregularis* (Morozova), sample KF 20.50 (8.5 m above K/Pg boundary), *E. trivialis* Subzone (*P. pseudobulloides* Zone), El Kef, Tunisia. (m) *Chiloguembeltria irregularis* (Morozova), sample KF 19.50 (7.5 m above K/Pg boundary), *E. trivialis* Subzone (*P. pseudobulloides* Zone), El Kef, Tunisia. (n) *Chiloguembeltria irregularis* (Morozova), sample KF 19.50 (7.5 m above K/Pg boundary), *E. trivialis* Subzone (*P. pseudobulloides* Zone), El Kef, Tunisia.

**Occurrence.** Lowermost Danian, from the lower part of Zone P $\alpha$  to the middle part of Zone P1b of Berggren and Pearson (2005), i.e. from the lower part of the *Parvularugoglobigerina longiapertura* Subzone (*Guembelitra cretacea* Zone) to the middle part of the *Subbotina triloculinoides* Subzone (*Parasubbotina pseudobulloides* Zone) of Arenillas et al. (2004). It is frequent in the *Eoglobigerina trivialis* Subzone (*Parasubbotina pseudobulloides* Zone), i.e. in P1a (Fig. 1).

**Remarks.** It differs from *Chg. danica* in the twisted triserial test that gives it an irregular appearance. It also differs from other *Chiloguembelitra* species with “regular” rather than twisted triserial tests (*Chg. hofkeri* sp. nov. and *Chg. trilobata* sp. nov.) in its higher spire, similar to *Chg. danica*. As was suggested by Arz et al. (2010), the species name *irregularis* may have been used as a “wastebasket” grouping earliest Danian species with a pustulate to rugose wall (Loeblich and Tappan, 1987) and both Maastrichtian and Danian aberrant forms with different types of wall texture. *Chg. irregularis* should thus not be confused with aberrant forms or with some specimens of *Guembelitra* with a relatively twisted test.

***Chiloguembelitra hofkeri* sp. nov.**

(Fig. 5(c); Fig. 12(h); Fig. 13(a)–(d))

1978 *Guembelitra danica* Hofker, p. 60, pl. 4, Fig. 14.

1987 *Guembelitra danica* (Hofker); Loeblich and Tappan, p. 452, part, pl. 484, Fig. 8.

non 1993 *Guembelitra danica* (Hofker); MacLeod, pl. 3, Figs. 1 and 5.

2007 *Guembelitra danica* (Hofker); Arenillas et al., p. 38, Figs. 13.14–17.

**Type-specimens.** Holotype MPZ 2016/108 (Fig. 13(a)). Paratype MPZ 2016/109 (Fig. 13(b)). MPZ 2016/110 (Fig. 13(c)). Paratype MPZ 2016/111 (Fig. 13(d)). Type-specimens deposited in the Museo de Ciencias Naturales de la Universidad de Zaragoza (Aragon Government, Spain).

**Diagnosis.** Test elongated, subconical, high-spined. Triserial arrangement, often slightly twisted, with 11–14 subspherical chambers distributed in 3.5–4.5 spiral whorls, with low rate of chamber enlargement. Outline subtriangular, lobate, with incised sutures. Aperture interiomarginal, umbilical-extraumbilical to extraumbilical, rounded or elongate, generally asymmetrical, with an imperforate lip. Wall surface microperforate, pustulate to rugose, with isolated, decentered pore-mounds, perforate and/or imperforate rugosities, and blunt pustules (papilla-type). Adult size range 120–180  $\mu$ m in height.

**Derivation of name.** Species dedicated to Jan Hofker for the discovery and definition of the Danian genus *Chiloguembelitra*.

**Type locality.** El Kef section, El Haria Formation, Tunisia.

**Type level.** 7.50 m above the Cretaceous/Paleogene boundary of the El Kef section (sample KF19.50), in the lower part of Zone P1a, or the middle part of the *Eoglobigerina trivialis* Subzone (*Parasubbotina pseudobulloides* Zone), lower Danian.

**Occurrence.** Lowermost Danian, from the upper part of Zone P0 to the middle part of Zone P1b of Berggren and Pearson (2005), i.e. from the upper part of the *Hedbergella holmdelensis* Subzone (*Guembelitra cretacea* Zone) to the middle part of the *S. triloculinoides* Subzone (*Parasubbotina pseudobulloides* Zone) of Arenillas et al. (2004). It is very frequent in the *Eoglobigerina trivialis* Subzone (*Parasubbotina pseudobulloides* Zone), i.e. in P1a (Fig. 1).

**Remarks.** It differs from *Chg. danica* in having a higher-spined test. The gross morphology of *Chg. hofkeri* sp. nov. is similar to the original holotype of *Chg. danica* illustrated by Hofker (1978). Nevertheless, because this holotype was invalidated (depository not given by the author), the name “*danica*” should be used to refer

to *Chiloguembelitra* specimens with a medium-spined test, such as the neotype designated by Jenkins et al. (1998). The difference in spire height of *Chg. hofkeri* sp. nov. from *Chg. danica* and *Chg. trilobata* sp. nov. is similar to that of *Guembelitra dammula* from *G. cretacea* and *G. blowi* (Arz et al., 2010). These two triplets of species differ from each other in the wall texture and the position and shape of the aperture. Danian specimens of *Chg. hofkeri* sp. nov. have commonly been attributed to *G. cretacea* (MacLeod, 1993; Olsson et al., 1999; Arenillas et al., 2000a, 2000b), but Arenillas et al. (2007) and Arz et al. (2010) have already pointed out the possible existence in the early Danian of a pseudocryptic species similar to *Guembelitra* spp. but with a rugose wall.

***Chiloguembelitra trilobata* sp. nov.**

(Fig. 13(e)–(h))

**Type-specimens.** Holotype MPZ 2016/112 (Fig. 13(e)). Paratype MPZ 2016/113 (Fig. 13(f)). MPZ 2016/114 (Fig. 13(g)). Paratype MPZ 2016/115 (Fig. 13(h)). Type-specimens deposited in the Museo de Ciencias Naturales de la Universidad de Zaragoza (Aragon Government, Spain).

**Diagnosis.** Test short subconical, low-spined. Triserial arrangement, often slightly twisted, with 8–11 subspherical chambers distributed in 2.5–3.5 spiral whorls, with a high rate of chamber enlargement. Outline subtriangular, lobate, with incised sutures. Aperture interiomarginal, umbilical-extraumbilical to extraumbilical, generally rounded and asymmetrical, with an imperforate lip. Wall surface microperforate, pustulate to rugose, with isolated, decentered pore-mounds, perforate and/or imperforate rugosities, and blunt pustules (papilla-type) and/or sharp pustules. Adult size range 90–120  $\mu$ m in height.

**Derivation of name.** Latin term *trilobata* referring to the shape of three lobes in the equatorial outline.

**Type locality.** El Kef section, El Haria Formation, Tunisia.

**Type level.** 7.50 m above the Cretaceous/Paleogene boundary of the El Kef section (sample KF19.50), in the uppermost part of Zone P $\alpha$ , or the lower part of the *Eoglobigerina trivialis* Subzone (*Parasubbotina pseudobulloides* Zone), lower Danian.

**Occurrence.** Lower Danian, from the lower part of Zone P $\alpha$  to the upper part of Zone P1b of Berggren and Pearson (2005), i.e. from the uppermost part of the *Parvularugoglobigerina longiapertura* Subzone (*Guembelitra cretacea* Zone) to the lower part of the *Globanomalina compressa* Subzone (*Parasubbotina pseudobulloides* Zone) of Arenillas et al. (2004). It is very frequent in the *Eoglobigerina trivialis* Subzone (*Parasubbotina pseudobulloides* Zone), i.e. in P1a (Fig. 1).

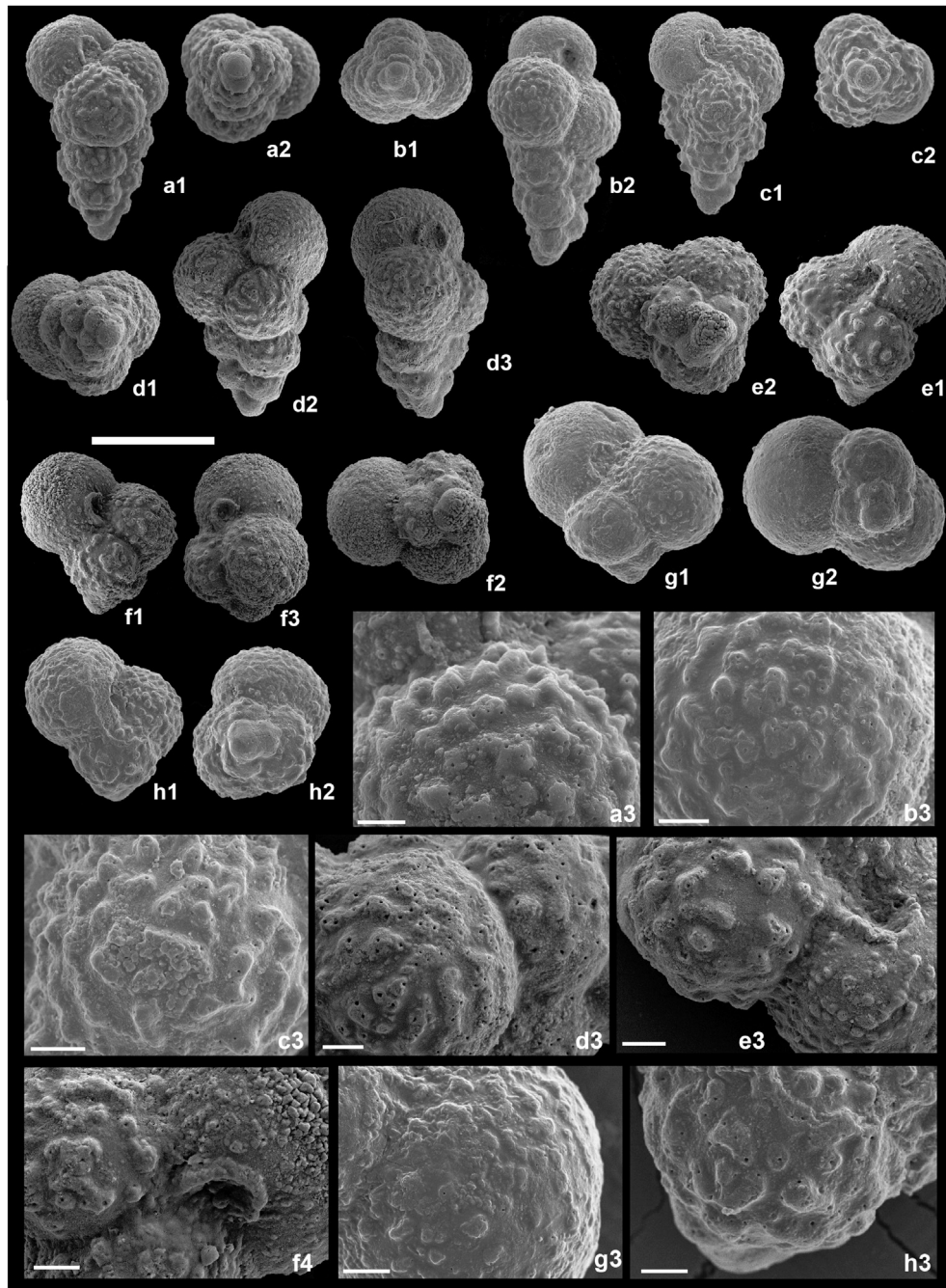
**Remarks.** It differs from *Chg. danica* in having a lower triserial test. Specimens of *Chg. trilobata* sp. nov. have been probably attributed to *Guembelitra blowi* (or *G. trifolia* for some authors; MacLeod, 1993; Arenillas et al., 2000a, 2000b) or *G. cretacea* (Olsson et al., 1999). Nevertheless, Arenillas et al. (2007) and Arz et al. (2010) pointed out the possible existence of pseudocryptic species of *Guembelitra* spp. in the lower Danian, referring to some of the *Chiloguembelitra* species defined here. The gross morphology and size of *Chg. trilobata* sp. nov. resemble those of *Trochoguembelitra alabamensis*, with which it shares the wall texture but from which it differs in the chamber arrangement (triserial vs. trochospiral).

***Chiloguembelitra biseriata* sp. nov.**

(Fig. 14(a)–(d))

? 1998 *Guembelitra danica* (Hofker); Jenkins et al., p. 64, part, pl. 1, Fig. 3.

? 1999 *Woodringina claytonensis* Loeblich and Tappan; Olsson et al., p. 242, pl. 68, Fig. 1.

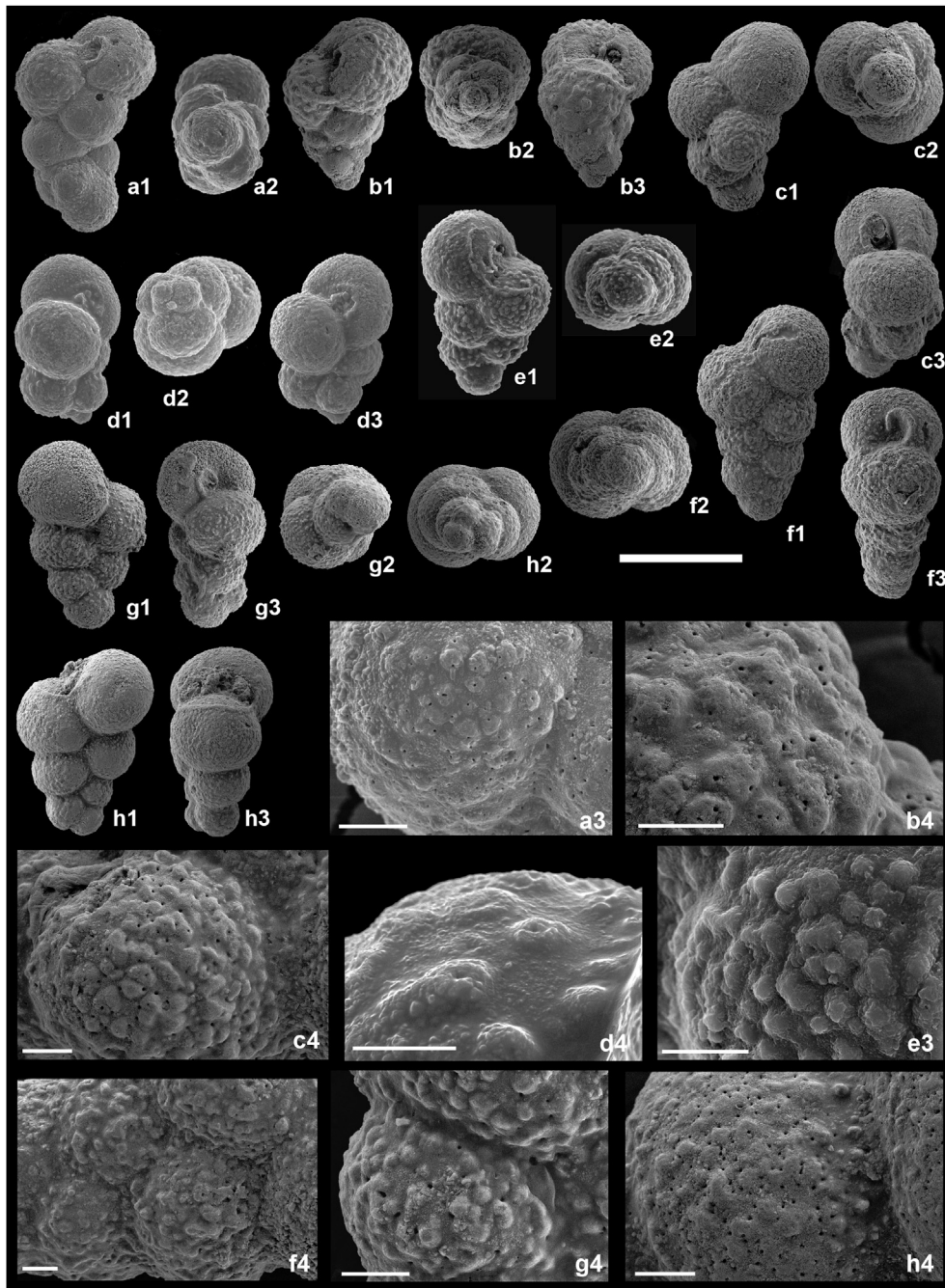


**Fig. 13.** Type-specimens of *Chiloguembeltria hofkeri* sp. nov. and *Chiloguembeltria trilobata* sp. nov. (scale bar = 100  $\mu$ m; scale bar of detail SEM-micrographs = 10  $\mu$ m). (a) *Chiloguembeltria hofkeri* sp. nov., Holotype MPZ 2016/108, sample KF 19.50 (7.5 m above K/Pg boundary), *E. trivialis* Subzone (*P. pseudobulloides* Zone), El Kef, Tunisia. (b) *Chiloguembeltria hofkeri* sp. nov., Paratype MPZ 2016/109, sample KF 20.50 (8.5 m above K/Pg boundary), *E. trivialis* Subzone (*P. pseudobulloides* Zone), El Kef, Tunisia. (c) *Chiloguembeltria hofkeri* sp. nov., Paratype MPZ 2016/110, sample KF 20.50 (8.5 m above K/Pg boundary), *E. trivialis* Subzone (*P. pseudobulloides* Zone), El Kef, Tunisia. (d) *Chiloguembeltria hofkeri* sp. nov., Paratype MPZ 2016/111, sample KF 19.50 (7.5 m above K/Pg boundary), *E. trivialis* Subzone (*P. pseudobulloides* Zone), El Kef, Tunisia. (e) *Chiloguembeltria trilobata* sp. nov., Holotype MPZ 2016/112, sample KF 19.50 (7.5 m above K/Pg boundary), *E. trivialis* Subzone (*P. pseudobulloides* Zone), El Kef, Tunisia. (f) *Chiloguembeltria trilobata* sp. nov., Paratype MPZ 2016/113, sample KF 19.50 (7.5 m above K/Pg boundary), *E. trivialis* Subzone (*P. pseudobulloides* Zone), El Kef, Tunisia. (g) *Chiloguembeltria trilobata* sp. nov., Paratype MPZ 2016/114, sample KF 21.25 (9.25 m above K/Pg boundary), *E. trivialis* Subzone (*P. pseudobulloides* Zone), El Kef, Tunisia. (h) *Chiloguembeltria trilobata* sp. nov., Paratype MPZ 2016/115, sample KF 20.50 (8.5 m above K/Pg boundary), *E. trivialis* Subzone (*P. pseudobulloides* Zone), El Kef, Tunisia.

**Type-specimens.** Holotype MPZ 2016/116 (Fig. 14(a)). Paratype MPZ 2016/117 (Fig. 14(b)). MPZ 2016/118 (Fig. 14(c)). Paratype MPZ 2016/119 (Fig. 14(d)). Type-specimens deposited in the Museo de Ciencias Naturales de la Universidad de Zaragoza (Aragon Government, Spain).

**Diagnosis.** Test subconical to flaring, with 7–10 subspherical chambers and a medium-to-high rate of chamber enlargement.

Triserial juvenile stage with 5–6 chambers distributed in 1.5–2 spiral whorls, and biserial final stage with 1–2 pairs of chambers in a twisted plane of biseriality. Outline subtriangular, lobate, with incised sutures. Aperture interiomarginal, lateral, rounded or elongate, generally asymmetrical, with an imperforate lip. Wall surface microperforate, pustulate to rugose, with isolated, decentered pore-mounds, perforate and/or imperforate rugosities, and



**Fig. 14.** Type-specimens of *Chiloguembeltria biseriata* sp. nov. and comparison with specimens of *Woodringina claytonensis* Loeblich (scale bar = 100  $\mu$ m; scale bar of detail SEM-micrographs = 10  $\mu$ m). (a) *Chiloguembeltria biseriata* sp. nov., Holotype MPZ 2016/116, sample KF 20.50 (8.5 m above K/Pg boundary), *E. trivialis* Subzone (*P. pseudobulloides* Zone), El Kef, Tunisia. (b) *Chiloguembeltria biseriata* sp. nov., Paratype MPZ 2016/117, sample KF 19.50 (7.5 m above K/Pg boundary), *E. trivialis* Subzone (*P. pseudobulloides* Zone), El Kef, Tunisia. (c) *Chiloguembeltria biseriata* sp. nov., Paratype MPZ 2016/118, sample KF 19.50 (7.5 m above K/Pg boundary), *E. trivialis* Subzone (*P. pseudobulloides* Zone), El Kef, Tunisia. (d) *Chiloguembeltria biseriata*, Paratype MPZ 2016/119, sample KF 18.50 (6.5 m above K/Pg boundary), *E. simplicissima* Subzone (*Pv. eugubina* Zone), El Kef, Tunisia. (e) *Woodringina claytonensis* Loeblich and Tappan, sample KF 20.50 (8.5 m above K/Pg boundary), *E. trivialis* Subzone (*P. pseudobulloides* Zone), El Kef, Tunisia. (f) *Woodringina claytonensis* Loeblich and Tappan, sample KF 19.50 (7.5 m above K/Pg boundary), *E. trivialis* Subzone (*P. pseudobulloides* Zone), El Kef, Tunisia. (g) *Woodringina claytonensis* Loeblich and Tappan, sample KF 19.50 (7.5 m above K/Pg boundary), *E. trivialis* Subzone (*P. pseudobulloides* Zone), El Kef, Tunisia. (h) *Woodringina claytonensis* Loeblich and Tappan, sample KF24.00 (12 m above the K/Pg boundary), *S. trilocolinoides* Subzone (*P. pseudobulloides* Zone), El Kef, Tunisia.

blunt pustules (papilla-type). Adult size range 120–160  $\mu$ m in height.

**Derivation of name.** Latin term *biseriata* referring to the *biseriate* final stage of its ontogeny.

**Type locality.** El Kef section, El Haria Formation, Tunisia.

**Type level.** 8.50 m above the Cretaceous/Paleogene boundary of the El Kef section (sample KF20.50), in the lower part of Zone P1a,

or middle part of the *Eoglobigerina trivialis* Subzone (*Parasubbotina pseudobulloides* Zone), lower Danian.

**Occurrence.** Lowermost Danian, from the lower part of Zone P $\alpha$  to the upper part of Zone P1a of Berggren and Pearson (2005), i.e. from the lower part of the *Parvularugoglobigerina longiapertura* Subzone (*Guembeltria cretacea* Zone) to the upper part of the *Subbotina trivialis* Subzone (*Parasubbotina pseudobulloides* Zone) of

Arenillas et al. (2004). It is not abundant, and is easily confused with *Woodringina claytonensis* (Fig. 1).

**Remarks.** It differs from other *Chiloguembeltria* species in its final biserial stage. The species *Chg. biseriata* sp. nov. has previously gone unnoticed because it is morphologically very similar to *Woodringina claytonensis*. However, *W. claytonensis* differs in its wall surface (pustulate or muricate rather than rugose, and without pore-mounds) and its reduced triserial initial stage (single whorl of three-chambered stage, usually pseudotriserial rather than triserial). Olsson et al. (1999) included these morphotypes within the phenotypic variability of *W. claytonensis*, adducing that some specimens of *Woodringina* bear scattered pore-mounds. However, typical *W. claytonensis* has a pustulate wall like other species of *Woodringina* and *Chiloguembelina*, consisting of small imperforate blunt pustules (papilla-type). Many pustules in the wall of *Woodringina* may have the same ontogenetic origin as the pore-mounds in *Guembeltria*, although others perhaps may not.

### Acknowledgements

We thank two anonymous reviewers for thoughtful and useful comments. This work was supported by the Spanish Ministerio de Economía y Competitividad [grant number CGL2015-64422-P], cofinanced by the European Regional Development Fund; by the Universidad de Zaragoza [grant number UZ2015-CIE-02]; and by the Departamento de Educación y Ciencia of the Aragonian Government cofinanced by the European Social Fund (ESF) [grant number DGA group E05]. The authors would like to acknowledge the use of the Servicio General de Apoyo a la Investigación-SAI, Universidad de Zaragoza. The authors are grateful to Rupert Glasgow for improvement of the English text.

### References

- Arenillas, I., Arz, J.A., 2000. *Parvularugoglobigerina eugubina* type-sample at Ceselli (Italy): planktic foraminiferal assemblage and lowermost Danian biostratigraphic implications. *Riv. Ital. Paleontol. S.* 106 (3), 379–390.
- Arenillas, I., Arz, J.A., 2013a. Origin and evolution of the planktic foraminiferal family Eoglobigerinidae Blow (1979) in the early Danian (Paleocene). *Rev. Mex. Cienc. Geol.* 30 (1), 159–177.
- Arenillas, I., Arz, J.A., 2013b. New evidence on the origin of nonspinose pitted-cancellate species of the early Danian planktic foraminifera. *Geol. Carpath.* 64 (3), 237–251.
- Arenillas, I., Arz, J.A., 2017. Benthic origin and earliest evolution of the first planktic foraminifera after the Cretaceous/Paleogene boundary mass extinction. *Hist. Biol.* 29 (1), 17–24. <http://dx.doi.org/10.1080/08912963.2015.1119133>.
- Arenillas, I., Arz, J.A., Molina, E., Dupuis, C., 2000a. An independent test of planktic foraminiferal turnover across the Cretaceous/Paleogene (K/P) boundary at El Kef, Tunisia: catastrophic mass extinction and possible survivorship. *Micropaleontology* 46 (1), 31–49.
- Arenillas, I., Arz, J.A., Molina, E., Dupuis, C., 2000b. The Cretaceous/Paleogene (K/P) boundary at Ain Settara, Tunisia: sudden catastrophic mass extinction in planktic foraminifera. *J. Foramin. Res.* 30 (3), 202–218.
- Arenillas, I., Arz, J.A., Molina, E., 2002. Quantifying the evolutionary turnover across the K/T boundary catastrophic planktic foraminiferal extinction event at El Kef, Tunisia. *GFF* 124, 121–126.
- Arenillas, I., Arz, J.A., Molina, E., 2004. A new high-resolution planktic foraminiferal zonation and subzonation for the lower Danian. *Lethaia* 37, 79–95.
- Arenillas, I., Arz, J.A., Grajales-Nishimura, J.M., Murillo-Muñeton, G., Alvarez, W., Camargo-Zanoguera, A., Molina, E., Rosales-Domínguez, C., 2006. Chicxulub impact event is Cretaceous/Paleogene boundary in age: new micropaleontological evidence. *Earth Planet. Sc. Lett.* 249 (3–4), 241–257.
- Arenillas, I., Arz, J.A., Nájuez, C., 2007. Morfología, Biometría y Taxonomía de foraminíferos planctónicos del Daniense basal: *Palaeglobigerina* n. gen. [Morphology, biometry and taxonomy of the lowermost Danian planktic foraminifera: *Palaeglobigerina* n. gen.]. *Rev. Esp. Paleontol.* 22 (1), 21–62. Spanish.
- Arenillas, I., Arz, J.A., Nájuez, C., 2010. Diversidad y evolución de la textura de la pared en guembeltridos (foraminíferos planctónicos) en el tránsito Cretácico-Paleógeno [Textural diversity and evolution of guembeltriids (planktic foraminifera) across the Cretaceous-Paleogene transition]. *Rev. Esp. Paleontol.* 25 (2), 87–105. Spanish.
- Arenillas, I., Arz, J.A., Nájuez, C., 2012. Smooth and rugose wall textures in earliest Danian trochospiral planktic foraminifera from Tunisia. *N. Jb. Geol. Paläont. Abh.* 266 (2), 123–142.
- Arenillas, I., Arz, J.A., Grajales-Nishimura, J.M., Rojas-Consuegra, R., 2016a. The Chicxulub impact is synchronous with the planktic foraminifera mass extinction at the Cretaceous/Paleogene boundary: new evidence from the Moncada section, Cuba. *Geol. Acta* 14 (1), 35–51.
- Arenillas, I., Arz, J.A., Nájuez, C., 2016b. New species of genus *Trochoguembeltria* from the lowermost Danian of Tunisia - biostratigraphic and evolutionary implications in planktic foraminifera. *Palaeontogr. Abt. A* 305 (4–6), 133–160.
- Arz, J.A., Arenillas, I., Nájuez, C., 2010. Morphostatistical analysis of Maastrichtian populations of *Guembeltria* from El Kef, Tunisia. *J. Foramin. Res.* 40 (2), 148–164.
- Ashkenazi-Polivoda, S., Rak, C., Almogi-Labin, A., Zsolt, B., Ovidia, O., Abramovich, S., 2014. Paleoeology of the K-Pg mass extinction survivor *Guembeltria* (Cushman): isotopic evidence from pristine foraminifera from Brazos River, Texas (Maastrichtian). *Paleobiology* 40 (1), 24–33.
- Berggren, W.A., Pearson, P.N., 2005. A revised tropical to subtropical Paleogene planktic foraminiferal zonation. *J. Foramin. Res.* 35 (4), 279–298.
- Blow, W.H., 1979. The Cainozoic Globigerinidae. In: Brill, E.J. (Ed.), *A Study of the Morphology, Taxonomy, Evolutionary Relationship and the Stratigraphical Distribution of Some Globigerinidae (Mainly Globigerinacea)*. Leiden, Netherlands, Vol. 1: xv+752 pp.; Vol. 2: 1413 pp.; Vol. 3: xxi, 264 pls.
- BouDagher-Fadel, M.K., 2012. Biostratigraphic and geological significance of planktic foraminifera (1st edition). *Dev. Palaeontol. Stratigr.* 22, 1–289.
- BouDagher-Fadel, M.K., 2015. Biostratigraphic and Geological Significance of Planktic Foraminifera, third ed. UCL Press, London. 298 pp, 12 charts.
- Brinkhuis, H., Zachariasse, W.J., 1988. Dinoflagellate cysts, sea level changes and planktic foraminifers across the Cretaceous-Tertiary boundary at El Haria, Northwest Tunisia. *Mar. Micropaleontol.* 13 (2), 153–191.
- Brönnimann, P., 1953. Note on planktonic foraminifera from Danian localities of Jutland, Denmark. *Eclogae Geol. Helv.* 45, 339–341.
- Brotzen, F., Pozaryska, T., 1961. Foraminifères du Paléocène et de l'Éocène inférieur en Pologne septentrionale; remarques paléogéographiques. *Rev. Micropaleontol.* 4, 155–166.
- Canudo, J.I., Keller, G., Molina, E., 1991. Cretaceous/Tertiary boundary extinction pattern and faunal turnover at Agost and Caravaca, SE Spain. *Mar. Micropaleontol.* 17 (3–4), 319–341.
- Chenet, A.L., Auidelleur, X., Fluteau, F., Courtillot, V.Y., Bajpai, S., 2007. <sup>40</sup>K-<sup>40</sup>Ar dating of the main Deccan large igneous province: further evidence of KTB age and short duration. *Earth Planet. Sc. Lett.* 263, 1–15.
- Cushman, J.A., 1927. An outline of a re-classification of the Foraminifera. *Contrib. Cushman Lab. Foramin. Res.* 3, 1–105.
- Cushman, J.A., 1933. Some New Foraminiferal Genera. *Contrib. Cushman Lab. Foramin. Res.* 9, 32–38.
- Cushman, J.A., 1940. Midway foraminifera from Alabama. *Contrib. Cushman Lab. Foramin. Res.* 16, 51–73.
- Delage, Y., Hérouard, E., 1896. *Traité de Zoologie Concrète, Tome 1, La Cellule et les Protozoaires*. Schleicher Frères, Paris.
- D'Hondt, S.L., 1991. Phylogenetic and stratigraphic analysis of earliest Paleocene biserial and triserial planktic foraminifera. *J. Foramin. Res.* 21 (2), 168–181.
- Fursenko, A.V., 1958. Osnovnye etapy razvitiya faun foraminifer v geologicheskome proshlom (Fundamental state of development of foraminiferal faunas in the geologic past). *Tr. Inst. Geol. Nauk, Akad. Nauk Belorusskoi SSR, Minsk* 1, 10–29.
- Georgescu, M.D., 2009. On the origins of superfamily Heterohelicacea Cushman, 1927 and the polyphyletic nature of planktic foraminifera. *Rev. Esp. Micropal.* 41 (1–2), 1–38.
- Georgescu, M.D., Arz, J.A., Macauley, R.V., Kukulski, R.B., Arenillas, I., Pérez-Rodríguez, I., 2011. Late Cretaceous (late Santonian-Maastrichtian) serial planktic and benthic foraminifera with pore mounds or pore mound-based ornamentation structures. *Rev. Esp. Micropal.* 43 (1–2), 109–139.
- Hammer, Ø., Harper, D.A.T., Ryan, P.D., 2001. PAST: paleontological statistics software package for education and data analysis. *Palaeontol. Electron* 4 (1), 9 p.
- Haque, A.F.M.M., 1956. The smaller Foraminifera of the Ranikot and the Laki of the Nammal Gorge, Salt Range, Paleontol. *Pakistan*, *Geol. Surv. Pakistan* 1, 1–300.
- Hildebrand, A.R., Penfield, G.T., Kring, D.A., Pilkington, M., Camargo, Z.A., Jacobsen, S.B., Boynton, W.V., 1991. Chicxulub crater: a possible Cretaceous/Tertiary boundary impact crater on the Yucatan Peninsula, Mexico. *Geology* 19, 867–871.
- Hofker, J., 1953. Types of genera described in Part III of the "Siboga Foraminifera". *Micropaleontologist* 7 (1), 26–28.
- Hofker, J., 1978. Analysis of a large succession of samples through the Upper Maastrichtian and the Lower Tertiary of Drill Hole 47.2, Shatsky Rise, Pacific, Deep Sea Drilling project. *J. Foramin. Res.* 8, 46–75.
- Huber, B.T., Olsson, R.K., Pearson, P.N., 2006. Taxonomy, biostratigraphy, and phylogeny of Eocene microperforate Planktic foraminifera (*Jenkinsina*, *Cassigerinelloita*, *Chiloguembelina*, *Streptochilus*, *Zeauvigerina*, *Tenuitella*, and *Cassigerinella*) and *Problematica* (*Dipsidripella*). In: Pearson, P.N., Olsson, R.K., Huber, B.T., Hemleben, C., Berggren, W.A. (Eds.), *Atlas of Eocene Planktic Foraminifera*, vol. 41. Cushman Foundation Special Publication, Virginia, U.S.A., pp. 461–508.
- Jenkins, D.C., Whittaker, J.E., Curry, D., 1998. Palaeogene triserial planktic foraminifera. *J. Micropaleontol.* 17, 61–70.
- Khalilov, D.M., 1956. O pelagicheskoy faune foraminifer Paleogenovykh otlozheniy Azerbaydzana. *Trudy Inst. Geol., Akad. Nauk Azerbaydzanskoy S.S.R.*, Baku. 17, 234–261.
- Kline, V.H., 1943. Clay County fossil: Midway foraminifera and ostracoda. *Miss. State*

- Geol. Surv. Bull. 53, 1–98.
- Koutsoukos, E.A., 2014. Phenotypic plasticity, speciations, and phylogeny in Early Danian planktic foraminifera. *J. Foramin. Res.* 44 (2), 109–142.
- Kroon, D., Nederbragt, A.J., 1990. Ecology and paleoecology of triserial planktic foraminifera. *Mar. Micropaleontol.* 16 (1–2), 25–38.
- Li, Q., 1987. Origin, phylogenetic development and systematic taxonomy of the *Tenuitella* plexus (Globigerinidae, Globigerinina). *J. Foramin. Res.* 17, 295–320.
- Li, Q., Radford, S.S., 1991. Evolution and biogeography of Paleogene microporiferate planktonic foraminifera. *Palaeogeogr. Palaeoclimatol. Palaeoecol.* 83 (1–3), 87–115.
- Li, Q., Sally, S., Radford, S.S., Banner, F.T., 1992. Distribution of microporiferate Tenuitellid planktonic foraminifers in Holes 747a and 749b, Kerguelen Plateau. *Proc. Ocean Drill. Program Sci. Res.* 120, 569–594.
- Liu, C., Olsson, R.K., 1992. Evolutionary radiation of microporiferate planktonic foraminifera following the K/T mass extinction event. *J. Foramin. Res.* 22 (4), 328–346.
- Loeblich Jr., A.R., Tappan, H., 1956. *Chiloguembelina*, a new tertiary genus of heterohelicidae (foraminifera). *J. Wash. Acad. Sci.* 46, 39–40.
- Loeblich Jr., A.R., Tappan, H., 1957. Planktonic foraminifera of Paleocene and early Eocene age from the Gulf and Atlantic coastal plains. *B. U. S. Nat. Mus.* 215, 173–198.
- Loeblich Jr., A.R., Tappan, H., 1984. Suprageneric classification of the Foraminifera (Protozoa). *Micropaleontology* 30, 1–70.
- Loeblich Jr., A.R., Tappan, H., 1987. Foraminiferal General and Their Classification, vol. 2. Van Nostrand Reinhold Company, New York, 970 pp., 847 pls.
- Longoria, J.F., 1974. Stratigraphic, morphologic and taxonomic studies of Aptian planktic foraminifera. *Rev. Esp. Micropaleontol. Extr. Number* 11–107.
- Luterbacher, H.P., Premoli Silva, I., 1964. Biostratigraphia del limite Cretaceous-Terciario nell Apennino Centrale [Biostratigraphy of the Cretaceous-Tertiary boundary in Central Apennines]. *Riv. Ital. Paleontol. S.* 70, 67–128. Italian.
- MacLeod, N., 1993. The Maastrichtian-Danian radiation of triserial and biserial planktic foraminifera: testing phylogenetic and adaptational hypotheses in the (micro) fossil record. *Mar. Micropaleontol.* 21, 47–100.
- Molina, E., Arenillas, I., Arz, J.A., 1998. Mass extinction in planktic foraminifera at the Cretaceous/Tertiary boundary in subtropical and temperate latitudes. *B. Soc. Geol. Fr.* 169 (3), 351–363.
- Molina, E., Alegret, L., Arenillas, I., Arz, J.A., Gallala, N., Hardenbol, J., von Salis, K., Steurbaut, E., Vandenberghe, N., Zaghbib-Turki, D., 2006. The global stratotype section and point of the Danian stage (Paleocene, Paleogene, “Tertiary”, Cenozoic) at El Kef, Tunisia: original definition and revision. *Episodes* 29 (4), 263–278.
- Molina, E., Alegret, L., Arenillas, I., Arz, J.A., Gallala, N., Grajales-Nishimura, M., Murillo-Muneton, G., Zaghbib-Turki, D., 2009. The global boundary stratotype section and point for the base of the Danian stage (Paleocene, Paleogene, “Tertiary”, Cenozoic): auxiliary sections and correlation. *Episodes* 32 (2), 84–95.
- Morozova, V.G., 1959. Stratigrafiya Datsko-Montskikh otlozhenii Kryma po foraminiferam (Stratigraphy of the Danian-Montian deposits of the Crimea according to the foraminifera). *Dokl. Akad. Nauk SSSR* 124, 1113–1116 [In Russian].
- Morozova, V.G., 1961. Datsko-Montskikh planktonnye foraminifery yuga SSSR: Paleontologicheskii Zhurnal, 1, 8–19.
- Nederbragt, A.J., 1991. Late Cretaceous biostratigraphy and development of Heterohelicidae (planktic foraminifera). *Micropaleontology* 37, 329–372.
- Olsson, R.K., 1960. Foraminifera of latest Cretaceous and earliest Tertiary age in the New Jersey Coastal Plain. *J. Paleontol.* 34, 1–58.
- Olsson, R.K., 1970. Planktonic foraminifera from base of tertiary, Millers Ferry, Alabama. *J. Paleontol.* 44, 598–604.
- Olsson, R.K., Hemleben, C., Berggren, W.A., Huber, B.T., 1999. Atlas of paleocene planktonic foraminifera. *Smithson. Contrib. Paleobiol.* 85, 1–252.
- Olsson, R.K., Hemleben, C., Berggren, W.A., Liu, C., 1992. Wall texture classification of planktonic foraminifera genera in the Lower Danian. *J. Foramin. Res.* 22, 195–213.
- Pandey, J., 1981. Cretaceous foraminifera of Um Sohryngkew River section, Meghalaya. *J. Paleontol. Soc. India* 25, 53–74.
- Pardo, A., Keller, G., 2008. Biotic effects of environmental catastrophes at the end of the cretaceous and early tertiary: *Guembelitria* and *Heterohelix* blooms. *Cretac. Res.* 29, 1058–1073.
- Punekar, J., Mateo, P., Keller, G., 2014. Effects of Deccan volcanism on paleoenvironment and planktic foraminifera: a global survey. *GSA Spec. Pap.* 505. [http://dx.doi.org/10.1130/214.2505\(04\)](http://dx.doi.org/10.1130/214.2505(04)).
- Salaj, J., 1986. The new *Postrugoglobigerina praedaubjergensis* Zone at the base of the stratotype of the marine Paleocene (El Kef, Tunisia). *Geol. Zb. Geol. Carpath. Bratisl.* 37, 35–58.
- Schoene, B., Samperton, K.M., Eddy, M.P., Keller, G., Adatte, T., Bowring, S.A., Khadri, S.F.R., Gerch, B., 2015. U-Pb geochronology of the Deccan Traps and relation to the end-Cretaceous mass extinction. *Science* 347 (6218), 182–184.
- Schulte, P., Alegret, L., Arenillas, I., Arz, J.A., Barton, P.J., Bown, P.R., Bralower, T.J., Christeson, G.L., Claeys, P., Cockell, C.S., Collins, G.S., Deutsch, A., Goldin, T.J., Goto, K., Grajales-Nishimura, J.M., Grieve, R.A.F., Gulick, S.P.S., Johnson, K.R., Kiessling, W., Koeberl, C., Kring, D.A., MacLeod, K.G., Matsui, T., Melosh, J., Montanari, A., Morgan, J.V., Neal, C.R., Norris, R.D., Pierazzo, E., Ravizza, G., Rebolledo-Vieyra, M., Reimold, W.U., Robin, E., Salge, T., Speijer, R.P., Sweet, A.R., Urrutia-Fucugauchi, J., Vajda, V., Whalen, M.T., Willumsen, P.S., 2010. The Chicxulub asteroid impact and mass extinction at the Cretaceous-Paleogene boundary. *Science* 327 (5970), 1214–1218.
- Smit, J., 1982. Extinction and evolution of planktonic foraminifera after a major impact at the Cretaceous/Tertiary boundary. *GSA Spec. Pap.* 190, 329–352.
- Smit, J., 1990. Meteorite impact, extinctions and the cretaceous-tertiary boundary. *Geol. Mijnb.* 69, 187–204.
- Tappan, H., 1940. Foraminifera from the Grayson Formation of northern Texas. *J. Paleontol.* 14, 93–126.
- Tyszka, J., 2006. Morphospace of foraminiferal shells: results from the moving reference model. *Lethaia* 39, 1–12.
- Voloshina, A.M., 1961. Nekotorye novye vidy Verkhhemelovkykh foraminifer Volyno-Podol'skoy plity (Some new species of Upper Cretaceous foraminifera from the Volhyn–Podol platform). *Paleontologicheskii Sbornik (L'vov)* 1, 71–81 [In Russian].

**4.2. Blooms of aberrant planktic foraminifera across the K/Pg boundary in the Western Tethys: causes and evolutionary implications.**

Arenillas, I., Arz, J. A., **Gilbert**, V., 2018. Blooms of aberrant planktic foraminifera across the K/Pg boundary in the Western Tethys: causes and evolutionary implications. *Paleobiology* 44, (3), 460–489. <https://doi.org/10.1017/pab.2018.16>.

El material suplementario de este artículo se encuentra en el apartado Anexos (Anexo I).

# Blooms of aberrant planktic foraminifera across the K/Pg boundary in the Western Tethys: causes and evolutionary implications

*Ignacio Arenillas, José A. Arz, and Vicente Gilabert*

**Abstract.**—We report a detailed study of the different categories and types of abnormal morphologies in planktic foraminifera recognizable in the lowermost Danian, mainly from the El Kef and Ain Settara sections, Tunisia. Various types of abnormalities in the test morphology were identified, including protuberances near the proloculus, abnormal chambers, double or twinned ultimate chambers, multiple ultimate chambers, abnormal apertures, distortion in test coiling, morphologically abnormal tests, attached twins or double tests, and general monstrosities. Detailed biostratigraphic and quantitative studies of the Tunisian sections documented a major proliferation of aberrant planktic foraminifera (between approximately 5% and 18% in relative abundance) during the first 200 Kyr of the Danian, starting immediately after the Cretaceous/Paleogene (K/Pg) boundary mass extinction (spanning from the *Guembelitra cretacea* Zone to the lower part of the *P. pseudobulloides* Zone). This contrasts with the proportionately low frequency of aberrant tests (generally <2%) identified within the uppermost Maastrichtian, suggesting more stable environmental conditions during the last ~50–100 Kyr of the Cretaceous. Two main pulses with abundant aberrant tests were recognized in the earliest Danian, the one recorded in the well-known K/Pg boundary clay being the more intense of those (maxima of >18%). These main pulses of aberrants coincide approximately with relevant quantitative and evolutionary turnovers in the planktic foraminiferal assemblages. In this paper, we explore the relation of these high values of the foraminiferal abnormality index with the environmental changes induced by the meteorite impact of Chicxulub in Yucatan, Mexico, and the massive eruptions of the Deccan Traps, India.

*Ignacio Arenillas, José A. Arz, and Vicente Gilabert. Departamento de Ciencias de la Tierra and Instituto Universitario de Investigación en Ciencias Ambientales de Aragón, Universidad de Zaragoza, E-50009, Spain. E-mail: ias@unizar.es*

Accepted: 3 April 2018

Published online: 13 July 2018

Data available from the Dryad Digital Repository: <https://doi.org/10.5061/dryad.n1q6527>

## Introduction

Asteroid impacts represent an extreme among natural disasters, inducing rapid and sharp environmental perturbations with important implications for the biosphere (Alvarez et al. 1992; Toon et al. 1997). After the Chicxulub asteroid impact (Yucatan, Mexico) at the Cretaceous/Paleogene (K/Pg) boundary (Hildebrand et al. 1991), a cloud of dust and fine ejecta scattered and contaminated the atmosphere, land, and oceans (Alvarez et al. 1980; Smit and Hertogen 1980). The cloud of pulverized impact material at Chicxulub was deposited slowly (probably over a few years), forming a thin (few millimeters) airfall layer evident in deep-marine sediments worldwide, with anomalous concentrations of iridium and other platinum-group metals, nickel-rich spinels, shocked quartz, and altered microtektites (Smit 1990;

Robin et al. 1991). The Chicxulub impact caused the blockage of sunlight, the inhibition of the photosynthesis, disruption of food chains, a sudden drop in global temperature, destruction of the ozone layer, and the production of toxins and acid rain (Smit and Romein 1985; Hsü and McKenzie 1985; Pope et al. 1997; Gerasimov 2002; Ocampo et al. 2006; Alegret et al. 2012; Bardeen et al. 2017), initiating one of the greatest mass extinctions in the history of life (Schulte et al. 2010).

In the earliest Danian oceans, a dark-clay bed was deposited above the K/Pg airfall layer under conditions of global climatic warming and alterations in oceanic productivity (Hsü and McKenzie 1985; D'Hondt et al. 1998; D'Hondt 2005; Coxall et al. 2006; Birch et al. 2016), with some regions showing a sharp decline in export productivity during approximately 2 Myr, and others a constant or rapidly reestablished



organic flux from the surface ocean to the deep seafloor (Hull and Norris 2011).

The dark-clay bed also contains high concentrations of heavy metals, which, though lower than in the airfall layer, are higher than in the sediments of the upper Maastrichtian and more modern lower Danian (Smit and ten Kate 1982; Dupuis et al. 2001; Hollis et al. 2003). The paleoenvironmental conditions recorded in the dark-clay bed seem therefore to reflect the long-term disruptive effects of the K/Pg impact event, revealing a time in which the ecosystems were starting to recover and ocean productivity to re-establish itself.

Planktic foraminifera, like other paleontological groups, suffered considerable, but not complete, extinction at the K/Pg boundary event (Smit 1982). The cause–effect relationship between the Chicxulub impact and the K/Pg mass extinction has been amply verified (see Smit 1990, 1999; Arenillas et al. 2000b, 2006), and the impact theory is correspondingly well established in the scientific community (Schulte et al. 2010). However, other evidence seems to suggest that the massive eruptions of the Deccan Traps, India, could have played an important role in the extinction, or at least in the paleoenvironmental changes that occurred during the Cretaceous/Paleogene transition (Courtilot et al. 1988; Chenet et al. 2007, 2009; Keller et al. 2011, among others). Recently, Schoene et al. (2015) has applied uranium-lead (U-Pb) zircon geochronology to Deccan rocks, showing three main eruptive phases or megapulses, the main one (phase 2) beginning approximately 250 Kyr before K/Pg boundary and lasting 750 Kyr.

The Deccan megapulses have been related to episodes of global warming and/or environmental stress across the K/Pg boundary (Keller and Pardo 2004; Pardo and Keller 2008; Punekar et al. 2014, 2016). Keller et al. (2011) proposed that phase 2 (responsible for ca. 80% of the total volume of Deccan Traps emissions) ended at or near the K/Pg boundary, spanning the last 280 Kyr of the Maastrichtian. Deccan-induced global warming and cooling episodes at the late Maastrichtian seem to be responsible for dwarfing episodes in some planktic foraminiferal species (Keller and Abramovich 2009; Omaña et al. 2012; Petersen et al. 2016), migrations (Olsson et al. 2001), and regional

assemblage changes (Keller 2003), however, without a significant decrease in global planktic foraminiferal diversity (Arenillas et al. 2000a,b). After the K/Pg boundary, small species began to appear following a model of “explosive” adaptive radiation (Smit 1982; Brinkhuis and Zachariasse 1988; Arenillas et al. 2002, 2004). One of the ancestors of the first Danian species was the opportunistic, triserial genus *Guembelitra*, which might be the only true survivor (Smit 1982, 2004). However, the main lineages of planktic foraminifers appearing in the Danian, whose descendants have reached the present day, could have a benthic origin (see Brinkhuis and Zachariasse 1988; Arenillas and Arz 2017). It must be emphasized that there are other relevant taxonomic and phylogenetic models, some of them highly supported among planktic foraminifer taxonomists. Among the most noteworthy proposals are those of Olsson et al. (1999), Apellaniz et al. (2002), Aze et al. (2011), and Koutsoukos (2014), which suggest that the genus *Muricohedbergella* was a survivor of the K/Pg extinction event and played an important phylogeny role for being the ancestral form of Danian genera such as *Globanomalina*, *Eoglobigerina*, and/or *Praemurica*.

Abnormal tests have long been reported in recent benthic foraminifera linked to regions with either high environmental variability (e.g., Polovodova and Schonfeld 2008; Ballent and Carignano 2008) or human-induced pollution (e.g., Yanko et al. 1998; Samir and El Din 2001; Frontalini and Coccioni 2008), showing that abnormal variations in morphology are a response to changes in ecological parameters such as temperature, pollution, carbonate solubility, dissolved oxygen, or the occurrence of rapid environmental fluctuations. The long-term effects of Chicxulub impact and the Deccan eruptions probably triggered similar ecological stress conditions, thus inducing similar malformations in planktic foraminiferal tests. Indeed, abnormal planktic foraminifers have been reported right above the K/Pg boundary, mainly in *Guembelitra* (Coccioni and Luciani 2006). Similar increases in abnormal planktic tests have been observed in warming episodes and episodes of ecological stress, such as the Cretaceous ocean anoxic events (Verga and Premoli Silva 2002) or the Paleocene–Eocene

Thermal Maximum (Luciani et al. 2007). However, studies on the aberrant planktic foraminifers of the K/Pg transition from a taxonomic and paleoenvironmental point of view are still very limited and fragmented.

Abnormalities are formed when the ontogenetic plan of the test is disrupted and this disruption generates an irregular shape in comparison with other specimens of the same species (Murray 2006). In recent foraminifera, abnormalities produced during the life and growth of an individual may be due either to mechanical or ecological causes (Boltovskoy and Wright 1976; Murray 2006). In the case of planktic foraminifera, the causes behind test abnormalities may be predation breakages, but abnormal planktic specimens seem to reflect mainly stressful environmental conditions (Montgomery, 1990; Luciani et al. 2007). In addition, abnormalities can also be produced by mutations. The phenotypic consequences of mutations can vary, but in the case of fossil foraminifera, the most interesting ones are those that affect the test morphology. Mutations can cause lethal or physiologically nonfeasible aberrations, but could have also generated new species, probably bringing on the early Danian evolutionary radiation mentioned earlier (Bou-Dagher-Fadel 2012; Arenillas et al. 2016).

In this paper, a wide variety of morphological abnormalities in planktic foraminiferal tests from the earliest Danian are described for the first time, mainly from Tunisian sections. We use a quantitative approach to identify changes in the abundance of aberrant tests and correlate them with evolutionary radiations and other shifts recognized in the planktic foraminiferal assemblages across the K/Pg boundary. The main aim is to inquire into the causes that could have triggered the proliferation of aberrant tests before and after the K/Pg boundary mass extinction, and the relation of these causes with the environmental changes induced by the Deccan eruptions and the Chicxulub impact.

### Material and Methods

*Geological Context and Micropaleontological Sampling.*—We studied samples from localities considered to be the most expanded and

continuous marine K/Pg sections worldwide, such as El Kef, Aïn Settara, and Elles (Tunisia), and Agost and Caravaca (Spain). The El Kef section was chosen to define the Global Boundary Stratotype Section and Point (GSSP) for the base of the Danian stage, or the K/Pg boundary (Molina et al. 2006), while Caravaca, Elles, and Aïn Settara were chosen as auxiliary sections of the GSSP (Molina et al. 2009). The K/Pg boundary is defined at the base of the bed informally known as the “K/Pg boundary clay,” specifically at the base of the 2- to 5-mm-thick airfall layer with high concentrations of iridium that coincides with the planktic foraminiferal extinction horizon (Smit 1990, 1999). The dark-clay bed overlying the K/Pg airfall layer is approximately 100 cm thick in El Kef, with a 50-cm-thick blackish clay overlain by a 50-cm-thick dark gray clay; it continues with 1-m-thick darkened gray marly clay and 60-cm-thick clayey marl, so the dark-clay bed thickness could be 200 cm or more in El Kef. It is characterized by low values of  $\delta^{13}\text{C}$  and  $\text{CaCO}_3$  content and high total organic carbon (TOC) values (Keller and Lindinger 1989). In Aïn Settara, the airfall layer is 5 to 10 mm thick, and the dark-clay bed is approximately 50 cm thick; this is also characterized by low values of  $\delta^{13}\text{C}$  and in  $\text{CaCO}_3$  content and high TOC values (Dupuis et al. 2001).

For the taxonomic studies, specimens were picked mainly from El Kef and Aïn Settara, where the foraminiferal test preservation is good (excellent at some samples), although specimens from other sections (Elles, Agost, and Caravaca) were used with the aim of conveniently illustrating some of the species and types of normal and abnormal growth morphologies identified in the lower Danian. Specimens considered to be normal forms are those that conform to some type of shape within the theoretical three-dimensional morphospace of serial and spiral foraminiferal tests proposed by Tyszka (2006). Taxonomic remarks and a systematic scheme for the normal forms of early Danian planktic foraminiferal species are provided in Supplementary Appendix A and Supplementary Figure 1.

All rock samples studied were disaggregated in water with diluted  $\text{H}_2\text{O}_2$ ,

washed through a 63  $\mu\text{m}$  sieve, and then oven-dried at 50°C. The quantitative analyses were based on representative splits (using a modified Otto microsplitter) of approximately 300 specimens per sample, quantifying the relative abundance of both normal and abnormal tests in each group of planktic foraminifera (Tables 1, 2). For the quantitative study, we restudied 39 samples from El Kef and 35 samples from Ain Settara (see Arenillas et al. 2000a, b). The specimens analyzed were mounted on microslides for a permanent record and identification. Planktic foraminifera were picked from the residues and selected for scanning electron microscopy (SEM), using the JEOL JSM 6400 and Zeiss MERLIN FE-SEM of the Electron Microscopy Service of the Universidad de Zaragoza (Spain). SEM photographs of the species considered here are provided in Supplementary Figures 2 and 3. For the illustration of these species, we used, in addition to El Kef and Ain Settara, other localities characterized by the good preservation of their foraminiferal tests, such as Ben Gurion (Israel), Deep Sea Drilling Project (DSDP) Site 305 (North Pacific), and Bajada del Jagüel (Argentina).

*Planktic Foraminiferal Biochronology.*—For the Maastrichtian, the biostratigraphic and quantitative study focused mainly on the *Plummerita hantkeninoides* Subzone, which spans the last 140 Kyr of the Cretaceous according to Husson et al. (2014). This biozone is defined by the total range of the nominate taxon and is equivalent to the alphanumeric Zone CF1 of Li and Keller (1998). For the lower Danian, we used the biozonation of Arenillas et al. (2004), and compared it with those of Li and Keller (1998) and Berggren and Pearson (2005) (the latter recently revised by Wade et al. 2011). Their equivalences are shown in Figure 1. The former is based on continuous, complete, and very expanded Tunisian and Spanish K/Pg sections such as El Kef, Ain Settara, Elles, Caravaca, Agost, and Zumaia. It includes six subbiozones: the *Muricohedbergella holmdelensis* and *Parvularugoglobigerina longiapertura* Subzones of the *Guembelitra cretacea* Zone, the *Parvularugoglobigerina sabina* and *Eoglobigerina simplicissima* Subzones of the *Pv. eugubina* Zone, and the *Eoglobigerina trivialis* and *Subbotina*

*triloculimoides* Subzones of the *P. pseudobulloides* Zone. The species ranges illustrated in Figure 1 are based on the stratigraphic distributions verified mainly in the El Kef stratotypic section. Note that the *Mh. holmdelensis* Subzone is equivalent to Zone P0 of Li and Keller (1998) and Berggren and Pearson (2005), whereas Zone P $\alpha$  (or P1a of Li and Keller 1998) spans approximately the *Pv. longiapertura*, *Pv. sabina*, and *E. simplicissima* Subzones.

Arenillas et al. (2004) calibrated numerical ages of the biozonal boundaries on the basis of biostratigraphic and magnetostratigraphic data from Agost, Spain, and the timescale of Röhl et al. (2001), who astronomically calibrated the C29r/C29n reversal at 255 Kyr after the K/Pg boundary. Subsequent radiometric, paleomagnetic, and astronomical dating/calibrations have given different results for the age of the K/Pg boundary as well as the duration of the magnetozones. Taking into account the Geologic Time Scale 2012 (GTS12; Gradstein et al. 2012), which gives an age for the C29r/C29n boundary of 352 Kyr after the K/Pg boundary, the *Mh. holmdelensis* Subzone would span the first 7 Kyr after the K/Pg boundary, the *Pv. longiapertura* Subzone from 7 to 25 Kyr, the *Pv. sabina* Subzone from 25 to 46 Kyr, the *E. simplicissima* Subzone from 46 to 79 Kyr, the *E. trivialis* Subzone from 79 to 282 Kyr, and the *S. triloculimoides* Subzone from 282 to 616 Kyr.

High-resolution quantitative studies of Tethyan sections make it possible to recognize three planktic foraminiferal acme-stages (PFAS) of high biochronological interest across the lowermost Danian in pelagic (oceanic and outer neritic) environments (see Arenillas et al. 2006): PFAS-1, dominated by the triserial *Guembelitra*; PFAS-2, dominated by tiny trochospiral, informally denominated parvularugoglobigerinids (*Parvularugoglobigerina* and *Palaeoglobigerina*); and PFAS-3, dominated by biserial *Woodringina* and *Chiloguembelina*. Following the GTS12, PFAS-1 would span the first 18 Kyr after the K/Pg boundary, PFAS-2 approximately from 18 to 62 Kyr, and PFAS-3 from 62 Kyr on. A second acme of triserials is identified in the lower part of PFAS-3, that is, in the transition between the *Pv. eugubina* and *P. pseudobulloides* Zones (Arenillas et al.

TABLE 1. Relative abundance (%) of planktic foraminiferal groups considered here and rates of aberrants at the El Kef section. Values for the hypotheses of both pattern A and pattern B are included. *A. m.*, *Abathophialus mayaroensis* Zone; *P. h.*, *Plummerita hantkeninoides* Subzone; *H. p.*, *Heterohelix* predominance; *P. e.*, *Parvularugoglobigerina eugubina* Zone; *P. s.*, *Parvularugoglobigerina sabina* Subzone. Samples are presented in centimeters below (–) and above (+) the K/Pg boundary. x, relative abundance <0.3%.

		El Kef															
		Maastrichtian															
Stage																	
Zone		<i>Abathophialus mayaroensis</i>															
Subzone		<i>Plummerita hantkeninoides</i>															
Acme-stage		<i>Heterohelix</i> predominance															
Sample		-1200	-1050	-900	-750	-540	-400	-250	-175	-135	-100	-70	-40	-20	-3		
Total number of counted specimens		330	345	324	341	350	340	320	343	306	321	329	373	335	329		
% Maastrichtian species		98.2	97.9	96.6	95.9	97.4	98.8	99.1	97.7	99.7	97.8	99.1	98.2	99.7	98.8		
% triserial		1.8	2.1	3.4	4.1	2.6	1.2	0.9	2.3	0.3	2.2	0.9	1.8	0.3	1.2		
Total number of aberrants		3	4	4	6	2	0	1	2	1	2	2	2	1	0		
FAI (aberrant rate in %)		0.9	1.2	1.2	1.8	0.6	0.6	0.3	0.6	0.3	0.6	0.6	0.5	0.5	0.3		
% other Maastrichtian aberrants		0.9	1.2	1.2	1.5	0.6	0.3	0.3	0.6	0.3	0.6	0.6	0.6	0.5	0.3		
% triserial aberrants					0.3												
Hypothesis of pattern A																	
Stage		Maastrichtian															
Zone		<i>A. m.</i>															
Subzone		<i>P. h.</i>															
Acme-stage		<i>H. p.</i>															
		Barren interzone (airfall layer)															
		PFAS-1															
		PFAS-2															
Sample		0	+0.1	+2	+7	+17	+37	+67	+97	+122	+147	+172	+197				
Total number of counted specimens		325		303	309	320	303	294	130	101	336	340	354				
% other Maastrichtian species		98.8		83.1	83.0	45.1	10.3	2.7	7.4	3.9	4.8	0.9	0.6				
% triserial		1.2		16.9	17.0	54.9	89.7	87.0	66.7	80.3	69.8	27.0	7.8				
% parvularugoglobigerinids						x	x	9.5	21.8	15.6	26.4	71.0	91.9				
% Danian biserial		1		1	7	25	41	55	23	9	27	37	38				
Total number of aberrants		0.3		0.3	2.3	7.8	13.5	18.7	17.7	8.9	8.0	10.9	10.7				
FAI (aberrant rate in %)		0.3		0.3	0.3	1.9	7.8	13.5	17.7	9.2	6.9	4.8	3.5				
% other Maastrichtian aberrants		0.3		0.3	1.9	7.8	13.5	17.7	1.0	8.5	2.0	3.3	7.4				
% triserial aberrants																	
% parvularugoglobigerinid aberrants																	
		Maastrichtian															
		<i>A. m.</i>															
		<i>P. h.</i>															
		<i>H. p.</i>															
		Danian															
		<i>Guembelitra cretacea</i>															
		<i>Parvularugoglobigerina longiapertura</i>															
		<i>P. s.</i>															



TABLE 1. CONTINUED

Stage	Danian													
	<i>Parvularugoglobigerina eugubina</i>						<i>Parasubbotina pseudobulloides</i>							
Subzone	<i>P. s.</i>		<i>Eoglobigerina simplicissima</i>		<i>Eoglobigerina tritialis</i>		<i>Subbotina triloculinoidea</i>							
Acme-stage	PFAS-2						PFAS-3							
Sample	+ 247	+ 297	+ 372	+ 447	+ 547	+ 647	+ 747	+ 847	+ 922	+ 992	+ 1107	+ 1197	+ 1277	+ 1347
Total number of counted specimens	356	358	381	409	360	677	473	366	460	398	369	408	405	470
% other Maastrichtian species	x	0.8	0.6	1.7	0.3	1.1	1.0	1.1	3.5	1.1	0.6	0.6		
% triserial	8.6	4.5	2.9	3.5	1.2	31.1	59.9	54.3	28.3	18.5	7.0	3.6	4.6	7.4
% parvularugoglobigerinids	90.3	70.1	70.1	53.5	11.6	7.7	0.2	0.5	0.4					
% Danian biserial	1.4	23.7	17.0	28.3	77.6	53.9	36.1	41.1	53.8	56.9	59.5	59.3	62.2	55.3
% other Danian species	26	11	27	33	30	67	52	32	22	19	14	13	10	17
Total number of aberrants	7.3	3.1	7.2	8.1	8.4	10.1	11.1	8.8	5.0	4.8	3.9	3.2	2.5	3.6
FAI (aberrant rate in %)	0.3	0.8	0.3	1.2	0.3	4.2	6.6	5.0	1.4	1.0	0.3	0.5		
% triserial aberrants	7.0	1.7	6.1	4.2	0.8	1.6	0.2	0.3						
% parvularugoglobigerinid aberrants														
% Danian biserial aberrants		0.6	0.8	2.0	6.4	3.9	4.3	3.6	2.9	2.5	3.0	1.5	2.0	2.3
% other Danian aberrants				0.7	0.8	0.3			0.7	1.3	0.6	1.2	0.5	1.3









2017). This acme has been attributed to the genus *Chiloguembelitra* Hofker, 1978, not *Guembelitra*, and spans approximately from 70 to 200 Kyr according to the GTS12.

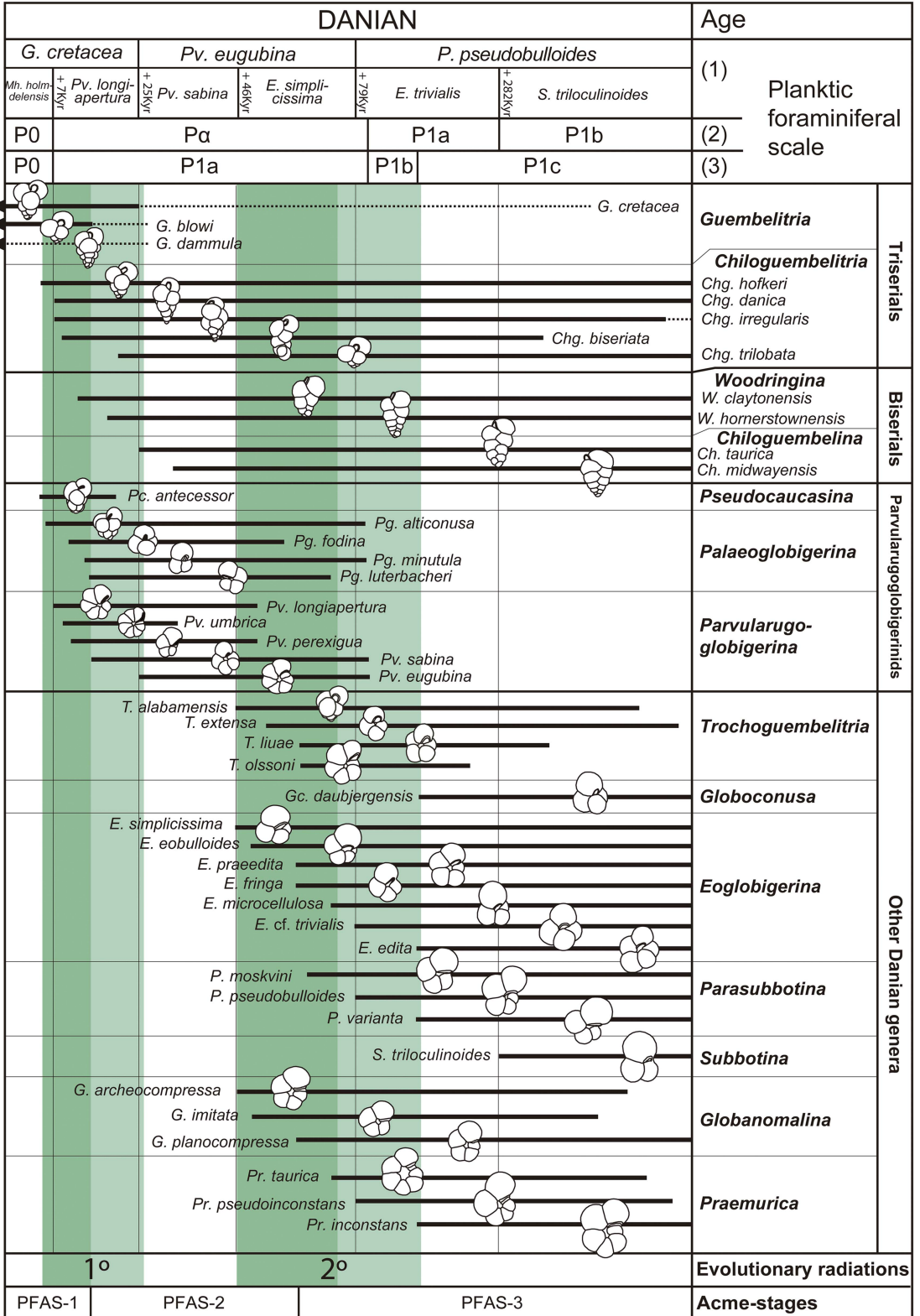
### Danian Planktic Foraminiferal Evolutionary Radiations

Many new species of trochospiral and biserial planktic foraminifers originated after the K/Pg boundary, as is shown in Figure 1 and described in Supplementary Appendix A. The systematic scheme in Supplementary Figure 1 is a good reflection of the morphological and textural diversity that appeared after the extinction event. As illustrated in Figure 1, the planktic foraminifera evolutionary radiation of the early Danian happened in two pulses (see also Arenillas et al. 2000a,b, 2017; Arenillas and Arz 2017). The first occurred between approximately 5 and 26 Kyr after the K/Pg boundary according to the GTS12, with the appearance of tiny, trochospiral species belonging to the parvularugoglobigerinids (*Pseudocaucasina*, *Palaeoglobigerina*, and *Parvularugoglobigerina*) and biserial taxa (*Woodringina* and *Chiloguembelina*), as well as triserial species of the genus *Chiloguembelitra* (Supplementary Figs. 1 and 2). The second evolutionary radiation occurred between approximately 46 and 110 Kyr after the K/Pg boundary according to the GTS12, giving rise to more ornamented, larger trochospiral species (Supplementary Figs. 1, 3) belonging to *Trochoguembelitra*, *Eoglobigerina*, *Parasubbotina*, *Globanomalina*, and *Praemurica*. Other genera appear shortly afterward, such as *Subbotina* and *Globoconusa*.

In the present work, the extinction and evolution of planktic foraminifers across the K/Pg boundary at the El Kef section were quantified using the evolutionary model proposed by Dean and McKinney (2001), which measures taxonomic turnovers using four metrics (Fig. 2): extinction rate ( $E_R$ ), speciation rate ( $N_R$ ), volatility ( $V$ ), and taxonomic flux ( $F$ ). Taxonomic flux  $F$  is used to estimate whether there are relative increases (positive values) or declines (negative values) in diversity. The volatility  $V$  indicates whether there is evolutionary stability (low values) or increased taxonomic turnover (high values). The method

developed by Dean and McKinney (2001), which is described in Supplementary Appendix B, was applied to the stratigraphic ranges of planktic foraminiferal species recognized in the El Kef section (Supplementary Fig. 4). The present quantification of the evolutionary pattern is an update of the one already made at El Kef by Arenillas et al. (2002), taking into account the taxonomic and biostratigraphic revisions made since then (see Supplementary Appendix A). The metrics were measured under two alternative hypotheses, as already proposed by Arenillas et al. (2002): (1) all 16 Cretaceous species identified in lower Danian levels are in situ (pattern A in Supplementary Table 1): *Muricohedbergella holmdelensis*, *Muricohedbergella monmouthensis*, *Heterohelix globulosa*, *Heterohelix planata*, *Heterohelix navarroensis*, *Heterohelix labellosa*, *Laeviheterohelix pulchra*, *Laeviheterohelix glabrans*, *Pseudoguembelina kempensis*, *Pseudoguembelina costulata*, *Globigerinelloides volutus*, *Globigerinelloides praeriedhillensis*, *Globigerinelloides yaucoensis*, *Guembelitra dammula*, *Guembelitra cretacea*, and *Guembelitra blowi* (see Supplementary Fig. 4); and (2) except for two *Guembelitra* species (*Guembelitra cretacea* and *Guembelitra blowi*), all Cretaceous species identified in lower Danian levels are reworked (pattern B in Supplementary Table 2).

According to these metrics, in both hypotheses (Fig. 2), four main evolutionary episodes were recognized: (1) an extremely high extinction rate coinciding with the catastrophic mass extinction at the K/Pg boundary; (2) a high speciation rate in the *Pv. longiapertura* Subzone coinciding with the first Danian evolutionary radiation, mainly of parvularugoglobigerinids; (3) a relatively high speciation rate in the *E. simplicissima* Subzone coinciding with the beginning of the second evolutionary radiation; and (4) a relatively high extinction rate in the basal part of the *E. trivialis* Subzone coinciding with the parvularugoglobigerinid extinction. Due to these evolutionary episodes, volatility is high at El Kef during approximately the first 200 Kyr of the Danian, which is also reflected by relevant fluctuations in the taxonomic flux. These data contrast with the extremely low volatility in the *P. hantkenioides* Subzone of the uppermost Maastrichtian (Fig. 2).



### Abnormal Specimens across the K/Pg Boundary

Our quantitative study of planktic foraminifers has revealed a strong proliferation of aberrant forms above the K/Pg boundary in the El Kef and Aïn Settara sections (Fig. 3). At El Kef, the abundance of aberrant tests (Foraminiferal Abnormality Index, or FAI) in PFAS-1 is as high as 18.7% of the total population of planktic foraminifera, of which almost 90% are abnormal forms of the triserial *Guembelitra*. At Aïn Settara, the abundance of aberrant forms in PFAS-1 reaches over 12%, of which almost 70% are aberrant tests belonging to *Guembelitra*. These data contrast with the total percentage of aberrant tests in studied Maastrichtian samples (Tables 1, 2), which almost never exceeds 2.5% in either section (except for the basal part of the Aïn Settara section, whose FAI is as high as 3.4–3.6%). These include a few aberrant specimens, mainly of *Heterohelix* and *Pseudoguembelina*.

These percentages increase if we assume that the Maastrichtian specimens found in Danian horizons are reworked (pattern B hypothesis), except for two *Guembelitra* species (curves with black shading in Fig. 3). In this case, the FAI in PFAS-1 reaches almost 20% in El Kef and 18% in Aïn Settara. It should be noted that, except for *Guembelitra*, the percentages of other aberrant Maastrichtian specimens in the Danian are similar to those estimated for Maastrichtian horizons (Tables 1, 2), in contrast with the strong increase in aberrant tests among the Danian *Guembelitra* specimens within the dark-clay bed. This suggests that all these Maastrichtian specimens (aberrants and non-aberrants alike) are in fact reworked. A high-resolution biostratigraphic analysis at the Moncada section, Cuba, revealed that, with the exception of *Guembelitra* species, there

were no cosmopolitan, generalist Cretaceous species in the lowermost Danian deposits, not even in Zone P0 and the dark-clay bed (Arenillas et al. 2016). This evidence led the authors to suggest that the planktic foraminiferal mass extinction at the K/Pg boundary was more severe and catastrophic than previously suggested and that the presence of Cretaceous species within the lowermost Danian deposits at most K/Pg localities may be the result of normal reworking/bioturbation processes worldwide (see also Huber 1996; Kaiho and Lamolda 1999; Huber et al. 2002). In any case, whether we consider the pattern A hypothesis or that of pattern B, the abundance curves indicate similar trends (Fig. 3).

Aberrant *Guembelitra* specimens have frequently been classified as *Guembelitra irregularis* (e.g., Coccioni and Luciani 2006). This species has no doubt been used as a “wastebasket” taxon that also includes the aberrant forms of both Maastrichtian and Danian guembelitriids (see discussion in Arz et al. 2010). However, we consider here that *irregularis* is a genuine Danian species, including normal triserial forms (see Supplementary Fig. 1), because the abnormal morphologies among guembelitriids are of another kind. Arenillas et al. (2017) attributed *irregularis* to the genus *Chiloguembelitra* instead of *Guembelitra*, on the basis of differences in the wall texture and position of the aperture. *Chiloguembelitra irregularis* groups Danian specimens with twisted triserial arrangements of irregular appearance, corresponding to the irregular morphophase of the model of Tyszka (2006). Nevertheless, if these specimens are also counted as abnormal forms, then the FAI during the earliest Danian is even more anomalous, reaching more than 23% in PFAS-1 at El Kef, according to the pattern B hypothesis (Fig. 3).

FIGURE 1. Biostratigraphic ranges of the early Danian species analyzed, based mainly on the El Kef and Aïn Settara sections, Tunisia; (1) planktic foraminiferal zonation and calibrated numerical ages of the biozonal boundaries proposed by Arenillas et al. (2004); (2) and (3) zonations of Berggren and Pearson (2005) and Li and Keller (1998), respectively; intervals with green shading indicate the first and second evolutionary radiations of the early Danian at El Kef (the shading in dark green indicates high speciation rates; see online version for color); dotted lines indicate uncertain ranges in the case of *Guembelitra* species (*G. cretacea*, *G. blowi*, and *G. dammula*) in the lower Danian, because these may actually correspond to reworked specimens and/or the ranges of morphologically similar species of *Chiloguembelitra* (*Chg. danica*, *Chg. trilobata*, and *Chg. hofkeri*, respectively). PFAS, planktic foraminiferal acme-stage.

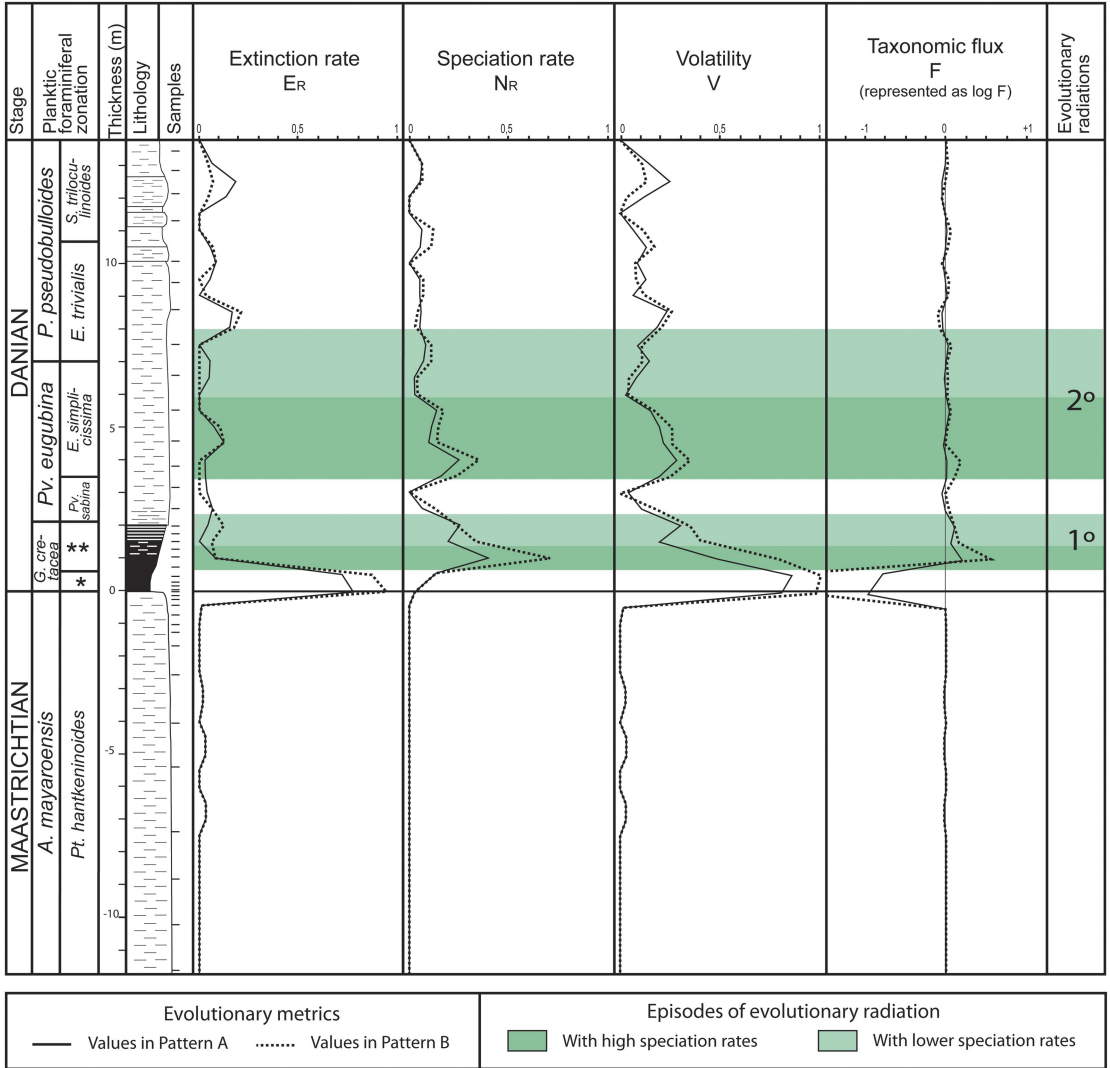


FIGURE 2. Evolutionary metrics (extinction and speciation rates, volatility, and taxonomic flux) at El Kef according to the model of Dean and McKinney (2001); solid line, hypothesis of pattern A; dotted line, hypothesis of pattern B; green shading, episodes of evolutionary radiation, with shading in dark green to indicate high speciation rates (see online version for color). \**Mh. holmdelensis* Subzone (= Zone P0); \*\**Pv. longiapertura* Subzone.

During the episode PFAS-1, abnormalities are frequent in all planktic foraminiferal groups, suggesting that ecological stress affected all pelagic environments during the early Danian. The FAI in the upper PFAS-1 is high not only in guembeltriids but also in parvarugoglobigerinids; for example, almost 40% of parvarugoglobigerinid specimens from the sample at 97 cm above the K/Pg boundary at El Kef have some type of abnormality. Subsequently, the abundance of aberrant tests decreases during PFAS-2 but

remains relatively high in both El Kef and Ain Settara, at around 3–10% (in both patterns A and B), suggesting that the environmental conditions remained unstable tens of thousands of years after the K/Pg boundary. Another increase in the FAI has been recognized across the boundary between the *Pv. eugubina* and *P. pseudobulloides* Zones (mainly in the *E. trivialis* Subzone, or Subzone P1a), rising to a maximum of 11% (in both patterns A and B) in El Kef and Ain Settara (Fig. 3). The increase in aberrant forms is more evident

among triserial and biserial specimens of the genera *Chiloguembelitra*, *Woodringina*, and *Chiloguembelina*. This interval coincides with the second bloom of triserials in the lower part of PFAS-3 (Fig. 3), in this case caused by *Chiloguembelitra* and not by *Guembelitra*. *Guembelitra* comprised opportunistic species whose relative abundance strongly increased in ecological stress conditions, mainly related to eutrophication episodes (see e.g., Keller and Pardo 2004). *Chiloguembelitra* replaced *Guembelitra* in the early Danian, occupying a similar ecological niche (Arenillas et al. 2017), so its blooms indicate similar conditions of ecological stress. Maxima in aberrant specimens thus seem to coincide with guembelitriid blooms in the early Danian, as occurs in PFAS-1 and the lower part of PFAS-3.

### A Compendium of Earliest Danian Abnormal Morphologies

Various types of abnormalities are present among the earliest Danian planktic foraminifers, severely complicating their taxonomic identification in some cases. Abnormal specimens have previously been reported in the lowermost Danian of other localities, mainly among *Guembelitra* (Coccioni and Luciani 2006) but also among parvularugoglobigerinids (Gerstel et al. 1986). Double and multiple tests of *Parasubbotina* and *Globoconusa* were also described by Ballent and Carignano (2008) in shallow environments of the Cerro Azul section, Argentina.

The terminology used here to describe the abnormalities identified in the earliest Danian (Figs. 4, 5) is based on those of Polovodova and Schönfeld (2008), Ballent and Carignano (2008), and Montgomery (1990) for both benthic and planktic foraminifera. The specimens illustrated in Figures 6 and 7 and Supplementary Figures 5, 6, and 7 come mainly from El Kef and Aïn Settara, but also from Elles, Agost, and Caravaca. The aberrant morphologies identified belong to the following categories:

1. Protuberance near the proloculus, which includes two types: (a) protruding proloculus (Fig. 4A1); and (b) second chamber abnormally

protruding beside the proloculus (Fig. 4A2), also known as a double- or twinned-chamber arrangement. The latter occurs during the calcification of juvenile individuals and may be a result of frustrated double tests (Stouff et al. 1999). During the early ontogenetic stage, two chambers can grow from the proloculus with subsequent development of an independent whorl from each of the second chambers; if a single whorl develops from one of these chambers, then the other appears as a protuberance on the proloculus (Polovodova and Schönfeld 2008).

2. Chamber abnormalities, which include six types: (a) aberrant shapes (Fig. 4B1); (b) reduced chamber sizes (Fig. 4B2); (c) overdeveloped chambers of the last whorl (Fig. 4B3); (d) additional chambers (Fig. 4B4); (e) protuberant chambers (Fig. 4B5); and (d) welded chambers (Fig. 4B6). Overdeveloped and reduced chambers have been related to environmental stress (Hecht and Savin 1972). For benthic foraminifera, Sujata et al. (2011) proposed that abnormal chambers are a result of specimens being subjected to temporary hyposaline conditions, which causes considerable dissolution and the subsequent regeneration of the chamber in an abnormal form. The same phenomenon could be applied to planktic foraminifera in conditions of acidified waters with increased carbonate dissolution, as occur in global warming–hyperthermal episodes (e.g., Luciani et al. 2007).

3. Abnormal ultimate chamber, which includes five types: (a) aberrant shape (Fig. 4C1); (b) kummerform, or reduced last chamber (Fig. 4C2); (c) overdeveloped or inflated last chamber (Fig. 4C3); (d) anomalous position (Fig. 4C4) causing, for example, the change from biserial/triserial to uniserial; and (e) bulla-like chamber (Fig. 4C5), that is, the last chamber partially or totally covering the umbilicus, resembling a bulla. The first three types are identified here in all the planktic foraminiferal groups and are frequently associated with a decrease in ornamentation. The bulla-like last chamber is typical of high trochospiral specimens with an intraumbilical or quasi-intraumbilical aperture, as in some species of *Palaeglobigerina* and *Parvularugoglobigerina*.

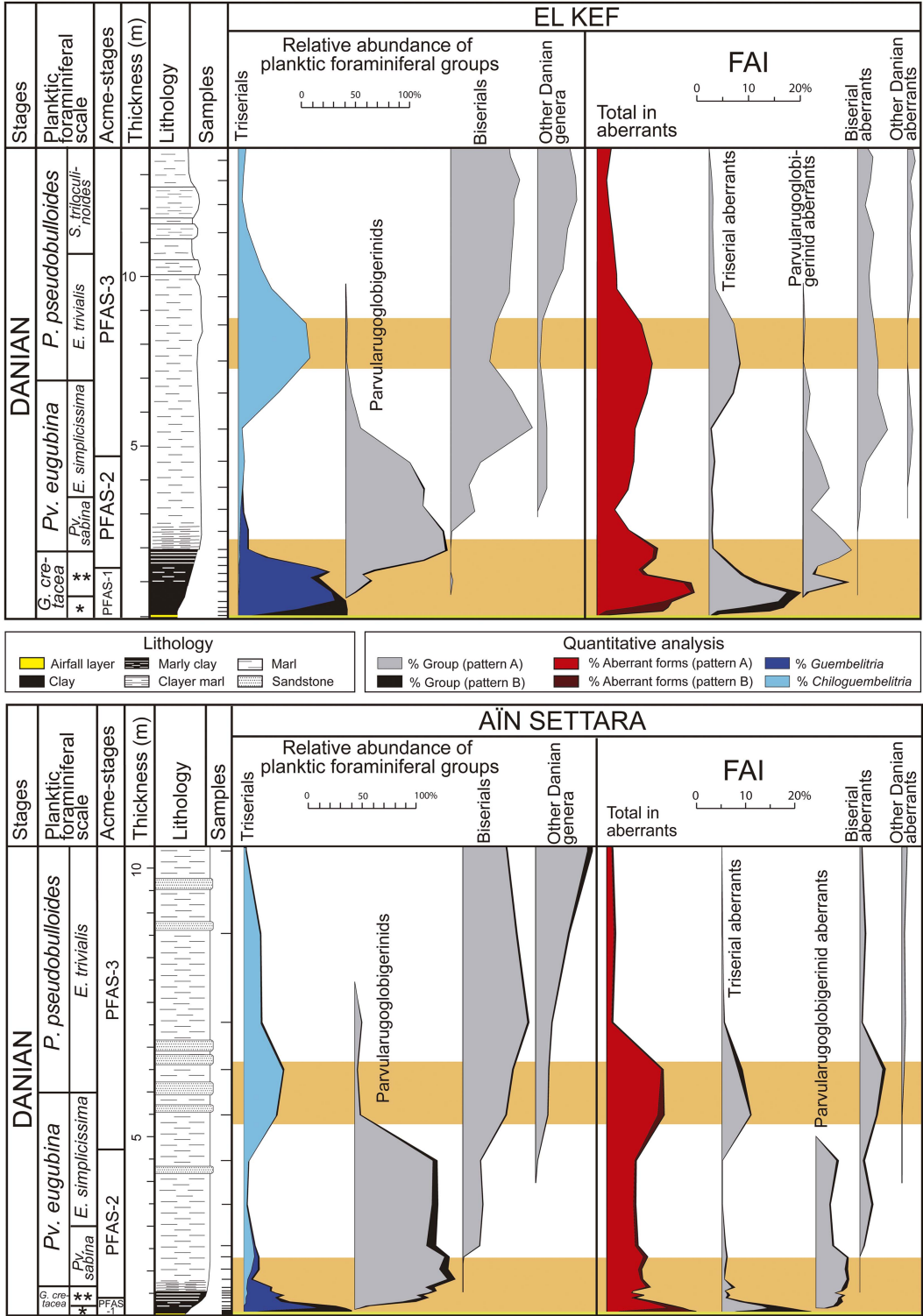


FIGURE 3. Quantitative stratigraphic distribution of planktic foraminiferal groups and aberrant forms across the K/Pg boundary in the El Kef and Aïn Settara sections. The triserial group includes *Guembeltria* and *Chiloguembeltria*; the parvularugoglobigerinids include *Pseudocaucasina*, *Palaeoglobigerina*, and *Parvularugoglobigerina*; the biserial group

Hecht and Savin (1972) reported that bulla-like abnormal chambers are more common in warmer waters and seem to develop on unusually long-lived specimens (Montgomery 1990). According to Bijma et al. (1992), abnormal last chambers could be induced by the ocean oxygen level, light quality, or feeding rate. Saclike overdeveloped chambers seem currently to be more common in upwelling areas characterized by waters that are more anoxic and richer in nutrients and in more yellow-green light conditions. Kummerform chambers are probably the result of the opposite conditions, that is, more oxygenated waters, oligotrophy, and light conditions (blue) typical of the open ocean.

4. Multiple ultimate chambers, which include two types: (a) double or twinned ultimate chambers (Fig. 4D1); and (b) proliferation of chambers in the last whorl(s) (Fig. 4D2). They are present mostly in triserial species (*Guembelitra*), but are also found here in the trochospiral *Palaeoglobigerina*. In *Guembelitra*, these additional chambers are usually disposed in several directions (multiserial forms). Many triserial specimens exhibit an ultimate tetraserial stage and have probably been misidentified as *Palaeoglobigerina alticonusa* and/or *Trochoguembelitra alabamensis* (see Supplementary Fig. 1). Others, mainly biserials, have two complete and identical ultimate chambers. According to Venturati (2006), twinned or bilobated chambers may be used as potential proxies for environmental stress. Montgomery (1990) suggested that specimens with multiple last chambers could also be some type of gerontic kummerforms, because these chambers tend to be downsized and similar in shape, and this could indicate long life.

5. Abnormal apertures, which include three types: (a) aberrant shape (e.g., gaping aperture), usually associated with abnormal ultimate chambers (Fig. 5E1); (b) additional aperture (Fig. 5E2); and (c) multiple apertures

(Fig. 5E3), usually associated with multiple ultimate chambers. According to Montgomery (1990), gaping apertures represent a strategy directly opposed to that of apertures covered by bullae, whose function is to protect them.

6. Distortion in test coiling, which includes three types: (a) excessively high spiral side or spiroconvex test (Fig. 5F1); (b) kinking (Fig. 5F2), that is, abnormal coiling due to a change in the direction of coiling, with two or more axes of rotation; and (c) twisting of entire test or extreme kinking (Fig. 5F3), that is, the umbilical side becomes the spiral side. Distortion in test coiling also seems to be a response to very stressed environments (Montgomery 1990; Polovodova and Schönfeld 2008).

7. Abnormal test, which includes four types: (a) lack of sculpture (Fig. 5G1); (b) poor development of the last whorl (Fig. 5G2); (c) overdevelopment of the last whorl (Fig. 5G3); and (d) compressed test (Fig. 5G4). Another test abnormality is a lack of ornamentation, but this type is not been analyzed here due to the difficulty of demonstrating the difference between abnormal alterations in the wall surface and the diagenetic processes of dissolution/recrystallization, which are usual in El Kef and Aïn Settara. As in the previous category, these abnormalities also seem to be a response to stressed environments (Polovodova and Schönfeld 2008), in some cases due to extremely stressful shifts in the environment (Montgomery 1990).

8. Attached twins or double tests, which include two types: (a) attached twins (Siamese) (Fig. 5H1), or even attached triplets (triamese) (Fig. 6.C); and (b) fused test (Fig. 5H2). If a second chamber beside the proloculus is followed by the development of an adjacent whorl, with two whorls with a similar number of chambers developing synchronously, attached twins are formed. Stouff et al. (1999) proposed

← includes *Woodringina* and *Chiloguembelina*; and other Danian genera include *Trochoguembelitra*, *Eoglobigerina*, *Parasubbotina*, *Globanomalina*, *Praemurica*, *Subbotina*, and *Globoconusa*. Curves with black shading represent the recalculated percentages assuming that, except for *Guembelitra*, the Maastrichtian specimens found in Danian horizons are reworked (pattern B hypothesis). Intervals with orange shading (see online version for color) represent terminal stress levels according to the model of Weinkauf et al. (2014). FAI, Foraminiferal Abnormality Index (% aberrant planktic foraminifera). \**Mh. holmdelensis* Subzone (= Zone P0); \*\**Pv. longiapertura* Subzone.



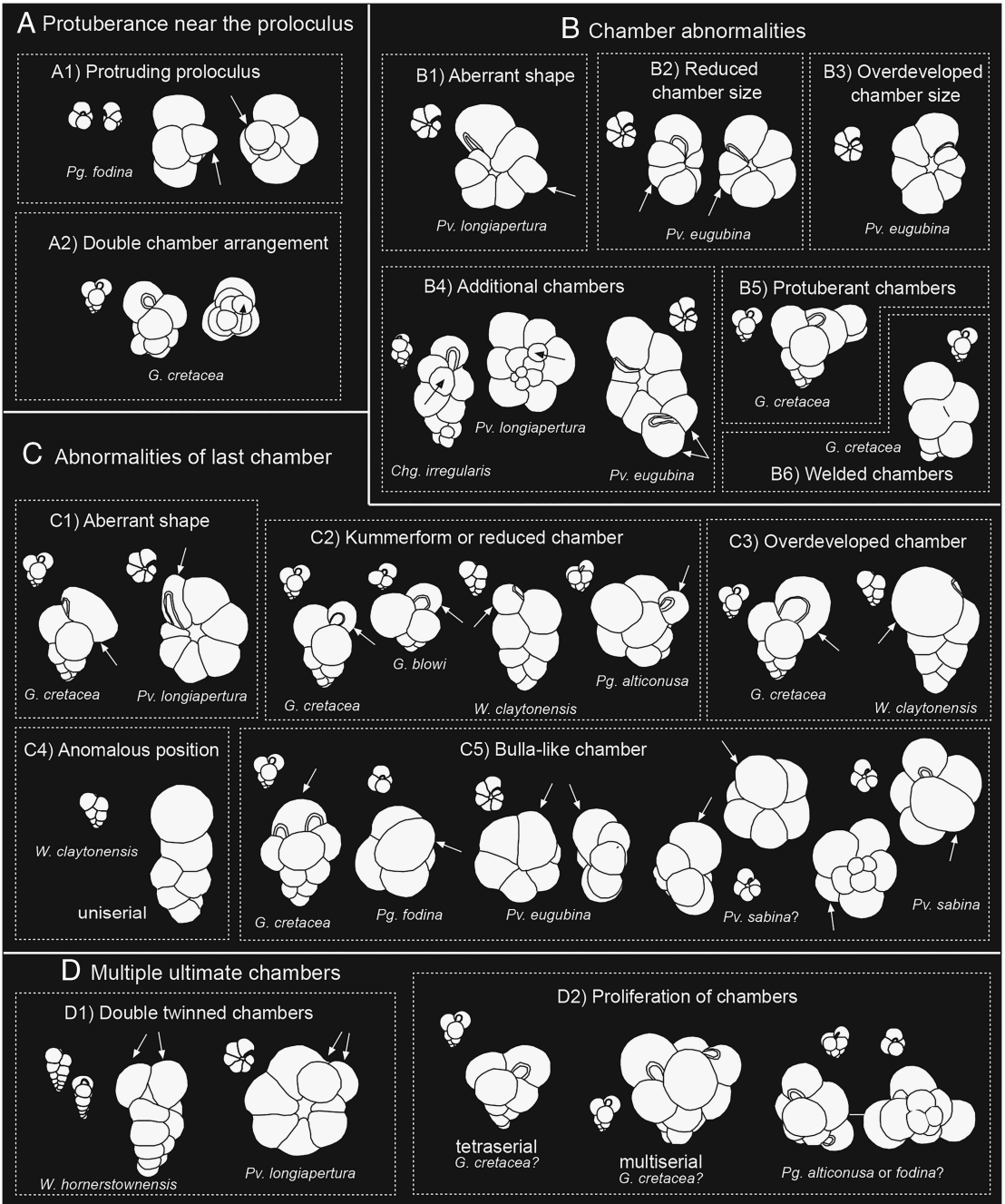


FIGURE 4. Schematic diagram of the main types of aberrant forms in the following categories: A, protuberances near the proloculus; B, chamber abnormalities; C, abnormalities of last chamber, including kummerforms; and D, multiple ultimate chambers, including double or twinned ultimate chambers (see explanation in text). Correlative normal forms are represented in miniature along with the abnormal forms.

that double tests in benthic foraminifera may result from: (i) an anomaly in the development of a single juvenile, building two or three second chambers or two third chambers, each one

possibly developing in an individual whorl; (ii) the early fusion of two juveniles, which both develop after their fusion; (iii) the attachment of a juvenile to a parental test after schizogony,

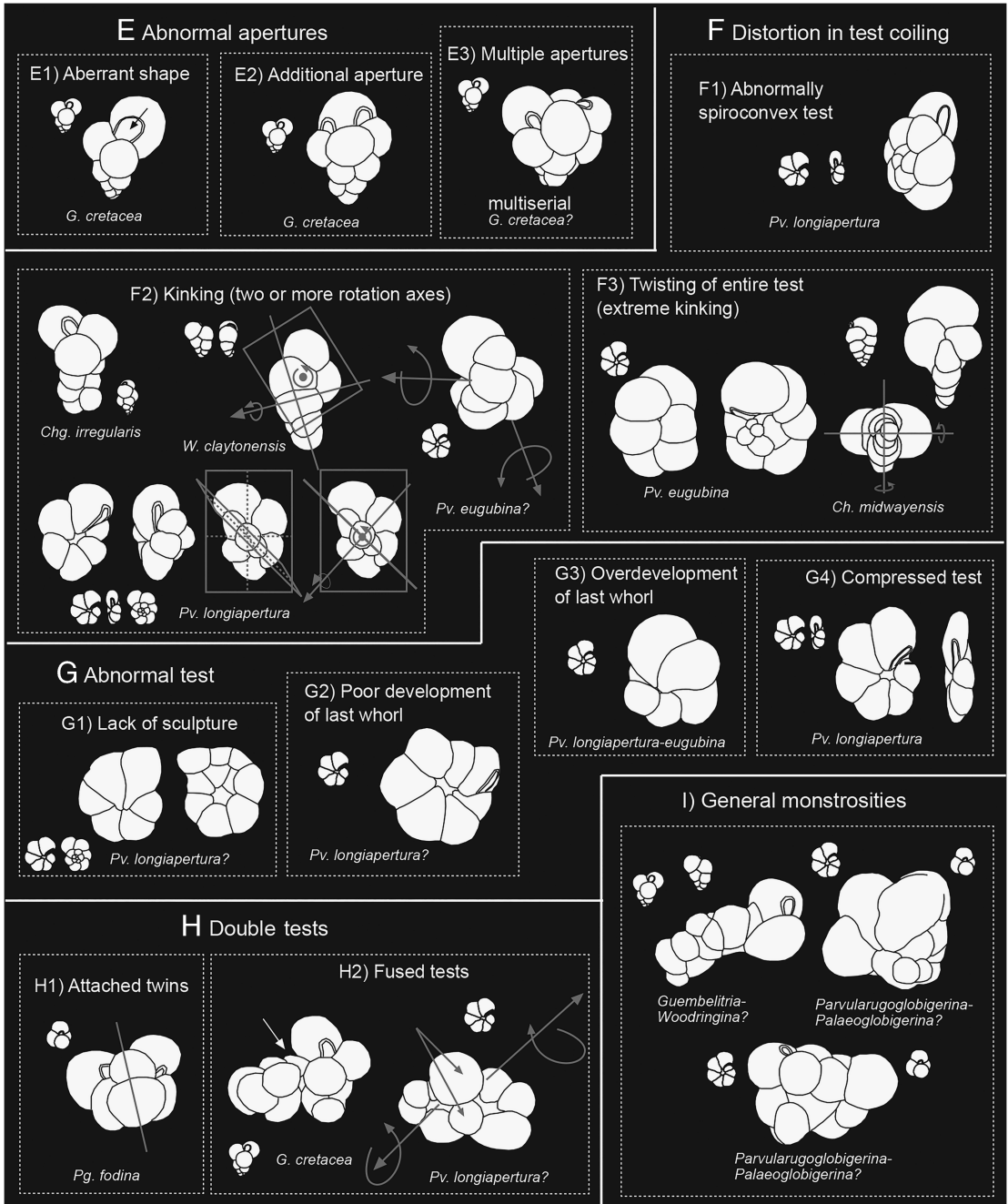


FIGURE 5. Schematic diagram of the main types of aberrant forms in the following categories (continuing from Fig. 4): E, abnormal apertures, including multiple apertures; F, distortion in test coiling, including kinking; G, morphologically abnormal tests; H, double tests, including attached twins or fused tests; and I, general monstrosities (see explanation in text). Correlative normal forms are represented in miniature along with the abnormal forms.

followed by the development of the juvenile specimen. According to Montgomery (1990), twinned specimens indicate reproductive difficulties in stressed environments.

9. General monstrosities (Fig. 5I): a conjunction of abnormal coiling due to several wrong directions of coiling, bulla-like kummerform chambers, double tests, and multiple ultimate

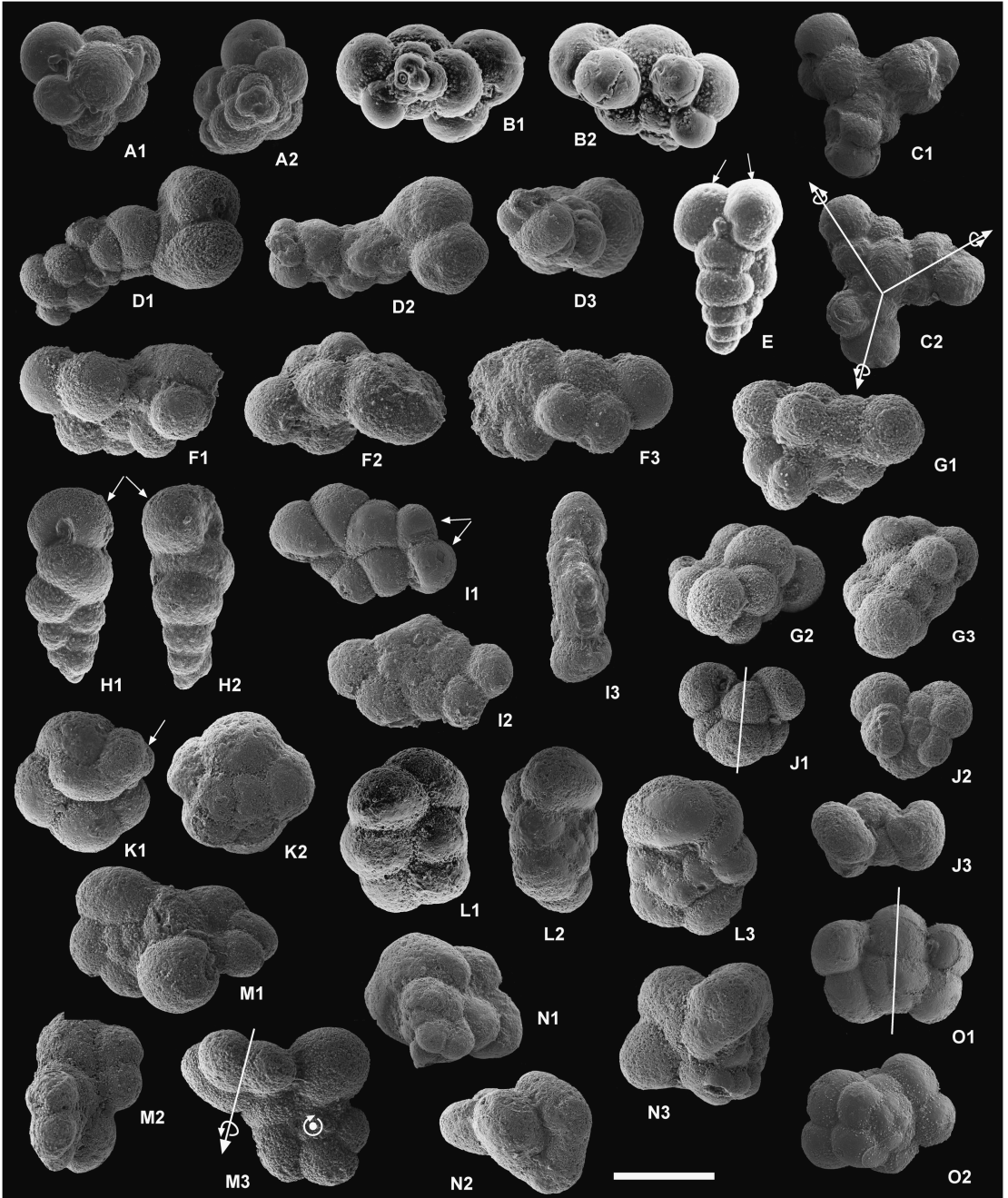


FIGURE 6. Examples of extreme aberrant forms of early Danian planktic foraminifera. Scale bar, 100 microns. A and B, *Guembelitra* spp., multiple ultimate chambers (racemiguembeliform multiserial test). C, *Guembelitra* sp. (probably *G. cretacea*), attached triplets (triamese). D, *Guembelitra* sp. or *Woodringina* sp., general monstrosity (probably attached twins with abnormal, kummerform, and protuberant chambers). E, *W. hornerstownensis*, double or twinned ultimate chambers. F, *Guembelitra* sp. or *Woodringina* sp., general monstrosity (probably attached twins with abnormal chambers). G, *Parvularugoglobigerina* sp. or *Palaeoglobigerina* sp., general monstrosity. H, *W. hornerstownensis*, last chamber in anomalous position, with test going from biserial to uniserial. i, *Pv. longiapertura*, additional chambers and apertures. J, *Palaeoglobigerina* sp. (probably *Pg. luterbacheri*), attached twins (Siamese). K, *Pv. sabina*, bulla-like ultimate chamber. L, *Pv. eugubina*, twisting of entire test (extreme kinking) and overdeveloped last chambers. M, *Parvularugoglobigerina* sp. (probably *Pv. longiapertura*), two specimens with fused tests. N, *Palaeoglobigerina* sp., general monstrosity. o, *Parvularugoglobigerina* sp.; additional chambers and apertures. All specimens come from El Kef, except for some from Ain Settara (E, F).

chambers can generate monstrous abnormalities. Montgomery (1990) proposed that monstrosities are probably crushed and repaired specimens resulting from extremely stressful shifts in their environment or increased predation by organisms such as copepods.

### Paleoenvironmental and Evolutionary Implications

*Uppermost Maastrichtian Evolutionary Stability in Open-Ocean Assemblages.*—According to Keller et al. (2011), Font et al. (2016), and Punekar et al. (2016), the main eruptive phase (phase 2) of the Deccan Traps may have been concentrated during the last ~50 or 100 Kyr of the Maastrichtian, triggering a short episode of global cooling—and ocean acidification—as a result of sulfate aerosol particles injected into the stratosphere and increased levels of mercury, an extremely toxic heavy metal. Opportunistic *Guembelitra* blooms have also been identified in the uppermost Maastrichtian, mainly in the shallow-marine environments of Israel, Egypt, Texas, and India, which suggests that the environmental deterioration and extinction began with the Deccan eruptions, several tens of thousands of years before the K/Pg boundary (Punekar et al. 2014; Keller et al. 2016). However, only minor *Guembelitra* blooms are present in the deep-marine environments of the Maastrichtian (Pardo and Keller 2008; Punekar et al. 2014). As proposed for warming episodes in the early Danian, *Guembelitra* acmes in shallow neritic environments could have also been under an orbital control related with small variations in sea level, temperature, acidity, and nutrients due to Milankovitch cycles (Quillévéré et al. 2008; Coccioni et al. 2010).

To test the hypothesis that the main eruptive phase (phase 2) of the Deccan Traps may have been concentrated during the last ~50 or 100 Kyr of the Maastrichtian, we have for the first time appraised the rate of aberrant planktic foraminifera in the upper part of the *P. hantkeninoides* Subzone from El Kef and Aïn Settara, as a proxy for ecological stress episodes. Our results indicate that there was a low frequency of aberrants (generally <2.5%) across this interval (Tables 1, 2), similar to the levels

recorded in recent deep-ocean sediments under “normal” environmental conditions and reflecting the natural background number of malformations among planktic foraminifera (Mancin and Darling 2015). Low extinction and speciation rates, as well as low volatility and taxonomic flux fluctuations (Figs. 2 and 8), corroborate the high evolutionary stability that prevailed during the latest Maastrichtian in El Kef.

*Proliferation of Aberrant Planktic Foraminifera, Chemical Pollution, and Global Warming during the Earliest Danian.*—The causes proposed to explain the abnormalities in planktic foraminiferal tests are still very vague, including biological factors (such as unusually high levels of intraspecific variability) or various chemical and physical stressors (see Mancin and Darling 2015). For example, Coccioni and Luciani (2006) speculated that blooms of aberrant *G. irregularis* across the K/Pg boundary are explained as the result of rapid and extreme fluctuations in climate and sea level, as well as intense volcanism and meteoritic impact events, which could have stressed surface waters. The higher values in the FAI identified here during the first 200 Kyr of the Danian (affecting not only *G. irregularis* but all the planktic foraminiferal groups), however, require a better understanding of how the long-term effects of the Chicxulub impact or the paleoenvironmental changes induced by the Deccan eruptions affected planktic foraminiferal assemblages during the early Danian.

Model calculations have suggested several short-term (hour- to decade-long) environmental perturbations caused by the Chicxulub impact (see reviews in Kring 2007; Schulte et al. 2010; Brugger et al. 2017; Artemieva et al. 2017). These include a global pulse of increased thermal radiation on the ground and wildfires caused by the atmospheric re-entry of the ejecta spherules, the production of acid rain, and an injection of dust and aerosol particles into the atmosphere, blocking the sunlight. Using TEX<sub>86</sub> paleothermometry, a short-term cooling (or “impact winter” phase) during the first months to decades following the Chicxulub impact has been documented at the Brazos River section

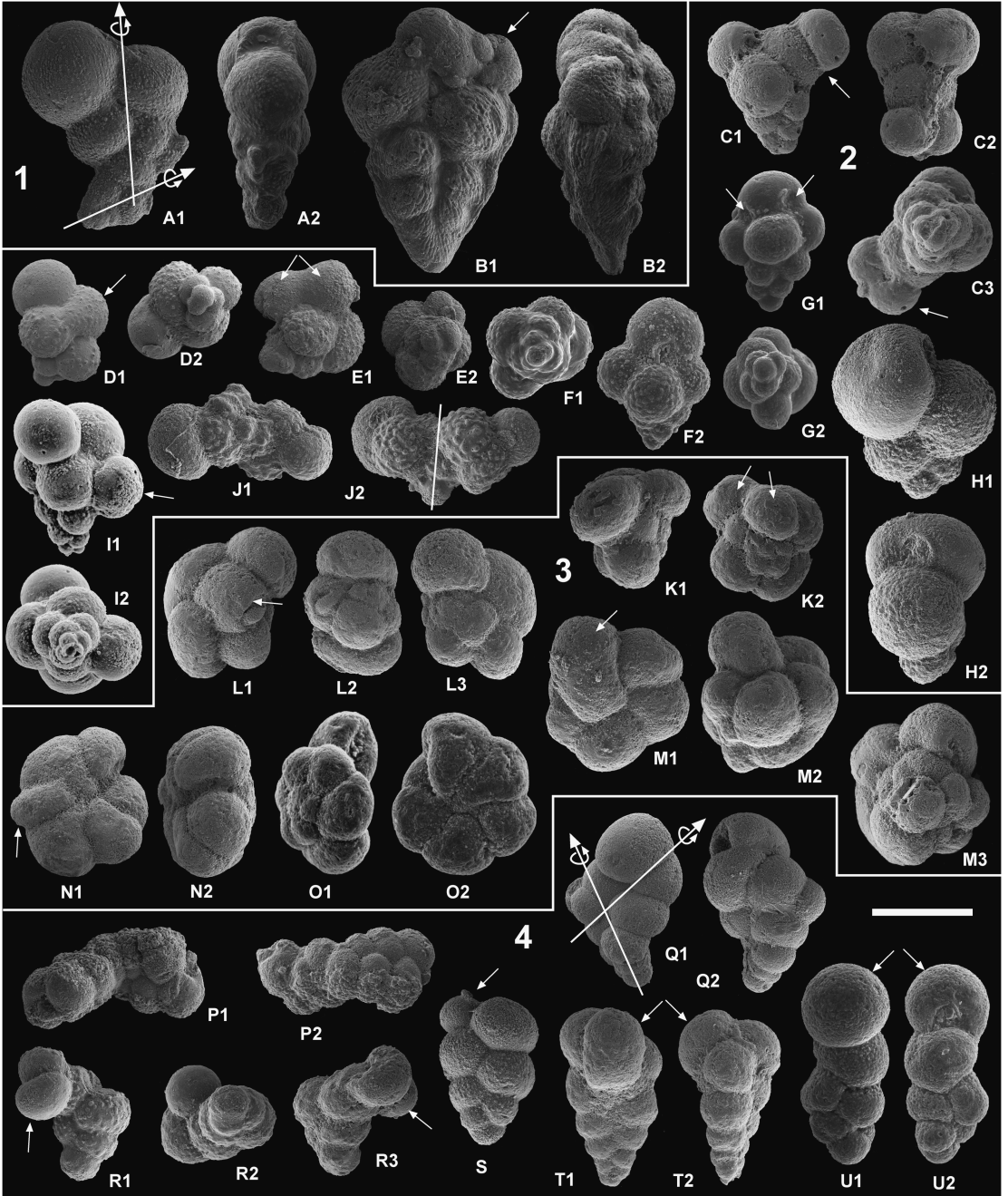


FIGURE 7. Examples of aberrant planktic foraminifera ordered by time intervals and environmental and evolutionary episodes. Scale bar, 100 microns. 1. Latest Maastrichtian: A, *Heterohelix globulosa*, kinking with change in the coiling direction. B, *Pseudoguembelina kempensis*, with multiple ultimate chambers. 2. PFAS-1 and transition between PFAS-1 and PFAS-2: C, *Guembelitra* sp. (probably *G. cretacea*), protuberant chambers. D and E, *Guembelitra* sp. (probably *G. cretacea*), welded chambers. F, *Guembelitra* sp. (probably *G. cretacea*), tetraserial form. G, *Guembelitra* sp. (probably *G. cretacea*), tetraserial form with multiple apertures. H, *W. claytonensis*, abnormal test with overdeveloped or inflated chambers. I, *Guembelitra* sp., multiple ultimate chambers (racemiguembeliform multiseriate test). J, *Chiloguembelitra* sp. (probably *Chg. trilobata*), attached twins (Siamese). 3. PFAS-2: K, *Pg. luterbacheri*, double twinned chambers. L, *Pv. sabina*, bulla-like ultimate chamber. M, *Parvularugoglobigerina* sp., bulla-like ultimate chamber. N, *Pv. eugubina*, protuberant aberrant chamber. O, *Pv. longiapertura*, abnormally spiroconvex test. 4. Lower part of PFAS-3 (*Chiloguembelitra* acme): P, *W. claytonensis*?, general monstrosities, probably attached twins (Siamese) with abnormal

in Texas (Vellekoop et al. 2014). Short-term global perturbations were likely major lethal factors for planktic foraminifera in the K/Pg mass extinction event (lasting months or a few years), but are insufficient to account for the increase of aberrants identified in the first 200 Kyr of the Danian.

Increased teratological forms in recent foraminifera are usually related with highly polluted areas (e.g., Alve 1991; Yanko et al. 1998; Geslin et al. 2002; Martin and Nesbitt 2015). Under the effect of extreme poisoning by heavy metals, the ability of foraminifera to constrain the shape of their shells is limited, leading to aberrant morphologies (Caron et al. 1987). The action of toxic heavy metals must have been very intense immediately after the Chicxulub impact. According to Erickson and Dickson (1987), a hypothetical 10-km-diameter chondritic impactor such as that of Chicxulub contains a mass of heavy metals, such as cobalt, nickel, copper, and mercury, comparable to or larger than the world ocean burden. Several heavy metals have relatively inefficient removal mechanisms, such as copper and nickel with greater than 1000-yr steady-state oceanic residence times. In addition, the worldwide sediments contaminated with heavy metals from the Chicxulub impact site may well have been eroded, removed, and resuspended in oceans for several thousand years (Smit and Romein 1985; Smit et al. 1996). Premovic et al. (2008) suggested that humics enriched in heavy metals were transported mainly by fluvial means into the ocean and deposited in the dark-clay bed. Enhanced levels of toxic heavy metals (e.g., nickel, zinc, chromium, cobalt, or copper) have been identified in the dark-clay bed, that is, in the first 10 Kyr after the K/Pg boundary, at Caravaca (Smit and ten Kate 1982), Aïn Set-tara (Dupuis et al. 2001), and Stevns Klint, Denmark (Premovic et al. 2008).

Chicxulub impact-linked chemical pollution could therefore be a major cause of the first bloom of aberrant planktic foraminifera within the dark-clay bed. In addition, the large amount of CO<sub>2</sub> gas devolatilized in the Chicxulub impact and the collapse of ocean productivity and the biological pump initiated intense global warming through the greenhouse effect after the post-impact winter phase (Kawaragi et al. 2009), persisting as another ecological stress factor for thousands of years. Isotopic data from El Kef indicate a sudden negative excursion in bulk-sediment  $\delta^{13}\text{C}$  and  $\delta^{18}\text{O}$  after the K/Pg boundary (Keller and Lindinger 1989), suggesting a warming episode and a decrease in biological productivity at the time of the dark-clay bed deposition and PFAS-1. According to the GTS12 and the bio-chronological scale of Arenillas et al. (2004), this negative  $\delta^{13}\text{C}$  excursion lasted for the first 20–25 Kyr of the Danian.

Another potential cause of the first peak of aberrant planktic foraminifera in PFAS-1 could be phytoplankton blooms concentrating toxins in the surface waters (Jiang et al. 2010; Schueth et al. 2015). Toxicity is a well-known product of modern plankton blooms (Castle and Rodgers 2009), and geographically heterogeneous spikes of phytoplankton groups are reported in the earliest Danian. For example, quantitative analyses with organic-walled marine dinoflagellate cyst assemblages in the lowermost Danian of El Kef show a relevant acme of the *Andalusiella-Palaeocystodinium* complex between 10 and 15 cm above the K/Pg boundary (Brinkhuis et al. 1998). This peak correlates approximately with the initial increase in aberrant tests of planktic foraminifera at El Kef, but not with the maximum values recorded between 37 and 97 cm above the K/Pg boundary (Fig. 3, Table 1). Although phytoplankton blooms may have favored the concentration of toxins in the surface-water layers, more studies are needed to establish the relationship between such blooms and

← chambers. Q, *W. hornerstownensis*, kinking with change in the coiling direction. R, *W. claytonensis*, kinking with change in the coiling direction and last chambers apparently protuberant. S, *W. claytonensis*, reduced last chamber (kummerform). T, *Ch. taurica*, last chamber in anomalous position, with test going from biserial to triserial. U, *W. claytonensis*, last chamber in anomalous position, with test going from biserial to uniserial. Most of the specimens come from El Kef, and the rest are from Aïn Settara (F, P, Q), Elles (G, K), Agost (O), and Caravaca (T).

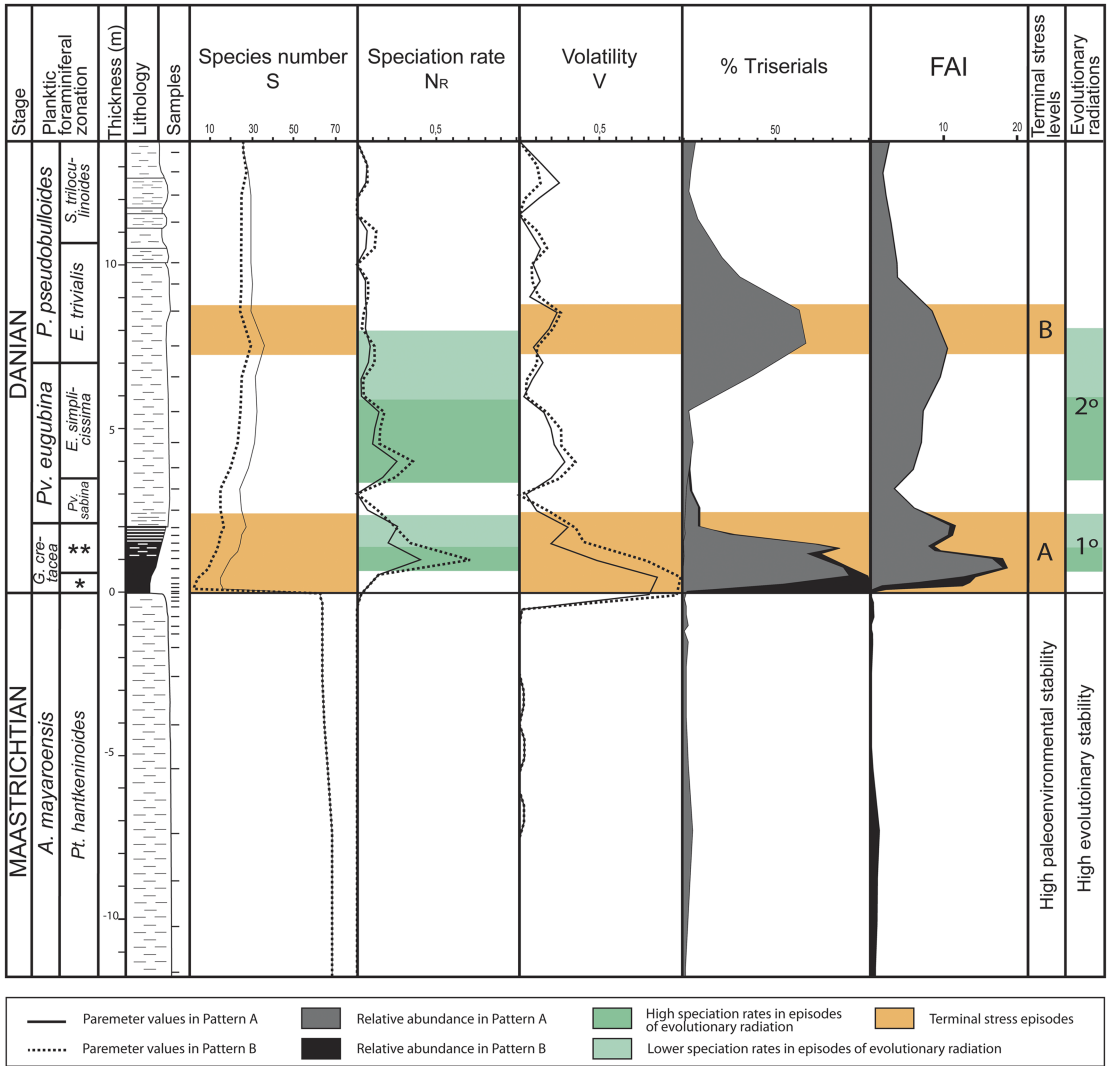


FIGURE 8. Shifts in specific richness (species number), speciation rate and volatility (according to the model of Dean and McKinney, 2001), relative abundance (%) of triserial specimens, and FAI (rate of aberrants in %) across the K/Pg boundary at El Kef; solid line and gray shading: hypothesis of pattern A; dotted line and black shading: hypothesis of pattern B; orange shading: terminal stress levels according to the model of Weinkauff et al. (2014), A corresponding to PFAS-1 and B to the *Chiloguembelitra* acme; green shading, evolutionary radiations, with shading in dark green to indicate high speciation rates (see online version for color). FAI, Foraminiferal Abnormality Index (% aberrant planktic foraminifera). \**Mh. holmdelensis* Subzone (= Zone P0); \*\**Pv. longiapertura* Subzone.

the proliferations of aberrant planktic foraminiferal tests in the early Danian. In any case, spikes of *Andalusiella*–*Palaeocystodinium* complex and other groups (such as the calcareous dinoflagellate cyst *Thoracosphaera* spp. or the nannofossil species *Braarudosphaera bigelowii*) identified in the Tethyan realm are usually explained as blooms of opportunistic taxa related to long-term environmental effects of the Chicxulub impact (Lamolda et al. 2005; Vellekoop et al. 2015).

On the basis of several independent stratigraphic, geochronological, geochemical, and tectonic constraints, Richards et al. (2015) hypothesized that the main Deccan eruptive phase (phase 2, >70% of the lava flows) could have been triggered by the Chicxulub impact during a relatively brief time interval on the order of one to several hundred thousand years. If this hypothesis by Richards et al. (2015) is correct, the long-term disruptive

effects of the Chicxulub impact could be combined in the early Danian with those of Deccan volcanism, including a chemical contamination of the ocean surface over a longer period of time. This hypothesis could explain why the values of the FAI at the El Kef and Aïn Settara sections remained high during at least the first 200 Kyr after the Chicxulub impact (including the interval PFAS-2).

As mentioned earlier, the second increase in aberrant forms coincides with the *Chiloguembelitra* bloom in the lower part of PFAS-3 (Figs. 3, 8). This episode spanned between approximately 70 and 200 Kyr after the K/Pg boundary, so it cannot be related to the long-term disruptive effects of the Chicxulub impact. On the contrary, it seems that it was caused by another independent, later period of intense ecological stress perhaps linked to the Deccan eruptions (phase 2 or 3). Quillévére et al. (2008) recognized in the lower Danian (in the *E. trivialis* Subzone, or Subzone P1a) a warming episode called Dan-C2 (the first hyperthermal episode of the Paleogene), which lasted approximately 100 Kyr. Although Dan-C2 and similar episodes could be a result of orbital cycles, Coccioni et al. (2010) proposed a possible link between this warming episode and the Deccan volcanism. According to this scenario, the second increase of the FAI, the *Chiloguembelitra* bloom, and the Dan-C2 episode could therefore be related. The low values of the FAI after the *Chiloguembelitra* bloom (in the *S. triloculinoides* Subzone, or Subzone P1b) suggest a period of greater environmental stability. This interval is widely dominated by biserial *Woodringina* and *Chiloguembelina*, typical of the PFAS-3 episode. Nevertheless, Coccioni et al. (2010) suggested that the predominance of biserials in Gubbio, along with other micropaleontological and geochemical proxies, was indicative of stressed ecological conditions (climatic warming and low oxygenation and acidification of ocean waters) during the Dan-C2 episode. According to this scenario, the whole PFAS-3 episode could be a record of the late eruptions of Deccan phase 2 or the first eruptions of phase 3. Moreover, the *Chiloguembelitra* bloom in the lower part of PFAS-3 could be the result of a more intense volcanic pulse during Dan-C2,

though not one recorded at Gubbio by Coccioni et al. (2010).

*Evolutionary Implications.*—Weinkauff et al. (2014) suggested that the phenotypic history of planktic foraminiferal assemblages allows the detection of threshold levels of ecological stress episodes that are likely to lead to extinction. According to these authors, an increase in interspecific morphological variability and abnormal forms can be observed at terminal stress levels immediately before extinction, indicating disruptive selection. In contrast, in periods of environmental stability and non-terminal stress levels, a decrease in morphological variability and abnormal forms is recognized, indicating stabilizing selection.

If the hypothesis that the massive eruptions of Deccan phase 2 were concentrated in the last 50 or 100 Kyr of the Maastrichtian and started a gradual mass extinction in planktic foraminifera before the K/Pg boundary (Punekar et al. 2016) is correct, a terminal stress episode with abundant aberrant forms should have been recorded below the K/Pg extinction horizon at El Kef and Aïn Settara. However, there is no evidence for such a scenario and, as in many sections worldwide, most Maastrichtian species suddenly become extinct at the K/Pg boundary following a catastrophic extinction pattern compatible with the short-term effects of the Chicxulub impact (Smit 1982, 1990; Huber 1996; Arz et al. 2000; Arenillas et al. 2000a,b; Huber et al. 2002; Molina et al. 2005; Gallala 2014). Similarly, latest Maastrichtian climatic fluctuations and environmental perturbations linked to Deccan volcanism had a relatively weak impact on the diversity of the calcareous nannoplankton assemblages before the K/Pg boundary, as evidenced in Elles and other sections worldwide (Thibault et al. 2016).

The first bloom of aberrants and PFAS-1 in the earliest Danian occurred in an interval in which the speciation rate was very high, especially in the lower part of the *Pv. longiapertura* Subzone, which also shows high volatility and relevant fluctuations in the taxonomic flux (Figs. 2 and 8). Arenillas et al. (2016) suggested that the speciation rate may have been increased in response to the long-term meteoritic pollution of the oceans, which may have caused increased mutation rates for at



least 10 to 20 Kyr after the K/Pg boundary and triggered the first evolutionary radiation of planktic foraminifera. Many mutations in planktic foraminifera are likely to have been lethal, causing mortality before the adult stage was reached. However, genetic mutations could have accelerated the evolution of planktic foraminifera in the early Danian, being amplified as a consequence of stressed and adverse environments (BouDagher-Fadel 2012). In addition, many other mutations would have been deleterious, producing malformations and teratological forms, as has been proposed for recent foraminifera (e.g., Mancin and Darling 2015). The high values of the FAI identified in the dark-clay bed and PFAS-1 at El Kef and Aïn Settara are consistent with this hypothesis. This interval occurred during the survival and recovery phases after the K/Pg boundary extinction according to the terminology of Kauffman and Erwin (1995), in which *Guembelitra* included the “disaster species” and the minute parvularugoglobigerinids the “progenitor species” (Molina 2015), although the latter had a benthic origin, as has recently been proposed by Arenillas and Arz (2017). The evolutionary history of the planktic foraminifera was restarted almost from scratch after the K/Pg boundary extinction, suggesting that all the latest Maastrichtian species went extinct at the K/Pg boundary, except for some species of *Guembelitra* (see also Smit 1982; Arenillas et al. 2016).

The second bloom of aberrants and the *Chiloguembelitra* acme appear to be better adjusted to a terminal stress episode, as proposed by Weinkauf et al. (2014). Nonterminal stress episodes could correspond to PFAS-2, dominated by parvularugoglobigerinids and characterized by an aberrant rate lower than in PFAS-1 and the *Chiloguembelitra* acme. It is not possible to speak of environmental stability in PFAS-2, because values of the FAI and volatility remain high. In fact, the speciation rate in the upper part of PFAS-2 is high (Fig. 8) as a consequence of the beginning of the second evolutionary radiation. Nevertheless, the maximum in species richness ( $S$  = species number) of the early Danian is reached during the beginning of the *Chiloguembelitra* acme (Fig. 8), which represents a terminal stress episode. This is because the species that emerged during the first

and second evolutionary radiations overlapped in time (Fig. 1). The parvularugoglobigerinids, which appeared in the first radiation, went extinct toward the end of the *Chiloguembelitra* acme, increasing the extinction rate (Fig. 8). Parvularugoglobigerinids were replaced definitively by the more ornamented, larger trochospiral species of the second evolutionary radiation. In this case, the *Chiloguembelitra* included the disaster species, and the species that appeared in the second radiation (those of *Eoglobigerina*, *Parasubbotina*, *Globanomalina*, and *Praemurica*, among others) were the progenitor species.

### Conclusions

1. A high-resolution, quantitative biostratigraphic study across the K/Pg boundary from open-ocean Tunisian sections (El Kef and Aïn Settara) revealed a proliferation of aberrant planktic foraminifera during approximately the first 200 Kyr of the Danian. Various categories and types of abnormalities were identified, including abnormal tests, extra chambers, attached twin tests, and general monstrosities.

2. The proliferation of aberrants occurred in two main pulses. The first was more intense and occurred during the first 20 to 25 Kyr after the K/Pg boundary, spanning the dark-clay bed. It is characterized by abnormal forms of triserials (*Guembelitra*), but also of parvularugoglobigerinids (*Parvularugoglobigerina* and *Palaeoglobigerina*) from just the first evolutionary radiation of Danian planktic foraminifera. The second pulse is recorded between approximately 70 and 200 Kyr after the K/Pg boundary and is characterized mainly by abnormal forms of triserials (*Chiloguembelitra*) and biserials (*Woodringina* and *Chiloguembelina*).

3. These two pulses of aberrants correlate respectively with the *Guembelitra* acme in PFAS-1 and the dark-clay bed and with the *Chiloguembelitra* acme in the lower part of PFAS-3, both of which have been interpreted as ecological stress episodes. The FAI during the parvularugoglobigerinid acme in PFAS-2 is lower, but remains high enough to suggest that environmental conditions were also unstable during this interval, in which the second evolutionary radiation of Danian planktic foraminifera occurred.

4. According to the data set available here, the high values of the FAI in PFAS-1 seems to be more related to long-term environmental effects of the Chicxulub impact. By contrast, the second bloom of aberrants during the *Chiloguembelitra* acme was caused by an independent, later period of ecological stress perhaps linked to the Deccan eruptions.

5. The absence of an ecological stress episode rich in abnormal tests during the latest Maastrichtian in both the El Kef and Aïn Settara locations, as well as the high values of the FAI during the first 200 Kyr of the Danian, could be compatible with the hypothesis that the Chicxulub impact triggered the main phase of the Deccan Traps. This would render the Deccan volcanism an unlikely candidate as the cause of the K/Pg boundary mass extinction.

### Acknowledgments

We thank I. Polovodova, C. M. Lowery, and two anonymous reviewers for their comments and critiques, which have greatly helped improve this paper. This study is a contribution to project CGL2015-64422-P (MINECO/FEDER-UE) and is also partially supported by the Departamento de Educación y Ciencia of the Aragonian Government, cofinanced by the European Social Fund (grant number DGA group E05). V.G. acknowledges support from the Spanish Ministerio de Economía, Industria y Competitividad (FPI grant BES-2016-077800). The authors would like to acknowledge the use of the Servicio General de Apoyo a la Investigación-SAI, Universidad de Zaragoza. The authors are grateful to Rupert Glasgow for improvement of the English text.

### Literature Cited

- Alegret, L., E. Thomas, and K. C. Lohmann. 2012. End-Cretaceous marine mass extinction not caused by productivity collapse. *Proceedings of the National Academy of Sciences USA* 109:728–732.
- Alvarez, L. W., W. Alvarez, F. Asaro, and H. V. Michel. 1980. Extraterrestrial cause for the Cretaceous–Tertiary extinction. *Science* 208:1095–1108.
- Alvarez, W., J. Smit, W. Lowrie, F. Asaro, S. V. Margolis, P. Claeys, M. Kastner, and A. R. Hildebrand. 1992. Proximal impact deposits at the Cretaceous–Tertiary boundary in the Gulf of Mexico: a restudy of DSDP Leg 77 Sites 536 and 540. *Geology* 20:697–700.
- Alve, E. 1991. Benthic foraminifera in sediment cores reflecting heavy metal pollution in Soerfjord, Western Norway. *Journal of Foraminiferal Research* 21:1–19.
- Apellaniz, E., X. Orue-Etxebarria, and H. P. Luterbacher. 2002. Evolution of the early Paleocene planktonic foraminifera: a Basque point of view. *Neues Jahrbuch für Geologie und Paläontologie, Abhandlungen* 225:157–194.
- Arenillas, I., and J. A. Arz. 2017. Benthic origin and earliest evolution of the first planktonic foraminifera after the Cretaceous/Paleogene boundary mass extinction. *Historical Biology* 29:17–24.
- Arenillas, I., J. A. Arz, E. Molina, and C. Dupuis. 2000a. The Cretaceous/Paleogene (K/P) boundary at Aïn Settara, Tunisia: sudden catastrophic mass extinction in planktic foraminifera. *Journal of Foraminiferal Research* 30:212–218.
- . 2000b. An independent test of planktonic foraminiferal turnover across the Cretaceous/Paleogene (K/P) boundary at El Kef, Tunisia: catastrophic mass extinction and possible survivorship. *Micropaleontology* 46:31–49.
- Arenillas, I., J. A. Arz, and E. Molina. 2002. Quantifying the evolutionary turnover across the K/T boundary catastrophic planktic foraminiferal extinction event at El Kef, Tunisia. *Geologica Föreningens Förhandlingar* 124:121–126.
- . 2004. A new high-resolution planktonic foraminiferal zonation and subzonation for the lower Danian. *Lethaia* 37:79–95.
- Arenillas, I., J. A. Arz, J. M. Grajales-Nishimura, G. Murillo-Muñetón, W. Alvarez, A. Camargo-Zanoguera, E. Molina, and C. Rosales-Domínguez. 2006. Chicxulub impact event is Cretaceous/Paleogene boundary in age: new micropaleontological evidence. *Earth and Planetary Science Letters* 249:241–257.
- Arenillas, I., J. A. Arz, J. M. Grajales-Nishimura, A. Meléndez, and R. Rojas-Consuegra. 2016. The Chicxulub impact is synchronous with the planktonic foraminifera mass extinction at the Cretaceous/Paleogene boundary: new evidence from the Moncada section, Cuba. *Geologica Acta* 14:35–51.
- Arenillas, I., J. A. Arz, and V. Gilabert. 2017. Revalidation of the genus *Chiloguembelitra* Hofker: implications for the evolution of early Danian planktonic foraminifera. *Journal of African Earth Sciences* 134:435–456.
- Artemieva, N., and J. Morgan, Expedition 364 Science Party 2017). Quantifying the release of climate-active gases by large meteorite impacts with a case study of Chicxulub. *Geophysical Research Letters* 44. doi: 10.1002/2017GL074879.
- Arz, J. A., I. Arenillas, E. Molina, and R. Sepúlveda. 2000. La estabilidad faunística de foraminíferos planctónicos en el Maastrichtense superior y su extinción en masa catastrófica en el límite K/T de Caravaca, España [The faunistic stability of planktonic foraminifera in the Upper Maastrichtian and their catastrophic mass extinction at the K/T boundary of Caravaca, Spain]. *Revista Geológica de Chile* 27:27–47.
- Arz, J. A., I. Arenillas, and C. Nález. 2010. Morphostatistical analysis of Maastrichtian populations of *Guembelitra* from El Kef, Tunisia. *Journal of Foraminiferal Research* 40:148–164.
- Aze, T., T. H. G. Ezard, A. Purvis, H. Coxall, D. R. M. Stewart, B. S. Wade, and P. N. Pearson. 2011. A phylogeny of Cenozoic macroperforate planktonic foraminifera from fossil data. *Biological Reviews* 86:900–927.
- Ballent, S. C., and A. P. Carignano. 2008. Morphological abnormalities in Late Cretaceous and early Paleocene foraminifer tests (northern Patagonia, Argentina). *Marine Micropaleontology* 67:288–296.
- Bardeen, C. G., R. R. Garcia, O. B. Toon, and A. J. Conley. 2017. On transient climate change at the Cretaceous–Paleogene boundary due to atmospheric soot injections. *Proceedings of the National Academy of Sciences USA* 114:E7415–E7424.
- Berggren, W. A., and P. N. Pearson. 2005. A revised tropical to subtropical Paleogene planktonic foraminiferal zonation. *Journal of Foraminiferal Research* 35:279–298.
- Bijma, J., C. Hemleben, H. Oberhänsli, and M. Spindler. 1992. The effect of increased water fertility on tropical spinose planktonic

- foraminifers in laboratory cultures. *Journal of Foraminiferal Research* 22:242–256.
- Birch, H.S., H. K. Coxall, P. N. Pearson, D. Kroon, and D. N. Schmidt. 2016. Partial collapse of the marine carbon pump after the Cretaceous–Paleogene boundary. *Geology* 44:287–290.
- Boltovskoy, E., and R. Wright. 1976). *Recent Foraminifera*. Dr. W. Junk b.v. Publishers, The Hague.
- BouDagher-Fadel, M. K. 2012). *Biostratigraphic and geological significance of planktonic foraminifera*, 1<sup>st</sup> ed. *Developments in Palaeontology and Stratigraphy* 22:1–289. Elsevier, Amsterdam.
- Brinkhuis, H., and W. J. Zachariasse. 1988. Dinoflagellate cyst, sea level changes and planktonic foraminifers across the Cretaceous–Tertiary boundary at El Haria, Northwest Tunisia. *Marine Micropaleontology* 13:153–191.
- Brinkhuis, H., J. P. Bujak, J. Smit, G. J. M. Versteegh, and H. Visscher. 1998. Dinoflagellate-based sea surface temperature reconstructions across the Cretaceous–Tertiary boundary. *Palaeogeography, Palaeoclimatology, Palaeoecology* 141:67–83.
- Brugger, J., G. Feulner, and S. Petri. 2017). Baby, it's cold outside: climate model simulations of the effects of the asteroid impact at the end of the Cretaceous. *Geophysical Research Letters* 44. doi: 10.1002/2016GL072241.
- Caron, D. A., J. W. F. Faber, and A. W. H. Bé. 1987. Growth of the spinose planktonic foraminifer *Orbulina universa* in laboratory culture and the effect of temperature on life processes. *Journal of Marine Biological Association of the United Kingdom* 67:343–358.
- Castle, J. W., and J. H. Rodgers, Jr. 2009. Hypothesis for the role of toxin-producing algae in Phanerozoic mass extinctions based on evidence from the geologic record and modern environments. *Environmental Geosciences* 16:1–23.
- Chenet, A.-L., X. Auidelleur, F. Fluteau, V. Y. Courtillot, and S. Bajpai. 2007. <sup>40</sup>K–<sup>40</sup>Ar dating of the main Deccan large igneous province: further evidence of KTB age and short duration. *Earth and Planetary Science Letters* 263:1–15.
- Chenet, A.-L., V. Courtillot, F. Fluteau, M. Gérard, X. Quidelleur, S. F. R. Khadri, K. V. Subbarao, and J. C. Zachos. 2009. Determination of rapid Deccan eruptions across the Cretaceous–Tertiary boundary using paleomagnetic secular variation. 2. Constraints from analysis of eight new sections and synthesis for a 3500-m-thick composite section. *Journal of Geophysical Research* 114:B06103.
- Coccioni, R., and V. Luciani. 2006. *Guenbelitria irregularis* bloom at the K-T boundary: morphological abnormalities induced by impact-related extreme environmental stress? Pp. 179–196. *in* C. Cockell, C. Koeberl, and I. Gilmour, eds. *Biological processes associated with impact events*. Springer, Berlin.
- Coccioni, R., F. Frontalini, G. Bancalà, E. Fornaciari, L. Jovane, and M. Sprovieri. 2010. The Dan-C2 hyperthermal event at Gubbio (Italy): global implications, environmental effects, and cause(s). *Earth and Planetary Science Letters* 297:298–305.
- Courtillot, V. E., G. Feraud, H. Maluski, D. Vandamme, M. G. Moreau, and J. Besse. 1988. Deccan flood basalts and the Cretaceous/Tertiary boundary. *Nature* 333:843–846.
- Coxall, H. K., S. L. D'Hondt, and J. C. Zachos. 2006. Pelagic ecosystem recovery after the K-T mass extinction. *Geology* 34:297–300.
- Dean, W. G., and M. L. McKinney. 2001. Taxonomic flux as a measure of evolutionary turnover. *Revista Española de Paleontología* 16:29–38.
- D'Hondt, S. 2005. Consequences of the Cretaceous/Paleogene mass extinction for marine ecosystems. *Annual Review of Ecology, Evolution and Systematics* 36:295–317.
- D'Hondt, S., P. Donaghay, J. C. Zachos, D. Luttenberg, and M. Lindinger. 1998. Organic carbon fluxes and ecological recovery from the Cretaceous–Tertiary mass extinction. *Science* 282:276–279.
- Dupuis, C., E. Steurbaut, E. Molina, R. Rauscher, N. P. Tribouillard, I. Arenillas, J. A. Arz, F. Robaszynski, M. Caron, E. Robin, J.R. Rocchia, and I. Lefèvre. 2001. The Cretaceous–Paleogene (K/P) boundary in the Ain Settara section (Kalaat-Senan, Central Tunisia): lithological, micropaleontological and geochemical evidence. *Bulletin de l'Institut Royal des Sciences Naturelles de Belgique* 71:169–190.
- Ericksen, D. J., and S. M. Dickson. 1987. Global trace-element biogeochemistry at the K/T boundary—oceanic and biotic response to a hypothetical meteorite impact. *Geology* 15:1014–1017.
- Font, E., T. Adatte, A. N. Sial, A. D. de Lacerda, G. Keller, and J. P. Punekar. 2016. Mercury anomaly, Deccan volcanism, and the end-Cretaceous mass extinction. *Geology* 44:171–174.
- Frontalini, F., and R. Coccioni. 2008. Benthic foraminifera for heavy metal pollution monitoring: a case study from the central Adriatic Sea coast of Italy. *Estuarine, Coastal and Shelf Science* 76:404–427.
- Gallala, N. 2014. Biostratigraphie, paleoecologie et zones d'acmé des foraminifères planctoniques au passage Crétacé-Paléogène dans la Téthys (Tunisie et Espagne) et l'Atlantique (France). [Biostratigraphy, paleoecology and acme-zones of planktic foraminifera of the Cretaceous/Paleogene transition in the Tethys (Tunisia and Spain) and the Atlantic realm (France)]. *Annales de Paléontologie* 100:193–215.
- Gerasimov, M. V. 2002. Toxins produced by meteorite impacts and their possible role in a biotic mass extinction. *Geological Society of America Special Paper* 356:705–717.
- Gerstel, J., R. Thunell, R. C. Zachos, and M. A. Arthur. 1986. The Cretaceous–Tertiary boundary event in the North Pacific; planktonic foraminiferal results from the Deep Sea Drilling Project 577, Shatsky Rise. *Paleoceanography* 1:97–117.
- Geslin, E., J. P. Debenay, W. Duleba, and C. Bonetti. 2002. Morphological abnormalities of foraminiferal tests in Brazilian environments: comparison between polluted and non-polluted areas. *Marine Micropaleontology* 45:151–168.
- Gradstein, F. M., J. G. Ogg, M. Schmitz, and G. Ogg eds. 2012. *The geologic time scale 2012*. Elsevier, Amsterdam.
- Hecht, A. D., and S. M. Savin. 1972. Phenotypic variation and oxygen isotope ratios in Recent planktonic foraminifera. *Journal of Foraminiferal Research* 2:55–67.
- Hildebrand, A. R., G. T. Penfield, D. A. Kring, M. Pilkington, A. Camargo, S. B. Jacobsen, and W. V. Boynton. 1991. Chicxulub crater: a possible Cretaceous/Tertiary boundary impact crater on the Yucatan Peninsula, Mexico. *Geology* 19:867–871.
- Hofker, J. 1978. Analysis of a large succession of samples through the Upper Maastrichtian and the Lower Tertiary of Drill Hole 472, Shatsky Rise, Pacific, Deep Sea Drilling Project. *Journal of Foraminiferal Research* 8:46–75.
- Hollis, C. J., K. A. Rodgers, C. P. Strong, B. D. Field, and K. M. Rogers. 2003. Paleoenvironmental changes across the Cretaceous/Tertiary boundary in the northern Clarence valley, south-eastern Marlborough, New Zealand. *New Zealand Journal of Geology and Geophysics* 46:209–234.
- Hsü, K. J., and J. A. McKenzie. 1985. "Strangelove" ocean in the earliest Tertiary. *American Geophysical Union, Geophysical Monograph Series* 32:487–892.
- Huber, B. T. 1996. Evidence for planktonic foraminifer reworking versus survivorship across the Cretaceous–Tertiary boundary at high latitudes. *Geological Society of America Special Paper* 307:319–334.
- Huber, B. T., K. G. MacLeod, and R. Norris. 2002. Abrupt extinction and subsequent reworking of Cretaceous planktonic foraminifera across the Cretaceous/Tertiary boundary: evidence for the subtropical North Atlantic. *Geological Society of America Special Paper* 356:277–290.
- Hull, P. M., and R. D. Norris. 2011. Diverse patterns of ocean export productivity change across the Cretaceous–Paleogene boundary: new insights from biogenic barium. *Paleoceanography* 26: PA3205. doi: 10.1029/2010PA002082.
- Husson, D., B. Galbrun, S. Gardin, and N. Thibault. 2014. Tempo and duration of short-term environmental perturbations across the Cretaceous–Paleogene boundary. *Stratigraphy* 11:159–171.

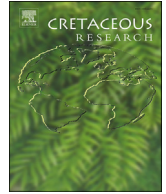
- Jiang, S., T. J. Bralower, M. E. Patzkowsky, L. R. Kump, and J. D. Schueth. 2010. Geographic controls on nannoplankton extinction across the Cretaceous/Paleogene boundary. *Nature Geoscience* 3:280–285.
- Kaiho, K., and M. A. Lamolda. 1999. Catastrophic extinction of planktonic foraminifera at the Cretaceous–Tertiary boundary evidenced by stable isotopes and foraminiferal abundance at Caravaca, Spain. *Geology* 27:355–358.
- Kauffman, E. G., and D. H. Erwin. 1995. Surviving mass extinctions. *Geotimes* 14:14–17.
- Kawaragi, K., Y. Sekine, T. Kadono, S. Sugita, S. Ohno, K. Ishibashi, K. Kurosawa, T. Matsui, and S. Ikeda. 2009. Direct measurements of chemical composition of shock-induced gases from calcite: an intense global warming after the Chicxulub impact due to the indirect greenhouse effect of carbon monoxide. *Earth and Planetary Science Letters* 282:56–64.
- Keller, G. 2003. Biotic effects of impacts and volcanism. *Earth and Planetary Science Letters* 215:249–264.
- Keller, G., and S. Abramovich. 2009. Lilliput effect in late Maastrichtian planktic foraminifera. Response to environmental stress. *Palaeogeography, Palaeoclimatology, Palaeoecology* 284:47–62.
- Keller, G., and M. Lindinger. 1989. Stable isotope, TOC and CaCO<sub>3</sub>, record across the Cretaceous/Tertiary boundary at El Kef, Tunisia. *Palaeogeography, Palaeoclimatology, Palaeoecology* 73:243–265.
- Keller, G., and A. Pardo. 2004. Disaster opportunists Guembelitriniidae—index for environmental catastrophes. *Marine Micropaleontology* 53:83–116.
- Keller, G., P. H. Bhowmick, H. Upadhyay, A. Dave, A. N. Reddy, B. C. Jaiprakash, and T. Adatte. 2011. Deccan volcanism linked to the Cretaceous–Tertiary boundary mass extinction: new evidence from ONGC wells in the Krishna–Godavari basin. *Journal Geological Society of India* 78:399–428.
- Keller, G., P. Mateo, and J. Punekar. 2016. Upheavals during the Late Maastrichtian: volcanism, climate and faunal events preceding the end-Cretaceous mass extinction. *Palaeogeography, Palaeoclimatology, Palaeoecology* 441:137–151.
- Koutsoukos, E. A. M. 2014. Phenotypic plasticity, speciation, and phylogeny in early Danian planktic foraminifera. *Journal of Foraminiferal Research* 44:109–142.
- Kring, D. A. 2007. The Chicxulub impact event and its environmental consequences at the Cretaceous/Tertiary boundary. *Palaeogeography, Palaeoclimatology, Palaeoecology* 255:4–21.
- Lamolda, M., M. C. Melinte, and K. Kaiho. 2005. Nannofloral extinction and survivorship across the K/T boundary at Caravaca, southeastern Spain. *Palaeogeography, Palaeoclimatology, Palaeoecology* 224:27–52.
- Li, L., and G. Keller. 1998. Maastrichtian climate, productivity and faunal turnovers in planktic foraminifera in South Atlantic DSDP sites 525A and 21. *Marine Micropaleontology* 33:55–86.
- Luciani, V., L. Giusberti, C. Agnini, J. Backman, E. Fornaciari, and D. Rio. 2007. The Paleocene–Eocene Thermal Maximum as recorded by Tethyan planktonic foraminifera in the Forada section (northern Italy). *Marine Micropaleontology* 64:189–214.
- Mancin, N., and K. Darling. 2015. Morphological abnormalities of planktonic foraminiferal tests in the SW Pacific Ocean over the last 550 ky. *Marine Micropaleontology* 120:1–19.
- Martin, R. A., and E. A. Nesbitt. 2015. Foraminiferal evidence of sediment toxicity in anthropogenically influenced embayments of Puget Sound, Washington, U.S.A. *Marine Micropaleontology* 121:97–106.
- Molina, E. 2015. Evidence and causes of the main extinction events in the Paleogene based on extinction and survival patterns of foraminifera. *Earth-Science Reviews* 140:166–181.
- Molina, E., L. Alegret, I. Arenillas, and J. A. Arz. 2005. The Cretaceous/Paleogene boundary at the Agost section revisited: paleoenvironmental reconstruction and mass extinction pattern. *Journal of Iberian Geology* 31:137–150.
- Molina, E., L. Alegret, I. Arenillas, J. A. Arz, N. Gallala, J. Hardenbol, K. von Salis, E. Steurbaut, N. Vandenberghe, and D. Zaghbib-Turki. 2006. The Global Stratotype Section and Point of the Danian stage (Paleocene, Paleogene, “Tertiary”, Cenozoic) at El Kef, Tunisia: original definition and revision. *Episodes* 29:263–278.
- Molina, E., L. Alegret, I. Arenillas, J. A. Arz, N. Gallala, M. Grajalés-Nishimura, G. Murillo-Muñeton, and D. Zaghbib-Turki. 2009. The Global Boundary Stratotype Section and Point for the base of the Danian stage (Paleocene, Paleogene, “Tertiary”, Cenozoic): auxiliary sections and correlation. *Episodes* 32:84–95.
- Montgomery, H. 1990. Abnormal terminal Cretaceous foraminifera of east-central Texas. *Texas Journal of Science* 42:37–44.
- Murray, J. W. 2006. *Ecology and applications of benthic foraminifera*. Cambridge University Press, Cambridge.
- Ocampo, A., V. Vajda, and E. Buffetaut. 2006. Unravelling the Cretaceous–Paleogene (KT) turnover: evidence from flora, fauna and geology. Pp. 197–220. *in* C. Cockell, C. Koeberl, and I. Gilmour, eds. *Biological processes associated with impact events*. Springer, Berlin.
- Olsson, R. K., C. Hemleben, W. A. Berggren, and B. T. Huber. 1999. Atlas of Paleocene planktonic Foraminifera. *Smithsonian Contributions to Paleobiology*. 85:1–252.
- Olsson, R. K., J. D. Wright, and K. G. Miller. 2001. Paleobiogeography of *Pseudotextularia elegans* during the latest Maastrichtian global warming event. *Journal of Foraminiferal Research* 31:275–282.
- Omaña, L., G. Alencáster, J. R. Torres Hernández, and R. López Doncel. 2012. Morphological abnormalities and dwarfism in Maastrichtian foraminifera from the Cárdenas Formation, Valles-San Luis Potosí Platform, Mexico: evidence of paleoenvironmental stress. *Boletín de la Sociedad Geológica Mexicana* 64:305–318.
- Pardo, A., and G. Keller. 2008. Biotic effects of environmental catastrophes at the end of the Cretaceous and Early Tertiary: *Guembelitra* and *Heterohelix* blooms. *Cretaceous Research* 29:1058–1073.
- Petersen, S. V., A. Dutton, and K. C. Lohmann. 2016. End-Cretaceous extinction in Antarctica linked to both Deccan volcanism and meteorite impact via climate change. *Nature Communications* 7:12079.
- Polovodova, I., and J. Schönfeld. 2008. Foraminiferal test abnormalities in the western Baltic sea. *Journal of Foraminiferal Research* 38:318–336.
- Pope, K. O., K. H. Baines, A. C. Ocampo, and B. A. Ivanov. 1997. Energy, volatile production, and climatic effects of the Chicxulub Cretaceous/Tertiary impact. *Journal of Geophysical Research* 102:21.
- Premovic, P. I., B. Z. Todorovic, and M. N. Stankovic. 2008. Cretaceous–Paleogene boundary (KP/B) Fish Clay at Højerup (Stevns Klint, Denmark): Ni, Co, and Zn of the black marl. *Geologica Acta* 6:369–382.
- Punekar, J., P. Mateo, and G. Keller. 2014. Effects of Deccan volcanism on paleoenvironment and planktic foraminifera: a global survey. *Geological Society of America Special Paper* 505:91–116.
- Punekar, J., G. Keller, H. M. Khozyem, T. Adatte, E. Font, and J. Spangenberg. 2016. A multi-proxy approach to decode the end-Cretaceous mass extinction. *Palaeogeography, Palaeoclimatology, Palaeoecology* 441:116–136.
- Quillévéré, F., R. D. Norris, D. Kroon, and P. A. Wilson. 2008. Transient ocean warming and shifts in carbon reservoirs during the early Danian. *Earth and Planetary Science Letters* 265:600–615.
- Richards, M. A., W. Alvarez, S. Self, L. Karlstrom, P. R. Renne, M. Manga, C. J. Sprain, J. Smit, L. Vanderkluysen, and S. A. Gibson. 2015. Triggering of the largest Deccan eruptions by the Chicxulub impact. *Geological Society of America Bulletin* 127:1507–1520.
- Robin, E., D. Boclet, Ph. Bonte, L. Froget, C. Jehanno, and R. Rocchia. 1991. The stratigraphic distribution of Ni-rich spinels in

- Cretaceous–Tertiary boundary rocks at El Kef (Tunisia), Caravaca (Spain) and Hole 761C (Leg 122). *Earth and Planetary Science Letters* 107:715–721.
- Röhl, U., J. G. Ogg, T. L. Geib, and G. Wefer. 2001. Astronomical calibration of the Danian time scale. In D. Kroon, R. D. Norris, and A. Klaus, eds. *Western North Atlantic Paleogene and Cretaceous palaeoceanography*. Geological Society of London Special Publication 183:163–183.
- Samir, A. M., and A. B. El Din. 2001. Benthic foraminiferal assemblages and morphological abnormalities as pollution proxies in two Egyptian bays. *Marine Micropaleontology* 41:193–129.
- Schoene, B., K. M. Samperton, M. P. Eddy, G. Keller, T. Adatte, S. A. Bowring, S. F. R. Khadri, and B. Gerch. 2015. U-Pb geochronology of the Deccan Traps and relation to the end-Cretaceous mass extinction. *Science* 347:182–184.
- Schueth, J. D., T. J. Bralower, S. Jiang, and M. E. Patzkowsky. 2015. The role of regional survivor incumbency in the evolutionary recovery of calcareous nannoplankton from the Cretaceous/Paleogene (K/Pg) mass extinction. *Paleobiology* 41:1–19.
- Schulte, P., L. Alegret, I. Arenillas, J. A. Arz, P. J. Barton, P. R. Bown, T. J. Bralower, G. L. Christeson, P. Claeys, C. S. Cockell, G. S. Collins, A. Deutsch, T. J. Goldin, K. Goto, J. M. Grajales-Nishimura, R. A. F. Grieve, S. P. S. Gulick, K. R. Johnson, W. Kiessling, C. Koeberl, D. A. Kring, K. G. MacLeod, T. Matsui, J. Melosh, A. Montanari, J. V. Morgan, C. R. Neal, D. J. Nichols, R. D. Norris, E. Pierazzo, G. Ravizza, M. Rebolledo-Vieyra, W. U. Reimold, E. Robin, T. Salge, R. P. Speijer, A. R. Sweet, J. Urrutia-Fucugauchi, V. Vajda, M. T. Whalen, and P. S. Willumsen. 2010. The Chicxulub asteroid impact and mass extinction at the Cretaceous–Paleogene boundary. *Science* 327:1214–1218.
- Smit, J. 1982. Extinction and evolution of planktonic foraminifera after a major impact at the Cretaceous/Tertiary boundary. *Geological Society of America Special Paper* 190:329–352.
- . 1990. Meteorite impact, extinctions and the Cretaceous/Tertiary Boundary. *Geologie en Mijnbouw* 69:187–204.
- . 1999. The global stratigraphy of the Cretaceous–Tertiary Boundary impact ejecta. *Annual Review of Earth and Planetary Sciences* 27:75–113.
- . 2004. The section of the Barranco del Gredero (Caravaca, SE Spain): a crucial section from the Cretaceous/Tertiary boundary impact extinction hypothesis. *Journal of Iberian Geology* 31:181–193.
- Smit, J., and J. Hertogen. 1980. An extraterrestrial event at the Cretaceous–Tertiary boundary. *Nature* 285:198–200.
- Smit, J., and A. J. T. Romein. 1985. A sequence of events across the Cretaceous–Tertiary boundary. *Earth and Planetary Science Letters* 74:155–170.
- Smit, J., and W. G. H. Z. ten Kate. 1982. Trace-element patterns at the Cretaceous–Tertiary boundary—consequences of a large impact. *Cretaceous Research* 3:307–332.
- Smit, J., T. B. Roep, W. Alvarez, A. Montanari, P. Claeys, J. M. Grajales-Nishimura, and J. Bermudez. 1996. Coarse-grained, clastic sandstone complex at the K/T boundary around the Gulf of Mexico: deposition by tsunami waves induced by the Chicxulub impact? *Geological Society of America Special Paper* 307:151–182.
- Stouff, V., J. P. Debenay, and M. Lesourd. 1999. Origin of double and multiple tests in benthic foraminifera: observations in laboratory cultures. *Marine Micropaleontology* 36:189–204.
- Sujata, K. R., R. Nigam, R. Saraswat, and V. N. Linshy. 2011. Regeneration and abnormality in benthic foraminifera *Rosalina leei*: implications in reconstructing past salinity changes. *Rivista Italiana di Paleontologia e Stratigrafia* 117:189–196.
- Thibault, N., B. Galbrum, S. Gardin, F. Minoletti, and L. Le Calonnec. 2016. The end-Cretaceous in the southwestern Tethys (Elles, Tunisia): orbital calibration of paleoenvironmental events before the mass extinction. *International Journal of Earth Sciences (Geologische Rundschau)* 105:771–795.
- Toon, O., D. Morrison, R. P. Turco, and C. Covey. 1997. Environmental perturbations caused by the impacts of asteroids and comets. *Reviews of Geophysics* 35:41–78.
- Tyszk, J. 2006. Morphospace of foraminiferal shells: results from the moving reference model. *Lethaia* 39:1–12.
- Vellekoop, J., A. Sluijs, J. Smit, S. Schouten, J. W. H. Weijers, J. S. S. Damsté, and H. Brinkhuis. 2014. Rapid short-term cooling following the Chicxulub impact at the Cretaceous–Paleogene boundary. *Proceedings of the National Academy of Sciences USA* 111:7537–7541.
- Vellekoop, J., J. Smit, B. van de Schootbrugge, J. W. H. Weijers, S. Galeotti, J. S. Sinninghe Damsté, and H. Brinkhuis. 2015. Palynological evidence for prolonged cooling along the Tunisian continental shelf following the K–Pg boundary impact. *Palaeogeography, Palaeoclimatology, Palaeoecology* 426:216–228.
- Venturati, A. 2006. Twin and bilobated chambered Cretaceous planktonic foraminifera: abnormal forms induced by high paleoenvironmental stress? Pp. 25–29 in *Proceedings of National Conference “Geosciences 2006,”* Sofia, Bulgaria.
- Verga, D., and I. Premoli Silva. 2002. Early Cretaceous planktonic foraminifera from the Tethys: the genus *Leupoldina*. *Cretaceous Research* 23:189–212.
- Wade, B. R., P. N. Pearson, W. A. Berggren, and H. Pälike. 2011. Review and revision of Cenozoic tropical planktonic foraminiferal biostratigraphy and calibration to the geomagnetic polarity and astronomical time scale. *Earth-Science Reviews* 104:111–142.
- Weinkauf, M. F. G., T. Moller, M. C. Koch, and M. Kucera. 2014. Disruptive selection and bet-hedging in planktonic Foraminifera: shell morphology as predictor of extinctions. *Frontiers in Ecology and Evolution* 2:1–12.
- Yanko, V., M. Ahmad, and M. Kaminski. 1998. Morphological deformities of benthic foraminiferal tests in response to pollution by heavy metals: implication for pollution monitoring. *Journal of Foraminiferal Research* 28:177–200.

**4.3. Influence of the Latest Maastrichtian Warming Event on planktic foraminiferal assemblages and ocean carbonate saturation at Caravaca, Spain.**

**Gilbert, V.,** Arz, J.A., Arenillas, I., Robinson, S.A., and Ferrer, D., 2021. Influence of the Latest Maastrichtian Warming Event on planktic foraminiferal assemblages and ocean carbonate saturation at Caravaca, Spain. *Cretaceous Research* 125, 104844. <https://doi.org/10.1016/j.cretres.2021.104844>.

El material suplementario de este artículo se encuentra en el apartado Anexos (Anexo II).



# Influence of the Latest Maastrichtian Warming Event on planktic foraminiferal assemblages and ocean carbonate saturation at Caravaca, Spain

Vicente Gilabert <sup>a, \*</sup>, José A. Arz <sup>a</sup>, Ignacio Arenillas <sup>a</sup>, Stuart A. Robinson <sup>b</sup>, Daniel Ferrer <sup>a</sup>

<sup>a</sup> Departamento de Ciencias de La Tierra, and Instituto Universitario de Investigación en Ciencias Ambientales de Aragón, Universidad de Zaragoza, E-50009 Zaragoza, C/ Pedro Cerbuna 12, 50009 Zaragoza, Spain

<sup>b</sup> Department of Earth Sciences, University of Oxford, South Parks Road, Oxford, OX1 3AN, UK

## ARTICLE INFO

### Article history:

Received 26 May 2020

Received in revised form

16 February 2021

Accepted in revised form 31 March 2021

Available online 14 April 2021

### Keywords:

Deccan volcanism

Stable isotopes

Mass extinction

Western Tethys

## ABSTRACT

A global warming episode in the Late Cretaceous, the Latest Maastrichtian Warming Event (LMWE), has been commonly linked to both the onset of massive Deccan Trap volcanism and the start of a planktic foraminiferal mass extinction prior to the Cretaceous/Paleogene boundary (KPB). The mechanisms that drove the LMWE are still under discussion, but radiometric dating of the onset of the main phase of the Deccan volcanism supports a temporal coincidence and permits a potential mechanistic link. Here we evaluate the planktic foraminiferal record, carbonate content and stable carbon and oxygen isotopes in the Caravaca section, in order to characterize paleoenvironmental change related to the LMWE. We identified negative  $\delta^{13}\text{C}$  and  $\delta^{18}\text{O}$  excursions in bulk carbonate from 66.35 to 66.14 Ma, i.e. ~310 to ~100 kyr before the KPB, which can be stratigraphically correlated to the LMWE and a major pulse of Deccan Traps volcanism. Within this warm interval, we identified high values in the fragmentation index of planktic foraminiferal tests, episodes of very high abundance of the low oxygen tolerant genus *Heterohelix*, a decrease of thermocline dwellers, dwarfing in *Contusotruncana contusa* tests, and an increase in the biserial morphotype of *Pseudoguembelina hariaensis* with elongated terminal chambers. However, the environmental disturbance during the LMWE did not cause changes in the planktic foraminiferal extinction rate. At Caravaca, the warming associated with LMWE was followed by a gradual cooling up to the KPB suggesting no extended interval of perturbed environments before the KPB extinction due to Deccan volcanism.

© 2021 Elsevier Ltd. All rights reserved.

## 1. Introduction

For more than 40 years there has been a debate about the tempo and causes of the end-Cretaceous mass extinction ~66 Ma ago, with the Chicxulub impact widely argued to be the major contributing factor (e.g., Alvarez et al., 1980; Hull et al., 2020; Kring, 2007; Schulte et al., 2010a; Smit, 1982). Nonetheless, more accurate magnetostratigraphic studies (Chenet et al., 2007, 2009) and radiogenic isotope dating of rocks from the Deccan Traps in India (Chenet et al., 2008), have fueled the debate over whether there was a single cause, the Chicxulub impact (Schulte et al., 2010a,b), or

a combination of causes, with uncertain relative contributions (Courtilot and Fluteau, 2010; Keller et al., 2010). Radiometric dating of intertrappean zircon crystals using the uranium-lead (U–Pb) geochronometer (Schoene et al., 2015, 2019), and new precise ages using  $^{40}\text{Ar}/^{39}\text{Ar}$  geochronology, have proven that the Deccan megaflores erupted during almost 1 Ma, fully spanning the magnetochron C29r (Renne et al., 2015; Sprain et al., 2019) in which the Cretaceous/Paleogene boundary (KPB) event occurred. Planktic foraminiferal biostratigraphic studies in the intertrappean marine sediments from the Krishna–Godavari Basin, SE India, are consistent with an onset of the Deccan main eruptive phase near the C29r/C30n reversal (Keller et al., 2008, 2012).

A decline in the marine  $^{187}\text{Os}/^{188}\text{Os}$  ratio (Robinson et al., 2009) provides the most unequivocal geochemical evidence for the timing in the marine sedimentary record of this latest Maastrichtian high-flux magma pulse. Although some authors have

\* Corresponding author.

E-mail addresses: [vgilabert@unizar.es](mailto:vgilabert@unizar.es) (V. Gilabert), [josearz@unizar.es](mailto:josearz@unizar.es) (J.A. Arz), [ias@unizar.es](mailto:ias@unizar.es) (I. Arenillas), [stuart.robinson@earth.ox.ac.uk](mailto:stuart.robinson@earth.ox.ac.uk) (S.A. Robinson), [danielferrer26795@gmail.com](mailto:danielferrer26795@gmail.com) (D. Ferrer).

suggested an increased input of volcanogenic Hg during the latest Maastrichtian (e.g., Sial et al., 2016; Font et al., 2016, Font et al., 2017) the patterns are not consistent between sites or through time (Percival et al., 2018), suggesting this proxy cannot be used as a reliable and consistent stratigraphic marker of Deccan volcanism. Alongside the geochemical evidence for volcanism, other records suggest that the carbonate system was perturbed during this time, possibly as a result of outgassing from the Deccan Traps (e.g. Kucera et al., 1997; Font et al., 2014; Punekar et al., 2014; Henehan et al., 2016; Keller et al., 2016; Dameron et al., 2017).

Global warming intervals during the KPB interval have been well documented from oxygen isotope ( $\delta^{18}\text{O}$ ) records for several decades, and have been commonly related to increased emissions of carbon dioxide greenhouse gases from the Deccan Traps (Stott and Kennett, 1990; Li and Keller, 1998a; Barrera and Savin, 1999). The magnitude of the temperature increase during the well-known Latest Maastrichtian Warming Event (LMWE) has been estimated to have been between 5 and 8 °C in the terrestrial realm from localities in North America (Nordt et al., 2003; Wilf et al., 2003) and NE China (Zhang et al., 2018). In the marine realm, contemporaneous warming episodes have been recognized in the North Atlantic Ocean ( $3.9 \pm 1.1$  °C in the ODP 174AX Bass River core by Woelders et al., 2018), the South Atlantic Ocean ( $\sim 2$  to 5 °C at ODP 1262 and DSDP 525A Sites by Barnett et al., 2018; Li and Keller, 1998a); Pacific Ocean ( $\sim 3$  °C at ODP 1209 Site by Westerhold et al., 2011); and the Southern Ocean ( $7.8 \pm 3.3$  °C at Seymour Island by Petersen et al., 2016). Recently, Hull et al. (2020) have modelled several scenarios for the timing of outgassing from the Deccan Traps and the climatic effects of volcanic emissions of  $\text{CO}_2$  and  $\text{SO}_2$ . Based on this modelling, Hull et al. (2020) suggest that the most likely scenario was one in which 50% of the degassing of the Deccan Traps occurred between 358 kyr (C29r/C30n reversal boundary) and 218 kyr before the KPB, with the other 50% of eruptive degassing events occurring in the early Danian.

Most of the evidence for the paleobiological response to the LMWE comes from marine records including, among others, blooms in the warm-water calcareous nannofossil *Micula murus* (Thibault et al., 2016), blooms of the planktic foraminiferal opportunistic species *Guembelitra cretacea* (Punekar et al., 2014), blooms in *Palyndinium grallator* dinoflagellate cysts (Vellekoop et al., 2019) and changes in bivalve assemblages (Petersen et al., 2016). According to some authors (Wilf et al., 2003; Keller et al., 2008, 2016; Gertsch et al., 2011; Keller, 2014), the age constraints for the LMWE and the terrestrial and marine paleobiological and geochemical data suggest that the global climate change triggered by Deccan volcanism started the end-Cretaceous extinctions. However, others found no evidence of extinctions or significant changes in the community structure of marine microbiota during the LMWE (see extensive compilation in Table S1 of Hull et al., 2020), suggesting that the environmental and climatic effects of Deccan Trap volcanism alone were insufficient to drive biotic extinctions.

To improve our knowledge about the role of the Deccan Traps in the complex paleoclimatic and paleobiological changes that took place during the latest Maastrichtian, we provide a detailed multiproxy analysis of the last  $\sim 400$  kyr of the Maastrichtian at the Caravaca section (SE Spain, western Tethys), including quantitative, biometric and taphonomic studies of planktic foraminifera, as well as bulk geochemical measurements (stable C- and O-isotopes,  $\text{CaCO}_3$  content). Several decades ago, the Caravaca section played a key role in testing the tempo and duration of biotic and environmental changes across the KPB (catastrophic vs gradual mass extinction; e.g. Smit, 1982 vs Canudo et al., 1991). However, most of the previous analyses performed at Caravaca have been focused only on the uppermost Maastrichtian rocks ( $\sim$ last meter), thereby

failing to capture the environmental influence of the late Maastrichtian Deccan eruptive phase.

## 2. Geological settings

The Caravaca section is located in southern Spain (Murcia region), about 4 km south of the town of Caravaca, in the Barranco del Gredero ravine ( $38^\circ 04' 36''$  N,  $1^\circ 52' 42''$  W). Geologically, the section lies in the Betic System (Subbetic Zone) which represents the westernmost edge of the Alpine Orogeny. Caravaca is one of the most complete, expanded, and well-exposed KPB outcrops in the world (Smit, 2004) and was designated as an auxiliary section for the Global Boundary Stratotype Section and Point (GSSP) for the base of the Danian Stage (Molina et al., 2009). On the basis of benthic foraminifera, Coccioni and Galeotti (1994) reported that the terminal Maastrichtian to basal Danian sedimentary rocks were deposited in an open marine middle-bathyal environment with a paleodepth of about 600–1000 m, similar to previous estimations of Smit (1982) (Fig. 1).

The uppermost Maastrichtian interval is defined as the Raspay Formation by Chacon (2002) and consists of 45 m of hemipelagic marlstones with some marly limestones intercalations. In this study, we focused only on the last 18.3 m immediately underlying the KPB since, from this level to downwards, the outcrop is no longer accessible.

The stratigraphic interval studied is thicker than that analyzed by Arz et al. (2000), which focused on the KPB mass extinction event, and consists mainly of limy marlstones and marly limestones (Fig. 2) rich in planktic foraminifera with rare, minor intercalations of siliciclastic turbidites. Lithologies have been distinguished on the basis of the  $\text{CaCO}_3$  content with 75–95% for marly limestones, 65–75% for limy marlstones and 35–65% for marlstones. From base to top we differentiated five lithologic intervals: 1) 2.4 m of greyish marly limestones; 2) 5.8 m of whitish limy marlstones with some centimetric to decimetric marly limestones intercalations and some scarce millimetric to centimetric siliciclastic turbidites; 3) 3.6 m of a gradual succession of whitish marlstones, limy marlstones and marly limestones. 4) 4.7 m of a rhythmic alternation between whitish limy marlstones with greyish marly limestones 20–40 cm thick; 5) 1.8 m of massive greyish marlstones with some centimetric to millimetric limy marlstone intercalations that get thinner towards the top. The KPB at Caravaca is marked by a 2 to 3 mm-thick rusty red layer that contains altered microtektites (Smit and Klaver, 1981), as well as anomalously high concentrations of Ir, Co, Cr, Ni, As, Sb, and Se (Smit and Ten Kate, 1982).

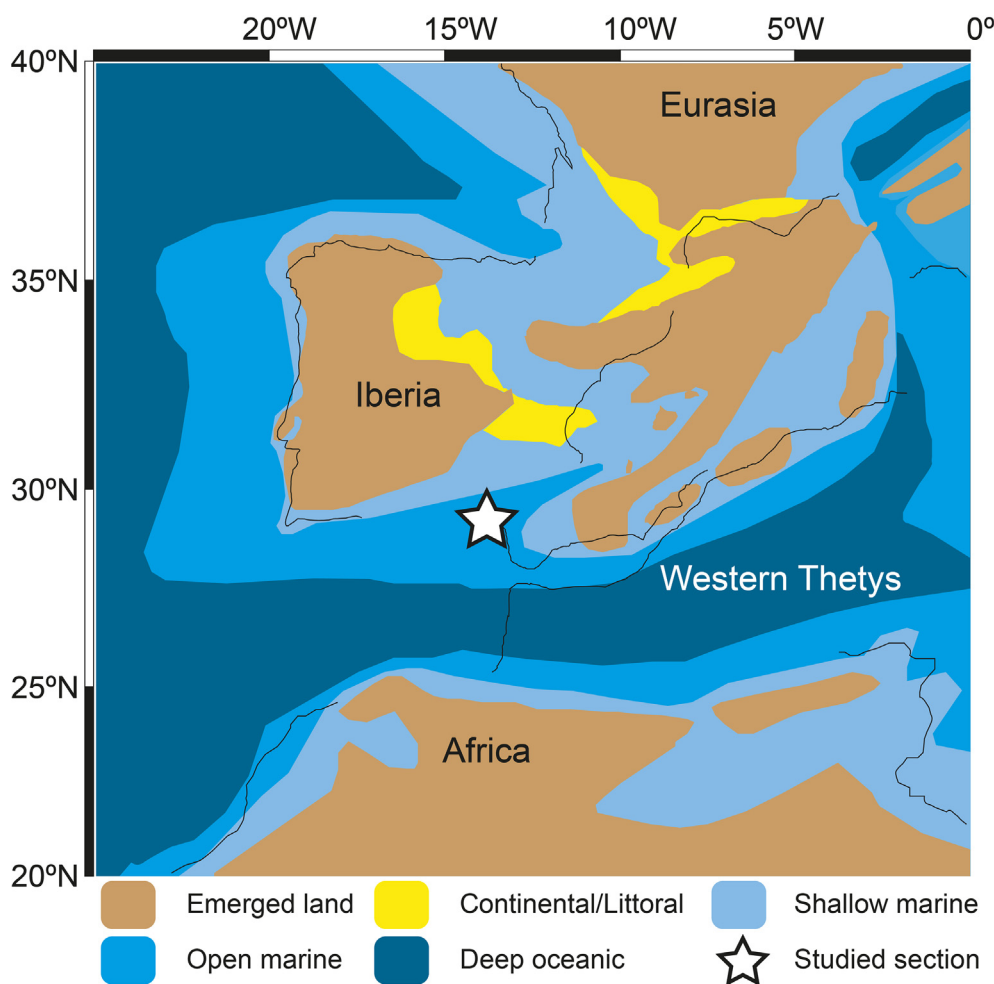
## 3. Material and methods

### 3.1. Micropaleontological methods

Fifty-eight samples were carefully disaggregated in 10% diluted  $\text{H}_2\text{O}_2$  for 2 h each, then washed and passed gently through 63, 100 and 1000  $\mu\text{m}$  mesh sieves, and finally dried in an oven at less than 50 °C. For planktic foraminiferal biostratigraphy, age model and specific richness determinations, we carried out an intensive scanning of the residue to minimize the Signor-Lipps effect (Signor and Lipps, 1982), trying to identify all the scarce species present in the samples (see Table 1 in the supplementary data).

Later, a subset of 35 samples was selected for paleoenvironmental analysis, using an Otto microsampler over the  $>63$   $\mu\text{m}$  size fraction to obtain a representative aliquot in each sample. We randomly picked about 500 whole planktic foraminifera tests per sample, and classified them at genus level in order to evaluate changes in the relative abundance of each genus. Changes in depth-habitat ecogroups were investigated using the deep-surface (D/S)





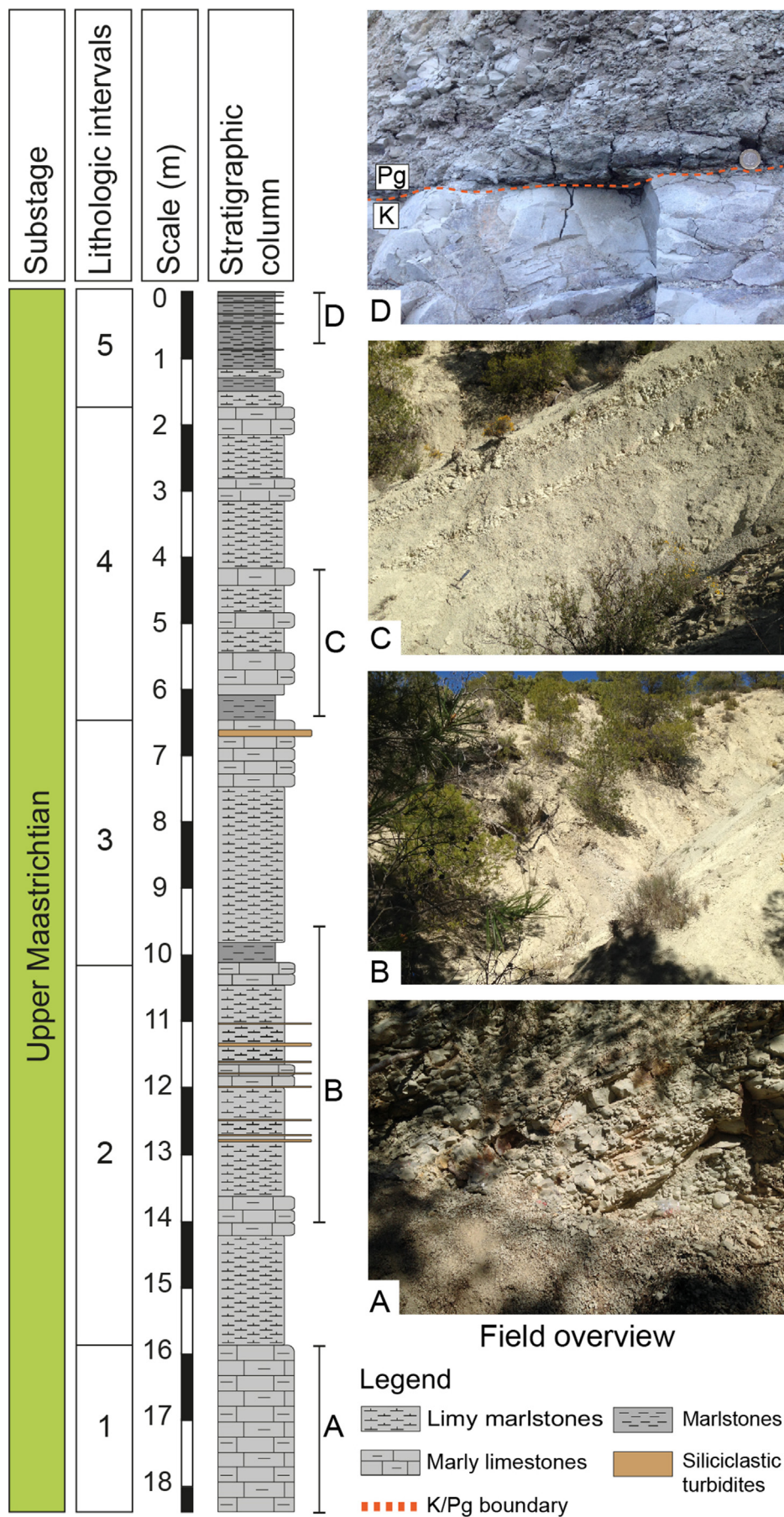
**Fig. 1.** Paleogeographic reconstruction of western Tethys, showing the position of the Caravaca section. Modified from ODSN Plate Tectonics Reconstruction Service and [Andeweg \(2002\)](#).

ratio, calculated as follows:  $D/S = [\text{thermocline dwellers}/(\text{thermocline dwellers} + \text{mixed layer dwellers})]$ . It is used as a proxy to analyze the water column state, with higher values suggesting more stable conditions with a deeper and wider thermocline or an increase in the suitability of the upper water column for planktic foraminifera. Interpretations of depth-habitat ecogroups are based mainly on stable isotope signatures and paleoecological data of planktic foraminiferal species from [D'Hondt and Zachos \(1993\)](#), [D'Hondt and Arthur \(1995\)](#), [Abramovich et al. \(2003\)](#), [Isaza-Londoño et al. \(2006\)](#), [Georgescu et al. \(2008\)](#), [Abramovich et al. \(2010, 2011\)](#), [Ashckenazi-Polivoda et al. \(2014\)](#), [Falzoni et al. \(2014, 2016\)](#), [Petruzzo et al. \(2020\)](#). We have adopted the depth ecology categories of [Petruzzo et al. \(2020\)](#) which differentiate between mixed layer, intermediate and thermocline dwelling planktic foraminifera ([Table 1](#)). Finally, in order to quantify the planktic/benthic (P/B) ratio and estimate changes in the paleobathymetry, we have picked the benthic foraminiferal specimens in each sample over the same split as the 500 whole planktic foraminiferal tests. The P/B ratio was calculated as follow:  $P/B = [\text{planktic foraminifera}/(\text{planktic} + \text{benthic foraminifera})] * 100$ .

For the taphonomic analysis, we additionally picked fragments of planktic foraminiferal tests over the same 35 sample set and  $>63 \mu\text{m}$  splits in order to identify episodes of enhanced fragmentation. Planktic foraminiferal test preservation is usually moderate to good ([Fig. 3](#)), but highly variable in some stratigraphic intervals

([Fig. 4](#)). The fragmentation index is a well-known taphonomic proxy of carbonate saturation state or dissolution of calcium carbonate ([Berger et al., 1982](#); [Malmgren, 1987](#)), and it is considered a better proxy to quantify these variables than other indicators such as weight percent  $\text{CaCO}_3$  or weight percent coarse fraction ([Henehan et al., 2016](#)). The fragmentation index (FI) measures the percentage of planktic foraminiferal fragments (specimens consisting of less than two-third on an entire test) in relation to the total number of whole tests, following [Berger et al. \(1982\)](#). We considered that the dissolution effects upon the composition of planktic foraminifera assemblages were substantially higher in samples with  $FI >40\%$ . This boundary has been previously used to distinguish between regimes of moderate and strong dissolution in other upper Cretaceous sections (e.g., [Malmgren, 1987](#); [Kucera et al., 1997](#)). The sample by sample results of this detailed quantitative taphonomic analysis are listed in [Table 2](#) in the [supplementary data](#).

We have also performed a biometric analysis in order to identify patterns of variation in test size over time in two selected species of planktic foraminifera ([Fig. 5](#)): the mixed layer dweller *Pseudoguembelina hariensis* and the intermediate dweller *Contusotruncana contusa*, one of the largest planktic foraminiferal species ever in evolutionary history. To avoid juvenile specimens, we studied the  $>100 \mu\text{m}$  size fraction, that was split into a representative aliquot using a microsplitter. Then, ten specimens of each



**Fig. 2.** Lithostratigraphic column, lithologic intervals and outcrop views of the Caravaca section. Differences between lithologies are based on CaCO<sub>3</sub> content: 75–95% for marly limestones, 65–75% for limy marlstones and 35–65% for marlstones.

**Table 1**  
Depth related ecogroups of planktic foraminiferal genera during the late Maastrichtian.

Genera	Taxonomic group	Depth ecologies	Average relative abundance
<i>Abathomphalus</i>	Globotruncanids	Thermocline <sup>1,2,3</sup>	<0.1%
<i>Archaeoglobigerina</i>	Rugoglobigerinids	Intermediate <sup>3</sup>	0.1%
<i>Contusotruncana</i>	Globotruncanids	Intermediate <sup>2,3,4,5,6</sup>	0.1%
<i>Globigerinelloides</i>	Globigerinelloids	Intermediate <sup>2,3</sup>	8.6%
<i>Globotruncana</i>	Globotruncanids	Thermocline <sup>1,2,3,6</sup>	1.9%
<i>Globotruncanella</i>	Globotruncanids	Thermocline <sup>1,2,3</sup>	0.8%
<i>Globotruncanita</i>	Globotruncanids	Thermocline <sup>1,2,3,6</sup>	1.6%
<i>Gublerina</i>	Heterohelicids	Thermocline <sup>1,2,7,10</sup>	0.1%
<i>Guembelitra</i>	Guembelitrids	Mixed layer <sup>3,8,9</sup>	1.4%
<i>Muricohedbergella</i>	Hedbergellids	Intermediate <sup>1,3,6</sup>	6.1%
<i>Heterohelix</i>	Heterohelicids	Intermediate <sup>1,2,3,4</sup>	66.2%
<i>Laeviheterohelix</i>	Heterohelicids	Thermocline <sup>1,2</sup>	1.0%
<i>Planoglobulina</i>	Heterohelicids	Intermediate <sup>1,2,3</sup>	0.2%
<i>Pseudoguembelina</i>	Heterohelicids	Mixed layer <sup>2,3,4,8</sup>	6.8%
<i>Pseudotextularia</i>	Heterohelicids	Intermediate <sup>1,2,3,4,6</sup>	0.8%
<i>Racemiguembelina</i>	Heterohelicids	Intermediate <sup>1,3,5,6</sup>	0.4%
<i>Rugoglobigerina</i>	Rugoglobigerinids	Mixed layer <sup>2,3,6,7,8</sup>	3.5%
<i>Plummerita</i>	Rugoglobigerinids	Mixed layer <sup>11</sup>	0.1%
<i>Schackoina</i>	Schackoinids	Mixed layer <sup>3</sup>	0.3%

References: <sup>1</sup>D'Hondt and Arthur (1995); <sup>2</sup>Abramovich et al. (2003); <sup>3</sup>Petrisso et al. (2020); <sup>4</sup>Abramovich et al. (2010); <sup>5</sup>Isaza-Londoño et al. (2006); <sup>6</sup>Falzone et al. (2016); <sup>7</sup>Falzone et al. (2014); <sup>8</sup>Ashckenazi-Polivoda et al. (2014); <sup>9</sup>D'Hondt and Zachos (1993); <sup>10</sup>Georgescu et al. (2008); <sup>11</sup>Abramovich et al. (2011).

species were randomly picked and mounted on standard 60-square micropaleontological slides. In case the aliquot did not contain ten specimens of a species, the splitting was repeated until the whole sample had been completely examined. For biometric analysis, we measured the test height and width of *P. hariaensis*, and height and length of *C. contusa* (see Fig. 5) using an Olympus UC30 digital camera connected to a Zeiss Discovery V.20 stereomicroscope, and the *Stream Image Analysis Software*. In the case of *P. hariaensis*, we differentiate two morphotypes, on the basis of the final serial arrangement of chambers: biserial, with elongated final chambers with subparallel pairs of the last few chambers (Figs. 4A and 5A), or multiserial with one or two sets of small subglobular chamberlets (Figs. 3H and 5B). Both morphotypes have previously been recognized within the inter-specific variability of *P. hariaensis* (e.g., Pl. 3, Figs. 9 and 11 of Coccioni and Premoli Silva, 2015). Biometric data and morphotype relative abundance of 507 specimens are given in Table 3 in the supplementary data.

Biometrically measured planktic foraminiferal specimens were also mounted on in a micropaleontological slide to provide a permanent record. Representative specimens of some relevant species were selected for scanning electron microscopy (SEM) analysis, and photographed using a JEOL JSM 6400 SEM at the Microscopy Service of the Universidad de Zaragoza. In order to ensure the replicability of this research, the micropaleontological material figured in this study is appropriately labelled with MPZ abbreviations (Museo Paleontológico de la Universidad de Zaragoza) and housed in the Natural Science Museum of the University of Zaragoza (Canudo, 2018).

### 3.2. Geochemical methods

The inorganic and organic carbonate content was measured using duplicate powdered subsamples from 87 samples that were weighed into ceramic boats, one of which was roasted in air at 420 °C for 12 h to remove organic carbon. The total carbon content of each subsample was determined using a Strohelein Coulomat 702 in the Department of Earth Sciences, University of Oxford. The difference between the amount of carbon determined in unroasted

and pre-roasted samples provided an estimate of Total Organic Carbon (TOC). Reproducibility of %C using this method is typically better than 0.1%. Assuming that all the inorganic carbon is present as CaCO<sub>3</sub> allows the CaCO<sub>3</sub>% to be calculated by multiplying the inorganic carbon value (from the pre-roasted sample) by 8.333 (recurring).

Stable carbon and oxygen isotopes ( $\delta^{13}\text{C}$ ,  $\delta^{18}\text{O}$ ) were measured using powdered bulk-rock from the same set of 87 samples. Samples were analyzed in the Department of Earth Sciences, University of Oxford using either a GasBench or a Kiel device attached to a ThermoFisher Delta V Advantage gas source isotope ratio mass spectrometer. Data are reported using the standard delta notation in per mil (‰) deviation on the VPDB scale. International and in-house standards were used to ensure the comparability between instruments and the precision and accuracy of the data. Repeated analyses of in-house standards suggest a reproducibility ( $\pm 1\sigma$ ) of <0.1 for both  $\delta^{13}\text{C}$  and  $\delta^{18}\text{O}$ .

## 4. Results

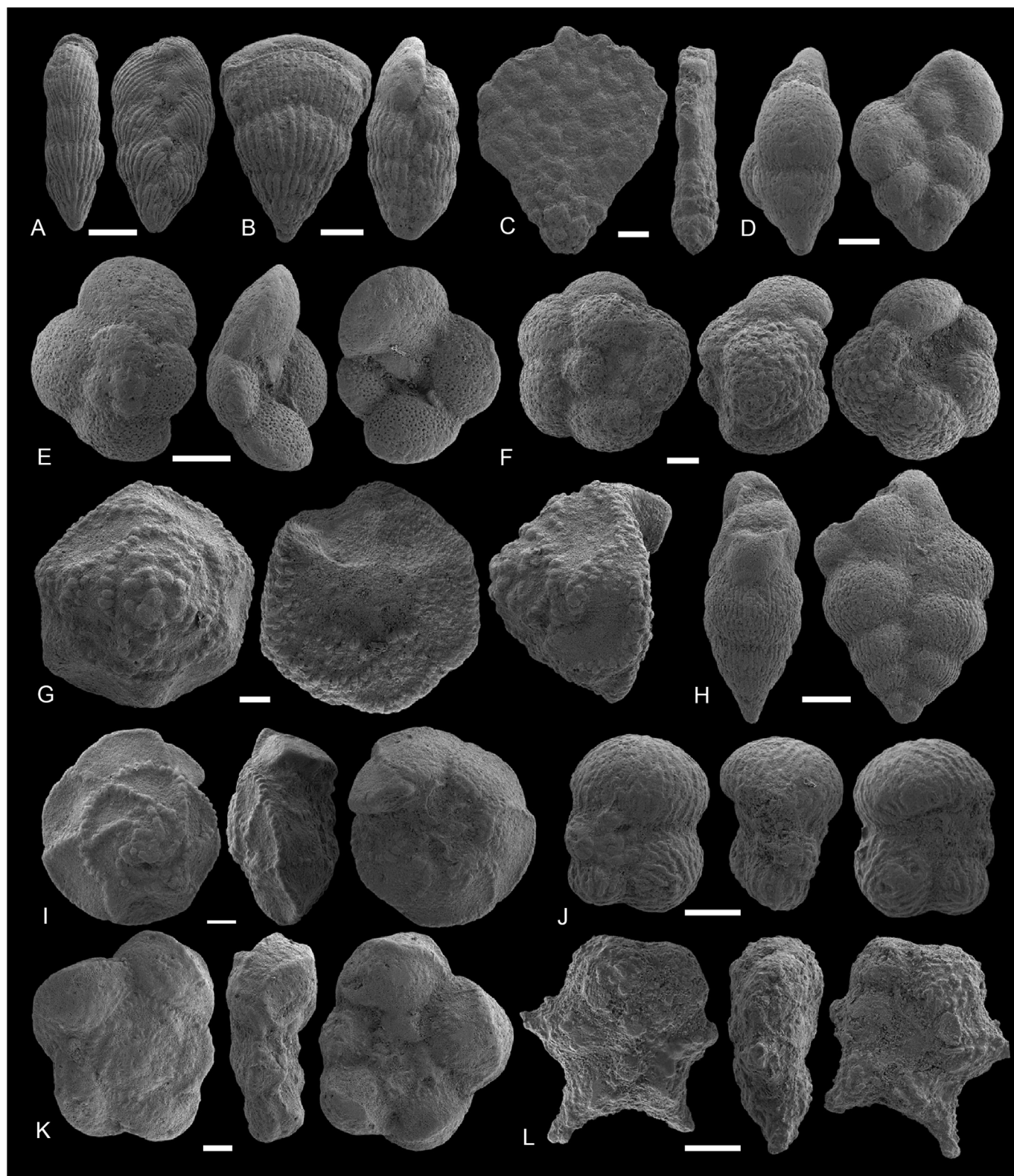
### 4.1. Planktic foraminiferal turnover

At Caravaca, planktic foraminiferal assemblages are characterized by a high diversity and a wide range of size and morphological variability of the tests. Species richness from the base to the top of the studied section remains very high with values between 63 and 69 species per sample. A total of 70 species belonging to 20 genera have been identified throughout the section (Fig. 6 and Table 1 in the supplementary data). Within the interval from 13.80 to 5.05 m below the KPB, the average species richness value is slightly lower (Fig. 7A). This is due to the disappearance of scarcer species, such as *Archaeoglobigerina cretacea*, *A. blowi*, *Globotruncanita falsocarata*, *Abathomphalus intermedius* and *Contusotruncana patelliformis*, that are absent in >20% of the analyzed samples. At Caravaca, we have identified the highest occurrences (HO) of only 4 species: HO of *A. cretacea* at 50 cm below the KPB, HO of *Gita. falsocarata* at 40 cm below the KPB, HO of *A. blowi* at 15 cm below the KPB, and HO of *Planoglobulina manuelensis* at 1 cm below the KPB. All remaining 66 planktic foraminiferal species have been identified in the uppermost sample, just 1 cm below the KPB (Table 1 in the supplementary data).

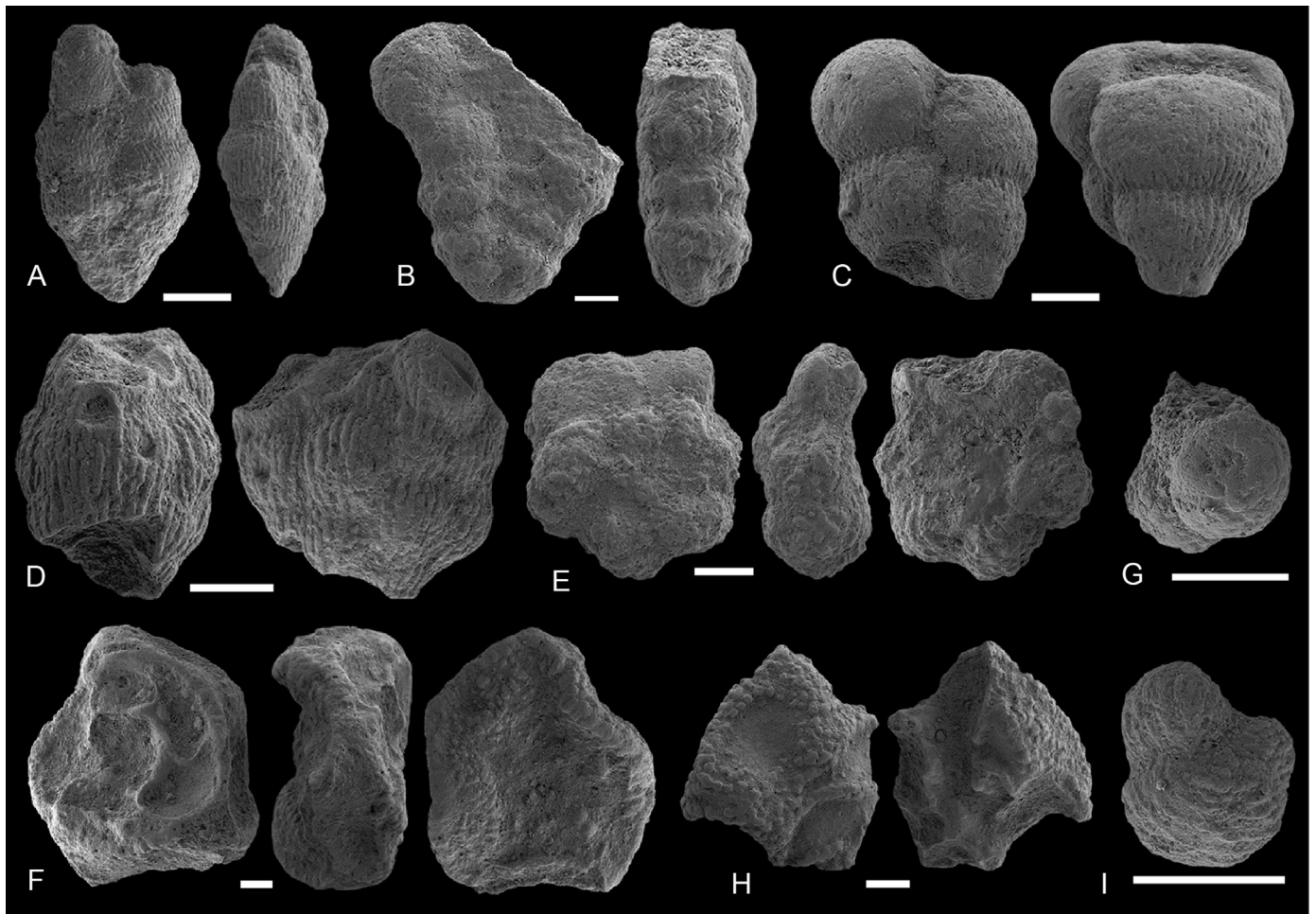
Quantitative data are shown in Table 2 of the supplementary material and plotted in Figs. 7 and 8. The P/B ratio always exceeds 95% (Fig. 7B), suggesting pelagic conditions and a relatively stable paleobathymetry throughout the Caravaca section. Given these broad and stable environmental conditions, it is no surprise that all Maastrichtian planktic foraminiferal ecogroups are well represented (e.g., heterohelicids, pseudoguembelinids, globotruncanids, rugoglobigerinids, hedbergellids, globigerinelloids and schackoinids).

Changes in the deep/surface (D/S) ratio allow us to differentiate three intervals (Fig 7C). In the lower part of the studied section (18.30–13.20 m below the KPB), the D/S ratio varies between 0.28 and 0.52, with an average of 0.39. The lowest D/S ratio values in the Caravaca section have been identified from 13.20 to 5.05 m below the KPB. Within this interval, D/S ratio values range between 0.0 and 0.45, with an average of 0.20. From 5.05 m to the KPB, D/S ratio values range between 0.29 and 0.47, with an average value of 0.39.

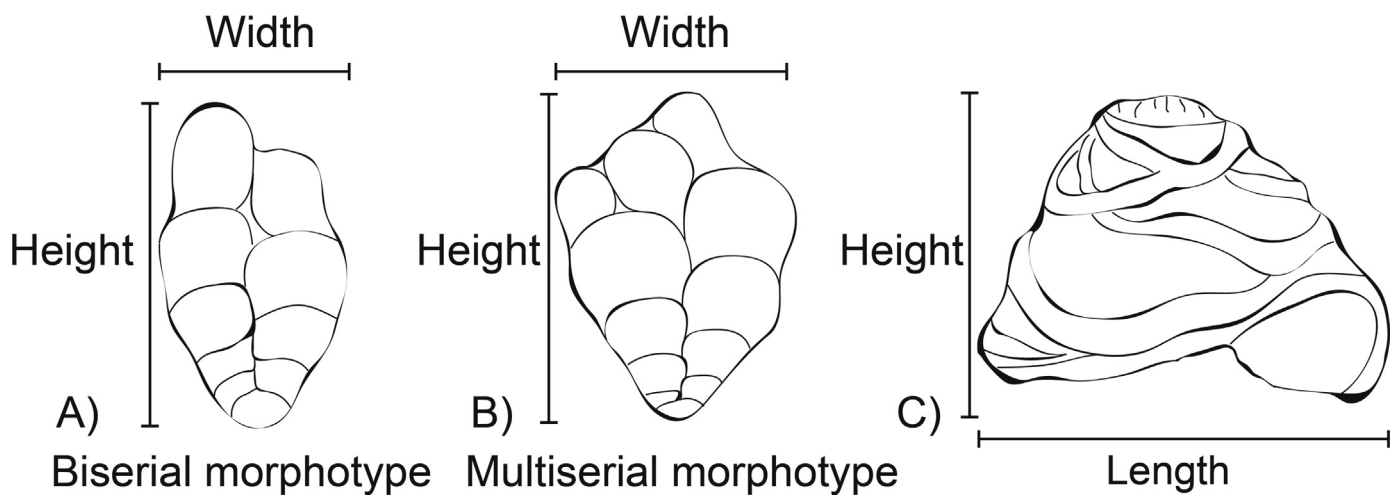
Planktic foraminiferal assemblages in the >63  $\mu\text{m}$  size fraction are dominated by the generalist *Heterohelix*, with an average relative abundance of about 66% (Fig. 8). Other common genera are *Globigerinelloides* (8.6%), *Pseudoguembelina* (6.8%) and *Muricohedbergella* (6.1%). On average, the least abundant genera are *Rugoglobigerina* (3.5%), *Globotruncana* (1.9%), and *Globotruncanita* (1.6%). In Fig. 8, other genera whose average relative abundance is



**Fig. 3.** Examples of moderate to good preserved tests of planktic foraminiferal species from the Caravaca section (scale bars = 100  $\mu$ m): **A**) *Pseudoguembelina costulata*, sample GR-0-2 (MPZ 2019/1), **B**) *Pseudotextularia elegans*, sample GR-0-2 (MPZ 2019/2), **C**) *Planoglobulina multicamerata*, sample GR-0-2 (MPZ 2019/3), **D**) *Pseudoguembelina palpebra*, sample GR-0-2 (MPZ 2019/4), **E**) *Globotruncanella petaloidea*, sample GR-0-2 (MPZ 2019/5), **F**) *Rugoglobigerina rotundata*, sample GR-4-6 (MPZ 2019/6), **G**) *Contusotruncana contusa*, sample GR-4-6 (MPZ 2019/7), **H**) *Pseudoguembelina hariaensis*, multiserial morphotype sample GR-4-6 (MPZ 2019/8), **I**) *Globotruncanita stuarti*, sample GR-4-6 (MPZ 2019/9), **J**) *Rugoglobigerina macrocephala*, sample GR-10 (MPZ 2019/10), **K**) *Abathomphalus mayaroensis*, sample GR-110 (MPZ 2019/11), **L**) *Plummerita hantkeninoides*, sample GR-630 (MPZ 2019/12).



**Fig. 4.** Examples of poor preservation and fragmentation in planktic foraminiferal tests from the Caravaca section (scale bars = 100  $\mu$ m): **A)** *Pseudoguembelina hariaensis*, biserial morphotype sample GR-1830 (MPZ 2019/13), **B)** *Gublerina cuvillieri*, sample GR-1380 (MPZ 2019/14), **C)** *Pseudotextularia nutalli*, sample GR-1020 (MPZ 2019/15), **D)** *Planoglobulina acervulinoides*, sample GR-655 (MPZ 2019/16), **E)** *Rugoglobigerina hexacamerata*, sample GR-1380 (MPZ 2019/17), **F)** *Contusotruncana contusa*, sample GR-1080 (MPZ 2019/18), **G)** fragment indet., sample GR-1290 (MPZ 2019/19), **H)** globotruncanid fragment sample GR-1290 (MPZ 2019/20), **I)** fragment indet., sample GR-655 (MPZ 2019/21).



**Fig. 5.** Biometric variables measured on the tests of selected species and morphotypes. A) Biserial morphotype of *Pseudoguembelina hariaensis*; B) Multiserial morphotype of *P. hariaensis*; C) *Contusotruncana contusa*.

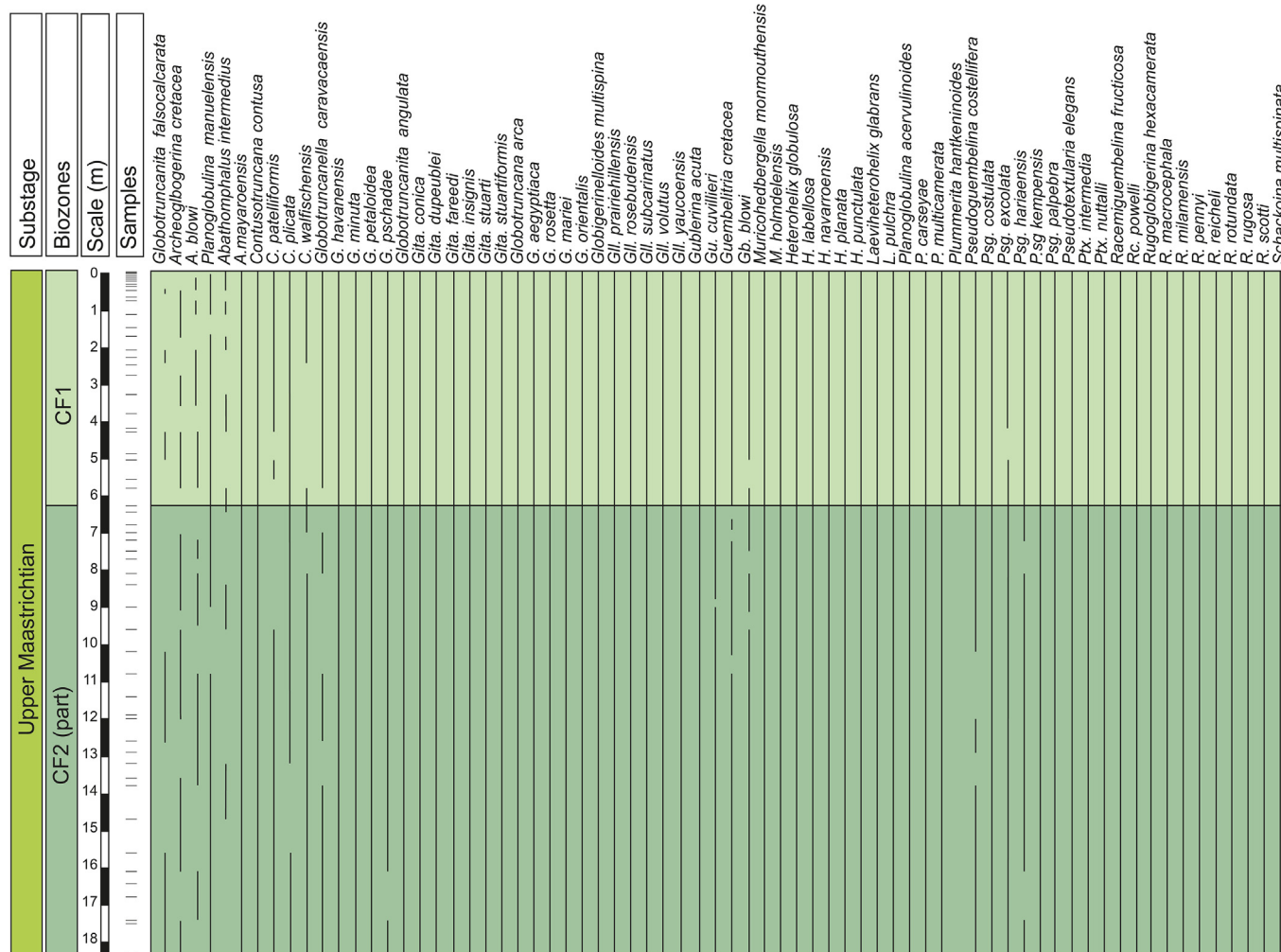


Fig. 6. Stratigraphic distribution of the late Maastrichtian planktic foraminiferal species.

<1% are grouped together. This group is composed of the following genera: *Abathomphalus*, *Archaeoglobigerina*, *Contusotruncana*, *Globotruncanella*, *Gublerina*, *Planoglobulina*, *Pseudotextularia*, *Racemiguembelina*, *Plummerita* and *Schackoina*.

4.1.1. Planktic foraminiferal size and morphological variation

We evaluated changes in test size of two planktic foraminiferal species: *Contusotruncana contusa* (intermediate dweller) and *Pseudoguembelina hariaensis* (mixed layer dweller). Biometric data are provided in Supplementary Table 3 and plotted in Fig. 9. The variation in test size of *C. contusa* is remarkable, especially between 13.8 and 5.05 m below the KPB (Fig. 9A). In this interval, the size reduction is close to 35% and occurs almost equally on both height and length of the test. Conversely, *P. hariaensis* was not affected by dwarfing, since its size progressively increases across the section (Fig. 9B). However, the relative abundance of the two morphotypes of *P. hariaensis* also varies remarkably between 13.2 and 5.05 m below the KPB (Fig. 9C). The biserial morphotype, with elongated final chambers, became more abundant within this depth interval, with a mean relative abundance of about 75%. Multiserial morphotypes, with small chamberlets, tend to dominate below and above this depth interval.

4.1.2. Planktic foraminiferal fragmentation index (FI)

We have recognized FI values higher than 40% in ten samples within two intervals: from 15.60 to 10.80 m and from 7.50 to 6.30 m

below the KPB (Table 2 in the supplementary data and Fig. 10A). Large oscillations in the FI are identified within both intervals, suggesting relatively rapid changes in carbonate dissolution intensity. Nonetheless, most of the studied section is below a moderate/strong dissolution limit of FI < 40% especially in the uppermost 6 m of the Maastrichtian. Linear regressions between FI and CaCO<sub>3</sub> content (Fig. 10B) and between FI and P/B ratios (Fig. 10C) show null and poor correlation coefficients.

4.2. Geochemistry

Total organic carbon (TOC) is less than 0.2%, or below detection limits in some samples, so, these data are not discussed further. % CaCO<sub>3</sub> varies from 55.4% to 82.0%, with a mean value of 72.7% ( $\pm 1\sigma = 5\%$ , n = 87). Stratigraphically there is little variability (Table 4 in the supplementary data), with small scale-fluctuations representing lithological differences between marlstones, marly limestones and limy marlstones.

Carbon-isotope ( $\delta^{13}C$ ) values vary between -0.60 and + 2.12‰ with a mean of +1.44‰ ( $\pm 1\sigma = 0.51\%$ , n = 87; Table 4 in the supplementary data). Oxygen-isotope ( $\delta^{18}O$ ) values vary between -3.17 and -1.80‰, with a mean of -2.21‰ ( $\pm 1\sigma = 0.26\%$ , n = 87). The isotopic data exhibit broad stratigraphic trends, with higher resolution variability superimposed upon these (Fig. 11). At a broad scale across the entire record, both carbon and oxygen isotopes exhibit a broad decrease to minimum values between 13.80

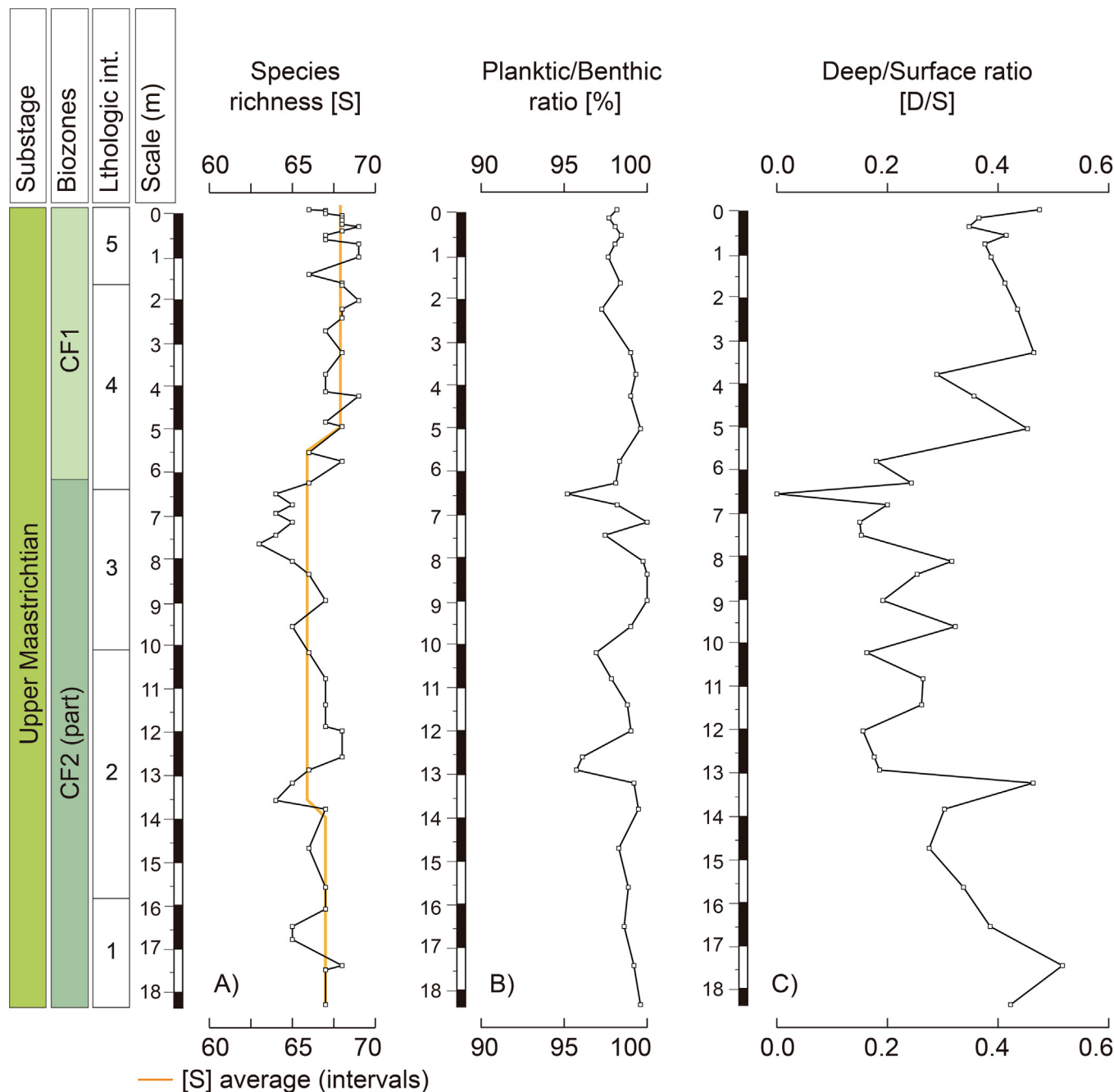


Fig. 7. Shifts in species richness (S), planktic/benthic (P/B) ratio and deep/surface (D/S) ratio.

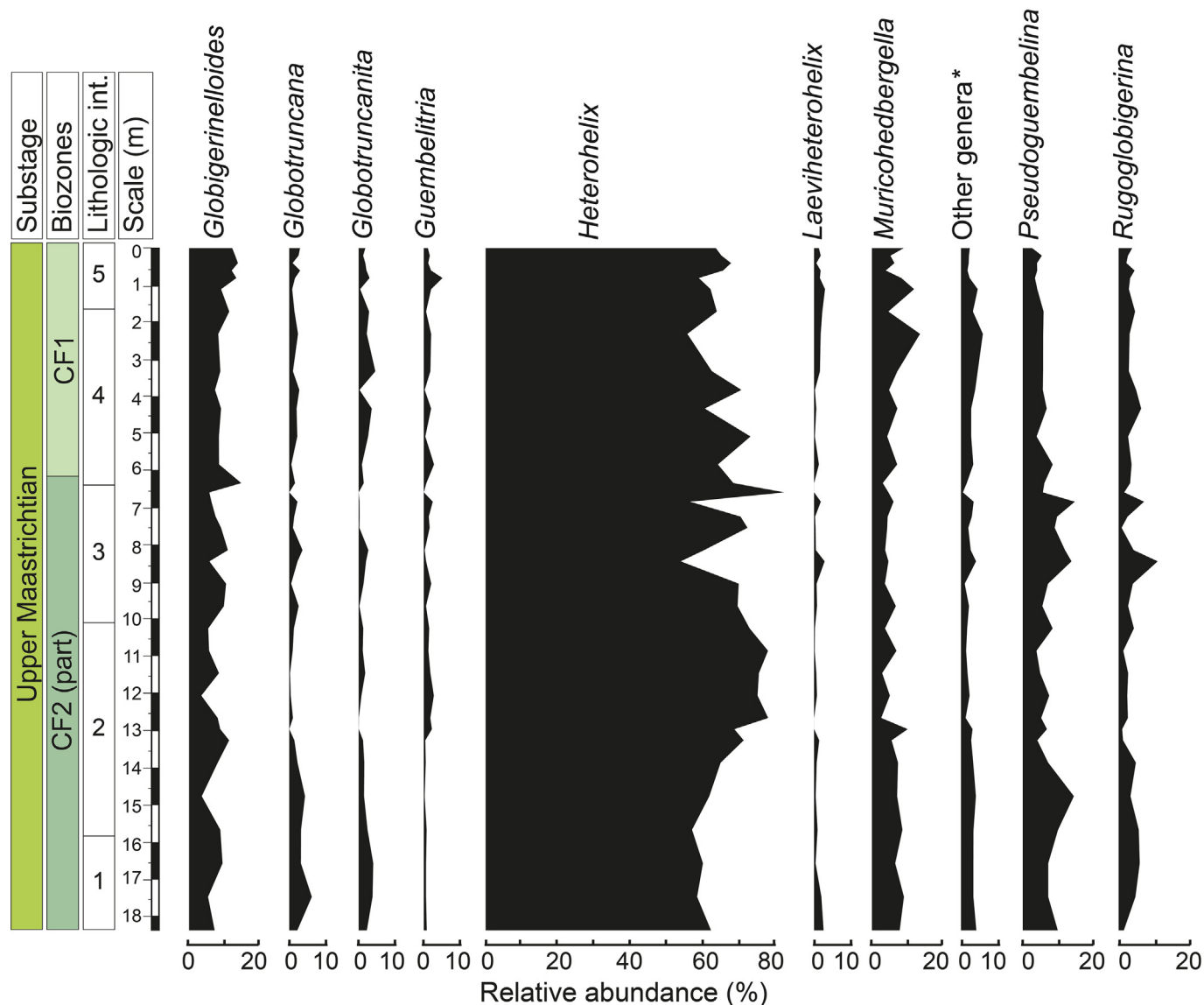
and 5.05 m below the boundary before increasing prior to the KP. In detail, there are notable negative excursions from the broad pattern in both  $\delta^{18}\text{O}$  and  $\delta^{13}\text{C}$ , occurring at 10.80 m, 6.55 m and 6.30 m below the KP.

### 5. Biostratigraphy and age model

Only the last two biozones of Li and Keller (1998b) alphanumerical scale, Zones CF1 (*Plummerita hantkeninoides*) and CF2 (*Pseudoguembelina palpebra*), have been identified at Caravaca (Fig. 6). The lowest occurrence (LO) of *Plummerita hantkeninoides*, the base of Zone CF1, is located 6.3 m below the KP. In this biohorizon, we found the first indubitable specimens of

*P. hantkeninoides* with well-developed tubulospines in the last whorl (Fig. 3L), although proto-*P. hantkeninoides* transitional forms with rugosities and some elongated chambers (but not true tubulospines) are found from 6.8 m below the KP. The HO of *Gansserina gansseri*, the base of Zone CF2, has not been recognized since it occurs >18.3 m below the KP, within strata that are no longer exposed and were, thus, inaccessible to us. Through the whole stratigraphic section, there is no evidence of erosive surfaces or abrupt changes in lithology, so we assume that the sedimentation rate was rather stable across the studied interval.

We have used the Husson et al. (2014) calibration for the Cretaceous part of the C29r magnetochron, which is based on the astrochronological age model from the Contessa Highway and



**Fig. 8.** Quantitative stratigraphic distribution of planktic foraminiferal genera. Other genera includes: *Abathomphalus*, *Archaeoglobigerina*, *Contusotruncana*, *Globotruncanella*, *Gublerina*, *Planoglobulina*, *Pseudotextularia*, *Racemiguembelina*, *Plummerita* and *Schackoina*.

Bottaccione sections near Gubbio, Italy. This age model provides a duration for the Cretaceous part of C29r of ~365 kyr, very similar to that given by GTS 2012 (~358 kyr, Gradstein et al., 2012). Following Renne et al. (2013), the KPB is dated at 66.04 Ma in both time scales. Husson et al. (2014) provided calibrated ages for micropaleontological data, such as the LO of *P. hantkeninoides* at 140 kyr before the KPB. The KPB and the LO of *P. hantkeninoides* have been used as tie points to estimate the linear sedimentation rate of the entire Caravaca section, resulting in an average of 4.5 cm/kyr.

At Bottaccione (Gubbio), the LO of *P. hantkeninoides* and HO of *G. gansseri* are, respectively, 1.4 and 4.7 m below the KPB (Husson et al., 2014; Coccioni and Premoli Silva, 2015). Assuming a constant sedimentation rate of 4.5 cm/kyr for Caravaca and correlating with planktic foraminiferal data from Gubbio, the HO of *G. gansseri* should be located 21.15 m below the KPB of Caravaca, so the studied section spans approximately the uppermost 80% of Zone CF2. In this age framework, the materials studied and discussed here span the last ~400 kyr of the Maastrichtian.

## 6. Global correlation of the isotope record and Latest Maastrichtian Warming Event

### 6.1. Veracity of the isotope records

Bulk stable-isotope records from pelagic marls, chalks and limestones have been used extensively for chemostratigraphic correlation and for reconstructing trends in Cretaceous climate (e.g., Scholle and Arthur, 1980; Jenkyns et al., 1994; Clarke and Jenkyns, 1999; Jarvis et al., 2006). However, before interpreting such data as a record of primary signals from Cretaceous seawater, diagenetic effects must be discounted. The  $\delta^{13}\text{C}$  and  $\delta^{18}\text{O}$  data from Caravaca presented here have values that are consistent with carbonate formation from Late Cretaceous seawater (Table 4 in the supplementary data) and are comparable to previous studies from the KPB interval itself at Caravaca (Kaiho and Lamolda, 1999; Sosa-Montes de Oca et al., 2016). A cross plot (Fig. 12C) shows that a positive correlation exists between  $\delta^{13}\text{C}$  and  $\delta^{18}\text{O}$ . Although this



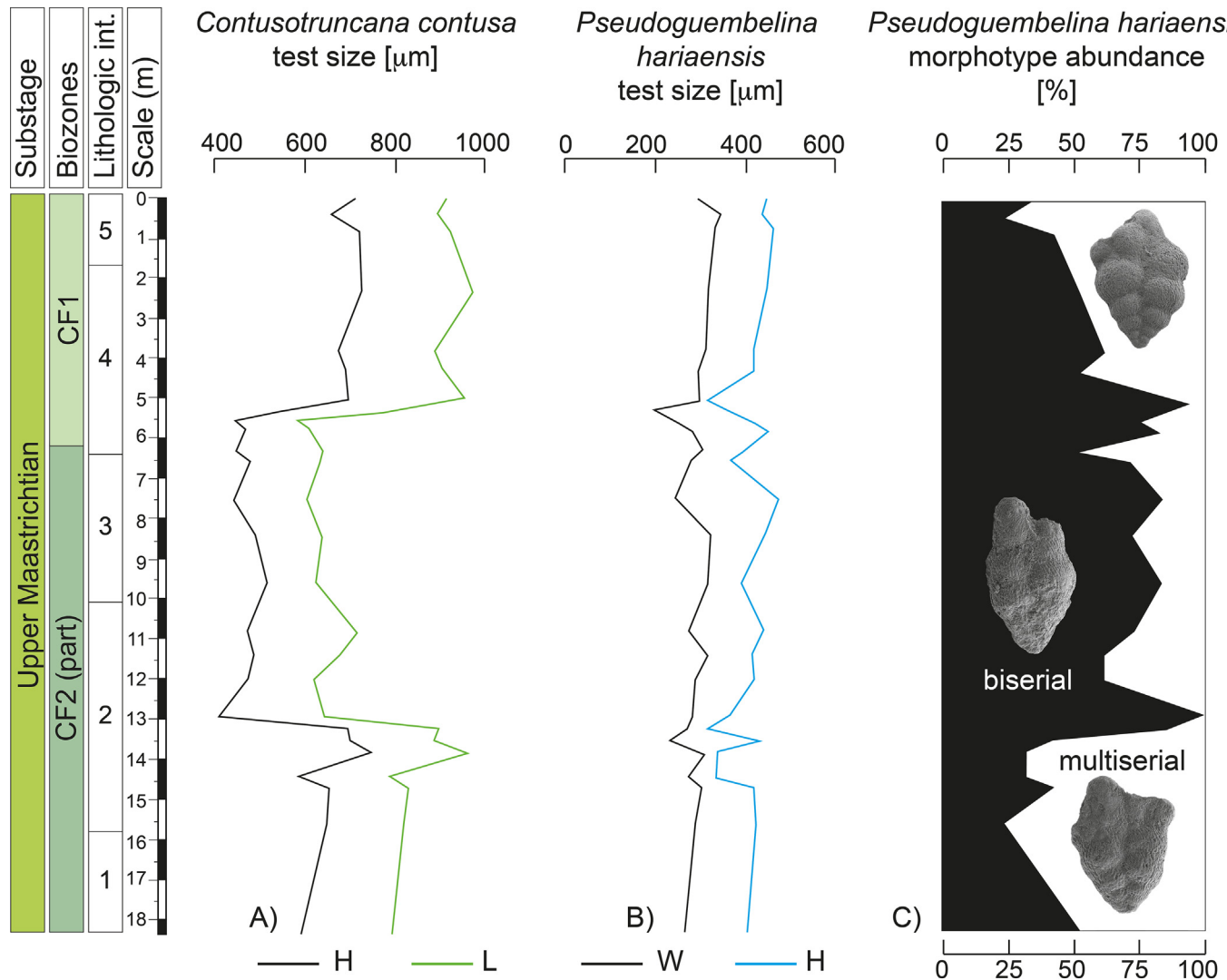


Fig. 9. Changes in the test size of *C. contusa* (A) and *P. hariaensis* (B), and in the relative abundance of *P. hariaensis* biserial morphotype (C).

relationship could be an indicator of a minor contribution of diagenetic calcite (with isotopically low  $\delta^{13}\text{C}$  and  $\delta^{18}\text{O}$  values).

Three samples, in particular, appear to have slightly lower  $\delta^{13}\text{C}$  and  $\delta^{18}\text{O}$  values than the remainder of the dataset and could, therefore, be outliers as a consequence of either unknown analytical issues, a more significant contribution of diagenetic calcite or short-term warming events associated with isotopically lighter DIC. When plotted stratigraphically, these three samples with relatively low  $\delta^{13}\text{C}$  and  $\delta^{18}\text{O}$  values (highlighted in Fig. 13) are offset from the remainder of the dataset. However, we note that they occur within intervals of relatively low background values and that ‘extreme’ values are within the broad range of possible seawater values recorded by pelagic sediments. We cannot exclude the possibility that these samples are outliers (as a consequence of diagenesis or analysis) but we have no analytical or geological justification for excluding them entirely from the dataset at this point.

Overall, the small range of oxygen-isotope values, their absolute value, and the moderate to good preservation of the planktic foraminifer are not consistent with extensive burial diagenesis nor the influence of meteoric waters. Furthermore, there is no relationship between  $\%\text{CaCO}_3$  and the stable-isotope data (Figs. 12A–B), suggesting that lithology exerts little control on the measured

isotope values. There are statistically significant negative relationships between the fragmentation index and both  $\delta^{13}\text{C}$  and  $\delta^{18}\text{O}$  (Figs. 12D–E), but with very weak correlation coefficients. These relationships could suggest that differential degrees of dissolution of some carbonate components (most likely planktic foraminifera) may be contributing to the covariance of  $\delta^{13}\text{C}$  and  $\delta^{18}\text{O}$ , but the weak regression coefficients suggest that, if true, this cannot be a major effect. We cannot constrain absolute paleotemperatures from the  $\delta^{18}\text{O}$  data with confidence due to varying sources of carbonate within the sediment, but given the dominance of calcareous plankton observed by us, the isotopic trends presented here likely reflect the average isotopic signature of the planktic dwellers of the upper part of the water column. In light of the considerations discussed here, we suggest that the stable-isotope data from Caravaca most likely reflect primary trends in Maastrichtian seawater chemistry and temperature.

## 6.2. Identifying the LMWE at Caravaca

The Maastrichtian was a relatively cool period in the Late Cretaceous, following the long-term cooling trend in the Campanian (e.g. Huber et al., 1995, 2018; Linnert et al., 2014; O’Brien et al.,

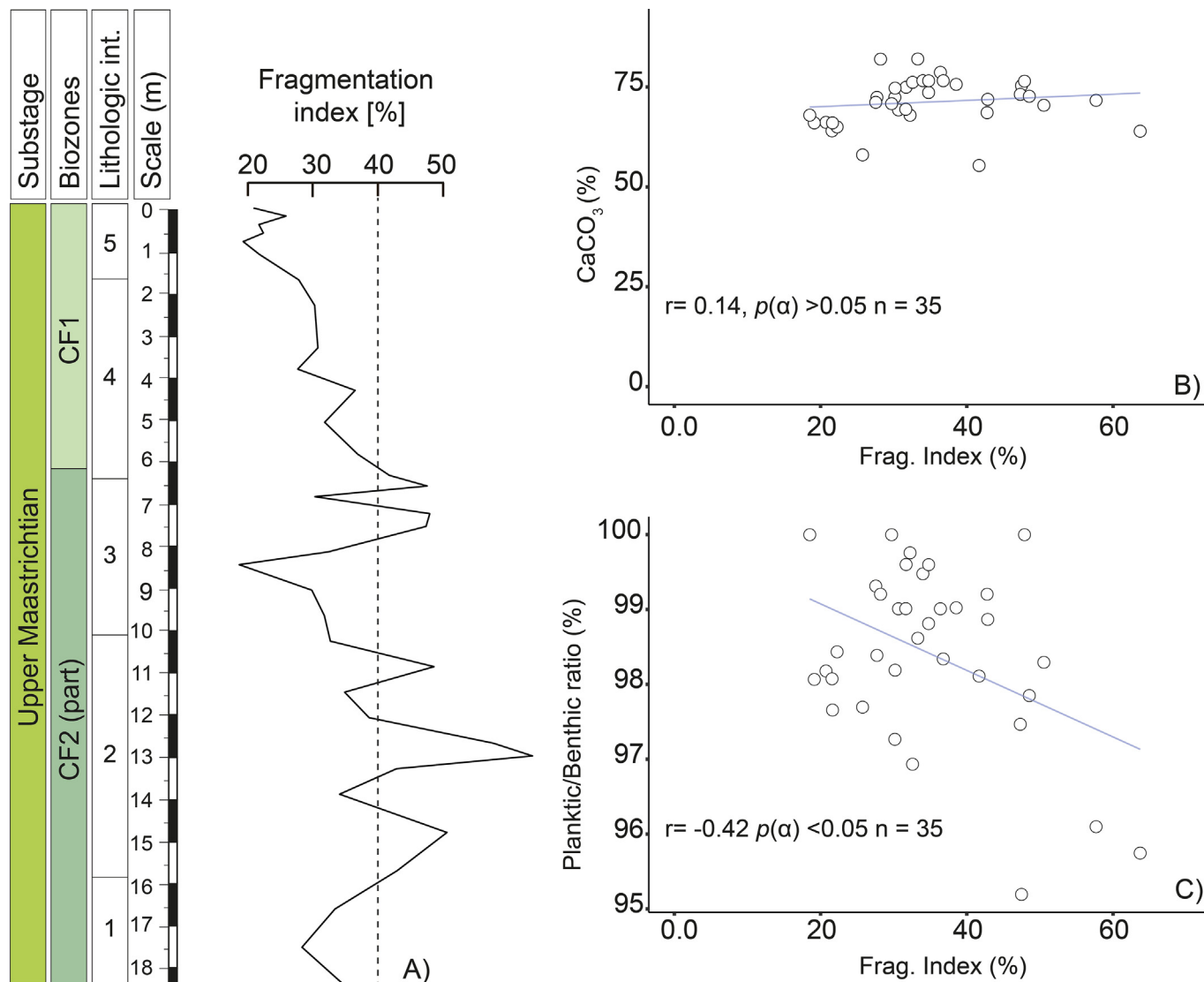


Fig. 10. Changes in fragmentation index (FI) (A), cross-plots between CaCO<sub>3</sub> and FI (B), and cross-plots between CaCO<sub>3</sub> and P/B ratio (C).

2017; O'Connor et al., 2019). During the Maastrichtian itself, a number of relatively minor fluctuations in climate have been recorded in widespread localities, most notably the brief warming episode of LMWE, ~300-150 kyr before the KPB (Barrera and Savin, 1999; MacLeod et al., 2005; Huber et al., 2018). The LMWE has previously been identified from globally distributed sites and sections, typically by δ<sup>18</sup>O and has been commonly related to the onset of the main eruptive phase of the Deccan Traps (e.g. Dessert et al., 2001; Keller et al., 2008; Tobin et al., 2012; Husson et al., 2014; Barnett et al., 2018, 2019; Schoene et al., 2019; Hull et al., 2020).

In Fig. 13, we compare the isotopic record from the Caravaca section with isotopic datasets from the Southern Ocean ODP Site 690 (Stott and Kennet, 1990), the South Atlantic DSDP Site 525A (Li and Keller, 1998a), the central Pacific Site ODP1209 (Westerhold et al., 2011), the South Atlantic ODP Site 1262 (Barnet et al., 2018), the Newfoundland Margin Site U1403 (Batenburg et al., 2018), the Gubbio section, Italy (Voigt et al., 2012) and Zumaia section, northern Spain (Batenburg et al., 2012). Age models for ODP Site 1209 (Westerhold et al., 2011), ODP Site 1262 (Barnet et al., 2018), IODP U1403 (Batenburg et al., 2018) and Zumaia (Batenburg et al., 2012) are based on cyclostratigraphy. Age models for the

other localities are based on interpolated ages using those estimated for the base of C29r, KPb and LO of *P. hantkeninoides* by Husson et al. (2014). For a better comparison of the different datasets, we applied the KPb age of 66.04 Ma estimated by Renne et al. (2013) to all localities.

At Caravaca and the ODP/IODP Sites (Fig. 13), the δ<sup>18</sup>O records all show an interval characterized by relatively low δ<sup>18</sup>O values between 66.35 and 66.14 Ma (i.e., between 310 and 100 kyr before the KPb), which was preceded and followed by higher δ<sup>18</sup>O isotope values. This interval has been previously recognized as the LMWE at some of these sites (e.g., Abramovich and Keller, 2003; Thibault and Gardin, 2010; Woelders et al., 2017; Barnett et al., 2018, 2019). As there are local differences between the different datasets, we propose, that the generally warm episode identified at the Caravaca section is the local isotopic record of the LMWE.

Previous work by Voigt et al. (2012) has postulated the existence of a consistent pattern of δ<sup>13</sup>C change immediately prior to the KPb at several sites, with relatively positive values around the C29r/C30n boundary (Kpg-2 event of Voigt et al., 2012), followed by a negative excursion (Kpg-3 event) before a final positive event within which the KPb itself occurs (not named by Voigt et al., 2012).

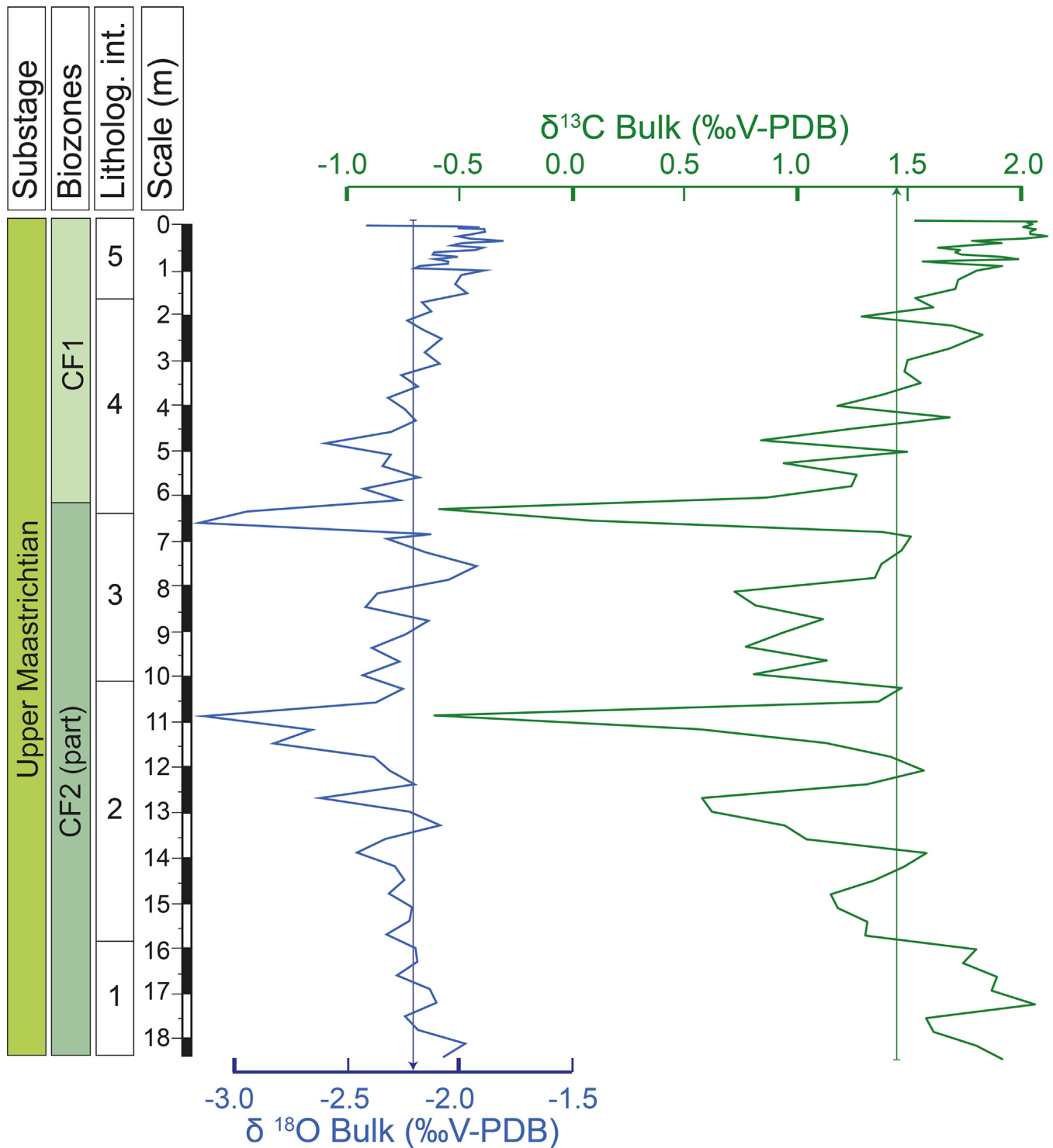


Fig. 11. Changes in  $\delta^{13}\text{C}$  and  $\delta^{18}\text{O}$  across the Caravaca section, the arrows mark the mean value for each isotope.

At Caravaca, it is possible that the positive values at the base of the section correspond to part of KPg-2, followed by lower  $\delta^{13}\text{C}$  values associated with the LMWE (KPg-3) and then a return to more positive values at the KPg. At Site 525, the highest occurrence of *G. gansseri* is associated with the KPg-2 event (Voigt et al., 2012), which, given that this same foraminiferal event must occur below the base of the section at Caravaca, implies that Caravaca contains only a partial record of the KPg-2 event. Fig. 13 illustrates that

precise correlation of the carbon isotope events prior to the KPg is problematic, as there is not perfect consistency between records of these (rather small magnitude) events when viewed at such high resolution, possibly as a consequence of age model limitations and uncertainties, sampling resolution, carbonate type, and/or site-specific oceanographic and diagenetic conditions. It is only during the last ~100 kyr of the Maastrichtian that there is a clearer consistency in  $\delta^{13}\text{C}$  trends with many records, including Caravaca,

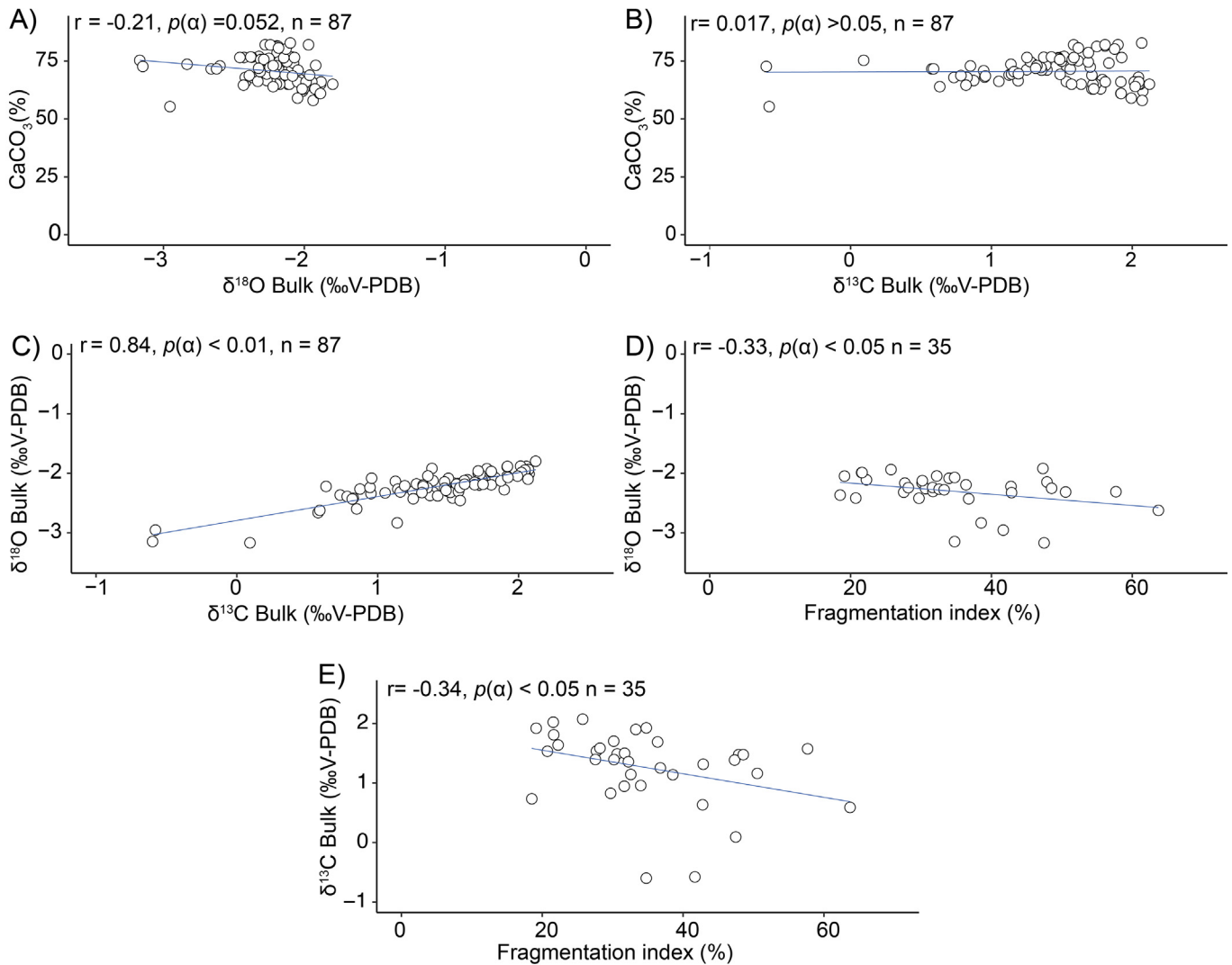


Fig. 12. Cross-plots between  $\text{CaCO}_3\%$  and  $\delta^{18}\text{O}$  (A),  $\text{CaCO}_3\%$  and  $\delta^{13}\text{C}$  (B),  $\delta^{18}\text{O}$  and  $\delta^{13}\text{C}$  (C),  $\delta^{13}\text{C}$  and FI (D), and  $\delta^{18}\text{O}$  and FI (E).

exhibiting a small increase in  $\delta^{13}\text{C}$  towards the KP (Fig. 13). Intriguingly, at both Zumaia and Caravaca, there are some remarkable negative excursions in  $\delta^{13}\text{C}$  bulk values (Fig. 13; Batenburg et al., 2012) which are very close in age at both localities. However, uncertainties in the precise age assignments of these isotope events, and questions over their veracity as primary seawater signals (as discussed in Section 6.1 above), prevents us from concluding that they are simultaneous events and requires further work in order to determine if these events have any significance.

## 7. Planktic foraminiferal response to LMWE

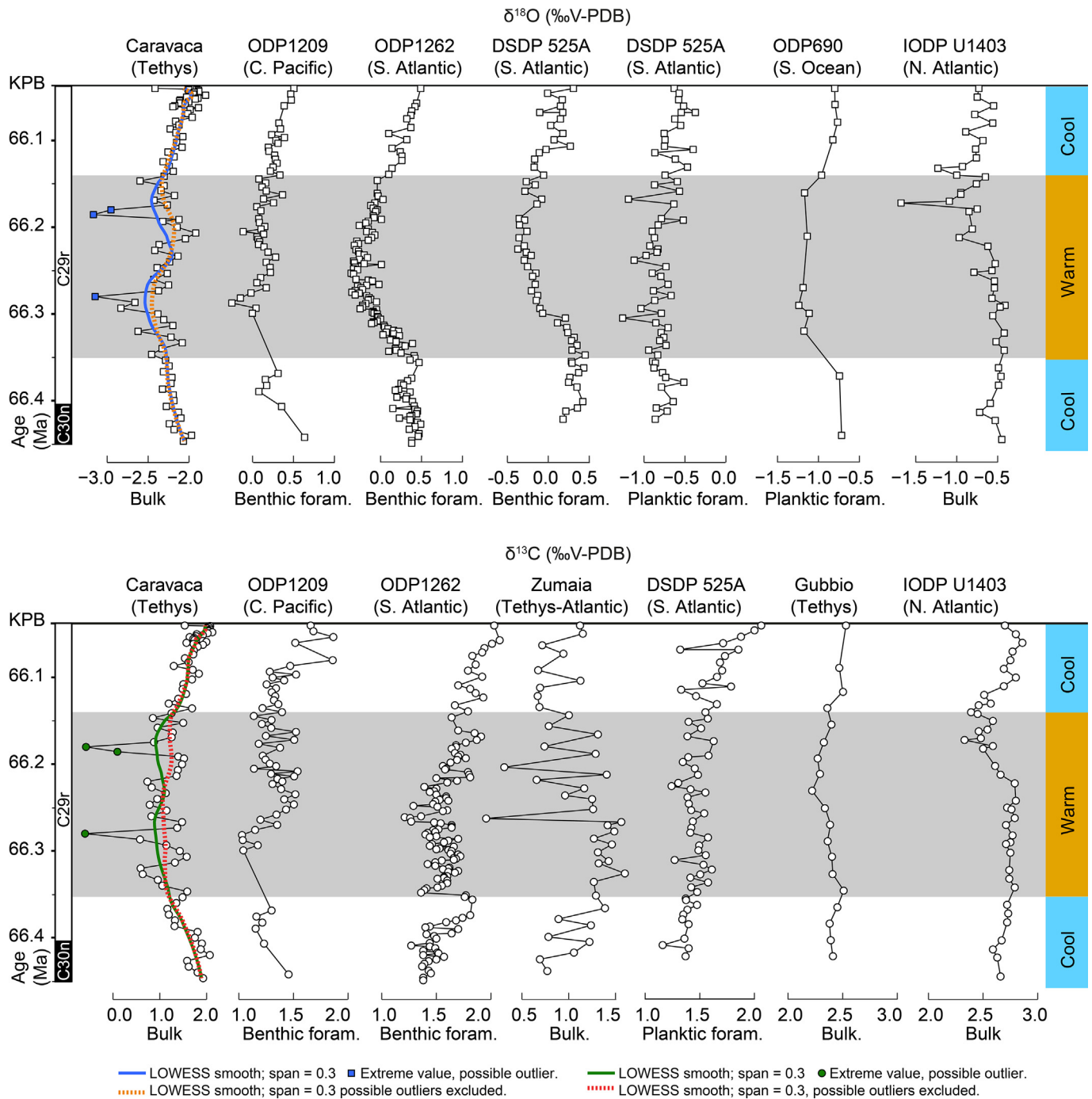
In this study, the planktic foraminiferal proxies presented provide evidence for environmental and climatic disturbances at Caravaca during the LMWE between 66.35 and 66.14 Ma, i.e. between 310 and 100 kyr before the KP (Figs. 14 and 15). The evidence for changes in the upper water column environment are as follows:

**First**, specific richness (S) slightly decreases during the LMWE, due to temporary disappearances (Lazarus effect) of some scarce species. Lazarus-taxa, such as *Gita. falsocalcarata*, *C. patelliformis* or *A. intermedius*, reappeared when the waters returned (marked by

an increase in  $\delta^{18}\text{O}$ ) to cooler conditions similar to the pre-LMWE phase.

**Second**, the Deep/Surface (D/S) ratio is 2–4 times higher in the pre- and post-LMWE intervals, compared to the LMWE itself. Similar ecological replacement has been observed in the late Maastrichtian at South Atlantic DSDP Site 525A, where the climate warming de-stratified the upper water column causing the removal of deep habitat niches (Abramovich and Keller, 2003).

**Third**, changes in the relative abundances of some genera, such as the increase in the low-oxygen tolerant genus *Heterohelix* (Pardo and Keller, 2008), indicate lower oxygen levels in the upper part of the water column during the LMWE. The relative abundance of *Heterohelix* increases in the intervals from 13.80 to 9.00 m and 7.50 to 5.05 m below the KP, reaching maximum values between 78 and 82% in the samples at 12.60, 10.80, and 6.55 m below the KP. Based on the  $\delta^{18}\text{O}$  record from Caravaca, the *Heterohelix* maxima coincide with the warmer events during the LMWE, probably driven by a decrease of seawater oxygen solubility in this area of the western Tethys. Seawater oxygen solubility is a limiting factor that decreases with increasing temperature since surface-water oxygen concentrations depend on the mixed-layer temperature (Helm et al., 2011). Between the two *Heterohelix* maxima, a discrete and



**Fig. 13.** Correlation of the  $\delta^{13}\text{C}$  and  $\delta^{18}\text{O}$  record from several upper Maastrichtian localities worldwide: Caravaca, this study; Southern Ocean ODP Site 690 (Stott and Kennet, 1990); South Atlantic DSDP Site 525A (Li and Keller, 1998a); central Pacific Site ODP1209 (Westerhold et al., 2011); South Atlantic ODP Site 1262 (Barnet et al., 2018); North Atlantic Newfoundland Margin Site U1403 (Batenburg et al., 2018); Zumaia (Batenburg et al., 2012); Gubbio (Voigt et al., 2012). Time-scale (Ma) is based on Husson et al. (2014).

temporary increase in *Pseudoguembelina*, globotruncanids and rugoglobigerinids is observed, which could reflect short intervals of better environmental conditions. Significantly, no increase in the disaster opportunist *Guembeltria* is identified across this interval (Fig. 8). *Guembeltria* blooms are often considered indicators of widespread high-stress conditions during the late Maastrichtian (Abramovich and Keller, 2002; Pardo and Keller, 2008; Punekar et al., 2014).

**Fourth**, an increase in the abundance of the biserial morphotype of *P. hariaensis* with elongated terminal chambers during the LMWE

could be related to a lower seawater oxygen solubility. Throughout the evolutionary history of the planktic foraminifera, the elongation of the terminal chambers is commonly associated with a reduced oxygenation of the water column (BouDagher-Fadel et al., 1997; Premoli Silva et al., 1999; Coccioni et al., 2006; Luciani et al., 2007). Luciani et al. (2007) considered the chamber elongation in planktic foraminifera as a recurring morphological character that constitutes an adaptation to facilitate oxygen uptake in a poorly oxygenated environment by increasing the surface/volume ratio of chambers.

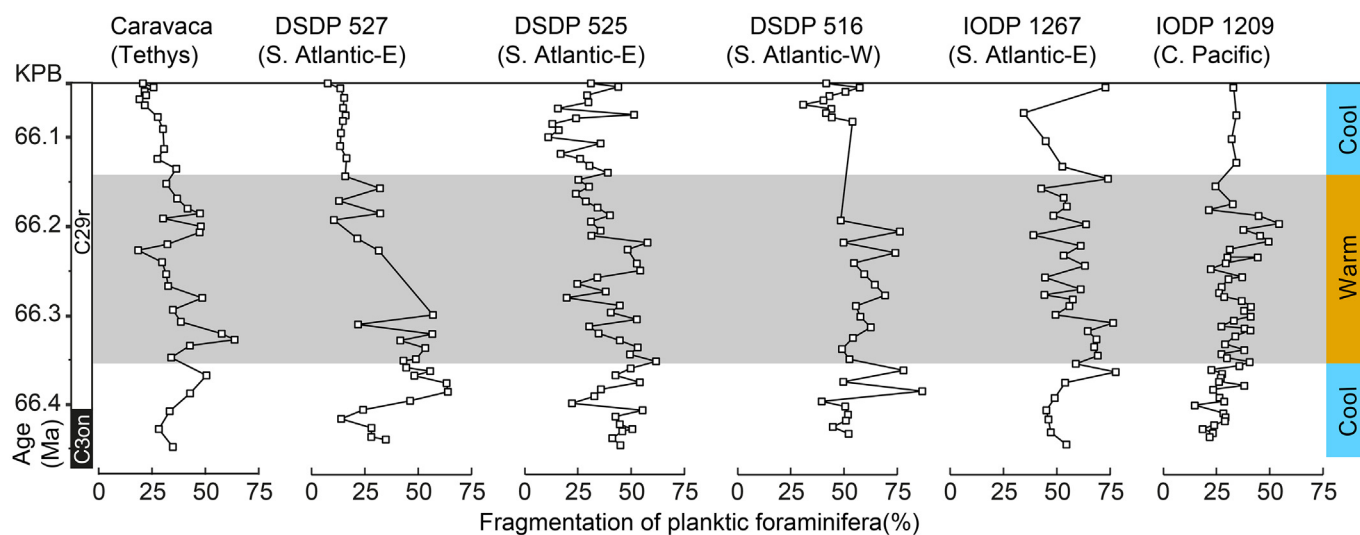


Fig. 14. Correlation of the planktic foraminiferal fragmentation record from several upper Maastrichtian localities worldwide: Caravaca, this study; South Atlantic DSDP 527, 525 and 516 (Kucera et al., 1997); South Atlantic IODP 1267 and Central Pacific IODP 1209 (Henehan et al., 2016). Time-scale (Ma) is based on Husson et al. (2014).

**Fifth**, the LO of *P. hantkeninoides* occurs within the upper part of the LMWE interval in Caravaca and many other localities (Husson et al., 2014). This species exhibits elongated chambers and well-developed tubulospines in the last whorl. We speculate that this morphology was an adaptation to inhabit deep waters with lower dissolved oxygen levels. Later, when global temperature decreased, and water-column stratification was reestablished, this species could migrate into fully oxygenated near-surface waters. A similar hypothesis was proposed by Coccioni et al. (2006), for planktic foraminiferal species with well-developed tubulospines such as the Eocene hantkeninids. However, further studies, from more localities, are necessary to establish the validity of a possible relationship between decreased dissolved oxygen during the LMWE and development of elongated terminal chambers in biserial morphotype of *P. hantkeninoides* and tubulospines in *P. hantkeninoides*.

**Sixth**, we observe a significant size reduction (close to 35%) of the tests of *Contusotruncana contusa* (Lilliput effect). Our biometric analyses indicate that the test sizes of *C. contusa* are around 1 mm-length before and after the LMWE interval. These test sizes are similar to those previously measured in samples by Kucera and Malmgren (1996) at Caravaca and El Kef samples for the terminal Cretaceous. However, Kucera and Malmgren (1996) analyzed only two samples from each site which were very close to the KP/B, and therefore fail to catch the influence of LMWE, which prevents us from making a detailed comparison. Notwithstanding this issue, it is noteworthy that Kucera and Malmgren (1996) determined that largest sized tests of *C. contusa* come from the Caravaca and El Kef section and are around twice the size of those reported at higher latitudes sites. Although they did not perform biometric analysis, Keller and Abramovich (2009) provided examples of the Lilliput effect in late Maastrichtian planktic foraminifera and concluded that this was a response to a stressed environment. According to MacLeod et al. (2000), a smaller test size implies stunted growth and early sexual maturity, which maximizes survival rates in high-stress environments where survival depends on rapid turnover, as was the case for the LMWE.

**Seventh**, the increase of the fragmentation index (FI) during the LMWE indicates increased dissolution intensity and/or poor preservation of  $\text{CaCO}_3$ . One possible explanation can be a lysocline shoaling, but this seems unlikely due to the poor linear correlation between the P/B ratio and the FI (Fig. 10C). In addition, the P/B ratio

remains stable along all the section, indicating no decline in planktic foraminiferal flux to the seafloor as the result of a rapid rise of the lysocline. The carbonate sediments of Caravaca were apparently deposited well above the foraminiferal lysocline, but FI indicates relatively poor preservation and high amounts of test dissolution in intervals from 15.60 to 10.80 m and 7.50 to 6.30 m below the KP/B. This apparent contradiction between FI and P/B ratio could be explained by local surface water becoming more acidic, perhaps due to a short-lived increase in the atmospheric partial pressure of  $\text{CO}_2$  (Henehan et al., 2016, 2019).

Although there are differences in absolute fragmentation index values between Caravaca and sites in the Pacific and South Atlantic (Fig. 14; Kucera et al., 1997; Henehan et al., 2016), a significant increase in fragmentation index can be observed close to the C30n/C29r boundary in all the localities, followed by relatively high values during the LMWE. In the last 100 kyr of the Maastrichtian, the fragmentation index seems to be more variable, but returned to values similar to the pre-LMWE interval, which is especially evident at Caravaca and DSDP 527. Other moderate to strong carbonate dissolution intervals broadly coeval with those identified in Fig. 14 have been also reported from South Atlantic DSDP Site 528 and Central Pacific DSDP Site 577 by D'Hondt (2005), albeit with a lower sampling resolution. According to the fragmentation records discussed here, it is suggested that widespread ocean acidification during the LMWE was probably linked to Deccan volcanism.

According to our data summarized in Fig. 15, the maximum in ecological stress, evidenced by the planktic foraminifera assemblages, occurred towards the end of the LMWE in the studied section. This event is recorded 6.55 m below the KTB and is characterized by the low values in  $\delta^{18}\text{O}$  and  $\delta^{13}\text{C}$ , the highest relative abundance of *Heterohelix* (82.3%), the lowest relative abundance of globotruncanids (0%), and the lowest D/S ratio (0%) (see Supplementary Tables 2 and 4). Maximum FI values seem to concentrate in the LMWE, but they do not coincide precisely with the excursions of both  $\delta^{18}\text{O}$  and  $\delta^{13}\text{C}$ .

In order to reduce the influence of the most extreme  $\delta^{18}\text{O}$  and  $\delta^{13}\text{C}$  values, smoothed curves were produced using the non-parametric Locally Weighted Scatterplot Smoothing (LOWESS; span = 0.3) and compared to the most relevant planktic foraminiferal proxies (Fig. 15). These smoothed records were generated both with and without the three 'extreme' values shown in Fig. 13

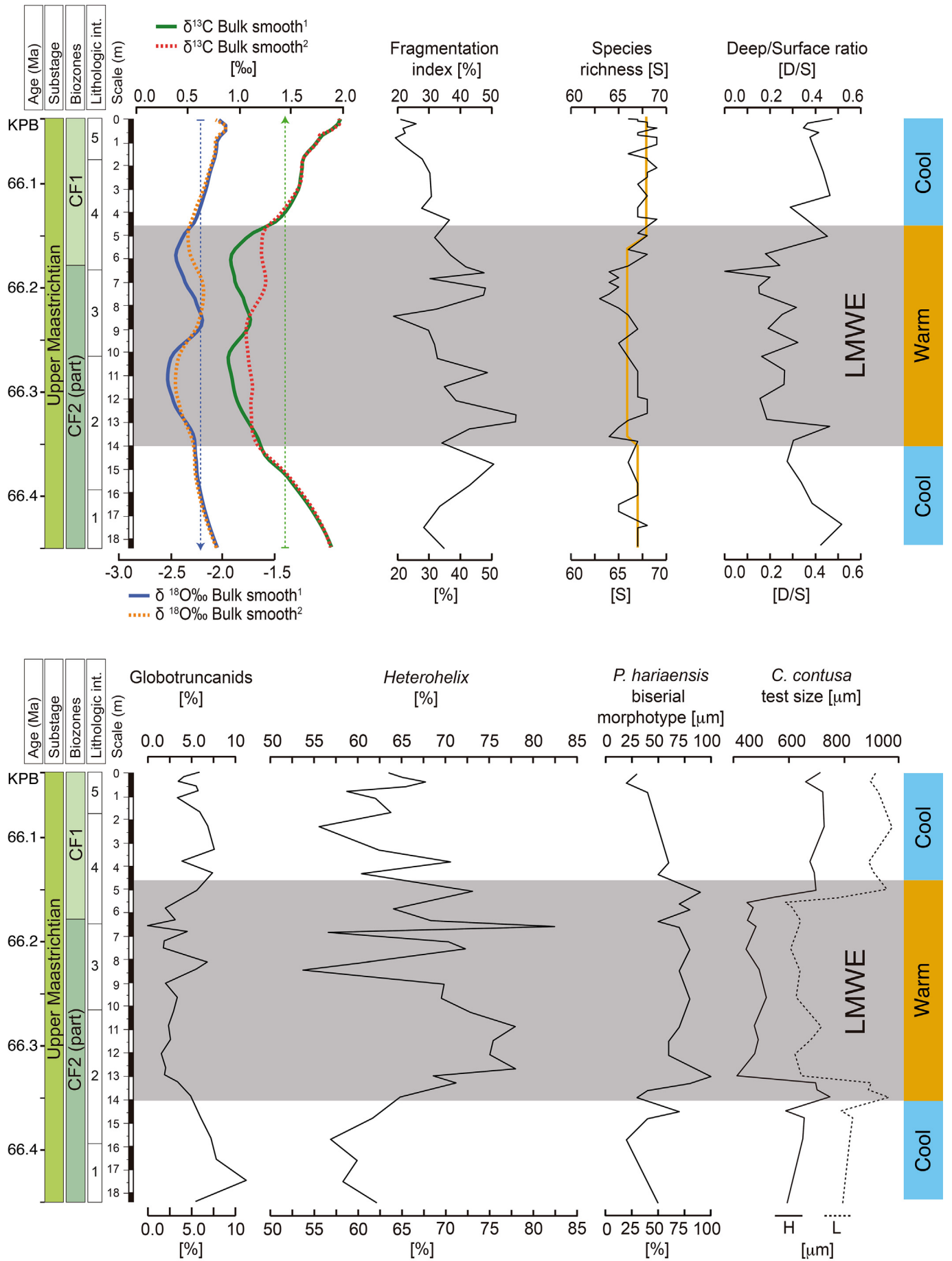


Fig. 15. Summary of the changes in most relevant planktic foraminiferal and geochemical proxies, and position of the LMWE in the Caravaca section. <sup>1</sup>Smoothing considering all the dataset, <sup>2</sup>Smoothing excluding three potential outliers discussed in Section 6.1.

(discussed in Section 6.1). Both approaches yield similar long-term trends but reduce the influence of the outlying datapoints. Both approaches exhibit two intervals of warming within the LMWE, although the timing of the younger interval is slightly shifted in the smoothed record that excludes the outlying data points. Overall, this comparison between isotopic and micropaleontological data supports the hypothesis that two warmer intervals could have occurred during the LMWE. Using the smoothed record that includes all the available data, the first warmer interval occurred between 66.32 and 66.26 Ma (i.e., between 280 and 220 kyr before the KPB) and the second between 66.19 and 66.15 Ma (i.e., between 150 and 110 kyr before the KPB). Both are characterized by maxima values of low oxygen tolerant genus *Heterohelix* and negative excursions of  $\delta^{18}\text{O}$  and  $\delta^{13}\text{C}$ . The intermediate interval is characterized by higher  $\delta^{18}\text{O}$  and  $\delta^{13}\text{C}$  values, a decrease in *Heterohelix*, and an increase in the globotruncanids, *Rugoglobigerina* and *Pseudoguembelina*, reliably related to cooler pulses within the LMWE interval. Recently, Woelders et al. (2018) compared multiple palaeotemperature proxies (stable oxygen isotope, Mg/Ca and  $\text{TEX}_{86}$ ) from the latest Maastrichtian of Bass River, New Jersey and, on this basis, proposed at least two warmer intervals within the LMWE (see Fig. 3 of Woelders et al., 2018). We suggest that these two intervals may correlate with those recognized in Caravaca.

## 8. Latest Maastrichtian cooling and return to pre-LMWE conditions

After the LMWE, a worldwide cooling is well documented at the end of Maastrichtian, from oceanic ODP/IODP sites (see Fig. 13) and outcrop sites in Seymour Island, Antarctica (Petersen et al., 2016), Argentina (Woelders et al., 2017), North America (Vellekoop et al., 2016; Woelders et al., 2018) and Tunisia (Thibault et al., 2016). The global temperature compilation of Hull et al. (2020) also shows that the climate cooled at this time, returning to pre-LMWE conditions. At Caravaca, this trend in cooling is evidenced by the increase in  $\delta^{18}\text{O}$  values recorded in the uppermost ~4.5 m of the section, i.e. during the last ~100 kyr of the Maastrichtian according to our age model (Fig. 15) and is consistent with the global pattern. The progressive decline in the FI values during this same interval suggests that surface waters were less corrosive after the LMWE up to the KPB. This contradicts the hypothesis that a major pulse of Deccan volcanism caused the most harmful effects, such as rapid warming and ocean acidification, just before the KPB (e.g., Font et al., 2014, 2017; Punekar et al., 2014, 2016; Keller et al., 2016; Schoene et al., 2019). Conversely, our results are consistent with the hypothesis of Henehan et al. (2019) in which ocean pH was stable over the last 100 kyr of the Cretaceous.

Planktic foraminiferal assemblages suffered minor reorganization during the LMWE but following the event the ecological proxies suggest a return to conditions similar to the pre-LMWE (Fig. 15). According to our data, water column stratification was reestablished during the end-Maastrichtian cooling, as suggested by the increase in the abundance of thermocline dwellers, especially globotruncanids, and the increase in the Deep/Surface ratio (Fig. 15 and Table S2). Species richness remained very high during the climate cooling, reaching the highest average value in species richness of the entire Caravaca section. Nevertheless, four HOs of planktic foraminiferal species (6% of the total number of species) have been recorded in the last 50 cm below the KPB (Fig. 6). However, three of these species (*A. blowi*, *P. manuelensis*, and *Gita. falsocalcarata*) have been identified just below the KPB in some western Tethyan sections including Agost, Spain (Molina et al., 1998), Ain Settara and El Kef, Tunisia (Arenillas et al., 2000a,b; Gallala, 2013), and Sidi Ziane and Djebel Zakhmoune, Algeria (Metsana-Oussaid et al., 2019). Therefore, the extinction rate before

the KPB was probably as low as 1.5%, since only *A. cretacea* actually became extinct just before the KPB, as part of the background extinction. Our data from Caravaca support high evolutionary stability during the latest Maastrichtian, and, therefore, indicate that the catastrophic planktic foraminiferal mass extinction at the KPB was caused by the Chicxulub impact (see Arenillas et al., 2000a, b, 2006; Arz et al., 2000; Lowery et al., 2018) and not by gradual environmental degradation induced by Deccan forcing as has been proposed by Keller (1988), Keller et al. (2012) and Punekar et al. (2014), among others.

## 9. Conclusions

In this work, we performed high-resolution micropaleontological and geochemical analyses of the last ~400 kyr of the Cretaceous from Caravaca (Spain, western Tethys), for the first time demonstrating the Latest Maastrichtian Warming Event (LMWE) in this section. As a warming indicator, we used the  $\delta^{18}\text{O}$  in bulk-rock to demonstrate the presence of a warm phase from ~66.35 to 66.14 Ma. Our data suggest that the LMWE at Caravaca included at least two shorter warming pulses marked by relatively lower  $\delta^{18}\text{O}$  and  $\delta^{13}\text{C}$  values, probably related to two massive and short periods of greenhouse gas injection during Deccan outgassing activity. Simultaneously with warming, high values of the fragmentation index (FI) of planktic foraminiferal tests are recorded, reaching significant values that exceed 40%; these values may be the result of changes in the carbonate saturation state of surface oceanic waters.

At Caravaca, planktic foraminiferal proxies suggest high-stress conditions (including warming, decreased water mass stratification and reduced oxygenation) during the LMWE, ending ~100 kyr before the Cretaceous/Paleogene boundary (KPB). Later, species richness and all ecological proxies return to values similar to the pre-LMWE interval.

At Caravaca, no evidence of a gradual mass extinction in planktic foraminifera has been recognized below the Ir-rich air-fall layer that is linked to the Chicxulub impact marking the KPB. Although the warming pulses of the LMWE are near the KPB and seem to have had global repercussions, our results indicate that the climate effects of greenhouse gas emissions linked to the Deccan volcanism were too weak to be an essential factor in the end-Cretaceous mass extinctions. Future work is needed to constrain the evidence of Deccan volcanism across the K/Pg boundary and its influence on the decline and posterior recovery of marine ecosystems in the early Danian. It is crucial to better know why the Deccan, one of the biggest igneous provinces in the history of Earth, apparently caused such a weak effect on marine ecosystems while other mass extinctions have been related to similar styles of large igneous province eruption.

## Acknowledgments

We deeply thank the editor and two anonymous reviewers for their useful, comprehensive and helpful comments and suggestions. This work was supported by MCIU (Ministerio de Ciencia, Innovación y Universidades)/AEI (Agencia Estatal de Investigación)/FEDER (Fondo Europeo de Desarrollo Regional), UE (grant number PGC2018-093890-B-I00), and by the Aragonian Government/FEDER, UE (grant number DGA groups E33\_17R and E33\_20R). Vicente Gilabert acknowledges support from the Spanish Ministerio de Economía, Industria y Competitividad (FPI grant number BES-2016-077800). The authors would like to acknowledge the use of the Servicio General de Apoyo a la Investigación-SAI, Universidad de Zaragoza. This research is part of the PhD thesis of the first author.



## References

- Abramovich, S., Keller, G., 2002. High stress late Maastrichtian paleoenvironment: Inference from planktonic foraminifera in Tunisia. *Palaeogeography, Palaeoclimatology, Palaeoecology* 178, 145–164. [https://doi.org/10.1016/S0031-0182\(01\)00394-7](https://doi.org/10.1016/S0031-0182(01)00394-7).
- Abramovich, S., Keller, G., 2003. Planktonic foraminiferal response to the latest Maastrichtian abrupt warm event: a case study from South Atlantic DSDP Site 525A. *Marine Micropaleontology* 48, 225–249. [https://doi.org/10.1016/S0377-8398\(03\)00021-5](https://doi.org/10.1016/S0377-8398(03)00021-5).
- Abramovich, S., Keller, G., Stüben, D., Berner, Z., 2003. Characterization of late Campanian and Maastrichtian planktonic foraminiferal depth habitats and vital activities based on stable isotopes. *Palaeogeography, Palaeoclimatology, Palaeoecology* 202, 1–29. [https://doi.org/10.1016/S0031-0182\(03\)00572-8](https://doi.org/10.1016/S0031-0182(03)00572-8).
- Abramovich, S., Yovel-Corem, S., Almogi-Labin, A., Benjamini, C., 2010. Global climate change and planktic foraminiferal response in the Maastrichtian. *Paleoceanography* 25 (2), PA2201. <https://doi.org/10.1029/2009PA001843>.
- Abramovich, S., Keller, G., Berner, Z., Cymbalista, M., Rak, C., 2011. Maastrichtian planktic foraminiferal biostratigraphy and paleoenvironment of Brazos River, Falls County, Texas. In: Keller, G., Adatte, T. (Eds.), *The End-Cretaceous Mass Extinction and the Chicxulub Impact in Texas*. Society for Sedimentary Geology Special Publication 100, pp. 123–156.
- Alvarez, L.W., Alvarez, W., Asaro, F., Michel, H.V., 1980. Extraterrestrial Cause for the Cretaceous-Tertiary Extinction. *Science* 208, 1095–1108. <https://doi.org/10.1126/science.208.4448.1095>.
- Andeweg, B., 2002. Cenozoic tectonic evolution of the Iberian Peninsula: effects and causes of changing stress fields. PhD thesis. Vrije Universiteit Amsterdam, Amsterdam, p. 192.
- Arenillas, I., Arz, J.A., Molina, E., Dupuis, C., 2000a. The Cretaceous/Paleogene (K/P) boundary at Ain Settara, Tunisia: sudden catastrophic mass extinction in planktic foraminifera. *Journal of Foraminiferal Research* 30, 202–218. <https://doi.org/10.2113/0300202>.
- Arenillas, I., Arz, J.A., Molina, E., Dupuis, C., 2000b. An independent test of planktonic foraminiferal turnover across the Cretaceous/Paleogene (K/P) boundary at El Kef, Tunisia: Catastrophic mass extinction and possible survivorship. *Micropaleontology* 46, 31–49.
- Arenillas, I., Arz, J.A., Grajales-Nishimura, J.M., Murillo-Muñeton, G., Alvarez, W., Camargo-Zanoguera, A., Molina, E., Rosales-Domínguez, C., 2006. Chicxulub impact event is Cretaceous/Paleogene boundary in age: new micropaleontological evidence. *Earth and Planetary Science Letters* 249, 241–257.
- Arz, J.A., Arenillas, I., Molina, E., Sepulveda, R., 2000. La estabilidad evolutiva de los foraminíferos planctónicos en el Maastrichtiense Superior y su extinción en el límite Cretácico/Terciario de Caravaca, España. *Revista Geologica de Chile* 27, 27–47.
- Ashkenazi-Polivoda, S., Rak, C., Almogi-Labin, A., Zsolt, B., Ovdia, O., Abramovich, S., 2014. Paleocology of the K-Pg mass extinction survivor *Guembelitra* (Cushman): isotopic evidence from pristine foraminifera from Brazos River, Texas (Maastrichtian). *Paleobiology* 40, 24–33. <https://doi.org/10.1666/13317>.
- Batenburg, S.J., Sprovieri, M., Gale, A.S., Hilgen, F.J., Hüsing, S., Laskar, J., Liebrand, D., Lirer, F., Orue-Etxebarria, X., Pelosi, N., Smit, J., 2012. Cyclostratigraphy and astronomical tuning of the Late Maastrichtian at Zumaia (Basque country, Northern Spain). *Earth and Planetary Science Letters* 359–360, 264–278. <https://doi.org/10.1016/j.epsl.2012.09.054>.
- Batenburg, S.J., Friedrich, O., Moriya, K., Voigt, S., Cournède, C., Moebius, I., Blum, P., Bornemann, A., Fiebig, J., Hasegawa, T., Hull, P.M., Norris, R.D., Röhl, U., Sexton, P.F., Westerhold, T., Wilson, P.A., IODP Expedition Scientists, 2018. Late Maastrichtian carbon isotope stratigraphy and cyclostratigraphy of the Newfoundland Margin (Site U1403, IODP Leg 342). *Newsletters on Stratigraphy* 51 (2), 245–260. <https://doi.org/10.1127/nos/2017/0398>.
- Barnet, J.S.K., Littler, K., Kroon, D., Leng, M.J., Westerhold, T., Röhl, U., Zachos, J.C., 2018. A new high-resolution chronology for the late Maastrichtian warming event: Establishing robust temporal links with the onset of Deccan volcanism. *Geology* 46 (2), 147–150. <https://doi.org/10.1130/G39771.1>.
- Barnet, J.S.K., Littler, K., Westerhold, T., Kroon, D., Leng, M.J., Bailey, I., Röhl, U., Zachos, J.C., 2019. A High-Fidelity Benthic Stable Isotope Record of Late Cretaceous–Early Eocene Climate Change and Carbon-Cycling. *Paleoceanography and Paleoclimatology* 34, 672–691. <https://doi.org/10.1029/2019PA003556>.
- Barrera, E., Savin, S.M., 1999. Evolution of late Campanian-Maastrichtian marine climates and oceans. In: Barrera, E., Johnson, C.C. (Eds.), *Evolution of the Cretaceous Ocean-Climate System*. Geological Society of America Special Paper 332, pp. 245–282.
- Berger, W.H., Bonneau, M.C., Parker, F.L., 1982. Foraminifera on the deep-sea floor: lysocline and dissolution rate. *Oceanologica Acta* 5, 249–258, 0399-1784/1982/249.
- BouDagher-Fadel, M.K., Banner, F.T., Whittaker, J.E., 1997. The Early evolutionary History of planktonic foraminifera. Chapman and Hall, New York, p. 269.
- Canudo, J.I., 2018. The collection of type fossils of the Natural Science Museum of the University of Zaragoza (Spain). *Geoheritage* 10, 385–392. <https://doi.org/10.1007/s12371-017-0228-1>.
- Canudo, J.I., Keller, G., Molina, E., 1991. Cretaceous/Tertiary boundary extinction pattern and faunal turnover at Agost and Caravaca, S.E. Spain. *Marine Micropaleontology* 17, 319–341. [https://doi.org/10.1016/0377-8398\(91\)90019-3](https://doi.org/10.1016/0377-8398(91)90019-3).
- Chacón, B., 2002. Las sucesiones hemipelágicas del final del Cretácico e inicio del Paleógeno en el SE de la Placa Ibérica: Estratigrafía de eventos y evolución de la cuenca. PhD thesis. Universidad Complutense, Madrid, p. 440.
- Chenet, A.L., Quidelleur, X., Fluteau, F., Courtillot, V., Bajpai, S., 2007. <sup>40</sup>K–<sup>40</sup>Ar dating of the Main Deccan large igneous province: Further evidence of KTB age and short duration. *Earth and Planetary Science Letters* 263, 1–15. <https://doi.org/10.1016/j.epsl.2007.07.011>.
- Chenet, A.L., Fluteau, F., Courtillot, V., Gérard, M., Subbarao, K.V., 2008. Determination of rapid Deccan eruptions across the Cretaceous-Tertiary boundary using paleomagnetic secular variation: Results from a 1200-m-thick section in the Mahabaleshwar escarpment. *Journal of Geophysical Research Solid Earth* 113. <https://doi.org/10.1029/2006JB004635>.
- Chenet, A.L., Courtillot, V., Fluteau, F., Gérard, M., Quidelleur, X., Khadri, S.F.R., Subbarao, K.V., Thordarson, T., 2009. Determination of rapid Deccan eruptions across the Cretaceous-Tertiary boundary using paleomagnetic secular variation: 2. Constraints from analysis of eight new sections and synthesis for a 3500-m-thick composite section. *Journal of Geophysical Research Solid Earth* 114, 1–38. <https://doi.org/10.1029/2008JB005644>.
- Clarke, L.J., Jenkyns, H.C., 1999. New oxygen isotope evidence for long-term Cretaceous climatic change in the Southern Hemisphere. *Geology* 27, 699–702.
- Coccioni, R., Galeotti, S., 1994. K-T boundary extinction: Geologically instantaneous or gradual event? Evidence from deep-sea benthic foraminifera. *Geology* 22, 779–782. [https://doi.org/10.1130/0091-7613\(1994\)022<0779:KTBEIG>2.3.CO;2](https://doi.org/10.1130/0091-7613(1994)022<0779:KTBEIG>2.3.CO;2).
- Coccioni, R., Premoli Silva, I., 2015. Revised Upper Albian-Maastrichtian planktonic foraminiferal biostratigraphy and magneto-stratigraphy of the classical Tethyan Gubbio section (Italy). *Newsletters on Stratigraphy* 48, 47–90. <https://doi.org/10.1127/nos/2015/0055>.
- Coccioni, R., Luciani, V., Marsili, A., 2006. Cretaceous oceanic anoxic events and radially elongated chambered planktonic foraminifera: Paleoclimatological and paleoceanographic implications. *Paleoceanography, Palaeoclimatology, Palaeoecology* 235, 66–92. <https://doi.org/10.1016/j.paleo.2005.09.024>.
- Courtillot, V., Fluteau, F., 2010. Cretaceous Extinctions: The volcanic hypothesis. *Science* 328, 973–974. <https://doi.org/10.1126/science.328.5981.975>.
- Dameron, S.N., Leckie, R.M., Clark, K., MacLeod, K.G., Thomas, D.J., Lees, J.A., 2017. Extinction, dissolution, and possible ocean acidification prior to the Cretaceous/Paleogene (K/Pg) boundary in the tropical Pacific. *Paleoceanography, Palaeoclimatology, Palaeoecology* 485, 433–454. <https://doi.org/10.1016/j.paleo.2017.06.032>.
- Dessert, C., Dupré, B., François, L.M., Schott, J., Gaillardet, J., Chakrapani, G., Bajpai, S., 2001. Erosion of Deccan Traps determined by river geochemistry: impact on the global climate and the 87Sr/86Sr ratio of seawater. *Earth and Planetary Science Letters* 188, 459–474. [https://doi.org/10.1016/S0012-821X\(01\)00317-X](https://doi.org/10.1016/S0012-821X(01)00317-X).
- D'Hondt, S., 2005. Consequences of the Cretaceous/Paleogene Mass Extinction for Marine Ecosystems. *Annual Review of Ecology, Evolution, and Systematics* 36, 295–317. <https://doi.org/10.1146/annurev.ecolsys.35.021103.105715>.
- D'Hondt, S., Arthur, M.A., 1995. Interspecies variation in stable isotopic signals of Maastrichtian planktonic foraminifera. *Paleoceanography* 10, 123–135. <https://doi.org/10.1029/94PA02671>.
- D'Hondt, S., Zachos, J.C., 1993. On stable isotopic variation and earliest Paleocene planktonic foraminifera. *Paleoceanography* 8, 527–547. <https://doi.org/10.1029/93PA00952>.
- Falzone, F., Petrizzo, M.R., Huber, B.T., MacLeod, K.G., 2014. Insights into the meridional ornamentation of the planktonic foraminiferal genus *Rugoglobigerina* (Late Cretaceous) and implications for taxonomy. *Cretaceous Research* 47, 87–104. <https://doi.org/10.1016/j.cretres.2013.11.001>.
- Falzone, F., Petrizzo, M.R., Clarke, L.J., MacLeod, K.G., Jenkyns, H.C., 2016. Long-term Late Cretaceous oxygen- and carbon isotope trends and planktonic foraminiferal turnover: A new record from the southern mid-latitudes. *Bulletin of the Geological Society of America* 128, 1725–1735. <https://doi.org/10.1130/B31399.1>.
- Font, E., Fabre, S., Nédélec, A., Adatte, T., Keller, G., Veiga-Pires, C., Ponte, J., Mirão, J., Khozyem, H., Spangenberg, J.E., 2014. Atmospheric halogen and acid rains during the main phase of Deccan eruptions: magnetic and mineral evidence. In: Keller, G., Kerr, A.C. (Eds.), *Volcanism, Impacts, and Mass Extinctions: Causes and Effects*. Geological Society of America Special Paper 505, pp. 353–368. [https://doi.org/10.1130/2014.2505\(18\)](https://doi.org/10.1130/2014.2505(18)).
- Font, E., Adatte, T., Sial, A.N., Drude de Lacerda, L., Keller, G., Punejar, J., 2016. Mercury anomaly, Deccan volcanism, and the end-Cretaceous mass extinction. *Geology* 44, 171–174. <https://doi.org/10.1130/G37451.1>.
- Font, E., Carlut, J., Rémazeilles, C., Mather, T.A., Nédélec, A., Mirão, J., Casale, S., 2017. End-Cretaceous akaganéite as a mineral marker of Deccan volcanism in the sedimentary record. *Scientific Reports* 7 (11453). <https://doi.org/10.1038/s41598-017-11954-y>.
- Gallala, N., 2013. Planktonic Foraminiferal Biostratigraphy and Correlation Across the Cretaceous-Paleogene Transition at the Tethyan and the Atlantic Realms. *Paleontology Journal* 2013, 1–20. <https://doi.org/10.1155/2013/643278>.
- Gradstein, F.M., Ogg, J.G., Schmitz, M., Ogg, G., 2012. *The Geological Time Scale 2012*. Elsevier Science Ltd., Boston, p. 1144. <https://doi.org/10.1016/C2011-1-08249-8>.
- Georgescu, M.D., Saupe, E.E., Huber, B.T., 2008. Morphometric and stratigraphic basis for phylogeny and taxonomy in Late Cretaceous gublerinid planktonic foraminifera. *Micropaleontology* 54, 397–424.
- Gertsch, B., Keller, G., Adatte, T., Garg, R., Prasad, V., Fleitmann, D., Berner, Z., 2011. Environmental effects of Deccan volcanism across the Cretaceous–Tertiary transition in Meghalaya, India. *Earth and Planetary Science Letters* 310, 272–285. <https://doi.org/10.1016/j.epsl.2011.08.015>.

- Helm, K.P., Bindoff, N.L., Church, J.A., 2011. Observed decreases in oxygen content of the global ocean: Global decreases in ocean oxygenic levels. *Geophysical Research Letters* 38, 1–6. <https://doi.org/10.1029/2011GL049513>.
- Henehan, M.J., Hull, P.M., Penman, D.E., Rae, J.W.B., Schmidt, D.N., 2016. Biogeochemical significance of pelagic ecosystem function: an end-Cretaceous case study. *Philosophical Transactions of the Royal Society B: Biological Sciences* 371 (20150510). <https://doi.org/10.1098/rstb.2015.0510>.
- Henehan, M.J., Ridgwell, A., Thomas, E., Zhang, S., Alegret, L., Schmidt, D.N., Rae, J.W.B., Witts, J.D., Landman, N.H., Greene, S.E., Huber, B.T., Super, J.R., Planavsky, N.J., Hull, P.M., 2019. Rapid ocean acidification and protracted Earth system recovery followed the end-Cretaceous Chicxulub impact. *Proceedings of the National Academy of Sciences of the United States of America* 116, 22500–22504. <https://doi.org/10.1073/pnas.1905989116>.
- Huber, B.T., Hodell, D.A., Hamilton, C.P., 1995. Middle–Late Cretaceous climate of the southern high latitudes: Stable isotopic evidence for minimal equator-to-pole thermal gradients. *The Geological Society of America Bulletin* 107 (10), 1164–1191. [https://doi.org/10.1130/0016-7606\(1995\)107<1164:MLCCOT>2.3.CO;2](https://doi.org/10.1130/0016-7606(1995)107<1164:MLCCOT>2.3.CO;2).
- Huber, B.T., MacLeod, K.G., Watkins, D.K., Coffin, M.F., 2018. The rise and fall of the Cretaceous Hot Greenhouse climate. *Global and Planetary Change* 167, 1–23. <https://doi.org/10.1016/j.gloplacha.2018.04.004>.
- Hull, P.M., Bornemann, A., Penman, D.E., Henehan, M.J., Norris, R.D., Wilson, P.A., Blum, P., Alegret, L., Batenburg, S.J., Bown, P.R., Bralower, T.J., Cournede, C., Deutsch, A., Donner, B., Friedrich, O., Jehle, S., Kim, H., Kroon, D., Lippert, P.C., Lorch, D., Moebius, I., Moriya, K., Peppe, D.J., Ravizza, G.E., Röhl, U., Schueth, J.D., Sepúlveda, J., Sexton, P.F., Sibert, E.C., Śliwińska, K.K., Summons, R.E., Thomas, E., Westerhold, T., Whiteside, J.H., Yamaguchi, T., Zachos, J.C., 2020. On impact and volcanism across the Cretaceous–Paleogene boundary. *Science* 367, 266–272. <https://doi.org/10.1126/science.aay5055>.
- Husson, D., Galbrun, B., Gardin, S., Thibault, N., 2014. Tempo and duration of short-term environmental perturbations across the Cretaceous–Paleogene boundary. *Stratigraphy* 11, 159–171. <https://hal.archives-ouvertes.fr/hal-01092775>.
- Isaza-Londoño, C., MacLeod, K.G., Huber, B.T., 2006. Maastrichtian North Atlantic warming, increasing stratification, and foraminiferal paleobiology at three timescales. *Paleoceanography* 21, 1–10. <https://doi.org/10.1029/2004PA001130>.
- Jarvis, I., Gale, A.S., Jenkyns, H.C., Pearce, M.A., 2006. Secular variation in Late Cretaceous carbon isotopes: a new  $\delta^{13}\text{C}$  carbonate reference curve for the Cenomanian – Campanian (99.6–70.6 Ma). *Geological Magazine* 143, 561–608. <https://doi.org/10.1017/S0016756800602421>.
- Jenkyns, H.C., Gale, A.S., Corfield, R.M., 1994. Carbon- and oxygen-isotope stratigraphy of the English Chalk and Italian Scaglia and its palaeoclimatic significance. *Geological Magazine* 131, 1–34. <https://doi.org/10.1017/S0016756800010451>.
- Kaiho, K., Lamolda, M.A., 1999. Catastrophic extinction of planktonic foraminifera at the Cretaceous–Tertiary boundary evidenced by stable isotopes and foraminiferal abundance at Caravaca, Spain. *Geology* 27, 355–358. [https://doi.org/10.1130/0091-7613\(1999\)027<0355:CEOPFA>2.3.CO;2](https://doi.org/10.1130/0091-7613(1999)027<0355:CEOPFA>2.3.CO;2).
- Keller, G., 1988. Extinctions, Survivorship and Evolution across the Cretaceous/Tertiary Boundary at El Kef, Tunisia. *Marine Micropaleontology* 13, 239–263. [https://doi.org/10.1016/0377-8398\(88\)90005-90009](https://doi.org/10.1016/0377-8398(88)90005-90009).
- Keller, G., 2014. Deccan volcanism, the Chicxulub impact, and the end-Cretaceous mass extinction: Coincidence? Cause and effect? In: Keller, G., Kerr, A.C. (Eds.), *Volcanism, Impacts, and Mass Extinctions: Causes and Effects*. Geological Society of America Special Paper 505, pp. 57–89. [https://doi.org/10.1130/2014.2505\(03\)](https://doi.org/10.1130/2014.2505(03)).
- Keller, G., Abramovich, S., 2009. Lilliput effect in late Maastrichtian planktic foraminifera: Response to environmental stress. *Paleoceanography, Palaeoclimatology, Palaeoecology* 284, 47–62. <https://doi.org/10.1016/j.palaeo.2009.08.029>.
- Keller, G., Adatte, T., Gardin, S., Bartolini, A., Bajpai, S., 2008. Main Deccan volcanism phase ends near the K-T boundary: evidence from the Krishna-Godavari Basin, SE India. *Earth and Planetary Science Letters* 268, 293–311. <https://doi.org/10.1016/j.epsl.2008.01.015>.
- Keller, G., Adatte, T., Pardo, A., Bajpai, S., Khosla, A., Samant, B., 2010. Cretaceous Extinctions: Evidence Overlooked. *Science* 328, 974–975. <https://doi.org/10.1126/science.328.5981.975>.
- Keller, G., Adatte, T., Bhowmick, P., Upadhyay, H., Dave, A., Reddy, A.N., Jaiprakash, B.C., 2012. Nature and timing of extinctions in Cretaceous–Tertiary planktic foraminifera preserved in Deccan intertrappean sediments of the Krishna–Godavari Basin, India. *Earth and Planetary Science Letters* 341–344, 211–221. <https://doi.org/10.1016/j.epsl.2012.06.021>.
- Keller, G., Puneekar, J., Mateo, P., 2016. Upheavals during the Late Maastrichtian: Volcanism, climate and faunal events preceding the end-Cretaceous mass extinction. *Paleoceanography, Palaeoclimatology, Palaeoecology* 441, 137–151. <https://doi.org/10.1016/j.palaeo.2015.06.034>.
- Kring, D.A., 2007. The Chicxulub impact event and its environmental consequences at the Cretaceous–Tertiary boundary. *Paleoceanography, Palaeoclimatology, Palaeoecology* 255, 4–21. <https://doi.org/10.1016/j.palaeo.2007.02.037>.
- Kucera, M., Malmgren, B.A., 1996. Latitudinal variation in the planktic foraminifer *Contusotruncana contusa* in the terminal Cretaceous ocean. *Marine Micropaleontology* 28, 31–52. [https://doi.org/10.1016/0377-8398\(95\)00078-X](https://doi.org/10.1016/0377-8398(95)00078-X).
- Kucera, M., Malmgren, B.A., Sturesson, U., 1997. Foraminiferal dissolution at shallow depths of the Walvis Ridge and Rio Grande Rise during the latest Cretaceous: Inferences for deep-water circulation in the South Atlantic. *Paleoceanography, Palaeoclimatology, Palaeoecology* 129, 195–212. [https://doi.org/10.1016/S0031-0182\(96\)00133-2](https://doi.org/10.1016/S0031-0182(96)00133-2).
- Li, L., Keller, G., 1998a. Abrupt deep-sea warming at the end of the Cretaceous. *Geology* 26, 995–998. [https://doi.org/10.1130/0091-7613\(1998\)026<0995:ADSWAT>2.3.CO;2](https://doi.org/10.1130/0091-7613(1998)026<0995:ADSWAT>2.3.CO;2).
- Li, L., Keller, G., 1998b. Diversification and extinction in Campanian–Maastrichtian planktic foraminifera of Northwestern Tunisia. *Eclogae Geologicae Helveticae* 91, 75–102.
- Linnert, C., Robinson, S.A., Lees, J.A., Bown, P.R., Rodríguez, I.P., Petrizzo, M.R., Falzoni, F., Littler, K., Arz, J.A., Russell, E.E., 2014. Evidence for global cooling in the Late Cretaceous. *Nature Communications* 5, 4194. <https://doi.org/10.1038/ncomms5194>.
- Lowery, C.M., Bralower, T.J., Owens, J.D., Rodríguez-Tovar, F.J., Jones, H., Smit, J., Whalen, M.T., Claeys, P., Farley, K., Gulick, S.P.S., Morgan, J.V., Green, S., Chenot, E., Christeson, G.L., Cocker, C.S., Coolen, M.J.L., Ferrière, L., Gebhardt, C., Goto, K., Kring, D.A., Lofi, J., Ocampo-Torres, R., Perez-Cruz, L., Pickersgill, A.E., Poelchau, M.H., Rae, A.S.P., Rasmussen, C., Rebollo-Vieyra, M., Riller, U., Sato, H., Tikoo, S.M., Tomioka, N., Urrutia-Fucugauchi, J., Vellekoop, J., Wittmann, A., Xiao, L., Yamaguchi, K.E., Zylberman, W., 2018. Rapid evidence of life at ground zero of the end-Cretaceous mass extinction. *Nature* 558, 288–291. <https://doi.org/10.1038/s41586-018-0163-6>.
- Luciani, V., Giuseberti, L., Agnini, C., Backman, J., Fornaciari, E., Rio, D., 2007. The Paleocene–Eocene Thermal Maximum as recorded by Tethyan planktonic foraminifera in the Forada section (northern Italy). *Marine Micropaleontology* 64, 189–214. <https://doi.org/10.1016/j.marmicro.2007.05.001>.
- MacLeod, N., Ortiz, N., Fefferman, N., Clyde, W., Schuster, C., MacLean, J., 2000. Phenotypic response of foraminifera to episodes of global environmental change. In: Culver, S.J., Rawson, P. (Eds.), *Biotic Response to Global Environmental Change: The Last 145 Million Years*. Cambridge University Press, Cambridge, pp. 51–78. <https://doi.org/10.1017/CBO9780511535505.006>.
- MacLeod, K.G., Huber, B.T., Isaza-Londoño, C., 2005. North Atlantic warming during global cooling at the end of the Cretaceous. *Geology* 33, 437–440. <https://doi.org/10.1130/G21466.1>.
- Malmgren, B.A., 1987. Differential dissolution of Upper Cretaceous planktonic foraminifera from a temperate region of the South Atlantic Ocean. *Marine Micropaleontology* 11, 251–271. [https://doi.org/10.1016/0377-8398\(87\)90001-6](https://doi.org/10.1016/0377-8398(87)90001-6).
- Metsana-Oussaid, F., Belhai, D., Arenillas, I., Arz, J.A., Gilibert, V., 2019. New sections of the Cretaceous–Paleogene transition in the southwestern Tethys (Médéa, northern Algeria): planktic foraminiferal biostratigraphy and biochronology. *Arabian Journal of Geosciences* 12. <https://doi.org/10.1007/s12517-019-4402-4>.
- Molina, E., Arenillas, I., Arz, J.A., 1998. Mass extinction in planktic foraminifera at the Cretaceous/Tertiary boundary in subtropical and temperate latitudes. *Bulletin de la Société Géologique de France* 169, 351–363.
- Molina, E., Alegret, L., Arenillas, I., Arz, J.A., Gallala, N., Grajales-Nishimura, M., Murillo-Muneton, G., Zaghbib-Turki, D., 2009. The Global Boundary Stratotype Section and Point for the base of the Danian Stage (Paleocene, Paleogene, “Tertiary”, Cenozoic): auxiliary sections and correlation. *Episodes* 32 (2), 84–95. <https://doi.org/10.18814/epiiugs/2009/v32i2/002>.
- Nordt, L., Atchley, S., Dworkin, S., 2003. Terrestrial evidence for two greenhouse events in the latest Cretaceous. *Geological Society of America Today* 13, 4–9. [https://doi.org/10.1130/1052-5173\(2003\)013<4:TEFTGE>2.0.CO;2](https://doi.org/10.1130/1052-5173(2003)013<4:TEFTGE>2.0.CO;2).
- O’Brien, C.L., Robinson, S.A., Pancost, R.D., Sinnighe Damsté, J.S., Schouten, S., Lunt, D.J., Alsenz, H., Bornemann, A., Bottini, C., Brassell, S.C., Farnsworth, A., Forster, A., Huber, B.T., Inglis, G.N., Jenkyns, H.C., Linnert, C., Littler, K., Markwick, P., McAnena, A., Mutterlose, J., Naafs, B.D.A., Püttmann, W., Sluijs, A., van Helmond, N.A.G.M., Vellekoop, J., Wagner, T., Wrobel, N.E., 2017. Cretaceous sea-surface temperature evolution: Constraints from TEX86 and planktonic foraminiferal oxygen isotopes. *Earth-Science Reviews* 172, 224–247. <https://doi.org/10.1016/j.earscirev.2017.07.012>.
- O’Connor, L.K., Robinson, S.A., Naafs, B.D.A., Jenkyns, H.C., Henson, S., Clarke, M., Pancost, R.D., 2019. Late Cretaceous Temperature Evolution of the Southern High Latitudes: A TEX86 Perspective. *Paleoceanography and Palaeoclimatology* 34, 436–454. <https://doi.org/10.1029/2018PA003546>.
- Pardo, A., Keller, G., 2008. Biotic effects of environmental catastrophes at the end of the Cretaceous and early Tertiary: *Guembelitra* and *Heterohelix* blooms. *Cretaceous Research* 29, 1058–1073. <https://doi.org/10.1016/j.cretres.2008.05.031>.
- Petersen, S.V., Dutton, A., Lohmann, K.C., 2016. End-Cretaceous extinction in Antarctica linked to both Deccan volcanism and meteorite impact via climate change. *Nature Communications* 7, 12079. <https://doi.org/10.1038/ncomms12079>.
- Petrizzo, M.R., Huber, B.T., Falzoni, F., MacLeod, K.G., 2020. Changes in biogeographic distribution patterns of southern mid-to high latitude planktonic foraminifera during the Late Cretaceous hot to cool greenhouse climate transition. *Cretaceous Research* 115 (104547). <https://doi.org/10.1016/j.cretres.2020.104547>.
- Percival, L., Jenkyns, H.C., Mather, T.A., Dickson, A.J., Batenburg, S.J., Ruhl, M., Hesselbo, S.P., Barclay, R., Jarvis, I., Robinson, S.A., Woelders, L., 2018. Does large igneous province volcanism always perturb the mercury cycle? Comparing the records of Oceanic Anoxic Event 2 and the end-Cretaceous to other Mesozoic events. *American Journal of Science* 318, 799–860. <https://doi.org/10.2475/08.2018.01>.
- Premoli Silva, I., Sliter, W.V., 1999. Cretaceous paleoceanography: evidence from planktonic foraminiferal evolution. In: Barrera, E., Johnson, C.C. (Eds.), *Evolution of the Cretaceous Ocean–Climate System*. Geological Society of America Special Paper 332, pp. 301–328. <https://doi.org/10.1130/0-8137-2332-9.301>.

- Punekar, J., Mateo, P., Keller, G., 2014. Environmental and biological effects of Deccan volcanism: a global survey. In: Keller, G., Kerr, A.C. (Eds.), *Volcanism, Impacts, and Mass Extinctions: Causes and Effects*. Geological Society of America Special Paper 505, pp. 91–116. [https://doi.org/10.1130/2014.2505\(04\)](https://doi.org/10.1130/2014.2505(04)).
- Punekar, J., Keller, G., Khozyem, H.M., Adatte, T., Font, E., Spangenberg, J., 2016. A multi-proxy approach to decode the end-Cretaceous mass extinction. *Palaeogeography, Palaeoclimatology, Palaeoecology* 441, 116–136. <https://doi.org/10.1016/j.palaeo.2015.08.025>.
- Renne, P.R., Deino, A.L., Hilgen, F.J., Kuiper, K.F., Mark, D.F., Mitchell, W.S., Morgan, L.E., Mundil, R., Smit, J., 2013. Time scales of critical events around the Cretaceous–Paleogene boundary. *Science* 339, 684–687. <https://doi.org/10.1126/science.1230492>.
- Renne, P.R., Sprain, C.J., Richards, M.A., Self, S., Vanderkluyzen, L., Pande, K., 2015. State shift in Deccan volcanism at the Cretaceous–Paleogene boundary, possibly induced by impact. *Science* 350, 76–78. <https://doi.org/10.1126/science.aac7549>.
- Robinson, N., Ravizza, G., Coccioni, R., Peucker-Ehrenbrink, B., Norris, R., 2009. A high-resolution marine  $^{187}\text{Os}/^{188}\text{Os}$  record for the late Maastrichtian: Distinguishing the chemical fingerprints of Deccan volcanism and the KP impact event. *Earth and Planetary Science Letters* 281, 159–168. <https://doi.org/10.1016/j.epsl.2009.02.019>.
- Schoene, B., Samperton, K.M., Eddy, M.P., Keller, G., Adatte, T., Bowring, S.A., Khadri, S.F.R., Gertsch, B., 2015. U–Pb geochronology of the Deccan Traps and relation to the end-Cretaceous mass extinction. *Science* 347, 182–184. <https://doi.org/10.1126/science.aaa0118>.
- Schoene, B., Eddy, M.P., Samperton, K.M., Keller, C.B., Keller, G., Adatte, T., Khadri, S.F.R., 2019. U–Pb constraints on pulsed eruption of the Deccan Traps across the end-Cretaceous mass extinction. *Science* 363, 862–866. <https://doi.org/10.1126/science.aau2422>.
- Scholle, P.A., Arthur, M.A., 1980. Carbon isotope fluctuations in Cretaceous pelagic limestones: potential stratigraphic and petroleum exploration tool. *American Association of Petroleum Geologists Bulletin* 64 (1), 67–87.
- Schulte, P., Alegret, L., Arenillas, I., Arz, J.A., Barton, P.J., Bown, P.R., Bralower, T.J., Christeson, G.L., Claeys, P., Cockell, C.S., Collins, G.S., Deutsch, A., Goldin, T.J., Goto, K., Grajales-Nishimura, J.M., Grieve, R.A.F., Gulick, S.P.S., Johnson, K.R., Kiessling, W., Koeberl, C., Kring, D.A., MacLeod, K.G., Matsui, T., Melosh, J., Montanari, A., Morgan, J.V., Neal, C.R., Nichols, D.J., Norris, R.D., Pierazzo, E., Ravizza, G., Rebolledo-Vieyra, M., Reimold, W.U., Robin, E., Salge, T., Speijer, R.P., Sweet, A.R., Urrutia-Fucugauchi, J., Vajda, V., Whalen, M.T., Willumsen, P.S., 2010a. The Chicxulub asteroid impact and mass extinction at the Cretaceous–Paleogene boundary. *Science* 327, 1214–1218. <https://doi.org/10.1126/science.1177265>.
- Schulte, P., Alegret, L., Arenillas, I., Arz, J.A., Barton, P.J., Bown, P.R., Bralower, T.J., Christeson, G.L., Claeys, P., Cockell, C.S., Collins, G.S., Deutsch, A., Goldin, T.J., Goto, K., Grajales-Nishimura, J.M., Grieve, R.A.F., Gulick, S.P.S., Johnson, K.R., Kiessling, W., Koeberl, C., Kring, D.A., MacLeod, K.G., Matsui, T., Melosh, J., Montanari, A., Morgan, J.V., Neal, C.R., D.J., Norris, R.D., Pierazzo, E., Ravizza, G., Rebolledo-Vieyra, M., Reimold, W.U., Robin, E., Salge, T., Speijer, R.P., Sweet, A.R., Urrutia-Fucugauchi, J., Vajda, V., Whalen, M.T., Willumsen, P.S., 2010b. Response – Cretaceous extinctions. *Science* 328, 975–976. <https://doi.org/10.1126/science.328.5981.975>.
- Sial, A.N., Chen, J., Lacerda, L.D., Frei, R., Tewari, V.C., Pandit, M.K., Gaucher, C., Ferreira, V.P., Cirilli, S., Peralta, S., Korte, C., Barbosa, J.A., Pereira, N.S., 2016. Mercury enrichment and Hg isotopes in Cretaceous–Paleogene boundary successions: Links to volcanism and palaeoenvironmental impacts. *Cretaceous Research* 66, 60–81. <https://doi.org/10.1016/j.cretres.2016.05.006>.
- Signor, P.W., Lipps, J.H., 1982. Sampling bias, gradual extinction patterns and catastrophes in the fossil record. *Geological Society of America Special Paper* 190, 291–296. <https://doi.org/10.1130/SPE190-p291>.
- Smit, J., 1982. Extinction and evolution of planktonic foraminifera after a major impact at the Cretaceous/Tertiary boundary. *Geological Society of America Special Paper* 190, 329–352. <https://doi.org/10.1130/SPE190-p329>.
- Smit, J., 2004. The section of the Barranco del Gredero (Caravaca, SE Spain): a crucial section for the Cretaceous/Tertiary boundary impact extinction hypothesis. *Journal of Iberian Geology* 31, 179–191. <https://doi.org/10.5209/JIGE.33967>.
- Smit, J., Klaver, G., 1981. Sanidine spherules indicate a large impact event. *Nature* 292, 47–49. <https://doi.org/10.1038/292047a0>.
- Smit, J., ten Kate, W.G.H.Z., 1982. Trace-element patterns at the Cretaceous–Tertiary boundary – Consequences of a large impact. *Cretaceous Research* 3, 307–332. [https://doi.org/10.1016/0195-6671\(82\)90031-3](https://doi.org/10.1016/0195-6671(82)90031-3).
- Sprain, C.J., Renne, P.R., Vanderkluyzen, L., Pande, K., Self, S., Mittal, T., 2019. The eruptive tempo of Deccan volcanism in relation to the Cretaceous–Paleogene boundary. *Science* 363, 866–870. <https://doi.org/10.1126/science.aav1446>.
- Sosa-Montes de Oca, C., Rodríguez-Tovar, F.J., Martínez-Ruiz, F., 2016. Geochemical and isotopic characterization of trace fossil infillings: New insights on trace-maker activity after the K/Pg impact event. *Cretaceous Research* 57, 391–401. <https://doi.org/10.1016/j.cretres.2015.03.003>.
- Stott, L.D., Kennett, J.P., 1990. The paleoceanographic and paleoclimatic signature of the Cretaceous/Paleogene boundary in the Antarctic: stable isotopic results from ODP Leg 113. In: *Proceedings of the Ocean Drilling Program. Scientific Results* 113, 829–848. <https://doi.org/10.2973/jodp.proc.sr.113.158.1990>.
- Thibault, N., Gardin, S., 2010. The calcareous nannofossil response to the end-Cretaceous warm event in the Tropical Pacific. *Palaeogeography, Palaeoclimatology, Palaeoecology* 291, 239–252. <https://doi.org/10.1016/j.palaeo.2010.02.036>.
- Thibault, N., Galbrun, B., Gardin, S., Minoletti, F., Le Callonnec, L.L., 2016. The end-Cretaceous in the southwestern Tethys (Elles, Tunisia): orbital calibration of paleoenvironmental events before the mass extinction. *International Journal of Earth Sciences (Geologische Rundschau)* 105, 771–795. <https://doi.org/10.1007/s00531-015-1192-0>.
- Tobin, T.S., Ward, P.D., Steig, E.J., Olivero, E.B., Hilburn, I.A., Mitchell, R.N., Diamond, M.R., Raub, T.D., Kirschvink, J.L., 2012. Extinction patterns,  $\delta^{18}\text{O}$  trends, and magnetostratigraphy from a southern high-latitude Cretaceous–Paleogene section: Links with Deccan volcanism. *Palaeogeography, Palaeoclimatology, Palaeoecology* 350–352, 180–188. <https://doi.org/10.1016/j.palaeo.2012.06.029>.
- Vellekoop, J., Esmeray-Senlet, S., Miller, K.G., Browning, J.V., Sluijs, A., van de Schoot-brugge, B., Sinninghe Damsté, J.S., Brinkhuis, H., 2016. Evidence for Cretaceous–Paleogene boundary bolide “impact winter” conditions from New Jersey, USA. *Geology* 44, 619–622. <https://doi.org/10.1130/G37961.1>.
- Vellekoop, J., Woelders, L., Sluijs, A., Miller, K.G., Speijer, R.P., 2019. Phytoplankton community disruption caused by latest Cretaceous global warming. *Biogeosciences* 16, 4201–4210. <https://doi.org/10.5194/bg-16-4201-2019>.
- Voigt, S., Gale, A.S., Jung, C., Jenkyns, H.C., 2012. Global correlation of upper Campanian–Maastrichtian successions using carbon-isotope stratigraphy: Development of a new Maastrichtian timescale. *Newsletters on Stratigraphy* 45, 25–53. <https://doi.org/10.1127/0078-0421/2012/0016>.
- Westerhold, T., Röhl, U., Donner, B., Mccarren, H.K., Zachos, J.C., 2011. A complete high-resolution Paleocene benthic stable isotope record for the central Pacific (ODP Site 1209). *Paleoceanography* 26, 1–13. <https://doi.org/10.1029/2010PA002092>.
- Wilf, P., Johnson, K.R., Huber, B.T., 2003. Correlated terrestrial and marine evidence for global climate changes before mass extinction at the Cretaceous–Paleogene boundary. *Proceedings of the National Academy of Sciences* 100, 599–604. <https://doi.org/10.1073/pnas.0234701100>.
- Woelders, L., Vellekoop, J., Kroon, D., Smit, J., Casadío, S., Prámparo, M.B., Dinarès-Turell, J., Peterse, F., Sluijs, A., Lenaerts, J.T.M., Speijer, R.P., 2017. Latest Cretaceous climatic and environmental change in the South Atlantic region. *Paleoceanography* 32. <https://doi.org/10.1002/2016PA00300703007>, 2016PA003007.
- Woelders, L., Vellekoop, J., Weltje, G.J., de Nooijer, L., Reichart, G.-J., Peterse, F., Claeys, P., Speijer, R.P., 2018. Robust multi-proxy data integration, using late Cretaceous paleotemperature records as a case study. *Earth and Planetary Science Letters* 500, 215–224. <https://doi.org/10.1016/j.epsl.2018.08.010>.
- Zhang, L., Wang, C., Wignall, P.B., Kluge, T., Wan, X., Wang, Q., Gao, Y., 2018. Deccan volcanism caused coupled pCO<sub>2</sub> and terrestrial temperature rises, and pre-impact extinctions in northern China. *Geology* 46, 271–274. <https://doi.org/10.1130/G39992.1>.

## Appendix A. Supplementary data

Supplementary data to this article can be found online at <https://doi.org/10.1016/j.cretres.2021.104844>.

## Appendix. Alphabetic list of all species mentioned in the paper

- Abathomphalus intermedius* (Bolli, 1951).  
*Abathomphalus mayaroensis* (Bolli, 1951).  
*Archaeoglobigerina blowi* Pessagno, 1967.  
*Archaeoglobigerina cretacea* (d’Orbigny, 1840).  
*Contusotruncana contusa* (Cushman, 1926).  
*Contusotruncana patelliformis* (Gandolfi, 1955).  
*Contusotruncana plicata* (White, 1928).  
*Contusotruncana walfischensis* (Todd, 1970).  
*Globigerinelloides multispina* (Lalicker, 1948).  
*Globigerinelloides praerhihensis* (Pessagno, 1967).  
*Globigerinelloides rosebudensis* Smith and Pessagno, 1973.  
*Globigerinelloides subcarinatus* (Brönnimann, 1952).  
*Globigerinelloides volutus* (White, 1928).  
*Globigerinelloides yaucoensis* (Pessagno, 1960).  
*Globotruncana aegyptiaca* Nakkady, 1950.  
*Globotruncana arca* (Cushman, 1926).  
*Globotruncana mariei* Banner and Blow, 1960.  
*Globotruncana orientalis* El Naggag, 1966.  
*Globotruncana rosetta* (Carsey, 1926).  
*Globotruncanella caravacaensis* Smit, 1982.  
*Globotruncanella havanensis* (Voorwijk, 1937).  
*Globotruncanella minuta* Caron and González Donoso, 1984.  
*Globotruncanella petaloidea* (Gandolfi, 1955).  
*Globotruncanella pschadae* (Keller, 1946).  
*Globotruncanella angulata* (Tilev, 1951).  
*Globotruncanita conica* (White, 1928).  
*Globotruncanita dupeublei* (Caron, González Donoso, Robaszynski and Wonders, 1984).  
*Globotruncanita falsocalcarata* (Kerdany and Abdelsalam, 1969).  
*Globotruncanita fareedi* (El Naggag, 1966).

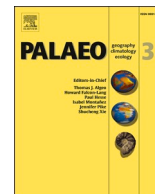
- Globotruncanita insignis* (Gandolfi, 1955).  
*Globotruncanita stuarti* (de Lapparent, 1918).  
*Globotruncanita stuartiformis* (Dalbiez, 1955).  
*Gublerina acuta* de Klsz, 1953.  
*Gublerina cuvillieri* Kikoine, 1948.  
*Guembeltria blowi* Arz, Arenillas and Nández, 2010.  
*Guembeltria cretacea* Cushman, 1933.  
*Heterohelix globulosa* (Ehrenberg, 1840).  
*Heterohelix labellosa* Nederbragt, 1991.  
*Heterohelix navarroensis* Loeblich, 1951.  
*Heterohelix punctulata* (Cushman, 1938).  
*Laeviheterohelix glabrans* (Cushman, 1938).  
*Laeviheterohelix pulchra* (Brotzen, 1936).  
*Muricohedbergella holmdelensis* (Olsson, 1964).  
*Muricohedbergella monmouthensis* (Olsson, 1960).  
*Planoglobulina acervulinoides* (Egger, 1899).  
*Planoglobulina carseyae* (Plummer, 1931).  
*Planoglobulina manuelensis* (Martin, 1972).  
*Planoglobulina multicamerata* (de Klsz, 1953).  
*Plummerita hantkeninoides* (Brönnimann, 1952).  
*Pseudoguembelina costellifera* Masters, 1976.  
*Pseudoguembelina costulata* (Cushman, 1938).  
*Pseudoguembelina excolata* (Cushman, 1926).  
*Pseudoguembelina hariaensis* Nederbragt, 1991.  
*Pseudoguembelina kempensis* Esker, 1968.  
*Pseudoguembelina palpebra* Brönnimann and Brown, 1953.  
*Pseudotextularia elegans* (Rzehak, 1891).  
*Pseudotextularia intermedia* de Klsz, 1953.  
*Pseudotextularia nuttalli* (Voorwijk, 1937).  
*Racemiguembelina fruticosa* (Egger, 1899).  
*Racemiguembelina powelli* Smith y Pessagno, 1973.  
*Rugoglobigerina hexacamerata* Brönnimann, 1952.  
*Rugoglobigerina macrocephala* Brönnimann, 1952.  
*Rugoglobigerina milamensis* Smith and Pessagno, 1973.  
*Rugoglobigerina pennyi* Brönnimann, 1952.  
*Rugoglobigerina reicheli* Brönnimann, 1952.  
*Rugoglobigerina rotundata* Brönnimann, 1952.  
*Rugoglobigerina rugosa* (Plumier, 1926).  
*Rugoglobigerina scotti* (Brönnimann, 1952).

**4.4. Multiproxy analysis of paleoenvironmental, paleoclimatic and paleoceanographic changes during the Early Danian in the Caravaca section (Spain)**

**Gilabert, V., Arenillas, I., Arz, J.A., Batenburg, S., Robinson, S.A., 2021.** Multiproxy analysis of paleoenvironmental, paleoclimatic and paleoceanographic changes during the Early Danian in the Caravaca section (Spain) *Palaeogeography, Palaeoclimatology, Palaeoecology*, 576, 110513.

<https://doi.org/10.1016/j.palaeo.2021.110513>.

El material suplementario de este artículo se encuentra en el apartado Anexos (Anexo III).



## Multiproxy analysis of paleoenvironmental, paleoclimatic and paleoceanographic changes during the early Danian in the Caravaca section (Spain)

Vicente Gilabert<sup>a,\*</sup>, Ignacio Arenillas<sup>a</sup>, José A. Arz<sup>a</sup>, Sietske J. Batenburg<sup>b</sup>, Stuart A. Robinson<sup>c</sup>

<sup>a</sup> Departamento de Ciencias de la Tierra, Instituto Universitario de Investigación en Ciencias Ambientales de Aragón, Universidad de Zaragoza, E-50009 Zaragoza, C/ Pedro Cerbuna 12, 50009 Zaragoza, Spain

<sup>b</sup> Departament de Dinàmica de la Terra i de l'Oceà, Facultat de Ciències de la Terra, Universitat de Barcelona, Martí i Franquès, 08028 Barcelona, Spain

<sup>c</sup> Department of Earth Sciences, University of Oxford, South Parks Road, Oxford OX1 3AN, UK

### ARTICLE INFO

Editor: Isabel Montanez

#### Keywords:

Deccan volcanism  
Dan-C2  
Acme-stage  
Mass extinction  
Western Tethys

### ABSTRACT

After the Chicxulub impact and mass extinction at the Cretaceous-Paleogene boundary (K-PgB), ecosystems haltingly recovered under unstable conditions. An early Danian (65.9 Ma) perturbation of the carbon cycle known as Dan-C2, which includes two carbon isotopic excursions (CIEs), has been ascribed to inputs of greenhouse gases through large-scale volcanism of the Deccan Traps. However, the relationship between Dan-C2, volcanism and environmental and climatic changes during the early Danian remains ambiguous. Based on stable isotopes, calcium carbonate content, magnetic susceptibility and planktic foraminifera, we present a paleoenvironmental, paleoclimatic and paleoceanographic reconstruction of the early Danian from the Caravaca section, Spain, one of the most complete and continuous K-PgB sections worldwide. The paleobiological response of planktic foraminifera suggests very volatile environmental conditions during the first 230 kyr of the Danian, as reflected in the rapid succession of opportunistic/generalist blooms and episodic high occurrences of aberrant specimens. According to our age model, the Dan-C2 has been identified at the Caravaca section from 65.92 to 65.74 Ma. No evidence of strong carbonate dissolution through ocean acidification was observed in the Dan-C2 interval or the rest of the studied section, excluding the K-PgB clay bed. We find that blooms of highly eutrophic *Chiloguembeltria* and increases in aberrant planktic foraminifera coincided with a major early Danian eruptive episode of Deccan Traps (Ambelani Formation), occurring before the Dan-C2. Conversely, during both Dan-C2 CIEs, less opportunistic taxa thrived, indicating changes in the upper part of the water column. This study demonstrates that the relationship between marine biota and climate change was very complex and rapidly changing during the early Danian. In addition, we propose that the Deccan volcanism had adverse effects on marine plankton, mostly through strong eutrophication, while an increased water column stratification during the Dan-C2 event resulted in a transient boost in the recovery of ecosystems.

### 1. Introduction

The Cretaceous-Paleogene boundary (K-PgB) is marked by one of the most devastating geological events that has occurred on Earth (Alvarez et al., 1980; Smit and Hertogen, 1980) caused by the impact of a ~ 10 km-diameter asteroid at the Yucatan Peninsula, Mexico, known as the Chicxulub asteroid (Hildebrand et al., 1991). It is widely understood that the asteroid impact caused a series of catastrophic environmental effects, including the blockage of solar radiation leading to a cold and

dark “impact winter”, ocean acidification, and pollution by toxic heavy metals, resulting in one of the greatest biotic crises on Earth (Kring, 2007; Premović, 2009; Schulte et al., 2010; Vellekoop et al., 2014, 2016; Gulick et al., 2019; Henehan et al., 2019; Gibbs et al., 2020). The environmental effects were lethal in the pelagic realm and caused the decimation of calcareous plankton at the K-PgB (Smit, 1982; Arenillas et al., 2000a, 2000b; Bown, 2005). Multiple lines of evidence have pointed to the Chicxulub impact as the main cause of the K-PgB mass extinction (e.g. Smit, 1999; Arenillas et al., 2006; Schulte et al., 2010;

\* Corresponding author.

E-mail addresses: [vgilabert@unizar.es](mailto:vgilabert@unizar.es) (V. Gilabert), [ias@unizar.es](mailto:ias@unizar.es) (I. Arenillas), [josearz@unizar.es](mailto:josearz@unizar.es) (J.A. Arz), [sbatenburg@ub.edu](mailto:sbatenburg@ub.edu) (S.J. Batenburg), [stuart.robinson@earth.ox.ac.uk](mailto:stuart.robinson@earth.ox.ac.uk) (S.A. Robinson).

<https://doi.org/10.1016/j.palaeo.2021.110513>

Received 5 January 2021; Received in revised form 26 May 2021; Accepted 31 May 2021

Available online 4 June 2021

0031-0182/© 2021 Elsevier B.V. All rights reserved.

Lowery et al., 2018; Henehan et al., 2019). Nonetheless, recent advances in radiometric dating constrain the eruptive phases of Deccan Traps volcanism (in India), as well as the Chicxulub impact, to a period of only a few hundred thousand years during magnetochron C29r (Chenet et al., 2007; Renne et al., 2015; Schoene et al., 2015, 2019; Sprain et al., 2019) thereby hindering a clear distinction between the specific roles of volcanism and impact in the K-PgB mass extinction. Consequently, these issues remain a topic of intense debate 40 years since the impact hypothesis was first proposed (Alvarez et al., 1980; Hull et al., 2020; Keller et al., 2020).

Discrepancies in the age of the K-PgB and its stratigraphic position within the Deccan Traps, as well as uncertainty regarding the eruptive rates of its main phases, result in two models of Deccan Traps eruptions, and a controversy about the role of Deccan volcanism in the K-PgB mass extinction and early Danian climate change (Burgess, 2019; Hull et al., 2020; Keller et al., 2020). Based on  $^{40}\text{Ar}/^{39}\text{Ar}$  dating, and volcano-stratigraphic and biostratigraphic evidence, it has been argued that the most voluminous Deccan eruptions occurred during the early Danian, corresponding to the emplacement of the Poladpur, Ambenali and Mahabaleswar Formations of the Wai subgroup (Jay and Widdowson, 2008; Renne et al., 2015; Richards et al., 2015; Sprain et al., 2019). However, based on U/Pb dating of the Deccan Traps Formations, it has been proposed that the volcanic phase with the highest eruptive rate (Poladpur Formation) occurred in the latest Maastrichtian, only tens of thousands of years prior the K-PgB (Schoene et al., 2015, 2019, 2021).

Although geochemical signatures ascribed to Deccan volcanism, such as  $^{187}\text{Os}/^{188}\text{Os}$  excursions and Hg enrichments, have been recognized prior to the K-PgB (Robinson et al., 2009; Font et al., 2016, 2018; Keller et al., 2020), several paleo-ecological and paleoclimate studies (e.g. Thibault and Gardin, 2010; Thibault et al., 2016; Hull et al., 2020; Gilabert et al., 2021) have shown that the influence of the Deccan volcanism during the latest Maastrichtian did not contribute to the K-PgB mass extinction (although this is disputed by some; e.g. Keller et al., 2020 and references therein). A broad temporal coincidence also exists between post-K-PgB Deccan volcanism and the first Danian hyperthermal event, known as Dan-C2 (Quillévéré et al., 2008), which has led some to speculate that the two are mechanistically linked (e.g. Coccioni et al., 2010; Punekar et al., 2014a; Krahl et al., 2020). However, others have suggested that the Dan-C2 event could be astronomically controlled (Quillévéré et al., 2008; Barnet et al., 2019; Sinnesael et al., 2019) and recent models of the  $\text{CO}_2$  emission rates of Deccan volcanism suggest that outgassing from Deccan volcanism alone was incapable of driving the magnitude of climate change observed during the early Danian (Hull et al., 2020; Fendley et al., 2020).

During the earliest Danian, planktic foraminiferal and calcareous nannoplankton assemblages were characterized by low diversity, a high single-species dominance, rapid evolutionary turnovers, and blooms of smaller generalist or opportunist taxa that could thrive under eutrophic and unstable conditions (Romein, 1977; Smit, 1982; Huber et al., 2002; Lamolda et al., 2005; Arenillas et al., 2006; Jiang et al., 2010; Jones et al., 2019; Lowery et al., 2020). Recently, it has been proposed that non-calcareous algal and microbial communities bloomed in the open ocean in the short-term aftermath of the Chicxulub impact (Bralower et al., 2020). According to Bralower et al. (2020), these microbial blooms probably contributed to rapid ecosystem recovery by removing nutrients and providing a food source for higher trophic orders, enhancing pelagic ocean habitability as evidenced by the rapid recovery of planktic foraminifera and calcareous nannoplankton after the impact.

The main planktic foraminiferal indicators of enhanced environmental stress across the K-PgB are the guembeltriid blooms (Kroon and Nederbragt, 1990; Keller and Pardo, 2004; Pardo and Keller, 2008; Ashckenazi-Polivoda et al., 2014; Punekar et al., 2014a, 2014b) and the increases in aberrant planktic foraminifera tests (Gerstel et al., 1986; Coccioni and Luciani, 2006; Arenillas et al., 2018). Worldwide, blooms of *Guembeltria* and its descendant *Chiloguembeltria* have been reported well above the K-PgB (Arenillas et al., 2018), and thus appear

genetically disconnected from the Chicxulub impact. However, the blooms did occur within the temporal range of Deccan volcanism in the Danian which points to a potential cause and effect relationship (Keller et al., 2012; Punekar et al., 2014a, 2014b; Arenillas et al., 2018). Similarly, an increase in aberrant foraminifera tests after the K-PgB has been shown to continue locally at the El Kef and Ain Settara sections (Tunisia) for several hundreds of thousands of years after the K-PgB (Arenillas et al., 2018), suggesting the persistence of stressed conditions.

Except for the immediate aftermath of the Chicxulub impact, the climatic and environmental changes that occurred during the first thousand years of the Danian leading up to the Dan-C2 event have not been exhaustively examined (e.g., Quillévéré et al., 2008; Barnet et al., 2019). To improve our understanding of the complex paleobiological changes that took place during the early Danian, and their potential relationship with the Deccan volcanism and the Dan-C2 event, we carried out a detailed analysis of the first ~750 kyr of the Danian at the Caravaca section (SE Spain, western Tethys). We took a multi-proxy approach: quantitative, diversity, taphonomic (fragmentation index) and teratological (percentage of aberrant specimens) analyses of planktic foraminifera, as well as bulk geochemical (stable C- and O-isotopes,  $\text{CaCO}_3$  content) and magnetic susceptibility measurements. Caravaca is a well-known section for its excellent exposure, completeness and continuity (Smit, 1982, 2004; Molina et al., 2009), and provides an exceptional opportunity to evaluate paleoclimatic, paleoceanographic and paleobiological changes during the early Danian.

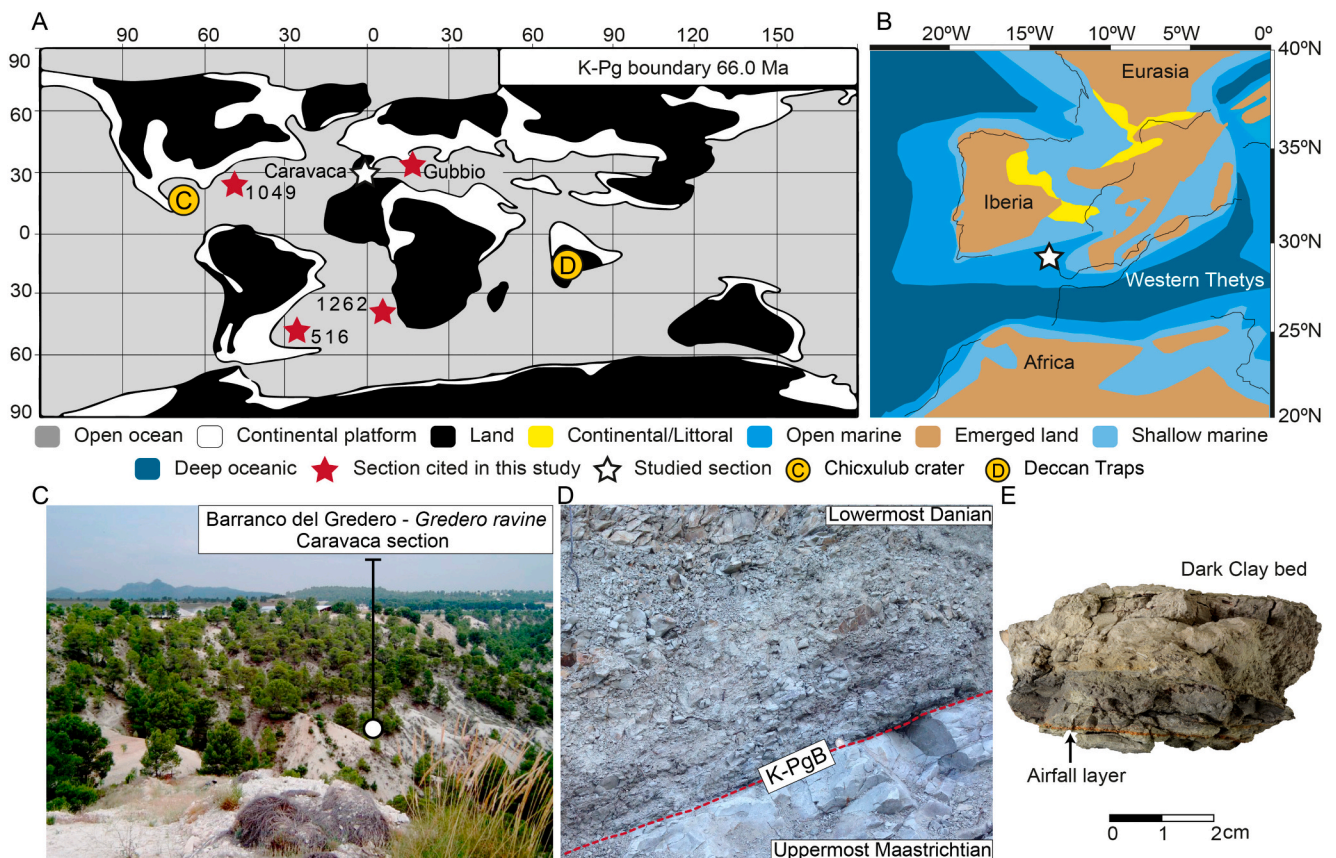
## 2. Material and methods

We revisited the Caravaca section, which is located in the Barranco del Gredero (38°04'36" N, 1°52'42" W), southwest of Caravaca de la Cruz, SE Spain (Fig. 1). The Danian part of this section consists mostly of hemipelagic marly limestones (Fig. 2), although it starts with the well-known K-PgB clay bed (Smit, 1982, 2004), consisting of a 1–2 mm-thick red air-fall layer and a 6 cm-thick dark clay bed, that is almost black in the lowermost 1.5 cm (Fig. 1E). This section was chosen as an auxiliary section of the Global Boundary Stratotype Section and Point (GSSP) for the base of the Danian Stage (Molina et al., 2009), as it represents one of the most continuous and complete K-PgB sections worldwide (Smit and Hertogen, 1980; Smit and Romein, 1985). Previous studies have focused on the K-PgB clay bed and the first one or two meters of the lowermost Danian, with a significantly lower resolution above this interval (Smit, 1982, 2004; Canudo et al., 1991; Coccioni and Galeotti, 1994; Kaiho and Lamolda, 1999; Arz et al., 2000; Lamolda et al., 2005; Vellekoop et al., 2018; Sepúlveda et al., 2019). In contrast, we sampled the first 820 cm of the Danian at high resolution, taking samples every 1–5 cm over the first 200 cm, and every 25–30 cm across the rest of the section.

### 2.1. Micropaleontological methods

For micropaleontological analyses, a total of 46 samples were disaggregated in  $\text{H}_2\text{O}_2$  for 3–4 h. These samples were washed and sieved under running water; the size fraction  $>63\ \mu\text{m}$  was collected, and the residue was oven-dried at 50 °C for 24 h. Representative splits of ca. 300 individuals per sample were studied for quantitative analyses, classifying the specimens at species level. Representative specimens from Caravaca were photographed with a JEOL JSM 6400 SEM (scanning electron microscope) at the Microscopy Service of the Universidad de Zaragoza (Spain).

For the Danian, we have used the planktic foraminiferal zonation of Arenillas et al. (2004), which was updated by Metsana-Oussaid et al. (2019). In Fig. 2, this biozonation has been compared with the more standardized zonation of Berggren and Pearson (2005), which was revised by Wade et al. (2011). Although the taxonomy used by the authors differs, the close correspondence of biozones and subbiozones is



**Fig. 1.** A) Paleogeographical location map of Caravaca and other localities worldwide: DSDP Site 516, ODP Sites 1262 and 1049, and Gubbio (Contessa Highway section). B) Detailed paleogeographical map of the Western Tethys, with the star indicating the position of Caravaca (modified from Andeweg, 2002). C) Caravaca section overview. D) Detail of the Cretaceous-Paleogene transition. E) Rock fragment of the first 3 cm of the K-PgB clay bed at Caravaca, which includes the 1–2 mm thick ejecta-rich air-fall layer and the basal part of dark clay bed.

illustrated in Fig. 2. The stratigraphic distribution of Danian planktic foraminiferal species across the Caravaca section is also illustrated in Fig. 2. SEM photographs of index-species and other relevant Danian species are displayed in Fig. 3.

To identify the planktic foraminiferal acme-stages (PFAS) proposed by Arenillas et al. (2006) for the lower Danian, we used quantitative data (Tables S1, S2) and the PAST software (v4.0.3, Hammer et al., 2001) for R-mode cluster analyses using the well-known Bray-Curtis index. We chose the Bray-Curtis similarity index since it is a more appropriate index for abundance data (i.e. species assemblages) than other distance measures, such as the common Euclidian distance (Beals, 1984; Ricotta and Podani, 2017). The Euclidean distance can lead to misleading results when species abundance data contains zeros (i.e. absences of certain taxa) as this method places more weight on the abundance differences between samples than on the similarities in the assemblage of species (Legendre and Gallagher, 2001). In contrast, in the Bray-Curtis index common and scarce species have relatively similar weights, which means that the assemblage (as opposed to the absolute abundances) becomes the more significant control on distance (Ricotta and Podani, 2017). The criteria for distinguishing the boundaries between PFAS are clear: PFAS-1 is characterized by a dominance of triserial guembeltriids (*Guembeltria*), PFAS-2 by the tiny trochospiral parvularugoglobigerinids (*Parvularugoglobigerina* and *Palaeglobigerina*), and PFAS-3 by biserial *Woodringina* and *Chiloguembelina*. All three acme-stages, first recognized in the Spanish sections of Zumaia (Arenillas et al., 1998) and Agost (Molina et al., 1998), have been identified in lower Danian sections worldwide (Arenillas et al., 2006, 2016; Gallala et al., 2009; Lowery et al., 2018; Renne et al., 2018).

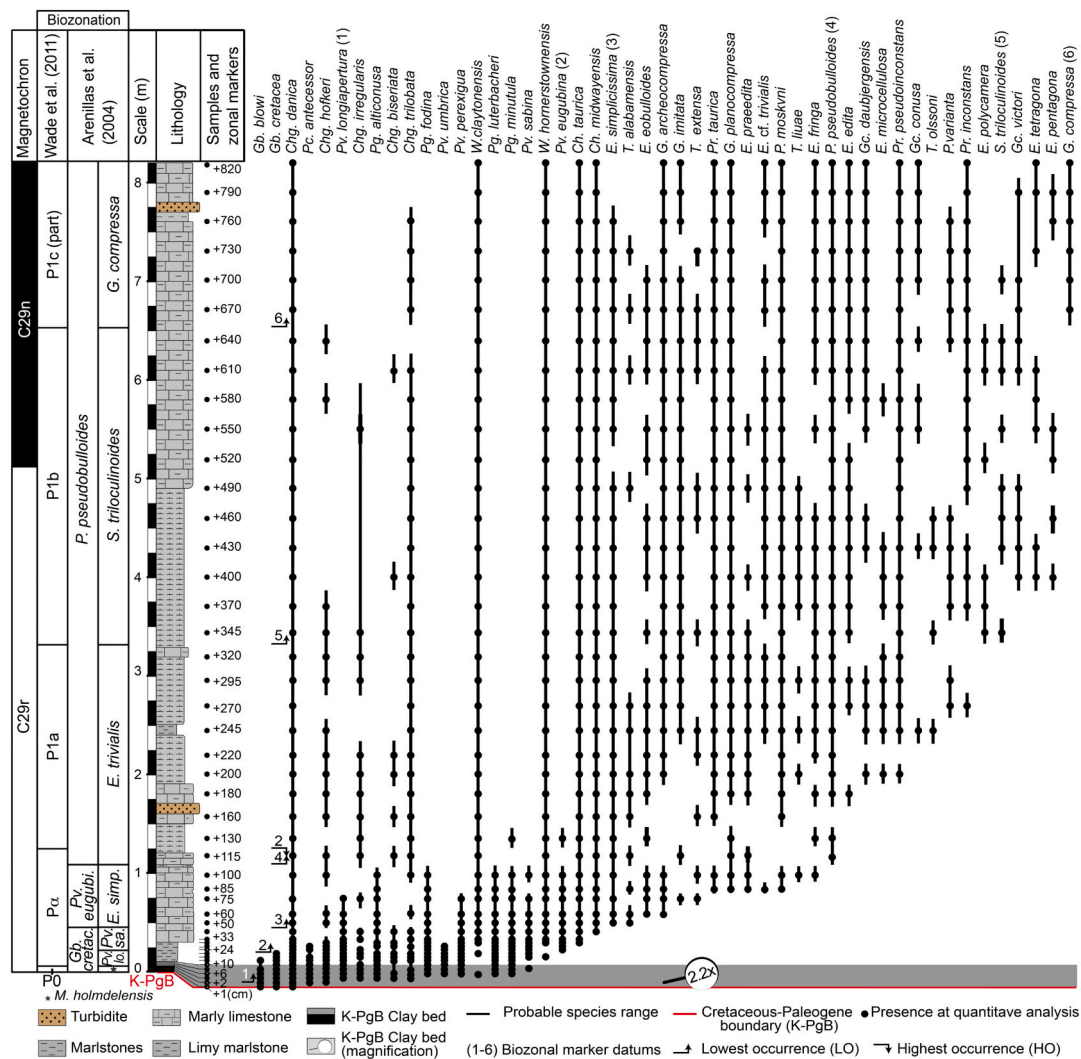
To reconstruct paleo-environmental change, we have used several

planktic foraminiferal proxies: paleoecological preferences of species, the abundance of aberrant specimens, fragmentation index, diversity indices and the planktic/benthic ratio. Early Danian planktic foraminiferal paleoecology has previously been interpreted based on the isotopic signatures of each species (e.g. Olsson et al., 1999; Aze et al., 2011; Birch et al., 2012). In order to discriminate between normal and abnormal specimens, we followed the compendium of aberrant morphologies of Arenillas et al. (2018) for early Danian planktic foraminifera. The fragmentation index (ratio of broken vs. complete foraminifera) was calculated following the method of Berger et al. (1982), and used to identify changes in carbonate preservation state. Benthic foraminifera were picked to evaluate potential dissolution processes by calculating the planktic/benthic (P/B) ratio (% planktic foraminifera of the total number of foraminifera), but they were not taxonomically classified.

## 2.2. Geochemical and geophysical methods

The inorganic and organic carbonate content was measured using duplicate subsamples from 70 samples that were weighed into ceramic boats, one of which was roasted in air at 420 °C for 12 h to remove organic carbon. The total carbon content (TC) of the unroasted subsample, and the Total Inorganic Carbon (TIC) of the roasted subsample, were determined using a Strohlein Coulomat 702, in the Department of Earth Sciences of the University of Oxford. The difference between the amount of carbon determined in unroasted and pre-roasted samples provided an estimate of Total Organic Carbon (TOC). Assuming the inorganic carbon content is all associated with  $\text{CaCO}_3$  allows the estimation of  $\text{CaCO}_3$  content using the equation from Stax and Stein (1993):





**Fig. 2.** Stratigraphic column and distribution of the Danian species at Caravaca. *Gb.* = *Guembeltria*; *Chg.* = *Chiloguembeltria*; *Pc.* = *Pseudocausasia*; *Pg.* *Palaeoglobigerina*; *Pv.* = *Parvularugoglobigerina*; *W.* = *Woodringina*; *Ch.* = *Chiloguembelina*; *E.* = *Eoglobigerina*; *T.* = *Trochoguembeltria*; *G.* = *Globanomalina*; *P.* = *Parasubbotina*; *Pr.* = *Praemurica*; *Gc.* = *Globoconusa*; *S.* = *Subbotina*.

$\text{CaCO}_3\% = \text{TIC} * 8.33$ . Reproducibility of %C using this method is typically better than 0.1%.

Measurements of stable carbon and oxygen isotope ratios ( $\delta^{13}\text{C}$ ,  $\delta^{18}\text{O}$ ) were performed on homogenized bulk powdered sediment from the same 70 samples. Samples were analyzed in the Department of Earth Sciences of the University of Oxford using a GasBench device attached to a ThermoFisher Delta V Advantage gas source isotope ratio mass spectrometer. Oxygen and carbon-isotopes are reported using the standard delta notation ( $\delta^{18}\text{O}$ ,  $\delta^{13}\text{C}$ ) in parts per mil (‰) on the Vienna PeeDee Belemnite (VPDB) scale. Calibration of samples to the VPDB scale was achieved using multiple analyses of an in-house standard, NOCZ, which has average values on the VPDB scale of  $-1.90\text{‰}$  for  $\delta^{18}\text{O}$  and  $2.18\text{‰}$  for  $\delta^{13}\text{C}$ . For  $\delta^{18}\text{O}$ , NOCZ has been calibrated to the VPDB scale by comparison with analyses of NBS-19 and NBS-18, which were assigned  $\delta^{18}\text{O}$  values of  $-2.20\text{‰}$  and  $-23.01\text{‰}$  respectively. For  $\delta^{13}\text{C}$ , NOCZ has been calibrated to the VPDB scale by comparison with analyses of NBS-19, which was assigned a value of  $1.95\text{‰}$ . Repeated analyses of in-house standards suggest a reproducibility ( $\pm 1\sigma$ ) of  $<0.1$  for both  $\delta^{13}\text{C}$  and  $\delta^{18}\text{O}$ .

The magnetic susceptibility (MS) of 70 samples was measured at the University of Zaragoza, Spain, with a Spinning Specimen Magnetic Susceptibility Anisotropy Meter KLY-35 Kappabridge. Samples were crushed in an agate mortar and measured in cylindrical plastic boxes of

$10\text{ cm}^3$  in volume. MS values are reported relative to mass ( $\text{m}^3/\text{kg}$ ).

### 3. Results

#### 3.1. Biostratigraphy and age model

At the Caravaca section, a total of 49 species and 14 genera of Danian planktic foraminifera (including species of the genus *Guembeltria*) have been identified. Relative abundances of each species are shown in the Supplementary Table 1. Seven subbiozones have been identified: *Mh. holmdelensis* and *Pv. longiapertura* Subzones (of the *G. cretacea* Zone), *Pv. sabina* and *E. simplicissima* Subzones (of the *Pv. eugubina* Zone), and *E. cf. trivialis*, *S. triloculinooides* and *G. compressa* (part) Subzones (of the *P. pseudobulloides* Zone). The stratigraphic interval studied corresponds to P $\alpha$ , P1a, P1b and (part of) P1c of Berggren and Pearson (2005) and Wade et al. (2011). At Caravaca, the bases of these subbiozones are at 0, 3, 22, 42, 107, 332 and 655 cm, respectively, above the K-PgB (Fig. 2).

To establish the age model at the Caravaca section, we linearly interpolated between the K-PgB, the top of the K-PgB dark clay bed, the C29r/C29n magnetic reversal and the C29n/C28r magnetic reversal. Based on the  $^{40}\text{Ar}/^{39}\text{Ar}$  calibrations of Sprain et al. (2018), we have assigned an age of 66.052 Ma to the K-PgB, 65.724 Ma to the C29r/C29n reversal and 65.075 Ma to the C29n/C28r reversal. Based on cosmic  $^3\text{He}$

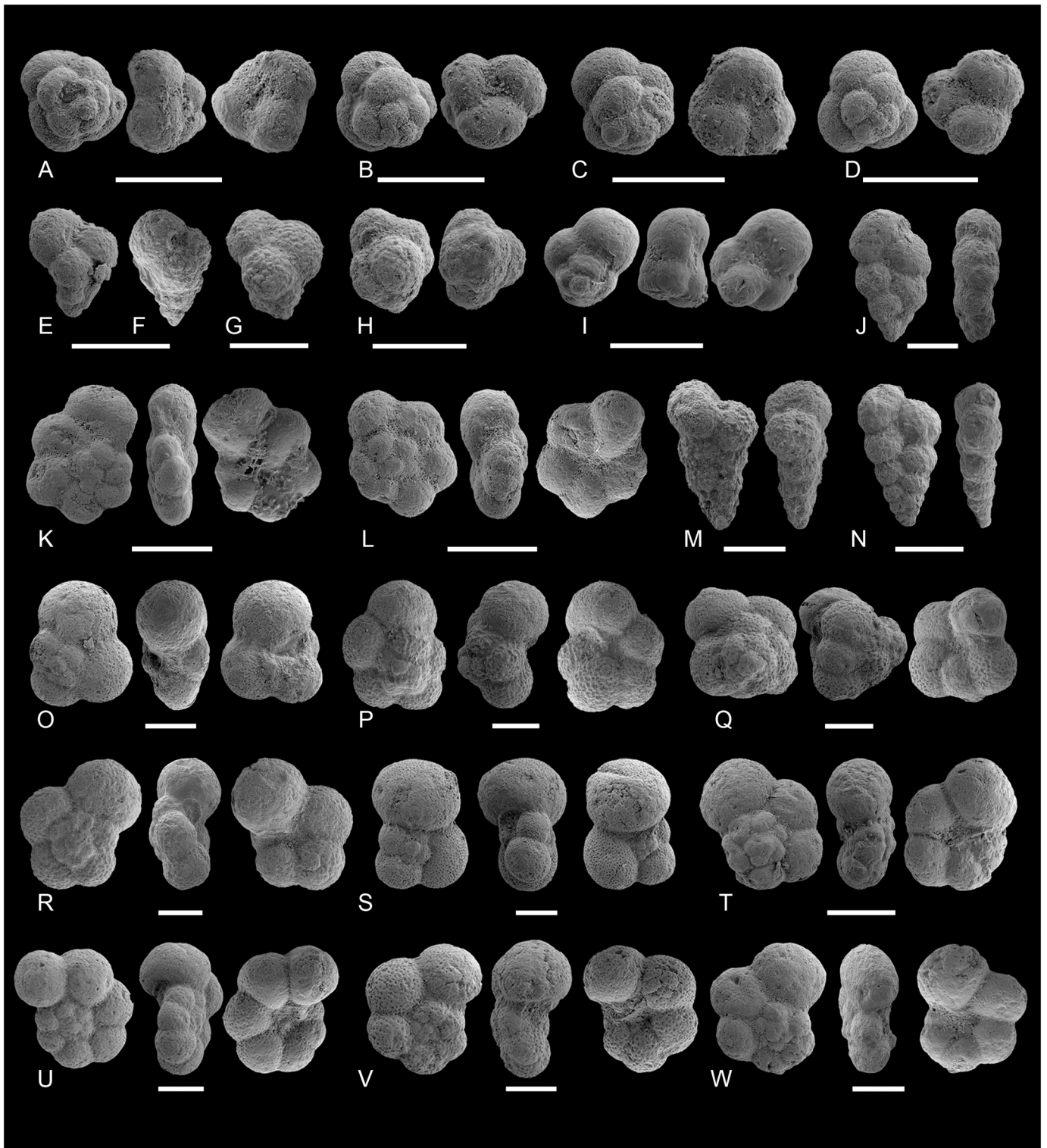


Fig. 3. SEM photographs of *Pseudocaucasina antecessor* (A-D); *Guembelitra cretacea* (E); *Chiloguembelitra hofkeri* (F); *Chiloguembelitra danica* (G); *Trochoguembelitra alabamensis* (H); *Palaeoglobigerina alticonusa* (I); *Chiloguembelina midwayensis* (J); *Parvularugoglobigerina longiapertura* (K); *Parvularugoglobigerina eugubina* (L); *Woodringina hornerstownensis* (M); *Chiloguembelina taurica* (N); *Eoglobigerina simplicissima* (O); *Eoglobigerina edita* (P); *Eoglobigerina pentagona* (Q); *Parasubbotina pseudobulloides* (R); *Subbotina triloculinoidea* (S); *Globanomalina archeocompressa* (T); *Praemurica taurica* (U); *Praemurica inconstans* (V); *Globanomalina compressa* (W). White bar scales = 100  $\mu$ m.

sedimentation rates, Mukhopadhyay et al. (2001) estimated a duration for deposition of the K-PgB dark clay bed of  $\sim$ 10 kyr. At Caravaca, the top of the K-PgB dark clay bed is  $\sim$ 6 cm above the K-PgB, and, according to Smit (1982) and Groot et al. (1989), the C29r/C29n and C29n/C28r

reversals are at 5.1 m and 9.8 m above the K-PgB respectively. Consequently, the average sedimentation rates at Caravaca are  $\sim$ 0.6 cm/kyr for the K-PgB dark clay bed, 1.58 cm/kyr for the Danian part of C29r and 0.72 cm/kyr for C29n. In total, the studied section spans approximately

the first 760 kyr of the Danian. According to this age model, the bases of *Mh. holmdelensis*, *Pv. longiapertura*, *Pv. sabina*, *E. simplicissima*, *E. cf. trivialis*, *S. triloculinoidea* and *G. compressa* Subzones occurred at 0, 5, 20, 33, 75, 219, and 528 kyr after the K-PgB, respectively. It is remarkable that *Pseudocausasina antecessor* (Arenillas and Arz, 2017) has been identified at Caravaca for the first time. Its Lowest Occurrence Data (LOD) is at 1.5 cm above the K-PgB, i.e. 2.5 kyr after the K-PgB. The LODs of its most direct evolutionary descendants, *Parvularugoglobigerina longiapertura* and *Palaeoglobigerina alticonusa*, are at 3 cm above the K-PgB, i.e. 5 kyr after the K-PgB.

### 3.2. Acme-stratigraphy

Planktic foraminiferal assemblages identified in the lower Danian of the Caravaca section are characterized by low diversities and high consecutive dominances of single taxon groups, corresponding to the succession of the three acme-stages PFAS of Arenillas et al. (2006). This is confirmed by the cluster analysis performed here (Fig. 4).

PFAS-1 spans the first 5 cm of the lower Danian of the Caravaca section (from the K-PgB to the lowermost part of *Pv. longiapertura* Subzone), i.e. the first 8 kyr after the K-PgB boundary according to our age model. PFAS-1 is dominated by triserial taxa, mainly *Guembelitra* and, to a lesser extent, its descendant *Chiloguembelitra*. *Guembelitra* is the only Cretaceous genus that increased its abundance after the K-PgB. In

addition, we have identified a bloom of *Pseudocausasina antecessor*, which starts within the PFAS-1 and ends at the lowermost part of PFAS-2. (Fig. 5, Table S1).

PFAS-2 is placed at 5 to 55 cm above the K-PgB at Caravaca (from the lowermost part of *Pv. longiapertura* Subzone to the middle part of the *E. simplicissima* Subzone), i.e. between 8 and 41 kyr after the K-PgB. This acme-stage is dominated by parvularugoglobigerinids, i.e. *Parvularugoglobigerina* and *Palaeoglobigerina* (the first evolutionary radiation of Danian species), comprising between 50 and 80% of the assemblages. The LODs of *Woodringina* and *Chiloguembelina*, the first Danian biserial taxa, occurred within PFAS-2, but their combined relative abundance never exceeds 3% except for the upper part of PFAS-2. Around 38 cm above the K-PgB (upper part of the *Pv. sabina* Subzone), biserial taxa show a sharp increase, but they do not exceed the parvularugoglobigerinids in abundance.

PFAS-3 has been recognized from 55 cm above the K-PgB to the top of the studied section (from the lower part of the *E. simplicissima* Subzone to the lower part of the *G. compressa* Subzone), i.e. between 41 kyr and at least 756 kyr after the K-PgB. The planktic foraminiferal assemblages in PFAS-3 comprise mostly biserial taxa, i.e. the genera *Woodringina* and *Chiloguembelina*, and especially the species *Woodringina hornerstownensis* (30.7% on average). Although PFAS-3 assemblages are dominated by biserial taxa throughout, several substages can be identified on the basis of changes in relative abundances of some other taxa. One of the most

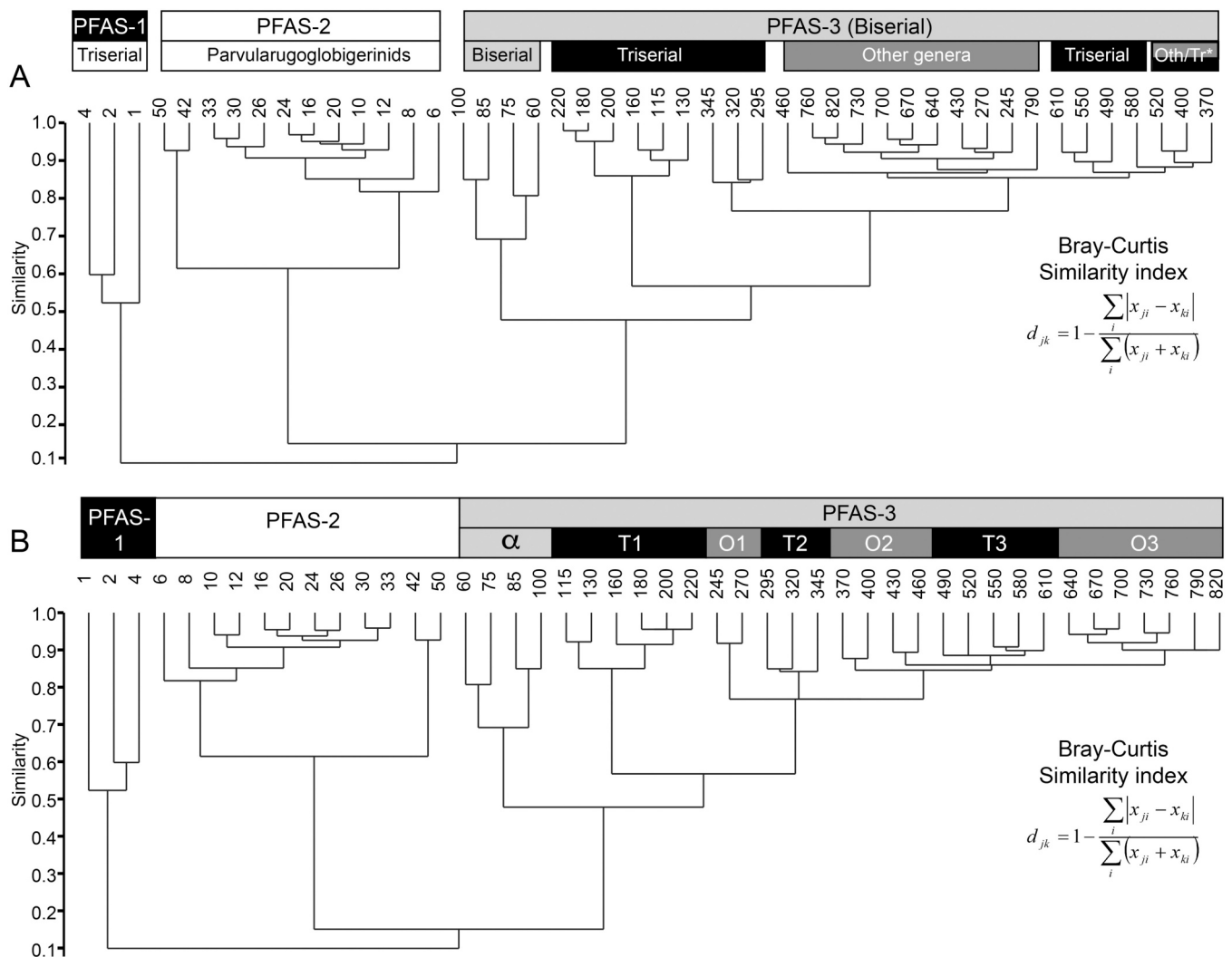


Fig. 4. A) Agglomerative clustering based on the unweighted paired group method with the arithmetic mean (UPGMA) and the Bray-Curtis similarity index. Oth/Tr\*. = Clusters with ambivalent affinity. B) Stratigraphically constrained dendrogram.

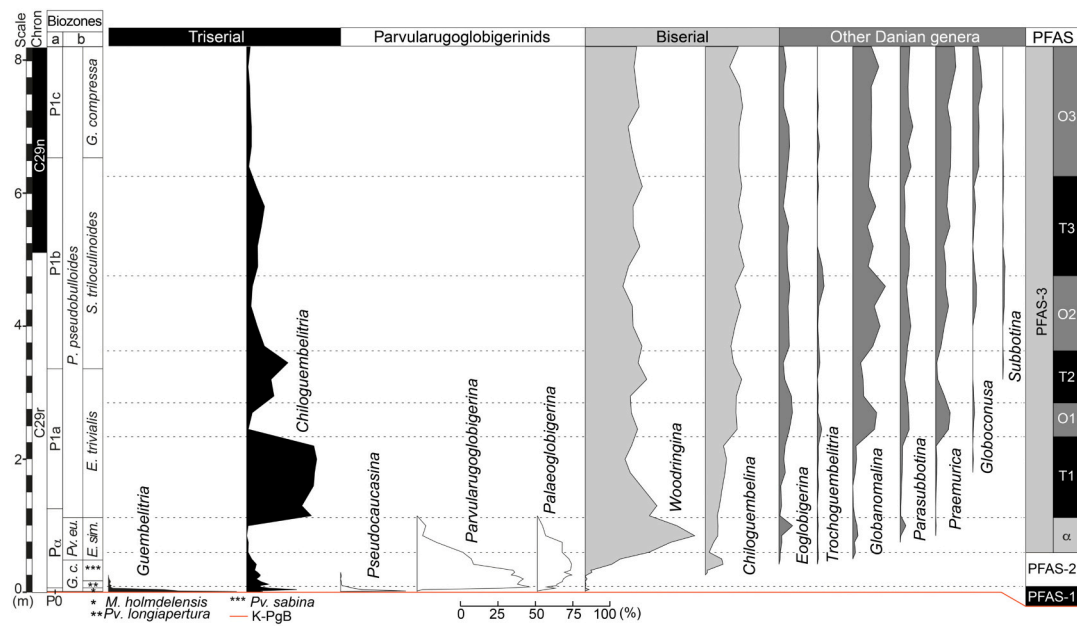


Fig. 5. Relative abundance of the Danian planktic foraminiferal genera and major groups at Caravaca. Biozones: a = (Wade et al., 2011); b = (Arenillas et al., 2004).

striking features within PFAS-3 at Caravaca is the occurrence of three successive blooms of the opportunist triserial *Chiloguembeltria* reaching maxima abundances of 48.5, 28.6, and 12.3% respectively. These *Chiloguembeltria* blooms are successively less intense and alternate in time with remarkable increases in the combined abundance of genera resulting from the second Danian evolutionary radiation, including *Eoglobigerina*, *Parasubbotina*, *Globanomalina*, *Praemurica*, and *Subbotina*, or “other genera” for short. The latter group reaches maxima abundance values of 43.1, 49.5 and 48.4% between each *Chiloguembeltria* bloom (Fig. 5). Cluster analyses strongly support the further division of PFAS-3 into 7 shorter substages following the alternation of major groups (Fig. 4), with each substage named as PFAS-3 plus a suffix: α, T1, O1, T2, O2, T3, O3. Stratigraphic and temporal boundaries of each stage and substage, with average relative abundances of major groups are listed in Table 1.

PFAS-3α is characterized almost exclusively by biserial *Woodringina* and *Chiloguembelina*, but mostly by *Woodringina* (Fig. 5). The LODs of *Eoglobigerina*, *Parasubbotina*, *Globanomalina*, *Praemurica* and *Trochoguembeltria* are at 55–85 cm above the K-PgB, forming the second evolutionary radiation of Danian species (Fig. 2 and Fig. 5). The Highest Occurrence Data (HOD) of *Palaeoglobigerina* and *Parvularugoglobigerina* are recognized towards the top of PFAS-3α, as these species were completely replaced by the incoming species of the second Danian evolutionary radiation.

PFAS-3T (1–3) are characterized by subsequent blooms of triserial

*Chiloguembeltria*. PFAS-3T1 witnessed the LOD of the genus *Globoconusa*, which occupies the same ecological niche as *Guembeltria* and *Chiloguembeltria* (see Olsson et al., 1999), although during each *Chiloguembeltria* bloom the relative abundance of *Globoconusa* remains extremely low with values <1% (0.1, 0.2, and 0.9%).

PFAS-3O (1–3) refers to the substages characterized by the higher relative abundance of the “other genera” combination. The genera *Globanomalina* (15.2%) and *Praemurica* (9.9%) are the most abundant genera during each PFAS-3O. It is noteworthy that the alternations between PFAS-3T and PFAS-3O occurred rapidly, especially between the first three alternations: T1-O1, O1-T2, and T2-O2 (Fig. 5 and Tables 1, 2).

### 3.3. Diversity indices

Standard diversity indices are summarized in Table 2 and shown in full in Table S2. We have calculated the average diversity values for PFAS-1-2 and for each substage of PFAS-3. The diversity indices provide evidence for rapid and abrupt environmental changes from PFAS-1 to the end of PFAS-3T1 (suggesting less resilient planktic foraminiferal assemblages), and more stable environmental conditions from PFAS-3O1 onwards (suggesting more resilient assemblages). However, it is noteworthy that the rapid evolutionary radiations which occurred during the PFAS-2 and PFAS-3α intervals (Figs. 2 and Fig. 5) highly influenced the values of the diversity indices. Conversely, from the base of

Table 1  
Stratigraphic height and age of PFAS and relative abundance of major groups.

PFAS	Height from K-PgB (cm)		Age from K-PgB (kyr)		Major groups relative abundance (%)			
	Base	Top	Base	Top	Triserial	Parvul.	Biserial	Others
PFAS-3O3	625	820*	487	756*	2.3%	0.0%	56.9%	40.8%
PFAS-3T3	475	625	311	487	8.8%	0.0%	59.5%	31.7%
PFAS-3O2	357	475	235	311	6.6%	0.0%	53.6%	39.8%
PFAS-3T2	282	357	187	235	21.4%	0.0%	58.8%	19.8%
PFAS-3O1	232	282	155	187	2.4%	0.0%	55.6%	41.9%
PFAS-3T1	107	232	75	155	45.2%	0.0%	49.0%	5.8%
PFAS-3α	55	107	41	75	0.8%	24.7%	67.0%	7.5%
PFAS-2	5	55	8.3	41	9.7%	83.4%	6.8%	0.1%
PFAS-1	K-PgB	5	0	8.3	76.1%	23.1%	0.9%	0.0%

Stratigraphic position and calibrated age of planktic foraminiferal acme-stages (PFAS) at Caravaca, and relative abundances of the major planktic foraminiferal groups.  
\* = Top of the studied section. Parvul. = Parvularugoglobigerinids.

**Table 2**  
Diversity indices and relative abundance of aberrant forms of major groups in each PFAS.

PFAS	Main diversity indices				Relative abundance of aberrant forms (%)				
	S	H'	1/ $\lambda$	E	Triserial	Parvul.	Biserial	Others	Total
PFAS-3O3	23	2.42	6.86	0.48	0.0%	0.0%	1.3%	1.3%	2.6%
PFAS-3T3	23	2.37	6.91	0.47	0.4%	0.0%	1.9%	1.4%	3.7%
PFAS-3O2	26	2.55	8.09	0.49	0.2%	0.0%	2.2%	1.7%	4.1%
PFAS-3T2	24	2.31	6.60	0.42	2.8%	0.0%	5.1%	2.2%	10.0%
PFAS-3O1	25	2.54	8.46	0.52	0.2%	0.0%	2.9%	2.4%	5.5%
PFAS-3T1	18	1.95	4.86	0.41	6.9%	0.0%	5.1%	0.5%	12.5%
PFAS-3 $\alpha$	20	1.88	4.24	0.33	0.0%	1.3%	4.6%	0.7%	6.6%
PFAS-2	15	1.71	3.95	0.40	1.0%	9.0%	0.7%	0.7%	11.5%
PFAS-1	6	1.26	3.13	0.64	17.3%	3.7%	0.0%	0.0%	21.0%

Average values of main diversity indices for each planktic foraminiferal acme-stage (PFAS), and relative abundance of the aberrant forms in total, and in each major group. S = Species richness; H' = Shannon-Weaver index; 1/ $\lambda$  = Inverse Simpson index; E = Evenness; Parvul. = Parvularugoglobigerinids.

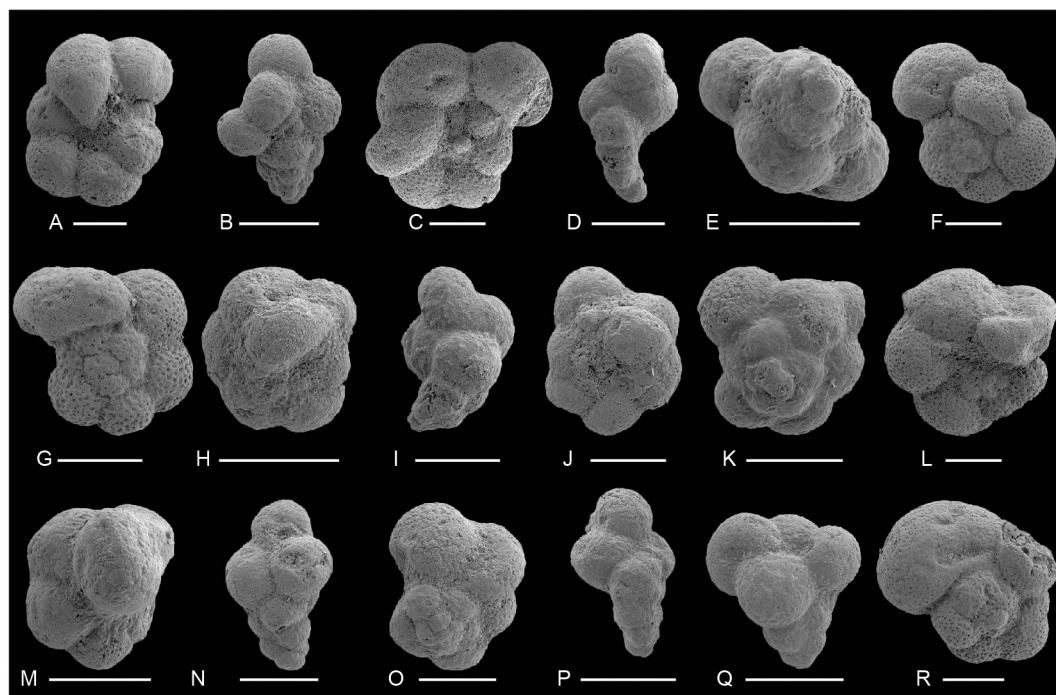
PFAS-3O1 to the top of the section, diversity indices show more gradual changes, showing slightly higher average diversity values in PFAS-3O substages than in the PFAS-3T substages (see Table 2).

### 3.4. Aberrant index

We have found abnormal specimens of *Guembelitra* and almost every incoming Danian species (Supplementary Table S3), whereas reworked Cretaceous specimens within Danian sediments display almost no aberrations. According to the terminology of Arenillas et al. (2018), the most common aberrant morphologies identified at Caravaca are: 1) chamber abnormalities: aberrant chamber shapes, reduced chamber sizes and overdeveloped chamber sizes; 2) an abnormal ultimate chamber: aberrant shape, anomalous position and bulla-like chamber; 3) multiple ultimate chambers: double or twinned ultimate chambers, and a proliferation of chambers; 4) distortion in test coiling; 5) abnormal tests. Some examples of these aberrations are illustrated in Fig. 6. The aberrant forms of planktic foraminifera are mainly abundant within the

first 357 cm (~230 kyr) of the Danian (i.e. from the K-PgB to the top of PFAS-3T2), close to the base of the *S. triloculinoide*s Subzone (Fig. 7).

PFAS-1 and PFAS-2 are characterized by high relative abundances of aberrant specimens (Fig. 7 and Table 2). The species most commonly displaying aberrant forms are either *G. cretacea* (14.4%) or *Ps. antecessor* (3.5%) for PFAS-1, and *Pv. longiapertura* (5.8%) for PFAS-2. The aberrant specimens of PFAS-3 $\alpha$  mainly belong to biserial taxa, especially to *Woodringina hornerstownensis* (3.1%). The average aberrant index during PFAS-3 $\alpha$  (6.6%) is significantly lower than during PFAS-2 (11.5%), while during PFAS-3T1 it reaches 12.5%, which is similar to that reached previously in PFAS-2. Triserial and biserial aberrant forms are dominant during PFAS-3T substages, especially for *Chg. danica* and *W. hornerstownensis* species. During PFAS-3T1, T2 and T3, aberrant forms of *Chg. danica* represent, respectively, 5.2, 1.6 and 0.3% on average of total planktic foraminiferal specimens, and 3.3, 2.5 and 1.0% for *W. hornerstownensis*. Each triserial bloom, i.e. PFAS-1, PFAS-3T1, PFAS-3T2 and to lesser extent PFAS-3T3, displays a transient increase of the aberrant index (Fig. 7 and Table 2). Conversely, during the blooming



**Fig. 6.** Examples of different aberrant morphologies within the studied specimens; (A) overdeveloped chamber size; (B) protuberant chamber; (C) aberrant shape; (D) overdeveloped chamber size + anomalous position; (E) proliferation of chambers; (F) aberrant chamber shape; (G) abnormal ultimate chamber; (H) bulla-like chamber; (I) distortion in test coiling and reduced ultimate chamber size; (J) additional chamber; (K) abnormal test; (L) abnormal ultimate chamber; (M) bulla-like chamber; (N) chamber in anomalous position; (O) abnormal test; (P) ultimate chambers in anomalous position and distortion in test coiling; (Q) proliferation of chambers; (R) overdeveloped ultimate chamber with aberrant shape.

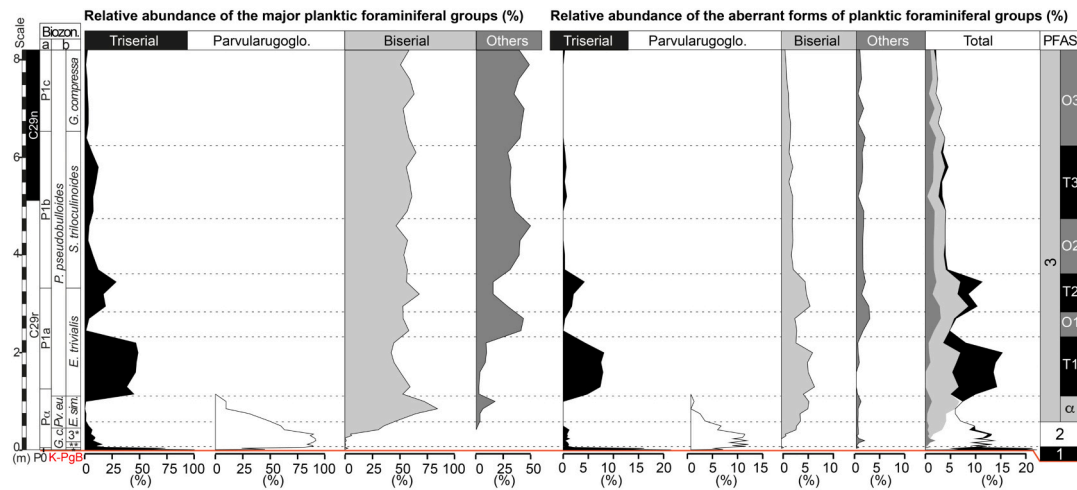


Fig. 7. Comparison of the quantitative results for the major groups of planktic foraminifera. Parvularuglo. = parvularuglobigerinids.

episodes of the “other genera”, i.e. PFAS-3O1, PFAS-3O2 and PFAS-3O3, there are fewer aberrant specimens. The most common biserial species with aberrant forms within PFAS-3O substages are *W. hornerstownensis* with respectively 1.8, 1.2 and 0.8% on average, and the most common aberrant specimens of the “other genera” belong to the species *Globanomalina archeocompressa* (0.55%) for PFAS-3O1, *Praemurica taurica* (0.4%) for PFAS-3O2 and *Pr. inconstans* (0.3%) for PFAS-3O3.

### 3.5. Carbonate preservation and magnetic susceptibility

At Caravaca, the CaCO<sub>3</sub> content ranges from 15.5 to 88.4% with a mean value of 73.78% (n = 70). The lowest CaCO<sub>3</sub> content has been identified in the K-PgB clay bed (0–6 cm, between 15.53 and 39.7%, and 28% on average). From 6 to 26 cm above the K-PgB, the CaCO<sub>3</sub> content increases sharply to 70%, and from 26 to 115 cm the average CaCO<sub>3</sub>

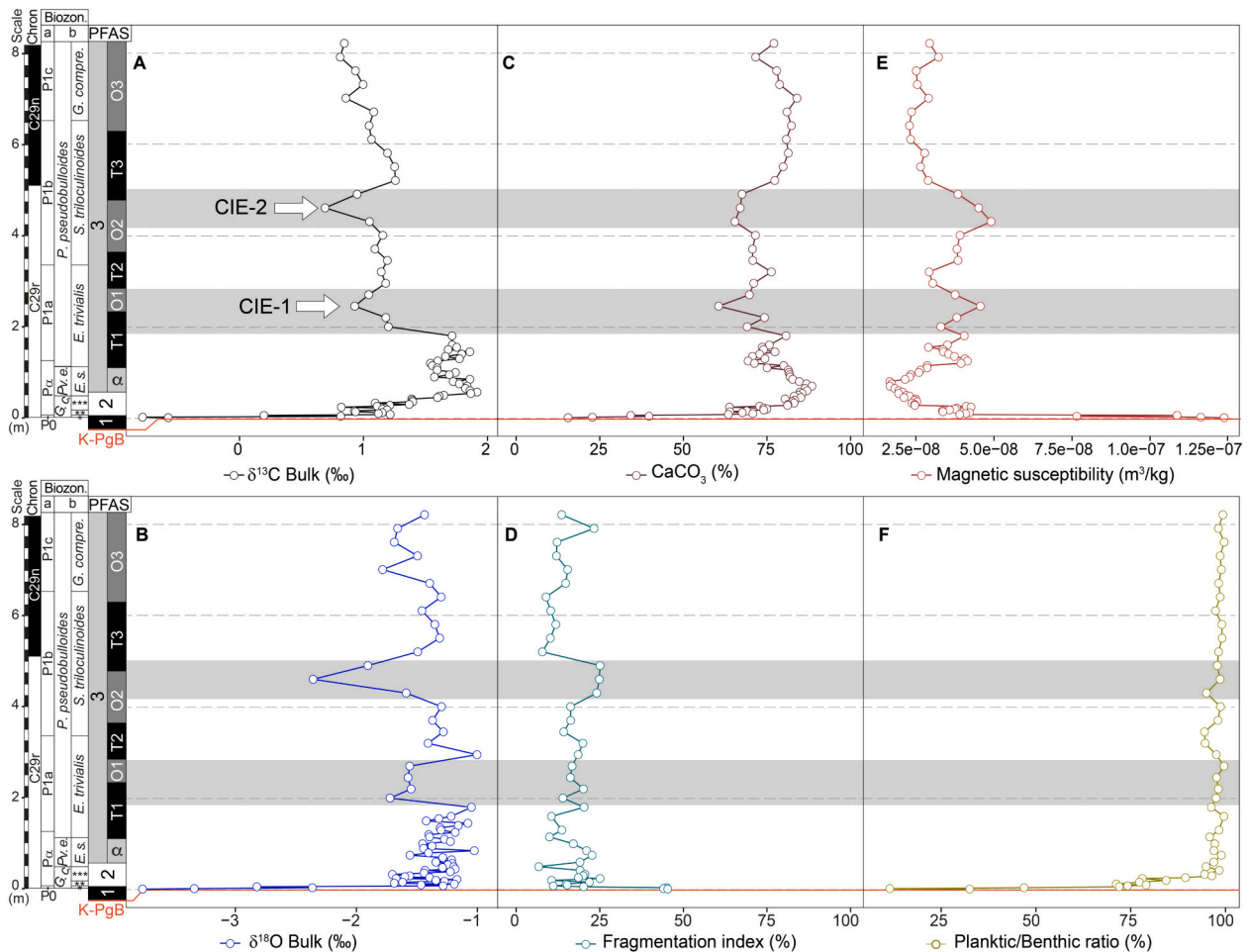


Fig. 8. A-B) Stable isotopes; C) Carbonate content; D) Fragmentation index; E) Magnetic susceptibility; and F) Planktic/Benthic ratio at Caravaca. Data can be found in Supplementary Table 4.

content is 83%. There is a decrease in the average CaCO<sub>3</sub> content from 115 to 520 cm above the K-PgB (71%) with two relatively low values identified at 245 (60.5%) and 430 (65.5%) cm above the K-PgB (Fig. 8C). Finally, from 520 cm to the top of section, the average CaCO<sub>3</sub> content is relatively stable at 80% on average.

Apparent dissolution features on tests, such as abrasion marks, broken and/or isolated chambers, or corroded walls, have been identified, but they are not abundant. The planktic foraminiferal preservation is moderate to good in most of the samples, with the exception of those from the dark K-PgB clay bed. We consider that samples with planktic foraminiferal fragmentation ratio or fragmentation index (FI) >40% represent intervals of strong dissolution (e.g., Kucera et al., 1997; Gilabert et al., 2021). Values of planktic foraminiferal fragmentation vary between 7 and 45% across the Caravaca section, with an average fragmentation of 18.3% ( $n = 46$ ). The average fragmentation values are high (45%) in the K-PgB dark clay bed, moderate (20%) between 6 and 520 cm, and low (13%) from 520 cm to the top of the section (Fig. 8D).

At Caravaca, the P/B ratio (Fig. 8F) ranges between 11 and 100%, with three distinct intervals: in the dark K-PgB clay bed P/B ratios range between 11 and 47%; from 6 to 26 cm above the K-PgB, they are between 72 and 89%; and from 30 cm to the top of the studied section, they are between 95 and 100%. Benthic foraminifera are more resistant to fragmentation and dissolution than planktic foraminifera, and the P/B ratio is expected to decrease with increasing dissolution intensity (Kucera et al., 1997). The significant, negative correlation  $r = -0.75$   $p < 0.01$  between FI and the P/B suggests that higher dissolution of planktic foraminifera is related to lower P/B values, which are limited to the K-PgB clay bed.

Magnetic susceptibility (MS) oscillates between  $1.67 \times 10^{-8}$  and  $1.23 \times 10^{-7}$  m<sup>3</sup>/kg across the Caravaca section, with a mean value of  $3.51 \times 10^{-8}$  m<sup>3</sup>/kg. MS values are within the standard range of values for lithified marine samples containing typical paramagnetic minerals (Ellwood et al., 2008). MS values increase between 115 and 520 cm above the K-PgB, with maxima at 245 and 430 cm, mirroring the CaCO<sub>3</sub> curve (Fig. 8C and E). The strong negative correlation between MS and CaCO<sub>3</sub> content suggests variations in the original detrital influx or variations in the flux of carbonate, causing variations in the concentration of paramagnetic minerals.

### 3.6. Stable isotopes (bulk carbonate $\delta^{13}\text{C}$ and $\delta^{18}\text{O}$ )

At Caravaca,  $\delta^{13}\text{C}$  and  $\delta^{18}\text{O}$  values for bulk carbonate show a moderate degree of correlation ( $r = 0.62$ ,  $p < 0.01$ ) and evolve in parallel in some intervals. However, values are comparable with those previously reported for the lower Danian at the Caravaca section (Kaiho et al., 1999; Sosa-Montes de Oca et al., 2016; Sepúlveda et al., 2019) and other sections worldwide (see compilation in Hull et al., 2020), suggesting little influence of diagenesis. Only in the K-PgB clay bed do %CaCO<sub>3</sub> and stable isotope values exhibit a significant correlation. In the rest of the studied section, the correlation between %CaCO<sub>3</sub> and  $\delta^{18}\text{O}$  or  $\delta^{13}\text{C}$  values is poor to very poor, with  $r = 0.54$  ( $p < 0.01$ ) between %CaCO<sub>3</sub> and  $\delta^{13}\text{C}$ , and  $r = 0.32$  ( $p < 0.01$ ) between %CaCO<sub>3</sub> and  $\delta^{18}\text{O}$ . This lack of significant correlation suggests that the lithology exerts very little control on the stable isotope values.

The  $\delta^{13}\text{C}$  values vary between  $-0.78\text{‰}$  and  $+1.92\text{‰}$  at Caravaca (Fig. 8A) with the lowest  $\delta^{13}\text{C}$  values registered within the K-PgB dark clay bed, ranging from  $-0.78\text{‰}$  to  $0.20\text{‰}$ . From 6 to 57 cm above the K-PgB,  $\delta^{13}\text{C}$  increases to the highest values of the section at  $\sim 1.92\text{‰}$ . Between the maximum  $\delta^{13}\text{C}$  value at 57 cm to 180 cm,  $\delta^{13}\text{C}$  displays very small oscillations between 1.92 and 1.71‰. From 180 cm to the top of the section,  $\delta^{13}\text{C}$  broadly displays a clear overarching trend to lower values, with two negative carbon isotopic excursions (CIEs) superimposed upon this trend. The first (CIE-1) has a minimum value of 0.93‰ at 245 cm and the second (CIE-2) a minimum value of 0.69‰, at 460 cm above the K-PgB.

The  $\delta^{18}\text{O}$  values are broadly invariant across much of the Caravaca

section, except for three distinct negative excursions (Fig. 8B), the first at the K-PgB and the other two coinciding approximately with the CIEs described above.  $\delta^{18}\text{O}$  values are the lowest of the whole section within the K-PgB clay bed ranging from  $-3.77\text{‰}$  to  $-2.82\text{‰}$ . The other two minima in  $\delta^{18}\text{O}$  occur at 200 cm above the K-PgB (slightly below the CIE-1), and 460 cm, coincident with CIE-2.

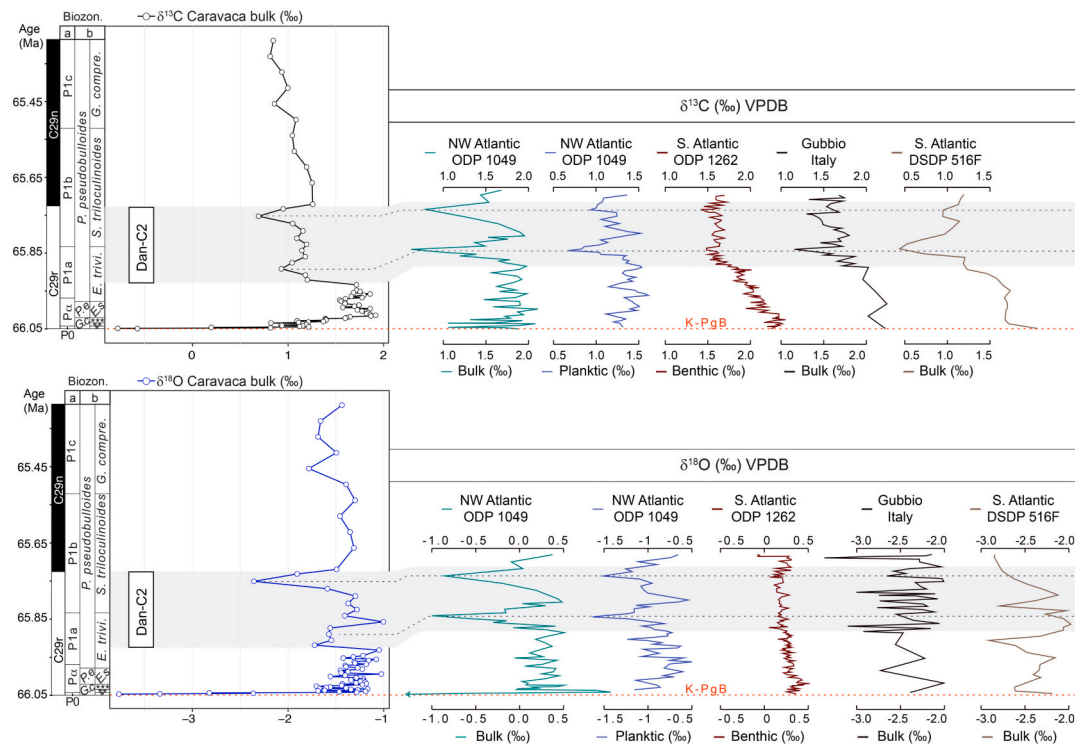
## 4. Recognizing the Dan-C2 event at Caravaca

The Dan-C2 event was first recognized in the NW Atlantic (ODP 1049), and SE Atlantic (DSDP 527 and 528) and defined as a pair of major, fairly symmetrical, negative excursions in  $\delta^{13}\text{C}$  and  $\delta^{18}\text{O}$  (Fig. 9), associated with decreased carbonate content and increased clay content and magnetic susceptibility values (Quillevéré et al., 2008). At Caravaca, the stratigraphic interval corresponding to Dan-C2, as defined in some Atlantic and Tethyan sections (Fig. 9), is recorded between 200 and 490 cm above the K-PgB, from the middle part of *E. cf. trivialis* (P1a) Subzone to the middle part of *S. trilocolinoides* (P1b) Subzone, i.e. between 130 and 315 kyr after the K-PgB according to our age model. The CIEs identified in Caravaca (CIE-1 and CIE-2) are within this stratigraphic interval and consequently they are correlated with the two characteristic negative excursions of Dan-C2 defined elsewhere (Quillevéré et al., 2008; Coccioni et al., 2010). Using our age model, the peak minimum values of CIE-1 and CIE-2 occur 158 and 295 kyr, respectively, after the K-PgB and each CIE has a duration of  $\sim 40$  kyr. In addition, both CIEs are associated with the lowest CaCO<sub>3</sub> content and the highest MS values. According to our age model, the entire Dan-C2 event lasted approximately 185 kyr, ending around the C29r/C29n magnetic reversal (Fig. 9 and Fig. 10A). The small discrepancies in the assigned ages of Dan-C2 between Caravaca and elsewhere (Fig. 9) are probably related to differences and uncertainties in the age models and/or variations in the local sedimentation rates between tie points that are not represented by linear interpolation. Nevertheless, all of different records suggest a broadly consistent age for Dan-C2 and a termination of the event near the C29r/C29n reversal.

## 5. Early Danian paleoenvironmental and paleoclimatic evolution

### 5.1. The K-PgB dark clay bed and PFAS-1 (*Guembeltria acme*): The aftermath of the Chicxulub impact

Worldwide, the K-PgB dark clay bed was deposited above the Chicxulub-linked air-fall layer under conditions of global climatic warming and alterations in oceanic productivity and acidity (D'Hondt et al., 1998; Coxall et al., 2006; Kawaragi et al., 2009; Birch et al., 2016; Henehan et al., 2016, 2019). At Caravaca, as in most continuous marine sections, the K-PgB dark clay bed is characterized by very low values in %CaCO<sub>3</sub>,  $\delta^{18}\text{O}$  and  $\delta^{13}\text{C}$  (Fig. 8A, B and Fig. 10D, E) (see Schulte et al., 2010, and references therein). In addition, the highest planktic foraminiferal fragmentation index values at Caravaca occur within the K-PgB dark clay bed. These geochemical and preservational changes have been directly related to the decimation of pelagic marine calcifiers at the K-PgB (Smit, 1982; Bown, 2005), and subsequent ocean acidification (Alegret et al., 2012; Henehan et al., 2019). At Caravaca, the P/B ratio across the K-PgB dark clay bed is very low, around 30% in comparison to the P/B ratio values for most of the Danian (Table S2). This decreased P/B ratio is more compatible with the sudden extinction of planktic foraminifera at the K-PgB than with rapid paleobathymetric changes, as previously shown by Alegret et al. (2003). Therefore, the K-PgB dark clay bed records a brief interval of time in which the ecosystems collapsed and the oceans acidified (D'Hondt et al., 1998; Arenillas et al., 2006, 2018; Kring, 2007; Henehan et al., 2019). Biological recovery, however, was relatively quick and oceanic productivity was rapidly re-established after the K-PgB (Sepúlveda et al., 2009, 2019; Lowery et al., 2018; Gibbs et al., 2020). Productivity may have been controlled by



**Fig. 9.** Worldwide correlation of the Dan-C2 event according to our age model and the  $\delta^{13}\text{C}$  and  $\delta^{18}\text{O}$  records from several localities: Caravaca (this report), ODP Site 1049 (Quillévére et al., 2008), DSDP Site 516 (Krahl et al., 2020), ODP Site 1262 (Barnet et al., 2019), and Contessa Highway (Gubbio) section (Coccioni et al., 2010).

blooms in the non-calcareous algal and microbial communities in the open ocean after the K-PgB event, which potentially provided a food supply for higher trophic levels such as calcareous plankton (Bralower et al., 2020).

The acme of the stress tolerant and opportunistic genus *Guembelitra* during PFAS-1 is recorded within the K-PgB dark clay bed, immediately above the air-fall layer. Contemporaneously, the start of an acme of the opportunist calcareous dinocyst *Thoracosphaera* (Fig. 10B) has been reported above the K-PgB at Caravaca (Lamolda et al., 2005, 2016) and in many other Tethyan sections (Romein, 1977; Smit, 1982; Pospichal, 1996; Gardin, 2002; Lamolda et al., 2005, 2016; Fornaciari et al., 2007; Thibault et al., 2018). The highest planktic foraminiferal aberrant index (21%) of the whole section occurs in PFAS-1 (Fig. 10C); a value which is comparable to other Tethyan and North Pacific localities (Gerstel et al., 1986; Coccioni and Luciani, 2006; Arenillas et al., 2018), suggesting stressed conditions on a global scale. Detrimental environmental effects such as eutrophication, warming, ocean acidification, low oxygenation, and the remobilization of pollutants and toxic heavy metals all occurred potentially in the aftermath of Chicxulub impact and can be attributed to it (Smit, 1999; Coccioni and Luciani, 2006; Ballent and Carignano, 2008; Omaña et al., 2012; Arenillas et al., 2018; Henehan et al., 2019). Nonetheless, a minor contribution by Deccan volcanism to some of these environmental changes cannot be entirely ruled out.

### 5.2. PFAS-2: Recovery and the first radiation of planktic foraminifera

Within PFAS-2, an initial recovery of planktic foraminiferal assemblages and a first evolutionary radiation took place. This first evolutionary radiation was mostly related to the evolution and proliferation of the tiny trochospiral species belonging to *Parvularugoglobigerina* and *Palaeoglobigerina* genera. Recently, Arenillas and Arz (2017) proposed that parvularugoglobigerinids originated from a benthic foraminifer that evolved into a planktic form, such as *Ps. antecessor*. Both *Parvularugoglobigerina* and *Palaeoglobigerina* genera radiated and proliferated

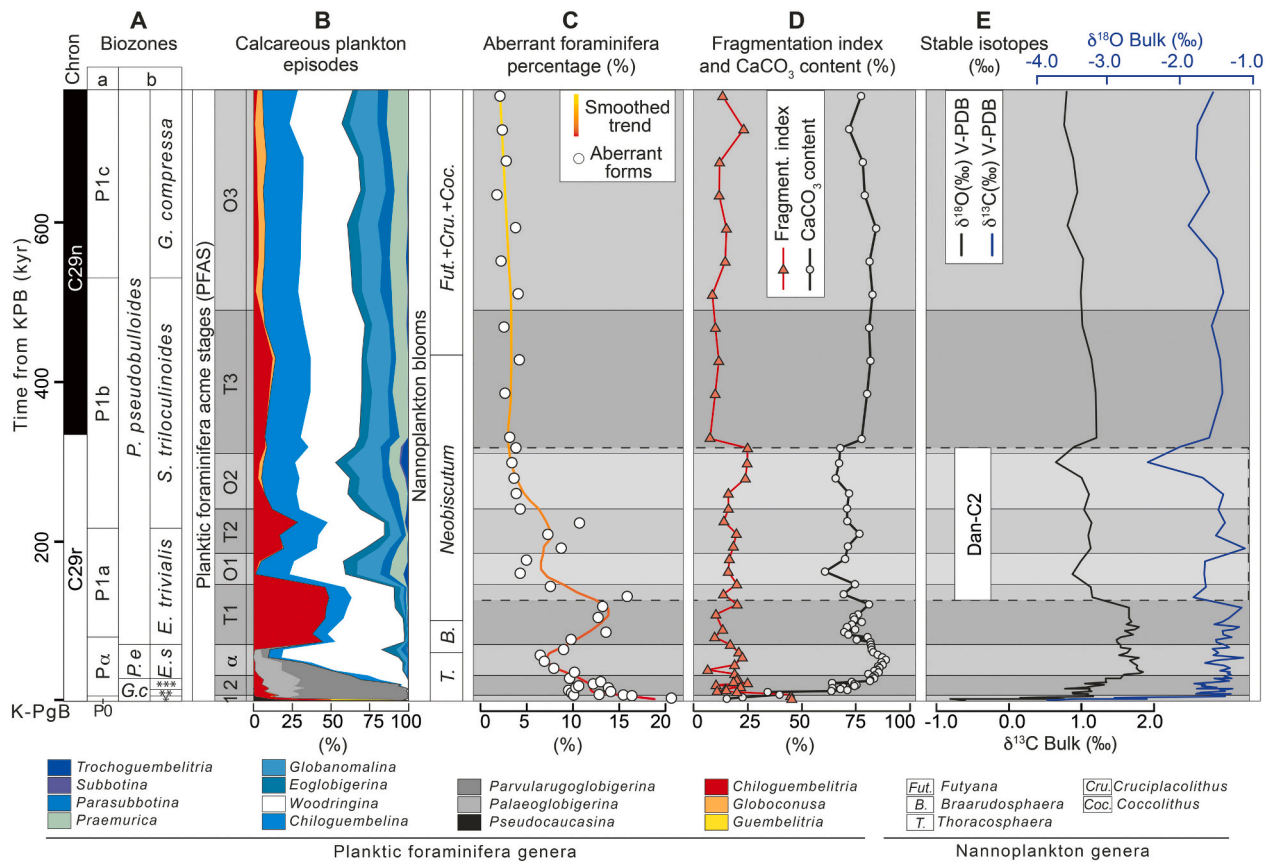
during PFAS-2, which, together with the continued dominance of *Thoracosphaera* (Lamolda et al., 2005, 2016) and the very high (11.5%) abundance of aberrant specimens, suggests that conditions remained unstable and stressed throughout PFAS-2.

At Caravaca, a rapid rebound (< 20 kyr) of the carbonate preservation state between PFAS-1 and PFAS-2 is supported by the rapid increase in %CaCO<sub>3</sub> and P/B ratios, and a decrease in the fragmentation index and MS values (Fig. 8). According to Henehan et al. (2016, 2019), the initial surface ocean acidification after the K-PgB, together with the extinction of calcifying organisms, would have led to a transient reduction in the marine alkalinity sink. With the return of marine calcifiers, the excess of alkalinity in seawater was removed leading to a rapid rebound and overshoot in surface ocean pH within 40 kyr after the K-PgB. This process likely explains the rapid increase in %CaCO<sub>3</sub> during PFAS-2. The  $\delta^{13}\text{C}$  values sharply increase through PFAS-2, returning to relatively stable background values similar to those recorded in the uppermost Maastrichtian of Caravaca (e.g. Kaiho et al., 1999; Sosa-Montes de Oca et al., 2016; Gilabert et al., 2021). This trend in  $\delta^{13}\text{C}$  also suggests that there was a rapid return of oceanic productivity (Sepúlveda et al., 2019).

### 5.3. Onset of PFAS-3 (PFAS-3 $\alpha$ ) and the second radiation of planktic foraminifera

The biserial taxa *Woodringina* and *Chiloguembelina* proliferated throughout PFAS-3 but especially during PFAS-3 $\alpha$ , when *Woodringina* was the dominant taxon (Fig. 5). A second radiation of Danian planktic foraminifera took place within PFAS-3 $\alpha$  with the first appearance of several incoming Danian genera including *Eoglobigerina*, *Globanomalina*, *Parasubbotina*, *Praemurica* and *Trochoguembelitra*. Most of these new genera seem to have occupied thermocline and subthermocline depths (see Olsson et al., 1999; Aze et al., 2011 and references therein) thus suggesting an initial reoccupation of deeper depth habitats and an incipient but increased water column stratification. The dominance of





**Fig. 10.** Synthesis of the results obtained in this study: A) Planktic foraminiferal biozonations: a = Wade et al. (2011); b = Arenillas et al. (2004); B) Relative abundances of Danian planktic foraminiferal genera, and correlation of the planktic foraminiferal acme-stages (PFAS) and calcareous nannoplankton blooms (see references in the text); C) Relative abundance of planktic foraminiferal aberrant specimens; D) Main carbonate sensitivity parameters; E) Bulk carbonate stable isotopes.

*Woodringina* during PFAS-3 $\alpha$  suggests relatively warm conditions (see Olsson et al., 1999 and references therein) during this stage. A similar bloom of biserial taxa at Gubbio has been interpreted as an overall reduction in oxygenation of the mixed layer in the oceans (Coccioni et al., 2010) similar to conditions during blooms of biserial taxa during the late Maastrichtian (Pardo and Keller, 2008).

During PFAS-3 $\alpha$ , *Thoracosphaera* was still the dominant calcareous nannoplankton genera although *Braarudosphaera* started to replace it as the dominant taxon, at least in the western Tethys (Romein, 1977; Smit, 1982; Lamolda et al., 2016). *Braarudosphaera* species are thought to have been abundant in the lower photic zone under low temperature, low salinity, and eutrophic conditions, and therefore *Braarudosphaera* species are typically considered opportunists and are associated with episodes of environmental stress (Bukry, 1974; Cunha and Shimabukuro, 1997; Kelly et al., 2003; Lamolda et al., 2005, 2016; Jones et al., 2019). The appearance of incoming species of planktic foraminifera and nannofossils characteristic of deeper water depth habitats suggests a first step for the recolonization of deeper niches. However, it is well-known that the entire reoccupation of the deeper ocean niches by planktic foraminifera, as well as the rebound of diversity levels comparable to pre-KBP levels, took several million years (Aze et al., 2011; Birch et al., 2012, 2016; Lowery and Fraass, 2019). Within PFAS-3 $\alpha$ , carbonate parameters (%CaCO<sub>3</sub> and the fragmentation index) are similar to those in PFAS-2.

#### 5.4. *Chiloguembeltria* blooms during PFAS-3 and the Dan-C2 event

Triserial guembeltriid blooms like those recorded during PFAS-3T substages are the most common planktic foraminiferal indicators of

high environmental stress (Kroon and Nederbragt, 1990; Coccioni and Luciani, 2006; Pardo and Keller, 2008; Punekar et al., 2014a, 2014b; Arenillas et al., 2018). In addition, during each triserial bloom identified at Caravaca, a rise in the aberrant index has been identified (Fig. 10B and C). Danian triserial guembeltriid blooms have been commonly ascribed to the effect of Deccan volcanism, and linked to the Dan-C2 event (Punekar et al., 2014a; Keller et al., 2016). At Caravaca, the two main *Chiloguembeltria* blooms (PFAS-3T1 and T2) are related to strong increases in the aberrant index (Fig. 7), suggesting higher stress conditions, similar to those reported in Tunisian sections (Arenillas et al., 2018).

A triserial guembeltriid acme, such as the bloom of *Guembeltria* (here *Chiloguembeltria*) during PFAS-3T1, has frequently been reported at other Tethyan localities (Arenillas et al., 2000a, 2000b, 2018; Keller, 2003; Coccioni et al., 2010; Punekar et al., 2014a, 2014b), always above the onset of the biserial acme of PFAS-3 (here PFAS-3 $\alpha$ ). In addition, this acme has been reported in the Gulf of Mexico (Arz et al., 2001; Abramovich et al., 2011), in the North Pacific (Smit and Romein, 1985), in the Western North Atlantic (Mateo et al., 2016), and in the Parathetys (Punekar et al., 2016). Therefore, PFAS-3T1 probably characterizes a global response to environmental stress.

During PFAS-3T1, the low-oxygenated sub-thermocline dweller *Chiloguembelina* (Boersma and Premoli Silva, 1989; Olsson et al., 1999; Aze et al., 2011; Luciani et al., 2020) became more abundant than during PFAS-3 $\alpha$ , suggesting the progressive reoccupation of the deeper-most niches initiated in PFAS-3 $\alpha$ . *Chiloguembelina* stabilized in abundance through the section (Fig. 5 and Fig. 10B) suggesting that the oxygen minimum zone did not show major changes during the studied interval. Nevertheless, near the end of PFAS-3T1 (around the onset of

Dan-C2), the *Braarudosphaera* bloom was followed by an acme of *Neobiscutum* species (Fig. 10B; Romein, 1977; Gardin and Monechi, 1998, Gardin, 2002; Lamolda et al., 2016; Thibault et al., 2018), suggesting rapidly changing ecological conditions in the upper part of the water column during the beginning of the Dan-C2 event.

Conversely to what may be expected, the minima of both Dan-C2 CIEs occurred during PFAS-3O substages instead of during triserial blooms. This lack of coincidence between the evidence for C-cycle perturbation and biotic stress was also noted in Italy (Coccioni et al., 2010) and can also be observed in the data reported by Punekar et al. (2014a) from Israel, Egypt and the USA. Since bulk  $\delta^{18}\text{O}$  and  $\delta^{13}\text{C}$  mostly reflect changes in the upper part of the water column it can be assumed that transient surface water warming occurred during both CIEs. No evidence of bottom water warming has been detected in the Dan-C2 interval, based on benthic foraminiferal  $\delta^{18}\text{O}$  (Fig. 9; see Barnett et al., 2019 and references therein). Instead, the warming indicated by the bulk oxygen isotope data may have led to a rapid thermal stratification of the upper part of the water column that caused a stronger thermal gradient between the near-surface waters and the thermocline, creating more differentiated ecological niches. The increase of the deeper water dwelling species (such as *Chiloguembelina*, *Eoglobigerina*, *Globanomalina* and *Parasubbotina*) during both CIEs agrees with transient but enhanced ocean stratification (Fig. 5 and Fig. 10B, E). The overall planktic foraminiferal assemblage response during Dan-C2 interval is represented by an alternation between the triserial blooms (PFAS-3T1, 2, 3) and increases in other genera (PFAS-3O1, 2) which are progressively less abrupt through time (Fig. 8 and Fig. 10B). These ecological alternations suggest rapidly changing conditions but also a slightly more resilient and stable ocean, compared to the very earliest Danian. During the Dan-C2 event,  $\text{CaCO}_3$  dissolution due to ocean acidification has been invoked (see Coccioni et al., 2010; Krahl et al., 2020 and references therein) but, at Caravaca, the dissolution-sensitive parameters (fragmentation index,  $\text{CaCO}_3$  content and P/B ratio) do not show evidence of strong dissolution, although we note that there are slight decreases in the % $\text{CaCO}_3$  content and slight increases in the fragmentation index within the Dan-C2 interval, roughly coincident with the two CIEs.

### 5.5. End of PFAS-3: Shift to a more stable ocean

The stabilization of the planktic foraminiferal assemblages at Caravaca seems to have been completed in PFAS-3O3, although there are some differences in comparison to the previous PFAS-3O substages. During PFAS-3O3, *Praemurica* significantly increases in abundance, and the triserial *Chiloguembelitra* is replaced by the trochospiral guembelitruid *Globoconusa* (Fig. 5, Fig. 10B and Table S2). The combined abundances of the *Chiloguembelitra* and *Globoconusa* genera is lower than the abundance reached by *Chiloguembelitra* in any of the preceding acme stages and substages, suggesting lower environmental stress conditions from PFAS-3O3 onwards.

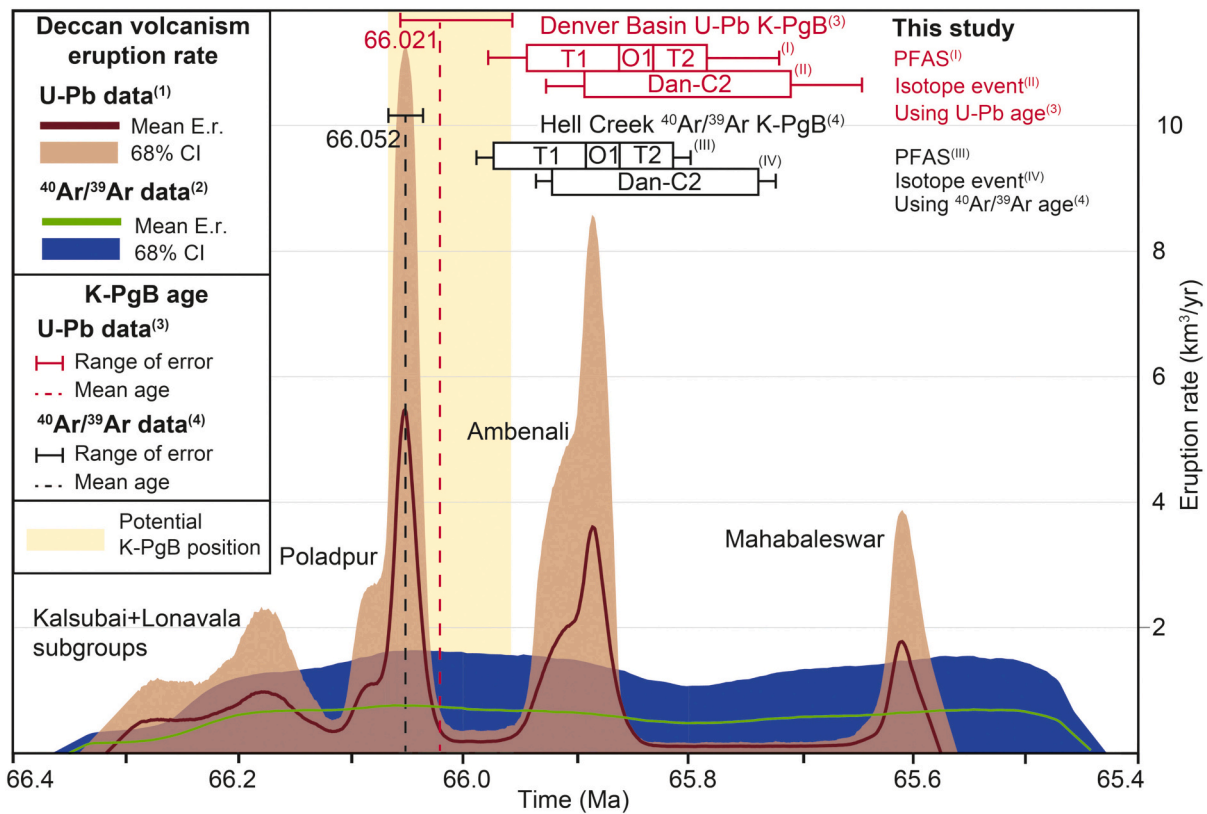
During PFAS-3O3 newly incoming nannoplankton taxa become dominant, including the r-selected opportunist *Futyana petalosa* and the first K-strategists *Cruciplacolithus* and *Coccolithus* (Romein, 1977; Gardin, 2002; Thibault et al., 2018; Jiang et al., 2019). *Cruciplacolithus* and *Coccolithus* are generally reported as oligotrophic taxa (Jiang et al., 2010, 2019), suggesting that the upper ocean waters at Caravaca became more oligotrophic during PFAS-3O3. Oligotrophic conditions at Caravaca are also supported by the very low abundance of *Chiloguembelitra* and by the rise of the *Praemurica* lineage, within which planktic foraminifera species first acquire symbionts during the Paleocene (Norris, 1996; Birch et al., 2012). In addition, carbonate content, magnetic susceptibility, fragmentation index, the P/B ratio and isotopic proxies show only minor oscillations in PFAS-3O3, suggesting relatively stable conditions (Fig. 8).

## 6. What was the environmental impact of the Deccan Traps during the earliest Danian?

For several decades, identifying the role of the Deccan Traps (India) in environmental and climatic change across the K-PgB has been difficult, mainly due to the uncertainties associated with radioisotopic dating (e.g., Courtillot et al., 1986; Vandamme et al., 1991; Chenet et al., 2007). However, recent improvements in radiometric methods have led to refined estimates of the duration of Deccan volcanism, at less than 1 Myr (Schoene et al., 2019; Sprain et al., 2019), and allowed for a more robust correlation between volcanism and climate change (e.g., Barnett et al., 2018; Hernandez Nava et al., 2021). Whether the major eruptive episodes of the Deccan Traps occurred before or after the K-PgB remains a topic of intense debate, since the timing has profound implications for the role of the Deccan Traps in the K-PgB mass extinction (Burgess, 2019; Hull et al., 2020; Keller et al., 2020). This controversy over the role of volcanism in the extinction event is mostly related to uncertainty over the stratigraphic position of the K-PgB within the Deccan Traps sequence.

Based on  $^{40}\text{Ar}/^{39}\text{Ar}$  dating, Sprain et al. (2018) reported an age of  $66.052 \pm 0.008/0.043$  for the K-PgB, supporting the hypothesis that the most voluminous formations of the Deccan Traps, which belong to the Wai subgroup (Poladpur, Ambenali and Mahabaleswar), are placed above the K-PgB (Jay and Widdowson, 2008; Renne et al., 2015; Richards et al., 2015; Sprain et al., 2019). According to the eruptive model of Sprain et al. (2019), the K-PgB is near the base of the Poladpur Formation, and thus the most voluminous eruptive episodes of the Deccan Traps may be early Danian in age. However, based on U-Pb dating, Clyde et al. (2016) reported an age of  $66.021 \pm 0.24/0.039$  Ma for the K-PgB, supporting the emplacement of the Poladpur Formation prior to the K-PgB (Schoene et al., 2015, 2019, 2021; Kasbohm et al., 2021; Fig. 11). According to the eruptive model of Schoene et al. (2019), the emplacement of the Poladpur Formation, (which achieved the highest eruption rate of Deccan volcanism) occurred in the latest Maastrichtian, preceding the K-PgB by only some tens of thousands of years. Schoene et al. (2021) recalculated the eruptive volumes of the model of Sprain et al. (2019) in terms of eruptive rate (Fig. 11), which clearly distinguishes between the mega-pulse eruptive model of Schoene et al. (2019) and the quasi-continuous eruptive model of Sprain et al. (2019).

The Rajahmundry Traps (RT, SE India) bear witness to the scale of early Danian Deccan volcanism, extending  $\sim 1000$  km from the erupting center and forming the longest lava flows on Earth (Self et al., 2008; Keller et al., 2011, 2012). The exposed flows of the RT have been dated as early Danian in age (Keller et al., 2008; Fendley et al., 2020) and have been geochemically assigned to the Ambenali and Mahabaleswar Formations in the Western Ghats (Baksi, 2001; Self et al., 2008). The age of the RT is also compatible with the recently published radiometric ages of the Ambenali and Mahabaleswar Formations (Schoene et al., 2019; Sprain et al., 2019). However, the eruption and outgassing rates in each phase of Deccan volcanism are considered potentially more important for climate change than the volume of basalt erupted (Self et al., 2006; Gertsch et al., 2011; Hernandez Nava et al., 2021). Recent estimations of the amount and rates of  $\text{CO}_2$  release from Deccan volcanism predict only minor increases in atmospheric  $\text{CO}_2$  compared to the background Cretaceous-Paleogene atmospheric reservoir (Self et al., 2006; Schmidt et al., 2016; Steinthorsdottir et al., 2016; Henehan et al., 2016; Fendley et al., 2020). Modelling of different climate sensitivities and volcanic outgassing scenarios suggest that Deccan volcanism alone was insufficient to have driven warming during the early Danian (Hull et al., 2020; Fendley et al., 2020). Conversely, the influence of volcanic  $\text{SO}_2$  and halogen emissions could have been profound at times of flood basalt emplacement (Self et al., 2006). Although volcanic aerosols have a short residence time in the troposphere of  $\sim 1$  week, flood basalt activity could have provided a semi-continuous  $\text{SO}_2$  supply (Self et al., 2006), which may have resulted in cooling and/or ocean acidification on geologic



**Fig. 11.** Age models and eruption rates for the Deccan Traps based on Fig. 4 of Schoene et al. (2021), compared with the age of key early Danian paleontological and climatic events as determined in the Caravaca section. The yellow band shows the most probable stratigraphic range for the K-PgB position within the Deccan Traps, considering both the range of error on U-Pb and  $^{40}\text{Ar}/^{39}\text{Ar}$  dates. Our preferred age model for Caravaca is anchored at the K-PgB using an  $^{40}\text{Ar}/^{39}\text{Ar}$  age of 66.052 Ma, but we also show how the relationship between Deccan volcanism and the PFAS-3T1, 3O1 and 3T2 and Dan-C2 events could vary by changing the age of the K-PgB to that derived from U-Pb (66.021 Ma). Error margins for both radiometric techniques are also shown and incorporated into the age estimates of early Danian events. E. r. = eruption rate; CI = Confidence interval (1) = (Schoene et al., 2019, 2) = (Sprain et al., 2019, 3) = (Clyde et al., 2016); (4) = (Sprain et al., 2018). (For interpretation of the references to colour in this figure legend, the reader is referred to the web version of this article.)

time scales (Gertsch et al., 2011; Courtillot and Fluteau, 2014).

Our data show no indications of ocean acidification or temperature changes in the first 50 kyr of the Danian, except within the K-PgB clay bed, and thus the effect of volcanic outgassing directly following the Chicxulub impact (Renne et al., 2015; Sprain et al., 2019) may have been obscured by the extinction of calcifying plankton (Henehan et al., 2019). Alternatively, our data could indicate that there was no significant Deccan volcanic activity during the earliest Danian. This would be in accordance with Schoene et al. (2019), who suggested that the Poladpur eruptive pulse occurred in the latest Maastrichtian and was followed by a period of volcanic inactivity in the Deccan for about 100 kyr, extending into the earliest Danian. The return to higher stressed environmental conditions at Caravaca occurred ~70 kyr after the K-PgB, as evidenced by the *Chiloguembeltria* bloom in PFAS-3T1, which is broadly coincident with the eruption of the Ambenali Formation (Schoene et al., 2019; Sprain et al., 2019). Recent pH estimates, based on boron isotopes, show initial surface water acidification after the K-PgB, followed by a rapid rebound and overshoot in surface ocean pH within 40 kyr, before pH values returned to pre-K-PgB background levels after ~120 kyr (Henehan et al., 2019). Previous ocean pH estimates predicted a rise in pH due to the extinction of calcifying organisms and the consequent transient reduction in the marine alkalinity sink (Caldeira et al., 1990; Henehan et al., 2016). The latter is supported by observations of improved deep-sea carbonate preservation during the time of the pH overshoot (e.g. Minoletti et al., 2005; Alegret and Thomas, 2013; Tobin et al., 2017) and by our own data (see Section 5.1 and 5.2).

At Caravaca, the aberrant index follows a declining trend during the first ~70 kyr of the Danian, from PFAS-1 to PFAS-3 $\alpha$ , suggesting a

reduction in the impact of the different environmental stressors with a rapid recovery of productivity. Conversely, during the following ~80 kyr (in PFAS-3T1), the opportunistic *Chiloguembeltria* bloomed at a global scale, and the aberrant index increased again (see Section 5.4), suggesting a new episode of environmental stress. Commonly, guembeltriid blooms are reported from shallow marine areas, often near volcanic provinces with a high nutrient flux (Pardo and Keller, 2008). However, these opportunistic taxa radiated and proliferated in the pelagic realm after the K-PgB (Olsson et al., 1999; Arenillas et al., 2000a, 2000b; Keller, 2003), suggesting that, during the early Danian, their ecological preferences of high nutrient availability were met in the open ocean. Although the uncertainties in the temporal correlation between Deccan Traps volcanic phases, the K-PgB, and climatic and paleobiological events are still significant, our data suggest that the *Chiloguembeltria* bloom (PFAS-3T1) is coeval with the emplacement of the Ambenali Formation (Fig. 11).

The emplacement of the Ambenali formation and the apparent co-occurrence with the Dan-C2 event in the upper part of C29r (Fig. 10A and D), has led some authors to link these two events mechanistically (Coccioni et al., 2010; Krahl et al., 2020; Puneekar et al., 2014a). However, the Dan-C2 event was not associated with bottom water warming (Quillévére et al., 2008; Coccioni et al., 2010; Barnet et al., 2019; Krahl et al., 2020) which raises questions as to whether this event can be considered a ‘true’ hyperthermal event or not (see discussion in Barnet et al., 2019). Ocean acidification has also been invoked during Dan-C2 (Coccioni et al., 2010; Krahl et al., 2020) but no convincing evidence has been identified during the Dan-C2 interval at Caravaca nor in other sections to support this (see Barnet et al., 2019). The exact mechanisms

that drove the Dan-C2 event are poorly resolved, and several hypotheses have been put forward: pulses of massive Deccan volcanic eruptions (Krahl et al., 2020); a combination of Deccan volcanism with an orbital configuration which perturbed the carbon cycle (e.g. Coccioni et al., 2010; Barnett et al., 2019; Sinnesael et al., 2019); and/or passive degassing of CO<sub>2</sub> due to the interaction of intrusive magma bodies with the crust (see Sprain et al., 2019; Fendley et al., 2020). The quasi-continuous eruptive model suggests that the Ambenali Formation represents a relatively long volcanic episode (Renne et al., 2015; Sprain et al., 2019). Although this scenario does not provide a relatively rapid trigger mechanism for environmental change, it still permits a hypothesis that the Deccan volcanism could add to emissions of CO<sub>2</sub> by passive degassing over longer timescales, contributing, albeit perhaps in a minor way, to early Danian climate change and the Dan-C2 event. Conversely, the hypothesis of a shorter (<100 kyr), more intense, volcanic pulse (Schoene et al., 2019) is not supported by geochemical evidence from marine records (Hull et al., 2020), and would imply a minimal impact of volcanic activity on climate. Regardless of the eruptive model favoured, and considering the estimated duration for the Ambenali eruptive episode, volcanic outgassing from the Deccan Traps by itself was probably insufficient to drive significant warming during the early Danian (Fendley et al., 2020; Hull et al., 2020), although it may have exacerbated environmental stress. Our age model allows us to suggest that the Ambenali phase coincided with the first Dan-C2 CIE, but not with the second CIE (Fig. 11). If Deccan volcanism was not the cause of the second CIE, then it seems that other factors, such as orbital forcing, are required to fully explain the Dan-C2 event.

Since the proposed warming for the Dan-C2 event is only observed in bulk and planktic foraminiferal isotopic records (Fig. 9), the increase in temperature probably only affected surface ocean waters. A transient but enhanced thermal stratification of the upper part of the water column may have resulted in more differentiated ecological niches. This is supported by our data at Caravaca, which show rapid turnovers of planktic foraminiferal assemblages in PFAS-3O1 and O2 coinciding approximately with both Dan-C2 CIEs. Remarkably, continental records of the first ~700 kyr of the Danian have documented increases in ecologic diversification of plants and mammals (suggested by increased species richness and taxonomic composition), coinciding with the warmer intervals of the early Danian (Lyson et al., 2019; Chiarenza et al., 2020). Therefore, if the Dan-C2 event influenced both marine and terrestrial ecosystems (driven by Deccan volcanism, orbital forcing, or a combination of those and additional mechanisms), it did not cause harmful environmental effects, but instead may have temporarily boosted the recovery of ecosystems.

## 7. Conclusions

High-resolution planktic foraminiferal, geochemical and paleomagnetic analyses of the first ~750 kyr of the Danian at Caravaca (Spain, western Tethys) were carried out. Planktic foraminiferal assemblages after the Cretaceous-Paleogene boundary (K-PgB) are characterized by a rapid succession of planktic foraminiferal acme-stages (PFAS). The first acme is of the triserial *Guembelitra* (PFAS-1), the second of the tiny trochospiral *Parvularugoglobigerina-Palaeoglobigerina* (PFAS-2), and the third of the biserial *Woodringina-Chiloguembelina* (PFAS-3). Within PFAS-3, seven shorter substages are distinguished: PFAS-3 $\alpha$  during the maximal bloom of biserials, PFAS-3T1, T2 and T3 for blooms of the triserial *Chiloguembelitra*, and PFAS-3O1, O2, O3 for increases in abundance of the trochospiral genera *Eoglobigerina*, *Praemurica*, *Globanomalina* and *Parasubbotina*. Triserial blooms and a high abundance of aberrant forms are striking evidence of enhanced environmental stress, occurring especially within PFAS-1 and PFAS-3T substages, during the first 230 kyr of the Danian.

On the basis of  $\delta^{18}\text{O}$  and  $\delta^{13}\text{C}$ , CaCO<sub>3</sub> content and magnetic susceptibility, the Dan-C2 event has been identified for the first time at the Caravaca section. The two carbon isotopic excursions (CIEs) that

characterize the Dan-C2 event have been linked to surface water warming that caused enhanced thermal stratification. During both CIEs, the PFAS-3T assemblages were rapidly replaced by the PFAS-3O assemblages containing less opportunistic taxa, probably because the water depth habitats became more differentiated. High carbonate dissolution is restricted to the K-PgB clay bed, while the Dan-C2 event and the rest of the section show no evidence of significant carbonate dissolution episodes. Although there are still uncertainties in radiometric dating, our data suggest that the first and largest *Chiloguembelitra* bloom (PFAS-3T1) coincided with the emplacement of the Ambenali Formation of the Deccan Traps. Conversely, the Dan-C2 event was decoupled from both the Ambenali eruptive pulse and the *Chiloguembelitra* bloom, starting long after these events had occurred. This suggests that volcanic outgassing of CO<sub>2</sub> was insufficient to drive warming, which only occurred only when the effects of volcanic CO<sub>2</sub> were combined with other factors such as a specific orbital configuration. More high-resolution multidisciplinary studies are needed to fully assess the relationship between Deccan Traps volcanism on early Danian climate, and its potential contribution in reshaping life on Earth after the end-Cretaceous mass extinction.

## Declaration of Competing Interest

The authors declare that they have no known competing financial interests or personal relationships that could have appeared to influence the work reported in this paper.

## Acknowledgements

We deeply thank the editor Isabel Montanez and two anonymous reviewers for their useful, comprehensive and helpful comments and suggestions. This work was supported by MCIU/AEI/FEDER, UE (grant number PGC2018-093890-B-I00), and by the Aragonian Government/FEDER, UE (grant number DGA groups E33\_17R and E33\_20R). Vicente Gilabert acknowledges support from the Spanish Ministerio de Economía, Industria y Competitividad (FPI grant number BES-2016-077800). The authors would like to acknowledge the use of the Servicio General de Apoyo a la Investigación-SAI, Universidad de Zaragoza. This research is part of the PhD thesis of the first author.

## Appendix A. Supplementary data

Supplementary data to this article can be found online at <https://doi.org/10.1016/j.palaeo.2021.110513>.

## References

- Abramovich, S., Keller, G., Berner, Z., Cymbalista, M., Rak, C., 2011. Maastrichtian Planktic Foraminiferal Biostratigraphy and Paleoenvironment of Brazos River, Falls County, Texas, U.S.A. In: Keller, G., Adatte, T. (Eds.), *The End-Cretaceous Mass Extinction and the Chicxulub Impact in Texas*. SEPM (Society for Sedimentary Geology), Tulsa, pp. 123–156. <https://doi.org/10.2110/sepm.100.123>.
- Alegret, L., Molina, E., Thomas, E., 2003. Benthic foraminiferal turnover across the Cretaceous/Paleogene boundary at Agost (southeastern Spain): Paleoenvironmental inferences. *Mar. Micropaleontol.* 48, 251–279. [https://doi.org/10.1016/S0377-8398\(03\)00022-7](https://doi.org/10.1016/S0377-8398(03)00022-7).
- Alegret, L., Thomas, E., 2013. Benthic foraminifera across the Cretaceous/Paleogene boundary in the Southern Ocean (ODP Site 690): Diversity, food and carbonate saturation. *Mar. Micropaleontol.* 105, 40–51. <https://doi.org/10.1016/j.marmicro.2013.10.003>.
- Alegret, L., Thomas, E., Lohmann, K.C., 2012. End-Cretaceous marine mass extinction not caused by productivity collapse. *Proc. Natl. Acad. Sci. U. S. A.* 109, 728–732. <https://doi.org/10.1073/pnas.1110601109>.
- Alvarez, L.W., Alvarez, W., Asaro, F., Michel, H.V., 1980. Extraterrestrial cause for the Cretaceous-Tertiary extinction. *Science* 208, 1095–1108. <https://doi.org/10.1126/science.208.4448.1095>.
- Andeweg, B., 2002. *Cenozoic tectonic evolution of the Iberian Peninsula: effects and causes of changing stress fields*. PhD thesis. Vrije Universiteit Amsterdam, Amsterdam (192 pp).
- Arenillas, I., Arz, J.A., 2017. Benthic origin and earliest evolution of the first planktonic foraminifera after the Cretaceous/Paleogene boundary mass extinction. *Hist. Biol.* 29, 25–42. <https://doi.org/10.1080/08912963.2015.1119133>.

- Arenillas, I., Arz, J.A., Molina, E., 1998. El límite Cretácico/Terciario de Zumaya, Osinaga y Músquiz (Pirineos): control bioestratigráfico y cuantitativo de hiatos con foraminíferos planctónicos. *Rev. Soc. Geol. Esp.* 11 (1–2), 127–138.
- Arenillas, I., Arz, J.A., Molina, E., Dupuis, C., 2000a. The Cretaceous/Paleogene (K/P) boundary at Aïn Settara, Tunisia: Sudden catastrophic mass extinction in planktic foraminifera. *J. Foraminif. Res.* 30, 202–218. <https://doi.org/10.2113/0300202>.
- Arenillas, I., Arz, J.A., Molina, E., Dupuis, C., 2000b. An independent test of planktic foraminiferal turnover across the Cretaceous/Paleogene (K/P) boundary at El Kef, Tunisia: Catastrophic mass extinction and possible survivorship. *Micropaleontology* 46, 31–49.
- Arenillas, I., Arz, J.A., Molina, E., 2004. A new high-resolution planktic foraminiferal zonation and subzonation for the lower Danian. *Lethaia* 37, 79–95. <https://doi.org/10.1080/00241160310005097>.
- Arenillas, I., Arz, J.A., Grajales-Nishimura, J.M., Meléndez, A., Rojas-Consuegra, R., 2016. The Chicxulub impact is synchronous with the planktonic foraminifera mass extinction at the Cretaceous/Paleogene boundary: New evidence from the Moncada section. *Cuba. Geol. Acta* 14, 35–51. <https://doi.org/10.1344/GeologicaActa2016.14.1.4>.
- Arenillas, I., Arz, J.A., Grajales-Nishimura, J.M., Murillo-Muñeton, G., Alvarez, W., Camargo-Zanoguera, A., Molina, E., Rosales-Domínguez, C., 2006. Chicxulub impact event is Cretaceous/Paleogene boundary in age: New micropaleontological evidence. *Earth Planet. Sci. Lett.* 249, 241–257. <https://doi.org/10.1016/j.epsl.2006.07.020>.
- Arenillas, I., Arz, J.A., Gilabert, V., 2018. Blooms of aberrant planktic foraminifera across the K/Pg boundary in the Western Tethys: Causes and evolutionary implications. *Paleobiology* 44, 460–489. <https://doi.org/10.1017/pab.2018.16>.
- Arz, J.A., Arenillas, I., Molina, E., Sepúlveda, R., 2000. La estabilidad evolutiva de los foraminíferos planctónicos en el Maestríchtien superior y su extinción en el límite Cretácico/Terciario de Caravaca, España. *Rev. geol. Chile* 27, 27–47. <https://doi.org/10.4067/S0716-0208200000100003>.
- Arz, J.A., Alegret, L., Arenillas, I., Liesa, C., Molina, E., Soria, A.R., 2001. Extinción de foraminíferos del límite Cretácico/Terciario en Coxquihui (México) y su relación con las evidencias de impacto. *Rev. Esp. Micropaleontol.* 33 (2), 221–236.
- Ashkenazi-Polivoda, S., Rak, C., Almogi-Labin, A., Zsolt, B., Ovadia, O., Abramovich, S., 2014. Paleocology of the K-Pg mass extinction survivor *Guembelitra* (Cushman): isotopic evidence from pristine foraminifera from Brazos River, Texas (Maestríchtien). *Paleobiology* 40, 24–33. <https://doi.org/10.1666/13317>.
- Aze, T., Ezard, T.H.G., Purvis, A., Coxall, H.K., Stewart, D.R.M., Wade, B.S., Pearson, P.N., 2011. A phylogeny of Cenozoic macroperforate planktonic foraminifera from fossil data. *Biol. Rev.* 86, 900–927. <https://doi.org/10.1111/j.1469-185X.2011.00178.x>.
- Baksi, A.K., 2001. The Rajahmundry Traps, Andhra Pradesh: Evaluation of their petrogenesis relative to the Deccan Traps. *Proc. Indian Acad. Sci. Earth Planet. Sci.* 110, 397–407. <https://doi.org/10.1007/BF02702903>.
- Ballent, S.C., Carignano, A.P., 2008. Morphological abnormalities in late Cretaceous and early Paleocene foraminifer tests (northern Patagonia, Argentina). *Mar. Micropaleontol.* 67, 288–296. <https://doi.org/10.1016/j.marmicro.2008.02.003>.
- Barnet, J.S.K., Littler, K., Kroon, D., Leng, M.J., Westerhold, T., Röhl, U., Zachos, J.C., 2018. A new high-resolution chronology for the late Maestríchtien warming event: establishing robust temporal links with the onset of Deccan volcanism. *Geology* 46, 147–150. <https://doi.org/10.1130/G39771.1>.
- Barnet, J.S.K., Littler, K., Westerhold, T., Kroon, D., Leng, M.J., Bailey, I., Röhl, U., Zachos, J.C., 2019. A High-Fidelity Benthic Stable Isotope Record of late Cretaceous-early Eocene climate Change and Carbon-Cycling. *Paleoceanogr. Paleoclimatology* 34, 672–691. <https://doi.org/10.1029/2019PA003556>.
- Beals, E.W., 1984. Bray-Curtis ordination: an effective strategy for analysis of multivariate ecological data. *Adv. Ecol. Res.* 14, 1–55. [https://doi.org/10.1016/S0065-2504\(08\)60168-3](https://doi.org/10.1016/S0065-2504(08)60168-3).
- Berger, W.H., Bonneau, M., Parker, F.L., Plateau, L., 1982. Foraminifera on the deep-sea floor: lysocline and dissolution rate. *Oceanol. Acta* 5, 249–258.
- Berggren, W.A., Pearson, P.N., 2005. A revised tropical to subtropical Paleogene planktonic foraminiferal zonation. *J. Foraminif. Res.* 35, 279–298. <https://doi.org/10.2113/35.4.279>.
- Birch, H.S., Coxall, H.K., Pearson, P.N., 2012. Evolutionary ecology of early Paleocene planktonic foraminifera: size, depth habitat and symbiosis. *Paleobiology* 38, 374–390. <https://doi.org/10.1666/11027.1>.
- Birch, H.S., Coxall, H.K., Pearson, P.N., Kroon, D., Schmidt, D.N., 2016. Partial collapse of the marine carbon pump after the Cretaceous-Paleogene boundary. *Geology* 44, 287–290. <https://doi.org/10.1130/G37581.1>.
- Boersma, A., Premoli Silva, I., 1989. Atlantic Paleogene biserial heterohelicid foraminifera and oxygen minima. *Paleoceanography* 4, 271–286.
- Bown, P., 2005. Selective calcareous nannoplankton survivorship at the Cretaceous-Tertiary boundary. *Geology* 33, 653–656. <https://doi.org/10.1130/G21566.1>.
- Bralower, T.J., Cosmidis, J., Heaney, P.J., Kump, L.R., Morgan, J.V., Harper, D.T., Lyons, S.L., Freeman, K.H., Grice, K., Wendler, J.E., Zachos, J.C., Artemieva, N., Chen, S.A., Gulick, S.P.S., House, C.H., Jones, H.L., Lowery, C.M., Nims, C., Schafer, B., Thomas, E., Vajda, V., 2020. Origin of a global carbonate layer deposited in the aftermath of the Cretaceous-Paleogene boundary impact. *Earth Planet. Sci. Lett.* 548, 116476. <https://doi.org/10.1016/j.epsl.2020.116476>.
- Bukry, D., 1974. Coccoliths as paleosalinity indicators - evidence from Black Sea. In: Degens, E.T., Ross, D.A. (Eds.), *The Black Sea—Geology, Chemistry, and Biology. AAPG Memoir* 20, Tulsa, pp. 353–363.
- Burgess, S., 2019. Deciphering mass extinction triggers. *Science* 363, 815–816. <https://doi.org/10.1126/science.aaw0473>.
- Caldeira, K., Rampino, M.R., Volk, T., Zachos, J.C., 1990. Biogeochemical modeling at mass extinction boundaries: Atmospheric carbon dioxide and ocean alkalinity at the K/T boundary. In: Kauffman, E.G., Walliser, O.H. (Eds.), *Extinction events in Earth history. Lecture Notes in Earth Sciences*, 30. Springer, Berlin, Heidelberg, pp. 333–345. <https://doi.org/10.1007/bfb0011156>.
- Canudo, J.I., Keller, G., Molina, E., 1991. Cretaceous/Tertiary boundary extinction pattern and faunal turnover at Agost and Caravaca, S.E. Spain. *Mar. Micropaleontol.* 17, 319–341. [https://doi.org/10.1016/0377-8398\(91\)90019-3](https://doi.org/10.1016/0377-8398(91)90019-3).
- Chenet, A.L., Quidelleur, X., Fluteau, F., Courtillot, V., Bajpai, S., 2007. <sup>40</sup>K–<sup>40</sup>Ar dating of the Main Deccan large igneous province: further evidence of KTB age and short duration. *Earth Planet. Sci. Lett.* 263, 1–15. <https://doi.org/10.1016/j.epsl.2007.07.011>.
- Chiarenza, A.A., Farnsworth, A., Mannion, P.D., Lunt, D.J., Valdes, P.J., Morgan, J.V., Allison, P.A., 2020. Asteroid impact, not volcanism, caused the end-Cretaceous dinosaur extinction. *Proc. Natl. Acad. Sci. U. S. A.* 117, 17084–17093. <https://doi.org/10.1073/pnas.2006087117>.
- Clyde, W.C., Ramezani, J., Johnson, K.R., Bowring, S.A., Jones, M.M., 2016. Direct high-precision U-Pb geochronology of the end-Cretaceous extinction and calibration of Paleocene astronomical timescales. *Earth Planet. Sci. Lett.* 452, 272–280. <https://doi.org/10.1016/j.epsl.2016.07.041>.
- Coccioni, R., Galeotti, S., 1994. K-T boundary extinction: Geologically instantaneous or gradual event? Evidence from deep-sea benthic foraminifera. *Geology* 22, 779–782. [https://doi.org/10.1130/0091-7613\(1994\)022<0779:KTBEIG>2.3.CO;2](https://doi.org/10.1130/0091-7613(1994)022<0779:KTBEIG>2.3.CO;2).
- Coccioni, R., Luciani, V., 2006. *Guembelitra irregularis* bloom at the K-T boundary: Morphological abnormalities induced by impact-related extreme environmental stress? In: Cockell, C., Gilmour, I., Koeberl, C. (Eds.), *Biological Processes Associated with Impact Events*. Springer-Verlag, Berlin, pp. 179–196. [https://doi.org/10.1007/3-540-25736-5\\_8](https://doi.org/10.1007/3-540-25736-5_8).
- Coccioni, R., Frontalini, F., Bancalà, G., Fornaciari, E., Jovane, L., Sprovieri, M., 2010. The Dan-C2 hyperthermal event at Gubbio (Italy): Global implications, environmental effects, and cause(s). *Earth Planet. Sci. Lett.* 297, 298–305. <https://doi.org/10.1016/j.epsl.2010.06.031>.
- Courtillot, V., Fluteau, F., 2014. A review of the embedded time scales of flood basalt volcanism with special emphasis on dramatically short magmatic pulses. In: Keller, G., Kerr, A.C. (Eds.), *Volcanism, Impacts, and Mass Extinctions: Causes and Effects*, *Geol. Soc. Am. Spec. Pap.*, vol. 505, pp. 301–317. [https://doi.org/10.1130/2014.2505\(15\)](https://doi.org/10.1130/2014.2505(15)).
- Courtillot, V., Besse, J., Vandamme, D., Montigny, R., Jaeger, J.-J., Cappetta, H., 1986. Deccan flood basalts at the Cretaceous/Tertiary boundary? *Earth Planet. Sci. Lett.* 80, 361–374.
- Coxall, H.K., D'Hondt, S., Zachos, J.C., 2006. Pelagic evolution and environmental recovery after the Cretaceous-Paleogene mass extinction. *Geology* 34, 297–300. <https://doi.org/10.1130/G21702.1>.
- Cunha, A.S., Shimabukuro, S., 1997. *Braarudosphaera* blooms and anomalous enrichments of *Nannococcus*: evidence from the Turonian South Atlantic, Santos Basin, Brazil. *J. Nannoplankt. Res.* 19, 51–55.
- D'Hondt, S., Donaghay, P., Zachos, J.C., Luttenberg, D., Lindinger, M., 1998. Organic carbon fluxes and ecological recovery from the Cretaceous-Tertiary mass extinction. *Science* 282, 276–279. <https://doi.org/10.1126/science.282.5387.276>.
- Ellwood, B.B., Tomkin, J.H., Ratcliffe, K.T., Wright, M., Kafafy, A.M., 2008. High-resolution magnetic susceptibility and geochemistry for the Cenomanian/Turonian boundary GSSP with correlation to time equivalent core. *Paleoceanogr. Paleoclimatol. Palaeoecol.* 261, 105–126. <https://doi.org/10.1016/j.palaeo.2008.01.005>.
- Fendley, I.M., Sprain, C.J., Renne, P.R., Arenillas, I., Arz, J.A., Gilabert, V., Self, S., Vanderkluyzen, L., Pande, K., Smit, J., Mittal, T., 2020. No Cretaceous-Paleogene boundary in exposed Rajahmundry Traps: a refined chronology of the longest Deccan lava flows from <sup>40</sup>Ar/<sup>39</sup>Ar dates, magnetostratigraphy, and biostratigraphy. *Geochemistry, Geophys. Geosystems* 21, 1–20. <https://doi.org/10.1029/2020gc009149>.
- Font, E., Adatte, T., Sial, A.N., de Lacerda, L.D., Keller, G., Punekar, J., 2016. Mercury anomaly, Deccan volcanism, and the end-Cretaceous mass extinction. *Geology* 44, 171–174. <https://doi.org/10.1130/G37451.1>.
- Font, E., Adatte, T., Andrade, M., Keller, G., Mbabi Bitchong, A., Carvalho, C., Ferreira, J., Diogo, Z., Mirão, J., 2018. Deccan volcanism induced high-stress environment during the Cretaceous–Paleogene transition at Zumaia, Spain: evidence from magnetic, mineralogical and biostratigraphic records. *Earth Planet. Sci. Lett.* 484, 53–66. <https://doi.org/10.1016/j.epsl.2017.11.055>.
- Fornaciari, E., Giusberti, L., Luciani, V., Tateo, F., Agnini, C., Backman, J., Oddone, M., Rio, D., 2007. An expanded Cretaceous-Tertiary transition in a pelagic setting of the Southern Alps (central-western Tethys). *Paleoceanogr. Paleoclimatol. Palaeoecol.* 255, 98–131. <https://doi.org/10.1016/j.palaeo.2007.02.044>.
- Gallala, N., Zaghib-Turki, D., Arenillas, I., Arz, J.A., Molina, E., 2009. Catastrophic mass extinction and assemblage evolution in planktic foraminifera across the Cretaceous/Paleogene (K/Pg) boundary at Bidart (SW France). *Mar. Micropaleontol.* 72, 196–209. <https://doi.org/10.1016/j.marmicro.2009.05.001>.
- Gardin, S., 2002. Late Maestríchtien to early Danian calcareous nannofossils at Elles (Northwest Tunisia). A tale of one million years across the K-T boundary. *Paleoceanogr. Paleoclimatol. Palaeoecol.* 178, 211–231. [https://doi.org/10.1016/S0031-0182\(01\)00397-2](https://doi.org/10.1016/S0031-0182(01)00397-2).
- Gardin, S., Monechi, S., 1998. Palaeoecological change in middle to low latitude calcareous nannoplankton at the Cretaceous/Tertiary boundary. *Bull. Soc. géol. Fr.* 169, 709–723.
- Gerstel, J., Thunell, R.C., Zachos, J.C., Arthur, M.A., 1986. The Cretaceous/Tertiary boundary event in the North Pacific: Planktonic foraminiferal results from Deep Sea Drilling Project Site 577, Shatsky rise. *Paleoceanography* 1, 97–117. <https://doi.org/10.1029/PA001i002p00097>.

- Gertsch, B., Keller, G., Adatte, T., Garg, R., Prasad, V., Berner, Z., Fleitmann, D., 2011. Environmental effects of Deccan volcanism across the Cretaceous-Tertiary transition in Meghalaya, India. *Earth Planet. Sci. Lett.* 310, 272–285. <https://doi.org/10.1016/j.epsl.2011.08.015>.
- Gibbs, S.J., Bown, P.R., Ward, B.A., Alvarez, S.A., Kim, H., Archontikis, O.A., Sauterey, B., Poulton, A.J., Wilson, J., Ridgwell, A., 2020. Algal plankton turn to hunting to survive and recover from end-Cretaceous impact darkness. *Sci. Adv.* 6, eab9123. <https://doi.org/10.1126/sciadv.abc9123>.
- Gilabert, V., Arz, J.A., Arenillas, I., Robinson, S.A., 2021. Influence of the latest Maastrichtian Warming Event on planktic foraminiferal assemblages and ocean carbonate saturation at Caravaca, Spain. *Cretac. Res.* 125, 104844. <https://doi.org/10.1016/j.cretres.2021.104844>.
- Groot, J.J., de Jonge, R.B.G., Langereis, C.G., ten Kate, W.G.H.Z., Smit, J., 1989. Magnetostratigraphy of the Cretaceous-Tertiary boundary at Agost (Spain). *Earth Planet. Sci. Lett.* 94, 385–397. [https://doi.org/10.1016/0012-821X\(89\)90155-6](https://doi.org/10.1016/0012-821X(89)90155-6).
- Gulick, S.P.S., Bralower, T.J., Ormó, J., Hall, B., Grice, K., Schaefer, B., Lyons, S., Freeman, K.H., Morgan, J.V., Artemieva, N., Kaskes, P., De Graaff, S.J., Whalen, M. T., Collins, G.S., Tiko, S.M., Verhagen, C., Christeson, G.L., Claeys, P., Coolen, M.J. L., Goderis, S., Goto, K., Grieve, R.A.F., McCall, N., Osinski, G.R., Rae, A.S.P., Riller, U., Smit, J., Vajda, V., Wittmann, A., 2019. The first day of the Cenozoic. *Proc. Natl. Acad. Sci. U. S. A.* 116, 19342–19351. <https://doi.org/10.1073/pnas.1909479116>.
- Hammer, Ø., Harper, D.A.T., Ryan, P.D., 2001. PAST: Paleontological statistics software package for education and data analysis. *Paleontol. Electron.* 4 (1), 9.
- Henehan, M.J., Hull, P.M., Penman, D.E., Rae, J.W.B., Schmidt, D.N., 2016. Biogeochemical significance of pelagic ecosystem function: an end-Cretaceous case study. *Philos. Trans. R. Soc. B Biol. Sci.* 371 <https://doi.org/10.1098/rstb.2015.0510>.
- Henehan, M.J., Ridgwell, A., Thomas, E., Zhang, S., Alegret, L., Schmidt, D.N., Rae, J.W. B., Wits, J.D., Landman, N.H., Greene, S.E., Huber, B.T., Super, J.R., Planavsky, N. J., Hull, P.M., 2019. Rapid Ocean acidification and protracted Earth system recovery followed the end-Cretaceous Chicxulub impact. *Proc. Natl. Acad. Sci. U. S. A.* 116, 22500–22504. <https://doi.org/10.1073/pnas.1905989116>.
- Hernandez Nava, A., Black, B.A., Gibson, S.A., Bodnar, R.J., Renne, P.R., Vanderkluyse, L., 2021. Reconciling early Deccan Traps CO<sub>2</sub> outgassing and pre-KPB global climate. *Proc. Natl. Acad. Sci. U. S. A.* 118, e2007797118 <https://doi.org/10.1073/pnas.2007797118>.
- Hildebrand, A.R., Penfield, G.T., Kring, D.A., Pilkington, M., Antonio, C.Z., Boynton, W. V., 1991. Chicxulub crater: a possible Cretaceous/Tertiary boundary impact crater on the Yucatan peninsula, Mexico. *Geology* 19, 867–871. [https://doi.org/10.1130/0091-7613\(1991\)019<0867:CCAPCT>2.3.CO;2](https://doi.org/10.1130/0091-7613(1991)019<0867:CCAPCT>2.3.CO;2).
- Huber, B.T., MacLeod, K.G., Norris, R.D., 2002. Abrupt extinction and subsequent reworking of Cretaceous planktonic foraminifera across the Cretaceous-Tertiary boundary: evidence from the subtropical North Atlantic. *Geol. Soc. Am. Spec. Pap.* 356, 277–289. <https://doi.org/10.1130/0-8137-2356-6.277>.
- Hull, P.M., Bornemann, A., Penman, D.E., Henehan, M.J., Norris, R.D., Wilson, P.A., Blum, P., Alegret, L., Batenburg, S.J., Bown, P.R., Bralower, T.J., Courmede, C., Deutsch, A., Donner, B., Friedrich, O., Jehle, S., Kim, H., Kroon, D., Lippert, P.C., Lorocho, D., Moebius, I., Moriya, K., Peppe, D.J., Ravizza, G.E., Röhl, U., Schueth, J. D., Septilveda, J., Sexton, P.F., Sibert, E.C., Śliwińska, K.K., Summons, R.E., Thomas, E., Westerhold, T., Whiteside, J.H., Yamaguchi, T., Zachos, J.C., 2020. On impact and volcanism across the Cretaceous-Paleogene boundary. *Science* 367, 266–272. <https://doi.org/10.1126/science.aay5055>.
- Jay, A.E., Widdowson, M., 2008. Stratigraphy, structure and volcanology of the SE Deccan continental flood basalt province: Implications for eruptive extent and volumes. *J. Geol. Soc. Lond.* 165, 177–188. <https://doi.org/10.1144/0016-76492006-062>.
- Jiang, S., Bralower, T.J., Patzkowsky, M.E., Kump, L.R., Schueth, J.D., 2010. Geographic controls on nanoplankton extinction across the Cretaceous/Paleogene boundary. *Nat. Geosci.* 3, 280–285. <https://doi.org/10.1038/ngeo775>.
- Jiang, S., Chen, X., Bernaola, G., 2019. Environmental controls on calcareous nanoplankton response to the Cretaceous/Paleogene mass extinction in the Tethys realm. *Palaeogeogr. Palaeoclimatol. Palaeoecol.* 515, 134–142. <https://doi.org/10.1016/j.palaeo.2017.12.044>.
- Jones, H.L., Lowery, C.M., Bralower, T.J., 2019. Delayed calcareous nanoplankton boom-bust successions in the earliest Paleocene Chicxulub (Mexico) impact crater. *Geology* 47, 753–756. <https://doi.org/10.1130/G46143.1>.
- Kaiho, K., Lamolda, M.A., 1999. Catastrophic extinction of planktonic foraminifera at the Cretaceous-Tertiary boundary evidenced by stable isotopes and foraminiferal abundance at Caravaca, Spain. *Geology* 27, 355–358. [https://doi.org/10.1130/0091-7613\(1999\)027<0355:CEOPFA>2.3.CO;2](https://doi.org/10.1130/0091-7613(1999)027<0355:CEOPFA>2.3.CO;2).
- Kaiho, K., Kajiwara, Y., Tazaki, K., Ueshima, M., Takeda, N., Kawahata, H., Arinobu, T., Ishiwatari, R., Hirai, A., Lamolda, M.A., 1999. Oceanic primary productivity and dissolved oxygen levels at the Cretaceous/Tertiary boundary: their decrease, subsequent warming, and recovery. *Paleoceanography* 14, 511–524. <https://doi.org/10.1029/1999PA900022>.
- Kasbohm, J., Schoene, B., Burgess, S., 2021. Radiometric constraints on the timing, tempo, and effects of large igneous province emplacement. In: Ernst, R.E., Dickson, J., Bekker, A. (Eds.), *Large Igneous Provinces: A Driver of Global Environmental and Biotic Changes*. American Geophysical Union. Carbon in Earth's Interior. John Wiley & Sons, Inc., pp. 27–82. <https://doi.org/10.1002/9781119507444.ch2> published by.
- Kawaragi, K., Sekine, Y., Kadono, T., Sugita, S., Ohno, S., Ishibashi, K., Kurosawa, K., Matsui, T., Ikeda, S., 2009. Direct measurements of chemical composition of shock-induced gases from calcite: an intense global warming after the Chicxulub impact due to the indirect greenhouse effect of carbon monoxide. *Earth Planet. Sci. Lett.* 282, 56–64. <https://doi.org/10.1016/j.epsl.2009.02.037>.
- Keller, G., 2003. *Guembelitrina* dominated late Maastrichtian planktic foraminiferal assemblages mimic early Danian in Central Egypt. *Mar. Micropaleontol.* 47, 71–99. [https://doi.org/10.1016/S0377-8398\(02\)00116-0](https://doi.org/10.1016/S0377-8398(02)00116-0).
- Keller, G., Pardo, A., 2004. Disaster opportunists Guembelitrinidae: Index for environmental catastrophes. *Mar. Micropaleontol.* 53, 83–116. <https://doi.org/10.1016/j.marmicro.2004.04.012>.
- Keller, G., Adatte, T., Gardin, S., Bartolini, A., Bajpai, S., 2008. Main Deccan volcanism phase ends near the K-T boundary: evidence from the Krishna-Godavari Basin, SE India. *Earth Planet. Sci. Lett.* 268, 293–311. <https://doi.org/10.1016/j.epsl.2008.01.015>.
- Keller, G.K., Bhowmick, P.K., Upadhyay, H., Dave, A., Reddy, A.N., Jaiprakash, B.C., Adatte, T., 2011. Deccan volcanism linked to the Cretaceous-Tertiary boundary mass extinction: New evidence from ONGC wells to the Krishna-Godavari Basin. *J. Geol. Soc. India* 78, 399–428. <https://doi.org/10.1007/s12594-011-0107-3>.
- Keller, G., Adatte, T., Bhowmick, P.K., Upadhyay, H., Dave, A., Reddy, A.N., Jaiprakash, B.C., 2012. Nature and timing of extinctions in Cretaceous-Tertiary planktic foraminifera preserved in Deccan intertrappean sediments of the Krishna-Godavari Basin, India. *Earth Planet. Sci. Lett.* 341–344, 211–221. <https://doi.org/10.1016/j.epsl.2012.06.021>.
- Keller, G., Puneekar, J., Mateo, P., 2016. Upheavals during the late Maastrichtian: Volcanism, climate and faunal events preceding the end-Cretaceous mass extinction. *Palaeogeogr. Palaeoclimatol. Palaeoecol.* 441, 137–151. <https://doi.org/10.1016/j.palaeo.2015.06.034>.
- Keller, G., Mateo, P., Monkenbusch, J., Thibault, N., Puneekar, J., Spangenberg, J.E., Abramovich, S., Ashkenazi-Polivoda, S., Schoene, B., Eddy, M.P., Samperton, K.M., Khadri, S.F.R., Adatte, T., 2020. Mercury linked to Deccan Traps volcanism, climate change and the end-Cretaceous mass extinction. *Glob. Planet. Change* 194, 103312. <https://doi.org/10.1016/j.gloplacha.2020.103312>.
- Kelly, D.C., Norris, R.D., Zachos, J.C., 2003. Deciphering the paleoceanographic significance of early Oligocene *Braarudosphaera* chalks in the South Atlantic. *Mar. Micropaleontol.* 49, 49–63. [https://doi.org/10.1016/S0377-8398\(03\)00027-6](https://doi.org/10.1016/S0377-8398(03)00027-6).
- Krahl, G., Bom, M.H.H., Kochhann, K.G.D., Souza, L.V., Savian, J.F., Fauth, G., 2020. Environmental changes occurred during the early Danian at the Rio Grande rise, South Atlantic Ocean. *Glob. Planet. Change* 191, 103197. <https://doi.org/10.1016/j.gloplacha.2020.103197>.
- Kring, D.A., 2007. The Chicxulub impact event and its environmental consequences at the Cretaceous-Tertiary boundary. *Palaeogeogr. Palaeoclimatol. Palaeoecol.* 255, 4–21. <https://doi.org/10.1016/j.palaeo.2007.02.037>.
- Kroon, D., Nederbragt, A.J., 1990. Ecology and paleoecology of triserial planktic foraminifera. *Mar. Micropaleontol.* 16, 25–38. [https://doi.org/10.1016/0377-8398\(90\)90027-J](https://doi.org/10.1016/0377-8398(90)90027-J).
- Kucera, M., Malmgren, B.A., Sturesson, U., 1997. Foraminiferal dissolution at shallow depths of the Walvis Ridge and Rio Grande rise during the latest Cretaceous: Inferences for deep-water circulation in the South Atlantic. *Palaeogeogr. Palaeoclimatol. Palaeoecol.* 129, 195–212. [https://doi.org/10.1016/S0031-0182\(96\)00133-2](https://doi.org/10.1016/S0031-0182(96)00133-2).
- Lamolda, M.A., Melinte, M.C., Kaiho, K., 2005. Nannofloral extinction and survivorship across the K/T boundary at Caravaca, southeastern Spain. *Palaeogeogr. Palaeoclimatol. Palaeoecol.* 224, 27–52. <https://doi.org/10.1016/j.palaeo.2005.03.030>.
- Lamolda, M.A., Melinte-Dobrincescu, M.C., Kaiho, K., 2016. Calcareous nannoplankton assemblage changes linked to paleoenvironmental deterioration and recovery across the Cretaceous-Paleogene boundary in the Betic Cordillera (Agost, Spain). *Palaeogeogr. Palaeoclimatol. Palaeoecol.* 441, 438–452. <https://doi.org/10.1016/j.palaeo.2015.10.003>.
- Legendre, P., Gallagher, E.D., 2001. Ecologically meaningful transformations for ordination of species data. *Oecologia* 129, 271–280. <https://doi.org/10.1007/s004420100716>.
- Lowery, C.M., Fraass, A.J., 2019. Morphospace expansion paces taxonomic diversification after end Cretaceous mass extinction. *Nat. Ecol. Evol.* 3, 900–904. <https://doi.org/10.1038/s41559-019-0835-0>.
- Lowery, C.M., Bralower, T.J., Owens, J.D., Rodríguez-Tovar, F.J., Jones, H., Smit, J., Whalen, M.T., Claeys, P., Farley, K., Gulick, S.P.S., Morgan, J.V., Green, S., Chenot, E., Christeson, G.L., Cockell, C.S., Coolen, M.J.L., Ferrière, L., Gebhardt, C., Goto, K., Kring, D.A., Lofi, J., Ocampo-Torres, R., Perez-Cruz, L., Pickersgill, A.E., Poelchau, M.H., Rae, A.S.P., Rasmussen, C., Rebolledo-Vieyra, M., Riller, U., Sato, H., Tikoo, S.M., Tomioka, N., Urrutia-Fucugauchi, J., Vellekoop, J., Wittmann, A., Xiao, L., Yamaguchi, K.E., Zylberman, W., 2018. Rapid recovery of life at ground zero of the end-Cretaceous mass extinction. *Nature* 558, 288–291. <https://doi.org/10.1038/s41586-018-0163-6>.
- Lowery, C.M., Bown, P.R., Fraass, A.J., Hull, P.M., 2020. Ecological Response of Plankton to Environmental Change: Thresholds for Extinction. *Annu. Rev. Earth Planet. Sci.* 48 <https://doi.org/10.1146/annurev-earth-081619-052818>.
- Luciani, V., D'Onofrio, R., Filippi, G., Moretti, S., 2020. Which was the habitat of early Eocene planktic foraminifer *Chiloguembelina*? Stable isotope paleobiology from the Atlantic Ocean and implication for paleoceanographic reconstructions. *Glob. Planet. Change* 191, 103216. <https://doi.org/10.1016/j.gloplacha.2020.103216>.
- Lyson, T.R., Miller, I.M., Bercovici, A.D., Weissenburger, K., Fuentes, A.J., Clyde, W.C., Hagadorn, J.W., Butrim, M.J., Johnson, K.R., Fleming, R.F., Barclay, R.S., Maccracken, S.A., Lloyd, B., Wilson, G.P., Krause, D.W., Chester, S.G.B., 2019. Exceptional continental record of biotic recovery after the Cretaceous–Paleogene mass extinction. *Science* 366, 977–983. <https://doi.org/10.1126/science.aay2268>.
- Mateo, P., Keller, G., Adatte, T., Spangenberg, J.E., 2016. Mass wasting and hiatuses during the Cretaceous-Tertiary transition in the North Atlantic: Relationship to the

- Chicxulub impact? *Palaeogeogr. Palaeoclimatol. Palaeoecol.* 441, 96–115. <https://doi.org/10.1016/j.palaeo.2015.01.019>.
- Metsana-Oussaid, F., Belhai, D., Arenillas, I., Arz, J.A., Gilabert, V., 2019. New sections of the Cretaceous-Paleogene transition in the southwestern Tethys (Médéa, northern Algeria): planktic foraminiferal biostratigraphy and biochronology. *Arab. J. Geosci.* 12 <https://doi.org/10.1007/s12517-019-4402-4>.
- Minoletti, F., De Rafelis, M., Renard, M., Gardin, S., Young, J., 2005. Changes in the pelagic fine fraction carbonate sedimentation during the Cretaceous-Paleocene transition: Contribution of the separation technique to the study of Bidart section. *Palaeogeogr. Palaeoclimatol. Palaeoecol.* 216, 119–137. <https://doi.org/10.1016/j.palaeo.2004.10.006>.
- Molina, E., Arenillas, I., Arz, J.A., 1998. Mass extinction in planktic foraminifera at the Cretaceous-Paleogene boundary in subtropical and temperate latitudes. *Bull. Soc. géol. Fr.* 169 (3), 351–363.
- Molina, E., Alegret, L., Arenillas, I., Arz, J.A., Gallala, N., Grajales-Nishimura, J.M., Murillo-Munetón, G., Zaghbib-Turki, D., 2009. The Global Boundary Stratotype Section and Point for the base of the Danian Stage (Paleocene, Paleogene, “Tertiary”, Cenozoic): Auxiliary sections and correlation. *Episodes* 32, 84–95. <https://doi.org/10.18814/epiiugs/2009/v32i2/002>.
- Mukhopadhyay, S., Farley, K.A., Montanari, A., 2001. A short duration of the Cretaceous-Tertiary boundary event: evidence from extraterrestrial Helium<sup>3</sup>. *Science* 291, 1952–1955. <https://doi.org/10.1126/science.291.5510.1952>.
- Norris, R.D., 1996. Symbiosis as an evolutionary innovation in the radiation of Paleocene planktic foraminifera. *Paleobiology* 22, 461–480. <https://doi.org/10.1017/S0094837300016468>.
- Olsson, R.K., Berggren, W.A., Hemleben, C., Huber, B.T., 1999. Atlas of Paleocene Planktonic Foraminifera. *Smithson. Contrib. Paleobiol.* 85, 1–252. <https://doi.org/10.5479/si.00810266.85.1>.
- Omaña, L., Alencáster, G., Hernández, J.R.T., Doncel, R.L., 2012. Morphological abnormalities and dwarfism in Maastrichtian foraminifera from the Cárdenas Formation, Valles-San Luis Potosí Platform, Mexico: Evidence of paleoenvironmental stress. *Bol. Soc. Geol. Mex.* 64, 305–318. <https://doi.org/10.18268/BSGM2012v64n3a4>.
- Pardo, A., Keller, G., 2008. Biotic effects of environmental catastrophes at the end of the Cretaceous and early Tertiary: *Guembelitra* and *Heterohelix* blooms. *Cretac. Res.* 29, 1058–1073. <https://doi.org/10.1016/j.cretres.2008.05.031>.
- Pospichal, J.J., 1996. Calcareous nannoplankton mass extinction at the Cretaceous/Tertiary boundary: an update. *Geol. Soc. Am. Spec. Pap.* 307, 335–360. <https://doi.org/10.1130/0-8137-2307-8.335>.
- Premović, P.I., 2009. Experimental evidence for the global acidification of surface ocean at the Cretaceous-Paleogene boundary: the biogenic calcite-poor spherule layers. *Int. J. Astrobiol.* 8, 193–206. <https://doi.org/10.1017/S1473550409990139>.
- Punekar, J., Mateo, P., Keller, G., 2014a. Effects of Deccan volcanism on paleoenvironment and planktic foraminifera: a global survey. *Spec. Geol. Soc. Am. Spec. Pap.* 505, 91–116. [https://doi.org/10.1130/2014.2505\(04\)](https://doi.org/10.1130/2014.2505(04)).
- Punekar, J., Keller, G., Khozyem, H., Hamming, C., Adatte, T., Tantai, A.A., Spangenberg, J.E., 2014b. Late Mastrichtian-early Danian high-stress environments and delayed recovery linked to Deccan volcanism. *Cretac. Res.* 49, 63–82. <https://doi.org/10.1016/j.cretres.2014.01.002>.
- Punekar, J., Keller, G., Khozyem, H.M., Adatte, T., Font, E., Spangenberg, J., 2016. A multi-proxy approach to decode the end-Cretaceous mass extinction. *Palaeogeogr. Palaeoclimatol. Palaeoecol.* 441, 116–136. <https://doi.org/10.1016/j.palaeo.2015.08.025>.
- Quillévéré, F., Norris, R.D., Kroon, D., Wilson, P.A., 2008. Transient Ocean warming and shifts in carbon reservoirs during the early Danian. *Earth Planet. Sci. Lett.* 265, 600–615. <https://doi.org/10.1016/j.epsl.2007.10.040>.
- Renne, P.R., Sprain, C.J., Richards, M.A., Self, S., Vanderkluyzen, L., Pande, K., 2015. State shift in Deccan volcanism at the Cretaceous-Paleogene boundary, possibly induced by impact. *Science* 350, 76–78. <https://doi.org/10.1126/science.aac7549>.
- Renne, P.R., Arenillas, I., Arz, J.A., Vajda, V., Gilabert, V., Bermúdez, H.D., 2018. Multi-proxy record of the Chicxulub impact at the Cretaceous-Paleogene boundary from Gorgonilla Island, Colombia. *Geology* 46, 547–550. <https://doi.org/10.1130/G40224.1>.
- Richards, M.A., Alvarez, W., Self, S., Karlstrom, L., Renne, P.R., Manga, M., Sprain, C.J., Smit, J., Vanderkluyzen, L., Gibson, S.A., 2015. Triggering of the largest Deccan eruptions by the Chicxulub impact. *Bull. Geol. Soc. Am.* 127, 1507–1520. <https://doi.org/10.1130/B31167.1>.
- Ricotta, C., Podani, J., 2017. On some properties of the Bray-Curtis dissimilarity and their ecological meaning. *Ecol. Complex.* 31, 201–205. <https://doi.org/10.1016/j.ecocom.2017.07.003>.
- Robinson, N., Ravizza, G., Cocconi, R., Peucker-Ehrenbrink, B., Norris, R., 2009. A high-resolution marine <sup>187</sup>Os/<sup>188</sup>Os record for the late Mastrichtian: Distinguishing the chemical fingerprints of Deccan volcanism and the K-P impact event. *Earth Planet. Sci. Lett.* 281, 159–168. <https://doi.org/10.1016/j.epsl.2009.02.019>.
- Romein, A.J.T., 1977. Calcareous nannofossils from the Cretaceous/Tertiary boundary interval in the Barranco del Gredero (Caravaca, Prov. Murcia, SE Spain). *Proc. K. Ned. Akad. Wet. Ser. B* 80, 256–279.
- Schmidt, A., Skeffington, R.A., Thordarson, T., Self, S., Forster, P.M., Rap, A., Ridgwell, A., Fowler, D., Wilson, M., Mann, G.W., Wignall, P.B., Carslaw, K.S., 2016. Selective environmental stress from Sulphur emitted by continental flood basalt eruptions. *Nat. Geosci.* 9, 77–82. <https://doi.org/10.1038/ngeo2588>.
- Schoene, B., Samperton, K.M., Eddy, M.P., Keller, G., Adatte, T., Bowring, S.A., Khadri, S.F.R., Gertsch, B., 2015. U-Pb geochronology of the Deccan Traps and relation to the end-Cretaceous mass extinction. *Science* 347, 182–184. <https://doi.org/10.1126/science.aaa0118>.
- Schoene, B., Eddy, M.P., Samperton, K.M., Keller, C.B., Keller, G., Adatte, T., Khadri, S.F.R., 2019. U-Pb constraints on pulsed eruption of the Deccan Traps across the end-Cretaceous mass extinction. *Science* 363, 862–866. <https://doi.org/10.1126/science.aau2422>.
- Schoene, B., Eddy, M.P., Keller, C.B., Samperton, K.M., 2021. An evaluation of deccan traps eruption rates using geochronologic data. *Geochronology* 3, 181–198. <https://doi.org/10.5194/gchron-3-181-2021>.
- Schulte, P., Alegret, L., Arenillas, I., Arz, J.A., Barton, P.J., Bown, P.R., Bralower, T.J., Christeson, G.L., Claeys, P., Cockell, C.S., Collins, G.S., Deutsch, A., Goldin, T.J., Goto, K., Grajales-Nishimura, J.M., Grieve, R.A.F., Gulick, S.P.S., Johnson, K.R., Kiessling, W., Koeberl, C., Kring, D.A., MacLeod, K.G., Matsui, T., Melosh, J., Montanari, A., Morgan, J.V., Neal, C.R., Nichols, D.J., Norris, R.D., Pierazzo, E., Ravizza, G., Rebolledo-Vieyra, M., Reimold, W.U., Robin, E., Salge, T., Speijer, R.P., Sweet, A.R., Urrutia-Fucugauchi, J., Vajda, V., Whalen, M.T., Willumsen, P.S., 2010. The Chicxulub asteroid impact and mass extinction at the Cretaceous-Paleogene boundary. *Science* 327, 1214–1218. <https://doi.org/10.1126/science.1177265>.
- Self, S., Widdowson, M., Thordarson, T., Jay, A.E., 2006. Volatile fluxes during flood basalt eruptions and potential effects on the global environment: a Deccan perspective. *Earth Planet. Sci. Lett.* 248, 518–532. <https://doi.org/10.1016/j.epsl.2006.05.041>.
- Self, S., Jay, A.E., Widdowson, M., Keszthelyi, L.P., 2008. Correlation of the Deccan and Rajahmundry Trap lavas: are these the longest and largest lava flows on Earth? *J. Volcanol. Geotherm. Res.* 172, 3–19. <https://doi.org/10.1016/j.jvolgeores.2006.11.012>.
- Sepúlveda, J., Wendler, J.E., Summons, R.E., Hinrichs, K.U., 2009. Rapid resurgence of marine productivity after the Cretaceous-Paleogene mass extinction. *Science* 326, 129–132. <https://doi.org/10.1126/science.1176233>.
- Sepúlveda, J., Alegret, L., Thomas, E., Haddad, E., Cao, C., Summons, R.E., 2019. Stable Isotope Constraints on Marine Productivity across the Cretaceous-Paleogene Mass Extinction. *Paleoceanogr. Palaeoclimatology* 34, 1195–1217. <https://doi.org/10.1029/2018PA003442>.
- Sinnesael, M., Montanari, A., Cocconi, R., Frontalini, F., Gattacceca, J., Snoeck, C., Wegner, W., Koeberl, C., Morgan, L.E., De Winter, N.J., DePaolo, D.J., Claeys, P., 2019. Multiproxy Cretaceous-Paleogene boundary event stratigraphy: an Umbria-Marche basinwide perspective. *Geol. Soc. Am. Spec. Pap.* 542, 133–158. [https://doi.org/10.1130/2019.2542\(07\)](https://doi.org/10.1130/2019.2542(07)).
- Smit, J., 1982. Extinction and evolution of planktonic foraminifera after a major impact at the Cretaceous/Tertiary boundary. *Geol. Soc. Am. Spec. Pap.* 190, 329–352. <https://doi.org/10.1130/SPE190-p329>.
- Smit, J., 1999. The global stratigraphy of the Cretaceous-Tertiary boundary impact ejecta. *Annu. Rev. Earth Planet. Sci.* 27, 75–113. <https://doi.org/10.1146/annurev.earth.27.1.75>.
- Smit, J., 2004. The section of the Barranco del Gredero (Caravaca, SE Spain): a crucial section for the Cretaceous/Tertiary boundary impact extinction hypothesis. *J. Iber. Geol.* 31, 179–191. <https://doi.org/10.5209/JIGE.33967>.
- Smit, J., Hertogen, J., 1980. An extraterrestrial event at the Cretaceous-Tertiary boundary. *Nature* 285, 198–200. <https://doi.org/10.1038/285198a0>.
- Smit, J., Romein, A.J.T., 1985. A sequence of events across the Cretaceous-Tertiary boundary. *Earth Planet. Sci. Lett.* 74, 155–170. [https://doi.org/10.1016/0012-821X\(85\)90019-6](https://doi.org/10.1016/0012-821X(85)90019-6).
- Sosa-Montes de Oca, C., Rodríguez-Tovar, F.J., Martínez-Ruiz, F., 2016. Geochemical and isotopic characterization of trace fossil infillings: New insights on tracemaker activity after the K/Pg impact event. *Cretac. Res.* 57, 391–401. <https://doi.org/10.1016/j.cretres.2015.03.003>.
- Sprain, C.J., Renne, P.R., Clemens, W.A., Wilson, G.P., 2018. Calibration of chron C29r: New high-precision geochronologic and paleomagnetic constraints from the Hell Creek region. *Montana Bull. Geol. Soc. Am.* 130, 1615–1644. <https://doi.org/10.1130/B31890.1>.
- Sprain, C.J., Renne, P.R., Vanderkluyzen, L., Pande, K., Self, S., Mittal, T., 2019. The eruptive tempo of Deccan volcanism in relation to the Cretaceous-Paleogene boundary. *Science* 363, 866–870. <https://doi.org/10.1126/science.aav1446>.
- Stax, R., Stein, R., 1993. Long-term changes in the accumulation of organic carbon in Neogene sediments, Ontong Java Plateau. *Proc., Sci. Results, ODP, Leg 130*, 573–584. <https://doi.org/10.2973/odp.proc.sr.130.039.1993>.
- Steinthorsdóttir, M., Vajda, V., Pole, M., 2016. Global trends of pCO<sub>2</sub> across the Cretaceous-Paleogene boundary supported by the first Southern Hemisphere stomatal proxy-based pCO<sub>2</sub> reconstruction. *Palaeogeogr. Palaeoclimatol. Palaeoecol.* 464, 143–152. <https://doi.org/10.1016/j.palaeo.2016.04.033>.
- Thibault, N., Gardin, S., 2010. The calcareous nannofossil response to the end-Cretaceous warm event in the Tropical Pacific. *Palaeogeogr. Palaeoclimatol. Palaeoecol.* 291, 239–252. <https://doi.org/10.1016/j.palaeo.2010.02.036>.
- Thibault, N., Galbrun, B., Gardin, S., Minoletti, F., Le Callonnec, L., 2016. The end-Cretaceous in the southwestern Tethys (Elles, Tunisia): orbital calibration of paleoenvironmental events before the mass extinction. *Int. J. Earth Sci.* 105, 771–795. <https://doi.org/10.1007/s00531-015-1192-0>.
- Thibault, N., Minoletti, F., Gardin, S., 2018. Offsets in the early Danian recovery phase in carbon isotopes: evidence from the biometrics and phylogeny of the *Cruciplacolithus* lineage. *Rev. Micropaleontol.* 61, 207–221. <https://doi.org/10.1016/j.revmic.2018.09.002>.
- Tobin, T.S., Bitz, C.M., Archer, D., 2017. Modeling climatic effects of carbon dioxide emissions from Deccan Traps volcanic eruptions around the Cretaceous-Paleogene boundary. *Palaeogeogr. Palaeoclimatol. Palaeoecol.* 478, 139–148. <https://doi.org/10.1016/j.palaeo.2016.05.028>.
- Vandamme, D., Courtillot, V., Besse, J., Montigny, R., 1991. Paleomagnetism and age determinations of the Deccan traps (India): results of a Nagpur–Bombay traverse and review of earlier work. *Rev. Geophys. Space Phys.* 29, 159–190.

- Vellekoop, J., Sluijs, A., Smit, J., Schouten, S., Weijers, J.W.H., Sinninghe Damsté, J.S., Brinkhuis, H., 2014. Rapid short-term cooling following the Chicxulub impact at the Cretaceous-Paleogene boundary. *Proc. Natl. Acad. Sci. U. S. A.* 111, 7537–7541. <https://doi.org/10.1073/pnas.1319253111>.
- Vellekoop, J., Esmeray-Senlet, S., Miller, K.G., Browning, J.V., Sluijs, A., van de Schootbrugge, B., Sinninghe Damsté, J.S., Brinkhuis, H., 2016. Evidence for Cretaceous-Paleogene boundary bolide “impact winter” conditions from New Jersey, USA. *Geology* 44. <https://doi.org/10.1130/G37961.1>.
- Vellekoop, J., Woelders, L., van Helmond, N.A.G.M., Galeotti, S., Smit, J., Slomp, C.P., Brinkhuis, H., Claey, P., Speijer, R.P., 2018. Shelf hypoxia in response to global warming after the Cretaceous-Paleogene boundary impact. *Geology* 46, 683–686. <https://doi.org/10.1130/G45000.1>.
- Wade, B.S., Pearson, P.N., Berggren, W.A., Pälike, H., 2011. Review and revision of Cenozoic tropical planktonic foraminiferal biostratigraphy and calibration to the geomagnetic polarity and astronomical time scale. *Earth-Science Rev.* 104, 111–142. <https://doi.org/10.1016/j.earscirev.2010.09.003>.



#### **4.5 Contribution of orbital forcing and Deccan volcanism to global climatic and biotic changes across the KPB at Zumaia, Spain**

**Gilbert, V., Batenburg, S.J., Arenillas.I., Arz, J.A., 2021.** Contribution of orbital forcing and Deccan volcanism to global climatic and biotic changes across the KPB at Zumaia, Spain. *Geology*. <https://doi.org/10.1130/G49214.1>. Publicado online como *Early Publication* el 30 de Agosto del 2021 (pendiente de asignación de volumen)  
El material suplementario de este artículo se encuentra en el apartado Anexos (Anexo IV).

# Contribution of orbital forcing and Deccan volcanism to global climatic and biotic changes across the Cretaceous-Paleogene boundary at Zumaia, Spain

Vicente Gilabert<sup>1</sup>, Sietske J. Batenburg<sup>2</sup>, Ignacio Arenillas<sup>1</sup> and José A. Arz<sup>1</sup>

<sup>1</sup>Departamento de Ciencias de la Tierra–Instituto Universitario de Investigación en Ciencias Ambientales de Aragón (IUCA), Universidad de Zaragoza, E-50009 Zaragoza, Spain

<sup>2</sup>Departament de Dinàmica de la Terra i de l'Oceà, Facultat de Ciències de la Terra, Universitat de Barcelona, 08028 Barcelona, Spain

## ABSTRACT

Untangling the timing of the environmental effects of Deccan volcanism with respect to the Chicxulub impact is instrumental to fully assessing the contributions of both to climate change over the Cretaceous-Paleogene boundary (KPB) interval. Despite recent improvements in radiometric age calibrations, the accuracy of age constraints and correlations is insufficient to resolve the exact mechanisms leading to environmental and climate change in the 1 m.y. across the KPB. We present new high-resolution planktic foraminiferal, geochemical, and geophysical data from the Zumaia section (Spain), calibrated to an updated orbitally tuned age model. We provide a revised chronology for the major carbon isotope excursions (CIEs) and planktic foraminiferal events and test temporal relationships with different models of the eruptive phases of the Deccan Traps. Our data show that the major CIEs near the KPB, i.e., the late Maastrichtian warming event (66.25–66.10 Ma) and the Dan-C2 event (65.8–65.7 Ma), are synchronous with the last and the first 405 k.y. eccentricity maximum of the Maastrichtian and the Danian, respectively, and that the minor Lower C29n event (65.48–65.41 Ma) is well constrained to a short eccentricity maximum. Conversely, we obtained evidence of abrupt environmental change likely related to Deccan volcanism at ca. 65.9 Ma, based on a bloom of opportunistic triserial guembeltriiids (*Chiloguembeltria*). The orbital, isotopic, and paleobiological temporal relationships with Deccan volcanism established here provide new insights into the role of Deccan volcanism in climate and environmental change in the 1 m.y. across the KPB.

## INTRODUCTION

The Cretaceous-Paleogene boundary (KPB) is one of the best-documented intervals in Earth's history and yet remains a subject of intensive research (Hull et al., 2020). Episodes of global climatic change during the ~1 m.y. across the KPB include, among others, the Late Maastrichtian Warming Event (LMWE) and the Danian Dan-C2 event. The LMWE is associated with a transient 2°–5° C global warming ~150–300 k.y. prior to the KPB (Woelders et al., 2017), and the Dan-C2 event with a 4° C sea-surface temperature rise ~200–300 k.y. after the KPB (Quillévéré et al., 2008). Recent improvements in radiometric dating (<sup>40</sup>Ar/<sup>39</sup>Ar and U-Pb) of Deccan volcanism (Schoene et al.,

2019; Sprain et al., 2019) suggest causal links between Deccan activity and climatic perturbations around the KPB (Barnet et al., 2018; Krahl et al., 2020). However, uncertainties in correlation mean that the timing of Deccan volcanism and its climatic effects over the KPB interval are still under intense discussion (e.g., Hull et al., 2020; Keller et al., 2020). Complete and expanded climate-sensitive archives with detailed age control are crucial to provide new insights into this classic problem.

The Zumaia outcrop in northwestern Spain (Fig. 1) is an auxiliary section for the Global Boundary Stratotype Section and Point (GSSP) for the base of the Danian (Molina et al., 2009). The KPB at Zumaia is marked by an altered

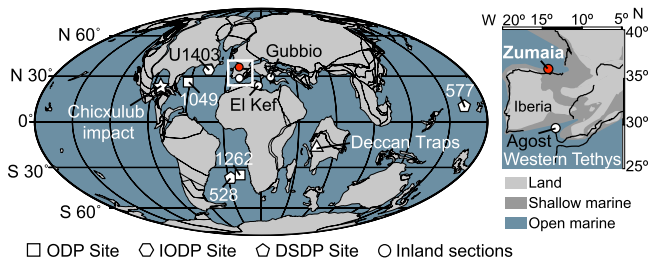
microtektite-rich airfall layer overlain by a 9-cm-thick blackish clay bed, which together form the KPB clay (Figs. S1B–S1E in the Supplemental Material<sup>1</sup>), separating the rhythmic marl-limestone alternations of Maastrichtian and Danian ages. The exceptional and cyclic exposure of the Zumaia outcrop (Fig. S1A) forms the basis of cyclostratigraphic age models (e.g., Batenburg et al. [2012] for the Maastrichtian, and Dinarès-Turell et al. [2014] for the Paleocene). We present integrated Maastrichtian and Danian astrochronologies over a 1-m.y.-long interval, providing ages for paleobiological and paleoclimate events identified in new high-resolution micropaleontological, geochemical, and geophysical data. Detailed age control of episodes of climate change during the KPB interval, i.e., the LMWE, Dan-C2, and the Lower C29n (LC29n) events, allows us to test to what degree Deccan volcanism and orbital forcing contributed to environmental change.

## METHODS AND AGE MODEL

We collected 171 rock samples in the 24.5-m-thick interval across the KPB at Zumaia for micropaleontological, geochemical, and geophysical analyses. Carbon isotope ( $\delta^{13}\text{C}$ ), calcium carbonate ( $\text{CaCO}_3$ ), magnetic susceptibility ( $\chi$ ), and foraminiferal analyses followed standard procedures.  $\delta^{13}\text{C}$  data were calibrated to the in-house NOCZ Carrara marble standard, showing analytical precision better than  $\pm 1\sigma$  ( $<0.1\text{‰}$  Vienna Pee Dee belemnite [VPDB]). See Text S1 in the Supplemental Material for detailed methods.

Our age model was constructed by correlating to the stable 405 k.y. component of long

<sup>1</sup>Supplemental Material. Text S1 (detailed methodology), Text S2 (geochemical and geophysical properties), Text S3 (detailed age models), Text S4 (further evidence of the stratigraphic continuity across the KPB at Zumaia), Tables S1–S5, and Figures S1–S5. Please visit <https://doi.org/10.1130/G49214.1> to access the supplemental material, and contact [editing@geosociety.org](mailto:editing@geosociety.org) with any questions.



**Figure 1. Paleogeographic reconstruction for the Cretaceous-Paleogene boundary (66 Ma), with localities cited in this study (after [https://www.odsn.de/odsn/services/paleomap/adv\\_map.html](https://www.odsn.de/odsn/services/paleomap/adv_map.html)). ODP—Ocean Drilling Program; IODP—International Ocean Discovery Program; DSDP—Deep Sea Drilling Project.**

eccentricity-modulated precession as identified by Batenburg et al. (2012) and Dinarès-Turell et al. (2014). The tie points for age calibration were the 405 k.y. maxima and minima extracted from the La2011 astronomical solution (Laskar et al., 2011) and a KPB age of 66.001 Ma (Dinarès-Turell et al., 2014). This age for the KPB differs from those of recent U-Pb and  $^{40}\text{Ar}/^{39}\text{Ar}$  dating efforts, which yielded results of  $66.016 \pm 0.05$  Ma (Schoene et al., 2019) and  $66.052 \pm 0.008/0.043$  Ma (Sprain et al., 2018), respectively, but falls within the uncertainties of these estimates. The stratigraphic position of the tie points is shown in Figure 2 and listed with ages in Table S1 in the Supplemental Material. We assume that each limestone-marlstone couplet represents a precession cycle, and the  $\text{CaCO}_3$  (%) and  $\chi$  ( $\text{m}^3/\text{kg}$ ) data support the identification of lithological alternations (Table S2; Fig. S2). Based on cosmic  $^3\text{He}$  sedimentation rates, the KPB clay spans the first  $\sim 10$  k.y. of the Danian (Mukhopadhyay et al., 2001), approximately half of a precession cycle. According to the 405 k.y. cyclostratigraphic framework of Dinarès-Turell et al. (2014), the interval between the KPB and the first Danian eccentricity minimum ( $\sim 50$  cm above the KPB) spans 34 k.y., which is compatible with the 1.5 precession cycles estimated here (Fig. 2). Calibrated ages assigned to each sample were linearly interpolated within each precession cycle between the tie points. This method has allowed us to account for large, orbitally driven changes in sedimentation rate in the Zumaia section, providing a detailed age calibration of the recognized paleobiological and paleoclimatic events in the 1 m.y. across the KPB (Table S2). Detailed methods, age model data, and stratigraphy are provided in Texts S1–S4.

## RESULTS

### Calibration of Planktic Foraminiferal Events

At Zumaia, the lowest occurrence datum (LOD) of *Plummerita hantkeninoides*, the index species of Biozone CF1, is at  $-4.55$  m (Fig. 2; Fig. S3; Table S3), i.e., 99 k.y. prior to the KPB. After intensive study, we recognized the LODs of the index species *Parvularugoglobigerina longiapertura*, *P. eugubina*, *Eoglobigerina simplicissima*, *Parasubbotina pseudobulloides*,

*Subbotina triloculinoides*, and *Globanomalina compressa* at 6, 23, 37, 100, 330, and 655 cm above the KPB, respectively (Fig. 2; Fig. S3; Table S4); i.e., 7, 18, 26, 68, 210, and 473 k.y. after the KPB, respectively. These datums mark the bases of the lower Danian biozones of Arenillas et al. (2004). Their equivalence with biozones P0, P $\alpha$ , P1a, P1b, and P1c of Wade et al. (2011) is shown in Figure 2.

The planktic foraminiferal assemblages remained relatively stable at Zumaia during the last  $\sim 400$  k.y. of the late Maastrichtian (Fig. S4), with only a minor and transient assemblage reorganization related to an increase in *Heterohelix* abundance ( $\sim 50\%$  to  $65\%$ – $80\%$ ) from 11 to 7.5 m below the KPB ( $\sim 250$ – $150$  k.y. prior to the KPB). Conversely, the lower Danian oligotaxitic assemblages are characterized by a rapid succession of planktic foraminiferal acme stages (PFAS of Arenillas et al., 2006) and blooms of opportunistic nannoplankton taxa (e.g., *Thoracosphaera*, *Braarudosphaera*, and *Neobiscutum*) (Bernaola et al., 2006, Table S2). We recognized PFAS-1 (acme of triserial *Guembelitra*) from the KPB up to 6 cm; PFAS-2 (acme of tiny trochospiral *Parvularugoglobigerina* and *Palaeoglobigerina*) from 6 to 55 cm; and PFAS-3 (acme of biserial *Woodringina* and *Chiloguembelina*) from 55 cm upward. A second bloom of triserial guembelitriids (*Chiloguembelitra*) is recognized in PFAS-3 from 195 to 400 cm (Table S4). According to our age model, the bases of the three main PFASs (1, 2, and 3) are calibrated to 0, 7, and 42 k.y. after the KPB, respectively, and the *Chiloguembelitra* bloom to 110 to 282 k.y.

### Calibration of Carbon Isotope Excursions (CIEs)

In the upper Maastrichtian of Zumaia, the main decrease in  $\delta^{13}\text{C}$  is recorded between 11.05 and 4.75 m ( $\sim 250$  and 100 k.y.) below the KPB, showing a distinctive gradual shift to the lowest  $\delta^{13}\text{C}$  values of the studied section, except for those reached at the KPB (Fig. 3C). From 55 cm (42 k.y.) above the KPB upward,  $\delta^{13}\text{C}$  shows an overall trend to lower isotopic values, interrupted by two distinctive negative CIEs (Fig. 3C). The first, with the shape of a double spike, is recorded between 3.15 and 4.30 m ( $\sim 200$  and 305 k.y.) above the KPB, and the

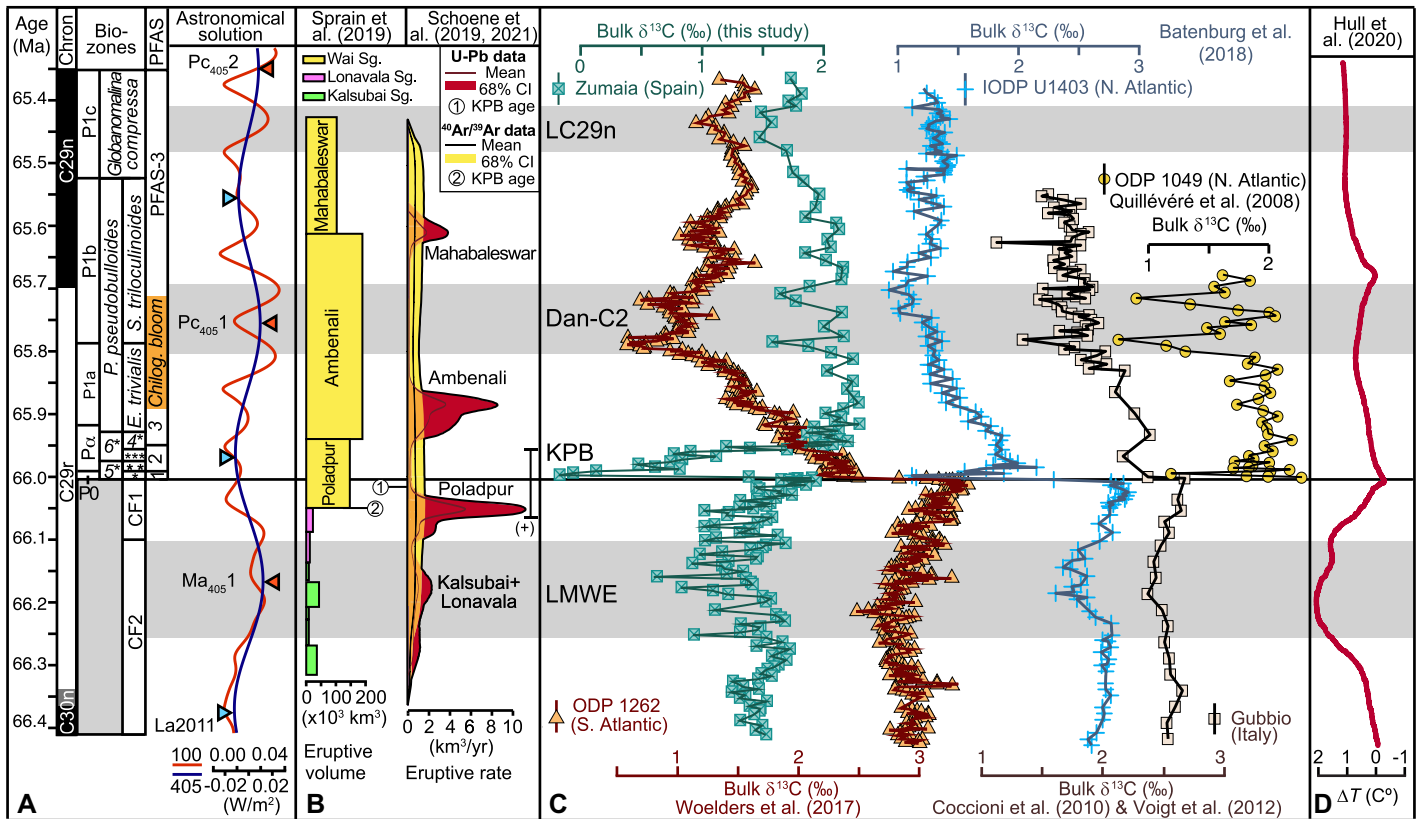
second between 7.1 and 7.9 m ( $\sim 520$  and 595 k.y.). We suggest that these isotopic events recognized at Zumaia correspond to the LMWE, Dan-C2, and LC29n events reported at Gubbio, Italy (Tethys; Coccioni et al., 2010; Voigt et al., 2012), Ocean Drilling Program (ODP) Site 1049 and International Ocean Discovery Program (IODP) Site U1403 (North Atlantic; Quillévéré et al., 2008; Batenburg et al., 2018), and ODP Site 1262 (South Atlantic; Woelders et al., 2017), confirming the global character of these carbon-cycle perturbations (Figs. 1 and 3).

## DISCUSSION AND CONCLUSION

To investigate the potential impact of volcanism, we focus on changes in carbon-cycle and climatic events before and after the KPB boundary, excluding the Chicxulub asteroid-induced KPB event. The astronomically calibrated  $\delta^{13}\text{C}$  record of Zumaia is compared in Figure 3 to those of other reference sites and sections from the Atlantic and Tethys Oceans and to the main period of Deccan Traps eruptions according to the models of Schoene et al. (2019) and Sprain et al. (2019). The LMWE, calibrated here to an age of 66.25–66.10 Ma, coincides with a minor eruptive phase of the Deccan Traps (Kalsubai and Lonavala subgroups) in both eruptive models (Fig. 3B). Recent carbon and  $\text{CO}_2$  estimations from Deccan outgassing suggest that this phase could have outgassed more  $\text{CO}_2$  than the main eruptive phases of the Wai subgroup, but this would still have been insufficient to explain the amplitude of LMWE warming (Hernandez Nava et al., 2021). However, both warming (Hull et al., 2020; Fig. 3D) and carbon-cycle changes follow the rhythm of long eccentricity (405 k.y. periodicity). The peak perturbation of the LMWE occurs at the eccentricity maximum  $\text{Ma}_{405.1}$  (Figs. 3A and 3C), rather than preceding it as suggested by Barnet et al. (2018), coinciding with increased amplitudes of orbital forcing and seasonality. We hypothesize that raised  $\text{CO}_2$  levels through Deccan outgassing during the late Maastrichtian may have amplified climate sensitivity to orbital forcing, resulting in the enhanced global climatic response of the LMWE. Similarly, late Paleocene–early Eocene hyperthermals have been linked to 405 k.y. eccentricity maxima during the emplacement of the North Atlantic igneous province (Barnet et al., 2019).

From the LMWE to the KPB, a gradual cooling is recognized worldwide (Woelders et al., 2017; Barnet et al., 2018; Hull et al., 2020). This pre-KPB cooling did not cause substantial changes in the foraminiferal assemblages of Zumaia, except for the extinction of *Archaeoglobigerina cretacea* (Fig. 2; Fig. S3). This points to planktic foraminiferal evolutionary and environmental stability during the latest Maastrichtian, as previously suggested (Gilbert et al., 2021a, and references therein). At





**Figure 3. Temporal correlation of planktic foraminiferal biozones and acme stages (PFAS) with the La2011 astronomical solution (Laskar et al., 2011) (A), Deccan eruptive models (B), bulk  $\delta^{13}C$  curves in several open-ocean localities on independent age models (C), and global temperature change across Cretaceous-Paleogene boundary (KPB) (D). Chron C29r-C30n and C29r-C29n reversals are based, respectively, on Batenburg et al. (2012) and Dinarès-Turell et al. (2014). \*—*Muricohedbergella holmdelensis*; \*\*—*Parvularugoglobigerina longiapertura*; \*\*\*—*Parvularugoglobigerina sabina*; 4\*—*Eoglobigerina simplicissima*; 5\*—*Guembelitra cretacea*; 6\*—*Parvularugoglobigerina eugubina*; E.—*Eoglobigerina*; S.—*Subbotina*; P.—*Parasubbotina*; Chilog.—*Chiloguembelitra*; Sg.—subgroup; colored triangles—405 k.y. eccentricity tie points; Pc<sub>405</sub>2, Pc<sub>405</sub>1—Paleocene eccentricity maxima 1 and 2; Ma<sub>405</sub>1—Maastrichtian eccentricity maximum 1; LMWE—late Maastrichtian warming event;  $\Delta T$ —temperature variation; (+)—uncertainty range for KPB within Deccan Traps, taken from Schoene et al. (2021); CI—confidence interval.**

We hypothesize that the massive input of nutrients to the surface ocean due to effusive Deccan volcanism may have been a stressor for pelagic ecosystems starting ~90 k.y. before the Dan-C2 event. The residence time of nutrients in the surface ocean may have been longer in the Danian due to the reduction in the efficiency of the biological pump (Birch et al., 2016), which could have allowed for a worldwide proliferation of opportunistic taxa in the open ocean for longer time intervals. Nonetheless, the absence of global changes in temperature and the carbon cycle prior to the Dan-C2 event suggests that orbital forcing was required to exacerbate the effect of long-term CO<sub>2</sub> emissions of Deccan volcanism during the Dan-C2 event. Our integrated stratigraphic results from Zumaia thus explain why the eruptive events of the Deccan Traps left a pronounced climatic signature only when they coincided with times of enhanced orbital forcing.

#### ACKNOWLEDGMENTS

We thank A. Gale and two anonymous reviewers for their constructive reviews. This work was supported by the Ministerio de Ciencia, Innovación y

Universidades (MCIU) / Agencia Estatal de Investigación (AEI) / Fondo Europeo de Desarrollo Regional (FEDER) (grant PGC2018-093890-B-I00), and by the Aragonese Government/FEDER (grant DGA group E33\_20R). V. Gilabert is supported by the Spanish Ministry of Economy and Competitiveness (MINECO) (FPI grant BES-2016-077800). We thank S.A. Robinson, A. Hilario, J.C. Larrasoña, and the Basque Coast UNESCO Global Geopark for support, and R. Glasgow for improving the English text. This research is part of the Ph.D. thesis of V. Gilabert.

#### REFERENCES CITED

Arenillas, I., Arz, J.A., and Molina, E., 2004, A new high-resolution planktic foraminiferal zonation and subzonation for the lower Danian: *Lethaia*, v. 37, p. 79–95, <https://doi.org/10.1080/00241160310005097>.  
 Arenillas, I., Arz, J.A., Grajalés-Nishimura, J.M., Murillo-Muñetón, G., Alvarez, W., Camarero-Zanoguera, A., Molina, E., and Rosales-Domínguez, C., 2006, Chicxulub impact event is Cretaceous/Paleogene boundary in age: New micropaleontological evidence: *Earth and Planetary Science Letters*, v. 249, p. 241–257, <https://doi.org/10.1016/j.epsl.2006.07.020>.  
 Arenillas, I., Arz, J.A., and Gilabert, V., 2018, Blooms of aberrant planktic foraminifera across the K/Pg boundary in the Western Tethys: Causes and evolutionary implications: *Paleobiology*, v. 44, p. 460–489, <https://doi.org/10.1017/pab.2018.16>.

Barnet, J.S.K., Littler, K., Kroon, D., Leng, M.J., Westerhold, T., Röhl, U., and Zachos, J.C., 2018, A new high-resolution chronology for the late Maastrichtian warming event: Establishing robust temporal links with the onset of Deccan volcanism: *Geology*, v. 46, p. 147–150, <https://doi.org/10.1130/G39771.1>.  
 Barnet, J.S.K., Littler, K., Westerhold, T., Kroon, D., Leng, M.J., Bailey, I., Röhl, U., and Zachos, J.C., 2019, A high-fidelity benthic stable isotope record of late Cretaceous–early Eocene climate change and carbon-cycling: *Paleoceanography and Paleoclimatology*, v. 34, p. 672–691, <https://doi.org/10.1029/2019PA003556>.  
 Batenburg, S.J., et al., 2012, Cyclostratigraphy and astronomical tuning of the Late Maastrichtian at Zumaia (Basque country, Northern Spain): *Earth and Planetary Science Letters*, v. 359–360, p. 264–278, <https://doi.org/10.1016/j.epsl.2012.09.054>.  
 Batenburg, S.J., et al., 2018, Late Maastrichtian carbon isotope stratigraphy and cyclostratigraphy of the Newfoundland Margin (Site U1403, IODP Leg 342): *Newsletters on Stratigraphy*, v. 51, p. 245–260, <https://doi.org/10.1127/nos/2017/0398>.  
 Bernaola, G., Baceta, J.I., Payros, A., Orue-Etxebarria, X., and Apellaniz, E., eds., 2006, *The Paleocene and lower Eocene of the Zumaia section (Basque Basin): Climate and Biota of the Early Paleo-*

- gene 2006, Post Conference Field Trip Guidebook: Bilbao, Spain, University of the Basque Country, 82 p.
- Birch, H.S., Coxall, H.K., Pearson, P.N., Kroon, D., and Schmidt, D.N., 2016, Partial collapse of the marine carbon pump after the Cretaceous-Paleogene boundary: *Geology*, v. 44, p. 287–290, <https://doi.org/10.1130/G37581.1>.
- Canudo, J.I., Keller, G., and Molina, E., 1991, Cretaceous/Tertiary boundary extinction pattern and faunal turnover at Agost and Caravaca, S.E. Spain: *Marine Micropaleontology*, v. 17, p. 319–341, [https://doi.org/10.1016/0377-8398\(91\)90019-3](https://doi.org/10.1016/0377-8398(91)90019-3).
- Coccioni, R., Frontalini, F., Bancalà, G., Fornaciari, E., Jovane, L., and Sprovieri, M., 2010, The Dan-C2 hyperthermal event at Gubbio (Italy): Global implications, environmental effects, and cause(s): *Earth and Planetary Science Letters*, v. 297, p. 298–305, <https://doi.org/10.1016/j.epsl.2010.06.031>.
- Coccioni, R., Bancalà, G., Catanzariti, R., Fornaciari, E., Frontalini, F., Giusberti, L., Jovane, L., Luciani, V., Savian, J., and Sprovieri, M., 2012, An integrated stratigraphic record of the Paleocene–lower Eocene at Gubbio (Italy): New insights into the early Paleogene hyperthermals and carbon isotope excursions: *Terra Nova*, v. 24, p. 380–386, <https://doi.org/10.1111/j.1365-3121.2012.01076.x>.
- D'Hondt, S., and Keller, G., 1991, Some patterns of planktic foraminiferal assemblage turnover at the Cretaceous-Tertiary boundary: *Marine Micropaleontology*, v. 17, p. 77–118, [https://doi.org/10.1016/0377-8398\(91\)90024-Z](https://doi.org/10.1016/0377-8398(91)90024-Z).
- Dinarès-Turell, J., Westerhold, T., Pujalte, V., Röhl, U., and Kroon, D., 2014, Astronomical calibration of the Danian stage (Early Paleocene) revisited: Settling chronologies of sedimentary records across the Atlantic and Pacific Oceans: *Earth and Planetary Science Letters*, v. 405, p. 119–131, <https://doi.org/10.1016/j.epsl.2014.08.027>.
- Fendley, I.M., et al., 2020, No Cretaceous-Paleogene boundary in exposed Rajahmundry Traps: A refined chronology of the longest Deccan lava flows from  $^{40}\text{Ar}/^{39}\text{Ar}$  dates, magnetostratigraphy, and biostratigraphy: *Geochemistry Geophysics Geosystems*, v. 21, e2020GC009149, <https://doi.org/10.1029/2020GC009149>.
- Gilbert, V., Arz, J.A., Arenillas, I., Robinson, S.A., and Ferrer, D., 2021a, Influence of the Latest Maastrichtian Warming Event on planktic foraminiferal assemblages and ocean carbonate saturation at Caravaca, Spain: *Cretaceous Research*, v. 125, 104844, <https://doi.org/10.1016/j.cretres.2021.104844>.
- Gilbert, V., Arenillas, I., Arz, J.A., Batenburg, S.J., and Robinson, S.A., 2021b, Multiproxy analysis of paleoenvironmental, paleoclimatic and paleoceanographic changes during the early Danian in the Caravaca section (Spain): *Palaeogeography, Palaeoclimatology, Palaeoecology*, v. 576, 110513, <https://doi.org/10.1016/j.palaeo.2021.110513>.
- Hernandez Nava, A., Black, B.A., Gibson, S.A., Bodnar, R.J., Renne, P.R., and Vanderkluyzen, L., 2021, Reconciling early Deccan Traps CO<sub>2</sub> outgassing and pre-KPB global climate: *Proceedings of the National Academy of Sciences of the United States of America*, v. 118, e2007797118, <https://doi.org/10.1073/pnas.2007797118>.
- Hull, P.M., et al., 2020, On impact and volcanism across the Cretaceous–Paleogene boundary: *Science*, v. 367, p. 266–272, <https://doi.org/10.1126/science.aay5055>.
- Keller, G., et al., 2020, Mercury linked to Deccan Traps volcanism, climate change and the end-Cretaceous mass extinction: *Global and Planetary Change*, v. 194, 103312, <https://doi.org/10.1016/j.gloplacha.2020.103312>.
- Krahl, G., Bom, M.H.H., Kochhann, K.G.D., Souza, L.V., Savian, J.F., and Fauth, G., 2020, Environmental changes occurred during the Early Danian at the Rio Grande Rise, South Atlantic Ocean: *Global and Planetary Change*, v. 191, 103197, <https://doi.org/10.1016/j.gloplacha.2020.103197>.
- Laskar, J., Gastineau, M., Delisle, J.-B., Farrés, A., and Fienga, A., 2011, Strong chaos induced by close encounters with Ceres and Vesta: *Astronomy and Astrophysics*, v. 532, L4, <https://doi.org/10.1051/0004-6361/201117504>.
- Li, L., and Keller, G., 1998, Maastrichtian climate, productivity and faunal turnovers in planktic foraminifera in South Atlantic DSDP sites 525A and 21: *Marine Micropaleontology*, v. 33, p. 55–86, [https://doi.org/10.1016/S0377-8398\(97\)00027-3](https://doi.org/10.1016/S0377-8398(97)00027-3).
- Molina, E., Alegret, L., Arenillas, I., Arz, J.A., Gallala, N., Grajales-Nishimura, J.M., Murillo-Muñetón, G., and Zaghbib-Turki, D., 2009, The Global Boundary Stratotype Section and Point for the base of the Danian Stage (Paleocene, Paleogene, “Tertiary”, Cenozoic): Auxiliary sections and correlation: *Episodes*, v. 32, p. 84–95, <https://doi.org/10.18814/epiugs/2009/v32i2/002>.
- Mukhopadhyay, S., Farley, K.A., and Montanari, A., 2001, A short duration of the Cretaceous-Tertiary boundary event: Evidence from extraterrestrial helium-3: *Science*, v. 291, p. 1952–1955, <https://doi.org/10.1126/science.291.5510.1952>.
- Quillévéré, F., Norris, R.D., Kroon, D., and Wilson, P.A., 2008, Transient ocean warming and shifts in carbon reservoirs during the early Danian: *Earth and Planetary Science Letters*, v. 265, p. 600–615, <https://doi.org/10.1016/j.epsl.2007.10.040>.
- Schoene, B., Eddy, M.P., Samperton, K.M., Keller, C.B., Keller, G., Adatte, T., and Khadri, S.F.R., 2019, U-Pb constraints on pulsed eruption of the Deccan Traps across the end-Cretaceous mass extinction: *Science*, v. 363, p. 862–866, <https://doi.org/10.1126/science.aau2422>.
- Schoene, B., Eddy, M.P., Keller, C.B., and Samperton, K.M., 2021, An evaluation of Deccan Traps eruption rates using geochronologic data: *Geochronology*, v. 3, p. 181–198, <https://doi.org/10.5194/gchron-3-181-2021>.
- Simmesael, M., et al., 2019, Multiproxy Cretaceous-Paleogene boundary event stratigraphy: An Umbria-Marche basinwide perspective, *in* Koeberl, C. and Bice, D.M., eds., 250 Million Years of Earth History in Central Italy: Celebrating 25 Years of the Geological Observatory of Coldigioco: Geological Society of America Special Paper 542, p. 133–158, [https://doi.org/10.1130/2019.2542\(07\)](https://doi.org/10.1130/2019.2542(07)).
- Smit, J., and Romein, A.J.T., 1985, A sequence of events across the Cretaceous-Tertiary boundary: *Earth and Planetary Science Letters*, v. 74, p. 155–170, [https://doi.org/10.1016/0012-821X\(85\)90019-6](https://doi.org/10.1016/0012-821X(85)90019-6).
- Sprain, C.J., Renne, P.R., Clemens, W.A., and Wilson, G.P., 2018, Calibration of chron C29r: New high-precision geochronologic and paleomagnetic constraints from the Hell Creek region, Montana: *Geological Society of America Bulletin*, v. 130, p. 1615–1644, <https://doi.org/10.1130/B31890.1>.
- Sprain, C.J., Renne, P.R., Vanderkluyzen, L., Pande, K., Self, S., and Mittal, T., 2019, The eruptive tempo of Deccan volcanism in relation to the Cretaceous-Paleogene boundary: *Science*, v. 363, p. 866–870, <https://doi.org/10.1126/science.aav1446>.
- Voigt, S., Gale, A.S., Jung, C., and Jenkyns, H.C., 2012, Global correlation of upper Campanian–Maastrichtian successions using carbon-isotope stratigraphy: Development of a new Maastrichtian timescale: *Newsletters on Stratigraphy*, v. 45, p. 25–53, <https://doi.org/10.1127/0078-0421/2012/0016>.
- Wade, B.S., Pearson, P.N., Berggren, W.A., and Pälike, H., 2011, Review and revision of Cenozoic tropical planktonic foraminiferal biostratigraphy and calibration to the geomagnetic polarity and astronomical time scale: *Earth-Science Reviews*, v. 104, p. 111–142, <https://doi.org/10.1016/j.earscirev.2010.09.003>.
- Woelders, L., et al., 2017, Latest Cretaceous climatic and environmental change in the South Atlantic region: *Paleoceanography*, v. 32, p. 466–483, <https://doi.org/10.1002/2016PA003007>.

Printed in USA



***Capítulo 5.***  
***Discusión***



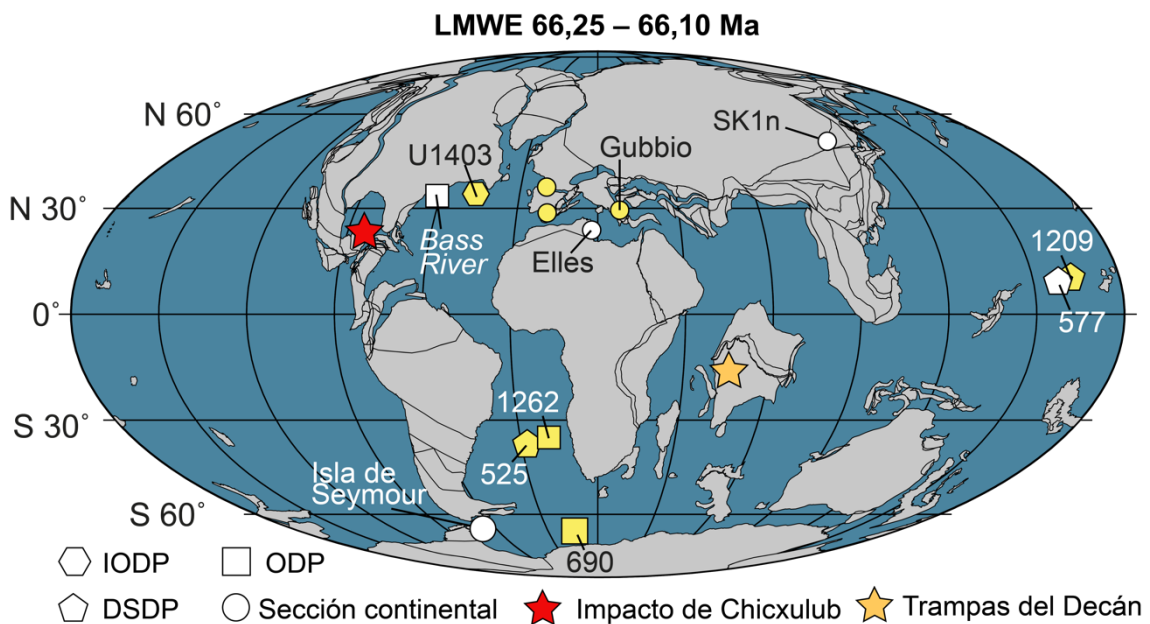


## 5. DISCUSIÓN

### 5.1 El evento de calentamiento del Maastrichtiense tardío (LMWE)

#### 5.1.1 Caracterización isotópica, calibración temporal y causas más probables

El llamado *Latest Maastrichtian Warming Event* (LMWE), que ocurrió entre ~150 y 300 ka antes del límite K/Pg, es considerado como el mayor episodio de calentamiento climático de todo el Maastrichtiense (Li y Keller, 1998b; MacLeod et al., 2005; Huber et al., 2018). Las curvas isotópicas del  $\delta^{18}\text{O}$  en foraminíferos bentónicos, en foraminíferos planctónicos y sobre roca total, y las curvas del  $\delta^{13}\text{C}$  en foraminíferos planctónicos y sobre roca total, se caracterizan en el LMWE por presentar una forma simétrica “en C” con un descenso y un ascenso gradual de los valores isotópicos (Gilabert et al., 2021a,c; Fig. 2). El  $\delta^{18}\text{O}$  y otros indicadores de paleotemperaturas, como el  $\text{TEX}_{86}$  o la relación Mg/Ca, indican un aumento de las temperaturas de entre 2 y 5 grados (Hull et al., 2020). Este calentamiento presenta un carácter global, evidenciado por el alto número y amplia distribución geográfica de las localidades en las que ha sido reconocido (Fig. 9).



**Figura 9.** Localización geográfica de las principales localidades donde se ha reportado el LMWE. En amarillo se han señalado los sondeos y secciones analizadas y correlacionadas en esta tesis doctoral (ver Gilabert et al., 2021a,c). SK1n = *Songke core 1* (norte).

El LMWE se ha reportado en secciones y sondeos terrestres, tanto de medios continentales, como los sondeos de Bass River en Norte América (Wilf et al., 2003) y de

Songke-1-norte (SK1n) en el Noreste de China (Zhang et al., 2018), como de medios marinos, como las secciones de Elles en Túnez (Thibault et al., 2016) y de la Isla de Seymour en el océano Antártico (Petersen et al., 2016). No obstante, este evento se ha identificado mayoritariamente en sondeos oceánicos entre los que destacan, por la información detallada que han proporcionado, el ODP 174 en el Atlántico Norte (Woelders et al., 2018), el DSDP 525A y el ODP1262 en el Atlántico Sur (Li y Keller, 1998b; Barnet et al., 2018), el ODP 690 en el Antártico (Stott y Kennet, 1990), y el ODP 1209 en el Pacífico central (Westerhold et al., 2011) (Fig. 9).

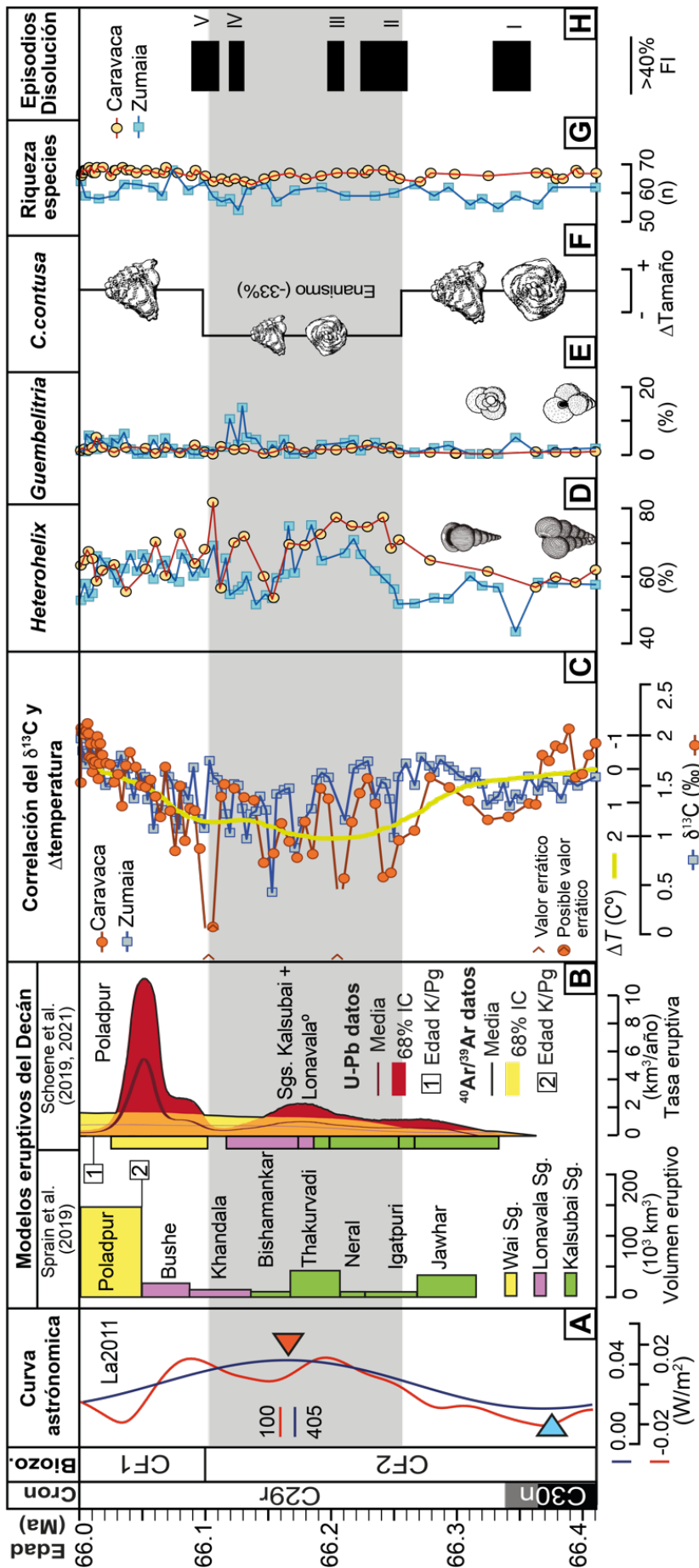
Tras analizar las evoluciones del  $\delta^{18}\text{O}$  y  $\delta^{13}\text{C}$  en Caravaca (Gilabert et al., 2021a) y del  $\delta^{13}\text{C}$  en Zumaia (Gilabert et al., 2021c), se pudo identificar por primera vez el LMWE en ambas secciones, mediante muestreos de alta resolución. Los registros isotópicos de Caravaca y Zumaia fueron comparados y correlacionados con los de otras localidades distribuidas en ambos hemisferios (Fig. 9). Para ello, se establecieron modelos de edad en ambas secciones, obteniendo resultados ligeramente diferentes para la edad y duración del LMWE. En Caravaca, se estimó una duración para el LMWE de  $\sim 210$  ka, tras ser datado mediante calibración magnetocronológica entre 310 y 100 ka antes del límite K/Pg (Gilabert et al., 2021a). Este artículo supuso un avance, ya que estudios previos estimaron una duración para el LMWE de  $> 300$  ka (Li y Keller, 1998b; Olsson et al., 2001; Abramovich et al., 2003; Petersen et al., 2016). En Zumaia, se calculó una duración para el LMWE de  $\sim 150$  ka, tras ser datado entre 250 y 100 ka antes del límite K/Pg mediante calibración astrocronológica (Gilabert et al., 2021c). Esta estimación es comparable con otras calibraciones astrocronológicas recientes de este evento (Thibault et al., 2016; Barnet et al., 2018). Por considerarlo más preciso, el modelo de edad obtenido en Zumaia se ha tomado como referencia en esta memoria para elaborar las Figs. 10 y 11, y para redactar el capítulo 5 de Discusión.

La similitud de los registros isotópicos del  $\delta^{13}\text{C}$  en Zumaia y Caravaca ha permitido establecer una correlación precisa entre ambos registros, tanto en el Maastrichtense más alto como en el Daniense. Utilizando el modelo de edad de Zumaia, se han recalibrado los eventos paleoambientales y paleobiológicos reconocidos en Caravaca (Anexo V; Tablas anexas 1, 2), actualizando el modelo de edad originalmente descrito en Gilabert et al. (2021a). Además, las curvas isotópicas en Zumaia y Caravaca pueden ser correlacionadas con bastante precisión con la curva que muestra la variación global de la temperatura propuesta por Hull et al. (2020), lo que indica que los cambios

paleoclimáticos identificados en ambas secciones siguen la tendencia climática global durante el tránsito K–Pg (Fig. 10).

Por otra parte, se ha considerado a menudo que el LMWE fue desencadenado por una desgasificación masiva en el Decán. Sin embargo, la relación causa-efecto entre ambos procesos (Thibault et al., 2016; Barnet et al., 2018; Keller et al., 2020; Gilabert et al., 2021a,c) no se pudo establecer hasta que no se mejoraron las dataciones radiométricas de las formaciones volcánicas del Decán (Renne et al., 2015; Schoene et al., 2015, 2019; Sprain et al., 2019). De acuerdo a estas dataciones, el LMWE se correlaciona cronológicamente con el emplazamiento de las formaciones volcánicas volumétricamente menores del Decán, es decir, aquellas que pertenecen a los Sgs. Kalsubai y Lonavala (Fig. 10A–C). Esto contradice la hipótesis previa que sugería que el LMWE estuvo relacionado con los mayores pulsos eruptivos del Decán (Chenet et al. 2008, Keller et al., 2012, Puneekar 2014a). Además, las recientes modelizaciones sobre el CO<sub>2</sub> procedente de la desgasificación masiva del Decán y el consecuente aumento de temperatura sugieren que el vulcanismo del Decán por si solo es insuficiente para explicar el calentamiento climático registrado durante el LMWE tal y como se ha propuesto recientemente (Hull et al., 2020; Hernandez Nava et al., 2021).

Un resultado importante de esta tesis doctoral es la correlación temporal directa que se ha establecido en Zumaia entre el LMWE, las variaciones orbitales de la curva astronómica y los episodios volcánicos del Decán (Fig. 10A–C). Esta correlación ha permitido relacionar el LMWE con el efecto climático combinado del vulcanismo del Decán y del forzamiento orbital. Según esta propuesta, la desgasificación masiva de CO<sub>2</sub> y de otros gases de efecto invernadero y su acumulación en la atmósfera durante el emplazamiento de los Sgs. Kalsubai y Lonavala potenciaron la sensibilidad climática ante los cambios orbitales de excentricidad larga (405 ka) de la Tierra, generando un mecanismo de retroalimentación positiva durante el LMWE que aumentó la temperatura a escala global (Fig. 10A–C). Esta hipótesis, propuesta por vez primera por Gilabert et al. (2021c), plantea un modelo alternativo que permite explicar el aumento de temperatura global observado en el LMWE, ya que las modelizaciones anteriores (Hull et al., 2020; Hernandez Nava et al., 2021), las cuales sólo tenían en cuenta el CO<sub>2</sub> volcanogénico emitido, no podían hacerlo. Esta hipótesis contradice por tanto los modelos previos que sugerían una relación causal más directa entre el LMWE y el vulcanismo del Decán, y que excluían el forzamiento orbital como factor del cambio climático (Barnet et al., 2018).



**Figura 10.** Marco de correlación temporal para el Maastrichtiense tardío: **A)** Biozonas de foraminíferos planctónicos y curva astronómica La 2011 (Laskar et al., 2011); **B)** Modelos eruptivos del Decán, y formaciones y subgrupos eruptivos del Decán; **C)** Variaciones del δ<sup>13</sup>C en Caravaca y Zumaia, correlacionadas según el mismo modelo de edad, junto a la curva del compendio de variación de temperatura global (ΔT) de Hull et al. (2020); **D)** Abundancia relativa (%) de *Heterohelix*; **E)** Abundancia relativa (%) de *Guembelitra*; **F)** Episodio de enanismo de *Contusotruncana contusa* en Caravaca; **G)** Variación de la riqueza específica; y **H)** Episodios de disolución. Biozon. = Biozona; FI = Índice de fragmentación.

5.1.2. Episodios de disolución del CaCO<sub>3</sub>

El análisis de las variaciones del índice de fragmentación a lo largo de los últimos 18 m del Maastrichtiense de Caravaca permitió establecer hasta cinco episodios (I-V) de elevada disolución de los carbonatos, los cuatro últimos dentro del intervalo estratigráfico en el que se ha registrado el LMWE (Gilabert et al., 2021a; Fig. 10H). En este trabajo se utilizó el umbral del 40% en el índice de fragmentación de las conchas de foraminíferos planctónicos para diferenciar un régimen de elevada disolución de carbonatos, tal como fue sugerido por Malgrem (1987) y Kucera et al. (1997). Los episodios de disolución identificados en Caravaca son comparables a otros reconocidos en distintas localidades durante el LMWE (Henehan et al., 2016; Batenburg et al., 2018; Gilabert et al., 2021a). En esta tesis doctoral se han interpretado como breves episodios de acidificación oceánica, probablemente causados por la desgasificación volcánica en el Decán y, en algunos casos, por configuraciones orbitales extremas. El modelo de edad disponible inicialmente para Caravaca (Gilabert et al., 2021a) impidió establecer una relación precisa entre los episodios de disolución y sus potenciales causas. Sin embargo, la recalibración de los episodios de disolución del LMWE en Caravaca según el modelo de edad de Zumaia (Gilabert et al., 2021c) ha permitido plantear que, al menos tres de ellos (I, II y IV) están probablemente relacionados genéticamente con el vulcanismo del Decán (Tabla 2).

Episodio de disolución	Edad (Ma)	Duración (ka)	Relación con V. Decán (1)	Relación con V. Decán (2)	Relación forzamiento orbital
V	66,11–66,09	~20	Final Fm. Khandala	Hiato eruptivo -inicio Fm. Poladpur	Máximo de excentricidad (P100)
IV	66,13–66,12	~10	Inicio Fm. Khandala	Final Fm. Khandala	–
III	66,21	<10	Inicio Fm. Thakurvadi	Final Fm. Thakurvadi	Máximo de excentricidad (P100)
II	66,26–66,23	~30	Emplazamiento Fm. Igatpuri	Transición Fm. Igatpuri - Neral	–
I	66,36–66,33	~30	Fase temprana del Decán*	Fase temprana* - Inicio Fm. Jawhar	–

**Tabla 2.** Propuesta de calibración temporal de los principales episodios de disolución y su relación con el vulcanismo del Decán y el forzamiento orbital. P100 = periodicidad de 100 ka (excentricidad corta). En azul aparecen marcados los causantes más probables de cada episodio de disolución. \* = Posiblemente relacionado con el emplazamiento de la provincia de Saurashtra al NW de la provincia principal del Decán (ver Hernandez Nava et al., 2021; Fig. 3). (1) Según Sprain et al. (2019); (2) Según Schoene et al. (2019).

Se llegó a esta conclusión tras correlacionar temporalmente los episodios de disolución del LMWE con la curva astronómica y los episodios volcánicos del Decán según los dos modelos eruptivos contemplados (mega-pulsos eruptivos o erupción casi-continua). No obstante, todavía es difícil determinar si el episodio I fue consecuencia del emplazamiento de las formaciones iniciales del Decán, como la Fm. Jawhar del Sg. Kalsubai (Fig. 10B,H), o si estuvo relacionado con una fase eruptiva anterior. En este sentido, se ha planteado que este primer episodio podría ser contemporáneo al emplazamiento de la Fm. Saurashtra, la cual aflora en la región homónima (Fig. 3 y Tabla 2) ya que de acuerdo a su datación  $^{40}\text{Ar}/^{39}\text{Ar}$ , antecede al emplazamiento del Sg. Kalsubai (Hernandez Nava et al., 2021). En cualquier caso, tanto la Fm. Saurashtra como las formaciones que componen los Sgs. Kalsubai y Lonavala se caracterizan por presentar los volúmenes y las tasas eruptivas más bajas de toda la secuencia eruptiva del Decán (Schoene et al., 2019; Sprain et al., 2019; Hernandez Nava et al., 2021; Fig. 10H). Sin embargo, hay evidencias de que estas erupciones tempranas fueron las que emitieron más  $\text{CO}_2$  de toda la historia eruptiva del Decán (Hernandez Nava et al. 2021). No obstante, esta hipótesis debe ser todavía contrastada y verificada.

En cuanto a los episodios III y V, es posible establecer un nexo temporal entre ellos y los dos máximos de excentricidad corta (100 ka) ocurridos durante el máximo de excentricidad larga (405 ka) que moduló el LMWE (Tabla 2 y Fig. 10A,H). Además, ambos coinciden con excursiones isotópicas del  $\delta^{13}\text{C}$  (Fig. 10C) y del  $\delta^{18}\text{O}$  (Gilabert et al., 2021a), lo que sugiere un escenario similar al de algunos eventos hipertermales del Paleoceno y Eoceno, en los cuales los máximos de excentricidad provocaron la liberación de  $\text{CO}_2$  enriquecido en  $^{12}\text{C}$  procedente de reservorios menores del carbono como la superficie oceánica, la atmósfera o los clatratos del fondo oceánico (Zachos et al., 2010). La rápida liberación de este  $\text{CO}_2$  no volcánogénico a la atmósfera pudo provocar un calentamiento climático similar durante el LMWE, y su absorción en las aguas oceánicas pudo ocasionar a su vez infrasaturación y disolución de los carbonatos. Esto último se evidencia también por enriquecimientos de Fe en los sedimentos oceánicos (Barnet et al., 2018; Batenburg et al., 2018) y aumentos del FI de foraminíferos planctónicos (Henehan et al., 2016; Gilabert et al., 2021a).

En resumen, tras la recalibración temporal de los episodios de disolución de Caravaca según el modelo de edad de Zumaia (Tabla 2), se sugiere que el emplazamiento de las formaciones basálticas menos voluminosas, pero más ricas en volátiles del Sg. Kalsubai fueron las causantes de la intensificación en la disolución de los carbonatos que

caracteriza los episodios I, II y IV, ya que estos no están relacionados con máximos de excentricidad corta. Por el contrario, el origen de los episodios III y V parece estar más relacionado con el forzamiento orbital en el rango de la excentricidad corta.

### 5.1.3. Influencia sobre las asociaciones de foraminíferos planctónicos

El LMWE no influyó de forma apreciable en la riqueza específica, ya que esta se mantuvo bastante estable en torno a 66 especies en Caravaca y a 59 en Zumaia (Fig. 10G) y no se produjo la extinción de ninguna especie (Gilabert et al., 2021a). A nivel cuantitativo, el cambio más destacable fue el aumento de la abundancia relativa del género *Heterohelix*, un taxón generalista y tolerante a condiciones de baja oxigenación al menos durante el Maastrichtiense tardío (Pardo y Keller, 2008). Este incremento se registra en ambas secciones durante la primera mitad del LMWE, entre ~66,25 y 66,17 Ma (Fig. 10C,D). La reducción de la cantidad de oxígeno disuelto en las capas de agua donde habitaban los foraminíferos planctónicos fue relacionado por Gilabert et al. (2021a) con el aumento de temperatura durante la primera fase de calentamiento del LMWE, ya que ambos factores están inversamente relacionados (Helm et al., 2011). El aumento en la temperatura durante el LMWE está bien reflejado en la curva de  $\Delta T$  de Hull et al. (2020), y permite correlacionarlo con un máximo de excentricidad larga (405 ka) coetáneo al aumento de la abundancia relativa de *Heterohelix* (Fig. 10A,C,D). En el punto en que la curva astronómica alcanza el máximo de excentricidad larga (Ma<sub>4051</sub>), la curva de  $\Delta T$  invierte su tendencia hacia un enfriamiento gradual. En este punto de inflexión (Fig. 10A,C), la abundancia de *Heterohelix* decrece rápidamente en ambas localidades hasta alcanzar valores similares a los previos al LMWE (Fig. 10D).

En esta tesis doctoral no se ha identificado durante el LMWE incremento alguno en la abundancia relativa de *Guembelitra*, un género oportunista e indicador de condiciones de estrés ambiental y de eutrofia (Kroon y Nederbragt, 1990; Abramovich y Keller, 2002; Pardo y Keller, 2008). La abundancia relativa promedio de *Guembelitra* durante el LMWE es muy baja (~1% en Caravaca y ~3% en Zumaia), y se mantiene bastante constante en el tiempo (Fig. 10D). Algunos autores han encontrado importantes episodios de apogeo de *Guembelitra* ligados al calentamiento del LMWE (Abramovich et al., 2010; Punekar et al., 2014a,b; Keller et al., 2016). Sin embargo, estos parecen estar restringidos a secciones de medios someros. Son estos medios donde las especies del género oportunista *Guembelitra* proliferan, debido a que las condiciones ambientales son más variables que en océano abierto y están fuera del rango de tolerancia del resto de especies



(Keller y Pardo, 2004; Pardo y Keller, 2008). También se han identificado además de *Guembelitra* similares en el Maastrichtiense superior de localidades próximas al Decán, debido probablemente a que presentaban condiciones locales en las aguas oceánicas superficiales de mayor estrés ambiental y eutrofia (Gertsch et al., 2011; Keller et al., 2012; Punekar et al., 2014a,b).

Otro efecto paleobiológico vinculado a los cambios paleoambientales del LMWE es una importante reducción en el tamaño de las conchas de *Contusotruncana contusa*, tal como se evidencia a partir de los análisis biométricos llevados a cabo en Caravaca. Este episodio de enanismo supuso una reducción promedio de su tamaño del ~33% (Fig. 10F), que pudo ser el resultado de una maduración sexual más temprana como adaptación a las condiciones de estrés ambiental (Gilabert et al., 2021a). Aunque no realizaron biometrías, Abramovich y Keller (2003) reportaron en el Atlántico Sur (DSDP 525A) episodios de enanismo equivalentes en varias especies de foraminíferos planctónicos.

En Caravaca no hay evidencias que sugieran cambios bruscos en los niveles de productividad y eutrofia coincidiendo con el LMWE. Por el contrario, la abundancia relativa de *Guembelitra* se mantiene baja y constante a lo largo de toda la sección (Fig. 10E). Por esta razón, el episodio de enanismo de *C. contusa* se ha asociado más bien a una reducción de su hábitat provocado por el incremento de la temperatura y la consiguiente reducción del gradiente térmico vertical entre las capas más superficiales y la más profundas. Los análisis isotópicos en conchas de foraminíferos realizados por Li y Keller (1998a) y Barnet et al. (2018) en los sondeos DSDP 525A y ODP 1262 (Atlántico Sur) también sugieren una debilitación del gradiente térmico de la columna de agua oceánica durante el LMWE.

Gilabert et al. (2021a) reconoció en Caravaca una reducción del índice P/S (profundos/superficiales) a la mitad (de 0.4 a 0.2) durante el LMWE. Esta reducción es compatible con un episodio de calentamiento climático, el cual pudo reducir la termoclina, perjudicando a las especies de hábitat profundo, y ampliar la capa de mezcla, lo que favoreció a las especies generalistas de hábitat superficial, como las de los heterohelícidos y trocoespiralados no carenados. El descenso del índice P/S durante el LMWE es paralelo a la reducción del tamaño de las conchas de *C. contusa* (Gilabert et al., 2021a, Fig. 10F). Ambos indicadores sugieren, por tanto, el mismo tipo de estrés ambiental, el cual se ha relacionado con una reducción del gradiente térmico vertical y la consiguiente pérdida temporal de nichos ecológicos profundos.

## 5.2. El enfriamiento progresivo en los últimos 100 ka del Maastrichtiense

Los últimos ~100 ka del Maastrichtiense se caracterizan, desde el punto de vista climático, por un rápido descenso de las temperaturas globales de entre ~2 a 5 °C respecto al LMWE, que implica un retorno a la tendencia general de enfriamiento global del Maastrichtiense (Stott y Kennett, 1990; Barrera, 1994; Li y Keller, 1998b; Wilf et al., 2003; Huber et al., 2018; Barnet et al., 2018; Hull et al., 2020). Los indicadores isotópicos y micropaleontológicos reflejan este retorno a las condiciones previas al LMWE tanto en Zumaia como en Caravaca (Gilabert et al., 2021a,c; Fig. 10). Este gradual enfriamiento climático finicretácico cuestiona el hipotético rol del vulcanismo del Decán en el clima de las últimas decenas de miles de años del Maastrichtiense. Según el modelo eruptivo de Schoene et al. (2019), entre ~100 y 30 ka antes del límite K/Pg se produjo de manera abrupta el mayor pulso volcánico del Decán, es decir, aquel que formó la Fm. Poladpur. Si este fue realmente el caso, debería haberse registrado en el Maastrichtiense tardío evidencias de un abrupto cambio climático y/o ambiental en vez de un enfriamiento gradual.

Según Gilabert et al (2021c), la Zona de *Plummerita hantkeninoides* abarca los últimos ~100 ka del Maastrichtiense, por lo que en esta biozona deberían haberse encontrado evidencias del emplazamiento de la Fm. Poladpur. Sin embargo, en Caravaca no se han identificado episodios de disolución de carbonatos relacionados con el pulso eruptivo Poladpur, salvo tal vez por la parte final del episodio V anteriormente descrito (Gilabert et al., 2021a; Fig. 10H). Por tanto, la hipótesis que relaciona la emisión de los basaltos de la Fm. Poladpur con una acidificación oceánica generalizada a finales del Maastrichtiense y un consiguiente deterioro de los ecosistemas pelágicos (Punekar et al., 2016; Font et al., 2018; Schoene et al. 2019; Keller et al., 2020) no ha podido ser corroborada en Caravaca. Esta hipótesis tampoco ha podido ser verificada en la curva de evolución del pH oceánico del Maastrichtiense tardío que Henehan et al. (2019) reportaron en Geulhemmerberg Cave (Países Bajos), Owl Creek y Brazos River (Estados Unidos), DSDP 465 y ODP 1209 (Pacífico), y ODP 1049 (Atlántico). En estas localidades, el pH oceánico se mantuvo también estable durante los últimos ~100 ka del Maastrichtiense.

Teniendo en cuenta los márgenes de error de la datación U-Pb de la Fm. Poladpur de Schoene et al. (2021), aunque son pequeños, aún cabe la posibilidad de que el mega-pulso eruptivo que la formó ocurriera tras el límite K/Pg. Si fue este el caso, esta datación aun

puede ser compatible con la hipótesis de Richards et al. (2015) de que el mega-pulso Poladpur fuera impulsado por el propio impacto de Chicxulub. Esta hipótesis explicaría por qué su señal isotópica y paleobiológica no se registra antes pero tampoco después del límite K/Pg, ya que pudo quedar enmascarada por los cambios climáticos y ambientales que provocó el impacto de Chicxulub. Por otro lado, en las últimas decenas de miles de años del Maastrichtiense no existió una configuración orbital propicia para maximizar el impacto climático asociado a la desgasificación del Decán, como había sucedido en el LMWE. En todo caso, si realmente el mega-pulso Poladpur tuvo lugar a finales del Maastrichtiense, parece que tuvo una influencia climática y paleobiológica muy pequeña. Desde el punto de vista micropaleontológico, solo se tradujo en una reorganización muy limitada de las asociaciones de foraminíferos planctónicos y en la extinción de *Archaeoglobigerina cretacea* (Gilabert et al., 2021a,c).

### 5.3. El evento del límite K/Pg.

#### 5.3.1 Definición y edad del límite Cretácico/Paleógeno

El GSSP de la base del Daniense o, lo que es lo mismo, del límite K/Pg se definió en la base de la capa de arcilla oscura en la localidad de El Kef (Cowie et al., 1989). Esta definición se impuso por votación con una aceptación del 75%, frente a la propuesta de otras localidades candidatas a albergar el GSSP (Brazos River, Stevns Klint y Zumaia) y frente a otros horizontes-guía como la base de la tsunamita, el primer registro del dinoflagelado *Danea californica*, y el máximo valor de contenido en iridio de la capa de arcilla. Sin embargo, la definición formal únicamente fue publicada en una nota breve en la revista *Episodes* y como parte del informe anual sobre las actividades de la Comisión Internacional de Estratigrafía (Cowie et al., 1989). No fue hasta 2006 cuando el presidente de la Subcomisión Internacional de Estratigrafía del Paleógeno lideró una publicación “en extenso” en la que se precisaba, de acuerdo a la descripción original, una definición inequívoca del GSSP de la base del Daniense y el criterio que debe seguirse para su correlación a escala global (Molina et al., 2006).

La base de la arcilla del límite K/Pg en El Kef se caracteriza por una capa de espesor milimétrico de color rojizo rica en iridio y en eyecta (vidrios de impacto, espinelas de níquel, cuarzos de choque). Sobre este nivel estratigráfico, que marca el límite K/Pg de acuerdo a su definición original, se depositó una capa de arcilla oscura de en torno a 50 cm de potencia, la cual muestra valores muy bajos de CaCO<sub>3</sub> y una excursión negativa de

~1 a 3‰ del  $\delta^{13}\text{C}$  en roca total y en foraminíferos planctónicos (Molina et al., 2006). Esta secuencia estratigráfica es fácilmente reconocible en todas aquellas secciones pelágicas distales a la estructura de impacto de Chicxulub que son continuas a través de límite K/Pg (Arenillas et al., 2006; Molina et al., 2009; Schulte et al., 2010), como es el caso de las estudiadas en esta tesis doctoral (Arenillas et al., 2018; Gilabert et al. 2021a,b,c).

Las dataciones del límite K/Pg varían en función de las técnicas de datación radiométrica usadas: según el método  $^{40}\text{Ar}/^{39}\text{Ar}$ , se ha datado entre  $66,038 \pm 0,025/0,049$  Ma (Renne et al., 2013) y en  $66,052 \pm 0,008/0,043$  Ma (Sprain et al., 2018); y según el método U-Pb, entre  $66,021 \pm 0,024/0,039$  Ma (Clyde et al., 2016) y  $66,016 \pm 0,050$  Ma (Schoene et al., 2019). Cualquiera de estas edades, con sus respectivos márgenes de error, son compatibles con la edad de referencia dada en la GTS 2020 (*Geological Time Scale 2020*; Gradstein et al., 2020), que es de 66,001 Ma, la cual está basada en calibraciones astrocronológicas realizadas en Zumaia y que se han basado en la excentricidad larga de 405 ka (Dinarés-Turell et al., 2014). Dado que tanto el modelo de edad de la GTS 2020 como el utilizado en la presente tesis doctoral se han basado en la sección de Zumaia, se ha considerado una edad para el límite K/Pg de 66,001 Ma.

### 5.3.2. Modelo de extinción y de supervivencia de los foraminíferos planctónicos

La alteración paleobiológica más destacable en el millón de años estudiados en esta tesis doctoral es sin lugar a dudas el evento de extinción masiva del límite K/Pg. Durante las últimas cuatro décadas, se han producido intensos debates entre los partidarios de un modelo de extinción masiva catastrófica, encabezados por Jan Smit (Smit, 1982), y los partidarios de un modelo de extinción masiva gradual, encabezados por Gerta Keller (Keller, 1988). Aunque no hay un consenso total, el modelo más ampliamente aceptado por la comunidad científica es el de una extinción masiva catastrófica, ya que es el que mejor se ajusta al registro bioestratigráfico de los foraminíferos planctónicos (Molina et al., 2006).

Las distribuciones estratigráficas de las especies a través del límite K/Pg, analizadas a partir de muestreos de alta resolución, confirman el modelo de extinción masiva catastrófica, tanto en El Kef (Anexo I, Supplementary Figure 4) como en Caravaca (Anexo II, Supplementary Table 1 y Anexo III, Supplementary Table 1) y Zumaia (Anexo IV, Supplementary Figure 3). Para evaluar la intensidad de la extinción, en esta tesis

doctoral se han planteado y comparado tres escenarios distintos en las tres secciones mencionadas (Tabla 3).

**Patrones de extinción en las asociaciones de foraminíferos planctónicos**

Sección	Sp <sup>1</sup>	Escenario 1		Escenario 2		Escenario 3	
		Sp <sup>2</sup>	Extinción (%)	Sp <sup>2</sup>	Extinción (%)	Sp <sup>2</sup>	Extinción (%)
Caravaca	66	33	50%	10	85%	2	97%
Zumaia	64	22	66%	7	89%	1	99%
El Kef	61	24	61%	8	87%	2	97%

**Tabla 3.** Comparación de los patrones de extinción según los distintos escenarios planteados. Sp<sup>1</sup> = nº especies identificadas inmediatamente por debajo del límite K/Pg; Sp<sup>2</sup> = nº especies cretácicas promedio reconocidas en las rocas danienses de cada sección y según cada escenario (datos tomados de Arenillas et al., 2018, y Gilabert et al., 2021a,b,c, y resumidos en el Anexo V, Tabla anexa 2)

Estos escenarios se han establecido según los siguientes criterios: Escenario 1) todos los ejemplares cretácicos identificados en el Daniense pertenecen a especies que sobrevivieron al evento de extinción; Escenario 2) solo las especies cretácicas que presentan un registro relativamente continuo en el Daniense (>3 muestras consecutivas desde el límite K/Pg) son consideradas especies supervivientes; y Escenario 3) únicamente las especies cretácicas que presentan en el Daniense un incremento relevante en su abundancia relativa respecto al que presentan en las últimas muestras del Maastrichtiense son consideradas especies supervivientes. Además, la correlación temporal de todos los eventos identificados en esta tesis doctoral (Fig. 11), ayuda a evaluar el modelo de extinción y supervivencia de los foraminíferos planctónicos a través del límite K/Pg.

En el Escenario 1, el porcentaje de especies extintas en el límite K/Pg es ~60%, lo que representa una tasa de extinción ya de por sí compatible con el modelo de extinción masiva catastrófica. Sin embargo, la mayoría de los especialistas en foraminíferos planctónicos han sugerido patrones de extinción más cercanos al propuesto en el Escenario 2, en el que se consideran solo entre 5 y 10 especies supervivientes (p. ej., Huber, 1996; Arz et al., 1999a,b; Gallala et al., 2009; Lowery et al., 2020). Las especies estimadas como supervivientes son las consideradas como más cosmopolitas y generalistas, y pertenecen a los géneros *Guembelitra*, *Heterohelix*, *Muricohedbergella*, *Globigerinelloides* y *Pseudoguembelina*. Salvo las de *Guembelitra*, la abundancia

relativa de estas especies desciende rápidamente tras el límite K/Pg, haciéndose residual en cuanto las nuevas especies danienses comienzan a proliferar (Arenillas et al., 2018; Gilabert et al., 2021b,c).

Por último, el Escenario 3 es el más extremo en cuanto a la tasa de extinción sugerida (~97%) y el que más se ajusta al modelo de extinción propuesto originalmente por Smit (1982). Según los resultados de esta tesis doctoral se puede concluir que hay un conjunto de evidencias que respaldan este último escenario, el cual resulta compatible con la teoría de que el impacto de Chicxulub fue la causa desencadenante de la extinción masiva.

La primera evidencia es la más directa y proviene del análisis cualitativo y cuantitativo de las asociaciones de foraminíferos planctónicos. Según este análisis, el horizonte de extinción masiva coincide con el nivel que contiene las evidencias de impacto en el límite K/Pg (Arenillas et al., 2018; Gilabert et al., 2021a,c). Además coincide con un rápido aumento de la acidificación oceánica, la cual duró ~1 ka (Gilabert et al., 2021b).

La segunda evidencia la proporciona el género oportunista *Guembelitra*, ya que es el único género maastrichtiense que incrementa su abundancia relativa tras el límite K/Pg y lo hace de manera brusca (Arenillas et al., 2018; Gilabert et al., 2021b,c; Fig. 11E). La proliferación de *Guembelitra* se observa no solo en su hábitat preferente, es decir, en medios neríticos relativamente someros (Pardo y Keller, 2008), sino también en medios oceánicos y neríticos externos como los estudiados en esta tesis doctoral (Fig. 11E). Arenillas et al. (2016b) pudieron corroborar la hipótesis de un sólo género superviviente (*Guembelitra*) tras analizar la sección de Moncada (Cuba), donde se ha identificado la arcilla del límite y todas las biozonas de foraminíferos planctónicos del Daniense inferior. Arenillas et al. (2016b) descubrieron que, en la parte basal del Daniense de Moncada, solo hay ejemplares del género *Guembelitra*, el cual presenta por tanto una abundancia relativa del 100%. Tras una búsqueda intensiva, no pudieron encontrar ejemplares de otros géneros cretácicos.

La tercera evidencia es el aumento brusco de la tasa de formas aberrantes tras el límite K/Pg, es decir, del número de especímenes de foraminíferos planctónicos con conchas de crecimiento anormal. Este aumento de formas aberrantes se ha atribuido al estrés ambiental extremo durante el Daniense más temprano provocado por las perturbaciones ambientales globales causadas por el impacto de Chicxulub (Arenillas et al., 2018; Gilabert et al., 2021b; Fig. 11H). Los factores ambientales concretos que causaron el incremento en el índice de foraminíferos aberrantes no se conocen con



exactitud, pero podrían estar relacionados con el aumento de la temperatura (Kawaragi et al., 2009; MacLeod et al., 2018), la acidificación oceánica (Alegret et al., 2012; Henehan et al., 2019; Gilabert et al., 2021b), la contaminación ambiental por metales pesados (Smit y Romein, 1985; Premović et al., 2008; Arenillas et al., 2016b) o la intensificación local de condiciones eutróficas justo inmediatamente después del límite K/Pg (Bralower et al., 2020). Estas perturbaciones ambientales derivadas del impacto, se estima que duraron entre <1 y 10 ka.

Lo que resulta más relevante es que, entre los ejemplares de géneros cretácicos identificados en el Daniense, solo se han observado tasas anómalas de aberrantes en *Guembelitra*, corroborando de este modo el Escenario 3. El resto de especies cretácicas, incluyendo las que han sido consideradas como potenciales supervivientes (como por ejemplo las especies de *Muricohedbergella* y algunas de *Heterohelix*), no se han reconocido en el análisis cuantitativo del Daniense inferior de Caravaca y Zumaia lo que sugiere una tasa de aberrantes muy poco abundante. En la misma línea, el estudio cuantitativo realizado en El Kef y Aïn Settara permitió el reconocimiento de un número muy bajo de ejemplares maastrichtienses con crecimientos aberrantes (Arenillas et al., 2018). Sin embargo, los valores obtenidos para estas especies son similares a los que tienen en el Maastrichtinse y por tanto no reflejan un aumento significativo, como por el contrario si hacen las especies y géneros Danienses (Arenillas et al., 2018). Por esta razón

**Figura 11 (página anterior).** Marco de correlación temporal para el Daniense inferior: **A)** Biozonas de foraminíferos planctónicos y curva astronómica La2011 (Laskar et al., 2011); **B)** Modelos eruptivos del vulcanismo del Decán; **C)** Variación del  $\delta^{13}\text{C}$  y curva de  $\Delta T$ . **D)** Variación de la riqueza específica en cada sección comparada con variación del nº de especies máximo según el modelo evolutivo de Arenillas et al. (2018); Nº sp. Paleógeno = nº de especies paleógenas reconocidas en el estudio cuantitativo; Nº sp. Cretácico = nº de especies cretácicas reconocidas en el estudio cuantitativo; \* Evolución sp. = variación del nº máximo de especies según el modelo evolutivo de Arenillas et al. (2018). **E)** Abundancia relativa de géneros triseriados (*Guembelitra* y *Chiloguembelitra*); **F)** Abundancia relativa de géneros biseriados (*Woodringina* y *Chiloguembelina*); **G)** abundancia relativa de parvularugoglobigerina (*Parvularugoglobigerina* y *Palaeoglobigerina*) y de otros (*Eoglobigerina*, *Parasubbotina*, *Globanomalina*, *Praemurica*, *Trochoguembelitra*, *Subbotina*); **H)** Abundancia relativa de foraminíferos aberrantes. Símbolos empleados en las biozonas del Daniense temprano: \* = *Muricohedbergella holmdelensis*; \*\* = *Parvularugoglobigerina longiapertura*; \*\*\* = *Pv. sabina*; 4\* = *Eoglobigerina simplicissima*; 5\* = *Guembelitra cretacea*; 6\* = *Pv. eugubina*. Con bandas grises se han marcado los intervalos correspondientes a los eventos Dan-C2 y LC29n.



en esta tesis doctoral se considera que los ejemplares de géneros cretácicos encontrados en el Daniense inferior son reelaborados, salvo los de *Guembelitra*.

Existe bastante aceptación en admitir que el género superviviente *Guembelitra* originó dos nuevos linajes danienses, el de los géneros biseriados *Woodringina* y *Chiloguembelina*, y el de los trocoespiralados *Trochoguembelitra* y *Globoconusa* (Olsson et al., 1999; Arenillas y Arz, 2017). Esta filogenia fue matizada tras la revalidación del género *Chiloguembelitra*, de manera que el origen de ambos linajes no ocurrió directamente desde *Guembelitra* sino a través de su descendiente *Chiloguembelitra* (Arenillas et al., 2017).

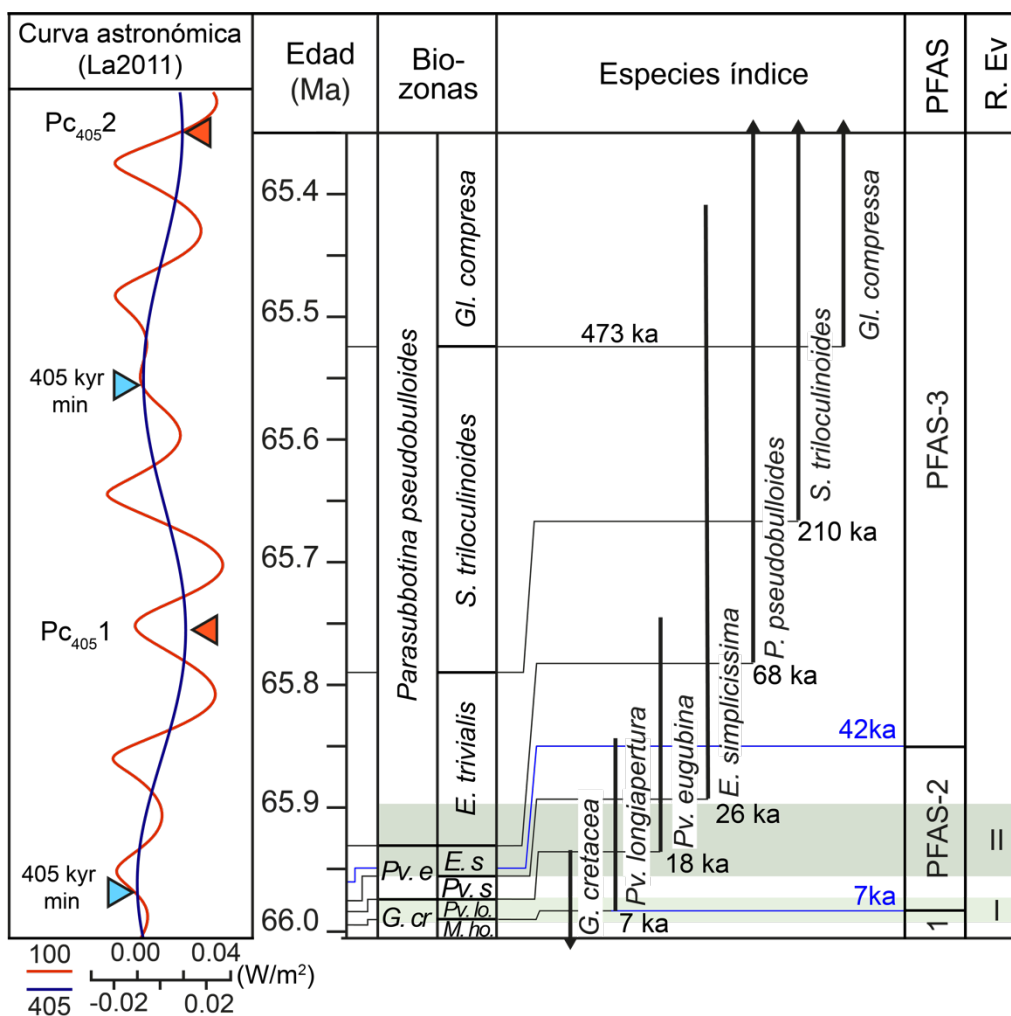
*Muricohedbergella* es considerado también, al igual que *Guembelitra*, como un género cretácico superviviente del evento de extinción del límite K/Pg (Huber et al., 2002). La hipótesis más comúnmente aceptada sugiere que *Muricohedbergella* es el ancestro de los foraminíferos planctónicos espiralados cenozoicos (Olsson et al., 1999; Aze et al., 2011), por lo que este género es comúnmente considerado como un superviviente de la extinción del límite K/Pg. Sin embargo, si la hipótesis del origen bentónico de foraminíferos planctónicos espiralados cenozoicos es verificada, la presunta evidencia filogenética de la supervivencia de *Muricohedbergella* quedaría por tanto refutada.

#### 5.4.2. Radiaciones evolutivas y reconocimiento de acmé-estadios

Las asociaciones de foraminíferos planctónicos del Daniense más temprano se caracterizan por una baja diversidad (Fig. 11D). Sin embargo, la tasa de especiación fue muy alta tras la extinción masiva del límite K/Pg. Según los estudios bioestratigráficos de alta resolución realizados en Caravaca, Zumaia, El Kef y Aïn Settara, en el Daniense temprano tuvieron lugar dos importantes radiaciones evolutivas de foraminíferos planctónicos (intervalos marcados como franjas verdes horizontales en las Figs. 11 y 12. La más antigua incluye a 16 especies de *Chiloguembelitra*, *Pseudocaucasina*, *Parvularugoglobigerina*, *Palaeoglobigerina*, *Woodringina* y *Chiloguembelina*, cuyos primeros registros se sitúan en la Subzona de *Parvularugoglobigerina longiapertura* de Arenillas et al. (2004), es decir, entre ~6 y 18 ka tras el límite K/Pg.

La segunda radiación evolutiva comprende la aparición de la mayoría de las especies trocoespiraladas de los géneros *Trochoguembelitra*, *Eoglobigerina*, *Parasubbotina*, *Globanomalina* y *Praemurica*. Durante este intervalo, *Palaeoglobigerina* y *Parvularugoglobigerina* se extinguen, siendo reemplazados por el nuevo conjunto de

géneros trocoespiraladas, los cuales alcanzaron un tamaño mayor. En esta segunda radiación se reconocen hasta 21 nuevas especies, cuyos primeros registros se sitúan en la Subzonas de *Eoglobigerina simplicissima* y *E. trivialis*, entre ~26 ka y ~100 ka tras el límite K/Pg. Posteriormente, entre ~140 y ~200 ka después del límite K/Pg aparecieron los géneros *Globoconusa* y *Subbotina*. Ambos géneros y los que caracterizan la segunda radiación evolutiva persistieron durante los siguientes 500 ka, aumentando su abundancia relativa hasta convertirse en los grupos predominantes de la asociaciones de foraminíferos planctónicos de las Subzonas de *Subbotina triloculinoides* y de *Globanomalina compressa* (Arenillas et al., 2018; Gilabert et al., 2021b,c).



Estas radiaciones evolutivas parecen ser en gran parte responsables de la sucesión de los tres acmé-estadios PFAS del Daniense inferior de Arenillas et al. (2006), los cuales han sido identificados en la cuatro secciones estudiadas en esta tesis doctoral: El Kef, Aïn Settara, Caravaca y Zumaia (Fig. 11A,E–G; Fig. 12; Arenillas et al., 2018; Gilabert et al., 2021b,c): **PFAS-1** (predominio de *Guembelitra*), **PFAS-2** (predominio de *Palaeoglobigerina* y *Parvularugoglobigerina*) y **PFAS-3** (predominio de *Woodringina* y *Chiloguembelina*). Estos PFAS se han reconocido en medios pelágicos oceánicos y neríticos externos principalmente en el Tetis, Atlántico Norte, Golfo de México y el Caribe (p. ej., Alegret et al., 2004; Arenillas et al., 2006, 2016, 2018; Gallala et al., 2009; Lowery et al., 2018, 2021; Renne et al., 2018; Gilabert et al., 2021b,c). Ninguno de ellos se repite en el tiempo, por lo que parecen estar ligados fundamentalmente a procesos evolutivos, resultando así una herramienta muy útil para llevar a cabo correlaciones bioestratigráficas.

Las radiaciones evolutivas del Daniense temprano permiten establecer biozonaciones de muy alta resolución (Arenillas et al., 2004; Wade et al., 2011). En la Fig. 12 se muestran los biohorizontes-guía utilizados en la biozonación de Arenillas et al. (2004), así como su calibración astrocronológica basada en el modelo de edad de Zumaia. Además, los horizontes que delimitan los PFAS han sido calibrados astrocronológicamente por primera vez en la sección de Zumaia por Gilabert et al. (2021c) (Fig. 11E,F,G y Fig. 12).

#### 5.4.3. Episodios de apogeo de *Chiloguembelitra* y vulcanismo del Decán

De acuerdo al modelo de mega-pulsos eruptivos planteado por Schoene et al. (2019, 2021) y descrito en el apartado 1.3.2. de esta memoria, el intervalo de tiempo entre el final del mega-pulso maastrichtiense de la Fm. Poladpur (hace ~66,04 Ma) y el primer mega-pulso eruptivo daniense que dio lugar a la Fm. Ambenali (hace ~65,92 Ma), el sistema eruptivo del Decán entró en un periodo de inactividad. Esta quiescencia eruptiva es compatible con nuestros datos geoquímicos y micropaleontológicos ya que, tras la intensa perturbación global de los ecosistemas que caracteriza los primeros ~10 ka del Daniense, los principales indicadores de estrés ambiental tendieron a decrecer, aunque todavía registrando valores elevados durante los primeros ~70 ka del Daniense (Arenillas et al., 2018; Gilabert et al., 2021b,c).

La tendencia hacia la estabilización ambiental fue interrumpida abruptamente hace ~65,9 Ma coincidiendo con el inicio de un episodio de apogeo de *Chiloguembeltria* (Arenillas et al., 2018; Gilabert et al. 2021b,c). Se trata de un episodio de proliferación de foraminíferos planctónicos triseriados que ha sido reconocido en numerosas localidades para esta edad, bien como episodios de apogeo de *Guembeltria* o de *Chiloguembeltria*. Es el caso del DSDP 577 (Pacífico; Smit y Romein 1985), Agost (España; Canudo et al., 1991), Gubbio (Italia; Coccioni et al., 2010), El Kef y Aïn Settara (Túnez; Arenillas et al., 2018), Caravaca (Gilabert et al., 2021b), Zumaia (Gilabert et al., 2021c) y ODP M0077 (interior del cráter de Chicxulub; Lowery et al., 2021).

Los resultados descritos en Arenillas et al. (2018) y Gilabert et al. (2021b,c) parecen indicar que existen sutiles diferencias temporales en el inicio y sobre todo en el final de este episodio. Este ligero desfase temporal entre unas localidades y otras (Fig. 11E) puede responder a diferencias ambientales locales y/o a una respuesta a las condiciones de productividad oceánica heterogénea tras el límite K/Pg (Birch et al., 2021). Con esta particularidad, el episodio de apogeo de *Chiloguembeltria* puede datarse en promedio entre ~65,90 y 65,75 Ma (es decir, entre 100 y 250 ka después del límite K/Pg) y por lo tanto tendría una duración de ~150 ka, lo que permite sugerir una correlación temporal muy alta con el emplazamiento de la Fm. Ambenali (Fig. 11B,E). Los principales modelos eruptivos (Schoene et al., 2019; Sprain et al., 2019) coinciden en la edad de la base de la Fm. Ambenali, pero la duración estimada para su emplazamiento es muy diferente. Según el modelo de Sprain et al. (2019), la Fm. Ambenali se formó en ~300 ka mientras que, según el modelo de Schoene et al. (2019), tan solo en ~100 ka. Teniendo en cuenta la duración estimada para el apogeo de *Chiloguembeltria* (~150 ka), parece más probable que éste fuera la respuesta a un pulso eruptivo más breve e intenso como el propuesto por Schoene et al. (2019).

Asociado al acmé de *Chiloguembeltria* se ha reconocido un aumento en el índice de foraminíferos aberrantes (FAI), que alcanza valores anormalmente altos y similares a los registrados en la arcilla del límite K/Pg (Fig. 11H). Estos valores del FAI evolucionan paralelamente al apogeo de *Chiloguembeltria*, lo que corrobora que ambos indicadores responden al mismo estresor ambiental. Dado que no hay evidencias de acidificación oceánica ni de cambios drásticos en la temperatura (Gilabert et al., 2021b,c; Hull et al., 2020) y que *Chiloguembeltria* prolifera bajo condiciones de estrés ambiental y/o eutrofia (Pardo y Keller, 2008; Arenillas et al., 2018), se ha sugerido que el factor desencadenante de ambas señales paleobiológicas fue la masiva liberación de nutrientes y metales

precedentes de la actividad eruptiva del Decán. Una ineficaz bomba biológica en el Daniense temprano (Henehan et al., 2019; Jiang et al., 2019; Birch et al., 2021) pudo aumentar el tiempo de residencia de estos nutrientes y metales volcanogénicos en la superficie oceánica. Esto explicaría la persistencia del acmé de *Chiloguembelitra* y de la abundancia de formas aberrantes a lo largo de los ~50 ka posteriores al final del emplazamiento de la Fm. Ambenali (Fig. 11B,E,H), según la edad estimada para esta formación por Schoene et al. (2019). En la misma línea, Arreguín-Rodríguez et al. (2021) reportaron cambios en las asociaciones de foraminíferos bentónicos en el Atlántico Sur (ODP 1262) que sugieren condiciones ligeramente más eutróficas en el fondo oceánico en un intervalo temporal aproximadamente similar al del acmé de *Chiloguembelitra*.

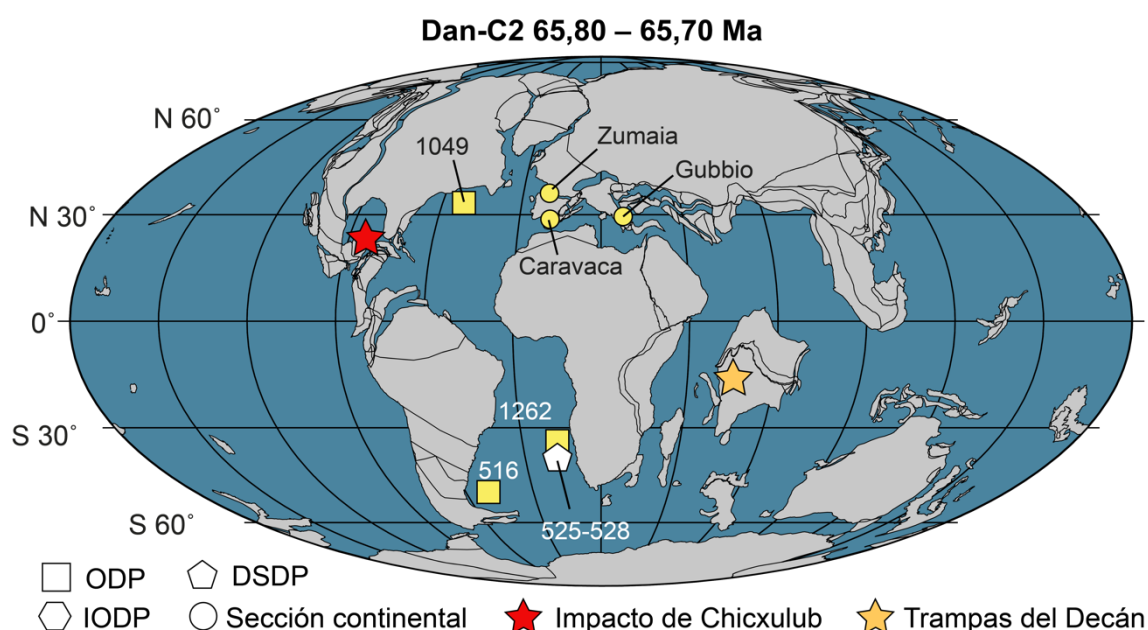
## 5.5. Los eventos Dan-C2 y LC29n

### 5.5.1. Características principales y calibración temporal

El evento Dan-C2 está estratigráficamente situado en torno al límite magnetoestratigráfico C29r/C29n (Quillévéré et al., 2008). Según estos autores, se caracteriza por una doble excursión negativa simétrica en  $\delta^{13}\text{C}$  y en  $\delta^{18}\text{O}$  (sobre roca total y en foraminíferos planctónicos), por una reducción del contenido de  $\text{CaCO}_3$  oceánico y por un incremento en la susceptibilidad magnética. Es la doble excursión negativa simétrica en el  $\delta^{13}\text{C}$  (doble CIE) lo que comúnmente se utiliza para reconocer en el registro estratigráfico este evento, ya que el  $\delta^{13}\text{C}$  es menos susceptible que el  $\delta^{18}\text{O}$  a los efectos de la diagénesis (Wendler, 2013). El evento Dan-C2 se ha identificado principalmente en sondeos oceánicos como el ODP 1049 (NO Atlántico; Quillévéré et al., 2008), el DSDP 516 (SO Atlántico; Krahl et al., 2020), los DSDPs 525 y 527 (SE Atlántico; Quillévéré et al., 2008) y el ODP 1262 (SE Atlántico; Woelders et al., 2017). También se ha identificado en Gubbio (Coccioni et al., 2010) y Caravaca (Gilabert et al., 2021b) en el Tetis occidental, así como en Zumaia (Gilabert et al., 2021c) dentro de la zona de transición entre el Tetis y el Atlántico Norte.

Teniendo en cuenta la señal isotópica del  $\delta^{18}\text{O}$  en foraminíferos planctónicos, en el Dan-C2 se produjo un aumento de temperatura de ~4 °C en la superficie oceánica (Quillévéré et al., 2008). Sin embargo, según la señal isotópica del  $\delta^{18}\text{O}$  sobre los foraminíferos bentónicos, no hubo calentamiento de las aguas del fondo oceánico (Westerhold et al., 2011; Barnet et al., 2019). Por otra parte, Coccioni et al. (2010) reconocieron en Gubbio un aumento del índice de fragmentación en ambas CIEs, por lo

que relacionaron el Dan-C2 con un episodio de acidificación oceánica. Sin embargo, esta posible acidificación oceánica y sus efectos no se han descrito en el resto de localidades antes citadas en la Fig. 13 (Quillévére et al., 2008; Barnet et al., 2019; Gilabert et al., 2021b,c). La ausencia de evidencias de una acidificación oceánica a escala global y de un aumento de las temperaturas en el fondo oceánico pone en duda de la naturaleza hipertermal del Dan-C2 (Barnet et al., 2019; Krhal et al., 2020; Hull et al., 2020; Arreguín et al., 2021). El Dan-C2 parece por tanto una perturbación relativamente pequeña del ciclo del carbono si lo comparamos con otros hipertermales del Paleógeno (Gilabert et al., 2021b,c).



**Figura 13.** Localización geográfica de las localidades donde se ha identificado el Dan-C2. En amarillo se han señalado los sondeos y secciones analizadas y correlacionadas en esta tesis doctoral (Gilabert et al., 2021b,c).

La duración del Dan-C2 se estimó inicialmente en ~100 ka, iniciándose ~250 ka después del límite K/Pg (Quillévére et al., 2008; Coccioni et al., 2010). No obstante, las calibraciones más recientes sugieren que comenzó un poco antes, ~150 o 200 ka tras el límite K/Pg (Barnet et al., 2019; Krahl et al., 2020). La recalibración astronómica del Dan-C2 en la sección de Zumaia (Fig. 11C) ha permitido datar su inicio en 200 ka tras el límite K/Pg, por lo que duró entre 65,8 y 65,7 Ma (Gilabert et al., 2021b,c; Fig. 11C).

Como la mayoría de hipertermales del Paleógeno, el evento Dan-C2 está modulado por los cambios en la excentricidad de la órbita de la Tierra (Coccioni et al.,

2010; Sinnesael et al., 2016, 2019; Barnet et al., 2019; Westerhold et al., 2020). Tanto Gilabert et al. (2021c) como Barnet et al. (2019) constataron que el Dan-C2 se correlaciona con el primer máximo de excentricidad larga (405 ka) del Daniense (Pc<sub>450</sub>1), y las 2 CIEs simétricas que lo caracterizan se correlacionan con 2 máximos de excentricidad corta (100 ka) vinculados al Pc<sub>450</sub>1. Aunque el Dan-C2 ha sido fuertemente ligado al forzamiento orbital, su proximidad en el tiempo con el emplazamiento de la Fm. Ambelani (Schoene et al., 2019; Sprain et al., 2019) ha llevado a varios autores a plantear una posible relación causa-efecto entre ambos episodios (Coccioni et al., 2010; Punekar et al., 2014a; Krhal et al., 2020). No obstante, modelizaciones y estimaciones recientes del volumen de CO<sub>2</sub> volcánico emitido desde el Decán sugieren que fue insuficiente para desencadenar un cambio climático significativo durante el Dan-C2 (Fendley et al., 2020; Hull et al., 2020). La comparación entre las dataciones radiométricas del pulso eruptivo Ambenali (Schoene et al., 2019) con las calibraciones astrocronológicas realizadas en Zumaia indican que este pulso eruptivo concluyó ~60 ka antes que el Dan-C2 (Gilabert et al., 2021c), por lo que no parecen tener una relación directa.

Por otra parte, a diferencia de los otros eventos descritos en esta tesis doctoral, el LC29n es muy poco conocido a escala global. Fue reconocido por primera vez por Coccioni et al. (2010) en Gubbio, donde se caracteriza por una sola excursión negativa del  $\delta^{13}\text{C}$  de ~0.5‰. Según estos autores, la duración del LC29n fue de ~38 ka y se inició ~75 ka después del Dan-C2. En Gubbio, el LC29n también coincide con un aumento moderado de la susceptibilidad magnética y una reducción también moderada en el contenido en CaCO<sub>3</sub>, aunque no hay evidencias de una disolución de carbonatos o de una acidificación oceánica relevante.

Según el registro isotópico del  $\delta^{13}\text{C}$  y la calibración astrocronológica llevada a cabo en el Daniense de Zumaia (Gilabert et al., 2021c), el LC29n se produjo entre 65,48 y 65,41 Ma, es decir, ~220 ka después del Dan-C2, una calibración similar a la estimada por Woelders et al. (2017) en el ODP 1262 (Atlántico Sur). En ambas localidades, los valores del  $\delta^{13}\text{C}$  descendieron entre ~0.2 y 0.3‰, siendo hasta la fecha las únicas secciones marinas en las que ha sido identificado con claridad. Como ocurre con el Dan-C2, en el evento LC29n no se ha reconocido un calentamiento del fondo oceánico (Westerhold et al., 2011; Barnet et al., 2019; Hull et al., 2020).

En cuanto a su origen, el LC29n no parece estar relacionado con el vulcanismo del Decán: según el modelo de pulsos eruptivos de Schoene et al. (2019), las erupciones del Decán finalizaron ~200 ka antes, y según el modelo de erupciones casi-continuas de

Sprain et al. (2019), lo hicieron aproximadamente coincidiendo con el inicio del LC29n. Como en el Dan-C2, el LC29n pudo ser causado principalmente por el forzamiento orbital, aunque en esta ocasión la contribución del vulcanismo del Decán es aún menos probable. Pickersgill et al. (2021) han propuesto recientemente que el impacto de Boltysch (Ucrania), cuyo cráter tienen un diámetro estimado de ~24 km, pudo estar relacionado con el LC29n. El impacto de Boltysch había sido previamente relacionado con el Dan-C2 (Gilmour et al., 2013, 2014; Jolley et al., 2017). Sin embargo, las nuevas dataciones de Pickersgill et al. (2021) con el método  $^{40}\text{Ar}/^{39}\text{Ar}$  dan una nueva edad de  $65,39 \pm 0,14/0,16$  Ma para el impacto de Boltysch, la cual es prácticamente indistinguible a la edad aquí estimada para el LC29n (entre 65,48 y 65,41). Es poco probable que un impacto relativamente tan pequeño como el de Boltysch causara por sí solo los cambios descritos en el evento LC29n (Pickersgill et al., 2021). Sin embargo, su coincidencia temporal con un máximo de excentricidad corta y con las últimas erupciones del vulcanismo del Decán apunta a que las causas que lo originaron son todavía inciertas.

#### 5.5.2. Efectos en las asociaciones de foraminíferos planctónicos.

El inicio del evento Dan-C2 ocurrió ~100 ka después del final del emplazamiento de la Fm. Ambenali y del inicio del episodio de apogeo de *Chiloguembelitra* y de incremento del FAI descritos en el apartado 5.4.3, por lo que el evento Dan-C2 no parece estar relacionado con ellos. De hecho, aunque se solapan parcialmente en el tiempo, la abundancia relativa de *Chiloguembelitra* y el valor del FAI disminuyeron rápidamente antes de concluir el Dan-C2 (Fig. 11E–H), lo que indica que este último tuvo un escaso impacto en las asociaciones de foraminíferos planctónicos.

Contrariamente a lo propuesto por Coccioni et al. (2010) en Gubbio, el análisis del índice de fragmentación en Caravaca sugiere que no hubo un incremento de la disolución del carbonato destacable durante el evento Dan-C2 (Gilabert et al., 2021b). Los resultados obtenidos por otros autores, como la ausencia de incrementos en la concentración de hierro en el sedimento (Barnet et al., 2019) o como la estabilidad en la abundancia de los diferentes grupos de foraminíferos bentónicos de conchas calcáreas (Arreguín-Rodríguez et al., 2021), corroboran que el Dan-C2 no está ligado a un aumento en la disolución de los carbonatos y/o de la acidez oceánica.

Hacia el final del Dan-C2 ~65,75 Ma, las asociaciones de foraminíferos planctónicos registran un cambio relevante, en el que las especies pertenecientes a los géneros de la segunda radiación evolutiva (*Eoglobigerina*, *Parasubbotina*, *Subbotina*, *Praemurica*,



*Globanomalina*) aumentan progresivamente su abundancia relativa, hasta alcanzar en conjunto entre el 40 y el 50% (Fig. 11G). La alta abundancia de estos géneros se mantuvo durante los 300 ka posteriores al final del Dan-C2, lo que ha sido interpretado como condiciones de creciente estabilidad ambiental (Gilabert et al. 2021b). En esta tesis doctoral no se han identificado cambios relevantes en las asociaciones de foraminíferos planctónicos que sugieran algún tipo de respuesta ligada al último mega-pulso eruptivo del Decán (Fm. Mahabaleswar).

Por lo que respecta al LC29n, tampoco se ha identificado un cambio significativo en las condiciones ambientales, climáticas y paleoceanográficas. En este evento, las asociaciones de foraminíferos planctónicos registran pequeñas fluctuaciones que resultan irrelevantes (Fig. 11E–H). Tampoco se han reportado episodios de disolución de carbonatos en el LC29n, ni en las localidades estudiadas en esta tesis doctoral ni en otras (Coccioni et al., 2010; Barnet et al., 2019), confirmando que se trata simplemente de una perturbación menor en el ciclo del carbono.

***Capítulo 6.***  
***Conclusiones***



## 6. CONCLUSIONES

Se han analizado los eventos climáticos acontecidos durante 1 Ma a través del límite K/Pg (LMWE, límite K/Pg, Dan-C2 y LC29n) y se ha evaluado su influencia en las asociaciones de foraminíferos planctónicos en tres secciones del Tetis occidental (Caravaca, El Kef y Aïn Settara) y en una sección de la zona de transición entre el Tetis y el Atlántico Norte (Zumaia). Los datos micropaleontológicos, geoquímicos y paleomagnéticos obtenidos se han integrado en un robusto modelo de edad calibrado astrocronológicamente. Este modelo ha permitido ponderar la influencia específica del impacto de Chicxulub, del vulcanismo del Decán y del control orbital en los principales cambios paleoclimáticos, paleoambientales y paleobiológicos a través del tránsito K–Pg, obteniendo las siguientes conclusiones:

I. El estudio bioestratigráfico de las cuatro secciones ha permitido reconocer las dos últimas biozonas del Maastrichtiense: Biozonas CF2 (o de *Pseudoguembelina palpebra*) y CF1 (o de *Plummerita hantkeninoides*), y las tres primeras biozonas del Daniense: Zonas de *Guembelitra cretacea*, de *Parvularugoglobigerina eugubina* y de *Parasubbotina pseudobulloides*. Estas últimas han sido divididas en 7 subbiozonas: Subzonas de *Muricohedbergella holmdelensis* y de *Parvularugoglobigerina longiapertura* (Zona de *G. cretacea*), Subzonas de *Parvularugoglobigerina sabina* y de *Eoglobigerina simplicissima* (Zona de *Pv. eugubina*), y Subzonas de *Eoglobigerina cf. trivialis*, de *Subbotina triloculinoides* y de *Globanomalina compressa* (Zona de *P. pseudobulloides*). Las biozonas danienses utilizadas en esta tesis doctoral equivalen aproximadamente a las Biozonas danienses estándar P0, P $\alpha$ , P1a, P1b y P1c. También se han reconocido los acmé-estadios de foraminíferos planctónicos PFAS 1 (acmé de *Guembelitra*), PFAS 2 (acmé de *Parvularugoglobigerina* y *Palaeoglobigerina*) y PFAS 3 (acmé de *Woodringina* y *Chiloguembelina*) del Daniense temprano.

II. Estas biozonas y los biohorizontes-guía que las definen han sido recalibrados magneto- y astrocronológicamente. Asumiendo una edad de 66,001 Ma para el límite K/Pg y utilizando la sección de Zumaia como referencia, la edad de la base de la Biozona CF1 ha sido estimada en 66,098 Ma, y las de las bases de las Subzonas de *Mh. holmdelensis*, *Pv. longiapertura*, *Pv. sabina*, *E. simplicissima*, *E. cf. trivialis*, *S. triloculinoides* y *Globanomalina compressa* en 66,001, 65,994, 65,983, 65,975, 65,933,

65,791 y 65,528 Ma respectivamente. De la misma manera, las bases de los acmé-estadios PFAS 1, 2 y 3 han sido calibradas astrocronológicamente en 66,001, 65,994 y 65,959 Ma respectivamente.

III. Los eventos LMWE, límite K/Pg, Dan-C2 y LC29n se han identificado en Caravaca y Zumaia basándose en su registro isotópico, en robustos modelos de edad y en la comparación y correlación con el registro de otras localidades. Se ha comprobado que tanto el LMWE, como el evento del límite K/Pg, se registran a escala mundial y por tanto que responden inequívocamente a cambios climáticos globales. Por el contrario, el Dan-C2 solo se ha reconocido en localidades del Atlántico y del Tetis, lo que sugiere su relación con un posible cambio climático más regional. El LC29n, hasta ahora, se ha registrado en muy pocas localidades, lo que nos impide determinar si es de naturaleza global.

IV. Asumiendo una edad de 66,001 Ma para el límite K/Pg y utilizando la sección de Zumaia como referencia, los eventos LMWE, Dan-C2 y LC29n se han calibrado astrocronológicamente entre 66,25 y 66,10 Ma, entre 65,8 y 65,7 Ma, y entre 65,48 y 65,41 Ma, respectivamente.

V. Solo se han reconocido episodios de acidificación oceánica y de disolución de carbonatos ligados al LMWE y al límite K/Pg, los cuales han quedado registrados como intervalos con elevados índices de fragmentación de las conchas de foraminíferos planctónicos. Durante el LMWE, estos episodios se correlacionan temporalmente con los máximos de excentricidad corta (100 ka) y con el emplazamiento de las formaciones volcánicas menos voluminosas del Decán.

VI. Los cambios en las asociaciones de foraminíferos planctónicos asociados a cada evento varían enormemente. El evento del límite K/Pg se ha atribuido a las perturbaciones ambientales globales desencadenadas por el impacto del asteroide de Chicxulub. Se caracteriza por una casi completa extinción instantánea a escala geológica, seguida de un acmé de *Guembelitra*, considerado el único género superviviente al evento del límite K/Pg, y de una etapa de proliferación de foraminíferos planctónicos aberrantes. El LMWE se caracteriza por una perturbación transitoria de las asociaciones de foraminíferos planctónicos. Durante el Dan-C2, las asociaciones no sufrieron ninguna perturbación

relevante sino más bien lo contrario, ya que se produjo la diversificación de nuevas especies de foraminíferos planctónicos. Finalmente, no se ha evidenciado ninguna respuesta paleobiológica en el LC29n.

VII. El único episodio de estrés ambiental relevante que no está relacionado con los efectos del impacto de Chicxulub, se caracteriza por el apogeo del género oportunista *Chiloguembelitra* y por el aumento de la tasa de formas aberrantes en los foraminíferos planctónicos, y ha sido atribuido al vulcanismo del Decán y concretamente al emplazamiento de la Fm. Ambenali ~100 ka tras el límite K/Pg.

VIII. El análisis morfológico, textural, biométrico y morfoestadístico del género daniense *Chiloguembelitra* ha permitido revalidar este género cuya validez taxonómica se había puesto en entredicho, al ser considerado como un sinónimo posterior de *Guembelitra*. *Chiloguembelitra* jugó un rol determinante en la evolución de varios linajes de foraminíferos planctónicos (chiloguembelínidos y globoconúsidos).

IX. El acmé de *Guembelitra* tras el límite K/Pg (PFAS 1) y los acmés de *Chiloguembelitra* posteriores se caracterizan también por la proliferación de formas aberrantes de foraminíferos planctónicos. Se ha realizado un estudio morfológico detallado de las diferentes categorías y tipos de estas formas anormales en El Kef y Aïn Settara, y de sus implicaciones en las reconstrucciones paleoambientales. Al igual que los acmés de guembelítridos, la proliferación de formas aberrantes es considerada un indicador de estrés ambiental.

X. Tras comparar las dataciones radiométricas de los episodios volcánicos del Decán y las calibraciones temporales de los eventos aquí estudiados, se concluye que el vulcanismo del Decán fue incapaz por si solo de provocar los cambios climáticos observados en el tránsito K–Pg a escala global. Se ha demostrado que el LMWE, el Dan-C2 y el LC29n fueron fuertemente modulados por los cambios orbitales de la Tierra.

## 6. CONCLUSIONS

The influence of the recognized climatic events 1 Ma across the K/Pg boundary (LMWE, K/Pg boundary, Dan-C2 and LC29n) on planktic foraminiferal assemblages has been analyzed in the studied samples of three sections of the western Tethys (Caravaca, El Kef and Aïn Settara) and one section belonging to the transitional zone between the Tethys and the North Atlantic realm (Zumaia). The micropaleontological, geochemical and paleomagnetic data obtained have been integrated into a robust astrochronologically calibrated age model. This age-model has allowed to disentangle the specific contributions of the Chicxulub impact, Deccan volcanism and orbital control on the main paleoclimatic, paleoenvironmental and paleobiological changes across the K–Pg transition, resulting in the following conclusions:

I. The biostratigraphic study of the four sections has made it possible to recognize the last biozones of the Maastrichtian: Biozones CF2 (or of *Pseudoguembelina palpebra*) and CF1 (or of *Plummerita hantkeninoides*), and the first three biozones of the Danian: Zones of *Guembelitra cretacea*, of *Parvularugoglobigerina eugubina* and *Parasubbotina pseudobulloides*. The last-mentioned Zone has been divided into 7 sub-biozones: The *Muricohedbergella holmdelensis* and *Parvularugoglobigerina longiapertura* subzones (Zone of *G. cretacea*), the *Parvularugoglobigerina sabina* and *Eoglobigerina simplicissima* subzones (Zone of *Pv. eugubina*) and the *Eoglobigerina cf. trivialis*, *Subbotina triloculinoides* and *Globanomalina compressa* subzones (Zone of *P. pseudobulloides*). The Danian biozones used in this PhD thesis are roughly equivalent to the standard Danian biozones P0, P $\alpha$ , P1a, P1b and P1c. The planktic foraminiferal acme-stages PFAS 1 (*Guembelitra* acme), PFAS 2 (*Parvularugoglobigerina* and *Palaeoglobigerina* acme) and PFAS 3 (*Woodringina* and *Chiloguembelina* acme) from the early Danian have also been recognized.

II. These biozones and the key-biohorizons that define them have been magneto- and astrochronologically recalibrated. Assuming an age of 66.001 Ma for the K/Pg boundary and using the astronomically calibrated age model developed in Zumaia as the reference, the age of the base of Biozone CF1 has been calibrated, at 66.098 Ma, as well as the bases of the Danian subzones: *Mh. holmdelensis*, *Pv. longiapertura*, *Pv. sabina*, *E. simplicissima*, *E. cf. trivialis*, *S. triloculinoides* and *Gl. compressa*, which have been

calibrated at 66.001, 65.994, 65.983, 65.975, 65.933, 65.791 and 65.528 Ma respectively. In the same way, the bases of the acme-stages PFAS 1, 2 and 3 have been calibrated at 66.001, 65.994 and 65.959 Ma respectively.

III. The LMWE, K/Pg boundary, the Dan-C2 and the LC29n events have been identified at Caravaca and Zumaia based on their isotopic signature, that was integrated into robust age models, allowing comparison and correlation with the isotopic record of other localities. It has been demonstrated that the LMWE and the K/Pg boundary event are worldwide events that unequivocally occurred in response to global changes. In contrast, the Dan-C2 has only been recognized in Atlantic and Tethyan localities, which suggests a probably more regional climate change. The LC29n is extremely poorly represented, having been reported only in a few localities, which prevents us from determining whether it is global or not.

IV. Assuming an age of 66.001 Ma for the K/Pg boundary and using the Zumaia section as a reference, the LMWE, Dan-C2 and LC29n events have been astronomically calibrated between 66.25 and 66.10 Ma, between 65.8 and 65.7 Ma, and between 65.48 and 65.41 Ma, respectively.

V. The episodes of oceanic carbonate dissolution and acidification have been recognized by the increase in fragmentation index among planktic foraminifera tests which have been chronologically linked to the LMWE and the K/Pg boundary. During the LMWE, carbonate dissolution episodes were temporally correlated with short eccentricity maxima (100 ka) and with the emplacement of the less voluminous volcanic formations of the Deccan.

VI. Planktic foraminifera assemblages show a very different ecological response to the different perturbations. The K/Pg boundary event has been attributed to global environmental disturbances triggered by the Chicxulub impact. It is characterized by an almost complete instantaneous extinction of planktic foraminifera on a geological scale, followed by an acme-stage of *Guembelitra*, considered the only surviving genus at the K/Pg boundary event, and by the proliferation stage of aberrant planktic foraminifera. The LMWE is characterized by a transient disturbance of planktic foraminifera assemblages. During the Dan-C2 event, the assemblages did not suffer any relevant



disturbance but rather the opposite, since the appearance of new species of planktic foraminifera occurred. Finally, no paleobiological response to LC29n has been detected.

VII. The only relevant episode of environmental stress unrelated to the long-term Chicxulub effects, is the acme-stage of the opportunistic genus *Chiloguembelitra* and the rebound in the increase of the planktic foraminiferal tests with aberrant growths. This rise in environmental stress has been related to the emplacement of the Ambenali Fm., which represents the third megapulse of Deccan Trap volcanism which occurred ~ 100 ka after the K/Pg boundary.

VIII. The morphological, textural, biometric and morpho-statistical analysis of the Danian genus *Chiloguembelitra* has allowed us to revalidate this genus, whose taxonomic validity had been questioned since it was considered a later synonym of *Guembelitra*. *Chiloguembelitra* played a determining role in the evolution of several lineages of planktic foraminifera (chiloguembelinid and globconusid).

IX. The *Guembelitra* acme after the K/Pg boundary (PFAS 1) and the subsequent *Chiloguembelitra* acme are also characterized by the proliferation of aberrant forms of planktic foraminifera. A detailed morphological study of the different categories and types of these abnormal forms, and their implications in paleoenvironmental reconstructions has been carried out at the El Kef and Aïn Settara sections. Similar to the acme of guembelitrids, the proliferation of aberrant forms is considered an indicator of environmental stress.

X. After comparing the radiometric dating of the volcanic episodes of the Deccan Traps and the temporal calibrations of the events studied here, it is concluded that the volcanism of the Deccan Traps alone was insufficient to cause the climatic changes observed in the K–Pg transition on a global scale. It has been demonstrated that the LMWE, the Dan-C2, and the LC29n events were strongly modulated by Earth's orbital variations.

# *Bibliografía*



**BIBLIOGRAFÍA**

- Abramovich, S., Keller, G., Stüben, D., Berner, Z., 2003. Characterization of late Campanian and Maastrichtian planktonic foraminiferal depth habitats and vital activities based on stable isotopes. *Palaeogeography, Palaeoclimatology, Palaeoecology* 202, 1–29.
- Abramovich, S., Yovel-Corem, S., Almogi-Labin, A., Benjamini, C., 2010. Global climate change and planktic foraminiferal response in the Maastrichtian. *Paleoceanography* 25, 1–15.
- Abramovich, S., Keller, G., 2002. High stress late Maastrichtian paleoenvironment: Inference from planktonic foraminifera in Tunisia. *Palaeogeography, Palaeoclimatology, Palaeoecology* 178, 145–164.
- Abramovich, S., Keller, G., 2003. Planktonic foraminiferal response to the latest Maastrichtian abrupt warm event: A case study from South Atlantic DSDP Site 525A. *Marine Micropaleontology* 48, 225–249.
- Alegret, L., Thomas, E., 2013. Benthic foraminifera across the Cretaceous/Paleogene boundary in the Southern Ocean (ODP Site 690): Diversity, food and carbonate saturation. *Marine Micropaleontology* 105, 40–51.
- Alegret, L., Arenillas, I., Arz, J.A., Molina, E., 2004. Foraminiferal event-stratigraphy across the Cretaceous/Paleogene boundary. *Neues Jahrbuch für Geologie und Paläontologie - Abhandlungen* 234, 25–50.
- Alegret, L., Thomas, E., Lohmann, K.C., 2012. End-Cretaceous marine mass extinction not caused by productivity collapse. *Proceedings of the National Academy of Sciences of the United States of America* 109, 728–732.
- Alvarez, L.W., Alvarez, W., Asaro, F., Michel, H. v., 1980. Extraterrestrial Cause for the Cretaceous-Tertiary Extinction. *Science* 208, 1095–1108.
- Arenillas, I., 1996. Los foraminíferos planctónicos del Paleoceno-Eoceno inferior: Sistemática, Bioestratigrafía, Cronoestratigrafía y Paleocianografía. tesis doctoral, Prensas Universitarias de Zaragoza (2000), Zaragoza, Spain. 413 pp.
- Arenillas, I., Arz, J.A., 2013a. New evidence on the origin of non-spinose pitted-cancellate species of the early Danian planktonic foraminifera. *Geologica Carpathica* 64, 237–251.

- Arenillas, I., Arz, J.A., 2013b. Origin and evolution of the planktic foraminiferal family Eoglobigerinidae Blow, 1979, during the early Danian (Paleocene). *Revista Mexicana de Ciencias Geológicas* 30, 159–177.
- Arenillas, I., Arz, J.A., 2017. Benthic origin and earliest evolution of the first planktonic foraminifera after the Cretaceous/Paleogene boundary mass extinction. *Historical Biology* 29, 25–42.
- Arenillas, I., Arz, J.A., Molina, E., Dupuis, C., 2000a. An independent test of planktic foraminiferal turnover across the Cretaceous/Paleogene (K/P) boundary at El Kef, Tunisia: Catastrophic mass extinction and possible survivorship. *Micropaleontology* 46, 31–49.
- Arenillas, I., Arz, J.A., Molina, E., Dupuis, C., 2000b. The Cretaceous/Paleogene (K/P) boundary at Ain Settara, Tunisia: Sudden catastrophic mass extinction in planktic foraminifera. *Journal of Foraminiferal Research* 30, 202–218.
- Arenillas, I., Arz, J.A., Molina, E., 2004. A new high-resolution planktic foraminiferal zonation and subzonation for the lower Danian. *Lethaia* 37, 79–95.
- Arenillas, I., Arz, J.A., Grajales-Nishimura, J.M., Murillo-Muñeton, G., Alvarez, W., Camargo-Zanoguera, A., Molina, E., Rosales-Domínguez, C., 2006. Chicxulub impact event is Cretaceous/Paleogene boundary in age: New micropaleontological evidence. *Earth and Planetary Science Letters* 249, 241–257.
- Arenillas, I., Arz, J.A., Náñez, C., 2010. Diversidad y evolución de la textura de la pared en guembelítridos (Foraminíferos planctónicos) del tránsito Cretácico-Paleógeno. *Revista Española de Paleontología* 25, 89–105.
- Arenillas, I., Arz, J.A., Náñez, C., 2016a. New species of the genus *Trochoguembelitra* from the lowermost Danian of Tunisia - Biostratigraphic and evolutionary implications in planktonic foraminifera. *Palaeontographica, Abteilung A: Paläozoologie - Stratigraphie* 305, 135–161.
- Arenillas, I., Arz, J.A., Grajales-Nishimura, J.M., Meléndez, A., Rojas-Consuegra, R., 2016b. The Chicxulub impact is synchronous with the planktonic foraminifera mass extinction at the Cretaceous/Paleogene boundary: New evidence from the Moncada section, Cuba. *Geologica Acta* 14, 35–51.
- Arenillas, I., Arz, J.A., Gilabert, V., 2017. Revalidation of the genus *Chiloguembelitra* Hofker: Implications for the evolution of early Danian planktonic foraminifera. *Journal of African Earth Sciences* 134, 435–456.

- Arenillas, I., Arz, J.A., Gilabert, V., 2018. Blooms of aberrant planktic foraminifera across the K/Pg boundary in the Western Tethys: Causes and evolutionary implications. *Paleobiology* 44, 460–489.
- Arreguín-Rodríguez, G.J., Barnet, J.S.K., Leng, M.J., Littler, K., Kroon, D., Schmidt, D.N., Thomas, E., Alegret, L., 2021. Benthic foraminiferal turnover across the Dan-C2 event in the eastern South Atlantic Ocean (ODP Site 1262). *Palaeogeography, Palaeoclimatology, Palaeoecology* 572.
- Arz, J.A., 1996. Los foraminíferos planctónicos del Campaniense y Maastrichtiense: Bioestratigrafía, Cronoestratigrafía y eventos paleoecológicos. tesis doctoral, Prensas Universitarias de Zaragoza (2000), Zaragoza, Spain, 419 pp.
- Arz, J., Arenillas, I., Molina, E., 1999a. Los efectos tafonómicos y “Signor-Lipps” sobre la extinción en masa de foraminíferos planctónicos en el límite Cretácico/Terciario de Elles (Tunicia). *Revista de la Sociedad Geológica de España* 12, 251–268.
- Arz, J.A., Arenillas, I., Molina, E., 1999b. Extinción de foraminíferos planctónicos en el tránsito Cretácico-Terciario de Zumaya (Guipúzcoa): ¿supervivencia o reelaboración? *Revista española de micropaleontología* 31, 297–304.
- Arz, J.A., Arenillas, I., Molina, E., Sepúlveda, R., 2000. La estabilidad evolutiva de los foraminíferos planctónicos en el Maastrichtiense Superior y su extinción en el límite Cretácico/Terciario de Caravaca, España. *Revista Geológica de Chile* 27, 27–47.
- Arz, J.A., Arenillas, I., Soria, A.R., Alegret, L., Grajales-Nishimura, J.M., Liesa, C.L., Meléndez, A., Molina, E., Rosales, M.C., 2001. Micropaleontology and sedimentology across the Cretaceous/Tertiary boundary at La Ceiba (Mexico): Impact-generated sediment gravity flows. *Journal of South American Earth Sciences* 14, 505–519.
- Arz, J.A., Molina, E., 2002. Bioestratigrafía y cronoeestratigrafía con foraminíferos planctónicos del Campaniense superior y Maastrichtiense de latitudes subtropicales y templadas (España, Francia y Tunicia). *Neues Jahrbuch für Geologie und Paläontologie - Abhandlungen* 224, 161–195.
- Ashkenazi-Polivoda, S., Rak, C., Almogi-Labin, A., Zsolt, B., Ovadia, O., Abramovich, S., 2014. Paleocology of the K-Pg mass extinction survivor *Guembelitra* (Cushman): isotopic evidence from pristine foraminifera from Brazos River, Texas (Maastrichtian). *Paleobiology* 40, 24–33.

- Artemieva, N., Morgan, J., 2017. Quantifying the release of climate-active gases by large meteorite impacts with a case study of Chicxulub. *Geophysical Research Letters* 44, 10,180–10,188.
- Aze, T., Ezard, T.H.G., Purvis, A., Coxall, H.K., Stewart, D.R.M., Wade, B.S., Pearson, P.N., 2011. A phylogeny of Cenozoic macroperforate planktonic foraminifera from fossil data. *Biological Reviews* 86, 900–927.
- Bardeen, C.G., Garcia, R.R., Toon, O.B., Conley, A.J., 2017. On transient climate change at the Cretaceous–Paleogene boundary due to atmospheric soot injections. *Proceedings of the National Academy of Sciences of the United States of America* 114, E7415–E7424.
- Barnet, J.S.K., Littler, K., Kroon, D., Leng, M.J., Westerhold, T., Röhl, U., Zachos, J.C., 2018. A new high-resolution chronology for the late Maastrichtian warming event: Establishing robust temporal links with the onset of Deccan volcanism. *Geology* 46, 147–150.
- Barnet, J.S.K., Littler, K., Westerhold, T., Kroon, D., Leng, M.J., Bailey, I., Röhl, U., Zachos, J.C., 2019. A high-Fidelity Benthic Stable Isotope Record of late Cretaceous–early Eocene Climate Change and Carbon-Cycling. *Paleoceanography and Paleoclimatology* 34, 672–691.
- Barrera, E., Savin, S.M., 1999. Evolution of late Campanian-Maastrichtian marine climates and oceans. In: Barrera, E., Johnson, C.C. (Eds.), *Evolution of the Cretaceous Ocean-Climate System*. Geological Society of America Special Paper 332, pp. 245–282.
- Batenburg, S.J., Sprovieri, M., Gale, A.S., Hilgen, F.J., Hüsing, S., Laskar, J., Liebrand, D., Lirer, F., Orue-Etxebarria, X., Pelosi, N., Smit, J., 2012. Cyclostratigraphy and astronomical tuning of the Late Maastrichtian at Zumaia (Basque country, Northern Spain). *Earth and Planetary Science Letters* 359–360, 264–278.
- Batenburg, S.J., Friedrich, O., Moriya, K., Voigt, S., Cournède, C., Moebius, I., Blum, P., Bornemann, A., Fiebig, J., Hasegawa, T., Hull, P.M., Norris, R.D., Röhl, U., Sexton, P.F., Westerhold, T., Wilson, P.A., Matsui, H., 2018. Late Maastrichtian carbon isotope stratigraphy and cyclostratigraphy of the Newfoundland Margin (Site U1403, IODP Leg 342). *Newsletters on Stratigraphy* 51, 245–260.
- Bé, A.W.H., Hutson, W.H., Be, A.W.H., 1977. Ecology of Planktonic Foraminifera and Biogeographic Patterns of Life and Fossil Assemblages in the Indian Ocean. *Micropaleontology* 23, 369–414.

- Berger, W.H., Bonneau, M., Parker, F.L., Plateau, L., 1982. Foraminifera on the deep-sea floor: lysocline and dissolution rate. *Oceanologica Acta* 5, 249–258.
- Berggren, W.A., Pearson, P.N., 2005. A revised tropical to subtropical Paleogene planktonic foraminiferal zonation. *Journal of Foraminiferal Research* 35, 279–298.
- Bérmudez, H.D., Cui, Y., 2020. Record of events associated with the Chicxulub Asteroid impact in a deep-marine tropical section: evidence from Gorgonilla Island, Colombian Pacific. *Geological Society of America Abstracts with Programs* 52, 6.
- Birch, H.S., Coxall, H.K., Pearson, P.N., 2012. Evolutionary ecology of early Paleocene planktonic foraminifera: size, depth habitat and symbiosis. *Paleobiology* 38, 374–390.
- Birch, H.S., Coxall, H.K., Pearson, P.N., Kroon, D., Schmidt, D.N., 2016. Partial collapse of the marine carbon pump after the Cretaceous-Paleogene boundary. *Geology* 44, 287–290.
- Birch, H., Schmidt, D.N., Coxall, H.K., Kroon, D., Ridgwell, A., 2021. Ecosystem function after the K/Pg extinction: decoupling of marine carbon pump and diversity. *Proceedings of the Royal Society B* 288, 20210863.
- Blow, W. H., 1979. *The Cainozoic Foraminiferida. I & II*. Leiden, E. J. Brill. 1413 pp.
- Bolli, H.M., 1957. The genera *Globigerina* and *Globorotalia* in the Paleocene-lower Eocene Lizard Springs formation of Trinidad, B.W.I. *Bulletin of the United States National Museum* 215, 97–124.
- Bolli, H.M., 1966. Zonation of Cretaceous to Pliocene marine sediments based on planktonic foraminifera. *Boletín de la Asociación Venezolana de Geología, Minería y Petróleo* 9, (1), 1–34.
- BouDagher-Fadel, M., 2015. *Biostratigraphic and Geological Significance of Planktonic Foraminifera*. UCL Press. 320 pp.
- Bown, P., 2005. Selective calcareous nannoplankton survivorship at the Cretaceous-Tertiary boundary. *Geology* 33, 653–656.
- Bralower, T.J., Cosmidis, J., Heaney, P.J., Kump, L.R., Morgan, J. v., Harper, D.T., Lyons, S.L., Freeman, K.H., Grice, K., Wendler, J.E., Zachos, J.C., Artemieva, N., Chen, S.A., Gulick, S.P.S., House, C.H., Jones, H.L., Lowery, C.M., Nims, C., Schaefer, B., Thomas, E., Vajda, V., 2020. Origin of a global carbonate layer deposited in the aftermath of the Cretaceous-Paleogene boundary impact. *Earth and Planetary Science Letters* 548, 116476.



- Brugger, J., Feulner, G., Petri, S., 2017. Baby, it's cold outside: Climate model simulations of the effects of the asteroid impact at the end of the Cretaceous. *Geophysical Research Letters* 44, 419–427.
- Canudo, J.I., Keller, G., Molina, E., 1991. Cretaceous/Tertiary boundary extinction pattern and faunal turnover at Agost and Caravaca, S.E. Spain. *Marine Micropaleontology* 17, 319–341.
- Caron, M., 1985. Cretaceous planktic foraminifera. In: Bolli, H.M., Saunders, J.B., Perch-Nielsen, K. (Eds.), *Plankton stratigraphy*. Cambridge University Press, Cambridge. pp.17–86.
- Chenet, A.L., Quidelleur, X., Fluteau, F., Courtillot, V., Bajpai, S., 2007.  $^{40}\text{K}$ - $^{40}\text{Ar}$  dating of the main Deccan large igneous province: Further evidence of KTB age and short duration. *Earth and Planetary Science Letters* 263, 1–15.
- Chenet, A.L., Fluteau, F., Courtillot, V., Gérard, M., Subbarao, K. V., 2008. Determination of rapid Deccan eruptions across the Cretaceous-Tertiary boundary using paleomagnetic secular variation: Results from a 1200-m-thick section in the Mahabaleshwar escarpment. *Journal of Geophysical Research: Solid Earth* 113, B04101.
- Chenet, A.L., Courtillot, V., Fluteau, F., Gérard, M., Quidelleur, X., Khadri, S.F.R., Subbarao, K. v., Thordarson, T., 2009. Determination of rapid Deccan eruptions across the Cretaceous-Tertiary boundary using paleomagnetic secular variation: 2. Constraints from analysis of eight new sections and synthesis for a 3500-m-thick composite section. *Journal of Geophysical Research: Solid Earth* 114, 1–38.
- Claeys, P., Kiessling, W., Alvarez, W., 2002. Distribution of Chicxulub ejecta at the Cretaceous-Tertiary boundary. *Special Paper of the Geological Society of America* 356, 55–68.
- Clarke, L.J., Jenkyns, H.C., 1999. New oxygen isotope evidence for long-term Cretaceous climatic change in the Southern Hemisphere. *Geology* 27, 699–702.
- Clyde, W.C., Ramezani, J., Johnson, K.R., Bowring, S.A., Jones, M.M., 2016. Direct high-precision U-Pb geochronology of the end-Cretaceous extinction and calibration of Paleocene astronomical timescales. *Earth and Planetary Science Letters* 452, 272–280.
- Coccioni, R., Luciani, V., 2006. *Guembelitra irregularis* Bloom at the K-T Boundary: Morphological Abnormalities Induced by Impact-related Extreme Environmental

- Stress?, In: Cockell C., Gilmour I., Koeberl C. (Eds.), *Biological Processes Associated with Impact Events*. Springer-Verlag, pp. 179–196.
- Coccioni, R., Frontalini, F., Bancalà, G., Fornaciari, E., Jovane, L., Sprovieri, M., 2010. The Dan-C2 hyperthermal event at Gubbio (Italy): Global implications, environmental effects, and cause(s). *Earth and Planetary Science Letters* 297, 298–305.
- Courtillot, V., 1999. *Evolutionary Catastrophes: The Science of Mass Extinctions*. Cambridge University Press, Cambridge. 171 pp.
- Courtillot, V., Besse, J., Vandamme, D., Montigny, R., Jaeger, J.J., Capetta, H., 1986. Deccan flood basalts at the Cretaceous/Tertiary boundary. *Earth and Planetary Science Letters* 80, 361–374.
- Courtillot, V. E., Feraud, G., Maluski, H., Vandamme, D., Moreau, M. G., Besse, J., 1988. Deccan flood basalts and the Cretaceous/Tertiary boundary, *Nature* 333, 843–846.
- Cowie, J.W., Zieger, W., Remane, J., 1989. Stratigraphic Commission accelerates progress, 1984–1989: *Episodes* 112, 79–83
- Coxall, H.K., Wilson, P.A., Pälike, H., Lear, C.H., and Backman, J., 2005. Rapid stepwise onset of Antarctic glaciation and deeper calcite compensation in the Pacific Ocean. *Nature* 433, 53–57.
- Coxall, H.K., D'Hondt, S., Zachos, J.C., 2006. Pelagic evolution and environmental recovery after the Cretaceous-Paleogene mass extinction. *Geology* 34, 297–300.
- Cramer, B.S., Wright, J.D., Kent, D. v., Aubry, M.P., 2003. Orbital climate forcing of  $\delta^{13}\text{C}$  excursions in the late Paleocene-early Eocene (chrons C24n-C25n). *Paleoceanography* 18, 1–25.
- Cramer, B.S., Toggweiler, J.R., Wright, J.D., Katz, M.E., Miller, K.G., 2009. Ocean overturning since the Late Cretaceous: Inferences from a new benthic foraminiferal isotope compilation. *Paleoceanography* 24, PA4216.
- Cramer, B., Miller, K., Barrett, P., Wright, J., 2011. Late Cretaceous–Neogene trends in deep ocean temperature and continental ice volume: reconciling records of benthic foraminiferal geochemistry ( $\delta^{18}\text{O}$  and Mg/Ca) with sea level history. *Journal of Geophysical Research: Oceans* (1978–2012) 116, C12023.
- DePalma, R.A., Smit, J., Burnham, D.A., Kuiper, K., Manning, P.L., Oleinik, A., Larson, P., Maurrasse, F.J., Vellekoop, J., Richards, M.A., Gurche, L., Alvarez, W., 2019. A seismically induced onshore surge deposit at the K-Pg boundary, North Dakota.

- Proceedings of the National Academy of Sciences of the United States of America 116, 8190–8199.
- D'Hondt, S., 2005. Consequences of the Cretaceous/Paleogene mass extinction for marine ecosystems. *Annual Review of Ecology, Evolution, and Systematics* 36, 295–317.
- D'Hondt, S., Zachos, J.C., 1993. On stable isotopic variation and earliest Paleocene planktonic foraminifera. *Paleoceanography* 8, 527–547.
- D'Hondt, S., Arthur, M.A., 1995. Interspecies variation in stable isotopic signals of Maastrichtian planktonic foraminifera. *Paleoceanography* 10, 123–135.
- D'Hondt, S., Donaghay, P., Zachos, J.C., Luttenberg, D., Lindinger, M., 1998. Organic Carbon Fluxes and ecological recovery for Cretaceous tertiary mass extinction. *Science* 282, 276–279.
- Dinarès-Turell, J., Westerhold, T., Pujalte, V., Röhl, U., Kroon, D., 2014. Astronomical calibration of the Danian stage (early Paleocene) revisited: Settling chronologies of sedimentary records across the Atlantic and Pacific Oceans. *Earth and Planetary Science Letters* 405, 119–131.
- Dupuis, C., Steurbaut, E., Molina, E., Rauscher, R., Tribovillard, N., Arenillas, I., Arz, J.A., Robaszynski, F., Caron, M., Robin, E., Rocchia, R., Lefevre, I., 2001. The Cretaceous-Palaeogene (K/P) boundary in the Aïn Settara section (Kalaat senan, Central Tunisia): Lithological, micropalaeontological and geochemical evidence. *Bulletin de l'Institut Royal des Sciences Naturelles de Belgique, Sciences de la Terre* 71, 169–190.
- Eddy, M.P., Schoene, B., Samperton, K.M., Keller, G., Adatte, T., Khadri, S.F.R., 2020. U-Pb zircon age constraints on the earliest eruptions of the Deccan Large Igneous Province, Malwa Plateau, India. *Earth and Planetary Science Letters* 540, 116249.
- Ernst, R.E., Bond, D.P.G., Zhang, S.H., Buchan, K.L., Grasby, S.E., Youbi, N., El Bilali, H., Bekker, A., Doucet, L.S., 2021. Large Igneous Province Record Through Time and Implications for Secular Environmental Changes and Geological Time-Scale Boundaries. In: Ernst, R.E., Dickson, A.J., Bekker, A. (Eds.), *Large Igneous Provinces*. *Geophysical Monograph Series*, 508 pp.
- Falzone, F., Petrizzo, M.R., Huber, B.T., MacLeod, K.G., 2014. Insights into the meridional ornamentation of the planktonic foraminiferal genus *Rugoglobigerina* (Late Cretaceous) and implications for taxonomy. *Cretaceous Research* 47, 87–104.

- Falzone, F., Petrizzo, M.R., Jenkyns, H.C., Gale, A.S., Tsikos, H., 2016. Planktonic foraminiferal biostratigraphy and assemblage composition across the Cenomanian-Turonian boundary interval at Clot Chevalier (Vocontian Basin, SE France). *Cretaceous Research* 59, 69–97.
- Fendley, I.M., Sprain, C.J., Renne, P.R., Arenillas, I., Arz, J.A., Gilabert, V., Self, S., Vanderkluyzen, L., Pande, K., Smit, J., Mittal, T., 2020. No Cretaceous-Paleogene Boundary in Exposed Rajahmundry Traps: A Refined Chronology of the Longest Deccan Lava Flows From  $^{40}\text{Ar}/^{39}\text{Ar}$  Dates, Magnetostratigraphy, and Biostratigraphy. *Geochemistry, Geophysics, Geosystems* 21, (9), e2020GC009149.
- Font, E., Adatte, T., Andrade, M., Keller, G., Mbabi Bitchong, A., Carvalho, C., Ferreira, J., Diogo, Z., Mirão, J., 2018. Deccan volcanism induced high-stress environment during the Cretaceous–Paleogene transition at Zumaia, Spain: Evidence from magnetic, mineralogical and biostratigraphic records. *Earth and Planetary Science Letters* 484, 53–66.
- Foster, G.L., Hull, P., Lunt, D.J., Zachos, J.C., 2018. Placing our current “hyperthermal” in the context of rapid climate change in our geological past. *Philosophical Transactions of the Royal Society A: Mathematical, Physical and Engineering Sciences* 376, 20170086.
- Frakes, L., Francis, J., Syktus, J., 1992. *Climate Modes of the Phanerozoic: The History of the Earth's Climate Over the Past 600 Million Years*. Cambridge University Press, Cambridge, 274 pp.
- Francis, J.E., Frakes, L., 1993. Cretaceous climates. *Sedimentology Review* 1, 17–30.
- Freeman, K.H., Hayes, J., 1992. Fractionation of carbon isotopes by phytoplankton and estimates of ancient CO<sub>2</sub> levels. *Global Biogeochemical Cycles* 6, 185–198.
- Friedrich, O., Norris, R.D., Erbacher, J., 2012. Evolution of middle to Late Cretaceous oceans—a 55 m.y. record of Earth's temperature and carbon cycle. *Geology* 40, 107–110.
- Gallala, N., Zaghbib-Turki, D., Arenillas, I., Arz, J.A., Molina, E., 2009. Catastrophic mass extinction and assemblage evolution in planktic foraminifera across the Cretaceous/Paleogene (K/Pg) boundary at Bidart (SW France). *Marine Micropaleontology* 72, 196–209.
- Gallala, N., 2013. Planktonic Foraminiferal Biostratigraphy and Correlation Across the Cretaceous-Paleogene Transition at the Tethyan and the Atlantic Realms. *Paleontology Journal* 2013, 1–20.

- Gertsch, B., Keller, G., Adatte, T., Garg, R., Prasad, V., Berner, Z., Fleitmann, D., 2011. Environmental effects of Deccan volcanism across the Cretaceous-Tertiary transition in Meghalaya, India. *Earth and Planetary Science Letters* 310, 272–285.
- Gibbs, S.J., Bown, P.R., Ward, B.A., Alvarez, S.A., Kim, H., Archontikis, O.A., Sauterey, B., Poulton, A.J., Wilson, J., Ridgwell, A., 2020. Algal plankton turn to hunting to survive and recover from end-Cretaceous impact darkness. *Science Advances* 6, eabc9123.
- Gibson, T.G., 1989. Planktonic benthonic foraminiferal ratios: Modern patterns and Tertiary applicability. *Marine Micropaleontology* 15, 29–52.
- Gilbert, V., Arz, J.A., Arenillas, I., Robinson, S.A., Ferrer, D., 2021a. Influence of the Latest Maastrichtian Warming Event on planktic foraminiferal assemblages and ocean carbonate saturation at Caravaca, Spain. *Cretaceous Research* 125, 104844.
- Gilbert, V., Arenillas, I., Arz, J.A., Batenburg, S.J., Robinson, S.A., 2021b. Multiproxy analysis of paleoenvironmental, paleoclimatic and paleoceanographic changes during the early Danian in the Caravaca section (Spain). *Palaeogeography, Palaeoclimatology, Palaeoecology* 576, 110513.
- Gilbert, V., Batenburg, S.J., Arenillas, I., Arz, J.A., 2021c. Contribution of orbital forcing and Deccan volcanism to global climatic and biotic changes across the Cretaceous-Paleogene boundary at Zumaia, Spain 49, 1–5.
- Gilmour, I., Gilmour, M., Jolley, D., Kelley, S., Kemp, D., Daly, R., Watson, J., 2013. A high-resolution nonmarine record of an early Danian hyperthermal event, Boltysch crater, Ukraine. *Geology* 41, 783–786.
- Gilmour, I., Jolley, D., Kemp, D., Kelley, S., Gilmour, M., Daly, R., Widdowson, M., 2014. The early Danian hyperthermal event at Boltysch (Ukraine): Relation to Cretaceous-Paleogene boundary events. *Special Paper of the Geological Society of America* 505, 133–146.
- Giorgioni, M., Jovane, L., Rego, E.S., Rodelli, D., Frontalini, F., Coccioni, R., Catanzariti, R., Özcan, E., 2019. Carbon cycle instability and orbital forcing during the Middle Eocene Climatic Optimum. *Scientific Reports* 2019 9:1 9, 1–10.
- Goldin, T.J., Melosh, H.J., 2009. Self-shielding of thermal radiation by Chicxulub impact ejecta: Firestorm or fizzle? *Geology* 37, 1135–1138.
- Gradstein, F.M.; Ogg, J.G.; Schmitz, M.D.; Ogg, G.M. *The Geologic Time Scale 2020*. Elsevier, 2020, 1357 pp.

- Grajales-Nishimura, J.M., Murillo, G., Rosales, M.C., Cedillo, E., and García, J., 2003. Heterogeneity of lithoclast composition in the deep-water carbonate breccias of the K/T Campeche. In: Bartolini, C., et al., (Eds.), *The circum-Gulf of Mexico and the Caribbean: Hydrocarbon habitats, basin formation, and plate tectonics: American Association of Petroleum Geologists Memoir 79*, pp. 312–329.
- Hammer, Ø., Harper, D.A.T., Ryan, P.D., 2001. PAST: Paleontological statistics software package for education and data analysis. *Paleontologia Electronica* 4, (1), 9.
- Haq, B.U., 2014. Cretaceous eustasy revisited. *Global and Planetary Change* 113, 44–58.
- Hart, M. B., 1980. A water depth model for the evolution of the planktonic Foraminiferida. *Nature* 286, (5770), 252–254.
- Helm, K.P., Bindoff, N.L., Church, J.A., 2011. Observed decreases in oxygen content of the global ocean: Global decreases in ocean oxygenic levels. *Geophysical Research Letters* 38, 1–6.
- Hemleben, C., Spindler, M., Anderson, O.R., 1989. *Modern planktonic Foraminifera*. New York (Springer), 363 pp.
- Henehan, M.J., Hull, P.M., Penman, D.E., Rae, J.W.B., Schmidt, D.N., 2016. Biogeochemical significance of pelagic ecosystem function: An end-Cretaceous case study. *Philosophical Transactions of the Royal Society B: Biological Sciences* 371, 20150510.
- Henehan, M.J., Ridgwell, A., Thomas, E., Zhang, S., Alegret, L., Schmidt, D.N., Rae, J.W.B., Witts, J.D., Landman, N.H., Greene, S.E., Huber, B.T., Super, J.R., Planavsky, N.J., Hull, P.M., 2019. Rapid ocean acidification and protracted Earth system recovery followed the end-Cretaceous Chicxulub impact. *Proceedings of the National Academy of Sciences of the United States of America* 116, 22500–22504.
- Hernandez Nava, A., Black, B.A., Gibson, S.A., Bodnar, R.J., Renne, P.R., Vanderkluysen, L., 2021. Reconciling early Deccan Traps CO<sub>2</sub> outgassing and pre-KPB global climate. *Proceedings of the National Academy of Sciences* 118, e2007797118.
- Hildebrand, A.R., Penfield, G.T., Kring, D.A., Pilkington, M., Antonio, C.Z., Boynton, W. v., 1991. Chicxulub crater: a possible Cretaceous/Tertiary boundary impact crater on the Yucatan Peninsula, Mexico. *Geology* 19, 867–871.
- Hofker, J., 1978. Analysis of a large succession of samples through the Maastrichtian and the lower Tertiary of Drill Hole 47.2, Shatsky Rise, Pacific, Deep Sea Drilling Project. *The Journal of Foraminiferal Research* 8, 46–75.

- Huber, B.T., 1996. Evidence for planktonic foraminifer reworking versus survivorship across the Cretaceous-Tertiary boundary at high latitudes. *Special Paper of the Geological Society of America* 307, 319–334.
- Huber, B.T., Hodell, D.A., Hamilton, C.P., 1995. Middle–Late Cretaceous climate of the southern high latitudes: stable isotopic evidence for minimal equator-to-pole thermal gradients. *Geological Society of America Bulletin* 107, 1164–1191.
- Huber, B.T., MacLeod, K.G., Norris, R.D., 2002. Abrupt extinction and subsequent reworking of Cretaceous planktonic foraminifera across the Cretaceous-Tertiary boundary: Evidence from the subtropical North Atlantic. *Special Paper of the Geological Society of America* 356, 277–289.
- Huber, B.T., MacLeod, K.G., Watkins, D.K., Coffin, M.F., 2018. The rise and fall of the Cretaceous Hot Greenhouse climate. *Global and Planetary Change* 167, 1–23.
- Hull, P.M., Bornemann, A., Penman, D.E., Henahan, M.J., Norris, R.D., Wilson, P.A., Blum, P., Alegret, L., Batenburg, S.J., Bown, P.R., Bralower, T.J., Cournede, C., Deutsch, A., Donner, B., Friedrich, O., Jehle, S., Kim, H., Kroon, D., Lippert, P.C., Loroch, D., Moebius, I., Moriya, K., Peppe, D.J., Ravizza, G.E., Röhl, U., Schueth, J.D., Sepúlveda, J., Sexton, P.F., Sibert, E.C., Śliwińska, K.K., Summons, R.E., Thomas, E., Westerhold, T., Whiteside, J.H., Yamaguchi, T., Zachos, J.C., 2020. On impact and volcanism across the Cretaceous-Paleogene boundary. *Science* 367, 266–272.
- Hsü, K. J., and J. A. McKenzie. 1985. “Strangelove” ocean in the earliest Tertiary. *American Geophysical Union, Geophysical Monograph Series* 32, 487–892.
- Isaza-Londoño, C., MacLeod, K.G., Huber, B.T., 2006. Maastrichtian North Atlantic warming, increasing stratification, and foraminiferal paleobiology at three timescales. *Paleoceanography* 21, 1–10.
- Jablonski, D., 2001. Lessons from the past: Evolutionary impacts of mass extinctions. *Proceedings of the National Academy of Sciences* 98, 5393–5398.
- Jay, A.E., Mac Niocaill, C., Widdowson, M., Self, S., Tuner, W., 2009. New Palaeomagnetic data from the Mahabaleshwar Plateau, Deccan Flood Basalt Province, India: Implications from the volcanostratigraphic architecture of Continental Flood Basalt Provinces. *Journal of Geological Society of London* 166, 1–12.

- Jay, A.E., Widdowson, M., 2008. Stratigraphy, structure and volcanology of the SE Deccan continental flood basalt province: Implications for eruptive extent and volumes. *Journal of the Geological Society* 165, 177–188.
- Jenkyns, H.C., 2010. Geochemistry of oceanic anoxic events. *Geochemistry, Geophysics, Geosystems* 11, Q03004.
- Jenkyns, H.C., Gale, A.S., Corfield, R.M., 1994. Carbon-and oxygen-isotope stratigraphy of the English Chalk and Italian Scaglia and its palaeoclimatic significance. *Geological Magazine* 131, 1–34.
- Jiang, S., Chen, X., Bernaola, G., 2019. Environmental controls on calcareous nannoplankton response to the Cretaceous/Paleogene mass extinction in the Tethys realm. *Palaeogeography, Palaeoclimatology, Palaeoecology* 515, 134–142.
- Jolley, D.W., Daly, R.J., Ebbinghaus, A., Kemp, D.B., Gilmour, I., mac Niocaill, C., Kelley, S.P., 2017. Centennial to decadal vegetation community changes linked to orbital and solar forcing during the Dan-C2 hyperthermal event. *Journal of the Geological Society* 174, 1019–1030.
- Jones, H.L., Lowery, C.M., Bralower, T.J., 2019. Delayed calcareous nannoplankton boom-bust successions in the earliest Paleocene Chicxulub (Mexico) impact crater. *Geology* 47, 753–756.
- Kaiho, K., Kajiwar, Y., Tazaki, K., Ueshima, M., Takeda, N., Kawahata, H., Arinobu, T., Ishiwatari, R., Hirai, A., Lamolda, M.A., 1999. Oceanic primary productivity and dissolved oxygen levels at the Cretaceous/Tertiary Boundary: Their decrease, subsequent warming, and recovery. *Paleoceanography* 14, 511–524.
- Kaiho, K., Oshima, N., Adachi, K., Adachi, Y., Mizukami, T., Fujibayashi, M., Saito, R., 2016. Global climate change driven by soot at the K-Pg boundary as the cause of the mass extinction. *Scientific Reports* 6, 1–13.
- Kawaragi, K., Sekine, Y., Kadono, T., Sugita, S., Ohno, S., Ishibashi, K., Kurosawa, K., Matsui, T., Ikeda, S., 2009. Direct measurements of chemical composition of shock-induced gases from calcite: an intense global warming after the Chicxulub impact due to the indirect greenhouse effect of carbon monoxide. *Earth and Planetary Science Letters* 282, 56–64.
- Keller, G., 1988. Extinction, Survivorship and Evolution of Planktic Foraminifera across the Cretaceous/Tertiary Boundary at El Kef, Tunisia. *Marine Micropaleontology* 13, 239–263.



- Keller, G., Lindinger, M., 1989. Stable isotope, TOC and CaCO<sub>3</sub> record across the cretaceous/tertiary boundary at El Kef, Tunisia. *Palaeogeography, Palaeoclimatology, Palaeoecology* 73, 243–265.
- Keller, G., 2003a. Biotic effects of impacts and volcanism. *Earth and Planetary Science Letters* 215, 249–264.
- Keller, G., 2003b. *Guembelitra*-dominated late Maastrichtian planktic foraminiferal assemblages mimic early Danian in central Egypt. *Marine Micropaleontology* 47, 71–99.
- Keller, G., 2005. Biotic effects of late Maastrichtian mantle plume volcanism: Implications for impacts and mass extinctions. *Lithos* 79, 317–341
- Keller, G., Pardo, A., 2004. Disaster opportunists *Guembelitrinidae*: Index for environmental catastrophes. *Marine Micropaleontology* 53, 83–116.
- Keller, G., Abramovich, S., 2009. Lilliput effect in late Maastrichtian planktic foraminifera: Response to environmental stress. *Palaeogeography, Palaeoclimatology, Palaeoecology* 284, 47–62.
- Keller, G., Barrera, E., Schmitz, B., Mattson, E., 1993. Long-term oceanic instability but no mass extinction or major  $\delta^{13}\text{C}$  shift in planktic foraminifera across the Cretaceous/Tertiary boundary in Northern high latitudes: Evidence from Nye Klov, Denmark, *Geological Society of America Bulletin* 105, 979–997.
- Keller, G., Li, L., and MacLeod, N., 1995, The Cretaceous/Tertiary boundary stratotype section at El Kef, Tunisia: How catastrophic was the mass extinction?. *Palaeogeography, Palaeoclimatology, Palaeoecology*, 119, 221–254.
- Keller, G., Li, L., MacLeod, N., 1996. The Cretaceous/Tertiary boundary stratotype section at El Kef, Tunisia: How catastrophic was the mass extinction? *Palaeogeography, Palaeoclimatology, Palaeoecology* 119, 221–254.
- Keller, G., Lopez-Oliva, J.G., Stinnesbeck, W., Adatte, T., 1997. Age, stratigraphy and deposition of near K/T siliciclastic deposits in Mexico: Relation to bolide impact? *Geological Society of America Bulletin* 109, 410–428.
- Keller, G., Stinnesbeck, W., Adatte, T., Stüben, D., 2003. Multiple impacts across the Cretaceous-Tertiary boundary: *Earth-Science Reviews* 62, 327–363.
- Keller, G., Adatte, T., Stinnesbeck, W., Rebolledo-Vieyra, M., Urrutia Fucugauchi, J., Kramar, U., Stueben, D., 2004. Chicxulub crater predates K-T mass extinction: *Proceedings of the National Academy of Sciences of the United States of America* 101, 3753–3758.

- Keller, G., Adatte, T., Gardin, S., Bartolini, A., Bajpai, S., 2008. Main Deccan volcanism phase ends near the K-T boundary: Evidence from the Krishna-Godavari Basin, SE India. *Earth and Planetary Science Letters* 268, 293–311.
- Keller, G., Adatte, T., Pardo Juez, A., Lopez-Oliva, J., 2009. New evidence concerning the age and biotic effects of the Chicxulub impact in NE Mexico: *Journal of the Geological Society of London* 166, 393–411.
- Keller, G., Adatte, T., Pardo, A., Bajpai, S., Khosla, A., Samant, B., 2010. Cretaceous Extinctions: Evidence Overlooked, *Science* 328, 974–975.
- Keller, G.K., Bhowmick, P.K., Upadhyay, H., Dave, A., Reddy, A.N., Jaiprakash, B.C., Adatte, T., 2011. Deccan volcanism linked to the Cretaceous-Tertiary boundary mass extinction: New evidence from ONGC wells in the Krishna-Godavari Basin. *Journal of the Geological Society of India* 78, 399–428.
- Keller, G., Adatte, T., Bhowmick, P.K., Upadhyay, H., Dave, A., Reddy, A.N., Jaiprakash, B.C., 2012. Nature and timing of extinctions in Cretaceous-Tertiary planktic foraminifera preserved in Deccan intertrappean sediments of the Krishna-Godavari Basin, India. *Earth and Planetary Science Letters* 341–344, 211–221.
- Keller, G., Punekar, J., Mateo, P., 2016. Upheavals during the Late Maastrichtian: Volcanism, climate and faunal events preceding the end-Cretaceous mass extinction. *Palaeogeography, Palaeoclimatology, Palaeoecology* 441, 137–151.
- Keller, G., Mateo, P., Monkenbusch, J., Thibault, N., Punekar, J., Spangenberg, J.E., Abramovich, S., Ashckenazi-Polivoda, S., Schoene, B., Eddy, M.P., Samperton, K.M., Khadri, S.F.R., Adatte, T., 2020. Mercury linked to Deccan Traps volcanism, climate change and the end-Cretaceous mass extinction. *Global and Planetary Change* 194, 103312.
- Kennett, J. P., Stott, L.D., 1991. Abrupt deep-sea warming, palaeoceanographic changes and benthic extinctions at the end of the Palaeocene. *Nature* 353, 412–414.
- Krahl, G., Bom, M.H.H., Kochhann, K.G.D., Souza, L. v., Savian, J.F., Fauth, G., 2020. Environmental changes occurred during the early Danian at the Rio Grande Rise, South Atlantic Ocean. *Global and Planetary Change* 191, 103197.
- Kring, D.A., 2007. The Chicxulub impact event and its environmental consequences at the Cretaceous-Tertiary boundary. *Palaeogeography, Palaeoclimatology, Palaeoecology* 255, 4–21.
- Kroon, D., Nederbragt, A.J., 1990. Ecology and paleoecology of triserial planktic foraminifera. *Marine Micropaleontology* 16, 25–38.

- Kucera, M., 2007. Chapter Six Planktonic Foraminifera as Tracers of Past Oceanic Environments. *Developments in Marine Geology* 1, 213–262.
- Kucera, M., Malmgren, B., (1996): Latitudinal variation in the planktic foraminifer *Contusotruncana contusa* in the terminal Cretaceous ocean. *Marine Micropaleontology*, 28(1), 31-52.
- Kucera, M., Malmgren, B.A., Sturesson, U., 1997. Foraminiferal dissolution at shallow depths of the Walvis Ridge and Rio Grande Rise during the latest cretaceous: Inferences for deep-water circulation in the South Atlantic. *Palaeogeography, Palaeoclimatology, Palaeoecology* 129, 195–212.
- Kuypers, M. M. M., Pancost, R. D., Damsté, J. S. S., 1999. A large and abrupt fall in atmospheric CO<sub>2</sub> concentration during Cretaceous times. *Nature* 399, 342–345.
- Lamolda, M.A., Melinte, M.C., Kaiho, K., 2005. Nannofloral extinction and survivorship across the K/T boundary at Caravaca, southeastern Spain. *Palaeogeography, Palaeoclimatology, Palaeoecology* 224, 27–52.
- Laskar, J., Gastineau, M., Delisle, J.-B., Farrés, A., Fienga, A., 2011. Strong chaos induced by close encounters with Ceres and Vesta. *Astronomy and Astrophysics* 532, 1–4.
- Lauretano, V., Littler, K., Polling, M., Zachos, J.C., Lourens, L.J., 2015. Frequency, magnitude and character of hyperthermal events at the onset of the Early Eocene Climatic Optimum. *Climate of the Past* 11, 1313–1324.
- Lear, C.H., Bailey, T.R., Pearson, P.N., Coxall, H.K., Rosenthal, Y., 2008. Cooling and ice growth across the Eocene-Oligocene transition. *Geology* 36, 251–254.
- Li, L., Keller, G., 1998a. Maastrichtian climate, productivity and faunal turnovers in planktic foraminifera in South Atlantic DSDP sites 525A and 21. *Marine Micropaleontology* 33, 55–86.
- Li, L., Keller, G., 1998b. Abrupt deep-sea warming at the end of the Cretaceous. *Geology* 26, 995–998.
- Lirer, F., 2000, A new technique for retrieving calcareous microfossils from lithified lime deposits. *Micropaleontology* 46, 365–369.
- Littler, K., Robinson, S.A., Bown, P.R., Nederbragt, A.J., Pancost, R.D., 2011. High sea-surface temperatures during the Early Cretaceous Epoch. *Nature Geosciences* 4, 169–172.
- Littler, K., Rohl, U., Westerhold, T., Zachos, J.C., 2014. A high-resolution benthic stable-isotope record for the South Atlantic: Implications for orbital-scale changes in Late

- Paleocene–Early Eocene climate and carbon cycling. *Earth and Planetary Science Letters* 401, 18–30.
- Linnert, Ch., Robinson, S.A., Lees, J.A., Bown, P.R., Pérez-Rodríguez, I., Petrizzo, M.R., Falzoni, F., Littler, K., Arz, J.A., Russell, E.E., 2014. Evidence for global cooling in the Late Cretaceous. *Nature Communications* 5, 4194.
- Loeblich Jr., A. R., y Tappan, H. (1987). *Foraminiferal general and their classification*. Van Nostrand Reinhold Company. 970 pp.
- Lowery, C.M., Fraass, A.J., 2019. Morphospace expansion paces taxonomic diversification after end Cretaceous mass extinction. *Nature Ecology and Evolution* 3, 900–904.
- Lowery, C.M., Bralower, T.J., Owens, J.D., Rodríguez-Tovar, F.J., Jones, H., Smit, J., Whalen, M.T., Claeys, P., Farley, K., Gulick, S.P.S., Morgan, J. v., Green, S., Chenot, E., Christeson, G.L., Cockell, C.S., Coolen, M.J.L., Ferrière, L., Gebhardt, C., Goto, K., Kring, D.A., Lofi, J., Ocampo-Torres, R., Perez-Cruz, L., Pickersgill, A.E., Poelchau, M.H., Rae, A.S.P., Rasmussen, C., Rebolledo-Vieyra, M., Riller, U., Sato, H., Tikoo, S.M., Tomioka, N., Urrutia-Fucugauchi, J., Vellekoop, J., Wittmann, A., Xiao, L., Yamaguchi, K.E., Zylberman, W., 2018. Rapid recovery of life at ground zero of the end-Cretaceous mass extinction. *Nature* 558, 288–291.
- Lowery, C.M., Bown, P.R., Fraass, A.J., Hull, P.M., 2020. Ecological Response of Plankton to Environmental Change: Thresholds for Extinction. *Annual Review of Earth and Planetary Sciences* 48, 403–429.
- Lowery, C. M., Jones, H. L., Bralower, T. J., Cruz, L. P., Gebhardt, C., Whalen, M. T., Chenot, E., Smit, J., Phillips, M. P., Choumiline, K., Arenillas, I., Arz, J. A., Garcia, F., Ferrand, M., & Gulick, S. P. S. (2021). Early Paleocene Paleoceanography and Export Productivity in the Chicxulub Crater. *Paleoceanography and Paleoclimatology*, 36, (11), e2021PA004241.
- Luciani, V., 1997. Planktonic foraminiferal turnover across the Cretaceous–Tertiary boundary in the Vajont valley (Southern Alps, northern Italy), *Cretaceous Research*, 18, 799–821.
- Luterbacher, H.P., 1964. Studies in some *Globorotalia* from the Paleocene and lower Eocene of the central Apennines. *Eclogae Geologicae Helvetiae* 57, (2), 631–730.
- Luterbacher, H.P., Premoli Silva, I., 1964. Biostratigrafia del limite Cretaceo-Terziario nell'Apennino Centrale. *Rivista Italiana di Paleontologia e Stratigrafia* 70, (1), 67–128.

- MacLeod, N., Keller G., 1994. Comparative biogeographic analysis of planktic foraminiferal survivorship across the Cretaceous/Tertiary (K/T) boundary, *Paleobiology*, 20, (2), 143–177.
- MacLeod, N., Ortiz, N., Fefferman, N., Clyde, W., Schuller, C., MacLean, J., 2000. Phenotypic response of foraminifera to episodes of global environmental change. In: Culver, S.J., Rawson, P. (Eds.), *Biotic Response to Global Environmental Change: The Last 145 Million Years*. Cambridge University Press, Cambridge, pp. 51–78.
- MacLeod, K.G., Huber, B.T., Pletsch, T., Röhl, U., Kucera, M., 2001. Maastrichtian foraminiferal and paleoceanographic changes on Milankovitch time scales. *Paleoceanography* 16, 133–154.
- MacLeod, K.G., Huber, B.T., Isaza-Londoño, C., 2005. North Atlantic warming during global cooling at the end of the Cretaceous. *Geology* 33, 437–440.
- MacLeod, K.G., Huber, B.T., Berrocoso, Á.J., Wendler, I., 2013. A stable and hot Turonian without glacial  $\delta^{18}\text{O}$  excursions is indicated by exquisitely preserved Tanzanian foraminifera. *Geology* 41, 1083–1086.
- Malmgren, B. A., 1987. Differential dissolution of Upper Cretaceous planktonic foraminifera from a temperate region of the South Atlantic Ocean. *Marine Micropaleontology* 11, (4), 251–271.
- Malmgren, B., Kennett, J.P., 1978. Test size variation in *Globigerina bulloides* in response to Quaternary palaeoceanographic changes. *Nature* 275, 123–124.
- Mancin, N., Darling, K., 2015. Morphological abnormalities of planktonic foraminiferal tests in the SW Pacific Ocean over the last 550 ky. *Marine Micropaleontology* 120, 1–19.
- Mateo, P., Keller, G., Punekar, J., Spangenberg, J.E., 2017. Early to Late Maastrichtian environmental changes in the Indian Ocean compared with Tethys and South Atlantic. *Palaeogeography, Palaeoclimatology, Palaeoecology* 478, 121–138.
- McGowran, B., 2008. *Biostratigraphy - Microfossils and Geological Time*. Cambridge University Press, 459 pp.
- McInerney, F. A., Wing, S. L., 2011. The Paleocene-Eocene Thermal Maximum: a Perturbation of Carbon Cycle, Climate, and Biosphere with Implications for the Future. *Annual Review of Earth and Planetary Sciences* 39, 489–516.
- Metsana-Oussaid, F., Belhai, D., Arenillas, I., Arz, J.A., Gilabert, V., 2019. New sections of the Cretaceous–Paleogene transition in the southwestern Tethys (Médéa, northern

- Algeria): planktic foraminiferal biostratigraphy and biochronology. *Arabian Journal of Geosciences* 12, 217.
- Miller, K.G., Fairbanks, R.G., Mountain, G.S., 1987. Tertiary oxygen isotope synthesis, sea level history, and continental margin erosion. *Paleoceanography* 2, 1–19.
- Miller, K.G., Wright, J.D., Browning, J.V., 2005. Visions of ice sheets in a greenhouse world. *Marine Geology* 217, 215–231.
- Milliman, J.D., 1993. Production and accumulation of calcium carbonate in the ocean: Budget of a non-steady state. *Global Biogeochemical Cycles* 7, 927–957.
- Molina, E., Arenillas, I., Arz, J.A., 1998. Mass extinction in planktic foraminifera at the Cretaceous/Tertiary boundary in subtropical and temperate latitudes. *Bulletin de la Société géologique de France* 169, (3), 351–363.
- Molina, E., Alegret, L., Arenillas, I., Arz, J.A., Gallala, N., Hardenbol, J., von Salis, K., Steurbaut, E., Vandenberghe, N., Zaghbib-Turki, D., Molina, E., Alegret, L., 2006. The global boundary stratotype section and point for the base of the Danian stage (Paleocene, Paleogene, “Tertiary”, Cenozoic) at El Kef, Tunisia. Original definition and revision. *Episodes* 29, 263–273.
- Molina, E., Alegret, L., Arenillas, I., Arz, J.A., Gallala, N., Grajales-Nishimura, J.M., Murillo-Muñetón, G., Zaghbib-Turki, D., 2009. The Global Boundary Stratotype Section and Point for the base of the Danian Stage (Paleocene, Paleogene, “Tertiary”, Cenozoic): Auxiliary sections and correlation. *Episodes* 32, 84–95.
- Morgan, J., Artemieva, N., Goldin, T., 2013. Revisiting wildfires at the K-Pg boundary. *Journal of Geophysical Research: Biogeosciences* 118, 1508–1520.
- Nederbragt, A.J., 1991. Late Cretaceous biostratigraphy and development of Heterohelicidae (planktic foraminifera). *Micropaleontology* 37, 329–372.
- Norris, R. D., Huber, B. T., Self-Trail, J., 1999. Synchronicity of the K-T oceanic mass extinction and meteorite impact: Blake Nose, western North Atlantic. *Geology* 27, (5), 419–422.
- Norris, R.D., Kirtland Turner, S., Hull, P.M., Ridgwell, A., 2013. Marine ecosystem responses to Cenozoic global change. *Science* 341, 492–498.
- O’Brien, C.L., Robinson, S.A., Pancost, R.D., Sinninghe Damsté, J.S., Schouten, S., Lunt, D.J., Alsenz, H., Bornemann, A., Bottini, C., Brassell, S.C., Farnsworth, A., Forster, A., Huber, B.T., Inglis, G.N., Jenkyns, H.C., Linnert, C., Littler, K., Markwick, P., McAnena, A., Mutterlose, J., Naafs, B.D.A., Püttmann, W., Sluijs, A., van Helmond, N.A.G.M., Vellekoop, J., Wagner, T., Wrobel, N.E., 2017. Cretaceous

- sea-surface temperature evolution: Constraints from TEX<sub>86</sub> and planktonic foraminiferal oxygen isotopes. *Earth-Science Reviews* 172, 224–247.
- Olsson, R.K., Berggren, W.A., Hemleben, C., Huber, B.T., 1999. Atlas of Paleocene Planktonic Foraminifera. *Smithsonian Contributions to Paleobiology*, 1–252.
- Olsson, R.K., Wright, J.D., Miller, K.G., 2001. Paleobiogeography of *Pseudotextularia elegans* during the latest Maastrichtian global warming event. *Journal of Foraminiferal Research* 31, 275–282.
- Olsson, R. K., Miller, K. G., Browning, J. V., Wright, J. D., Cramer, B. S., 2002. Sequence stratigraphy and sea-level change across the Cretaceous-Tertiary boundary on the New Jersey passive margin. *Geological Society of America Special Paper* 356, 97–108.
- Pardo, A., Keller, G., 2008. Biotic effects of environmental catastrophes at the end of the Cretaceous and early Tertiary: *Guembelitra* and *Heterohelix* blooms. *Cretaceous Research* 29, 1058–1073.
- Paull, C.K., Caress, D.W., Gwiazda R., Urrutia-Fucugauchi J., Rebolledo-Vieyra M., Lundsten E., Anderson K., Sumner E.J., 2014. Cretaceous–Paleogene boundary exposed: Campeche Escarpment, Gulf of Mexico. *Marine Geology* 357, 392–400.
- Pearson, P.N., Foster, G.L., Wade, B.S., 2009. Atmospheric carbon dioxide through the Eocene-Oligocene climate transition. *Nature* 461, 1110–1113.
- Pérez-Rodríguez, I., 2013. Biocronoestratigrafía y evolución ambiental del Coniaciense superior al Maastrichtiense con foraminíferos planctónicos. tesis doctoral. Universidad de Zaragoza, Zaragoza, 346 pp.
- Petersen, S. v., Dutton, A., Lohmann, K.C., 2016. End-Cretaceous extinction in Antarctica linked to both Deccan volcanism and meteorite impact via climate change. *Nature Communications* 7, 12079.
- Petruzzo, M.R., Huber, B.T., Falzoni, F., MacLeod, K.G., 2020. Changes in biogeographic distribution patterns of southern mid-to high latitude planktonic foraminifera during the Late Cretaceous hot to cool greenhouse climate transition. *Cretaceous Research* 115, 104547.
- Pickersgill, A.E., Mark, D.F., Lee, M.R., Kelley, S.P., Jolley, D.W., 2021. The Boltsh impact structure: An early Danian impact event during recovery from the K-Pg mass extinction. *Science Advances* 7, 1–10.
- Polovodova, I., Schönfeld, J., 2008. Foraminiferal test abnormalities in the western Baltic Sea. *Journal of Foraminiferal Research* 38, 318–336.

- Poulsen, C.J., Gendaszek, A.S., Jacob, R.L., 2003. Did the rifting of the Atlantic Ocean cause the Cretaceous thermal maximum? *Geology* 31, 115–118.
- Premoli Silva, I., Sliter, W.V., 1999. Cretaceous paleoceanography: evidence from planktonic foraminiferal evolution. In: Barrera, E., Johnson, C.C. (Eds.), *The Evolution of the Cretaceous Ocean- Climate System*. Geological Society of America Special Paper 332. Colorado, Boulder, pp. 301–328.
- Manu Prasanth, MP, Hari, KR, Santosh, M., 2019. Tholeiitic basalts of Deccan large igneous province, India: An overview. *Geological Journal* 54, 2980–2993.
- Premović, P.I., Stanković, M.N., Pavlović, M.S., Djordjević, M.G., 2008. Cretaceous - Paleogene boundary Fish Clay at Højerup (Stevns Klint, Denmark): Zn, Pb and REE in kerogen. *Journal of the Serbian Chemical Society* 73, 453–461.
- Punekar, J., Mateo, P., Keller, G., 2014a. Effects of Deccan volcanism on paleoenvironment and planktic foraminifera: A global survey. *Special Paper of the Geological Society of America* 505, 91–116.
- Punekar, J., Keller, G., Khozyem, H., Hamming, C., Adatte, T., Tantawy, A.A., Spangenberg, J.E., 2014b. Late Maastrichtian-early Danian high-stress environments and delayed recovery linked to Deccan volcanism. *Cretaceous Research* 49, 63–82.
- Punekar, J., Keller, G., Khozyem, H.M., Adatte, T., Font, E., Spangenberg, J., 2016. A multi-proxy approach to decode the end-Cretaceous mass extinction. *Palaeogeography, Palaeoclimatology, Palaeoecology* 441, 116–136.
- Raup, D.M., Sepkoski J.J., 1982. Mass extinctions in the marine fossil record. *Science* 215, 1501–1503.
- Quillévéré, F., Norris, R.D., Kroon, D., Wilson, P.A., 2008. Transient ocean warming and shifts in carbon reservoirs during the early Danian. *Earth and Planetary Science Letters* 265, 600–615.
- Renne, P.R., Deino, A.L., Hilgen, F.J., Kuiper, K.F., Mark, D.F., Mitchell, W.S., Morgan, L.E., Mundil, R., Smit, J., 2013. Time scales of critical events around the Cretaceous-Paleogene boundary. *Science* 339, 684–687.
- Renne, P.R., Sprain, C.J., Richards, M.A., Self, S., Vanderkluysen, L., Pande, K., 2015. State shift in Deccan volcanism at the Cretaceous-Paleogene boundary, possibly Induced by Impact. *Science* 350, 76–78.
- Renne, P.R., Arenillas, I., Arz, J.A., Vajda, V., Gilabert, V., Bermúdez, H.D., 2018. Multi-proxy record of the Chicxulub impact at the Cretaceous- Paleogene boundary from Gorgonilla Island, Colombia. *Geology* 46.



- Richards, M.A., Alvarez, W., Self, S., Karlstrom, L., Renne, P.R., Manga, M., Sprain, C.J., Smit, J., Vanderkluyzen, L., Gibson, S.A., 2015. Triggering of the largest Deccan eruptions by the Chicxulub impact. *Bulletin of the Geological Society of America* 127, 1507–1520.
- Robaszynski, F., Caron, M., Gonzalez-Donoso, J.M., Wonders A.H., Ewgpf., 1983-1984. Atlas of late Cretaceous Globotruncanids, *Revue de Micropaléontologie* 36, (3-4), 145–305.
- Rosenberg, Y.O., Ashckenazi-Polivoda, S., Abramovich, S., Thibault, N., Chin, S., Feinstein, S., Bartov, Y., Amrani, A., 2021. Resilience of primary and export productivity in a eutrophic ecosystem following the Cretaceous-Paleogene mass extinction. *Global and Planetary Change* 196, 103371.
- Schiebel, R., 2002. Planktic foraminiferal sedimentation and the marine calcite budget. *Global Biogeochemical Cycles* 16, 3–1.
- Schiebel, R., Hemleben, C., 2005. Modern planktic foraminifera. *Paläontologische Zeitschrift* 79, 135–148.
- Schiebel, R., Smart, S.M., Jentzen, A., Jonkers, L., Morard, R., Meilland, J., Michel, E., Coxall, H.K., Hull, P.M., de Garidel-Thoron, T., Aze, T., Quillévéré, F., Ren, H., Sigman, D.M., Vonhof, H.B., Martínez-García, A., Kučera, M., Bijma, J., Spero, H.J., Haug, G.H., 2018. Advances in planktonic foraminifer research: New perspectives for paleoceanography. *Revue de Micropaleontologie* 61, 113–138.
- Schmidt, D.N., Lazarus, D., Young, J.R., Kucera, M., 2006. Biogeography and evolution of body size in marine plankton. *Earth-Science Reviews* 78, 239–266.
- Schoene, B., Samperton, K.M., Eddy, M.P., Keller, G., Adatte, T., Bowring, S.A., Khadri, S.F.R., Gertsch, B., 2015. U-Pb geochronology of the Deccan Traps and relation to the end-Cretaceous mass extinction. *Science* 347, 182–184.
- Schoene, B., Eddy, M.P., Samperton, K.M., Keller, C.B., Keller, G., Adatte, T., Khadri, S.F.R., 2019. U-Pb constraints on pulsed eruption of the Deccan Traps across the end-Cretaceous mass extinction. *Science* 363, 862–866.
- Schoene, B., Eddy, M.P., Keller, C.B., Samperton, K.M., 2021. An evaluation of Deccan Traps eruption rates using geochronologic data. *Geochronology* 3, 181–198.
- Schulte, P., Deutsch, A., Salge, T., Berndt, J., Kontny, A., MacLeod, K.G., Neuser, R.D., Krumm, S., 2009. A dual-layer Chicxulub ejecta sequence with shocked carbonates from the Cretaceous-Paleogene (K-Pg) boundary, Demerara Rise, western Atlantic. *Geochimica et Cosmochimica Acta* 73, 1180–1204.

- Schulte, P., Alegret, L., Arenillas, I., Arz, J.A., Barton, P.J., Bown, P.R., Bralower, T.J., Christeson, G.L., Claeys, P., Cockell, C.S., Collins, G.S., Deutsch, A., Goldin, T.J., Goto, K., Grajales-Nishimura, J.M., Grieve, R.A.F., Gulick, S.P.S., Johnson, K.R., Kiessling, W., Koeberl, C., Kring, D.A., MacLeod, K.G., Matsui, T., Melosh, J., Montanari, A., Morgan, J. v., Neal, C.R., Nichols, D.J., Norris, R.D., Pierazzo, E., Ravizza, G., Rebolledo-Vieyra, M., Reimold, W.U., Robin, E., Salge, T., Speijer, R.P., Sweet, A.R., Urrutia-Fucugauchi, J., Vajda, V., Whalen, M.T., Willumsen, P.S., 2010. The Chicxulub asteroid impact and mass extinction at the Cretaceous-Paleogene boundary. *Science* 327, 1214–1218.
- Self, S., Jay, A.E., Widdowson, M., Keszthelyi, L.P., 2008. Correlation of the Deccan and Rajahmundry Trap lavas: Are these the longest and largest lava flows on Earth? *Journal of Volcanology and Geothermal Research* 172, 3–19.
- Sepúlveda, J., Wendler, J.E., Summons, R.E., Hinrichs, K.U., 2009. Rapid resurgence of marine productivity after the Cretaceous-Paleogene mass extinction. *Science* 326, 129–132.
- Sharpton, V.L., Dalrymple, G.B., Marin, L.E., Ryder, G., Shuaraytz, B.C., Urrutia-Fucugauchi, J., 1992. New links between the Chicxulub impact structure and the Cretaceous/Tertiary boundary: *Nature* 359, 819–821.
- Sinnesael, M., de Vleeschouwer, D., Coccioni, R., Claeys, P., Frontalini, F., Jovane, L., Savian, J.F., Montanari, A., 2016. High-resolution multiproxy cyclostratigraphic analysis of environmental and climatic events across the Cretaceous-Paleogene boundary in the classic pelagic succession of Gubbio (Italy). *Special Paper of the Geological Society of America* 524, 115–137.
- Sinnesael, M., Montanari, A., Coccioni, R., Frontalini, F., Gattacceca, J., Snoeck, C., Wegner, W., Koeberl, C., Morgan, L.E., de Winter, N.J., DePaolo, D.J., Claeys, P., 2019. Multiproxy Cretaceous-Paleogene boundary event stratigraphy: An Umbria-Marche basinwide perspective. In: Koeberl, C., Bice, D.M. (Eds.), *250 Million Years of Earth History in Central Italy: Celebrating 25 Years of the Geological Observatory of Coldigioco*. Geological Society of America, pp. 133–158.
- Smit, J., 1982. Extinction and evolution of planktonic foraminifera after a major impact at the Cretaceous/Tertiary boundary. *Special Paper of the Geological Society of America* 190, 329–352.
- Smit, J., 1999. The global stratigraphy of the Cretaceous-Tertiary boundary impact ejecta. *Annual Review of Earth and Planetary Sciences* 27, 75–113.

- Smit, J., Hertogen, J., 1980. An extraterrestrial event at the Cretaceous-Tertiary boundary. *Nature* 285, 198–200.
- Smit, J., Romein, A.J.T., 1985. A sequence of events across the Cretaceous-Tertiary boundary. *Earth and Planetary Science Letters* 74, 155–170.
- Smit, J., Roep, T.B., Alvarez, W., Montanari, A., Claeys, P., Grajales-Nishimura, J.M., Bermudez, J., 1996. Coarse-grained clastic sandstone complex at the K/T boundary around the Gulf of Mexico: Deposition by tsunami waves induced by the Chicxulub impact. In: Ryder, G., Fastovsky, D.E., Gartner, S. (Eds.), *The Cretaceous-Tertiary event and other catastrophes in Earth history: Geological Society of America Special Paper 307*, pp. 151–182.
- Smith, C.C., Pessagno, E.A., 1973. Planktonic foraminifera and stratigraphy of the Corsicana Formation (Maestrichtian) north-central Texas. Special publication - Cushman Foundation for Foraminiferal Research 12, 68 pp.
- Soria, A.R., Liesa, C.L., Mata, M.P., Arz, J.A., Alegret, L., Arenillas, I., Melendez, A., 2001. Slumping and a sandbar deposit at the Cretaceous-Tertiary boundary in the El Tecolote section (northeastern Mexico): An impact-induced sediment gravity flow. *Geology* 29, 231–234.
- Sprain, C.J., Renne, P.R., Clemens, W.A., Wilson, G.P., 2018. Calibration of chron C29r: New high-precision geochronologic and paleomagnetic constraints from the Hell Creek region, Montana. *Bulletin of the Geological Society of America* 130, 1615–1644.
- Sprain, C.J., Renne, P.R., Vanderkluyzen, L., Pande, K., Self, S., Mittal, T., 2019. The eruptive tempo of deccan volcanism in relation to the Cretaceous-Paleogene boundary. *Science* 363, 866–870.
- Stainforth, R.M., Lamb, J.L., Luterbacher, H., Beardand, J.H., Jeffords, R.M., 1975. Cenozoic planktonic foraminiferal zonation and characteristics of index form. *The University of Kansas Paleontological Contributions* 62, 1–425.
- Stax, R., Stein, R., 1993. Long-term changes in the accumulation of organic carbon in Neogene sediments, Ontong Java Plateau. *Proceedings of the Ocean Drilling Program, Scientific Results College Station, TX (Ocean Drilling Program)*, 130, 573–584.
- Stinnesbeck, W., Keller, G., Adatte, T., Lopez-Oliva, J.G., and MacLeod, N., 1996. Cretaceous-Tertiary boundary clastic deposits in northeastern Mexico: Impact tsunami or sea level lowstand? In: MacLeod, N., Keller, G., (Eds.), *Cretaceous-*

- Tertiary mass extinctions: Biotic and environmental changes: New York, W.W. Norton and Company, pp. 471–518.
- Stinnesbeck, W., Keller, G., Adatte, T., Harting, M., Stuben, D., Istrate, G., Kramar, U., 2004. Yaxcopoil-1 and the Chicxulub impact: *International Earth Sciences (Geologische Rundschau)* 93, 1042–1065.
- Stott, L.D., Kennett, J.P., 1990. The paleoceanographic and paleoclimatic signature of the Cretaceous/Paleogene boundary in the Antarctic: stable isotopic results from ODP Leg 113, Proc., scientific results, ODP, Leg 113, Weddell Sea, Antarctica.
- Stüben, D., Kramar, U., Berner, Z.A., Meudt, M., Keller, G., Abramovich, S., Adatte, T., Hambach, U., Stinnesbeck, W., 2003. Late Maastrichtian paleoclimatic and paleoceanographic changes inferred from Sr/Ca ratio and stable isotopes. *Palaeogeography, Palaeoclimatology, Palaeoecology* 199, 107–127.
- Takayama, H., Tada, R., Matsui, T., Iturralde-Vinent, M.A., Oji, T., Tajika, E., Kiyokawa, S., García, D.G., Okada, H., Hasegawa, T., and Toyoda, K., 2000. Origin of the Peñalver Formation in northwestern Cuba and its relation to K/T boundary impact event: *Sedimentary Geology* 135, 295–320.
- Tarduno, J., Brinkman, D.B., Renne, P.R., Cottrell, R.D., Scher, H., Castillo, P., 1998. Evidence for extreme climatic warmth from Late Cretaceous Arctic vertebrates: *Science* 282, 2241–2244.
- Thibault, N., Galbrun, B., Gardin, S., Minoletti, F., le Callonnec, L., 2016. The end-Cretaceous in the southwestern Tethys (Elles, Tunisia): orbital calibration of paleoenvironmental events before the mass extinction. *International Journal of Earth Sciences* 105, 771–795.
- Thomas, E., Zachos, J.C., Bralower, T.J., 2000. Deep-sea environments on a warm earth: latest Paleocene-early Eocene. In: Huber, B.T., Macleod, K.G., Wing, S.L. (Eds.), *Warm Climates in Earth History*. Division III Faculty Publications. Cambridge University Press, Cambridge, pp. 132–160.
- Thomas, E., Shackleton, N.J., 1996. The Paleocene-Eocene benthic foraminiferal extinction and stable isotope anomalies. *Geological Society of London, Special Publication* 101, 401–441.
- Toon, O.B., Zahnle, K., Morrison, D., Turco, R.P., Covey, C., 1997. Environmental perturbations caused by the impacts of asteroids and comets. *Reviews of Geophysics* 35, 41–78.

- Toumarkine, M., Luterbacher, H.P., 1985. Paleocene and Eocene planktic foraminifera. In: Bolli, H.M., Saunders, J.B., Perch-Nielsen, K. (Eds.), *Plankton stratigraphy*. Cambridge University Press, pp. 87–154
- Urrutia-Fucugauchi, J., Marin, L., Trejo-Garcia, A., 1996. UNAM Scientific Drilling Program of Chicxulub Impact Structure-Evidence for a 300 kilometer crater diameter. *Geophysical Research Letters* 23, 1565–1568.
- Urrutia Fucugauchi, J., Chavez Aguirre, J.M., Perez Cruz, L., de la Rosa, J.L., 2008. Impact ejecta and carbonate sequence in the eastern sector of Chicxulub crater. *Comptes Rendus Geosciences* 341, 801–810.
- Urrutia-Fucugauchi, J., Pérez-Cruz, L. 2016. Chicxulub Asteroid Impact: An Extreme Event at the Cretaceous/Paleogene Boundary. Wiley, American Geophysical Union Monograph 242, 99–111.
- Vandamme, D., Courtillot, V., Besse, J., Montigny, R., 1991. Paleomagnetism and age determinations of the Deccan traps (India): results of a Nagpur–Bombay traverse and review of earlier work. *Reviews of Geophysics* 29, 159–190.
- Vellekoop, J., Sluijs, A., Smit, J., Schouten, S., Weijers, J.W.H., Sinninghe Damsté, J.S., Brinkhuis, H., 2014. Rapid short-term cooling following the Chicxulub impact at the Cretaceous-Paleogene boundary. *Proceedings of the National Academy of Sciences of the United States of America* 111, 7537–7541.
- Vellekoop, J., Esmeray-Senlet, S., Miller, K.G., Browning, J. v, Sluijs, A., van de Schootbrugge, B., Sinninghe Damsté, J.S., Brinkhuis, H., 2016. Evidence for Cretaceous-Paleogene boundary bolide “impact winter” conditions from New Jersey, USA. *Geology* 44, (8), 619–622.
- Vincent, E., Berger, W. H., 1981. Planktonic foraminifera and their use in paleoceanography. In: Emiliani, C. (Ed.), *The Sea*, vol. 7, *The Ocean in Lithosphere*. John Wiley, New York, pp. 1025–1119
- Wade, B. S., Pearson, P. N., Berggren, W. A., Pälike, H., 2011. Review and revision of Cenozoic tropical planktonic foraminiferal biostratigraphy and calibration to the geomagnetic polarity and astronomical time scale. *Earth-Science Reviews* 104, (1–3), 111–142.
- Wang, Y., Huang, C., Sun, B., Quan, C., Wu, J., Lin, Z., 2014. Paleo-CO<sub>2</sub> variation trends and the Cretaceous greenhouse climate. *Earth Sciences Review* 129, 136–147.

- Ward, W., Keller, G., Stinnesbeck, W., Adatte, T., 1995. Yucatan subsurface stratigraphy: Implications and constraints for the Chicxulub impact: *Geology* 23, 873–876.
- Wendler, I., 2013. A critical evaluation of carbon isotope stratigraphy and biostratigraphic implications for Late Cretaceous global correlation. *Earth-Science Reviews* 126, 116–146.
- Westerhold, T., Rhl, U., Donner, B., McCarren, H.K., Zachos, J.C., 2011. A complete high-resolution Paleocene benthic stable isotope record for the central Pacific (ODP Site 1209). *Paleoceanography* 26, 1–13.
- Westerhold, T., Marwan, N., Drury, A.J., Liebrand, D., Agnini, C., Anagnostou, E., Barnet, J.S.K., Bohaty, S.M., de Vleeschouwer, D., Florindo, F., Frederichs, T., Hodell, D.A., Holbourn, A.E., Kroon, D., Lauretano, V., Littler, K., Lourens, L.J., Lyle, M., Pälike, H., Röhl, U., Tian, J., Wilkens, R.H., Wilson, P.A., Zachos, J.C., 2020. An astronomically dated record of Earth's climate and its predictability over the last 66 million years. *Science* 369, 1383–1388.
- Wignall, P. (2005). The Link between Large Igneous Province Eruptions and Mass Extinctions. *Elements* 5, 293–297.
- Wilf, P., Johnson, K.R., Huber, B.T., 2003. Correlated terrestrial and marine evidence for global climate changes before mass extinction at the Cretaceous-Paleogene boundary. *Proceedings of the National Academy of Sciences* 100, 599–604.
- Woelders, L., Vellekoop, J., Kroon, D., Smit, J., Casadío, S., Prámparo, M.B., Dinarès-Turell, J., Peterse, F., Sluijs, A., Lenaerts, J.T.M., Speijer, R.P., 2017. Latest Cretaceous climatic and environmental change in the South Atlantic region. *Paleoceanography* 32, 466–483.
- Woelders, L., Vellekoop, J., Weltje, G.J., de Nooijer, L., Reichart, G.-J., Peterse, F., Claeys, P., Speijer, R.P., 2018. Robust multi-proxy data integration, using late Cretaceous paleotemperature records as a case study. *Earth and Planetary Science Letters* 500, 215–224.
- Wu, G., Berger, W.H., 1989. Planktonic foraminifera: Differential dissolution and the Quaternary stable isotope Record in the west equatorial Pacific. *Paleoceanography* 4, 181–198.
- Yanko, V., Ahmad, M., Kaminski, M., 1998. Morphological deformities of benthic foraminiferal tests in response to pollution by heavy metals; implications for pollution monitoring. *Journal of Foraminiferal Research* 28, 177–200.

- Young, J. R., Wade, B. S., & Huber, B. T. (2017). pforams@mikrotax website. <http://www.mikrotax.org/pforams>
- Zachos, J.C., Arthur, M.A., Dean, W.E., 1989. Geochemical evidence for suppression of pelagic marine productivity at the Cretaceous/Tertiary boundary. *Nature* 337, 61–64.
- Zachos, J.C., Lohmann, K.C., Walker, J.C.G., Wise, S.W., 1993. Abrupt climate change and transient climates during the Paleogene: a marine perspective. *Journal of Geology* 101, 191–213.
- Zachos, J.C., Quinn, T.M., Salamy, K.A., 1996. High resolution (10<sup>4</sup> years) deep-sea foraminiferal stable isotope records of the Eocene-Oligocene climate transition. *Paleoceanography* 11, 251–266.
- Zachos, J., Pagani, H., Sloan, L., Thomas, E., Billups, K., 2001. Trends, rhythms, and aberrations in global climate 65 Ma to present. *Science* 292, 686–693.
- Zachos, J.C., Röhl, U., Schellenberg, S.A., Sluijs, A., Hodell, D.A., Kelly, D.C., Thomas, E., Nicolo, M., Raffi, I., Lourens, L.J., McCarren, H., Kroon, D., 2005. Paleoclimate: Rapid acidification of the ocean during the Paleocene-Eocene thermal maximum. *Science* 308, 1611–1615.
- Zachos, J.C., Schouten, S., Bohaty, S., Quattlebaum, T., Sluijs, A., Brinkhuis, H., Gibbs, S.J., and Bralower, T.J., 2006. Extreme warming of mid-latitude coastal ocean during the Paleocene-Eocene Thermal Maximum: Inferences from TEX<sub>86</sub> and isotope data. *Geology* 34, 737.
- Zachos, J.C., Dickens, G.R., Zeebe, R.E., 2008. An early Cenozoic perspective on greenhouse warming and carbon-cycle dynamics. *Nature* 451, 279–283.
- Zachos, J.C., McCarren, H., Murphy, B., Röhl, U., and Westerhold, T., 2010. Tempo and scale of late Paleocene and early Eocene carbon isotope cycles: Implications for the origin of hyperthermals. *Earth and Planetary Science Letters* 299, 242–249.
- Zeebe, R.E., Westerhold, T., Littler, K., and Zachos, J.C., 2017. Orbital forcing of the Paleocene and Eocene carbon cycle. *Paleoceanography* 32, 440–465.
- Zhang, L., Wang, C., Wignall, P.B., Kluge, T., Wan, X., Wang, Q., Gao, Y., 2018. Deccan volcanism caused coupled *p*CO<sub>2</sub> and terrestrial temperature rises, and pre-impact extinctions in northern China. *Geology* 46, 271–274.

***Anexos.***  
***Material***  
***suplementario***





## ANEXOS

**Anexo I. Material suplementario de Arenillas et al. (2018)**, (2 apéndices de texto, bibliografía, 7 figuras y 2 tablas).

**SUPPLEMENTARY APPENDIX A. Taxonomic Remarks**

The planktic foraminiferal taxonomy used in this paper is based on detailed morphological, morphostatistical and textural studies of specimens from the most continuous, complete and expanded sections worldwide (Arenillas and Arz, 2000, 2007, 2013*a,b*, 2017; Arenillas et al. 2007, 2012, 2016; Arz et al. 2010). Specimens illustrated in Supplementary Figures 2 and 3 come mainly from El Kef and Aïn Settara, but also from Ben Gurion (Israel), Bajada del Jagüel (Argentina) and DSDP Site 305 (North Pacific).

After the K/Pg boundary, two main evolutionary lineages emerged, one of tiny globigeriniform, trochospiral tests informally called parvularugoglobigerinids (*Palaeoglobigerina* Arenillas, Arz and Nández, 2007, and *Parvularugoglobigerina* Hofker, 1978) with a smooth wall-texture, and the other of triserial tests (*Chiloguembelitra*) with a rugose wall-texture (Arenillas and Arz 2017; Arenillas et al. 2017). The benthic genus *Caucasina* Khalilov, 1951, seems to be the ancestor of parvularugoglobigerinids (Brinkhuis and Zachariasse 1988), with *Pseudocaucasina* Arenillas and Arz, 2017 encompassing the intermediate morphotypes (Arenillas and Arz 2017). On the basis of transitional specimens, Arenillas and Arz (2013*a*) suggested an evolution from smooth-walled *Palaeoglobigerina* to a spinose, cancellate lineage, first *Eoglobigerina* (initially with a pitted wall), and then *Parasubbotina* and *Subbotina*. Likewise, Arenillas and Arz (2013*b*) suggested an evolution from smooth-walled *Parvularugoglobigerina* to pitted *Globanomalina*, and then to non-spinose, cancellate *Praemurica* (wall-textures shown in Supplementary Fig. 1).

*Guembelitra* is the ancestor of *Chiloguembelitra* (Hofker 1978; Arenillas et al. 2017). This taxon played an important role in the evolution of early Danian guembelitriids, as it seems to be the most immediate ancestor of two lineages, one biserial and culminating in *Chiloguembelina* and another trochospiral and culminating in *Globoconusa* (Arenillas and Arz 2000; Arenillas et al. 2010). For the latter, Arenillas et al. (2012, 2016) proposed *Trochoguembelitra* as an intermediate taxon; this shares its wall-texture with *Chiloguembelitra* and, like the latter, may be triserial in its juvenile stage (Supplementary Fig. 1). *Woodringina*, with a mixed triserial-biserial test, is the intermediate taxon between *Chiloguembelitra* and the wholly biserial *Chiloguembelina*. This biserial lineage is characterized by a finely pustulate wall-texture, which tends to be smoother in *Chiloguembelina* (Supplementary Fig. 1).

#### SUPPLEMENTARY APPENDIX A. - References

- Arenillas, I., and J. A. Arz. 2000. *Parvularugoglobigerina eugubina* type-sample at Ceselli (Italy): planktic foraminiferal assemblage and lowermost Danian biostratigraphic implications. *Rivista Italiana di Paleontologia e Stratigrafia* 106:379–390.
- . 2007. Análisis morfoestadístico del género *Palaeoglobigerina* (Foraminifera, Globigerinida) del Paleoceno basal, y descripción de una nueva especie. [Morphostatistical analysis of the basal Paleocene genus *Palaeoglobigerina* (Foraminifera, Globigerinida), and description of a new species]. *Revista Española de Micropaleontología* 39:1–28.
- . 2013a. Origin and evolution of the planktic foraminiferal Family Eoglobigerinidae Blow (1979) in the early Danian (Paleocene). *Revista Mexicana de Ciencias Geológicas* 30:159–177.

- . 2013b. New evidence on the origin of nonspinose pitted-cancellate species of the early Danian planktonic foraminifera. *Geologica Carpathica* 64:237–251.
- . 2017. Benthic origin and earliest evolution of the first planktonic foraminifera after the Cretaceous/Paleogene boundary mass extinction. *Historical Biology* 29: 17–24.
- Arenillas, I., J. A. Arz, and C. Nájuez. 2007. Morfología, Biometría y Taxonomía de foraminíferos planctónicos del Daniense basal: *Palaeoglobigerina* n. gen. [Morphology, biometry and taxonomy of the lowermost Danian planktonic foraminifera: *Palaeoglobigerina* n. gen.]. *Revista Española de Paleontología* 22(1):21–62.
- . 2012. Smooth and rugose wall textures in earliest Danian trochospiral planktic foraminifera from Tunisia. *Neues Jahrbuch für Geologie und Paläontologie, Abhandlungen* 266:123–142.
- . 2016. New species of genus *Trochoguembelitra* from the lowermost Danian of Tunisia – biostratigraphic and evolutionary implications in planktonic foraminifera. *Palaeontographica Abteilung A* 305:133–160.
- Arenillas, I., J. A. Arz, and V. Gilabert. 2017. Revalidation of the genus *Chiloguembelitra* Hofker: implications for the evolution of early Danian planktonic foraminifera. *Journal of African Earth Sciences* 134:435–456.
- Arz, J. A., I. Arenillas, and C. Nájuez. 2010. Morphostatistical analysis of Maastrichtian populations of *Guembelitra* from El Kef, Tunisia. *Journal of Foraminiferal Research* 40:148–164.
- Brinkhuis, H., and W. J. Zachariasse. 1988. Dinoflagellate cyst, sea level changes and planktonic foraminifers across the Cretaceous-Tertiary boundary at El Haria, Northwest Tunisia. *Marine Micropaleontology* 13:153–191.

Hofker, J. 1978. Analysis of a large succession of samples through the Upper Maastrichtian and the Lower Tertiary of Drill Hole 47.2, Shatsky Rise, Pacific, Deep Sea Drilling Project. *Journal of Foraminiferal Research* 8:46–75.

#### **SUPPLEMENTARY APPENDIX B.** Evolutionary model of planktic foraminifera across the K/Pg boundary

The evolutionary model proposed by Dean and McKinney (2001) includes four metrics: extinction rate ( $E_R$ ), speciation rate ( $N_R$ ), taxonomic flux ( $F$ ) and volatility ( $V$ ). These are calculated for consecutive stratigraphic intervals of approximately the same thickness and duration (Supplementary Fig. 4). The number, position and resolution of intervals are chosen by the researcher. In order to measure the metric turnovers in the greatest detail, we chose two series of overlapping intervals of 100 cm thickness (each interval between approximately 10 and 20Kyr in duration). The interval boundaries of the first series fall within the middle parts of the second series of intervals, and vice versa. The K/Pg boundary was made to coincide with the boundary between intervals 12 and 13 and with the middle part of interval 13' (Supplementary Fig. 4).

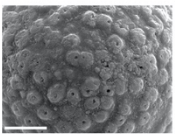



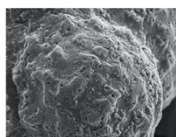




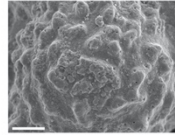





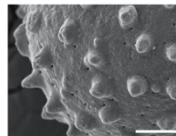

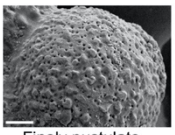


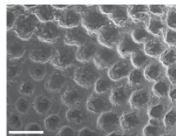







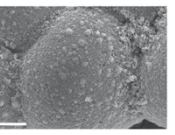


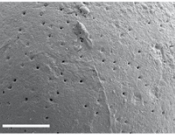

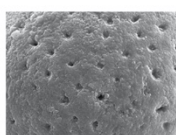
















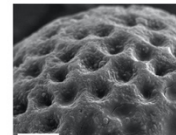



Four parameters were measured in each interval (Supplementary Tables 1 and 2): the number of identified species ( $G$ ), of extinct species ( $E$ ), of new species ( $N$ ) and of stable species ( $S$ ), all quantified from stratigraphic range data. A stable species in a particular interval is the one that persists across the entire interval. We used the K-Pg planktic foraminiferal biostratigraphic data from Arenillas et al. (2000) and subsequent modifications (see Arenillas and Arz 2017; Arenillas et al. 2017) and calculated the Dean and McKinney (2001) metrics for the pattern A hypothesis (Supplementary Table 1), with sixteen Cretaceous survivors (see Supplementary Fig. 4), and the pattern B hypothesis,

with two Cretaceous survivors (*Guembelitra cretacea* and *G. blowi*) and the rest considered to be reworked specimens (Supplementary Table 2). The extinction ( $E_R$ ) and speciation ( $N_R$ ) rates in each interval were expressed as  $E_R = E/G$  and  $N_R = N/G$ , respectively. The taxonomic flux was defined as  $F = (G-E+N+S)/[S+G((E+S)/(N+S))]$  and  $\log F$  was used to estimate the relative increase (positive value) or decline (negative value) in diversity in each interval. Finally, evolutionary variability was measured in terms of volatility,  $V = (G-S)/G$ , where low values indicate evolutionary stability and high values imply evolutionary turnovers.

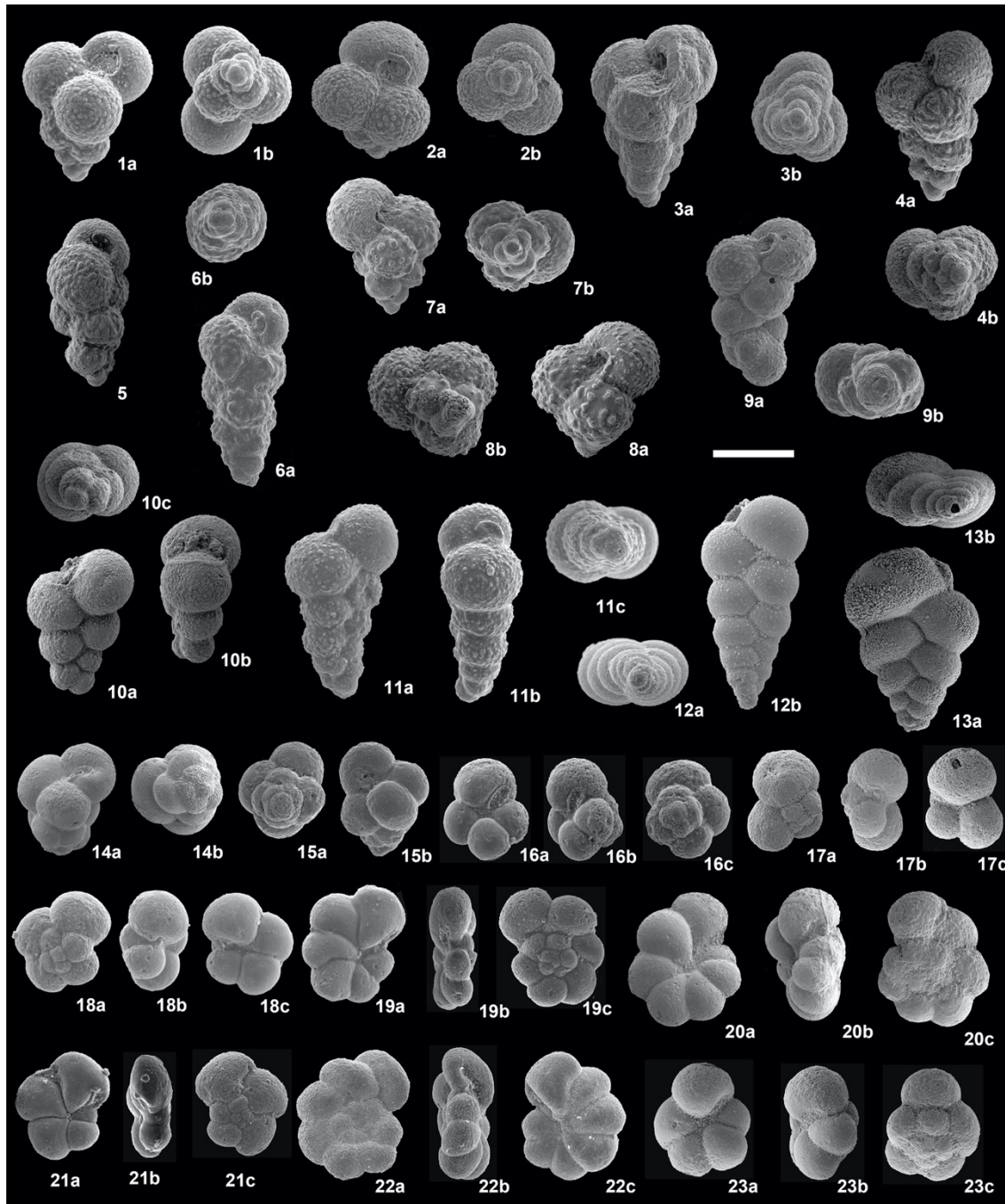
### Supplementary APPENDIX B - References

- Arenillas, I., and J. A. Arz. 2017. Benthic origin and earliest evolution of the first planktonic foraminifera after the Cretaceous/Paleogene boundary mass extinction. *Historical Biology* 29:17–24.
- Arenillas, I., J. A. Arz, E. Molina, and C. Dupuis. 2000. An independent test of planktonic foraminiferal turnover across the Cretaceous/Paleogene (K/P) boundary at El Kef, Tunisia: Catastrophic mass extinction and possible survivorship. *Micropaleontology* 46:31–49.
- Arenillas, I., J. A. Arz, and V. Gilabert. 2017. Revalidation of the genus *Chiloguembelitra* Hofker: implications for the evolution of early Danian planktonic foraminifera. *Journal of African Earth Sciences* 134:435–456.
- Dean, W. G., and M. L. McKinney. 2001. Taxonomic flux as a measure of evolutionary turnover. *Revista Española de Paleontología* 16:29–38.

SUPPLEMENTARY FIGURES AND TABLES

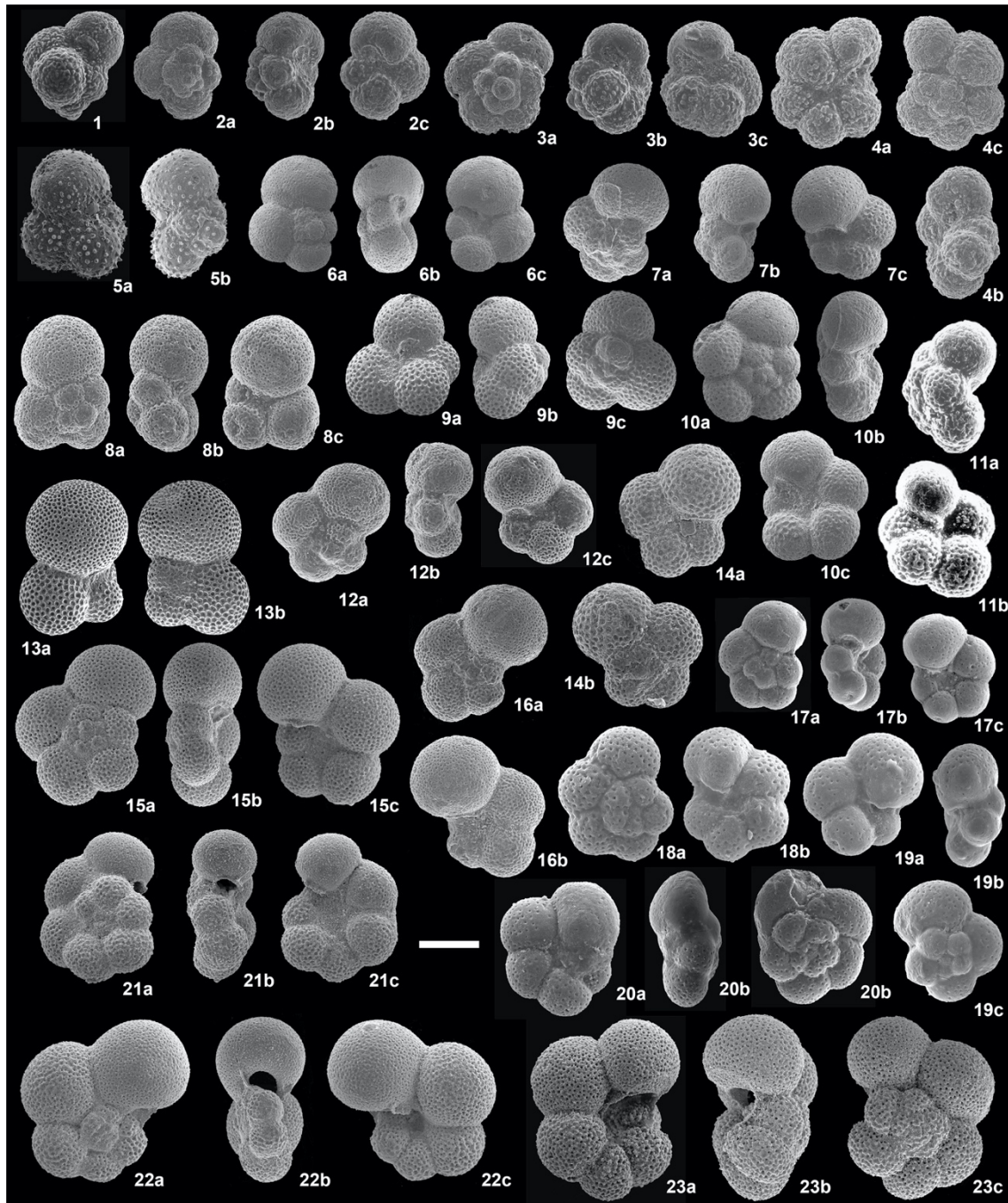
Wall-texture	Genus	Species	Wall-texture	Genus	Species	
 Pore-mounded	<i>Guembelitra</i> Cushman, 1933	 <i>G. cretacea</i> Cushman, 1933  <i>G. dammula</i> Voloshina, 1961  <i>G. blowi</i> Arz, Arenillas & Nájuez, 2010	 Perforate rugose Pustulate rugose	<i>Trochoguembelitra</i> Arenillas & Arz, 2016a	 <i>T. alabamensis</i> Liu & Olsson, 1992  <i>T. extensa</i> (Blow, 1979)  <i>T. liuae</i> Arenillas & Arz, 2016a  <i>T. olssoni</i> Arenillas & Arz, 2016a	
 Perforate rugose Pustulate rugose	<i>Chiloguembelitra</i> Hofker, 1978	 <i>Chg. hofkeri</i> Arenillas, Arz & Gilabert, 2017  <i>Chg. danica</i> Hofker, 1978  <i>Chg. trilobata</i> Arenillas, Arz & Gilabert, 2017  <i>Chg. irregularis</i> (Morozova, 1961)  <i>Chg. biseriata</i> Arenillas, Arz & Gilabert, 2017	 Pustulate	<i>Globoconusa</i> Khalilov, 1956	 <i>Gc. daubjergensis</i>	
 Finely pustulate	<i>Woodringina</i> Loeblich & Tappan, 1957	 <i>W. claytonensis</i> Loeblich & Tappan, 1957  <i>W. hornerstownensis</i> Olsson, 1960	 Spinose cancellate	<i>Eoglobigerina</i> Morozova, 1959	 <i>E. simplicissima</i> (Blow, 1979)  <i>E. fringa</i> (Subbotina, 1950)  <i>E. microcellulosa</i> (Morozova, 1961)  <i>E. cf. trivialis</i> (Subbotina, 1953)  <i>E. eobuloides</i> Morozova, 1959  <i>E. praedita</i> Blow, 1979  <i>E. edita</i> (Subbotina, 1953)	
 Smoothed pustulate	<i>Chiloguembelina</i> Loeblich & Tappan, 1956	 <i>Ch. taurica</i> Morozova, 1961  <i>Ch. midwayensis</i> (Cushman, 1940)				
 Smooth	<i>Pseudocaucasina</i> Arenillas & Arz, 2016b	 <i>Pc. antecessor</i> Arenillas & Arz, 2016b	 Pitted	<i>Parasubbotina</i> Olsson, Hemleben, Berggren & Liu, 1992	 <i>P. moskvini</i> (Shutskaya, 1953)  <i>P. pseudobuloides</i> (Plummer, 1927)  <i>P. varianta</i> (Subbotina, 1953)	
	<i>Palaeoglobigerina</i> Arenillas, Arz & Nájuez, 2007	 <i>Pg. alticonusa</i> (Li, McGowan & Boersma, 1995)  <i>Pg. fodina</i> (Blow, 1979)  <i>Pg. minutula</i> (Luterbacher & Premoli Silva, 1964)  <i>Pg. luterbacheri</i> Arenillas & Arz			<i>Subbotina</i> Brotzen & Pozaryska, 1961	 <i>S. trilocolinoides</i> (Plummer, 1927)
	<i>Parvularugoglobigerina</i> Hofker, 1978	 <i>Pv. perexigua</i> Li, McGowan & Boersma, 1995  <i>Pv. umbrica</i> (Luterbacher & Premoli Silva, 1964)  <i>Pv. longiapertura</i> (Blow, 1979)  <i>Pv. eugubina</i> (Luterbacher & Premoli Silva, 1964)  <i>Pv. sabina</i> (Luterbacher & Premoli Silva, 1964)			<i>Globanomalina</i> Haque, 1956	 <i>G. archeocompressa</i> (Blow, 1979)  <i>G. imitata</i> (Subbotina, 1953)  <i>G. planocompressa</i> (Shutskaya 1965)
			 Non-spinose cancellate	<i>Praemurica</i> Olsson, Hemleben, Berggren & Liu, 1992	 <i>Pr. taurica</i> (Morozova, 1961)  <i>Pr. pseudoinconstans</i> (Blow, 1979)  <i>Pr. inconstans</i> (Subbotina, 1953)	

SUPPLEMENTARY FIGURE 1. Systematic scheme of early Danian planktic foraminifera (normal forms) with notes on test wall structure according to the taxonomy used here. The first evolutionary radiation occurred between approximately 5 and 26Kyr after the K/Pg boundary includes the appearance of species belonging to the genera *Pseudocaucasina*, *Palaeoglobigerina*, *Parvularugoglobigerina*, *Chiloguembelitra*, *Woodringina* and *Chiloguembelina* appeared. The second evolutionary radiation occurred between approximately 46 and 110Kyr after the K/Pg boundary includes the appearance of species belonging to the genera *Trochoguembelitra*, *Eoglobigerina*, *Parasubbotina*, *Globanomalina* and *Praemurica*.



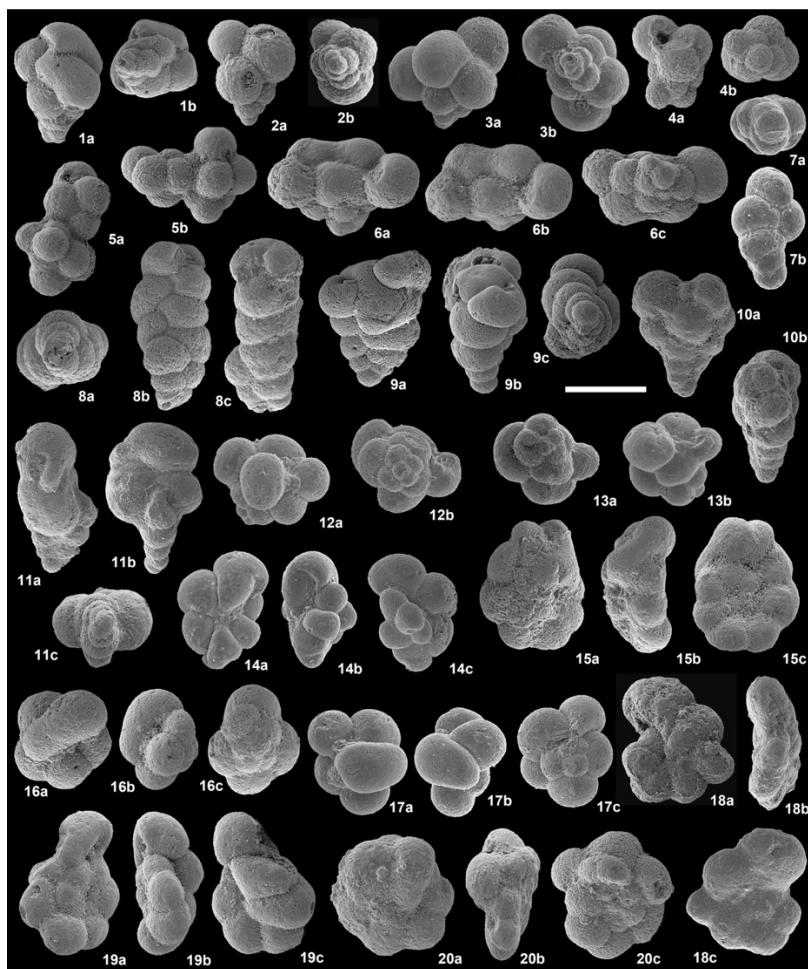
**SUPPLEMENTARY FIGURE 2.** Normal forms of early Danian species of the first evolutionary radiation (scale bar = 100 microns). 1. *Guembelitra cretacea*; 2. *Guembelitra blowi*; 3. *Guembelitra dammula*; 4. *Chiloguembelitra danica*; 5-6. *Chiloguembelitra irregularis*; 7. *Chiloguembelitra hofkeri*; 8. *Chiloguembelitra trilobata*; 9. *Chiloguembelitra biseriata*; 10. *Woodringina claytonensis*; 11. *Woodringina hornerstownensis*; 12. *Chiloguembelina taurica*; 13. *Chiloguembelina midwayensis*; 14. *Pseudocaucasina antecessor*; 15. *Palaeoglobigerina alticonusa*; 16. *Palaeoglobigerina fodina*; 17. *Palaeoglobigerina minutula*; 18. *Palaeoglobigerina luterbacheri*; 19. *Parvularugoglobigerina longiapertura*; 20. *Parvularugoglobigerina eugubina*; 21. *Parvularugoglobigerina perexigua*; 22. *Parvularugoglobigerina umbrica*; 23. *Parvularugoglobigerina sabina*. All specimens come from El Kef, except for some from Ain Settara (10, 11, 19) and DSDP Site 305 (12).



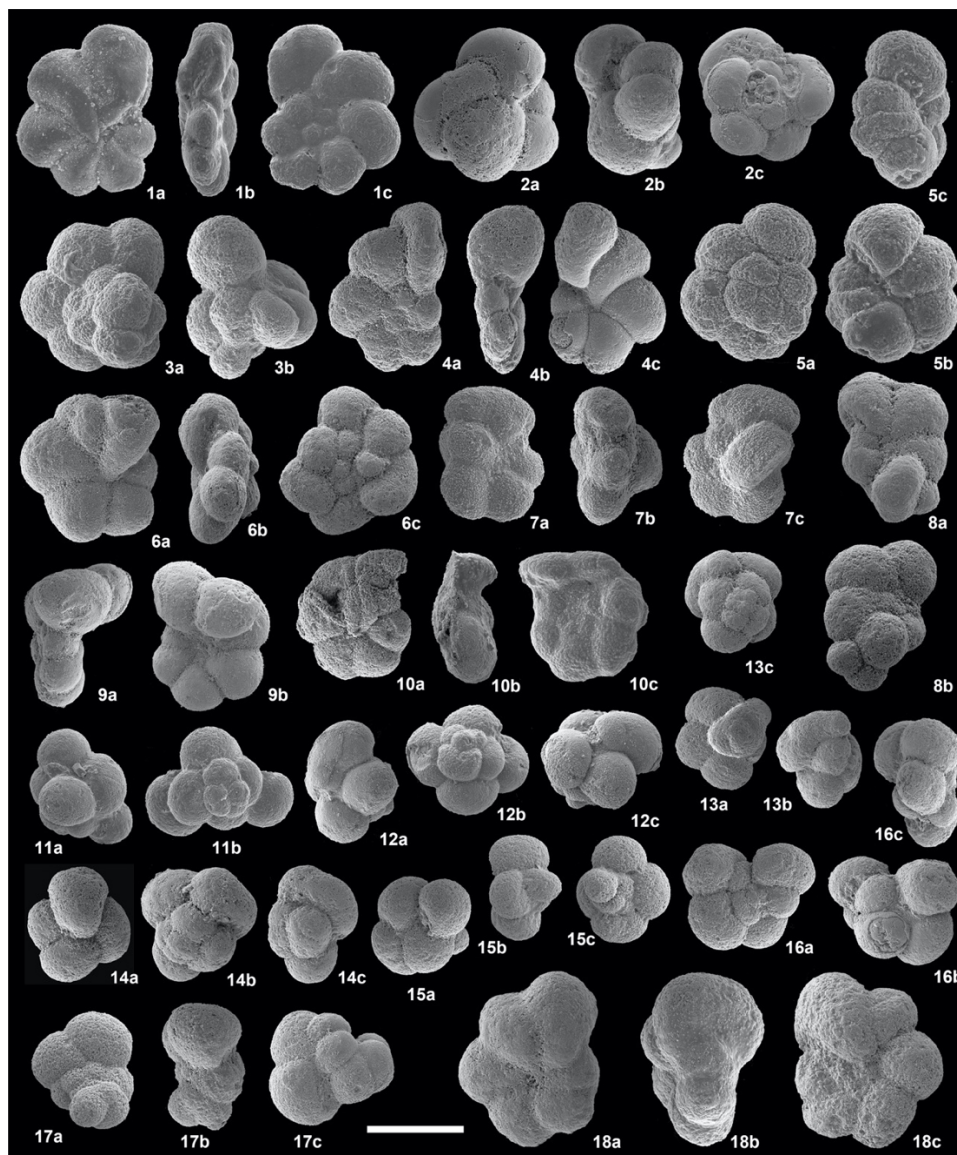


**SUPPLEMENTARY FIGURE 3.** Normal forms of early Danian species of the second evolutionary radiation (scale bar = 100 microns). 1. *Trochoguembelitra alabamensis*; 2. *Trochoguembelitra extensa*; 3. *Trochoguembelitra liuae*; 4. *Trochoguembelitra olssoni*; 5. *Globoconusa daubjergensis*; 6. *Eoglobigerina simplicissima*; 7. *Eoglobigerina eobulloides*; 8. *Eoglobigerina microcellulosa*; 9. *Eoglobigerina* cf. *trivialis*; 10. *Eoglobigerina praeedita*; 11. *Eoglobigerina edita*; 12. *Eoglobigerina fringa*; 13. *Subbotina triloculinooides*; 14. *Parasubbotina moskvini*; 15. *Parasubbotina pseudobulloides*; 16. *Parasubbotina varianta*; 17-18. *Globanomalina archeocompressa*; 19. *Globanomalina imitata*; 20. *Globanomalina planocompressa*; 21. *Praemurica taurica*; 22. *Praemurica pseudoinconstans*; 23. *Praemurica inconstans*. All specimens come from El Kef, except for some from Bajada del Jagüel (5), Ben Gurion (9, 12, 14, 16), DSDP Site 305 (15, 21, 22, 23) and Ain Settara (18).

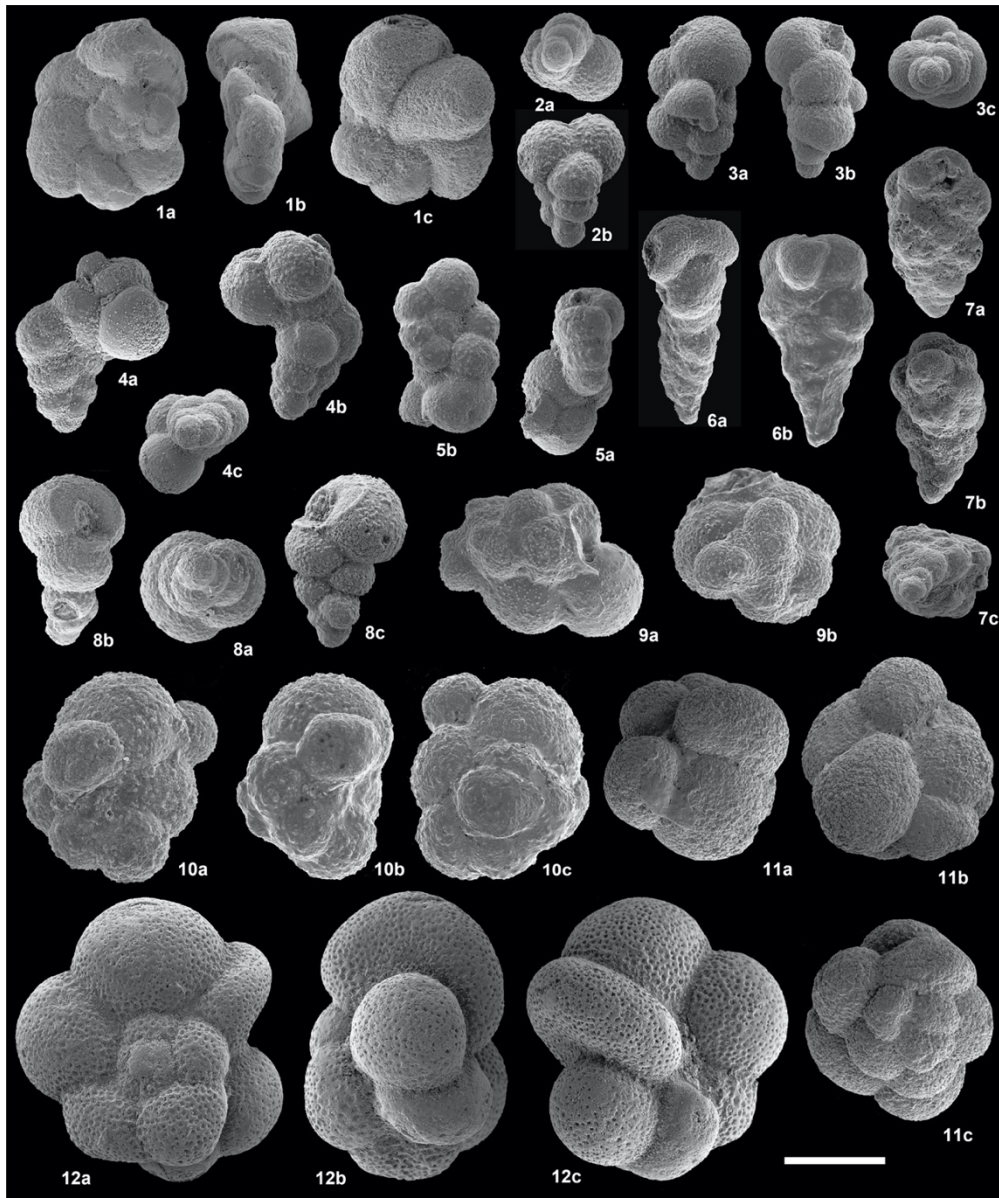




**SUPPLEMENTARY FIGURE 5.** Examples of aberrant planktic foraminiferal forms from acme-stage PFAS-1, and transition between acme-stages PFAS-1 and PFAS-2 (scale bar = 100 microns). 1. *Guembelitra* sp. (probably *G. cretacea*), lack of sculpture in the test due to aberrant ultimate chambers. 2. *Chiloguembelitra* sp. (probably *Chg. danica*), reduced last chamber (kummerform). 3. *Guembelitra* spp., multiple ultimate chambers (racemiguembeliform multiserial test). 4. *Guembelitra* sp. (probably *G. cretacea*), second chamber abnormally protruding beside the proloculus. 5. *Guembelitra* sp. (probably *G. cretacea*), two specimens with fused tests. 6. *Guembelitra* sp. (probably *G. cretacea*), attached twins (Siamese). 7. *W. claytonensis*, kinking with change in the coiling direction. 8. *W. hornerstownensis*, kinking with change in the coiling direction. 9-10. *W. hornerstownensis*, multiple ultimate chambers (planoglobuliniiform multiserial test). 11. *Ch. midwayensis*, kinking with change in the coiling direction of 90°. 12. *Palaeoglobigerina* sp. (probably *Pg. alticonusa*), multiple ultimate chambers and apertures (multiserial test). 13. *Palaeoglobigerina* sp. (probably *Pg. fodina*), multiple ultimate chambers (multiserial test). 14. *Pv. longiapertura*, kinking with two axes of rotation. 15. *Parvularugoglobigerina* sp. (probably *Pv. umbrica*), lack sculpture of the test, with multiple bulla-like chambers. 16-17. *Pv. sabina*, overdeveloped or bulla-like ultimate chamber. 18. *Pv. longiapertura*, aberrant antepenultimate chamber. 19. *Pv. longiapertura*, twisting of entire test (extreme kinking) and overdeveloped chambers. 20. *Parvularugoglobigerina* sp. (probably *Pv. longiapertura*), double or twinned ultimate chambers. Most of the specimens come from El Kef, and the rest are from Aïn Settara (9, 14, 17), Caravaca (10, 19), Elles (11) and Agost (15, 16, 18, 20).



**SUPPLEMENTARY FIGURE 6.** Examples of aberrant planktic foraminiferal forms from PFAS-1 and PFAS-2 (scale bar = 100 microns). 1. *Pv. longiapertura*, abnormally compressed test and aberrant ultimate chambers. 2. *Pv. sabina*, bulla-like ultimate chamber. 3. *Parvularugoglobigerina* sp. (probably *Pv. longiapertura*), twisting of entire test (extreme kinking). 4. *Pv. longiapertura*, abnormally compressed test and aberrant ultimate chamber. 5. *Pv. eugubina*, aberrant chamber (second chamber of the last whorl). 6. *Pv. longiapertura*, protuberant additional chamber. 7. *Pv. longiapertura*, inflated additional chamber. 8. *Pv. longiapertura*, test with two additional chambers. 9. *Pv. eugubina*, protuberant aberrant chamber. 10. *Pv. longiapertura*, poor development of last whorl. 11. *Palaeoglobigerina* sp. (probably *Pg. fodina*), multiple ultimate chambers (multiserial test). 12-14. *Palaeoglobigerina* sp. (*Pg. alticonusa* or *Pg. fodina*), bulla-like ultimate chamber with additional apertures. 15. *Palaeoglobigerina* sp. (probably *Pg. fodina*), second chamber abnormally protruding beside the proloculus. 16. *Palaeoglobigerina* sp. (probably *Pg. fodina* or *Pg. luterbacheri*), attached twins (Siamese). 17. *Palaeoglobigerina* sp. (probably *Pg. fodina*), twisting of entire test (extreme kinking). 18. *Pv. eugubina*, overdeveloped last chamber with aperture in equatorial position, and test going from trochospiral to planispiral. All specimens come from El Kef, except for some from Elles (1, 9) and Agost (10).



**SUPPLEMENTARY FIGURE 7.** Examples of aberrant planktic foraminiferal forms from PFAS-3, mainly from the *Chiloguembelitra* acme (scale bar = 100 microns). 1. *Pv. eugubina*, overdevelopment of the last whorl. 2. *W. claytonensis*, protuberant last chamber in anomalous position, with test going from biserial to triserial. 3. *W. claytonensis*, lack of sculpture in the test with both abnormal and protuberant chambers. 4. *W. hornerstownensis*, kinking with change in the coiling direction and reduced last chamber (kummerform). 5. *Woodringina* sp. (probably *W. claytonensis*), general monstrosity, probably attached twins (Siamese) or test with extreme kinking. 6. *Ch. taurica*, welded chambers. 7. *Ch. taurica*, multiple ultimate chambers (multiserial test). 8. *W. claytonensis*, overdeveloped ultimate chamber. 9. *Trochoguembelitra* sp. (probably *T. extensa*), general monstrosity (proliferation of generally kummerform chambers, kinking, chambers abnormally protruding beside the proloculus, multiple apertures, etc.). 10. *T. liuae*, bulla-like ultimate chambers. 11. *T. liuae*, double or twinned ultimate chambers. 12. *Praemurica* sp. (probably *Pr. pseudoinconstans*), lack of sculpture in the test, with bulla-like antepenultimate chamber and two kummerform last chambers. All specimens come from El Kef, except for some from Ain Settara (5), Caravaca (6), and Agost (7).

## EL KEF - HYPOTHESIS OF PATTERN A

Interval	G	E	N	S	Er	Nr	V	F	log F
1'	68	0	0	68	0.00	0.00	0.00	1.00	0.00
1	68	0	0	68	0.00	0.00	0.00	1.00	0.00
2'	68	0	0	68	0.00	0.00	0.00	1.00	0.00
2	68	0	0	68	0.00	0.00	0.00	1.00	0.00
3'	68	0	0	68	0.00	0.00	0.00	1.00	0.00
3	68	0	0	68	0.00	0.00	0.00	1.00	0.00
4'	68	0	0	68	0.00	0.00	0.00	1.00	0.00
4	68	0	0	68	0.00	0.00	0.00	1.00	0.00
5'	68	0	0	68	0.00	0.00	0.00	1.00	0.00
5	68	0	0	68	0.00	0.00	0.00	1.00	0.00
6'	68	2	0	66	0.03	0.00	0.03	0.97	-0.01
6	68	2	0	66	0.03	0.00	0.03	0.97	-0.01
7'	66	0	0	66	0.00	0.00	0.00	1.00	0.00
7	66	0	0	66	0.00	0.00	0.00	1.00	0.00
8'	66	2	0	64	0.03	0.00	0.03	0.97	-0.01
8	66	2	0	64	0.03	0.00	0.03	0.97	-0.01
9'	64	0	0	64	0.00	0.00	0.00	1.00	0.00
9	64	1	0	63	0.02	0.00	0.02	0.98	-0.01
10'	64	1	0	63	0.02	0.00	0.02	0.98	-0.01
10	63	0	0	63	0.00	0.00	0.00	1.00	0.00
11'	63	0	0	63	0.00	0.00	0.00	1.00	0.00
11	63	0	0	63	0.00	0.00	0.00	1.00	0.00
12'	63	0	0	63	0.00	0.00	0.00	1.00	0.00
12	63	1	0	62	0.02	0.00	0.02	0.98	-0.01
13'	65	50	2	13	0.77	0.03	0.80	0.10	-0.98
13	71	51	9	11	0.72	0.13	0.85	0.17	-0.76
14'	25	2	10	13	0.08	0.40	0.48	1.57	0.20
14	25	0	5	20	0.00	0.20	0.20	1.25	0.10
15'	27	1	7	19	0.04	0.26	0.30	1.31	0.12
15	27	2	2	24	0.07	0.07	0.11	1.00	0.00
16'	26	1	0	25	0.04	0.00	0.04	0.96	-0.02
16	30	1	5	24	0.03	0.17	0.20	1.16	0.07
17'	32	1	8	23	0.03	0.25	0.28	1.30	0.11
17	32	4	3	25	0.13	0.09	0.22	0.96	-0.02
18'	35	3	4	28	0.09	0.11	0.20	1.03	0.01
18	31	0	4	26	0.00	0.13	0.16	1.15	0.06
19'	33	0	1	32	0.00	0.03	0.03	1.03	0.01
19	33	2	1	30	0.06	0.03	0.09	0.97	-0.01
20'	36	2	3	31	0.06	0.08	0.14	1.03	0.01
20	34	0	3	31	0.00	0.09	0.09	1.10	0.04
21'	36	5	2	29	0.14	0.06	0.19	0.91	-0.04
21	35	6	2	27	0.17	0.06	0.23	0.87	-0.06
22'	33	0	2	31	0.00	0.06	0.06	1.06	0.03
22	32	2	2	28	0.06	0.06	0.13	1.00	0.00
23'	32	3	0	29	0.09	0.00	0.09	0.90	-0.04
23	32	2	2	28	0.06	0.06	0.13	1.00	0.00
24'	30	0	2	28	0.00	0.07	0.07	1.07	0.03
24	30	0	0	30	0.00	0.00	0.00	1.00	0.00
25'	30	4	0	26	0.13	0.00	0.13	0.86	-0.07
25	32	6	2	24	0.19	0.06	0.25	0.85	-0.07
26'	28	2	2	24	0.07	0.07	0.14	1.00	0.00
26	26	0	0	26	0.00	0.00	0.00	1.00	0.00

**SUPPLEMENTARY TABLE 1.** Values of parameters (G, E, N and S) and metrics (Er, Nr, F and V) in each interval of the El Kef section for pattern A hypothesis (meaning of parameters and metrics in SUPPLEMENTARY APPENDIX A).

EL KEF - HYPOTHESIS OF PATTERN B									
Interval	G	E	N	S	E <sub>R</sub>	N <sub>R</sub>	V	F	log F
1'	68	0	0	68	0.00	0.00	0.00	1.00	0.00
1	68	0	0	68	0.00	0.00	0.00	1.00	0.00
2'	68	0	0	68	0.00	0.00	0.00	1.00	0.00
2	68	0	0	68	0.00	0.00	0.00	1.00	0.00
3'	68	0	0	68	0.00	0.00	0.00	1.00	0.00
3	68	0	0	68	0.00	0.00	0.00	1.00	0.00
4'	68	0	0	68	0.00	0.00	0.00	1.00	0.00
4	68	0	0	68	0.00	0.00	0.00	1.00	0.00
5'	68	0	0	68	0.00	0.00	0.00	1.00	0.00
5	68	0	0	68	0.00	0.00	0.00	1.00	0.00
6'	68	2	0	66	0.03	0.00	0.03	0.97	-0.01
6	68	2	0	66	0.03	0.00	0.03	0.97	-0.01
7'	66	0	0	66	0.00	0.00	0.00	1.00	0.00
7	66	0	0	66	0.00	0.00	0.00	1.00	0.00
8'	66	2	0	64	0.03	0.00	0.03	0.97	-0.01
8	66	2	0	64	0.03	0.00	0.03	0.97	-0.01
9'	64	0	0	64	0.00	0.00	0.00	1.00	0.00
9	64	1	0	63	0.02	0.00	0.02	0.98	-0.01
10'	64	1	0	63	0.02	0.00	0.02	0.98	-0.01
10	63	0	0	63	0.00	0.00	0.00	1.00	0.00
11'	63	0	0	63	0.00	0.00	0.00	1.00	0.00
11	63	0	0	63	0.00	0.00	0.00	1.00	0.00
12'	63	0	0	63	0.00	0.00	0.00	1.00	0.00
12	63	1	0	62	0.02	0.00	0.02	0.98	-0.01
13'	65	61	2	2	0.94	0.03	0.97	0.01	-2.11
13	71	62	9	0	0.87	0.13	1.00	0.04	-1.43
14'	14	1	10	3	0.07	0.71	0.79	3.56	0.55
14	15	1	5	9	0.07	0.33	0.40	1.42	0.15
15'	17	2	4	11	0.12	0.24	0.35	1.17	0.07
15	16	1	2	13	0.06	0.13	0.19	1.07	0.03
16'	15	0	0	15	0.00	0.00	0.00	1.00	0.00
16	20	0	5	15	0.00	0.25	0.25	1.33	0.12
17'	23	0	8	15	0.00	0.35	0.35	1.53	0.19
17	23	3	3	17	0.13	0.13	0.26	1.00	0.00
18'	27	3	4	20	0.11	0.15	0.26	1.05	0.02
18	24	0	4	20	0.00	0.17	0.17	1.20	0.08
19'	25	0	1	24	0.00	0.04	0.04	1.04	0.02
19	25	0	1	24	0.00	0.04	0.04	1.04	0.02
20'	28	0	3	25	0.00	0.11	0.11	1.12	0.05
20	28	0	3	25	0.00	0.11	0.11	1.12	0.05
21'	29	5	1	23	0.17	0.03	0.21	0.84	-0.07
21	28	6	1	21	0.21	0.04	0.25	0.79	-0.10
22'	26	1	2	23	0.04	0.08	0.12	1.04	0.02
22	25	0	2	23	0.00	0.08	0.08	1.09	0.04
23'	25	2	0	23	0.08	0.00	0.08	0.92	-0.04
23	28	2	3	23	0.07	0.11	0.18	1.04	0.02
24'	26	0	3	23	0.00	0.12	0.12	1.13	0.05
24	26	0	0	26	0.00	0.00	0.00	1.00	0.00
25'	26	1	0	25	0.04	0.00	0.04	0.96	-0.02
25	28	2	2	24	0.07	0.07	0.14	1.00	0.00
26'	27	1	2	24	0.04	0.07	0.11	1.04	0.02
26	26	0	0	26	0.00	0.00	0.00	1.00	0.00

**SUPPLEMENTARY TABLE 2.** Values of parameters (G, E, N and S) and metrics (E<sub>r</sub>, N<sub>r</sub>, F and V) in each interval of the El Kef section for pattern B hypothesis (meaning of parameters and metrics in SUPPLEMENTARY APPENDIX A).

Anexo II. Material suplementario de Gilabert et al. (2021a), (4 Tablas).

Archivos originales de las tablas en formato xlsx. se encuentran en la carpeta (Anexos).

Sample number	cm below KFB	Species	Species richness (S)
GR-0-2	-1	<i>Archaeoglobigerina blowi</i>	66
GR-3	-3	<i>A. cretacea</i>	67
GR-4	-4	<i>Abathomphalus intermedius</i>	67
GR-15	-15	<i>A. mayaroensis</i>	68
GR-20	-20	<i>Contusotruncana contusa</i>	68
GR-25	-25	<i>C. patelliformis</i>	68
GR-35	-35	<i>C. plicata</i>	68
GR-40	-40	<i>C. walfischensis</i>	68
GR-60	-60	<i>Globotruncanella</i>	69
GR-70	-70	<i>G. havanensis</i>	69
GR-80	-80	<i>G. minuta</i>	69
GR-110	-110	<i>G. petaloidea</i>	69
GR-150	-150	<i>G. pschadae</i>	69
GR-175	-175	<i>Globotruncanita angulata</i>	69
GR-210	-210	<i>G. conica</i>	69
GR-230	-230	<i>G. dupeblei</i>	69
GR-250	-250	<i>G. falsocalcarata</i>	69
GR-280	-280	<i>G. fareedi</i>	69
GR-300	-300	<i>G. insignis</i>	69
GR-420	-420	<i>G. stuarti</i>	69
GR-430	-430	<i>G. stuartiformis</i>	69
GR-490	-490	<i>Globotruncana arca</i>	69
GR-505	-505	<i>G. aegyptiaca</i>	69
GR-580	-580	<i>G. rosetta</i>	69
GR-630	-630	<i>G. marie</i>	69
GR-655	-655	<i>G. orientalis</i>	69
GR-680	-680	<i>Globigerinelloides multispina</i>	69
GR-700	-700	<i>G. prairiehillensis</i>	69
GR-720	-720	<i>G. rosebudensis</i>	69
GR-770	-770	<i>G. subcarinatus</i>	69
GR-810	-810	<i>G. volutus</i>	69
GR-840	-840	<i>G. yaucoensis</i>	69
GR-900	-900	<i>Gublerina acuta</i>	69
GR-950	-950	<i>G. cuvillieri</i>	69
GR-1080	-1080	<i>Guembeltria blowi</i>	69
GR-1140	-1140	<i>G. cretacea</i>	69
GR-1190	-1190	<i>Muricohedbergella</i>	69
GR-1200	-1200	<i>M. holmdelensis</i>	69
GR-1250	-1250	<i>Heterohelix globulosa</i>	69
GR-1280	-1280	<i>H. labellosa</i>	69
GR-1320	-1320	<i>H. navarroensis</i>	69
GR-1360	-1360	<i>H. planata</i>	69
GR-1380	-1380	<i>H. punctulata</i>	69
GR-1470	-1470	<i>Laeviheterohelix glabrans</i>	69
GR-1580	-1580	<i>L. pulchra</i>	69
GR-1680	-1680	<i>Planoglobulina acervulinoides</i>	69
GR-1740	-1740	<i>P. carseyae</i>	69
GR-1750	-1750	<i>P. multicaemata</i>	69
		<i>P. manuelensis</i>	69
		<i>Plummeria hantkeninoides</i>	69
		<i>Pseudoguembelina costellifera</i>	69
		<i>P. costulata</i>	69
		<i>P. excolata</i>	69
		<i>P. hariaensis</i>	69
		<i>P. kempensis</i>	69
		<i>P. palpebra</i>	69
		<i>Pseudotextularia elegans</i>	69
		<i>P. intermedia</i>	69
		<i>P. nuttalli</i>	69
		<i>Racemiguembelina fructicosa</i>	69
		<i>R. powelli</i>	69
		<i>Rugoglobigerina hexacamerata</i>	69
		<i>R. macrocephala</i>	69
		<i>R. milamensis</i>	69
		<i>R. pennyi</i>	69
		<i>R. reicheli</i>	69
		<i>R. rotundata</i>	69
		<i>R. rugosa</i>	69
		<i>R. scotti</i>	69
		<i>Schackoina multispinata</i>	69

Supplementary Table 1. Stratigraphic distribution of planktic foraminifera across the Caravaca section, and specific richness in each sample.



Sample number	cm below KPB	Relative abundance (%) of planktic foraminifera genera																				N	Planktic Benthic ratio P/B (%)	Depth-ranking ecogroups (%)					Fragmentation I.	
		Abathomphalus+	Archaeoglobigerina*	Contusotruncana*	Globigerinelloides*	Globotruncana+	Globotruncanella+	Globotruncanita+	Gublerina+	Guembelitra^	Muricohedbergella*	Heterohelix*	Laeviheterohelix+	Planoglobulina*	Pseudotextularia*	Pseudoguembelina^	Racemiguembelina*	Rugoglobigerina^	Plummerita^	Schackoina^	Globotruncanids+			Mixed	Intermediate	Thermocline	Deep/Surface ratio	>2/3 test	Fragments	(F) Fragmentation Index (%)
GR-02	-1	0.0%	0.0%	0.0%	11.9%	3.0%	1.1%	1.8%	0.0%	1.1%	8.7%	63.5%	1.3%	0.2%	0.6%	2.6%	0.0%	2.5%	0.0%	0.6%	5.9%	539	98.2%	8%	85%	7%	0.47	539	141	21%
GR-20	-20	0.0%	0.0%	0.0%	12.7%	2.5%	0.4%	1.2%	0.0%	1.6%	5.1%	65.0%	1.8%	0.2%	0.7%	5.3%	0.0%	2.1%	0.5%	0.4%	4.1%	551	97.7%	10%	84%	6%	0.37	551	191	26%
GR-40	-40	0.0%	0.0%	0.3%	13.4%	0.3%	0.5%	1.8%	0.2%	1.2%	6.2%	67.7%	1.8%	0.0%	0.6%	3.9%	0.5%	2.1%	0.2%	0.0%	3.5%	682	98.1%	7%	89%	4%	0.35	682	182	22%
GR-80	-80	0.0%	0.0%	0.0%	11.7%	3.0%	0.4%	2.2%	0.0%	2.0%	3.8%	65.4%	1.8%	0.0%	0.6%	4.0%	0.5%	4.4%	0.0%	0.0%	5.8%	503	98.4%	10%	82%	7%	0.41	503	144	22%
GR-380	-80	0.0%	0.0%	0.2%	13.0%	1.6%	1.0%	3.0%	0.0%	5.1%	8.1%	58.1%	1.8%	0.2%	0.4%	3.4%	0.4%	3.2%	0.0%	0.2%	5.8%	500	97.1%	12%	81%	7%	0.38	507	120	19%
GR-110	-110	0.0%	0.0%	0.4%	8.6%	0.3%	1.8%	0.4%	0.2%	2.0%	11.6%	62.0%	3.0%	0.4%	0.6%	4.0%	0.4%	4.5%	0.0%	0.8%	3.4%	488	98.4%	12%	84%	6%	0.39	500	138	22%
GR-170	-110	0.0%	0.0%	0.2%	11.1%	1.4%	1.4%	2.9%	0.2%	2.0%	4.5%	63.7%	2.3%	0.0%	0.4%	5.7%	0.0%	4.5%	0.0%	0.8%	3.4%	488	98.4%	12%	80%	6%	0.41	488	187	28%
GR-230	-230	0.0%	0.0%	0.0%	8.0%	2.4%	2.2%	2.2%	0.0%	2.0%	13.3%	55.6%	1.8%	0.6%	1.8%	5.6%	0.8%	3.0%	0.0%	0.6%	6.9%	498	97.3%	11%	80%	9%	0.44	488	215	30%
GR-330	-330	0.0%	0.0%	0.0%	8.6%	1.0%	2.0%	4.6%	0.0%	1.8%	7.0%	62.4%	1.8%	0.2%	0.7%	5.5%	0.4%	2.8%	0.0%	0.4%	7.6%	500	99.0%	11%	80%	9%	0.46	500	221	31%
GR-430	-380	0.0%	0.7%	0.0%	7.1%	2.8%	1.9%	0.2%	0.2%	2.0%	4.7%	70.5%	0.2%	0.0%	0.2%	6.6%	0.5%	4.5%	0.0%	0.4%	7.4%	434	99.3%	11%	85%	4%	0.46	500	165	28%
GR-530	-505	0.0%	0.0%	0.0%	8.8%	2.0%	1.8%	3.6%	0.2%	2.0%	6.0%	60.4%	0.6%	0.0%	0.2%	6.6%	0.6%	6.2%	0.2%	0.0%	5.6%	500	99.0%	15%	87%	8%	0.36	500	286	36%
GR-630	-580	0.0%	0.0%	0.0%	8.3%	2.2%	0.8%	2.6%	0.0%	4.4%	7.0%	73.0%	0.2%	0.0%	1.2%	3.8%	0.6%	2.6%	0.0%	0.6%	5.6%	533	98.3%	7%	87%	6%	0.45	500	232	32%
GR-630	-630	0.0%	0.5%	0.0%	14.4%	1.6%	0.2%	1.4%	0.0%	0.7%	3.0%	68.3%	0.0%	0.0%	0.5%	6.0%	0.4%	3.5%	0.0%	0.6%	3.2%	571	98.1%	15%	81%	3%	0.18	533	310	37%
GR-655	-655	0.0%	0.0%	0.0%	6.2%	1.6%	0.0%	0.0%	0.0%	0.0%	4.7%	82.3%	0.0%	0.0%	0.0%	4.7%	0.0%	1.5%	0.0%	0.5%	0.0%	198	95.2%	7%	87%	0%	0.24	198	179	40%
GR-680	-720	0.0%	0.0%	0.2%	6.1%	2.3%	1.8%	0.2%	0.3%	2.4%	5.9%	56.6%	1.6%	0.4%	0.4%	14.3%	0.4%	7.0%	0.0%	0.5%	1.9%	488	98.2%	7%	93%	0%	0.00	488	179	47%
GR-720	-720	0.3%	0.0%	0.0%	7.3%	1.4%	0.0%	0.3%	0.3%	1.4%	4.3%	70.3%	0.3%	0.0%	0.8%	8.9%	0.4%	2.4%	0.0%	1.0%	1.8%	370	100.0%	14%	86%	2%	0.15	500	449	47%
GR-750	-750	0.0%	0.0%	0.0%	8.8%	1.0%	0.6%	0.2%	0.0%	1.6%	4.2%	72.2%	0.4%	0.0%	0.0%	8.8%	0.5%	1.1%	0.0%	0.5%	1.9%	500	97.5%	16%	86%	2%	0.15	500	340	48%
GR-810	-810	0.0%	0.0%	0.0%	10.7%	3.6%	0.5%	2.7%	0.2%	0.2%	4.5%	60.2%	0.5%	0.5%	0.7%	11.7%	0.5%	4.1%	0.0%	0.2%	6.8%	412	99.8%	16%	86%	8%	0.32	412	196	32%
GR-840	-840	0.2%	0.0%	0.0%	5.6%	2.3%	1.2%	2.0%	0.2%	0.6%	4.5%	53.8%	2.9%	0.0%	1.4%	13.4%	0.6%	10.7%	0.0%	0.6%	5.5%	484	100.0%	25%	86%	9%	0.25	484	110	19%
GR-900	-900	0.2%	0.0%	0.0%	10.2%	0.5%	0.0%	1.4%	0.3%	0.6%	3.6%	69.8%	0.7%	0.0%	0.4%	7.0%	0.3%	3.9%	0.0%	0.0%	2.0%	589	99.0%	13%	84%	3%	0.19	589	249	30%
GR-960	-960	0.0%	0.2%	0.2%	9.6%	2.8%	0.4%	0.2%	0.2%	0.6%	6.6%	69.8%	0.8%	0.0%	1.0%	5.4%	0.2%	2.8%	0.0%	0.2%	3.4%	501	99.0%	14%	87%	4%	0.32	501	232	32%
GR-1020	-1020	0.0%	0.3%	0.0%	5.5%	1.3%	0.0%	1.3%	0.0%	1.5%	6.8%	72.8%	0.2%	0.0%	0.6%	8.2%	0.4%	4.2%	0.0%	0.8%	2.4%	474	96.9%	14%	83%	3%	0.16	474	229	33%
GR-1080	-1080	0.0%	0.0%	0.3%	9.6%	2.8%	0.9%	0.3%	1.1%	0.0%	7.5%	75.3%	0.2%	0.0%	0.6%	4.8%	0.0%	2.8%	0.0%	0.2%	3.0%	637	97.8%	10%	87%	3%	0.26	637	601	49%
GR-1140	-1140	0.0%	0.0%	0.0%	3.4%	0.4%	0.2%	0.2%	0.2%	1.8%	2.8%	75.0%	0.8%	0.0%	0.0%	7.3%	0.0%	2.2%	0.0%	1.4%	1.6%	499	98.0%	14%	84%	3%	0.16	507	318	39%
GR-1200	-1200	0.0%	0.0%	0.0%	8.2%	0.2%	0.6%	1.8%	0.2%	2.2%	4.9%	75.0%	0.8%	0.0%	0.0%	4.8%	0.0%	2.5%	0.0%	0.3%	2.1%	394	96.1%	10%	88%	2%	0.18	394	537	56%
GR-1260	-1260	0.0%	0.0%	0.0%	7.9%	1.0%	1.0%	0.8%	0.0%	1.8%	2.8%	68.5%	0.0%	0.0%	0.0%	6.7%	0.0%	1.0%	0.0%	0.2%	3.4%	315	95.7%	10%	88%	5%	0.19	315	553	64%
GR-1320	-1320	0.0%	0.2%	0.0%	11.0%	1.4%	0.9%	1.2%	0.2%	0.4%	5.4%	71.1%	1.4%	0.0%	1.0%	4.0%	0.4%	1.7%	0.0%	0.2%	3.4%	489	99.2%	6%	89%	5%	0.46	489	373	43%
GR-1380	-1380	0.0%	0.0%	0.2%	7.9%	2.3%	0.0%	1.5%	0.0%	0.5%	7.2%	64.8%	0.7%	0.2%	1.4%	7.0%	0.5%	4.7%	0.0%	0.2%	6.0%	571	99.5%	12%	82%	5%	0.30	571	294	34%
GR-1470	-1470	0.0%	0.0%	0.0%	3.5%	4.3%	0.0%	1.6%	0.4%	0.2%	6.9%	61.7%	0.4%	0.2%	2.6%	14.1%	0.7%	3.3%	0.0%	0.0%	6.0%	461	98.3%	18%	82%	7%	0.28	461	471	51%
GR-1580	-1580	0.0%	0.0%	0.0%	8.5%	3.2%	3.2%	0.8%	4.0%	0.2%	6.4%	56.9%	0.4%	0.8%	1.0%	9.7%	0.5%	5.8%	0.0%	0.0%	7.8%	524	98.6%	15%	78%	8%	0.34	524	393	43%
GR-1650	-1650	0.0%	0.0%	0.0%	9.2%	3.3%	0.6%	4.0%	0.2%	6.4%	59.9%	0.4%	0.8%	1.0%	7.0%	0.5%	5.8%	0.0%	0.0%	7.8%	489	98.6%	13%	78%	8%	0.39	489	249	33%	
GR-1740	-1740	0.0%	0.0%	0.2%	5.2%	6.2%	1.0%	3.8%	0.6%	8.9%	58.3%	2.0%	1.0%	0.6%	0.6%	7.0%	0.4%	4.8%	0.0%	0.0%	11.2%	489	99.2%	12%	75%	13%	0.52	489	196	28%
GR-1830	-1830	0.0%	0.0%	0.2%	2.8%	2.2%	0.8%	0.8%	0.3%	0.8%	62.1%	0.8%	1.0%	0.8%	0.9%	9.1%	0.4%	1.5%	0.0%	0.0%	4.5%	497	99.2%	12%	79%	9%	0.42	497	265	35%
Average ->		0.0%	0.1%	0.1%	8.9%	1.9%	0.8%	1.6%	0.1%	1.4%	61.1%	66.2%	1.0%	0.2%	0.6%	6.9%	0.4%	3.5%	0.0%	0.3%	4.5%	492	98.4%	12%	82%	6%	0.31	492	276	35%

Note: ^ = mixed layer dweller, \* = intermediate dweller, + = thermocline dweller, N = total number of studied specimens in each sample.

**Supplementary Table 2.** Relative abundance (%) of planktic foraminifera genera (^ = mixed layer dweller; \* = intermediate dweller, + = thermocline dweller), N = total number of studied specimens in each sample, planktic/benthic (P/B) ratio, depth-habitat ecogroups (%), Deep/surface ratio, and fragmentation index.

Contusotruncana contusa											Pseudoguembelina hariaensis										
cm below KPB	H (µm)	L (µm)	Average (H)	Average (L)	cm below KPB	H (µm)	L (µm)	Average (H)	Average (L)	cm below KPB	H (µm)	W (µm)	Average (H)	Average (W)	Morphotype	cm below KPB	H (µm)	W (µm)	Average (H)	Average (W)	Morphotype
-1	822	729			-840	444	535			-1	498	314			Biserial	-840	449	307			Multiserial
-1	822	988			-840	497	719			-1	390	255			Multiserial	-840	338	213			Biserial
-1	691	872			-840	432	529			-1	430	246			Biserial	-840	525	354			Biserial
-1	745	985			-840	485	579			-1	409	318			Multiserial	-840	423	287			Biserial
-1	799	971	716	923	-840	464	585	494	640	-1	448	323	404	289	Multiserial	-840	481	340	453	312	Biserial
-1	832	983			-840	402	584			-1	399	308			Multiserial	-840	477	317			Biserial
-1	762	943			-840	441	604			-1	369	249			Multiserial	-840	515	336			Biserial
-1	763	917			-840	505	673			-1	347	276			Multiserial	-840	460	327			Multiserial
-1	639	899			-840	521	715			-1	302	254			Biserial	-840	434	272			Biserial
-1	802	972			-840	746	873			-1	443	347			Multiserial	-840	432	366			Multiserial
-40	707	954			-960	516	620			-40	441	354			Multiserial	-960	502	342			Biserial
-40	685	972			-960	462	549			-40	529	421			Multiserial	-960	353	261			Multiserial
-40	704	860			-960	549	606			-40	354	272			Multiserial	-960	343	271			Biserial
-40	737	977			-960	496	603			-40	430	291			Biserial	-960	531	407			Multiserial
-40	691	853	662	906	-960	555	707	516	629	-40	340	287	433	333	Multiserial	-960	336	240	427	305	Biserial
-40	659	881			-960	440	615			-40	441	299			Multiserial	-960	476	333			Biserial
-40	625	931			-960	532	635			-40	464	385			Multiserial	-960	422	287			Biserial
-40	606	846			-960	485	587			-40	448	386			Multiserial	-960	409	292			Biserial
-40	627	943			-960	610	800			-40	464	352			Multiserial	-960	336	219			Biserial
-40	665	840			-960	515	571			-40	416	304			Biserial	-960	561	394			Biserial
-80	737	896			-1080	518	753			-80	337	244			Multiserial	-1080	408	288			Biserial
-80	645	877			-1080	430	681			-80	418	294			Biserial	-1080	404	258			Biserial
-80	675	827			-1080	-	-			-80	354	209			Multiserial	-1080	412	301			Biserial
-80	845	977			-1080	-	-			-80	418	272			Biserial	-1080	307	231			Biserial
-80	740	888	720	927	-1080	-	-	474	717	-80	487	330	431	320	Biserial	-1080	341	285	376	271	Multiserial
-80	710	843			-1080	-	-			-80	444	342			Multiserial	-1080	334	244			Biserial
-80	707	1041			-1080	-	-			-80	557	342			Multiserial	-1080	437	280			Biserial
-80	616	833			-1080	-	-			-80	418	315			Multiserial	-1080	374	224			Biserial
-80	743	1005			-1080	-	-			-80	441	319			Biserial	-1080	326	235			Multiserial
-80	780	986			-1080	-	-			-80	437	334			Multiserial	-1080	421	361			Multiserial
-230	701	957			-1140	444	645			-230	392	254			Multiserial	-1140	396	249			Biserial
-230	731	948			-1140	450	570			-230	398	285			Multiserial	-1140	413	262			Biserial
-230	742	960			-1140	436	655			-230	592	333			Biserial	-1140	334	270			Biserial
-230	677	1002			-1140	513	656			-230	565	407			Multiserial	-1140	398	288			Multiserial
-230	780	1003			-1140	751	1009	487	678	-230	392	294	448	308	Multiserial	-1140	522	382	426	303	Biserial
-230	677	1036			-1140	445	717			-230	455	270			Biserial	-1140	424	299			Multiserial
-230	758	1002			-1140	393	629			-230	442	349			Biserial	-1140	443	299			Multiserial
-230	692	874			-1140	412	609			-230	454	321			Biserial	-1140	381	328			Multiserial
-230	782	978			-1140	484	659			-230	457	368			Multiserial	-1140	495	325			Biserial
-230	711	1007			-1140	545	628			-230	430	303			Biserial	-1140	463	331			Multiserial
-380	630	893			-1200	585	639			-380	358	245			Biserial	-1200	506	309			Multiserial
-380	651	838			-1200	535	692			-380	539	320			Biserial	-1200	422	274			Multiserial
-380	684	949			-1200	527	722			-380	537	394			Multiserial	-1200	343	252			Biserial
-380	730	861			-1200	431	638			-380	358	211			Biserial	-1200	443	315			Multiserial
-380	596	746	677	896	-1200	402	465	474	621	-380	406	285	433	303	Multiserial	-1200	342	230	406	278	Biserial
-380	749	910			-1200	399	586			-380	346	293			Multiserial	-1200	376	276			Biserial
-380	794	956			-1200	448	547			-380	419	275			Multiserial	-1200	348	260			Biserial
-380	640	854			-1200	406	595			-380	409	277			Biserial	-1200	358	284			Multiserial
-380	717	973			-1200	589	649			-380	462	360			Biserial	-1200	394	291			Multiserial
-380	617	875			-1200	417	680			-380	494	265			Biserial	-1200	386	267			Multiserial
-430	837	1015			-1290	470	725			-430	436	314			Multiserial	-1290	344	235			Biserial
-430	696	936			-1290	422	675			-430	434	283			Multiserial	-1290	361	264			Biserial
-430	667	950			-1290	328	588			-430	437	302			Multiserial	-1290	482	270			Biserial
-430	730	964			-1290	432	625			-430	514	297			Biserial	-1290	477	314			Biserial
-430	659	784	692	910	-1290	409	617	412	646	-430	332	242	406	285	Biserial	-1290	318	236	402	274	Biserial
-430	654	869			-1290	-	-			-430	444	332			Biserial	-1290	437	303			Biserial
-430	696	999			-1290	-	-			-430	344	265			Multiserial	-1290	360	280			Biserial
-430	645	874			-1290	-	-			-430	392	308			Multiserial	-1290	426	315			Biserial
-430	615	838			-1290	-	-			-430	355	250			Biserial	-1290	386	267			Biserial
-430	724	972			-1290	-	-			-430	370	252			Biserial	-1290	429	256			Biserial
-505	888	1160			-1320	595	971			-505	448	355			Biserial	-1320	396	272			Biserial
-505	672	984			-1320	554	816			-505	394	300			Biserial	-1320	427	308			Biserial
-505	758	949			-1320	759	928			-505	356	262			Biserial	-1320	355	248			Biserial
-505	759	938			-1320	700	1001			-505	390	285			Biserial	-1320	396	241			Biserial
-505	611	1056			-1320	783	899	698	912	-505	505	364	406	289	Biserial	-1320	347	391	355	263	Multiserial
-505	736	1013			-1320	695	889			-505	447	310			Biserial	-1320	276	187			Biserial
-505	599	809			-1320	835	946			-505	266	191			Biserial	-1320	352	270			Biserial
-505	661	824			-1320	580	840			-505	517	386			Biserial	-1320	400	261			Biserial
-505	767	938			-1320	695	929			-505	372	228			Biserial	-1320	285	215			Biserial
-505	640	812	</																		

Sample number	cm below KPB	$\delta^{13}\text{C}$ (‰, VPDB)	$\delta^{18}\text{O}$ (‰, VPDB)	CaCO <sub>3</sub> %	Sample number	cm below KPB	$\delta^{13}\text{C}$ (‰, VPDB)	$\delta^{18}\text{O}$ (‰, VPDB)	CaCO <sub>3</sub> %
GR-1	-1	1.53	-2.42	66%	GR-605	-605	0.87	-2.27	67%
GR-3	-3	2.07	-2.01	62%	GR-630	-630	-0.58	-2.95	55%
GR-5	-5	2.03	-1.91	65%	GR-655	-655	0.09	-3.17	75%
GR-7	-7	2.04	-2.00	68%	GR-680	-680	1.39	-2.12	75%
GR-9	-9	2.06	-1.88	65%	GR-690	-690	1.52	-2.32	77%
GR-15	-15	2.01	-1.88	66%	GR-720	-720	1.47	-2.15	76%
GR-20	-20	2.07	-1.94	58%	GR-750	-750	1.39	-1.92	73%
GR-25	-25	2.05	-2.00	65%	GR-780	-780	1.36	-2.04	71%
GR-30	-30	2.05	-1.95	66%	GR-810	-810	0.73	-2.37	68%
GR-35	-35	2.12	-1.80	65%	GR-840	-840	0.83	-2.42	68%
GR-40	-40	2.02	-1.99	64%	GR-870	-870	1.13	-2.14	69%
GR-45	-45	1.79	-2.03	67%	GR-900	-900	0.95	-2.24	71%
GR-50	-50	1.92	-1.89	61%	GR-930	-930	0.78	-2.39	69%
GR-55	-55	1.78	-1.92	63%	GR-960	-960	1.14	-2.27	69%
GR-60	-60	1.64	-2.11	65%	GR-990	-990	0.82	-2.43	65%
GR-65	-65	1.73	-2.12	65%	GR-1020	-1020	1.47	-2.25	76%
GR-70	-70	1.71	-2.00	63%	GR-1050	-1050	1.37	-2.37	77%
GR-75	-75	1.74	-2.11	65%	GR-1080	-1080	-0.60	-3.15	73%
GR-80	-80	1.92	-2.05	66%	GR-1110	-1110	0.58	-2.66	72%
GR-85	-85	1.99	-2.05	59%	GR-1140	-1140	1.14	-2.83	74%
GR-90	-90	1.57	-2.18	65%	GR-1170	-1170	1.43	-2.38	77%
GR-95	-95	1.72	-2.20	65%	GR-1200	-1200	1.57	-2.31	76%
GR-100	-100	1.92	-1.89	61%	GR-1230	-1230	1.32	-2.20	73%
GR-110	-110	1.81	-1.99	66%	GR-1260	-1260	0.59	-2.62	72%
GR-130	-130	1.73	-2.02	63%	GR-1290	-1290	0.63	-2.22	64%
GR-150	-150	1.71	-1.96	69%	GR-1320	-1320	0.96	-2.08	69%
GR-170	-170	1.54	-2.16	72%	GR-1350	-1350	1.05	-2.33	66%
GR-190	-190	1.62	-2.12	75%	GR-1380	-1380	1.59	-2.46	77%
GR-210	-210	1.30	-2.23	74%	GR-1410	-1410	1.48	-2.29	76%
GR-230	-230	1.70	-2.16	72%	GR-1440	-1440	1.35	-2.24	72%
GR-250	-250	1.83	-2.08	74%	GR-1470	-1470	1.16	-2.31	70%
GR-280	-280	1.69	-2.15	75%	GR-1500	-1500	1.19	-2.21	70%
GR-305	-305	1.50	-2.09	77%	GR-1530	-1530	1.32	-2.22	73%
GR-330	-330	1.49	-2.26	69%	GR-1560	-1560	1.31	-2.32	72%
GR-355	-355	1.56	-2.18	72%	GR-1590	-1590	1.81	-2.19	81%
GR-380	-380	1.39	-2.32	71%	GR-1620	-1620	1.75	-2.19	81%
GR-405	-405	1.19	-2.24	67%	GR-1650	-1650	1.90	-2.28	82%
GR-430	-430	1.69	-2.19	79%	GR-1680	-1680	1.87	-2.13	80%
GR-455	-455	1.25	-2.30	71%	GR-1710	-1710	2.07	-2.10	83%
GR-480	-480	0.85	-2.60	73%	GR-1740	-1740	1.58	-2.24	82%
GR-505	-505	1.50	-2.31	75%	GR-1770	-1770	1.62	-2.18	81%
GR-530	-530	0.95	-2.34	68%	GR-1800	-1800	1.81	-1.97	82%
GR-555	-555	1.28	-2.18	75%	GR-1830	-1830	1.92	-2.07	77%
GR-580	-580	1.25	-2.43	77%	-	-	-	-	-

Supplementary Table 4. Geochemical results: bulk  $\delta^{18}\text{O}$  and  $\delta^{13}\text{C}$  data (‰ VPDB) and CaCO<sub>3</sub> content.



Height	Supplementary Table 2																											
	Relative abundance of Danian Planktic foraminifera genera (%)										Major groups (%)			Diversity Indices					Planktic / benthic ratio (%)		Fragmentation index (%)							
820	Guembeltria	Chiloguembeltria	Woodringina	Chiloguembelina	Palaeoglobbigerina	Parvularugoglobbigerina	Pseudocaucasina	Trochoguembeltria	Globoconusa	Eoglobbigerina	Parasubbotina	Subbotina	Globanomalina	Praemurica	Triserial	Parvularugoglobbigerinids	Biserial	Other Danian genera	(S) Species	(H') Shanon-Weaver index	(λ) Simpson	(1/λ) Inverse Simpson index	Fisher alpha	Equitability	Berger Parker	(E) Evenness	Planktic / benthic ratio (%)	Fragmentation index (%)
790	2.4	3.57	2.27	1.68	3.5	3.1	6.6	5.6	5.0	5.9	5.9	1.1	1.1	1.1	1.1	1.1	1.1	2.4	2.32	0.16	6.43	4.90	0.78	0.32	0.51	99%	14%	
760	0.9	3.39	1.68	2.1	6.4	3.2	5.3	6.4	3.2	5.3	5.3	1.1	1.1	1.1	1.1	1.1	1.1	2.2	2.49	0.13	7.54	5.35	0.80	0.30	0.55	98%	23%	
730	2.5	3.73	2.37	2.5	3.9	3.2	5.6	3.9	3.2	5.6	5.6	1.1	1.1	1.1	1.1	1.1	1.1	2.4	2.32	0.16	6.10	5.58	0.75	0.33	0.46	100%	12%	
700	3.3	2.98	2.33	3.3	4.4	6.9	8.7	4.4	6.9	8.7	8.7	1.1	1.1	1.1	1.1	1.1	1.1	2.4	2.49	0.13	7.71	6.32	0.78	0.27	0.50	99%	12%	
670	3.3	3.20	2.33	3.3	4.0	7.3	5.1	4.0	7.3	5.1	5.1	1.1	1.1	1.1	1.1	1.1	1.1	2.4	2.56	0.13	7.61	7.05	0.79	0.28	0.50	98%	15%	
640	1.4	3.51	2.34	1.4	4.3	6.2	7.5	4.3	6.2	7.5	7.5	1.1	1.1	1.1	1.1	1.1	1.1	2.4	2.40	0.15	6.65	6.28	0.75	0.31	0.45	99%	9%	
610	6.6	3.95	2.52	6.6	0.8	0.8	4.7	0.8	4.7	2.7	0.4	10.9	8.5	6.6	6.6	6.6	6.6	2.6	2.34	0.15	6.63	7.21	0.72	0.30	0.40	97%	10%	
580	12.3	3.31	2.27	12.3	1.9	2.9	3.2	1.9	2.9	3.2	3.2	15.9	7.8	12.3	12.3	12.3	12.3	2.1	2.37	0.13	7.64	5.10	0.78	0.25	0.51	99%	12%	
550	10.2	3.32	2.57	10.2	0.9	6.6	3.0	0.9	6.6	3.0	0.3	10.2	9.9	10.2	10.2	10.2	10.2	2.5	2.37	0.15	6.85	6.26	0.73	0.30	0.42	99%	10%	
490	7.7	3.00	2.67	7.7	5.6	6.3	6.2	5.6	6.3	6.2	1.5	10.6	7.0	7.7	7.7	7.7	7.7	2.2	2.28	0.16	5.96	5.65	0.77	0.33	0.51	98%	8%	
460	3.9	2.62	2.04	3.9	3.3	1.1	5.9	3.3	1.1	5.9	6.2	4.3	1.1	3.9	3.9	3.9	3.9	2.2	2.50	0.13	7.46	5.99	0.80	0.28	0.53	98%	25%	
430	3.0	3.27	2.44	3.0	4.7	2.5	7.5	4.7	2.5	7.5	1.1	2.26	6.8	4.3	4.3	4.3	4.3	2.6	2.62	0.11	9.17	7.01	0.80	0.23	0.53	99%	25%	
400	7.3	3.31	2.05	7.3	1.0	2.3	6.3	1.0	2.3	6.3	1.0	1.9	8.9	3.0	3.0	3.0	3.0	2.8	2.55	0.13	7.84	7.53	0.77	0.27	0.46	95%	24%	
370	12.2	3.93	1.76	12.2	1.8	1.8	7.1	1.8	1.8	7.1	0.4	5.5	0.7	12.2	12.2	12.2	12.2	2.4	2.49	0.13	7.50	6.17	0.78	0.29	0.50	98%	16%	
345	28.6	3.66	1.94	28.6	0.7	0.7	3.9	0.7	0.7	3.9	2.9	7.2	1.4	16.8	16.8	16.8	16.8	2.2	2.25	0.17	6.00	6.34	0.71	0.32	0.39	94%	14%	
320	16.8	4.27	2.31	16.8	0.4	0.4	8.5	0.4	0.4	8.5	5.0	7.5	6.0	18.9	18.9	18.9	18.9	2.2	2.09	0.20	4.92	5.60	0.68	0.38	0.37	95%	20%	
295	18.9	3.13	2.14	18.9	0.4	0.4	5.8	0.4	0.4	5.8	5.8	7.5	6.0	3.8	3.8	3.8	3.8	2.6	2.59	0.11	8.88	6.99	0.80	0.24	0.51	98%	19%	
270	3.8	3.19	2.12	3.8	1.0	1.0	3.1	1.0	1.0	3.1	0.3	7.2	6.2	4.7	4.7	4.7	4.7	2.4	2.62	0.11	9.30	6.45	0.82	0.25	0.57	100%	17%	
245	1.0	3.63	1.19	1.0	0.8	0.8	4.2	0.8	0.8	4.2	1.6	2.2	0.3	4.6	4.6	4.6	4.6	2.5	2.46	0.13	7.62	6.54	0.77	0.29	0.47	98%	16%	
220	4.65	3.21	1.25	4.65	0.6	0.6	4.2	0.6	0.6	4.2	1.5	2.2	0.3	4.6	4.6	4.6	4.6	2.1	1.97	0.23	4.37	5.08	0.65	0.37	0.34	98%	20%	
200	4.85	2.76	1.46	4.85	0.7	0.7	4.2	0.7	0.7	4.2	1.5	2.6	0.7	4.8	4.8	4.8	4.8	2.3	2.16	0.18	5.33	6.03	0.69	0.35	0.38	98%	14%	
180	4.70	3.11	1.36	4.70	0.3	0.3	4.3	0.3	0.3	4.3	1.3	2.6	0.7	4.7	4.7	4.7	4.7	1.9	2.11	0.17	5.82	4.50	0.72	0.29	0.44	96%	20%	
160	4.63	3.85	1.19	4.63	0.8	0.8	4.3	0.8	0.8	4.3	1.3	1.7	0.7	4.6	4.6	4.6	4.6	2.5	1.83	0.23	4.32	3.23	0.69	0.33	0.45	100%	11%	
130	3.82	4.97	9.7	3.82	0.3	0.3	1.7	0.3	0.3	1.7	0.3	0.3	0.4	3.8	3.8	3.8	3.8	1.8	1.81	0.22	4.59	2.80	0.70	0.34	0.47	98%	14%	
115	4.48	4.45	8.2	4.48	0.6	0.6	0.6	0.6	0.6	0.6	0.3	1.3	0.3	4.4	4.4	4.4	4.4	1.5	1.84	0.22	4.54	3.27	0.68	0.32	0.42	96%	10%	
100	1.0	6.35	8.7	1.0	3.5	6.1	3.9	3.5	6.1	3.9	0.4	3.6	0.4	1.0	1.0	1.0	1.0	2.4	2.03	0.23	4.42	6.07	0.64	0.39	0.32	97%	17%	
85	7.58	8.5	5.7	7.58	0.4	0.4	0.4	0.4	0.4	0.4	0.4	1.1	1.1	8.5	8.5	8.5	8.5	1.8	1.59	0.33	3.00	4.29	0.55	0.52	0.27	97%	21%	
60	1.1	5.92	5.6	1.1	1.9	1.9	1.9	1.9	1.9	1.9	1.9	1.1	1.1	6.0	6.0	6.0	6.0	1.9	1.80	0.27	3.71	4.68	0.61	0.47	0.32	99%	23%	
50	1.0	4.41	2.5	1.0	0.7	0.7	0.7	0.7	0.7	0.7	0.7	1.0	1.0	4.8	4.8	4.8	4.8	1.9	2.10	0.17	5.83	4.44	0.71	0.31	0.43	97%	19%	
42	3.4	2.43	1.13	3.4	2.1	3.7	3.7	2.1	3.7	3.7	0.7	1.9	0.7	3.4	3.4	3.4	3.4	1.6	2.36	0.12	8.55	3.64	0.85	0.21	0.66	95%	7%	
30	6.7	18.3	12.1	6.7	2.8	3.9	3.9	2.8	3.9	3.9	0.7	1.9	0.7	6.7	6.7	6.7	6.7	1.6	2.46	0.10	10.20	3.86	0.89	0.15	0.73	98%	19%	
26	5.5	3.9	1.2	5.5	1.4	1.4	1.4	1.4	1.4	1.4	1.4	1.4	1.4	5.5	5.5	5.5	5.5	1.4	1.88	0.25	3.95	3.36	0.71	0.46	0.47	96%	20%	
24	9.4	9.4	1.1	9.4	2.3	6.5	6.5	2.3	6.5	6.5	0.4	9.4	0.5	9.4	9.4	9.4	9.4	1.6	1.83	0.29	3.45	3.69	0.66	0.51	0.39	89%	19%	
20	0.4	6.7	1.3	0.4	2.0	7.0	7.0	2.0	7.0	7.0	0.5	9.1	0.5	9.4	9.4	9.4	9.4	1.4	1.68	0.32	3.10	3.33	0.64	0.54	0.38	78%	25%	
16	1.4	9.8	0.6	1.4	1.4	1.4	1.4	1.4	1.4	1.4	0.5	7.1	0.5	1.4	1.4	1.4	1.4	1.6	1.46	0.43	2.32	3.86	0.53	0.64	0.27	84%	11%	
12	0.6	15.2	0.6	0.6	1.4	1.4	1.4	1.4	1.4	1.4	0.6	1.4	0.6	1.4	1.4	1.4	1.4	1.4	1.41	0.45	2.23	3.36	0.53	0.66	0.29	77%	22%	
10	2.0	9.4	0.5	2.0	1.4	1.4	1.4	1.4	1.4	1.4	0.5	1.4	0.5	1.4	1.4	1.4	1.4	1.5	1.49	0.42	2.37	3.96	0.55	0.64	0.30	71%	15%	
8	1.2	9.5	0.4	1.2	1.4	1.4	1.4	1.4	1.4	1.4	0.5	1.4	0.5	1.4	1.4	1.4	1.4	1.5	1.25	0.51	1.95	3.74	0.46	0.71	0.23	79%	15%	
6	3.0	16.2	0.4	3.0	1.4	1.4	1.4	1.4	1.4	1.4	0.5	1.4	0.5	1.4	1.4	1.4	1.4	1.6	1.63	0.36	2.82	3.88	0.59	0.57	0.32	72%	20%	
4	3.8	34.7	2.7	3.8	1.4	1.4	1.4	1.4	1.4	1.4	0.5	1.4	0.5	1.4	1.4	1.4	1.4	1.1	2.00	0.19	5.19	3.55	0.83	0.37	0.67	47%	44%	
2	4.8	4.4	6.5	4.8	1.4	1.4	1.4	1.4	1.4	1.4	0.5	1.4	0.5	1.4	1.4	1.4	1.4	5	1.17	0.37	2.74	1.69	0.73	0.45	0.65	11%	44%	
1	8.9	11.1	1.1	8.9	1.4	1.4	1.4	1.4	1.4	1.4	0.5	1.4	0.5	1.4	1.4	1.4	1.4	3	0.60	0.68	1.47	0.86	0.55	0.81	0.61	33%	45%	

Supplementary Table 2. Relative abundance of planktic foraminifera genera, major groups, main diversity indices, Planktic/Benthic ratio and Fragmentation index across the Caravaca section.



Supplementary Table 4									
Geochemistry and geophysic measurements									
Height	Magnetic susceptibility (m <sup>3</sup> /kg)	CaCO <sub>3</sub> (%)	δ <sup>13</sup> C (‰) VPDB	δ <sup>18</sup> O (‰) VPDB	Cm from K-PgB	Magnetic susceptibility (m <sup>3</sup> /kg)	CaCO <sub>3</sub> (%)	δ <sup>13</sup> C (‰) VPDB	δ <sup>18</sup> O (‰) VPDB
105	2.65E-08	81.38	1.59	-1.22	820	2.94E-08	77.08	0.85	-1.44
100	2.60E-08	81.58	1.74	-1.45	790	3.22E-08	71.61	0.81	-1.66
95	2.33E-08	81.81	1.69	-1.37	760	2.51E-08	77.89	0.94	-1.69
90	2.30E-08	81.94	1.57	-1.45	730	2.55E-08	78.78	1.00	-1.50
85	2.16E-08	82.67	1.86	-1.03	700	2.91E-08	83.97	0.86	-1.78
80	1.66E-08	84.68	1.72	-1.40	670	2.36E-08	80.97	1.08	-1.39
75	1.72E-08	86.82	1.77	-1.56	640	2.29E-08	82.32	1.04	-1.30
70	1.67E-08	88.44	1.84	-1.29	610	2.33E-08	80.77	1.06	-1.46
65	1.83E-08	86.38	1.82	-1.21	580	2.78E-08	81.38	1.19	-1.35
60	1.96E-08	86.98	1.86	-1.34	550	2.65E-08	79.84	1.25	-1.31
57	2.07E-08	84.85	1.92	-1.21	520	2.89E-08	77.32	1.26	-1.49
54	1.95E-08	85.51	1.87	-1.24	490	3.85E-08	67.54	0.95	-1.91
50	2.20E-08	84.38	1.65	-1.20	460	4.51E-08	67.01	0.69	-2.36
48	2.30E-08	83.15	1.61	-1.29	430	4.91E-08	65.41	1.05	-1.59
45	2.12E-08	85.13	1.60	-1.18	400	3.91E-08	71.57	1.16	-1.30
42	2.49E-08	80.41	1.39	-1.43	370	3.81E-08	70.65	1.09	-1.37
39	2.46E-08	83.32	1.39	-1.22	345	3.85E-08	70.75	1.19	-1.28
36	2.53E-08	82.59	1.40	-1.44	320	2.93E-08	76.32	1.14	-1.41
33	2.38E-08	83.08	1.10	-1.70	295	3.04E-08	71.03	1.18	-1.00
30	2.46E-08	81.28	1.37	-1.56	270	3.76E-08	69.76	1.04	-1.56
28	2.47E-08	81.14	1.21	-1.60	245	4.57E-08	60.55	0.93	-1.57
26	4.11E-08	72.79	1.11	-1.39	220	3.81E-08	74.26	1.18	-1.55
24	4.26E-08	63.79	0.82	-1.67	200	3.30E-08	69.10	1.20	-1.72
22	3.81E-08	74.04	1.17	-1.17	180	4.05E-08	80.71	1.71	-1.05
20	3.76E-08	74.99	1.15	-1.34	160	3.51E-08	75.71	1.72	-1.22
18	3.58E-08	74.05	1.19	-1.27	155	2.90E-08	73.58	1.75	-1.32
16	3.35E-08	68.93	0.93	-1.62	150	3.36E-08	73.97	1.68	-1.42
14	3.37E-08	63.92	0.94	-1.69	145	3.38E-08	77.39	1.86	-1.08
12	4.21E-08	67.61	1.15	-1.19	140	3.55E-08	72.81	1.79	-1.16
10	4.09E-08	70.80	1.12	-1.47	135	3.73E-08	70.66	1.66	-1.31
8	3.91E-08	63.46	1.21	-1.28	130	4.07E-08	74.39	1.77	-1.30
6	1.09E-07	34.26	0.20	-2.82	125	4.15E-08	69.36	1.60	-1.18
4	7.65E-08	39.70	0.82	-2.36	120	3.95E-08	71.25	1.54	-1.40
2	1.16E-07	22.76	-0.78	-3.34	115	2.86E-08	80.02	1.56	-1.40
1	1.24E-07	15.53	-0.58	-3.77	110	2.86E-08	75.06	1.59	-1.27

**Supplementary Table 4.** Geochemical results: bulk δ<sup>18</sup>O and δ<sup>13</sup>C data (‰ VPDB), CaCO<sub>3</sub> content, and magnetic susceptibility.

**Anexo IV. Material suplementario de Gilabert et al. (2021c)**, (4 textos, 5 figuras, 5 tablas y bibliografía suplementaria).

Archivos originales de las tablas en formato xlsx. se encuentran en la carpeta (Anexos).

#### **Text S1: Detailed Methodology**

**Sampling:** For the micropaleontological, geochemical and geophysical analysis, we sampled 24.5 m across the Cretaceous/Paleogene boundary (KPB) of the Zumaia section. A total of 171 samples were taken, of which 103 samples were from the 16-m-thick Maastrichtian interval and 68 from the 8.5-m-thick Danian interval. The sample spacing for the Maastrichtian was of 15–20 cm, except for the 2 m below the KPB, which were sampled every 5–10 cm. The Danian interval was sampled every 2.5–5 cm across the first 80 cm and every 15 cm further upwards.

**Micropaleontology:** We follow the disaggregating technique of Lirer (2000) which employs dilute acetic acid for 3-4 hours to liberate calcareous microfossils from strongly lithified calcareous rocks such as those from Zumaia. The disaggregated samples were then washed through a 63  $\mu\text{m}$  sieve and oven-dried at 50 °C. When quantitative analysis was possible, the samples were split with a microsplitter to obtain a representative aliquot of ca. 300 specimens per sample.

**Calcium carbonate content:** The calcium carbonate content of each rock sample was estimated with a manocalcimeter by measuring and recording the carbon dioxide pressure rise produced by acid attack on the rock sample. 171 rock samples were analyzed, which were mechanically powdered to avoid the secondary calcite veins. The analyses were performed by adding 5ml of 5M HCl to one gram of powdered sample in the reaction cell, which is independent of the atmospheric pressure.



**Carbon isotope analyses:** Measurements of  $\delta^{13}\text{C}$  were performed on homogenized bulk powdered sediment from the same 171 samples. Samples were analyzed in the Department of Earth Sciences of the University of Oxford, using a GasBench device attached to a ThermoFisher Delta V Advantage gas source isotope ratio mass spectrometer. Carbon isotopes are reported using the standard delta notation ( $\delta^{13}\text{C}$ ) in parts per mill (‰) on the Vienna PeeDee Belemnite (VPDB) scale. Calibration of samples to the VPDB scale was achieved using multiple analyses of an in-house standard. For the  $\delta^{13}\text{C}$ , the in-house standard, NOCZ, has an average value of 2.18‰. The NOCZ standard was calibrated to the VPDB scale by comparison with analyses of NBS-19 and NBS-18, which were assigned values of +1.95‰ and -5.014‰, respectively. Repeated analyses of in-house standards suggest a reproducibility ( $\pm 1\sigma$ ) of <0.1.

**Magnetic susceptibility:** The magnetic susceptibility (MS) of the 171 samples was measured at the University of Zaragoza, Spain, with a Kappabridge KLY-35 spinning specimen magnetic susceptibility anisotropy meter. Samples were crushed in an agate mortar and measured in cylindrical plastic boxes 10 cm<sup>3</sup> in volume. MS values are reported relative to mass (m<sup>3</sup>/kg).

### **Text S2: Geochemical and geophysical properties.**

The  $\delta^{13}\text{C}$ , CaCO<sub>3</sub> and magnetic susceptibility data from Zumaia presented here (Figs. 3, S2 and Table S2) are comparable to previous studies from the KP interval at Zumaia (e.g., Batenburg et al., 2012; Dinarés-Turell et al., 2003, 2014). Fig. S2 shows that  $\delta^{13}\text{C}$  and CaCO<sub>3</sub> exhibit a limited degree of correlation, although this is variable through the section. Covariation of  $\delta^{13}\text{C}$  and carbonate content at the KP and the first 50 cm of the Danian is ascribed to the KP mass extinction that caused the decimation of the marine calcifiers, causing a sudden decrease in carbonate production (Smit, 1982; Bown, 2005;

Henehan et al., 2019). The generally poor correlation in the 1 m.y. across the KPBP suggests that the lithology of the Zumaia section is not the dominant control on  $\delta^{13}\text{C}$  values, which is consistent with reported carbonate concentrations and  $\delta^{13}\text{C}$  values for the Late Cretaceous and early Danian (e.g., Hull et al., 2020). A strong negative correlation between magnetic susceptibility and  $\text{CaCO}_3$  content (Fig. S2) suggests that variations in the original fluxes of detrital material and carbonate were the main driver of variations in the concentration of paramagnetic minerals. Although we could not replicate the detailed sampling of Danian rocks of ten Kate and Sprenger (1993) due to coastal erosion, previous studies indicate that the thin layers in between indurated Danian limestones beds are marls (e.g., ten Kate and Sprenger, 1993; Dinarès-Turell et al., 2003, 2014; Hilgen et al., 2010, 2015). Rather than dissolution of  $\text{CaCO}_3$ , the formation of marls was likely driven by increases in siliciclastic input during extremes of the precessional cycle, in a time of overall low production of  $\text{CaCO}_3$  in the aftermath of the extinction of marine calcifiers at the KPBP (e.g., Smit, 1982; Bown, 2005; Schulte et al., 2010).

### **Text S3: Age models**

The age model presented here is based on the identification of the 405 k.y. component of eccentricity-modulated precession in the lithological alternations at Zumaia, following the studies by Batenburg et al. (2012) for the Maastrichtian interval and by Dinarès-Turell et al. (2014) for the Danian interval, anchored to a KPBP age of 66.001 Ma, as in the 405 k.y. age model of Dinarès-Turell et al. (2014) (Table S1). The 405 k.y. periodicity, also known as long eccentricity, is the only reliable tuning target beyond 52 Ma (Laskar et al., 2011). Lithological patterns are tied to eccentricity minima and maxima, with maximal lithological contrast taken to reflect eccentricity maxima, and minimal contrast between lithologies considered to reflect eccentricity minima. Lithological alternations, i.e.

limestone-marl couplets or more gradual variations in lithology, were interpreted to reflect precession-driven cyclicity (manuscript Fig. 2), following the work of Dinarès-Turell et al. (2014), Hilgen et al. (2015) and Batenburg et al. (2012). In between tie-points, precessional cycles were ascribed ages by assuming an equal duration per precessional cycle (Table S2), an approximation which allows considerable differences in sedimentation rate within 405 k.y. cycles to be accounted for. This approach is in line with that of Batenburg et al. (2012) in providing astronomically calibrated ages for bio-, chemo- and magneto-stratigraphic events.

To correlate and compare the  $\delta^{13}\text{C}$  curve of Zumaia with data from other localities (ODP 1262, South Atlantic; ODP 1049 and IODP U1403, North Atlantic; and Gubbio, Italy), we anchored the  $\delta^{13}\text{C}$  curves to the same KPB age, aligned the different tie-points in each locality (Table S5), and assumed a constant sedimentation rate between the tie-points.

#### **Text S4: Stratigraphic continuity across the KPB at Zumaia**

The Zumaia section was designated one of the auxiliary sections of the GSSP for the base of the Danian due to its continuity and good exposure (Molina et al., 2009). The KPB is easily identifiable at Zumaia because there is an abrupt change of facies from the uppermost Maastrichtian reddish marls to the KPB blackish clay bed (Fig. S1B). The first 2 cm of the Danian exhibits calcite veins as the result of small-scale tectonic shear stress at the Maastrichtian/Danian contact (Fig. S1B), which favored the growth of millimetric to centimetric fractures filled with calcite. Nevertheless, moving laterally across the outcrop, sites can be found where the KPB sequence is better exposed and is less affected by calcite veins. At Zumaia, the KPB is well marked by a millimeter-thick airfall layer consisting of altered microtektites, referred to as microkrystites by Smit (1999), and a

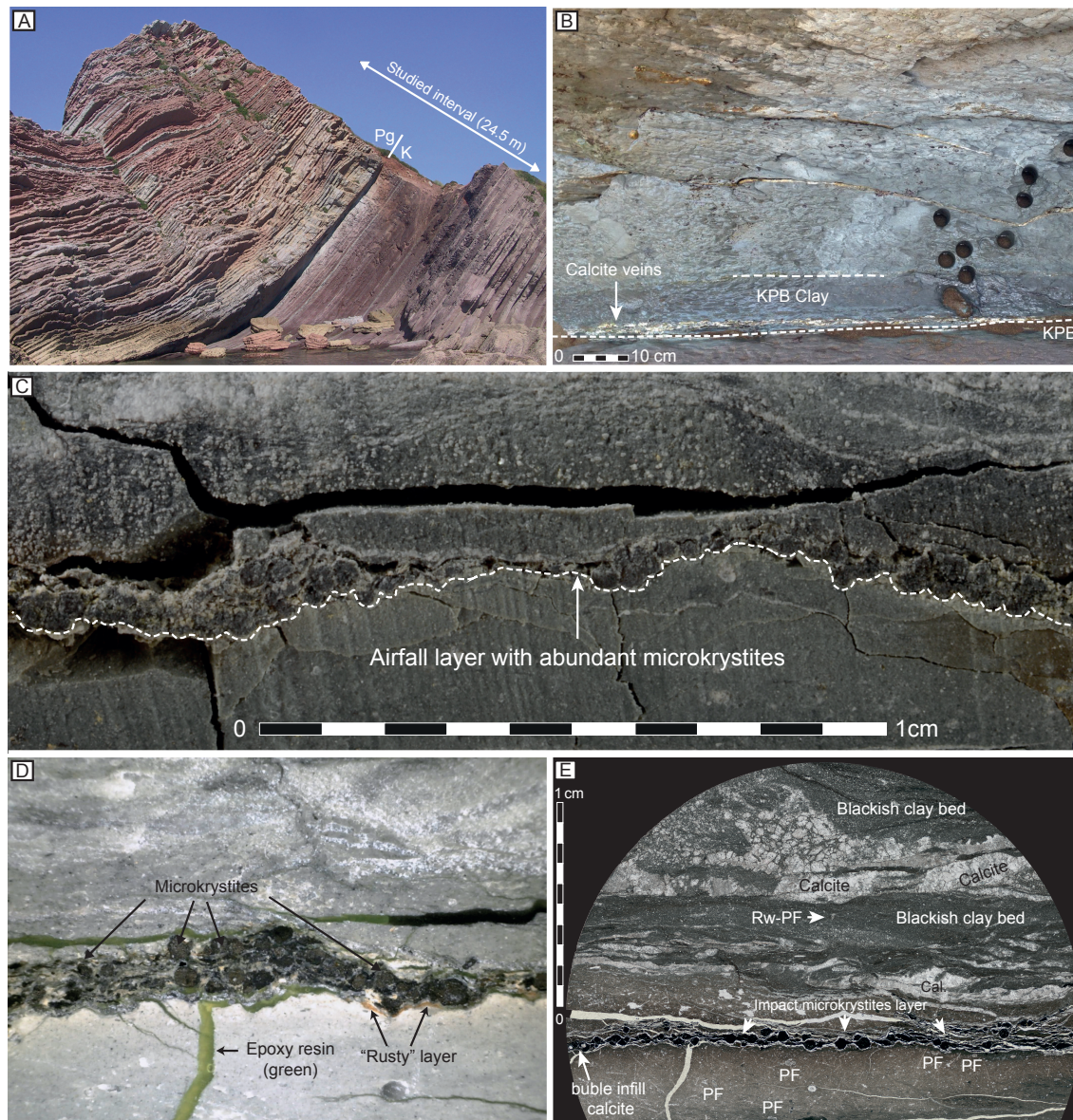
“rusty” layer (Fig. S1C-E). According to Smit (1990), the airfall layer at Zumaia has an anomalous iridium concentration of up to 26.3 ppb, which is similar to other iridium anomalies identified in well-known KPB sections such as Caravaca (Smit, 1982) and Agost (Ruíz et al., 1992). At Zumaia, the mass extinction horizon of planktic foraminifera coincides with the airfall layer at the base of the KPB Clay (Fig. S3).

Our lithological, cyclostratigraphic, micropaleontological and geochemical observations refute the recent suggestion by Font et al. (2018) that there would be a ~150 k.y. hiatus across the KPB. Above and below the boundary clay, rhythmic alternations of marls and limestones at Zumaia have proven instrumental for the tuning and correlation of sections worldwide (ten Kate and Sprenger, 1993; Westerhold et al., 2008; Batenburg et al., 2012; Dinares-Turell et al., 2014; Hilgen et al., 2015; this work), and even for intercalibrating astrochronology and radiometric dating (Kuiper et al., 2008). We recognized 13.5 precession cycles in the ~4-m-thick interval between the KPB and the C29r/C29n reversal, which represents the first ~300 k.y. of the Danian, in line with previous cyclostratigraphic studies for this interval at Zumaia (Dinarès-Turell et al., 2003, 2014; Hilgen et al., 2010, 2015). A hiatus of ~150 k.y. as proposed by Font et al. (2018) implies that the lithological alternations only represent 6–7 precession cycles with an average thickness of ~0.6 m per precession cycle, similar to lithological couplets in the Maastrichtian (~0.7 m average thickness; Batenburg et al., 2012). Such a low number of cycles is not in agreement with the bedding patterns, and a constant sedimentation rate is not in agreement with the change in lithology from predominantly marl in the uppermost Maastrichtian to predominantly limestone in the lowermost Danian at Zumaia, ascribed to a sharp drop in siliciclastic supply (Dinarès-Turell et al., 2003). Abrupt changes in sedimentation rate are commonly recognized at other localities in the early Danian (e.g., Smit, 1999; D’Hondt et al., 2005; Dameron et al., 2017).

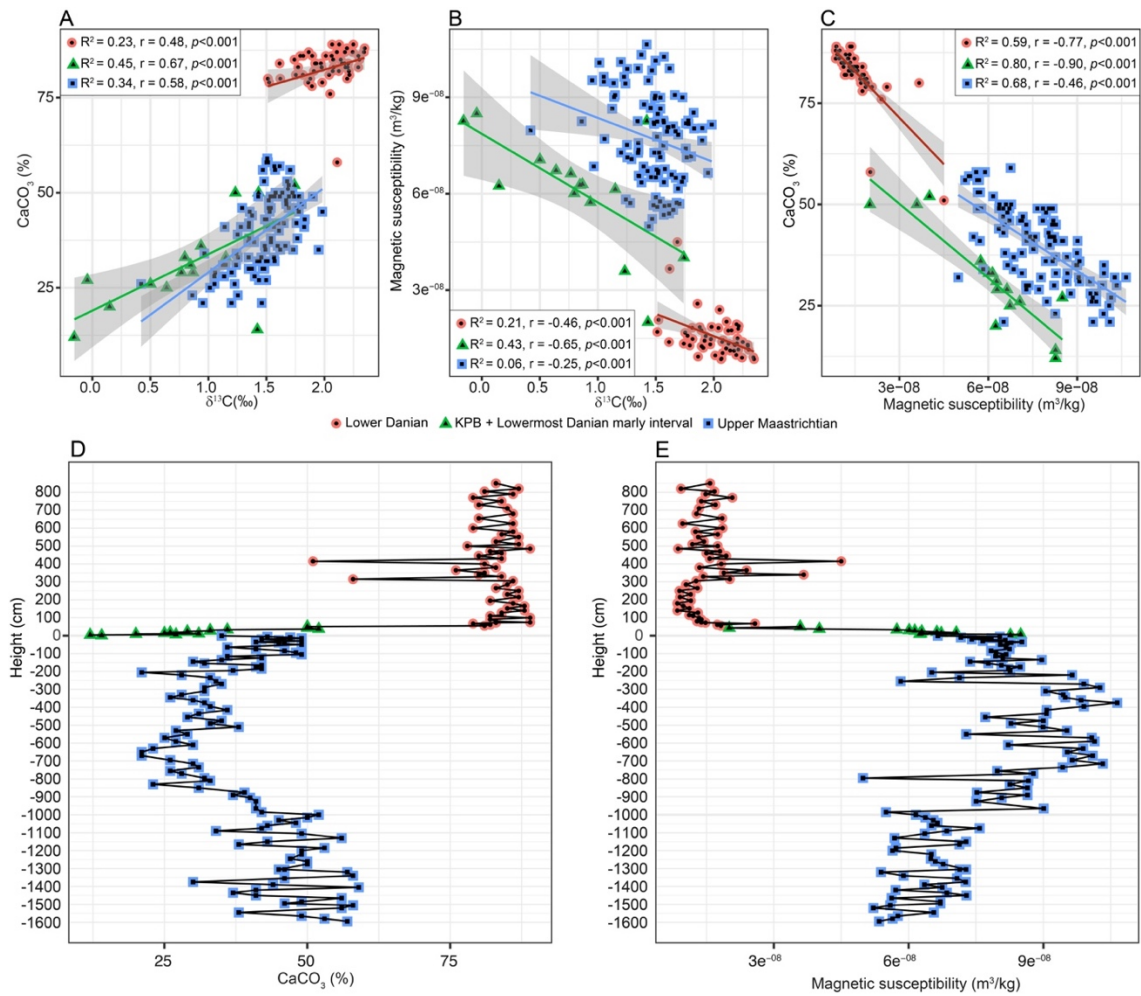
Unlike the biostratigraphic study of Font et al. (2018), we were able to recognize the complete sequence of biozones and bioevents of planktic foraminifera across the KPBB interval of Zumaia. For the Maastrichtian, these include the lowest occurrence datum (LOD) of *Plummerita hantkeninoides* and the highest occurrence datum (HOD) of *Archaeoglobigerina cretacea* (Fig. S3, Tables S3 and S4), in stratigraphic positions directly correlatable to those recognized in other reference sections such as El Kef (Tunisia; Arenillas et al., 2000a), Aïn Setara (Tunisia; Arenillas et al., 2000b), Caravaca (Spain; Gilabert et al., 2021), and Agost (Spain; Molina et al., 2005). All the lowermost Danian biozones of Arenillas et al. (2004) and Wade et al. (2011) and all the planktic foraminiferal acme-stages (PFAS) of Arenillas et al. (2006) are identified in this section (Figs. 2, 3, S2, S3, S4, Tables S3 and S4). The PFAS have been reported worldwide, mainly in the Tethys, North Atlantic and Gulf of Mexico-Caribbean regions (Arenillas et al., 2000a,b, 2018; Alegret et al., 2004; Gallala et al., 2009; Renne et al., 2018; Lowery et al., 2018), and consequently they have been considered a very useful tool for biostratigraphic correlation. Their identification in the lowermost Danian provides additional support in assessing the stratigraphic continuity of the Zumaia section across the KPBB. Danian nannoplankton assemblages typically display a similar acme stage sequence worldwide (e.g., Jiang et al., 2010; Jones et al., 2019; Gibbs et al., 2020), which has been recognized at Zumaia by Bernaola et al. (2006) above the KPBB (Table S2).

The geochemical and isotope-stratigraphic record at Zumaia also supports the completeness of the stratigraphic record. We recognize all the isotopic events identified worldwide across the KPBB (see main text), including the sharp decrease in  $\text{CaCO}_3$  and  $\delta^{13}\text{C}$  that is recognized worldwide (Molina et al., 2009; Schulte et al., 2010; Sepulveda et al., 2019; Fig. 3 and Table S2).

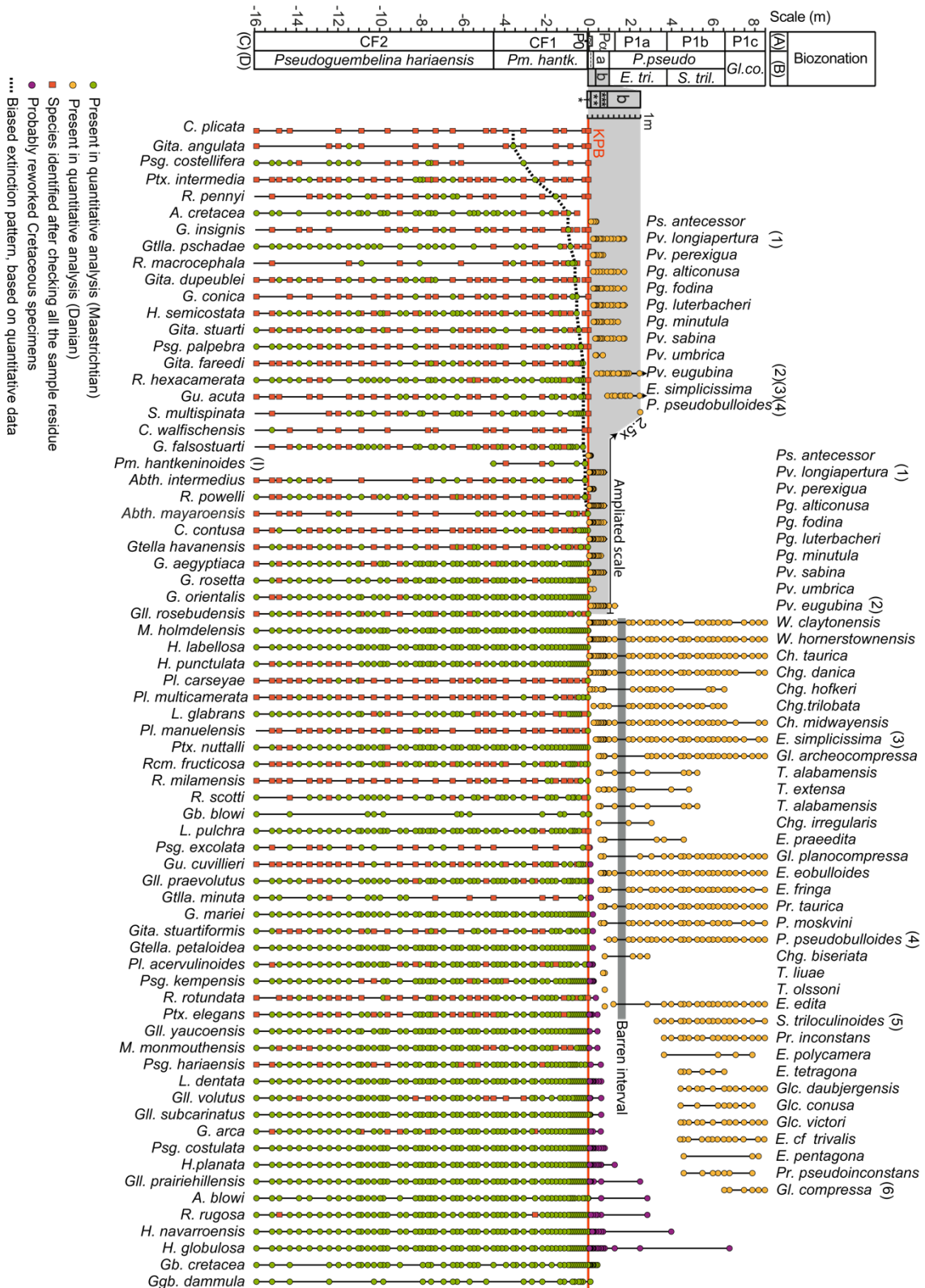
## Supplementary figures S1-S5



**Figure S1:** Cretaceous-Paleogene transition of Zumaia at different scales. A) Field overview of the Zumaia outcrop, illustrating the rhythmic lithological patterns across the upper Maastrichtian (reddish-marl-dominated upper part of the Zumaia-Algorri Formation) and lower Danian (limestone-dominated lower part of the Aitzgorri Formation). B) Detailed field view of the boundary interval; the KPB is located at the base of the KPB Clay. C) Magnified view of the airfall layer with abundant microkrystites in concordant contact with the underlying Maastrichtian sediments. D) Detail of ejecta-rich airfall layer, illustrating lateral changes in thickness. E) Thin-section micrograph of the airfall layer under a petrographic microscope; several *in situ* planktic foraminifera specimens in the reddish Maastrichtian marls can also be recognized, and only one reworked specimen in the overlying blackish clay bed.

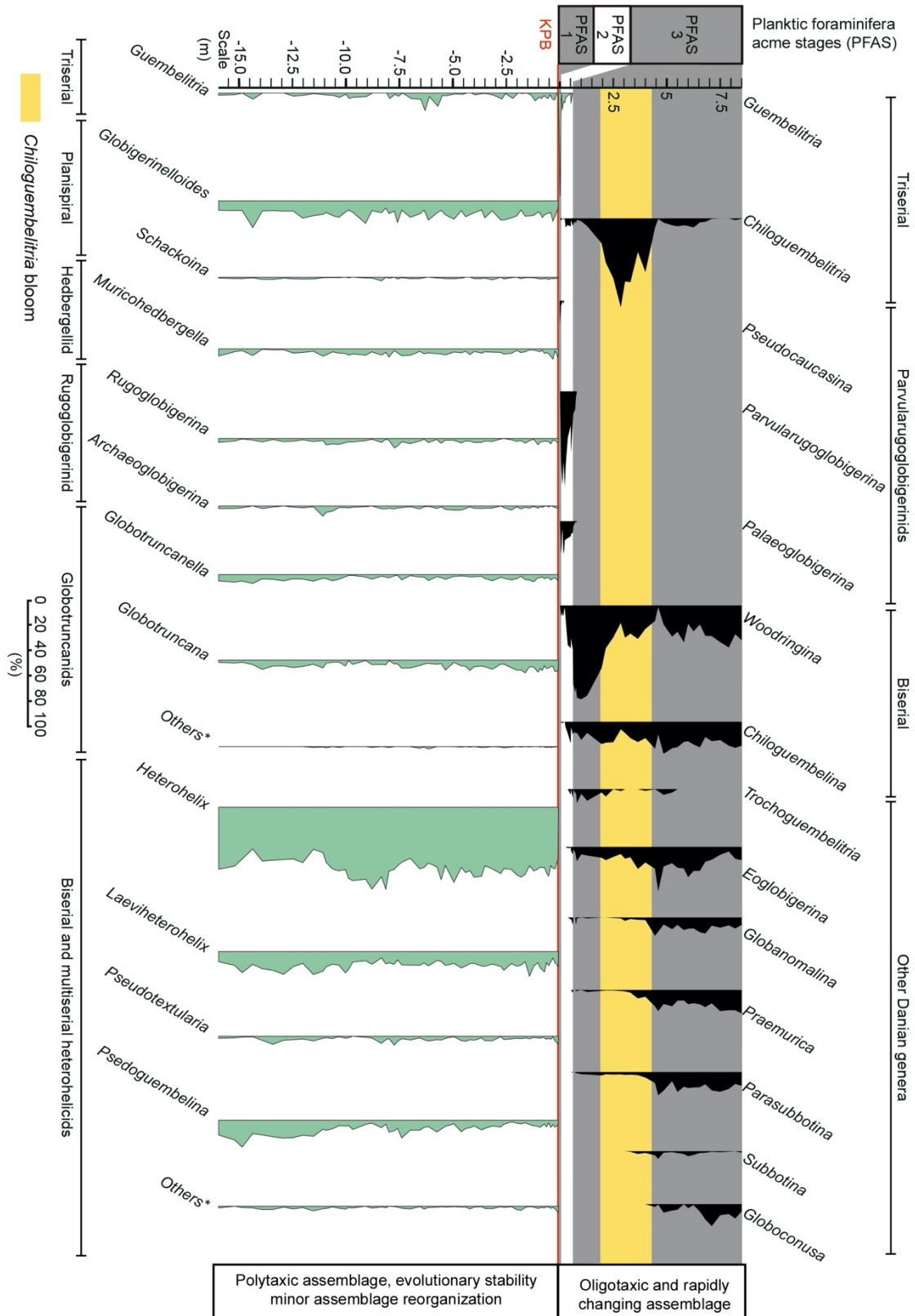


**Figure S2:** Cross-plots between CaCO<sub>3</sub> and δ<sup>13</sup>C (A), magnetic susceptibility and δ<sup>13</sup>C (B), CaCO<sub>3</sub> and magnetic susceptibility, the gray shadow in each plot represents the standard error. Changes in the values of CaCO<sub>3</sub> (D) and magnetic susceptibility (E) across the Zumaia section.

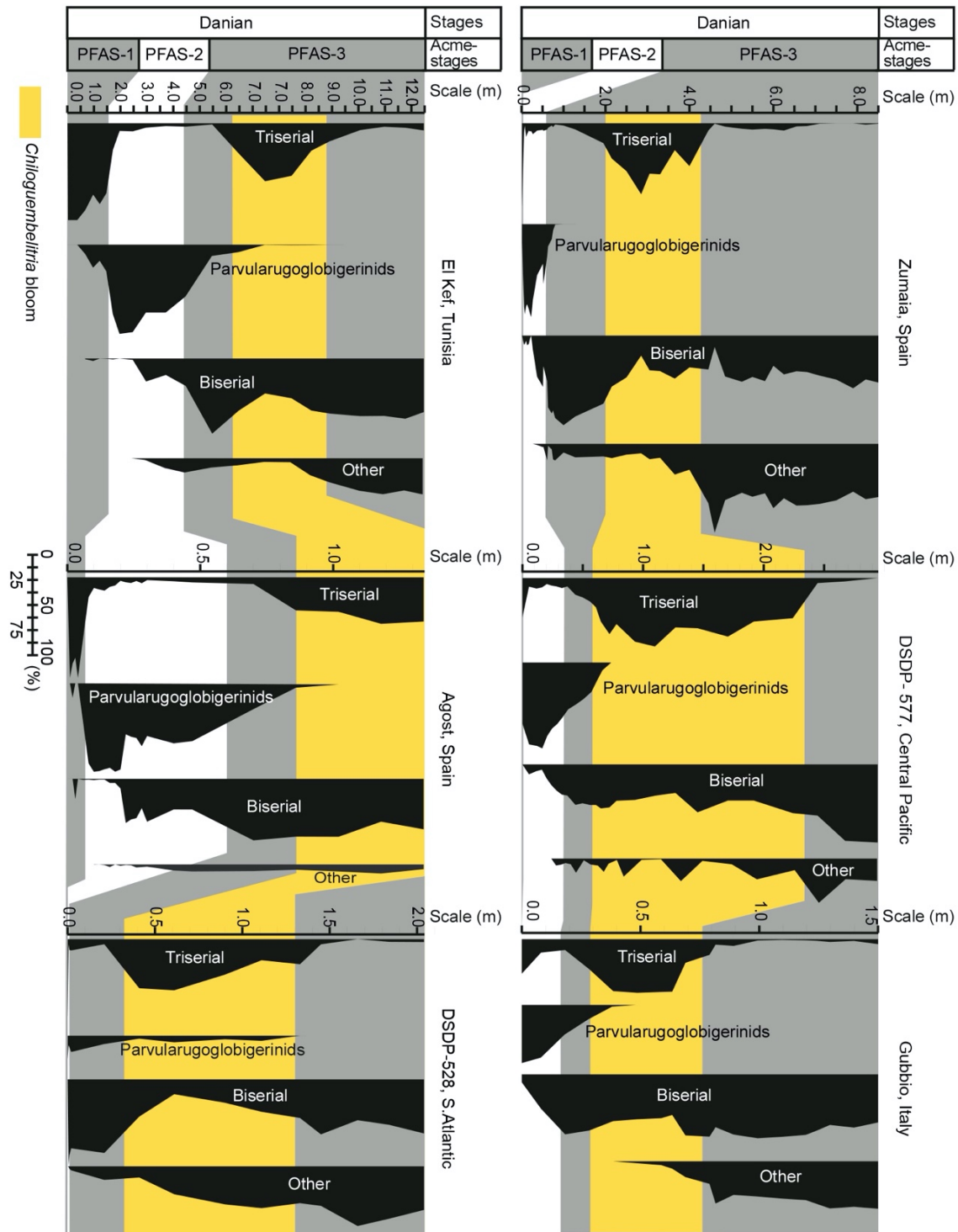




**Figure S3:** Stratigraphic ranges of the late Maastrichtian and early Danian planktic foraminiferal species recognized at the Zumaia section. Dashed line represents the extinction pattern based only on quantitative data, showing a biased extinction pattern. Lowest occurrence datums (LODs) of the species numbered from (1) to (6) are the base of the biozones and subbiozones of Arenillas et al. (2004). (I) LOD of *Plummerita hantkeninoides* is the base of the uppermost Maastrichtian Biozone CF1 of Li and Keller (1998). Biozonations: A – Wade et al. (2011); B – Arenillas et al. (2004); C – Li and Keller (1998); D – Arz and Molina (2002). C– *Contusotruncana*; Gita– *Globotruncanita*; Psg.–*Pseudoguembelina*; R. *Rugoglobigerina*; A–*Archaeoglobigerina*; G.–*Globotruncana*; Gtlla.–*Globotruncanella*; H.–*Heterohelix*; Gu.–*Gublerina*; S.–*Schackoina*; Pm.–*Plummerita*; Abth.–*Abathomphalus*; Gll.–*Globigerinelloides*; M.–*Muricohedbergella*; Pl.–*Planoglobulina*; L.– *Laeviheterohelix*; Ptx.–*Pseudotextularia*; Rcm.–*Racemiguembelina*; Gb.–*Guembelitra* for the Maastrichtian. Ps.–*Pseudocaucasina*; Pv.–*Parvularugoglobigerina*; Pg.–*Palaeoglobigerina*; E.–*Eoglobigerina*; P.–*Parasubbotina*; W.–*Woodringina*; Ch.–*Chiloguembelina*; Chg.– *Chiloguembelitra*; Gl.–*Globanomalina*; T.–*Trochoguembelitra*; Pr.–*Praemurica*; S.–*Subbotina*; Glc.–*Globoconusa* for the Danian.



**Figure S4:** Quantitative analysis of planktic foraminifera based on the >63 microns sieved fraction. (Others\* Globotruncanids) – *Abathomphalus* + *Contusotruncana* + *Globotruncanita*; (Others\* Biserial and multiserial heterohelicids) – *Racemiguembelina* + *Planoglobulina* + *Gublerina*.



**Figure S5:** Correlation of the lowermost Danian PFAS at Zumaia (this study), El Kef (Tunisia; Arenillas et al., 2018), DSDP-577 (Central Pacific; Smit and Romein, 1985), Agost (Spain; Canudo et al., 1991), Gubbio (Italy; Coccioni et al., 2010) and DSDP 528 (South Atlantic; D’Hondt and Keller, 1991). Triserial taxa = *Guembeltria* and *Chiloguembeltria*. Parvularugoglobigerinids (tiny trochospiral taxa): *Parvularugoglobigerina* and *Palaeoglobigerina*. Biserial taxa: *Woodringina* and *Chiloguembelina*. Other taxa: *Eoglobigerina*, *Parasubbotina*, *Subbotina*, *Globanomalina* and *Praemurica* (*Trochoguembeltria* and *Globoconusa* are also included here).

## Supplementary Tables S1-S5

TABLE S1. TIE-POINTS FOR THE ASTRONOMICALLY CALIBRATED AGE MODEL OF THE CRETACEOUS-PALEOGENE TRANSITION AT ZUMAIA

Height from KPB (cm)	Age La2011 (Ma)	Age model tie-points	Source	Description
865	65.353	405-k.y. max. $PC_{405}2$	(Dinarès-Turell et al., 2014)	Stratigraphic heights for tie points are based on our fieldwork measurements correlated to previous reports from the Zumaia section.
615	65.555	405-k.y. min.	(Dinarès-Turell et al., 2014)	
365	65.760	405-k.y. max. $PC_{405}1$	(Dinarès-Turell et al., 2014)	
50	65.967	405- k.y. min.	(Dinarès-Turell et al., 2014)	
9	65.991	KPB clay bed top	(Mukhopadhyay, et al., 2001)	
0	66.001	KPB	(Dinarès-Turell et al., 2014)	
-830	66.172	405-k.y. max. $Ma_{405}1$	(Batenburg et al., 2012)	
-1505	66.374	405- k.y. min.	(Batenburg et al., 2012)	

**Table S1:** Tie-points for the astronomically calibrated age model of the Cretaceous-Paleogene transition at Zumaia. Min.–Minima; max.–maxima. All the ages are based on the La2011 astronomical solution (Laskar et al., 2011); the KPB age is based on the 405 k.y. calibration by Dinarès-Turell et al. (2014); the 405 eccentricity maxima follow the nomenclature of Husson et al. (2011).

TABLE S2. ASTRONOMICALLY CALIBRATED AGE MODEL FOR THE CRETACEOUS-PALEOGENE TRANSITION AT ZUMAIA

Height from KPB (cm)	Age (Ma)	$\delta^{13}C$ Bulk (‰)	$CaCO_3$ (%)	Magnetic suceptibility ( $kg/m^3$ )	Time from KPB (k.y.)	Main paleobiologic and isotopic events
850	65.364	1.773	83	1.581E-08	636.69	
820	65.389	1.865	87	9.313E-09	611.82	
805	65.401	1.753	81	1.677E-08	600.27	
790	65.408	1.817	86	1.481E-08	592.73	End of Lower C29n event
770	65.418	1.524	79	2.076E-08	582.68	
750	65.434	1.614	84	1.385E-08	566.60	
730	65.459	1.513	80	1.700E-08	542.48	
710	65.480	1.741	85	1.337E-08	521.38	Onset of Lower C29n event
680	65.514	1.793	86	1.279E-08	486.90	
655	65.528	1.879	80	1.852E-08	472.76	LOD of <i>Globanomalina compressa</i>
625	65.549	2.012	86	9.687E-09	452.04	
600	65.570	1.981	79	1.860E-08	430.93	
580	65.586	1.895	86	1.256E-08	415.43	
565	65.595	2.153	84	1.750E-08	405.74	
550	65.605	2.177	87	1.317E-08	396.05	
525	65.621	2.079	83	1.444E-08	379.90	
510	65.633	2.107	87	1.186E-08	367.62	
500	65.642	1.893	78	1.750E-08	358.58	
485	65.654	2.067	89	8.700E-09	346.52	
470	65.666	2.210	82	1.799E-08	335.21	
460	65.673	2.204	84	1.499E-08	327.68	
445	65.685	2.196	80	1.939E-08	316.37	
430	65.696	1.930	84	1.571E-08	305.06	End of Dan-C2 event
415	65.707	1.686	51	4.500E-08	293.76	

400	65.719	1.814	81	1.830E-08	281.70	End of <i>Chiloguembelitra</i> bloom, end of <i>Neobiscutum parvulum</i> * bloom, LOD of <i>Cruciplacolithus primus</i> (large)*, onset of <i>Futyania petalosa</i> * bloom
380	65.737	2.200	83	1.345E-08	263.61	
365	65.760	2.050	76	2.392E-08	241.00	
350	65.776	2.215	81	1.886E-08	225.48	
340	65.784	1.620	80	3.664E-08	216.85	
330	65.791	1.920	84	1.428E-08	209.95	LOD of <i>Subbotina trilocolinoides</i>
315	65.801	2.110	58	2.020E-08	199.60	Onset of Dan-C2 event
305	65.812	2.293	86	1.270E-08	189.25	
285	65.830	2.076	85	1.045E-08	170.62	
265	65.847	2.292	83	1.300E-08	154.06	
250	65.859	2.243	87	8.991E-09	141.64	
230	65.872	2.301	85	1.148E-08	128.63	
215	65.881	2.341	87	9.110E-09	119.76	
195	65.891	2.211	82	1.153E-08	109.90	Onset of <i>Chiloguembelitra</i> bloom, LOD of <i>Futyania petalosa</i> *
180	65.898	2.063	86	8.506E-09	103.00	
165	65.905	2.194	88	9.833E-09	96.10	
152	65.910	2.141	85	1.121E-08	90.72	End of <i>Cyclagelosphaera reinhardtii</i> * bloom
140	65.915	2.347	88	8.523E-09	85.75	
128	65.920	1.969	84	1.311E-08	80.78	HOD of <i>Parvularugoglobigerina eugubina</i>
115	65.926	2.174	84	1.116E-08	75.40	
110	65.928	1.909	82	1.204E-08	73.10	
100	65.933	2.127	89	1.335E-08	68.50	LOD of <i>Parasubbotina pseudobulloides</i> , onset of <i>Neobiscutum parvulum</i> * bloom
90	65.937	2.072	82	1.387E-08	63.90	
80	65.942	2.182	83	1.291E-08	59.30	
74	65.945	2.249	89	1.387E-08	56.43	
72	65.945	1.976	83	1.479E-08	55.62	
67	65.949	1.860	79	2.580E-08	52.42	
61	65.954	2.124	82	1.741E-08	47.46	
55	65.959	2.040	81	1.822E-08	42.49	Onset of PFAS-3
50	65.967	1.233	50	3.589E-08	34.00	
43	65.971	1.432	50	2.007E-08	29.89	
37	65.975	1.741	52	4.014E-08	26.38	LOD of <i>Eoglobigerina simplicissima</i>
33	65.977	0.936	36	5.738E-08	24.04	
30	65.979	0.797	33	6.013E-08	22.29	
27	65.981	1.150	33	6.138E-08	20.53	
23	65.983	0.867	29	6.293E-08	18.19	LOD of <i>Parvularugoglobigerina eugubina</i>
20	65.985	0.767	29	6.628E-08	16.44	Onset of <i>Braarudosphaera bigelowii</i> * bloom
17	65.987	0.500	26	7.062E-08	14.68	
14	65.989	0.640	25	6.727E-08	12.93	
11	65.990	0.846	31	6.271E-08	11.17	
9	65.992	0.148	20	6.247E-08	10.00	Onset of <i>Cyclagelosphaera reinhardtii</i> * bloom

6	65.995	-0.044	27	8.496E-08	6.60	LOD of <i>Parvularugoglobigerina longiapertura</i> , onset of PFAS-2
4	65.997	-0.156	12	8.266E-08	4.40	
1	66.000	1.422	14	8.266E-08	1.10	LOD of <i>Pseudocaucasina antecessor</i> , onset of PFAS-1, and onset of <i>Thoracosphaera operculata</i> * bloom
0	66.001					KPB mass extinction, HOD of <i>Plummerita hantkeninoides</i> . Airfall layer (microkrystites)
-1	66.001	1.950	35	6.650E-08	-0.34	
-6	66.003	1.830	43	8.032E-08	-1.71	
-10	66.004	1.805	47	7.163E-08	-2.73	
-15	66.005	1.694	49	7.842E-08	-4.10	
-20	66.006	1.758	42	7.409E-08	-5.47	
-25	66.008	1.982	45	8.152E-08	-6.83	
-30	66.009	1.899	49	7.653E-08	-8.20	
-35	66.011	1.826	41	8.523E-08	-9.56	
-40	66.012	1.780	45	8.280E-08	-11.30	
-45	66.014	1.760	46	8.191E-08	-13.04	
-50	66.016	1.901	49	8.042E-08	-14.78	HOD of <i>Archaeoglobigerina cretacea</i>
-65	66.021	1.486	36	8.169E-08	-20.00	
-75	66.024	1.512	41	8.247E-08	-23.48	
-85	66.028	1.692	46	7.835E-08	-26.95	
-95	66.031	1.670	48	7.945E-08	-29.97	
-105	66.034	1.782	49	8.171E-08	-32.52	
-115	66.036	1.597	36	7.936E-08	-35.07	
-125	66.039	1.650	42	8.100E-08	-37.62	
-135	66.041	1.491	35	8.966E-08	-40.17	
-145	66.044	1.351	30	7.369E-08	-42.72	
-155	66.046	1.510	32	7.775E-08	-45.27	
-165	66.049	1.604	42	8.066E-08	-47.82	
-175	66.051	1.517	41	8.486E-08	-49.73	
-185	66.053	1.569	42	8.222E-08	-51.65	
-195	66.055	1.343	37	8.259E-08	-53.56	
-205	66.056	1.460	21	6.516E-08	-55.47	
-220	66.059	1.051	28	9.642E-08	-58.34	
-235	66.062	1.255	33	7.133E-08	-61.21	
-255	66.066	1.242	34	5.824E-08	-65.04	
-270	66.069	1.619	35	9.901E-08	-67.68	
-290	66.072	1.570	32	1.026E-07	-70.63	
-310	66.075	1.496	32	9.047E-08	-73.57	
-330	66.078	1.136	28	9.442E-08	-76.51	
-345	66.080	1.052	26	9.486E-08	-78.72	
-360	66.082	1.467	30	9.839E-08	-80.93	
-375	66.084	1.422	32	1.065E-07	-83.13	
-395	66.087	1.346	33	9.901E-08	-86.08	
-415	66.091	1.664	36	9.074E-08	-90.33	
-435	66.096	1.149	31	9.071E-08	-94.58	
-455	66.100	1.057	29	7.708E-08	-98.83	LOD of <i>Plummerita hantkeninoides</i>
-475	66.104	1.730	35	8.999E-08	-103.08	End of Late Maastrichtian Warming event
-490	66.107	1.565	33	8.277E-08	-106.04	
-510	66.110	1.539	38	8.993E-08	-109.36	

-530	66.114	1.436	27	9.526E-08	-112.69	
-550	66.117	1.200	29	7.281E-08	-116.02	
-570	66.120	1.013	25	1.008E-07	-119.34	
-590	66.124	1.498	27	1.014E-07	-122.67	
-610	66.127	1.483	30	8.217E-08	-126.00	
-630	66.130	1.254	23	9.886E-08	-129.32	
-650	66.134	0.952	21	9.532E-08	-132.65	
-670	66.137	1.199	21	1.010E-07	-135.98	
-695	66.141	1.226	26	9.640E-08	-140.13	
-715	66.144	1.375	30	1.033E-07	-143.46	
-735	66.149	1.238	31	9.429E-08	-148.24	
-755	66.154	0.420	26	7.972E-08	-153.03	
-770	66.158	1.399	28	8.778E-08	-156.61	
-795	66.164	1.440	32	4.983E-08	-162.59	
-810	66.168	1.456	33	8.668E-08	-166.69	
-830	66.172	0.861	23	8.253E-08	-171.00	
-850	66.179	1.124	31	8.646E-08	-177.62	
-875	66.185	1.252	39	7.521E-08	-184.45	
-890	66.190	1.539	37	8.648E-08	-188.55	
-905	66.194	1.609	40	8.073E-08	-192.65	
-925	66.199	1.564	41	7.504E-08	-198.11	
-965	66.212	1.140	41	9.010E-08	-211.28	
-985	66.219	1.650	42	5.497E-08	-218.24	
-1000	66.225	1.692	52	6.162E-08	-223.80	LOD <i>Micula prinsii</i> *
-1015	66.231	1.725	50	6.372E-08	-229.54	
-1030	66.236	1.356	45	6.552E-08	-235.28	
-1045	66.241	1.520	48	6.642E-08	-240.23	
-1060	66.245	1.500	43	6.510E-08	-243.60	
-1075	66.248	1.349	42	7.581E-08	-246.98	
-1090	66.251	0.965	34	6.853E-08	-250.35	
-1105	66.255	1.570	49	6.359E-08	-253.73	Onset of Late Maastrichtian Warming event
-1130	66.261	1.704	56	5.686E-08	-259.97	
-1150	66.268	1.487	43	7.279E-08	-266.93	
-1165	66.273	1.766	38	7.132E-08	-272.14	
-1185	66.280	1.679	53	5.719E-08	-278.63	
-1200	66.283	1.616	49	5.641E-08	-282.46	
-1220	66.289	1.738	49	6.506E-08	-287.56	
-1245	66.295	1.672	47	6.495E-08	-293.94	
-1260	66.299	1.637	50	6.595E-08	-297.96	
-1275	66.303	1.578	50	6.769E-08	-302.37	
-1305	66.312	1.538	46	7.138E-08	-311.20	
-1305	66.312	1.528	45	7.278E-08	-311.20	
-1320	66.317	1.615	57	5.387E-08	-315.62	
-1340	66.322	1.500	58	5.887E-08	-320.72	
-1355	66.326	1.291	46	7.078E-08	-324.54	
-1375	66.331	1.347	30	7.271E-08	-329.64	
-1390	66.334	1.376	44	6.352E-08	-333.47	
-1405	66.339	1.507	59	6.750E-08	-337.93	
-1420	66.344	1.280	41	5.713E-08	-342.71	
-1435	66.348	1.394	37	6.853E-08	-347.50	
-1450	66.353	1.348	41	7.287E-08	-352.28	
-1465	66.359	1.574	56	5.622E-08	-357.70	

-1485	66.366	1.430	49	6.709E-08	-365.35
-1495	66.370	1.521	46	6.709E-08	-369.17
-1505	66.374	1.513	58	5.591E-08	-373.00
-1520	66.378	1.469	56	5.216E-08	-377.10
-1545	66.385	1.351	38	6.562E-08	-383.93
-1565	66.390	1.536	49	5.762E-08	-389.40
-1580	66.398	1.480	53	5.642E-08	-396.91
-1595	66.412	1.568	57	5.342E-08	-411.26

---

*Note:* \* Nannoplankton datums for Zumaia section are taken from Bernaola et al. (2006)

---

**Table S2:** Astronomically calibrated age model for the Cretaceous-Paleogene transition at Zumaia.



TABLE S3. RELATIVE ABUNDANCE OF PLANKTIC FORAMINIFERAL SPECIES IN THE UPPER MAASTRICHTIAN OF ZUMAIA

Height from NPB	Planktic foraminiferal species (%)		Total species
-150'	1.6	0.3	306
-145'	1.4	0.3	305
-140'	0.3	0.3	304
-135'	0.3	0.3	303
-130'	0.3	0.3	302
-125'	0.3	0.3	301
-120'	0.3	0.3	300
-115'	0.3	0.3	299
-110'	0.3	0.3	298
-105'	0.3	0.3	297
-100'	0.3	0.3	296
-95'	0.3	0.3	295
-90'	0.3	0.3	294
-85'	0.3	0.3	293
-80'	0.3	0.3	292
-75'	0.3	0.3	291
-70'	0.3	0.3	290
-65'	0.3	0.3	289
-60'	0.3	0.3	288
-55'	0.3	0.3	287
-50'	0.3	0.3	286
-45'	0.3	0.3	285
-40'	0.3	0.3	284
-35'	0.3	0.3	283
-30'	0.3	0.3	282
-25'	0.3	0.3	281
-20'	0.3	0.3	280
-15'	0.3	0.3	279
0'	0.3	0.3	278
5'	0.3	0.3	277
10'	0.3	0.3	276
15'	0.3	0.3	275
20'	0.3	0.3	274
25'	0.3	0.3	273
30'	0.3	0.3	272
35'	0.3	0.3	271
40'	0.3	0.3	270
45'	0.3	0.3	269
50'	0.3	0.3	268
55'	0.3	0.3	267
60'	0.3	0.3	266
65'	0.3	0.3	265
70'	0.3	0.3	264
75'	0.3	0.3	263
80'	0.3	0.3	262
85'	0.3	0.3	261
90'	0.3	0.3	260
95'	0.3	0.3	259
100'	0.3	0.3	258
105'	0.3	0.3	257
110'	0.3	0.3	256
115'	0.3	0.3	255
120'	0.3	0.3	254
125'	0.3	0.3	253
130'	0.3	0.3	252
135'	0.3	0.3	251
140'	0.3	0.3	250
145'	0.3	0.3	249
150'	0.3	0.3	248
155'	0.3	0.3	247
160'	0.3	0.3	246
165'	0.3	0.3	245
170'	0.3	0.3	244
175'	0.3	0.3	243
180'	0.3	0.3	242
185'	0.3	0.3	241
190'	0.3	0.3	240
195'	0.3	0.3	239
200'	0.3	0.3	238
205'	0.3	0.3	237
210'	0.3	0.3	236
215'	0.3	0.3	235
220'	0.3	0.3	234
225'	0.3	0.3	233
230'	0.3	0.3	232
235'	0.3	0.3	231
240'	0.3	0.3	230
245'	0.3	0.3	229
250'	0.3	0.3	228
255'	0.3	0.3	227
260'	0.3	0.3	226
265'	0.3	0.3	225
270'	0.3	0.3	224
275'	0.3	0.3	223
280'	0.3	0.3	222
285'	0.3	0.3	221
290'	0.3	0.3	220
295'	0.3	0.3	219
300'	0.3	0.3	218
305'	0.3	0.3	217
310'	0.3	0.3	216
315'	0.3	0.3	215
320'	0.3	0.3	214
325'	0.3	0.3	213
330'	0.3	0.3	212
335'	0.3	0.3	211
340'	0.3	0.3	210
345'	0.3	0.3	209
350'	0.3	0.3	208
355'	0.3	0.3	207
360'	0.3	0.3	206
365'	0.3	0.3	205
370'	0.3	0.3	204
375'	0.3	0.3	203
380'	0.3	0.3	202
385'	0.3	0.3	201
390'	0.3	0.3	200
395'	0.3	0.3	199
400'	0.3	0.3	198
405'	0.3	0.3	197
410'	0.3	0.3	196
415'	0.3	0.3	195
420'	0.3	0.3	194
425'	0.3	0.3	193
430'	0.3	0.3	192
435'	0.3	0.3	191
440'	0.3	0.3	190
445'	0.3	0.3	189
450'	0.3	0.3	188
455'	0.3	0.3	187
460'	0.3	0.3	186
465'	0.3	0.3	185
470'	0.3	0.3	184
475'	0.3	0.3	183
480'	0.3	0.3	182
485'	0.3	0.3	181
490'	0.3	0.3	180
495'	0.3	0.3	179
500'	0.3	0.3	178
505'	0.3	0.3	177
510'	0.3	0.3	176
515'	0.3	0.3	175
520'	0.3	0.3	174
525'	0.3	0.3	173
530'	0.3	0.3	172
535'	0.3	0.3	171
540'	0.3	0.3	170
545'	0.3	0.3	169
550'	0.3	0.3	168
555'	0.3	0.3	167
560'	0.3	0.3	166
565'	0.3	0.3	165
570'	0.3	0.3	164
575'	0.3	0.3	163
580'	0.3	0.3	162
585'	0.3	0.3	161
590'	0.3	0.3	160
595'	0.3	0.3	159
600'	0.3	0.3	158
605'	0.3	0.3	157
610'	0.3	0.3	156
615'	0.3	0.3	155
620'	0.3	0.3	154
625'	0.3	0.3	153
630'	0.3	0.3	152
635'	0.3	0.3	151
640'	0.3	0.3	150
645'	0.3	0.3	149
650'	0.3	0.3	148
655'	0.3	0.3	147
660'	0.3	0.3	146
665'	0.3	0.3	145
670'	0.3	0.3	144
675'	0.3	0.3	143
680'	0.3	0.3	142
685'	0.3	0.3	141
690'	0.3	0.3	140
695'	0.3	0.3	139
700'	0.3	0.3	138
705'	0.3	0.3	137
710'	0.3	0.3	136
715'	0.3	0.3	135
720'	0.3	0.3	134
725'	0.3	0.3	133
730'	0.3	0.3	132
735'	0.3	0.3	131
740'	0.3	0.3	130
745'	0.3	0.3	129
750'	0.3	0.3	128
755'	0.3	0.3	127
760'	0.3	0.3	126
765'	0.3	0.3	125
770'	0.3	0.3	124
775'	0.3	0.3	123
780'	0.3	0.3	122
785'	0.3	0.3	121
790'	0.3	0.3	120
795'	0.3	0.3	119
800'	0.3	0.3	118
805'	0.3	0.3	117
810'	0.3	0.3	116
815'	0.3	0.3	115
820'	0.3	0.3	114
825'	0.3	0.3	113
830'	0.3	0.3	112
835'	0.3	0.3	111
840'	0.3	0.3	110
845'	0.3	0.3	109
850'	0.3	0.3	108
855'	0.3	0.3	107
860'	0.3	0.3	106
865'	0.3	0.3	105
870'	0.3	0.3	104
875'	0.3	0.3	103
880'	0.3	0.3	102
885'	0.3	0.3	101
890'	0.3	0.3	100
895'	0.3	0.3	99
900'	0.3	0.3	98
905'	0.3	0.3	97
910'	0.3	0.3	96
915'	0.3	0.3	95
920'	0.3	0.3	94
925'	0.3	0.3	93
930'	0.3	0.3	92
935'	0.3	0.3	91
940'	0.3	0.3	90
945'	0.3	0.3	89
950'	0.3	0.3	88
955'	0.3	0.3	87
960'	0.3	0.3	86
965'	0.3	0.3	85
970'	0.3	0.3	84
975'	0.3	0.3	83
980'	0.3	0.3	82
985'	0.3	0.3	81
990'	0.3	0.3	80
995'	0.3	0.3	79
1000'	0.3	0.3	78

Table S3: Relative abundance of planktic foraminiferal species in the upper Maastrichtian of Zumaia.



TABLE S4. RELATIVE ABUNDANCE OF PLANKTIC FORAMINIFERAL SPECIES IN THE LOWER DANIAN OF ZUMAIA

Height from KPB	Cretaceous specimens within Danian rocks (probably reworked)																				Total Danian + Cretaceous specimens													
(cm)	<i>Archeoglobigerina blowi</i>	<i>Gobigerinelloides prairiehillensis</i>	<i>Gobigerinelloides praevolitus</i>	<i>Gobigerinelloides rosebundenensis</i>	<i>Gobigerinelloides yaucoensis</i>	<i>Gobigerinelloides subcarinatus</i>	<i>Gobigerinelloides volutus</i>	<i>Gobotruncana aegyptiaca</i>	<i>Gobotruncana arca</i>	<i>Gobotruncana linneliana</i>	<i>Gobotruncana mariei</i>	<i>Gobotruncana sp.</i>	<i>Gobotruncanella pelaloida</i>	<i>Gobotruncanella minuta</i>	<i>Gobotruncanella stuartiformis</i>	<i>Guberna cuvillieri</i>	<i>Heterohelix globulosa</i>	<i>Heterohelix navarroensis</i>	<i>Heterohelix planata</i>	<i>Laeviheterohelix dentata</i>	<i>Laeviheterohelix glabrans</i>	<i>Laeviheterohelix pulchra</i>	<i>Muricohedbergella holmdelensis</i>	<i>Muricohedbergella monimouthensis</i>	<i>Planoglobulina acervulinoides</i>	<i>Pseudoguembellina costulata</i>	<i>Pseudoguembellina excolata</i>	<i>Pseudoguembellina hariaensis</i>	<i>Pseudoguembellina kempensis</i>	<i>Pseudotextularia elegans</i>	<i>Rugoglobigerina rotundata</i>	<i>Rugoglobigerina rugosa</i>	(n)	
850																																		274
820																																		149
790																																		305
750																																		274
710																																		246
680																	0.3																	332
655																																		290
625																																		277
600																																		283
580																																		181
550																																		272
525																																		294
485																																		270
460																																		250
445																																		276
400																	0.3																	301
365																																		286
330																																		246
305																																		269
285	0.4																														0.4			269
250		0.4															0.8																	255
215																																		276
195																																		152
128																	0.4		0.4															264
100																																		222
80																	0.4										0.4							258
74																																		222
72													0.4				1.5	0.7										0.4						274
63	0.4	0.4				0.4	0.4					1.2				6.4	0.8	1.2	0.4							0.4	1.2				1.2		249	
67								0.4											0.4									0.4						269
55																	3.6	2.4	0.8	0.4														247
43						0.5											2.5	1.0						0.5			0.8				0.5		2.0	200
37												2.5					4.2	5.0	2.1	1.3											0.4	0.4		239
27		0.9															7.9	4.0	0.9	1.3							2.2							227
23								0.4		0.4		0.4		0.4			6.1	2.4		1.6						0.4	1.6			0.9		0.4		247
20																	10.3	4.8	4.0	1.1						0.4	5.5		0.7	0.4				272
17		0.5													0.5		2.6	1.0	0.5							2.1			1.5					194
14	3.3	3.3						0.6									6.6	2.2	0.6	1.7						1.1		0.6	2.8	0.6		0.6		181
11		1.8				0.4	1.3								0.4		8.4	3.1	2.2	0.9					0.4	1.8								225
9		1.2			0.4	0.4	0.4										15.5	9.8	6.9	3.3						2.4	0.8		2.0	0.8				245
6		2.2				1.1											12.4	7.1	5.2	2.6		0.4								0.7		0.4		267
1	4.9	2.9	2.0	2.0			1.0	1.0		2.0	1.0	1.0			2.0	1.0	24.5	2.9	6.9	3.9	1.0		2.9	10.8		1.0			2.0	2.0				102

Table S4 (continued): Relative abundance of planktic foraminiferal species in the lower Danian of Zumaia.

TABLE S5. AGE MODEL TIE-POINTS FOR OTHER CRETACEOUS-PALEOGENE SECTIONS

Section	Tie-point	Age (Ma)	Height from KPB (m)	Datum source
Gubbio (Contessa)	C29r/C29n	65.7	1	(Coccioni et al., 2010)
Gubbio (Bottaccione)	KPB	66.001	0	(Voigt et al., 2012; Coccioni et al., 2010)
Gubbio (Bottaccione)	FO ( <i>P. hantkeninoides</i> )	66.1	-1.4	(Coccioni and Premoli-Silva, 2015)
Gubbio (Bottaccione)	$\delta^{13}\text{C}$ minimum below C30n/C29r	66.52	-5.5	(Voigt et al., 2012; Batenburg et al., 2018)
Site	Tie-point	Age (Ma)	Depth (mbsf)	Datum source
ODP 1049	C29r/C29n	65.7	106.63	(Quillévéré et al. 2008)
ODP 1049	K/Pg boundary	66.001	113	(Quillévéré et al. 2008)
Site	Tie-point	Age (Ma)	Depth (mcd)	Datum source
ODP 1262	405-k.y. max. Pc <sub>405</sub> 2	65.353	213.4	(Dinarès-Turell et al., 2014)
ODP 1262	405-k.y. min.	65.555	214.58	(Dinarès-Turell et al., 2014)
ODP 1262	405-k.y. max. Pc <sub>405</sub> 1	65.76	215.33	(Dinarès-Turell et al., 2014)
ODP 1262	405-k.y. min.	65.967	216.4	(Dinarès-Turell et al., 2014)
ODP 1262	KPB	66.001	216.71	(Dinarès-Turell et al., 2014)
ODP 1262	405-k.y. max. Ma <sub>405</sub> 1	66.172	219.96	(Woelders et al., 2017)
ODP 1262	405-k.y. min.	66.374	223.73	(Woelders et al., 2017)
ODP 1262	405-k.y. min.	66.782	230.64	(Woelders et al., 2017)
Site	Tie-point	Age (Ma)	Depth (mcd)	Datum source
IODP U1403	405-k.y. max. Pc <sub>405</sub> 2	65.356	245.06	(Hull et al., 2020)
IODP U1403	405-k.y. min.	65.559	246.39	(Hull et al., 2020)
IODP U1403	405-k.y. max. Pc <sub>405</sub> 1	65.762	246.94	(Hull et al., 2020)
IODP U1403	405-k.y. min.	65.965	247.48	(Hull et al., 2020)
IODP U1403	KPB	66.001	247.7	(Hull et al., 2020)
IODP U1403	405-k.y. max. Ma <sub>405</sub> 1	66.171	248.92	(Hull et al., 2020)
IODP U1403	405-k.y. min.	66.374	251.04	(Batenburg et al., 2018)
IODP U1403	405-k.y. min.	66.782	254.96	(Batenburg et al., 2018)

**Table S5:** Age model tie-points for other Cretaceous-Paleogene sections. All the ages are based on the La2011 astronomical solution (Laskar et al., 2011); the KPB age is based on the 405 k.y. eccentricity calibration of Dinarès-Turell et al. (2014); the 405 eccentricity maxima follow the nomenclature of Husson et al. (2011). The ages for KPB and C29r/C29n are based on the astronomical tuning of Dinarès-Turell et al. (2014). The age for the  $\delta^{13}\text{C}$  minimum below C30n/C29r is based on the astronomical tuning of Batenburg et al. (2018). min.–Minima; max.–maxima.

### Supplementary references cited

- Alegret, L., Arenillas, I., Arz, J.A., and Molina, E., 2004, Foraminiferal event-stratigraphy across the Cretaceous/Tertiary boundary: Neues Jahrbuch für Geologie und Paläontologie, Abhandlungen, v. 234, no. 1-3, p. 25–50, <https://doi.org/0.1127/NJGPA/234/2004/25>.
- Arenillas, I., Arz, J.A., Molina, E., and Dupuis, C., 2000a, An independent test of planktonic foraminiferal turnover across the Cretaceous/Paleogene (K/P) boundary

- at El Kef, Tunisia: Catastrophic mass extinction and possible survivorship: *Micropaleontology*, v. 46, p. 31–49.
- Arenillas, I., Arz, J.A., Molina, E., and Dupuis, C., 2000b, The Cretaceous/Paleogene (K/P) boundary at Ain Settara, Tunisia: sudden catastrophic mass extinction in planktic foraminifera: *Journal of Foraminiferal Research*, v. 30, p. 202–218, <https://doi.org/10.2113/0300202>.
- Arenillas, I., Arz, J.A., and Molina, E., 2004, A new high-resolution planktic foraminiferal zonation and subzonation for the lower Danian: *Lethaia*, v. 37, p. 79–95, <https://doi.org/10.1080/00241160310005097>.
- Arenillas, I., Arz, J.A., Grajales-Nishimura, J.M., Murillo-Muñetón, G., Alvarez, W., Camargo-Zanoguera, A., Molina, E., and Rosales-Domínguez, C., 2006, Chicxulub impact event is Cretaceous/Paleogene boundary in age: New micropaleontological evidence: *Earth and Planetary Science Letters*, v. 249, p. 241–257, <https://doi.org/10.1016/j.epsl.2006.07.020>.
- Arenillas, I., Arz, J.A., and Gilabert, V., 2018, Blooms of aberrant planktic foraminifera across the K/Pg boundary in the Western Tethys: Causes and evolutionary implications: *Paleobiology*, v. 44, p. 460–489, <https://doi.org/10.1017/pab.2018.16>
- Arz, J.A., and Molina, E., 2002, Bioestratigrafía y cronoestratigrafía con foraminíferos planctónicos del Campaniense superior y Maastrichtiense de latitudes subtropicales y templadas (España, Francia y Tunicia): *Neues Jahrbuch für Geologie und Paläontologie, Abhandlungen*, v. 224, p. 161–195, <https://doi.org/10.1127/njgpa/224/2002/161>.
- Batenburg, S.J. et al., 2012, Cyclostratigraphy and astronomical tuning of the Late Maastrichtian at Zumaia (Basque country, Northern Spain): *Earth and Planetary Science Letters*, v. 359–360, p. 264–278, <https://doi.org/10.1016/j.epsl.2012.09.054>.
- Batenburg, S.J. et al., 2018, Late Maastrichtian carbon isotope stratigraphy and cyclostratigraphy of the Newfoundland Margin (Site U1403, IODP Leg 342): *Newsletters on Stratigraphy*, v. 51, p. 245–260, <https://doi.org/10.1127/nos/2017/0398>.
- Bernaola G., Baceta J.I., Payros A., Orue-Etxebarria X. and Apellaniz E., 2006. The Paleocene and lower Eocene of the Zumaia section (Basque Basin): *in* *Climate and Biota of the Early Paleogene 2006. Post Conference Field Trip Guidebook*, Bilbao, Spain 82 p.

- Bown, P., 2005, Selective calcareous nannoplankton survivorship at the Cretaceous-Tertiary boundary: *Geology*, v. 33, p. 653–656, doi:10.1130/G21566.1.
- Canudo, J.I., Keller, G., and Molina, E., 1991, Cretaceous/Tertiary boundary extinction pattern and faunal turnover at Agost and Caravaca, S.E. Spain: *Marine Micropaleontology*, v. 17, p. 319–341, [https://doi.org/10.1016/0377-8398\(91\)90019-3](https://doi.org/10.1016/0377-8398(91)90019-3).
- Coccioni, R., and Silva, I.P., 2015, Revised upper Albian-Maastrichtian planktonic foraminiferal biostratigraphy and magneto-stratigraphy of the classical tethyan Gubbio section (Italy): *Newsletters on Stratigraphy*, v. 48, p. 47–90, <https://doi.org/10.1127/nos/2015/0055>.
- Coccioni, R., Frontalini, F., Bancalà, G., Fornaciari, E., Jovane, L., and Sprovieri, M., 2010, The Dan-C2 hyperthermal event at Gubbio (Italy): Global implications, environmental effects, and cause(s): *Earth and Planetary Science Letters*, v. 297, p. 298–305, <https://doi.org/10.1016/j.epsl.2010.06.031>.
- Dameron, S.N., Leckie, R.M., Clark, K., MacLeod, K.G., Thomas, D.J., and Lees, J.A., 2017, Extinction, dissolution, and possible ocean acidification prior to the Cretaceous/Paleogene (K/Pg) boundary in the tropical Pacific: *Palaeogeography, Palaeoclimatology, Palaeoecology*, v. 485, p. 433–454, <https://doi.org/10.1016/j.palaeo.2017.06.032>.
- D'Hondt, S., 2005, Consequences of the Cretaceous/Paleogene mass extinction for marine ecosystems: *Annual Review of Ecology, Evolution, and Systematics*, v. 36, p. 295–317, <https://doi.org/10.1146/annurev.ecolsys.35.021103.105715>.
- D'Hondt, S., and Keller, G., 1991, Some patterns of planktic foraminiferal assemblage turnover at the Cretaceous-Tertiary boundary: *Marine Micropaleontology*, v. 17, p. 77–118, [https://doi.org/10.1016/0377-8398\(91\)90024-Z](https://doi.org/10.1016/0377-8398(91)90024-Z).
- Dinarès-Turell, J., Baceta, J.I., Pujalte, V., Orue-Etxebarria, X., Bernaola, G., and Lorito, S., 2003, Untangling the Palaeocene climatic rhythm: An astronomically calibrated Early Palaeocene magnetostratigraphy and biostratigraphy at Zumaia (Basque basin, northern Spain): *Earth and Planetary Science Letters*, v. 216, p. 483–500, [https://doi.org/10.1016/S0012-821X\(03\)00557-0](https://doi.org/10.1016/S0012-821X(03)00557-0).
- Dinarès-Turell, J., Westerhold, T., Pujalte, V., Röhl, U., and Kroon, D., 2014, Astronomical calibration of the Danian stage (Early Paleocene) revisited: Settling chronologies of sedimentary records across the Atlantic and Pacific Oceans: *Earth*

- and *Planetary Science Letters*, v. 405, p. 119–131, <https://doi.org/10.1016/j.epsl.2014.08.027>.
- Font, E., Adatte, T., Andrade, M., Keller, G., Mbabi Bitchong, A., Carvalho, C., Ferreira, J., Diogo, Z., and Mirão, J., 2018, Deccan volcanism induced high-stress environment during the Cretaceous–Paleogene transition at Zumaia, Spain: Evidence from magnetic, mineralogical and biostratigraphic records: *Earth and Planetary Science Letters*, v. 484, p. 53–66, <https://doi.org/10.1016/j.epsl.2017.11.055>.
- Gallala, N., Zaghbib-Turki, D., Molina, E., Arenillas, I., and Arz, J.A., 2009, Planktic foraminiferal catastrophic mass extinction and assemblage evolution across the Cretaceous/Paleogene (K/Pg) boundary at Bidart (SW France): *Marine Micropaleontology*, v. 72, p. 196–209, <https://doi.org/10.1016/j.marmicro.2009.05.001>.
- Gibbs, S.J., Bown, P.R., Ward, B.A., Alvarez, S.A., Kim, H., Archontikis, O.A., Sauterey, B., Poulton, A.J., Wilson, J., and Ridgwell, A., 2020, Algal plankton turn to hunting to survive and recover from end-Cretaceous impact darkness: *Science Advances*, v. 6, p. eabc9123, <https://doi.org/10.1126/sciadv.abc9123>.
- Gilabert, V., Arz, J.A., Arenillas, I., and Robinson, S.A., 2021, Influence of the Latest Maastrichtian Warming Event on planktic foraminiferal assemblages and ocean carbonate saturation at Caravaca, Spain: *Cretaceous Research*, v., 125, 104844, <https://doi.org/10.1016/j.cretres.2021.104844>.
- Hilgen, F.J., Kuiper, K.F., and Lourens, L.J., 2010, Evaluation of the astronomical time scale for the Paleocene and earliest Eocene: *Earth and Planetary Science Letters*, v. 300, p. 139–151, <https://doi.org/10.1016/j.epsl.2010.09.044>.
- Hilgen, F.J., Abels, H.A., Kuiper, K.F., Lourens, L.J., and Wolthers, M., 2015, Towards a stable astronomical time scale for the Paleocene: Aligning Shatsky Rise with the Zumaia - Walvis Ridge ODP site 1262 composite: *Newsletters on Stratigraphy*, v. 48, p. 91–110, <https://doi.org/10.1127/nos/2014/0054>.
- Hull, P.M. et al., 2020, On impact and volcanism across the Cretaceous-Paleogene boundary: *Science*, v. 367, p. 266–272, <https://doi.org/10.1126/science.aay5055>.
- Husson, D., Galbrun, B., Laskar, J., Hinnov, L.A., Thibault, N., Gardin, S., and Locklair, R.E., 2011, Astronomical calibration of the Maastrichtian (Late Cretaceous): *Earth and Planetary Science Letters*, v. 305, p. 328–340, <https://doi.org/10.1016/j.epsl.2011.03.008>.

- Jiang, S., Bralower, T.J., Patzkowsky, M.E., Kump, L.R., and Schueth, J.D., 2010, Geographic controls on nannoplankton extinction across the Cretaceous/Palaeogene boundary: *Nature Geoscience*, v. 3, p. 280–285, <https://doi.org/10.1038/ngeo775>.
- Jones, H.L., Lowery, C.M., and Bralower, T.J., 2019, Delayed calcareous nannoplankton boom-bust successions in the earliest Paleocene Chicxulub (Mexico) impact crater: *Geology*, v. 47, <https://doi.org/10.1130/G46143.1>.
- Kuiper, K.F., Deino, A., Hilgen, F.J., Krijgsman, W., Renne, P.R., and Wijbrans, J.R., 2008, Synchronizing rock clocks of earth history: *Science*, v. 320, p. 500–504, <https://doi.org/10.1126/science.1154339>.
- Laskar, J., Gastineau, M., Delisle, J.-B., Farrés, A., and Fienga, A., 2011, Strong chaos induced by close encounters with Ceres and Vesta: *A&A*, v. 532, p. 4, <https://doi.org/10.1051/0004-6361/201117504>.
- Li, L., and Keller, G., 1998, Maastrichtian climate, productivity and faunal turnovers in planktic foraminifera in South Atlantic DSDP sites 525A and 21: *Marine Micropaleontology*, v. 33, p. 55–86, [https://doi.org/10.1016/S0377-8398\(97\)00027-3](https://doi.org/10.1016/S0377-8398(97)00027-3).
- Lirer, F., 2000, A new technique for retrieving calcareous microfossils from lithified lime deposits: *Micropaleontology*, v. 46, p. 365–369.
- Lowery, C.M. et al., 2018, Rapid recovery of life at ground zero of the end-Cretaceous mass extinction: *Nature*, v. 558, p. 288–291, <https://doi.org/10.1038/s41586-018-0163-0>.
- Molina, E., Alegret, L., Arenillas, I., and Arz, J.A., 2005, The Cretaceous/Paleogene boundary at the Agost section revisited: paleoenvironmental reconstruction and mass extinction pattern: *Journal of Iberian Geology*, v.31, p.135-148.
- Molina, E., Alegret, L., Arenillas, I., Arz, J.A., Gallala, N., Grajales-Nishimura, J.M., Murillo-Muñetón, G., and Zaghbib-Turki, D., 2009, The Global Boundary Stratotype Section and Point for the base of the Danian Stage (Paleocene, Paleogene, “Tertiary”, Cenozoic): Auxiliary sections and correlation: *Episodes*, v. 32, p. 84–95, <https://doi.org/10.18814/epiiugs/2009/v32i2/002>.
- Mukhopadhyay, S., Farley, K.A., and Montanari, A., 2001, A short duration of the Cretaceous-Tertiary boundary event: Evidence from extraterrestrial <sup>3</sup>Helium: *Science*, v. 291, p. 1952–1955, <https://doi.org/10.1126/science.291.5510.1952>.



- Quillévére, F., Norris, R.D., Kroon, D., and Wilson, P.A., 2008, Transient ocean warming and shifts in carbon reservoirs during the early Danian: *Earth and Planetary Science Letters*, v. 265, p. 600–615, <https://doi.org/10.1016/j.epsl.2007.10.040>.
- Renne, P., Arenillas, I., Arz, J.A., Bermúdez, H., Vajda, V., Gilabert, V., 2018, Multi-proxy record of the Chicxulub impact at the Cretaceous/Paleogene boundary from Gorgonilla Island, Colombia: *Geology*, v. 46, no. 6, p. 547–550, <https://doi.org/10.1130/G40224.1>.
- Ruíz, F.M., Huertas, M.O., Palomo, I., and Barbieri, M., 1992, The geochemistry and mineralogy of the Cretaceous-Tertiary boundary at Agost (southeast Spain): *Chemical Geology*, v. 95, p. 265–281, [https://doi.org/10.1016/0009-2541\(92\)90016-X](https://doi.org/10.1016/0009-2541(92)90016-X).
- Sepúlveda, J., Alegret, L., Thomas, E., Haddad, E., Cao, C., and Summons, R.E., 2019, Stable Isotope Constraints on Marine Productivity Across the Cretaceous-Paleogene Mass Extinction: *Paleoceanography and Paleoclimatology*, v. 34, p. 1195–1217, <https://doi.org/10.1029/2018PA003442>.
- Schulte, P. et al., 2010, The Chicxulub asteroid impact and mass extinction at the Cretaceous-Paleogene boundary: *Science*, v. 327, p. 1214–1218, <https://doi.org/10.1126/science.1177265>.
- Smit, J., 1982, Extinction and evolution of planktonic foraminifera after a major impact at the Cretaceous/Tertiary boundary: *Special Paper of the Geological Society of America*, v. 190, p. 329–352, <https://doi.org/10.1130/SPE190-p329>.
- Smit, J., 1990, Meteorite impact, extinctions and the Cretaceous-Tertiary Boundary: *Geologie en Mijnbouw*, v. 69, p. 187–204.
- Smit, J., 1999, The global stratigraphy of the Cretaceous-Tertiary boundary impact ejecta: *Annual Review of Earth and Planetary Sciences*, v. 27, p. 75–113, <https://doi.org/10.1146/annurev.earth.27.1.75>.
- Smit, J., and Romein, A.J.T., 1985, A sequence of events across the Cretaceous-Tertiary boundary: *Earth and Planetary Science Letters*, v. 74, p. 155–170, [https://doi.org/10.1016/0012-821X\(85\)90019-6](https://doi.org/10.1016/0012-821X(85)90019-6).
- ten Kate, W.G.H.Z., and Sprenger, A., 1993, Orbital cyclicities above and below the Cretaceous/Paleogene boundary at Zumaya (N Spain), Agost and Rellou (SE Spain): *Sedimentary Geology*, v. 87, p. 69–101, [https://doi.org/10.1016/0037-0738\(93\)90037-6](https://doi.org/10.1016/0037-0738(93)90037-6).

- Voigt, S., Gale, A.S., Jung, C., and Jenkyns, H.C., 2012, Global correlation of upper Campanian- Maastrichtian successions using carbon-isotope stratigraphy: Development of a new Maastrichtian timescale: *Newsletters on Stratigraphy*, v. 45, p. 25–53, <https://doi.org/10.1127/0078-0421/2012/0016>.
- Wade, B.S., Pearson, P.N., Berggren, W.A., and Pälike, H., 2011, Review and revision of Cenozoic tropical planktonic foraminiferal biostratigraphy and calibration to the geomagnetic polarity and astronomical time scale: *Earth-Science Reviews*, v. 104, p. 111–142, <https://doi.org/10.1016/j.earscirev.2010.09.003>.
- Westerhold, T., Röhl, U., Raffi, I., Fornaciari, E., Monechi, S., Reale, V., Bowles, J., and Evans, H.F., 2008, Astronomical calibration of the Paleocene time: *Palaeogeography, Palaeoclimatology, Palaeoecology*, v. 257, p. 377–403, <https://doi.org/10.1016/j.palaeo.2007.09.016>.
- Woelders, L. et al., 2017, Latest Cretaceous climatic and environmental change in the South Atlantic region: *Paleoceanography*, v. 32, p. 466–483, <https://doi.org/10.1002/2016PA003007>.

## Anexo V. (Material suplementario elaborado para esta tesis doctoral), (2 Tablas).

TABLA ANEXA 1: SECCIÓN DE CARAVACA

Altura respecto al límite K/Pg	Edad Según (1)	$\delta^{13}\text{C}$ roca total (2)	Edad muestras estudio cualitativo según (1)	Nº de especies (2)	Edad muestras cuantitativo según (1)	<i>Guembeliria</i> (2)	<i>Heterohelix</i> (2)	Índice de Fragmentación (2)	Edad, muestras biométrías (2)	<i>Contusotruncana contusa</i> (Altura, $\mu\text{m}$ ) (2)	<i>Contusotruncana contusa</i> (Anchura, $\mu\text{m}$ ) (2)
(cm)	(Ma)	(‰)	(Ma)	(n)	(Ma)	(%)	(%)	(%)	(Ma)	( $\mu\text{m}$ )	( $\mu\text{m}$ )
-1	66,001	1,53	66,001	66	66,001	1,1	63,5	20,7	66,001	716,30	923,40
-3	66,001	2,07	66,001	67	66,004	1,6	65,0	25,7	66,007	661,60	905,70
-5	66,002	2,03	66,002	67	66,007	1,2	67,7	21,6	66,014	719,80	927,30
-7	66,002	2,04	66,003	67	66,010	2,0	65,4	22,3	66,037	725,70	976,70
-9	66,002	2,06	66,003	68	66,014	5,1	58,7	19,1	66,061	677,40	895,50
-15	66,003	2,01	66,004	68	66,018	2,0	62,0	21,6	66,069	692,30	910,10
-20	66,004	2,07	66,005	68	66,028	0,6	63,7	27,7	66,080	700,60	958,30
-25	66,005	2,05	66,007	68	66,037	2,0	55,6	30,2	66,084	544,50	773,90
-30	66,006	2,05	66,007	69	66,053	1,8	62,4	30,7	66,088	450,60	589,30
-35	66,007	2,12	66,009	68	66,061	0,2	70,5	27,5	66,092	468,80	614,30
-40	66,007	2,02	66,010	67	66,069	2,0	60,4	36,4	66,100	452,60	648,80
-45	66,008	1,79	66,012	67	66,080	0,4	73,0	31,7	66,107	480,33	635,33
-50	66,009	1,92	66,014	69	66,092	2,8	64,0	36,8	66,131	444,78	606,56
-55	66,010	1,78	66,018	69	66,100	0,7	68,3	41,7	66,155	494,00	639,60
-60	66,010	1,64	66,025	66	66,107	0,0	82,3	47,5	66,180	516,00	629,30
-65	66,011	1,73	66,028	68	66,113	2,4	56,6	30,2	66,205	474,00	717,00
-70	66,012	1,71	66,029	68	66,124	1,4	70,3	47,9	66,218	487,00	677,70
-75	66,013	1,74	66,034	69	66,131	1,6	72,2	47,3	66,230	473,90	621,30
-80	66,014	1,92	66,037	68	66,147	0,2	60,2	32,2	66,249	412,20	646,00
-85	66,014	1,99	66,040	68	66,155	0,6	53,8	18,5	66,255	697,60	912,40
-90	66,015	1,57	66,045	67	66,168	2,0	69,8	29,7	66,268	703,10	889,60
-95	66,016	1,72	66,053	68	66,180	0,6	69,5	31,7	66,280	746,00	966,60
-100	66,017	1,92	66,061	67	66,193	1,5	72,8	32,6	66,311	587,00	803,60
-110	66,018	1,81	66,067	67	66,205	1,3	77,9	48,5	66,326	653,50	832,80
-130	66,021	1,73	66,069	69	66,218	1,8	75,3	34,8	66,364	650,10	823,00
-150	66,025	1,71	66,078	67	66,230	2,8	75,0	38,5	66,412	592,80	792,00
-170	66,028	1,54	66,080	68	66,243	1,8	77,9	57,7			
-190	66,031	1,62	66,089	66	66,249	2,2	68,5	63,7			
-210	66,034	1,30	66,092	68	66,255	0,4	71,1	42,8			
-230	66,037	1,70	66,100	66	66,280	0,5	64,8	34,0			
-250	66,040	1,83	66,107	64	66,326	0,2	61,7	50,5			
-280	66,045	1,69	66,113	65	66,364	0,8	56,9	42,9			
-305	66,049	1,50	66,118	64	66,380	0,6	59,9	33,3			
-330	66,053	1,49	66,124	65	66,396	0,6	58,3	28,2			
-355	66,057	1,56	66,131	64	66,412	0,8	62,1	34,8			
-380	66,061	1,39	66,137	63							
-405	66,065	1,19	66,147	65							
-430	66,069	1,69	66,155	66							
-455	66,073	1,25	66,168	67							
-480	66,076	0,85	66,180	65							
-505	66,080	1,50	66,193	66							
-530	66,084	0,95	66,205	67							
-555	66,088	1,28	66,218	67							
-580	66,092	1,25	66,228	67							
-605	66,096	0,87	66,230	68							

-630	66,100	-0,58	66,243	68
-655	66,107	0,09	66,249	66
-680	66,113	1,39	66,255	65
-690	66,116	1,52	66,272	64
-720	66,124	1,47	66,280	67
-750	66,131	1,39	66,326	66
-780	66,139	1,36	66,364	67
-810	66,147	0,73	66,373	67
-840	66,155	0,83	66,380	65
-870	66,161	1,13	66,386	65
-900	66,168	0,95	66,396	68
-930	66,174	0,78	66,398	67
-960	66,180	1,14	66,412	67
-990	66,186	0,82		
-1020	66,193	1,47		
-1050	66,199	1,37		
-1080	66,205	-0,60		
-1110	66,211	0,58		
-1140	66,218	1,14		
-1170	66,224	1,43		
-1200	66,230	1,57		
-1230	66,236	1,32		
-1260	66,243	0,59		
-1290	66,249	0,63		
-1320	66,255	0,96		
-1350	66,268	1,05		
-1380	66,280	1,59		
-1410	66,295	1,48		
-1440	66,311	1,35		
-1470	66,326	1,16		
-1500	66,343	1,19		
-1530	66,359	1,32		
-1560	66,364	1,31		
-1590	66,370	1,81		
-1620	66,375	1,75		
-1650	66,380	1,90		
-1680	66,386	1,87		
-1710	66,391	2,07		
-1740	66,396	1,58		
-1770	66,401	1,62		
-1800	66,407	1,81		
-1830	66,412	1,92		

---

Nota: (1) = (Gilabert et al., 2021c); (2) (Gilabert et al., 2021a),

---

TABLA ANEXA 1: SECCIÓN DE ZUMAIA

Altura respecto al límite K/Pg (cm)	Edad (Ma)	$\delta^{13}C$ C roca total (‰)	Edad muestras estudio cuantitativo (Ma)	<i>Heterohelix</i> (%)	<i>Guenbelitria</i> (%)	Edad muestras estudio cualitativo (Ma)	Nº de especies (n)
-1	66,001	1,95	66,001	52,9	1,0	66,001	64
-6	66,003	1,83	66,005	58,0	0,7	66,005	59
-10	66,004	1,80	66,008	53,9	5,6	66,016	58
-15	66,005	1,69	66,011	55,0	4,7	66,028	59
-20	66,006	1,76	66,014	66,2	1,4	66,036	63
-25	66,008	1,98	66,016	61,5	4,3	66,046	63
-30	66,009	1,90	66,021	64,3	3,4	66,059	62
-35	66,011	1,83	66,024	63,2	2,0	66,066	59
-40	66,012	1,78	66,028	60,7	4,3	66,075	68
-45	66,014	1,76	66,031	58,2	3,2	66,087	61
-50	66,016	1,90	66,036	62,5	6,1	66,100	64
-65	66,021	1,49	66,041	66,4	1,4	66,107	59
-75	66,024	1,51	66,046	61,7	0,0	66,114	57
-85	66,028	1,69	66,051	66,7	0,3	66,120	58
-95	66,031	1,67	66,055	65,7	0,0	66,127	54
-105	66,034	1,78	66,059	59,3	4,3	66,134	61
-115	66,036	1,60	66,066	63,8	0,3	66,149	63
-125	66,039	1,65	66,069	64,9	4,7	66,158	57
-135	66,041	1,49	66,075	59,4	1,7	66,172	61
-145	66,044	1,35	66,080	58,5	0,3	66,194	62
-155	66,046	1,51	66,082	66,7	0,3	66,212	59
-165	66,049	1,60	66,087	65,4	1,4	66,236	59
-175	66,051	1,52	66,091	60,1	0,0	66,251	60
-185	66,053	1,57	66,096	63,8	0,0	66,268	63
-195	66,055	1,34	66,100	61,1	1,1	66,283	59
-205	66,056	1,46	66,107	69,3	0,7	66,295	62
-220	66,059	1,05	66,114	57,6	2,1	66,312	56
-235	66,062	1,25	66,117	65,5	2,0	66,322	58
-255	66,066	1,24	66,120	54,7	10,5	66,334	55
-270	66,069	1,62	66,127	56,1	2,9	66,348	59
-290	66,072	1,57	66,130	57,1	13,9	66,366	56
-310	66,075	1,50	66,134	60,1	5,0	66,378	62
-330	66,078	1,14	66,141	51,6	4,3	66,412	62
-345	66,080	1,05	66,149	54,5	0,0		
-360	66,082	1,47	66,154	53,5	2,5		
-375	66,084	1,42	66,158	59,7	1,0		
-395	66,087	1,35	66,164	60,7	4,3		
-415	66,091	1,66	66,168	75,1	0,0		
-435	66,096	1,15	66,172	61,1	0,0		

-455	66,100	1,06	66,185	75,4	0,0
-475	66,104	1,73	66,194	64,8	2,8
-490	66,107	1,57	66,212	67,0	3,4
-510	66,110	1,54	66,219	71,0	4,2
-530	66,114	1,44	66,225	66,7	1,0
-550	66,117	1,20	66,236	61,7	3,4
-570	66,120	1,01	66,245	59,4	1,9
-590	66,124	1,50	66,251	56,3	1,5
-610	66,127	1,48	66,255	51,8	1,3
-630	66,130	1,25	66,268	52,0	0,4
-650	66,134	0,95	66,283	53,6	1,8
-670	66,137	1,20	66,295	53,4	2,5
-695	66,141	1,23	66,312	60,0	0,0
-715	66,144	1,38	66,322	57,3	0,0
-735	66,149	1,24	66,334	56,7	0,0
-755	66,154	0,42	66,348	43,6	4,9
-770	66,158	1,40	66,366	58,3	0,0
-795	66,164	1,44	66,378	58,1	1,3
-810	66,168	1,46	66,412	57,6	1,7
-830	66,172	0,86			
-850	66,179	1,12			
-875	66,185	1,25			
-890	66,190	1,54			
-905	66,194	1,61			
-925	66,199	1,56			
-965	66,212	1,14			
-985	66,219	1,65			
-1000	66,225	1,69			
-1015	66,231	1,72			
-1030	66,236	1,36			
-1045	66,241	1,52			
-1060	66,245	1,50			
-1075	66,248	1,35			
-1090	66,251	0,96			
-1105	66,255	1,57			
-1130	66,261	1,70			
-1150	66,268	1,49			
-1165	66,273	1,77			
-1185	66,280	1,68			
-1200	66,283	1,62			
-1220	66,289	1,74			
-1245	66,295	1,67			
-1260	66,299	1,64			
-1275	66,303	1,58			
-1305	66,312	1,54			
-1305	66,312	1,53			
-1320	66,317	1,61			

-1340	66,322	1,50
-1355	66,326	1,29
-1375	66,331	1,35
-1390	66,334	1,38
-1405	66,339	1,51
-1420	66,344	1,28
-1435	66,348	1,39
-1450	66,353	1,35
-1465	66,359	1,57
-1485	66,366	1,43
-1495	66,370	1,52
-1505	66,374	1,51
-1520	66,378	1,47
-1545	66,385	1,35
-1565	66,390	1,54
-1580	66,398	1,48
-1595	66,412	1,57

---

Nota: (1) = (Gilabert et al., 2021c); (2) (Gilabert et al., 2021a),

---

**Tabla Anexa 1.** Compilación de los resultados obtenidos en la presente tesis doctoral para la elaboración de la figura de síntesis, Figura 10.

TABLA ANEXA 2: SECCIÓN DE CARAVACA

Altura respecto al límite K/Pg (cm)	Edad recalibrada según (1) (Ma)	$\delta^{13}C$ roca total (2,3) (%)	Edad muestras estudio cuantitativo según (1) (Ma)	P/B (2,3) (%)	Triseriados (2,3) (%)	Parvularugoglobigerinidos (3) (%)	Biseriados (3) (%)	Otros géneros (3) (%)	Aberrantes total (3) (%)	Edad muestras estudio cualitativo según (1) (Ma)	Nº de especies total (2,3) (n)	Nº de especies (Daniense) (3) (n)	Nº de especies (Cretácico) (2,3) (n)
820,0	65,364	0,85	65,364	98,97	2,45		58,39	39,16	2,08	65,364	21	20	1
790,0	65,388	0,81	65,388	98,77	0,93		50,62	48,45	2,17	65,388	24	22	2
760,0	65,412	0,94	65,412	100,00	2,13		59,22	38,65	2,45	65,412	22	22	0
730,0	65,435	1,00	65,435	99,65	2,46		63,03	34,51	2,11	65,435	25	24	1
700,0	65,459	0,86	65,459	100,00	3,27		53,09	43,64	3,27	65,459	24	24	0
670,0	65,505	1,08	65,505	99,64	3,27		55,27	41,45	2,55	65,505	27	26	1
640,0	65,546	1,04	65,546	99,30	1,42		58,52	40,06	3,87	65,546	25	24	1
610,0	65,580	1,06	65,580	99,23	6,59		64,73	28,68	3,47	65,580	28	26	2
580,0	65,615	1,19	65,615	98,72	12,34		55,84	31,82	4,55	65,615	24	21	3
550,0	65,650	1,25	65,650	100,00	10,18		58,98	30,84	3,29	65,650	26	26	0
520,0	65,685	1,26	65,685	99,26	7,43		60,97	31,60	3,35	65,685	20	18	2
490,0	65,696	0,95	65,696	98,20	7,69		56,78	35,53	4,03	65,696	25	23	2
460,0	65,707	0,69	65,707	98,24	3,94		46,59	49,46	3,94	65,707	27	26	1
430,0	65,722	1,05	65,722	98,38	2,97		57,10	39,93	3,95	65,722	30	28	2
400,0	65,737	1,16	65,737	97,73	7,28		53,64	39,07	3,97	65,737	31	27	4
370,0	65,750	1,09	65,750	98,99	12,20		56,95	30,85	4,41	65,750	26	24	2
345,0	65,760	1,19	65,760	96,48	28,57		56,04	15,38	11,31	65,760	26	24	2
320,0	65,766	1,14	65,766	97,58	16,85		67,74	15,41	8,51	65,766	23	22	1
295,0	65,772	1,18	65,772	96,90	18,86		52,67	28,47	10,32	65,772	29	26	3
270,0	65,778	1,04	65,778	97,40	3,85		53,08	43,08	6,11	65,778	25	24	1
245,0	65,784	0,93	65,784	97,66	1,03		58,22	40,75	4,79	65,784	26	25	1
220,0	65,795	1,18	65,795	98,11	46,47		44,55	8,97	8,01	65,795	23	21	2
200,0	65,803	1,20	65,803	96,14	48,51		42,16	9,33	15,33	65,803	24	23	1
180,0	65,812	1,71	65,812	98,09	47,02		44,70	8,28	13,96	65,812	21	19	2
160,0	65,830	1,72	65,830	99,19	46,31		50,41	3,28	13,52	65,830	15	14	1
155,0	65,841	1,75	65,892	96,97	38,19		59,38	2,43	14,24	65,892	14	13	1
150,0	65,851	1,68	65,922	98,77	44,79	0,00	52,68	2,52	9,97	65,922	17	15	2
145,0	65,861	1,86	65,938	97,19	0,97	9,68	72,26	17,10	7,40	65,938	28	24	4
140,0	65,871	1,79	65,945	97,27	0,00	9,61	84,34	6,05	5,96	65,945	21	18	3
135,0	65,881	1,66	65,954	97,46	1,12	30,71	64,79	3,37	5,95	65,954	21	19	2
130,0	65,892	1,77	65,966	97,83	0,95	48,89	46,67	3,49	6,98	65,966	22	19	3
125,0	65,902	1,60	65,975	97,69	3,42	59,59	35,62	1,37	9,80	65,975	19	16	3
120,0	65,912	1,54	65,977	88,64	6,67	62,92	30,42		9,92	65,977	22	16	6
115,0	65,922	1,56	65,980	91,49	5,51	89,37	5,12		13,18	65,980	19	13	6
110,0	65,933	1,59	65,981	79,34	7,48	86,45	6,07		13,02	65,981	19	14	5
105,0	65,933	1,59	65,982	89,46	9,39	89,53	1,08		12,14	65,982	25	16	9
100,0	65,934	1,74	65,983	84,21	9,09	90,91	0,00		10,71	65,983	24	14	10



95,0	65,935	1,69	65,985	86,41	7,11	91,63	1,26	13,71	65,985	24	16	8
90,0	65,936	1,57	65,988	82,58	11,21	88,79	0,00	9,63	65,988	24	14	10
85,0	65,937	1,86	65,990	77,93	15,79	83,63	0,58	13,29	65,990	25	15	10
80,0	65,942	1,72	65,991	83,61	11,39	88,12	0,50	9,80	65,991	27	15	12
75,0	65,948	1,77	65,992	75,52	10,67	89,33	0,00	12,25	65,992	24	14	10
70,0	65,953	1,84	65,994	67,13	19,15	80,43	0,43	10,25	65,994	31	16	15
65,0	65,959	1,82	65,995	27,99	73,33	24,00	2,67	21,33	65,995	30	11	19
60,0	65,964	1,86	65,998	11,61	54,84	45,16		19,35	65,998	19	5	14
57,0	65,967	1,92	65,999	8,91	100,00			22,22	65,999	36	3	33
54,0	65,970	1,87	66,001	98,18	1,11				66,001	66	0	66
50,0	65,975	1,65	66,004	97,70	1,63				66,001	67	0	67
48,0	65,975	1,61	66,007	98,07	1,21				66,002	67	0	67
45,0	65,976	1,60	66,010	98,43	1,99				66,003	67	0	67
42,0	65,977	1,39	66,014	98,07	5,13				66,003	68	0	68
39,0	65,978	1,39	66,018	97,66	2,00				66,004	68	0	68
36,0	65,979	1,40	66,028	98,39	0,61				66,005	68	0	68
33,0	65,980	1,10	66,037	97,27	2,01				66,007	68	0	68
30,0	65,981	1,37	66,053	99,01	1,80				66,007	69	0	69
28,0	65,982	1,21	66,061	99,31	0,23				66,009	68	0	68
26,0	65,982	1,11	66,069	99,01	2,00				66,010	67	0	67
24,0	65,983	0,82	66,080	99,60	0,40				66,012	67	0	67
22,0	65,984	1,17	66,092	98,34	2,81				66,014	69	0	69
20,0	65,985	1,15	66,100	98,11	0,70				66,018	69	0	69
18,0	65,987	1,19							66,025	66	0	66
16,0	65,988	0,93							66,028	68	0	68
14,0	65,989	0,94							66,029	68	0	68
12,0	65,990	1,15							66,034	69	0	69
10,0	65,991	1,12							66,037	68	0	68
8,0	65,992	1,21							66,040	68	0	68
6,0	65,994	0,20							66,045	67	0	67
4,0	65,995	0,82							66,053	68	0	68
2,0	65,998	0,78							66,061	67	0	67
1,0	65,999	0,58							66,067	67	0	67
-1,0	66,001	1,53							66,069	69	0	69
-3,0	66,001	2,07							66,078	67	0	67
-5,0	66,002	2,03							66,080	68	0	68
-7,0	66,002	2,04							66,089	66	0	66
-9,0	66,002	2,06							66,092	68	0	68
-15,0	66,003	2,01							66,100	66	0	66
-20,0	66,004	2,07										
-25,0	66,005	2,05										
-30,0	66,006	2,05										
-35,0	66,007	2,12										
-40,0	66,007	2,02										
-45,0	66,008	1,79										
-50,0	66,009	1,92										
-55,0	66,010	1,78										
-60,0	66,010	1,64										

-65,0	66,011	1,73
-70,0	66,012	1,71
-75,0	66,013	1,74
-80,0	66,014	1,92
-85,0	66,014	1,99
-90,0	66,015	1,57
-100,0	66,016	1,72
-110,0	66,017	1,92
-130,0	66,018	1,81
-150,0	66,021	1,73
-170,0	66,025	1,71
-190,0	66,028	1,54
-210,0	66,031	1,62
-230,0	66,034	1,30
-250,0	66,037	1,70
-280,0	66,040	1,83
-305,0	66,045	1,69
-330,0	66,049	1,50
-355,0	66,053	1,49
-380,0	66,057	1,56
-405,0	66,061	1,39
-430,0	66,065	1,19
-455,0	66,069	1,69
-480,0	66,073	1,25
-505,0	66,076	0,85
-530,0	66,080	1,50
-555,0	66,084	0,95
-580,0	66,088	1,28
-605,0	66,092	1,25
-630,0	66,096	0,87

---

Nota: (1) = (Gilabert et al., 2021c); (2) (Gilabert et al., 2021a); (3) Gilabert et al., 2021b; (4) (Arenillas et al., 2018); (NP) No publicado, Triseriados = *Guembeltria* + *Chiloguembeltria*; Parvularugoglobigerinidos = *Parvularugoglobigerina* + *Palaeoglobigerina* + *Pseudocaucasina*; Biseriados = *Woodringina* + *Chiloguembelina*; Otros géneros = *Globanomalina*, *Praemurica*, *Subbotina*, *Parasubbotina*, *Globoconusa*, *Trochoguembeltria*, *Eoglobigerina*.

---

TABLA ANEXA 2: SECCIÓN DE ZUMAIA

Altura respecto al límite K/Pg (cm)	Edad (1) (Ma)	$\delta^{13}C$ roca total (1) (‰)	Edad muestras estudio cuantitativo (1) (Ma)	Triseriados (1) (%)	P/B (NP) (%)	Parvulamoglobigerinidos (1) (%)	Biseriados (1) (%)	Otros géneros (1) (%)	Aberrantes total (NP) (%)	Edad muestras estudio cualitativo (1) (Ma)	Nº de especies total (1) (n)	Nº de especies (Daniense) (1) (n)	Nº de especies (Cretácico) (1) (n)
850	65,364	1,77	65,364	0,36	100		46,72	52,92	2,55	65,364	21	20	1
820	65,389	1,86	65,389	1,34	98,68		43,62	55,03	2,01	65,389	19	18	1
805	65,401	1,75	65,408	0,00	97,44		52,46	47,54	0,66	65,408	21	20	1
790	65,408	1,82	65,434	0,00	96,82		43,80	56,20	1,46	65,434	20	19	1
770	65,418	1,52	65,480	0,41	98,40		39,84	59,76	1,22	65,480	20	19	1
750	65,434	1,61	65,514	2,72	98,22		36,25	61,03	1,81	65,514	23	21	2
730	65,459	1,51	65,528	3,10	95,71		35,52	61,38	0,34	65,528	26	25	1
710	65,480	1,74	65,549	7,22	98,93		38,63	54,15	2,89	65,549	22	21	1
680	65,514	1,79	65,570	6,01	95,93		30,04	63,96	2,47	65,570	24	23	1
655	65,528	1,88	65,586	5,52	100,00		45,30	49,17	3,31	65,586	17	16	1
625	65,549	2,01	65,605	6,25	98,91		41,18	52,57	2,21	65,605	23	22	1
600	65,570	1,98	65,621	5,44	98,33		45,92	48,64	3,40	65,621	22	21	1
580	65,586	1,89	65,654	3,33	98,54		40,74	55,93	4,81	65,654	23	22	1
565	65,595	2,15	65,673	0,40	100,00		11,20	88,40	2,40	65,673	22	21	1
550	65,605	2,18	65,685	7,25	98,92		33,70	59,06	6,52	65,685	23	22	1
525	65,621	2,08	65,719	42,67	98,04		31,67	25,67	6,67	65,719	21	19	2
510	65,633	2,11	65,760	26,67	97,60		42,81	30,53	8,07	65,760	21	20	1
500	65,642	1,89	65,791	50,81	97,62		35,37	13,82	10,98	65,791	17	16	1
485	65,654	2,07	65,812	50,19	97,82		34,57	15,24	11,52	65,812	16	15	1
470	65,666	2,21	65,830	70,68	98,88		19,92	9,40	15,79	65,830	19	16	3
460	65,673	2,20	65,859	47,62	98,44		41,67	10,71	10,32	65,859	18	15	3
445	65,685	2,20	65,881	35,14	98,92		50,72	14,13	7,97	65,881	17	16	1
430	65,696	1,93	65,891	19,74	98,06		67,76	12,50	7,24	65,891	15	14	1
415	65,707	1,69	65,920	6,11	98,13	0,45	80,53	12,91	12,21	65,920	17	14	3
400	65,719	1,81	65,933	2,25	99,11	0,00	89,64	8,11	10,36	65,933	12	11	1
380	65,737	2,20	65,942	1,17	96,97	0,39	82,03	16,41	15,23	65,942	20	17	3
365	65,760	2,05	65,945	3,76	98,67	6,39	74,44	15,41	12,61	65,945	23	22	1
350	65,776	2,22	65,945	2,25	96,73	14,86	77,48	5,41	10,90	65,945	18	13	5
340	65,784	1,62	65,949	4,51	85,26	22,18	71,43	1,88	9,35	65,949	18	12	6
330	65,791	1,92	65,952	6,17	97,08	32,16	45,37	16,30	11,28	65,952	27	23	4
315	65,801	2,11	65,959	6,45	91,90	39,25	51,08	3,23	8,37	65,959	23	17	6
305	65,812	2,29	65,971	7,48	90,73	59,35	30,37	2,80	17,20	65,971	20	13	7
285	65,830	2,08	65,975	7,25	78,46	50,78	40,93	1,04	12,44	65,975	24	15	9
265	65,847	2,29	65,981	10,75	76,23	75,27	13,98		15,59	65,981	24	16	8
250	65,859	2,24	65,983	7,69	71,23	92,31	0,00		15,38	65,983	20	8	12
230	65,872	2,30	65,985	8,08	63,26	88,89	3,03		14,14	65,985	20	11	9
215	65,881	2,34	65,987	7,34	80,45	84,18	8,47		16,38	65,987	20	12	8
195	65,891	2,21	65,989	10,87	62,73	79,71	9,42		19,57	65,989	24	11	13
180	65,898	2,06	65,990	13,48	68,99	81,46	5,06		14,61	65,990	23	12	11
165	65,905	2,19	65,992	2,24	47,02	89,55	8,21		14,93	65,992	25	11	14

152	65,910	2,14	65,995	8,52	52,38	82,39	9,09	11,93	65,995	26	13	13
140	65,915	2,35	66,000	81,82	17,05	18,18			66,000	25	3	22
128	65,920	1,97	66,001	0,98	100,00				66,001	64	64	64
115	65,926	2,17	66,005	0,68	100,00				66,005	59	59	59
110	65,928	1,91	66,008	5,59	100,00				66,016	58	58	58
100	65,933	2,13	66,011	4,67	100,00				66,028	59	59	59
90	65,937	2,07	66,014	1,41	99,30				66,036	63	63	63
80	65,942	2,18	66,021	4,32	100,00				66,046	63	63	63
74	65,945	2,25	66,024	3,40	98,70				66,059	62	62	62
72	65,945	1,98	66,028	1,97	100,00				66,066	59	59	59
67	65,949	1,86	66,031	4,33	98,60				66,075	68	68	68
61	65,954	2,12	66,036	3,19	99,32				66,087	61	61	61
55	65,959	2,04	66,041	6,14	98,57				66,100	64	64	64
50	65,967	1,23	66,046	1,45	98,99							
43	65,971	1,43	66,051	0,00	99,02							
37	65,975	1,74	66,055	0,33	100,00							
33	65,977	0,94	66,059	0,00	99,64							
30	65,979	0,80	66,066	4,29	99,68							
27	65,981	1,15	66,069	0,32	98,92							
23	65,983	0,87	66,075	4,71	98,37							
20	65,985	0,77	66,080	1,66	100,00							
17	65,987	0,50	66,082	0,35	98,99							
14	65,989	0,64	66,087	0,34	98,95							
11	65,990	0,85	66,091	1,41	100,00							
9	65,992	0,15	66,096	0,00	99,67							
6	65,995	-0,04	66,100	0,00	98,61							
4	65,997	-0,16										
1	66,000	0,65										
0	66,001	1,42										
-1	66,001	1,95										
-6	66,003	1,83										
-10	66,004	1,80										
-15	66,005	1,69										
-20	66,006	1,76										
-25	66,008	1,98										
-30	66,009	1,90										
-35	66,011	1,83										
-40	66,012	1,78										
-45	66,014	1,76										
-50	66,016	1,90										
-65	66,021	1,49										
-75	66,024	1,51										
-85	66,028	1,69										
-95	66,031	1,67										
-105	66,034	1,78										
-115	66,036	1,60										
-125	66,039	1,65										
-135	66,041	1,49										
-145	66,044	1,35										
-155	66,046	1,51										
-165	66,049	1,60										

-175	66,051	1,52
-185	66,053	1,57
-195	66,055	1,34
-205	66,056	1,46
-220	66,059	1,05
-235	66,062	1,25
-255	66,066	1,24
-270	66,069	1,62
-290	66,072	1,57
-310	66,075	1,50
-330	66,078	1,14
-345	66,080	1,05
-360	66,082	1,47
-375	66,084	1,42
-395	66,087	1,35
-415	66,091	1,66
-435	66,096	1,15
-455	66,100	1,06

---

Nota: (1) = (Gilabert et al., 2021c); (2) (Gilabert et al., 2021a); (3) Gilabert et al., 2021b; (4) (Arenillas et al., 2018); (NP) No publicado, Triseriados = *Guembeltria* + *Chiloguembeltria*; Parvularugoglobigerinidos = *Parvularugoglobigerina* + *Palaeoglobigerina* + *Pseudocaucasina*; Biseriados = *Woodringina* + *Chiloguembelina*; Otros géneros = *Globanomalina*, *Praemurica*, *Subbotina*, *Parasubbotina*, *Globoconusa*, *Trochoguembeltria*, *Eoglobigerina*,

---

TABLA ANEXA 2: SECCIÓN DE EL KEF

Altura respecto al límite K/Pg (cm)	Edad recalibrada según (1) (Ma)	Triseriados (4) (%)	Parvularugoglobigerinidos (4) (%)	Biseriados (4) (%)	Otros géneros (4) (%)	Aberrantes total (4) (%)	Edad muestras estudio cualitativo (4) según (1) (Ma)	Nº de especies total (4) (n)	Nº d especies (Daniense) (4) (n)	Nº d especies (Cretácico) (4) (n)
1347	65,600	7,4		55,30	27,9	3,6	65,60	26	26	0
1277	65,631	4,6		62,20	35,4	2,5	65,64	29	28	1
1197	65,667	3,6		59,30	36,2	3,2	65,75	29	26	3
1107	65,708	7,0		59,50	31,1	3,9	65,82	32	28	4
992	65,759	18,5		56,90	22,6	4,8	65,86	30	25	5
922	65,791	28,3	0,4	53,80	12,7	5,0	65,90	31	28	3
847	65,824	54,3	0,5	41,10	2,9	8,8	65,94	32	28	4
747	65,869	59,9	0,2	36,10	2,2	11,1	65,95	31	25	6
647	65,914	31,1	7,7	53,90	5,4	10,1	65,96	29	24	5
547	65,959	1,2	11,6	77,60	9,1	8,4	65,97	29	23	6
447	65,969	3,5	53,5	28,30	8,9	8,1	65,97	26	20	6
372	65,976	2,9	70,1	17,00	8,6	7,2	65,98	22	16	6
297	65,983	4,5	70,1	23,70	0,8	3,1	65,99	21	15	6
247	65,988	8,6	90,3	1,40	0,0	7,3	66,00	16	6	10
197	65,992	7,9	92,1	0,00	0,0	10,7	66,00	16	6	10
172	65,995	27,3	71,8	0,90	0,0	11,0	66,00	21	2	19
147	65,996	72,3	27,4	0,30	0,0	8,3	66,00	26	2	24
122	65,997	83,5	16,5	0,00	0,0	9,3	66,00	61	0	61
97	65,997	73,7	23,7	2,50	0,0	19,5	66,00	60	0	60
67	65,999	89,8	9,5	0,70	0,0	19,3	66,00	59	0	59
37	66,000	100	0,0		0,0	15,1	66,00	61	0	61
17	66,000	100			0,0	14,2	66,01	58	0	58
7	66,001	100			0,0	13,2	66,01	61	0	61
2	66,001	100			0,0	2,0	66,01	61	0	61
-1	66,001	1,2			0,0	0,0	66,02	62	0	62
-3	66,001	1,2			0,0	0,3	66,02	59	0	59
-20	66,003	0,3					66,03	62	0	62
-40	66,004	1,8					66,05	63	0	63
-70	66,007	0,9					66,06	66	0	66
-100	66,009	2,2					66,08	63	0	63
-135	66,012	0,3					66,09	64	0	64
-175	66,015	2,3					66,10	66	0	66
-250	66,022	0,9								
-400	66,034	1,2								
-540	66,046	2,6								
-750	66,063	4,1								
-900	66,075	3,4								
-1050	66,088	2,1								
-1200	66,100	1,8								

Nota: (1) = (Gilabert et al., 2021c); (2) (Gilabert et al., 2021a); (3) Gilabert et al., 2021b; (4) (Arenillas et al., 2018); (NP) No publicado, Triseriados = *Guembelitra* + *Chiloguembelitra*; Parvularugoglobigerinidos = *Parvularugoglobigerina* + *Palaeoglobigerina* + *Pseudocaucasina*; Biseriados = *Woodringina* + *Chiloguembelina*; Otros géneros = *Globanomalina*, *Praemurica*, *Subbotina*, *Parasubbotina*, *Globoconusa*, *Trochoguembelitra*, *Eoglobigerina*,

TABLA ANEXA 2: SECCIÓN DE AÏN SETTARA

Altura respecto al límite K/Pg	Edad recalibrada según (1)	Triseriados (4)	Parvularugoglobigerinidos (4)	Biseriados (4)	Otros géneros (4)	Aberrantes total (4)
(cm)	(Ma)	(%)	(%)	(%)	(%)	(%)
1040	65,600	2,2	0,0	44,1	53,7	1,6
860	65,723	15,4	0,0	52,4	32,2	2
660	65,858	16,6	5,2	64	24,6	1,7
560	65,925	38,4	2,5	48,2	15,9	10,8
460	65,961	35,8	5	47,2	22	11
360	65,965	4,5	76,3	17,3	1,9	5,9
260	65,970	3,4	76,5	20,1	0,0	5,8
160	65,974	10,2	74	15,8	0,0	6,2
130	65,977	13,5	86,1	0,4	0,0	8,7
110	65,978	14,2	85,8	0,0	0,0	7,2
80	65,981	7,4	92,6	0,0	0,0	7,4
60	65,983	26,9	73,1	0,0	0,0	8,9
55	65,985	24,4	75,6	0,0	0,0	5,8
50	65,986	29,5	70,5	0,0	0,0	4,9
45	65,987	37,3	627	0,0	0,0	7,7
40	65,989	31,4	68,6	0,0	0,0	6
30	65,992	42,4	57,6	0,0	0,0	10
20	65,995	85,4	14,6	0,0	0,0	14,2
15	65,996	94,4	5,6	0,0	0,0	15,2
10	65,998	100	0,0	0,0	0,0	16
5	65,999	100	0,0	0,0	0,0	17,9
-1	66,001	4,7				
-2	66,001	3,4				
-6	66,002	0,9				
-11	66,003	4,2				
-13	66,003	1,8				
-21	66,004	1,8				
-31	66,006	2				
-40	66,007	1,3				
-90	66,015	2,7				
-140	66,023	1,7				
-240	66,038	1				
-340	66,054	2,5				
-540	66,085	6				
-640	66,100	6,9				

Nota: (1) = (Gilabert et al., 2021c); (2) (Gilabert et al., 2021a); (3) Gilabert et al., 2021b; (4) (Arenillas et al., 2018); (NP) No publicado, Triseriados = *Guembelitra* + *Chiloguembelitra*; Parvularugoglobigerinidos = *Parvularugoglobigerina* + *Palaeoglobigerina* + *Pseudocaucasina*; Biseriados = *Woodringina* + *Chiloguembelina*; Otros géneros = *Globanomalina*, *Praemurica*, *Subbotina*, *Parasubbotina*, *Globoconusa*, *Trochoguembelitra*, *Eoglobigerina*,

**Tabla Anexa 2.** Compilación de los resultados obtenidos en la presente tesis doctoral para la elaboración de la figura de síntesis, Figura 11.

# *Apéndices*





**APÉNDICE I. Listado de trabajos que componen esta tesis doctoral.**

-Arenillas, I., Arz, J. A., **Gilbert**, V., 2017. Revalidation of the genus *Chiloguembelitra* Hofker: Implications for the evolution of early Danian planktonic foraminifera. *Journal of African Earth Sciences* 134, 435–456.

Factor de impacto: 1.532 - 122/189 Q3 Geociencias, Multidisciplinar: El doctorando contribuyó en el reconocimiento y extracción de especímenes de *Chiloguembelitra* para su posterior análisis biométrico, así como en la discusión, escritura y revisión del manuscrito.

-Arenillas, I., Arz, J. A., **Gilbert**, V., 2018. Blooms of aberrant planktic foraminifera across the K/Pg boundary in the Western Tethys: causes and evolutionary implications. *Paleobiology* 44, (3), 460–489.

Factor de impacto: 2.354 - 6/57 Q1 Paleontología: El doctorando contribuyó en el reconocimiento y extracción de especímenes de foraminíferos planctónicos con malformaciones, así como en la discusión, interpretación de resultados, escritura, revisión del manuscrito, y preparación y edición de figuras.

-**Gilbert**, V., Arz, J.A., Arenillas, I., Robinson, S.A., and Ferrer, D., 2021. Influence of the Latest Maastrichtian Warming Event on planktic foraminiferal assemblages and ocean carbonate saturation at Caravaca, Spain. *Cretaceous Research* 125, 104844.

Factor de impacto: 2.176 - 8/55 Q1 Paleontología (datos SCI 2020): El doctorando realizó la clasificación a nivel de género de los foraminíferos planctónicos maastrichtienses, fotografió los especímenes en el SEM, calculó el índice de fragmentación, participó en los análisis biométricos, y preparó las muestras para los análisis isotópicos y calcimetrías. El doctorado se encargó de la conceptualización, investigación, elección y utilización de metodología, así como de la escritura y elaboración de las figuras del manuscrito.

-**Gilbert**, V., Arenillas, I., Arz, J.A., Batenburg, S., Robinson, S.A., 2021. Multiproxy analysis of paleoenvironmental, paleoclimatic and paleoceanographic changes

during the Early Danian in the Caravaca section (Spain) *Palaeogeography, Palaeoclimatology, Palaeoecology* 576, 110513.

Factor de impacto: 3.318 - 2/54 Q1 Paleontología (datos SCI 2020): El doctorando realizó la clasificación a nivel de especie de los foraminíferos planctónicos del Daniense y Maastrichtiense, fotografió los especímenes en el SEM, calculó el índice de fragmentación, reconoció y cuantificó el porcentaje de especímenes aberrantes, preparó las muestras para isótopos estables, calcimetrías y susceptibilidad magnética. El doctorado se encargó de la conceptualización, investigación, elección y utilización de metodología, así como de la escritura y elaboración de las figuras del manuscrito.

**-Gilabert, V., Batenburg, S.J., Arenillas.I., Arz, J.A., 2021.** Contribution of orbital forcing and Deccan volcanism to global climatic and biotic changes across the KPB at Zumaia, Spain. *Geology*. <https://doi.org/10.1130/G49214.1>. Publicado online como *Early Publication* el 30 de Agosto del 2021 (pendiente de asignación de volumen).

Factor de impacto: 5.399 - 1/61 Q1 Geología (datos SCI 2020). El doctorando realizó la clasificación a nivel de especie de los foraminíferos planctónicos del Daniense y Maastrichtiense, desarrolló un modelo de edad calibrado astrocronológicamente, preparó las muestras para isótopos estables, calcimetrías y susceptibilidad magnética. El doctorado se encargó de la conceptualización, investigación, elección y utilización de metodología, así como de la escritura y elaboración de las figuras del manuscrito.

## APÉNDICE II. Cartas de aceptación.

Según normativa de Tesis Doctorales de la Universidad de Zaragoza, se adjunta carta de aceptación del artículo titulado: *Contribution of orbital forcing and Deccan volcanism to global climatic and biotic changes across the KPB*, en la revista *Geology*, donde está aceptado y publicado online, pero todavía sin número de volumen y páginas en la versión impresa.

# GEOLOGY

THE GEOLOGICAL SOCIETY  
OF AMERICA®

[Manuscript Home](#) [Author Instructions](#) [Reviewer Instructions](#) [Contact](#) [Journal home](#) [Logout](#)

[Close Window](#)

[Print Email](#)

**Date:** 07-16-2021 01:41

**Last Sent:** 07-16-2021 01:41

**Triggered By:** Redacted

**BCC:** Redacted

**Subject:** G49214R1 Decision Letter from GEOLOGY

**Message:** July 16, 2021

RE: G49214R1  
GEOLOGY

Dear Dr. Gilabert:

I am pleased to inform you that your revised manuscript G49214R1 "Contribution of orbital forcing and Deccan volcanism to global climatic and biotic changes across the KPB at Zumaia, Spain" has been accepted for publication in GEOLOGY.

It was accepted on July 16, 2021. My congratulations for a great paper!

If you will be requesting Gold Open Access, the GEOLOGY OA Article Processing Fee is US\$2500. Please contact Lyne Yohe, Managing Editor of GEOLOGY, at [lyohe@geosociety.org](mailto:lyohe@geosociety.org) to complete the request process.

If you have not already done so, please send electronic copies of your final figure files (in native graphics format and high-resolution PDF format) to us at [geology@geosociety.org](mailto:geology@geosociety.org) or [lyohe@geosociety.org](mailto:lyohe@geosociety.org).

We will soon be sending you a copyedited version of your paper, for your approval, prior to typesetting.

Any questions you might have about your manuscript should be directed to [geology@geosociety.org](mailto:geology@geosociety.org).

Thank you for submitting your work to this journal.

Sincerely,  
Urs Schaltegger  
Science Editor  
GEOLOGY

-----